2-2013

Techno-Economic Feasibility Study of Ammonia Plants Powered by Offshore Wind

Eric R. Morgan
University of Massachusetts Amherst, aixeric@gmail.com

TECHNO-ECONOMIC FEASIBILITY STUDY OF AMMONIA PLANTS POWERED BY OFFSHORE WIND

A Dissertation Presented

by

ERIC R. MORGAN

Submitted to the Graduate School of the
University of Massachusetts Amherst in partial fulfillment
of the requirements for the degree of

DOCTOR OF PHILOSOPHY

February 2013

Department of Mechanical and Industrial Engineering

A TECHNO-ECONOMIC FEASIBILITY STUDY OF AMMONIA PLANTS POWERED BY OFFSHORE WIND

A Dissertation Presented

By

ERIC R. MORGAN

Approved as to style and content by:

Jon G. McGowan, Chair

James F. Manwell, Member

Senay Solak, Member

Donald L. Fisher, Department Head
Department of Mechanical and Industrial Engineering

DEDICATION

To my children, Brighid and Sawyer

ACKNOWLEDGEMENTS

I am grateful to the many people that have helped me get to this point in my career. I could not have done this alone. I would like to first thank my committee members: Jim Manwell and Senay Solak of the University of Massachusetts. Their assistance, guidance and support were pivotal in helping me finish this dissertation. I am indebted to my mentor and friend, Jon McGowan, for embracing research on wind-powered ammonia and supporting me every step of the way. He told me to "go big", and so I did. Thank you.

I would like to thank kind people at the Wind Energy Center for their warmth and friendship over the course of my four-year stay. During many of our weekly meetings students, staff and faculty asked questions that proved invaluable to my research. Some of the questions that were posed took three years to answer – that's the kind of questioning that makes a PhD worth it. My life and career benefited from the work that Jon Black, Charlie McClelland, Dan Finn-Foley and Bob Hyers did with me on behalf of "Apera Technology". The brief time we spent on that endeavor forever changed how I think of engineering, technology and business.

I have fond memories of going on tower trips with Tony Ellis et al. (despite the brutally early mornings). Tromping around New England with friends to put up or take down towers can be rewarding. I saw many things that I never expected; the hands-on experience that I got from those trips still proves useful.

I would like to thank Fred Letson and Nico Lustig for smoothing the edges of academic life. All those late nights playing board games together have a special place in my heart. Thanks to Jon Lewis who once told me that my dog had excellent "thrust vectors". Jon, that was priceless and unforgettable, like many of your insights.

My former colleagues at UMass Lowell started me down this path back in 2005 when I entered the Civil and Environmental Engineering Department. Donald Leitch taught me how to be a professional and dignified engineer back when I still had an adolescent mentality. Thanks to John Duffy who gave me the opportunity to be a paid graduate student. For that, I am appreciative. Dan Golumb opened up the world of industrial chemistry via an amazing course, and two coal-fired electricity plant tours. His course was a remarkable experience that I still draw from. Kiwi smashed mathematics and engineering together to form a beautiful course that every engineer should take. I took it and reaped the benefits.

I thank my parents yet again for embodying their phrase “the kids always come first”. From my earliest memories they gave all they had so that I could get to this point. Now that I'm here, I am as proud of them as they are of me. My brother, Tom, provided valuable insight into chemistry, engineering, writing and life throughout my college career. Thanks for the inspiration and friendship, little brother. I would like to thank Liz and Charles Holt who opened their home to me and my family so that I could complete this dissertation. With your help, I worked my way out of the basement. I would like to thank my wife, Frances, for always being there, day or night, holiday or weekday, when I needed her. She made many sacrifices so that I could be a student, and finish being a student. I cannot thank you enough. Also, thanks to my kids, Brighid and Sawyer, for helping me to keep everything in perspective.

ABSTRACT

A TECHNO-ECONOMIC FEASIBILITY STUDY OF AMMONIA PLANTS POWERED BY OFFSHORE WIND

FEBRUARY 2013

ERIC R. MORGAN, B.S., UNIVERSITY OF MASSACHUSETTS AMHERST

M.S., UNIVERSITY OF MASSACHUSETTS LOWELL

Ph.D., UNIVERSITY OF MASSACHUSETTS AMHERST

Directed by: Professor Jon G. McGowan

Ammonia production with offshore wind power has the potential to transform energy and fertilizer markets within the United States. The vast offshore wind resource can be converted directly into liquid ammonia using existing technologies. The liquid ammonia can then be transported around the country via rail, truck, barge or pipeline and used as either a fertilizer or a fuel. This thesis reviews the technologies required for all-electric, wind-powered ammonia production and offers a simple design of such a system. Cost models based on the physical equipment necessary to produce ammonia with wind power are developed; offshore wind farm cost models are also developed for near-shore, shallow, wind farms in the United States. The cost models are capable of calculating the capital costs of small industrial-sized ammonia plants coupled with an offshore wind farm. A case study for a utility-tied, all-electric ammonia plant in the Gulf of Maine is used to assess the lifetime economics of such a system. Actual utility grid prices and offshore wind are incorporated into a systems-level simulation of the ammonia plant. The results show that significant utility grid backup is required for an all-electric ammonia plant built with present-day technologies. The levelized cost of one metric ton of ammonia is high

relative to ammonia produced with natural gas or coal, but is not as susceptible to spikes in ammonia feedstock prices. A sensitivity analysis shows that the total levelized cost of ammonia is driven in large part by the cost of producing electricity with offshore wind. Major cost reductions are possible for systems that have long lifetimes, low operations and maintenance costs, or for systems that qualify for Renewable Energy Credits.

PREFACE

Ammonia production represents the opportunity to simultaneously produce two disparate commodities: energy and food. At present, ammonia-based fertilizers feed about 3 billion people by enabling more food to be grown on a given area of land. Ammonia can be also be used as a synthetic fuel in diesel engines, internal combustion engines and gas turbines. If enough ammonia can be sustainably produced, it could displace the need for fossil fuels in the future. Thus, sustainable manufacture of ammonia for feeding the world's population and, perhaps, fueling vehicles, represents a worthy endeavor for scientists and engineers of today, just as it was for engineers one hundred years ago. This thesis couples ammonia production with offshore wind power, a mature form of renewable energy that is poised for worldwide expansion in the near future. Why choose offshore wind power to produce ammonia when it is already known to be expensive? Offshore wind power is slated to move further from shore and onto floating structures. These structures could potentially be remote enough that electrical cables are not practical. Thus, ammonia could be synthesized on site and shipped back to shore, or around the world. This idea is not new: the Applied Physics Laboratory at The Johns Hopkins University investigated ammonia production with Ocean Thermal Energy Conversion (OTEC) in the 1970s and 1980s. Given the immensity of the ocean and the significant offshore wind resource that it represents, it is possible that floating offshore wind power could generate ammonia fertilizers and fuels for the entire planet in the future. This thesis investigates the simple case of offshore wind powering an ammonia synthesis facility located onshore. The economics for such a system represent a best case scenario for ammonia production, as it is currently practiced. If significant government incentives are created for ammonia production, it is possible to competitively manufacture ammonia for both fertilizers and fuel.

TABLE OF CONTENTS

Page

ACKNOWLEDGEMENTS v

ABSTRACT vii

PREFACE ix

LIST OF TABLES xv

LIST OF FIGURES xix

CHAPTER

1 – THESIS OVERVIEW AND BACKGROUND 1

2 – AMMONIA PRODUCTION 5

2.1 Traditional Ammonia Production 6

2.1.1 Conventional Steam Reforming 9

2.1.2 Partial Oxidation 12

2.1.3 Electrolytic Ammonia 13

2.1.4 Syngas Compression 14

2.1.5 Synthesis of Ammonia 15

2.1.6 Technical Requirements 18

2.1.7 Environmental Issues 20

3 – OFFSHORE WIND POWER 25

3.1 State-of-the-Art 27

3.1.1 Electrical Connection 31

3.1.2 Current Trends 35

3.2 Environmental 42

3.2.1 Birds 42

3.2.2 Fish and Marine Mammals 44

3.2.3 Benthos 44

3.3 Power Curves 44

3.3.1 Wind Farm Power Curve 48

4 – REVIEW OF ALL-ELECTRIC AMMONIA SUBSYSTEM ANALOGUES 53

4.1 Hydrogen Production 53
4.1.1 Electrolyzers 53
4.1.1 Thermodynamics of electrolyzers 61
4.2 Nitrogen Production Methods 65
4.2.1 Cryogenic Air Separation 66
4.2.2 Pressure Swing Adsorption (PSA) 67
4.2.3 Membrane Separation 69
4.2.4 Inert Gas Generators 70
4.3 Gas Compressors 71
4.4 Desalination of water 74
4.4.1 Thermal processes 75
4.4.2 Membrane Processes 78
4.4.3 Other desalination processes 80
4.5 Product Storage 81
4.5.1 Ammonia 82
4.5.2 Hydrogen 84
4.5.3 Nitrogen and Oxygen 88
4.5.4 Purified Water 88
4.6 Energy Storage 88
4.6.1 Sodium Sulfur 89
4.7 Literature Review of Ammonia Subsystems 92
4.7.1 Survey of Ammonia Production Subsystems Powered by Renewable Energy 97
5 – SYSTEM SELECTION AND TECHNICAL FEASIBILITY 113
5.1 Electric Ammonia Plant Flow Rates 113
5.2 All-Electric Ammonia Plant Equipment Selection 115
5.2.1 Nitrogen Subsystem 115
5.2.2 Hydrogen Subsystem 116
5.2.3 Water Desalination 117
5.2.4 Synthesis Loop 119
5.2.5 Final Subsystem Selection 119
5.3 Flexible Ammonia Production 120
6 – THE ECONOMICS OF AMMONIA PLANTS 123

6.1 Capital Costs 123
6.1.1 Pressure Factors 125
6.1.2 Materials Factors 126
6.2 Manufacturing Costs 128
6.2.1 Raw materials 129
6.2.2 Waste Treatment 130
6.2.3 Utilities 130
6.2.4 Operating labor 131
6.3 Ammonia Synthesis Loop 132
6.3.1 Compression power for the feed stream 136
6.3.2 Compression in the recycle stream 139
6.3.3 Drivers 140
6.3.4 Power Requirements for Compression 141
6.3.5 Ammonia Synthesis Reactor and Flash Drum 141
6.3.6 Heat Exchangers 145
6.3.7 Pumps 151
6.3.8 Synthesis Loop Capital Costs 152
6.3.9 Synthesis Loop Manufacturing Costs 158
6.4 Hydrogen Production/Electrolyzers 159
6.4.1 Overview of Electrolysis Economics 160
6.4.2 Large Scale Electrolyzers 162
6.4.3 Results 173
6.4.4 Conclusions 177
6.5 Air Separation 177
6.5.1 Compression and expansion 181
6.5.2 Drivers 182
6.5.3 Heat Exchangers 183
6.5.4 Towers 185
6.5.5 Economics of Air Separation 186
6.6 Mechanical Vapor Compression 193
6.6.1 Mathematical model 194
6.6.2 Economics of MVC 197
6.7 Ammonia Storage 201

6.7.1 Economics of Ammonia Storage 204
6.8 Total Overall Costs 206
6.9 Total Power Requirements in the Ammonia Synthesis Process 209
6.9.1 Synthesis Loop 209
6.9.2 Air Separation Power 209
6.9.3 Mechanical Vapor Compression 210
6.9.4 Electrolyzers 211
6.9.5 Ammonia Storage 211
6.9.6 Total Power Required 211
6.10 Manufacturing Costs for Ammonia Synthesis 213
7 – WIND POWER ECONOMICS 216
7.1 Rotor Nacelle Assembly (RNA) and Tower 216
7.1.1 Cost Escalation Method 218
7.1.2 Application of the cost escalation method 220
7.1.3 Comparison with Wind Turbine Prices 224
7.1.4 Conclusions 227
7.2 European Cost Data 228
7.2.1 Variations in Inflation Indices 230
7.2.2 Currency Exchange and PPPs 232
7.2.3 Translating Historical Foreign Costs to Real US Dollars 234
7.2.4 Example Cost Conversion Calculations 236
7.2.5 Discussion of Conversion Results 240
7.2.6 Conclusions 246
7.3 European Equipment Costs 247
7.3.1 Foundation/Substructure 248
7.3.2 Wind Farm Cables 252
7.4 Results and Validation 263
8 – BASELINE NH_3 – OFFSHORE WIND PLANT 273
8.1 Gulf of Maine Wind Resource 273
8.2 Baseline Wind Farm Specifications 277
8.3 Power Production 278
8.4 Levelized Costs 279

8.4.1 Levelized Cost of Energy 280
8.4.2 Levelized Cost of Ammonia 282
8.5 Deviations from the Base Case 293
8.5.1 Hydrogen Storage Systems versus Battery Systems 294
8.5.2 Tax Incentives and Investment Strategies 304
8.5.3 Sensitivity Calculations 305
9 – SUMMARY AND FUTURE WORK 310
9.1 Future Work 312
APPENDIX – MATLAB SIMULATION CODE 316
REFERENCES 376

LIST OF TABLES

Table Page

Table 1 – The typical composition of syngas for the Kellogg Ammonia Process 9

Table 2 – Gas composition following carbon dioxide removal [27] 11

Table 3 – Ammonia production emissions for a 1200 metric ton/d steam reforming plant [43] 22

Table 4 – Ammonia production emissions for a 1200 metric ton/d partial oxidation plant [43] 23

Table 5 – Ammonia toxicity to humans [48] 24

Table 6 – Support structure types used in offshore wind farms [51] 29

Table 7 – Worldwide offshore wind farm data (references in table) 33

Table 8 – Array efficiencies based on turbine spacing [104] 50

Table 9 – Principle gases of dry air [127] 65

Table 10 – Application range of nitrogen separation processes [128] 65

Table 11 – Typical composition of dissolved solids in seawater [143] 75

Table 12 – Energy consumption of desalination systems assuming seawater with 35,000 ppm TDS [141] *calculated using parenthetical value in mechanical power column 81

Table 13 – Properties of anhydrous ammonia [31] 83

Table 14 – Features of ammonia storage tanks [28] 84

Table 15 – Selected solar hydrogen plant installations. 98

Table 16 – Major hydrogen systems that include wind power that have been installed since 2000. 103

Table 17 -- Worldwide solar powered Reverse-Osmosis plants [262] 108

Table 18 – Worldwide solar distillation plants [261] 109

Table 19 – Advantages and disadvantages for different autonomous desalination systems [278] 111

Table 20 – The flow rates of nitrogen, hydrogen and water through an electric ammonia plant 114

Table 21 – Characteristics of the three major electrical desalination processes [141, 145, 281] 118

Table 22 – Subsystem selection for an all-electric ammonia plant 120

Table 23 – Cost parameters used in this study, from [296] 125

Table 24 – Bare module cost factors for ammonia synthesis equipment 127

Table 25 – Direct manufacturing costs for chemical plants [296] 129

Table 26 – Stream table for a simple ammonia synthesis loop 135

Table 27 –Coefficients used in calculating the specific heats of the gases present in the synloop [310] 137

Table 28 – Assumed operating conditions and parameters of the ammonia synthesis loop 138

Table 29 – The power requirements for the compressors and the drivers for various ammonia plants 141

Table 30 – Stream table for an ammonia synthesis loop [34] 147

Table 31 – Heat exchanger temperature data from the synloop 148

Table 32 – Summary of calculations for redistributed gases to displace inerts 148

Table 33 – Approximate U-values for the major heat exchangers present in an ammonia synloop 150

Table 34 – The approximate surface area of each of the major heat exchangers within the compressor train and synloop 151

Table 35 – Summary of the sizes and costs of the equipment required for a synloop 153

Table 36 – Cost parameters used in this study 154

Table 37 – The bare module cost factors for the synthesis loop equipment 157

Table 38 – State of the art hydrogen production technology from electrolysis of water [314] 159

Table 39 – Baseline operating parameters for a Norsk Hydro 5040 Atmospheric electrolyzer [116, 288] 160

Table 40 – Exchange rates for Norwegian kroner and US dollars for 2002 and 2005 [319] 163

Table 41 – General inflation for the US and Norway 163

Table 42 – The costs in 2005$ of a Norsk Hydro electrolyzer using two methods 163

Table 43 – The averaging approach to currency conversion across time, as applied to electrolyzer costs 165

Table 44 – Cost breakdown of a Norsk Hydro electrolyzer 165

Table 45 – Assumed scaling exponents for the equipment analyzed in this study 167

Table 46 – Scaling exponents for the balance of plant equipment 172

Table 47 – The scenarios used for sensitivity analysis 175

Table 48 – Column dimensions for an ASU [328] 180

Table 49 – The compressors for an ASU 182

Table 50 – Compressor drivers and ratings for an ASU 183

Table 51 – Major heat exchangers, sizes and heat duties in an ASU 185

Table 52 – Columns specifications for an air separation unit 186

Table 53 – The cost constants for the major pieces of equipment in an ASU 186

Table 54 – Coefficients for the bare module cost factor of heat exchangers and towers 187

Table 55 – Compressors used in an ASU 188

Table 56 – The drives used in conjunction with the compressors in an ASU 189

Table 57 – Total bare module cost factors for the distillation towers in an ASU 189

Table 58 – Tower cost data for an ASU 190

Table 59 – Equipment list and costs for a 250 tonne/day GN_2 ASU plant 192

Table 60 – Parameters used in the MVC model [335] 197

Table 61 – The approximate sizes of the equipment in a MVC distillation plant 197

Table 62 – Cost constants for the MVC equipment [296] 198

Table 63 – Equipment list for a 500 m^3/day distillation plant 199

Table 64 – A stream table for the ammonia refrigeration loop shown in Figure 54 203

Table 65 – Cost constants to be used for ammonia storage [296] 204

Table 66 – Summary of the operating labor required for an all-electric 300 tpd ammonia plant, based on Equation 50 215

Table 67 – Wind turbine components and associated NAICS codes (*General inflation) [110] 219

Table 68 – Specifications for a Vestas V82 1.65MW wind turbine 220

Table 69 – The original and inflated costs of all the components 222

Table 70 – A comparison of turbine cost changes for the LBNL analysis and the present work (2010$/kW) 226

Table 71 – Wind farms built in the UK with reliable capital cost information [49] 237

Table 72 – Example calculations for representing the cost of Blyth Offshore wind farm in 2010 US dollars 238

Table 73 – Actual and calculated array cable lengths 255

Table 74 – XLPE AC Cable Data 256

Table 75 – Cost constants to be used with Equation 146 257

Table 76 – Eight wind farms used in the offshore wind farm validation 270

Table 77 – Baseline wind farm specifications 278

Table 78 – Assumptions for calculating the LCOE using Equation 157 281

Table 79 – Results from the simulation of the baseline wind-ammonia plant 290

Table 80 – Economic assumptions for the LCOA calculation 291

Table 81 – Energy storage characteristics and costs for batteries [405] 297

LIST OF FIGURES

Figure Page

Figure 1 – Electrolytic ammonia process flow diagram 14

Figure 2 – Process flow of ammonia synthesis loop 16

Figure 3 – The US offshore wind resource [50] 27

Figure 4 – Offshore wind turbine structures for shallow water. From L-R: monopile, tripod, and gravity foundations [60] 28

Figure 5 – The jacket type structure for offshore wind installations. [61] 28

Figure 6 – Electrical layouts for offshore wind farms 32

Figure 7 – Cabling specifications for the Lillgrund offshore wind farm [67] 35

Figure 8 – Worldwide offshore wind power development 1991-2010 (References: see Table 7) 37

Figure 9 – Offshore wind capacity by country (November 2010) (References: see Table 7) 38

Figure 10 – Average distance from shore, water depth and wind farm size (References: see Table 7) 39

Figure 11 – Turbine rotor diameter and wind farm size trends in European waters, 2000-2010 (References: see Table 7) 40

Figure 12 – The progression of offshore wind into deeper water further from shore (References: see Table 7) 41

Figure 13 – Bird tracks derived from RADAR at the Nysted offshore wind farm [101] 43

Figure 14 – The power curve for a GE 1.5sl wind turbine [103] 45

Figure 15 – A power curve for a generic 3 MW wind turbine 48

Figure 16 – A normalized composite power curve for a theoretical 300 MW wind farm 51

Figure 17 – Normalized power curves for a single turbine and a wind farm [111] 52

Figure 18 –Schematic of an alkaline electrolyzer 55

Figure 19 – Schematic of a Proton Exchange Membrane (PEM) electrolyzer 56

Figure 20 – Schematic of a Mercury Cell for chlorine and hydrogen production 59

Figure 21 – Schematic of a Diaphragm cell 60
Figure 22 – Membrane cell for chlorine and hydrogen production. 61
Figure 23 – Competitive range of air separation technologies [129] 66
Figure 24 – A basic schematic of cryogenic air separation 67
Figure 25 – Schematic of a PSA adsorption nitrogen generator [132] 68
Figure 26 – Schematic of a membrane nitrogen generator 69
Figure 27 – Hierarchy of compressor types [136] 71
Figure 28 – Competitive ranges for compressors [137] 72
Figure 29 – Boiling point variation of water with pressure 76
Figure 30 – The principle of reverse osmosis 80
Figure 31 – Volumetric and gravimetric energy densities of some alternative fuels 86
Figure 32 – Underground natural gas storage facilities in the United States [167] 87
Figure 33 – Electricity storage options [171] 89
Figure 34 – Schematic of a sodium sulfur cell [175] 91
Figure 35 – Possible pairings of solar and wind energy systems with desalination technologies 106
Figure 36 – A simple ammonia synthesis loop in Aspen Plus 135
Figure 37 – Fluid compression power for the feed gas in an all-electric ammonia synthesis loop 139
Figure 38 – Pressure drop as a function of space velocity for granular ammonia catalyst [308] 143
Figure 39 – Approximate diameters for an ammonia reactor for various ammonia capacities and operating pressures. 144
Figure 40 – The volume of ammonia synthesis reactors for various ammonia plant capacities and operating pressures 144
Figure 41 – An ammonia synthesis loop with a 3 bed reactor [34] 146
Figure 42 – A grassroots cost plot of small all-electric ammonia synthesis loops 157
Figure 43 – Tornado chart for the simple lifetime cost of a Norsk Hydro 5040 electrolyzer 161

Figure 44 – The schematic of an electrolysis plant [317] 169

Figure 45 – The capital costs for scaled subsystems within a Norsk Hydro alkaline electrolyzer 174

Figure 46 – The total uninstalled costs for scaled and unscaled electrolyzers 175

Figure 47 – The effect of different scaling exponents on the uninstalled costs of alkaline electrolyzers 176

Figure 48 – Tornado chart for the scaling of equipment in an alkaline electrolyzer 177

Figure 49 – A schematic on an air separation unit (ASU) for the production of nitrogen, oxygen and argon [328] 179

Figure 50 – A schematic of a cryogenic air separation facility [328] 180

Figure 51 – Capital Costs of an ASU 191

Figure 52 – A Schematic of a mechanical vapor compression (MVC) plant [335] 193

Figure 53 – Grass roots cost (top) and unit product cost (bottom) for MVC plants of various sizes 200

Figure 54 – A simplified ammonia storage compression loop 201

Figure 55 – Grass roots cost for an ammonia storage facility 206

Figure 56 – Capital cost curve for an all-electric ammonia plant 207

Figure 57 – Capital cost breakdown of a 300 t/d all-electric ammonia plant with electrolyzer scaling 208

Figure 58 – Capital cost breakdown of a 300 t/d all-electric ammonia plant without electrolyzer scaling 208

Figure 59 – Power requirements of all-electric ammonia facilities 212

Figure 60 – The power requirement breakdown for an all-electric ammonia plant 213

Figure 61 – Cost contributions for the parts in a wind turbine 223

Figure 62 – Cost and price trends in wind turbines 226

Figure 63 – Percent change in the GDP deflator indices in Europe, the UK and the US and Denmark over the period 1990 to 2010 [320-321, 360] 232

Figure 64 – Exchange rates and PPPs for several countries with offshore wind farms [319, 361, 367] 234

Figure 65 – The capital costs for offshore wind farms in the UK, calculated using pure exchange rates 239

Figure 66 – The capital costs for offshore wind farms in the UK calculated using PPPs..... 240

Figure 67 – The conversion factors for GBP to 2010 USD using exchange-inflate, inflate-exchange, and the average over all combinations for the period 2000-2010 with traditional exchange rates (top) and PPPs (bottom) 242

Figure 68 – The conversion factors for EUR to 2010 USD using exchange-inflate, inflate-exchange, and the average over all combinations for the period 2000-2010 with traditional exchange rates (top) and PPPs (bottom) 244

Figure 69 – Forces acting on an offshore wind turbine with a monopile substructure 249

Figure 70 – An example of tapered cables used in the Lillgrund wind farm 253

Figure 71 – Rectangular offshore wind farm setup showing the influence of spacing on the inter-turbine cable length..... 254

Figure 72 – The offshore substation installed at Lillgrund [373] 262

Figure 73 – Inputs to the power production and cost models 265

Figure 74 – Calculated capital cost breakdown of the baseline offshore wind farm 267

Figure 75 – A visual comparison of the offshore wind economic model and the actual costs 271

Figure 76 – Calculated installed capital costs of offshore wind farms in the United States. 272

Figure 77 – Calculated normalized capital costs for offshore wind farms in the United States 272

Figure 78 – Gulf of Maine Bathymetry [392] 274

Figure 79 – Comparison of averaged wind data from 1984-2008 for Matinicus Rock and Mt. Desert Rock 275

Figure 80 – Range of average monthly wind speeds at Mt. Desert Rock, 1985-2008..... 276

Figure 81 – Wind rose for the Mt. Desert Rock site in the Gulf of Maine. 277

Figure 82 – Calculated average weekly power output from a fictitious 300 MW wind farm in the Gulf of Maine..... 279

Figure 83 – LCOE for offshore wind farms ranging from 3 MW to 300 MW 282

Figure 84 – Average Weekly Electricity Price Based on LMPs 284

Figure 85 – The projected weekly revenue from the baseline wind farm 285

Figure 86 – Tornado chart for a conventional natural gas fired ammonia plant 288

Figure 87 – Capital cost breakdown of an offshore wind/NH_3 plant 292

Figure 88 – Simulation logic for H_2 storage 298

Figure 89 – Dimensionless analysis of H_2 storage for a wind-driven ammonia plant 299

Figure 90 – The inter-timestep decision process. 301

Figure 91 – Logic scheme for the flexible ammonia plant 302

Figure 92 – Contour plot of the LCOA NPV for various plant configurations 303

Figure 93 – Contour plot for the LCOA with the cost of electricity doubled 304

Figure 94 – Sensitivity analysis of an offshore wind powered ammonia plant. Baseline = $1224/tonne 307

Figure 95 – Tornado chart for an offshore wind powered ammonia plant 308

SYMBOLS AND ACRONYMS

a	annuity factor	[-]
A	Area	[m_2]
A	Plant Capacity	[tons/day]
AC	Alternating Current	[Hz]
AEP	Annual Energy Production	[kWh/year]
AMSL	Above Mean Sea Level	[m]
Ap	Cable Cost Constant	[-]
Ap	Surface Density of Fins on a HX	$[\frac{m^2}{m^3}]$
aq	Aqueous	[-]
Ar	Argon	[-]
b	Loan Interest Rate	[%]
B	Constant for Process Type	[-]
B_1, B_2	Pressure Factor Constants	[-]
B_p	Cable Cost Constant	[-]
Br	Bromine	[-]
C	Cost	[$]
CAES	Compressed Air Energy Storage	[-]
C_{BM}	Bare Module Cost	[$]
C_{Cap}	Total Capital Investment Cost	[$]
C_D	Drag Coefficient	[-]
CH_4	Methane	[-]
Cl_2	Chlorine	[-]
C_{life}	Lifetime Cost	[$]
C_m	Inertia Coefficient	[-]
C_n	New Capital Investment	[$]
C_n	Cost in Year n	[$]
CO	Carbon Monoxide	[-]
$C_{O\&M}$	Annual Operation and Maintenance (O&M) Cost	[$]
CO_2	Carbon Dioxide	[-]
COE	Cost of Energy	[$/kWh]
COL	Cost of Operating Labor	[$]
COM	Cost of Manufacture	[$]
C_p	Coefficient of Performance	[-]
C_p	Specific Heat Capacity at Constant Pressure	$[\frac{J}{kg\,K}]$
C_p	Cable Cost Constant	[-]
CPI	Consumer Price Index	[-]
CRF	Capital Recovery Factor	[-]
CRM	Cost of Raw Materials	[$]
CRSS	Central Receiver Solar System	[-]
CUT	Cost of Utilities	[$]
CWT	Cost of Waste Treatment	[$]
d	Water Depth	[m]
D	Diameter	[m]
DC	Direct Current	[-]
dm	Differential Mass	[kg]

dn	Number of Drawings of Specifications	[-]
DOWEC	Dutch Offshore Wind Energy Converter	[-]
dt	Differential Time	[s]
dT	Differential Temperature	[K]
dV	Differential Volume	[m^3]
$d\Phi_B$	Change in Magnetic Flux	[Wb]
E	Voltage	[V]
E	Energy	[kWh]
E	Purchased Equipment Cost	[$]
e-	Electron	[-]
E_a	Annual Energy Produced	[kWh/year]
ED	Electrodialysis	[-]
EDR	Reversible Electrodialysis	[-]
E_L	Purchased Equipment Labor Cost	[$]
E_y	Annual Energy Produced	[kWh/year]
F	Future Sum of Money	[$]
F	Faraday Constant	[Electric Charge/mole]
f_1	Parameter Related to Faraday Efficiency	[mA^2/cm^4]
f_2	Parameter Related to Faraday Efficiency	[-]
F_{BM}	Bare Module Cost Factor	[-]
FCI	Fixed Capital Investment	[$]
FCR	Fixed Charge Rate	[1/year]
f_d	Unit Cost for a Drawing of Specification	[$]
f_e	Unit Cost of Engineering	[$]
f_F	Construction or Field Expense Factor	[-]
f_l	Cost Factor	[-]
F_m	Materials Factor	[-]
F_p	Cost Factor	[-]
FRB	Flow Redox Batteries	[-]
f_x	Specific Material Cost	[$]
f_y	Specific Material Labor Cost	[$]
g	Gravity	[m/s^2]
GIS	Geographic Information System	[-]
H	Height	[m]
H_2O	Water	[-]
H_2S	Hydrogen Sulfide	[-]
He	Engineering Employee Hours	[-]
HHV	Higher Heating Value	[kJ]
I	Current	[Amp]
I	Cost Index	[-]
I	Interest Earned	[$]
i	Inflation Rate	[%]
ICC	Initial Capital Cost	[$]
I_i	Cost Index of Desired Currency in Year i	[-]
INTA	Instituto Nacional de Técnica Aeroespacial	[-]
IX	Ion Exchange	[-]
j	A Portion of a Membrane	[-]
J_i	Cost Index of Known Currency in Year i	[-]
k	Wave Number	[1/m]
k	Interest/Discount Rate	[%]
k_1, k_2	Reaction Constants	[-]

K_1, K_2, K_3	Cost Constants	[-]
KOH	Potassium Hydroxide	[-]
kV	Kilovolts	[V]
kVA	Kilo-Volt Amps	[VA]
L	Length	[m]
LLC	Lease Land Cost	[$]
LMTD	Log Mean Temperature Difference	[K]
LRC	Levelized Replacement Cost	[$]
m	Mass	[kg]
$\dot{m}$	Mass Flow Rate	[kg/s]
M	Labor Employee Hours for a Specific Material	[-]
M	Overturning Moment	$[\frac{kgm^2}{s^2}]$
M_b	Brine Flowrate	[kg/s]
M_d	Distillate Flowrate	[kg/s]
MEB	Multi Effect Boiling	[-]
MED	Multi Effect Distillation	[-]
M_f	Feedwater Flowrate	[kg/s]
Mg	Magnesium	[-]
MSF	Multi Stage Flash	[-]
MVA	Mega Volt Amps	[-]
Mx	Specific Material Quantity	[-]
N	Number of Interest Periods	[-]
N	Number of Windings	[-]
N	Number of Compression Stages	[-]
n	Scaling Exponent	[-]
n	Adiabatic Exponent	[-]
n	Number of Years	[-]
n	Economic Lifetime of the Wind Farm	[years]
N_2	Nitrogen	[-]
NaCl	Sodium Chloride	[-]
NaOH	Sodium Hydroxide	[-]
NaS	Sodium Sulfur Battery	[-]
n_C	Number of Electrolysis Cells	[-]
n_F	Current Efficiency	[-]
NH_3	Ammonia	[-]
NH_{3OM}	O&M for NH_3 Plant	[$/year]
Nm^3	Normal Cubic Meters (gas at STP equivalent)	[m^3]
Nnp	Number of Pieces of Equipment	[-]
N_{OL}	Number of Operators per Shift	[-]
NREL	National Renewable Research Laboratory	[-]
NSF	National Science Foundation	[-]
NT	Number of Wind Turbines on the Farm	[-]
n_{wt}	Number of Wind Turbines	[-]
O_2	Oxygen	[-]
OM_{cost}	Operations and Maintenance Cost	[$]
OWECS	Offshore Wind Energy Conversion System	[-]
OWPAP	Offshore Wind Powered Ammonia Plant	[-]
p	Partial Pressure	[bar]
P	Permeability	[cm/s]
P	Processing Steps for Manufacture	[-]

P	Principal	[$]
P	Pressure	[bar]
P(V)	Power of the Wind Turbine at Wind Speed V	[W]
P_a	Annual Payment	[$/year]
P_d	Downpayment	[$]
PEM	Proton Exchange Membrane	[-]
PEMFC	Proton Exchange Membrane Fuel Cell	[-]
PPI	Producer Price Index	[-]
ppm	Parts Per Million	[-]
PSA	Pressure Swing Adsorption	[-]
PV	Photovoltaic	[-]
P_{WT}	Power of the Wind Turbine	[W] or [MW]
$\dot{Q}$	Cooling Power	[J/s]
r	Reaction Rate	$[\frac{kg\ NH_3}{\frac{m^3 catalyst}{s}}]$
r	Discount Rate	[%]
R	Radius	[m]
R	Universal Gas Constant	$[\frac{bar\ m^3}{K\ mol}]$
r_1, r_2	Parameter Related to Electrolyte Ohmic Resistance	[Ωm^2]
RO	Reverse Osmosis	[-]
s	Coefficient for Overvoltage on Electrodes	[V]
S	Equipment Size	[m_3],[kW],etc
SAPHYS	Stand-Alone Small Size Photovoltaic Hydrogen Energy System	[-]
S_k	Exchange Rate in Year k	[-]
S_n	Rated Power	[VA]
SSAS	Solid State Ammonia Synthesis	[-]
STP	Standard Temperature and Pressure	[-]
SWB	Solar-Wasserstoff-Bayern	[-]
t	Time in a Sequence (a Given Time t)	[-]
t	Metric Tons	[1000 kg]
T	Temperature	[K]
t_1, t_2, t_3	Empirical Overvoltage Coefficients	[m^2/V]
TDS	Total Dissolved Solids	[-]
t_{soil}	Soiling Loss on Turbine Blades	[%]
TVC	Thermal Vapor Compression	[-]
TW	Terawatts	[W]
U	Wind Speed	[m/s]
U	Voltage	[V]
v	Velocity	[m/s]
V	Voltage	[V]
V	Volume	[m^3]
V	Vanadium	[-]
v_{in}	Cut-in Wind Speed	[m/s]
v_o	Downstream Wind Velocity	[m/s]
v_{out}	Cut-out Wind Speed	[m/s]
VRB	Vanadium Redox Battery	[-]
VVC	Vacuum Vapor Compression	[-]
w	Mass Fraction	[-]

W	Power	[W]
WindPACT	Wind Partnerships for Advanced Component Technology	[-]
WTG	Wind Turbine Generator	[-]
X	Plant Capacity Per Day	[t/d]
X	Salt Concentration of Brine	[ppm]
Y	Operator Labor	$[\frac{hours*processing\ step}{ton}]$
z	Transferred Electrons	[-]
Z_2	Reactor Diameter	[m]
z_H	Height	[m]
Zn	Zinc	[-]
ZnO	Zinc Oxide	[-]
ZnS	Zinc Sulfide	[-]
z_o	Reference Height	[m]
$\Delta G°$	Change in Gibbs Free Energy	[J/mol]
$\Delta H°$	Change in System Enthalpy	[J/mol]
$\Delta S°$	Change in Entropy	[J/molK]
α	Selectivity of a Membrane	[-]
γ	Adiabatic Exponent	[-]
ζ	Wave Amplitude	[m]
η	Efficiency	[-]
η_{Avail}	Wind Farm Availability	[%]
η_{Elec}	Wind Farm Electrical Efficiency	[%]
η_{Farm}	Wind Farm Efficiency	[%]
η_{mech}	Wind Farm Mechanical Efficiency	[%]
λ	Latent Heat	[kJ/kg]
λ	Tip Speed Ratio	[-]
Φ	Power Angle	[rad]
$\phi(V)$	Wind Speed Distribution	[-]
ω	Angular Speed of Rotation	[rad/s]
ρ	Density	[kg/m^3]
ρ_{cat}	Bulk Density of the Catalyst	[kg/L]

CHAPTER 1

THESIS OVERVIEW AND BACKGROUND

Offshore wind in the United States is a vast and wholly untapped resource, capable of providing gigawatts of power. While it is unlikely that the entire resource will ever be fully developed, storage for large scale deployment must be seriously considered. Ammonia offers an attractive chemical storage option for wind power because ammonia plants are scalable to gigawatt-hour sizes; ammonia is easily stored for long periods of time; a mature global infrastructure already exists; and ammonia is an industrial chemical that can be used either as a fuel or a fertilizer.

This thesis discusses the marriage of offshore wind power and industrial ammonia production. In particular, the following topics are addressed:

- The relevant chemical equipment that is necessary and suitable for all-electric wind-driven ammonia production
- The feasibility of creating a standalone ammonia plant
- Cost modeling for all major subsystems of an ammonia plant
- Cost modeling of an offshore wind farm located in the United States
- The levelized cost of an offshore-wind powered ammonia facility

Within each of these topics, a variety of sub-topics are discussed. Notably, cost update methods for wind turbines and European equipment were developed so that plausible cost models for wind turbines could be incorporated. Furthermore, a cost scaling method for industrial-sized electrolytic hydrogen production plants was also developed.

The thesis unites two topics that are infrequently paired, and thus opens new opportunities in both ammonia production and wind energy. First, wind power and ammonia are both given a broad overview to establish fundamental system design principles. Industrial ammonia production is thoroughly detailed enough to create an understanding of the operational requirements. Offshore wind power is then discussed using the European experience as a template for production in the United States. Finally, the two disparate topics are combined through a simulation model that predicts the power outputs, ammonia production capacity and total costs of an offshore-wind powered ammonia plant.

This thesis implicitly challenges the notion that wind turbines exclusively make electricity. Indeed, for many years they were used to grind grain, pump water, or generate heat, yet now all large turbines are assumed to produce electricity. Wind-powered ammonia production removes the constraints of the utility grid, and creates a commodity that can be transported via rail, barge, or truck.

Currently, there is neither in-depth technical discussion in the literature regarding wind powered ammonia nor consideration given to the costs of ammonia manufactured using offshore wind power. To better understand how offshore wind power can assist in the manufacture of ammonia, more research is needed.

This thesis reviews the required technology; establishes a feasible system based on state-of-the-art components; and estimates the overall costs of wind powered ammonia production based on the feasible system. This work illustrates the strengths, weaknesses and costs of an offshore wind powered ammonia facility.

While there are a myriad of possibilities in which wind power could assist ammonia production, only two scenarios will be considered herein:

- A “flexible” offshore ammonia plant capable of high ramp rates powered entirely by wind, with grid backup when necessary
- A traditional grid-assisted offshore wind-powered ammonia plant

Each scenario proposes replacing the major subsystems in an ammonia plant with wind-powered analogs. For example, the steam reforming process that typically produces hydrogen and nitrogen in a traditional ammonia facility can be replaced with wind powered electrolyzers and an air separation unit to achieve the same results.

The work is divided into four main sections. The first section deals with researching the requirements of an ammonia plant. The second section addresses equipment selection in which equipment is evaluated according to the ammonia plant requirements. The third section formulates a parametric simulation in which the feasible systems are modeled and simulated using a three-year-long wind and utility grid data set. The fourth section discusses the economics of the chosen system. The capital costs as well as operation and maintenance costs will be considered for the entire system. The net present value of the entire wind farm and ammonia plant will be used to levelize the costs of producing one metric ton of ammonia.

Chapter 2 provides an introduction to conventional ammonia synthesis and outlines the technical requirements. Chapter 3 discusses the basics of offshore wind power, the current trends, and estimates of power production. Chapter 4 presents a review of the potential wind-powered replacements for all the major ammonia synthesis subsystems and presents the relevant literature. Chapter 5 details the equipment selection for an all-electric ammonia synthesis plant powered by wind and discusses the potential for flexible ammonia production. Chapter 6 reviews the fundamentals of chemical plant economics and provides a framework for determining the capital costs and manufacturing costs for an all-electric ammonia plant. Chapter 7 provides cost modeling of offshore wind farms in the United States through the use of turbine cost scaling and

equipment cost translation methods. Chapter 8 outlines the overall computer model that is used to determine the levelized costs of ammonia and the power generation potential of offshore wind, respectively. Chapter 8 also presents the full results of applying the computer model to a baseline ammonia plant powered by offshore wind. The sensitivity of the levelized cost of ammonia to several key parameters is presented. Chapter 9 summarizes the conclusions of this study, shows how the model may be enhances to, and offers new research opportunities. Appendix A contains the Matlab code that was used in the analysis.

CHAPTER 2

AMMONIA PRODUCTION

Ammonia production, as it is currently practiced, is economically and environmentally unsustainable in the long term. In 2006, ammonia produced by the Haber-Bosch process represented 1.4% of the world consumption of fossil fuel [1], mainly through the use of natural gas and coal. Worldwide production in 2008 was approximately 133 million metric tons, of which about 8 million metric tons were produced in the United States [2]. Natural gas and coal based ammonia production release 2.7 metric tons and 3.4 metric tons of the greenhouse gas carbon dioxide, respectively, for every metric ton produced [3].Because more than eighty percent of ammonia is used for fertilizer manufacture, ammonia production will increase commensurate with population growth, which is projected to rise 30% by 2050 [4-5]. At the same time, natural gas – the main feedstock for ammonia, is expected to become more expensive over the next 20 years as demand outpaces supply [6]. Thus, any significant disruption in natural gas supply can have devastating effects on the world population through decreased fertilizer production.

In order to improve sustainability, ammonia production can be achieved by replacing fossil fuels with renewable energy in the manufacturing process. In fact, some of the earliest ammonia plants used only hydroelectric power to produce ammonia from water and air. Several large scale electrolytic hydrogen facilities have been built since 1928 when hydrogen was first produced via hydroelectric power in Norway [7-9]. By the 1970s, plants in India, Egypt, Zimbabwe, Peru, Iceland and Canada were also producing fertilizers from electrolytic hydrogen [10], the largest of these facilities being the 180 megawatt plant in Egypt. By 1998 only seven hydroelectric

ammonia facilities were still active in the world, accounting for roughly 0.5% of total worldwide ammonia production [10].

Despite early interest in hydroelectric ammonia production, limited research has been conducted on wind powered ammonia production in the last 50 years. Beginning in the early 1960s wind powered ammonia production was investigated by the United States Army through an initiative called the "Energy Depot Concept" [11-13]. Later, in the 1970s, ammonia production using wind power in a standalone system was explored extensively by Lockheed California Company and the National Science Foundation [14-16]. While both the US Army and Lockheed/NSF found that wind power could be used to produce ammonia, neither constructed a wind-ammonia prototype plant; neither discussed the economics of building a wind powered ammonia plant in any significant depth.

In the early 1970s, William Heronemus, a professor at the University of Massachusetts, proposed using offshore wind power to produce hydrogen [17]. Since that time, significant offshore wind power has been developed in Europe, but only for electricity production. At the time of this writing, no offshore wind farms exist in the United States even though coastal and offshore wind regimes along much of the east and west coasts, as well as the Great Lakes, are classified as "excellent", "outstanding" or "superb" [18]. This extensive wind resource can be exploited and converted to ammonia – a hydrogen carrier and a valuable liquid commodity that can be transported and sold throughout the world.

2.1 Traditional Ammonia Production

Ammonia has the chemical formula NH_3 and consists of 82.4% nitrogen and 17.6% hydrogen by weight. Thus, nitrogen and hydrogen must be mixed in the proper proportions and reacted together to form ammonia. Chemical and thermodynamic analyses reveal that the reaction is not

spontaneous at standard temperature and pressure (STP), but is spontaneous at high temperatures and pressures in the presence of a catalyst. This fact is due to the strong triple bond present in the nitrogen molecule (941 kJ/mol) as well as the relatively strong (432 kJ/mol) single bond in the hydrogen molecule [19]. While there are numerous configurations for ammonia synthesis plants, the underlying process for each is the same: production and purification of the nitrogen and hydrogen synthesis gas (usually referred to as "syngas"); compression of the syngas; and conversion of the nitrogen and hydrogen into ammonia over a catalyst [20].

Since Fritz Haber first published his two famous patents in the early 1900s [21-22] industrial ammonia synthesis has changed very little [23]. A mixture of hydrogen gas (H_2) and nitrogen gas (N_2) reacts over a promoted iron catalyst at temperatures of 400-500°C and pressures ranging from 100 to 250 bar.

Ammonia syngas is produced using two main techniques: steam reforming of natural gas and partial oxidation of heavy oil feedstocks or coal. Each process consists of several basic steps which include feedstock purification, syngas production, syngas purification, syngas compression and ammonia synthesis.

In addition to the aforementioned processes for syngas production, other methods exist which are of marginal importance today. These include water electrolysis which yields hydrogen with oxygen as a byproduct; electrolysis of sodium chloride which yields hydrogen as a byproduct; the steam-iron ore process for the production of hydrogen from passing steam over iron ore; hydrogen from catalytic reformers; hydrogen from acetylene plants; hydrogen from ethylene plants; hydrogen from butadiene plants and nitrogen production from air by the combustion of oxygen and hydrogen [24-25].

The iron catalyst is susceptible to both permanent and temporary poisoning by compounds present in the syngas. Permanent poisoning reduces catalyst activity and performance which are

not regained when the poison is removed from the syngas. Examples of permanent poisons include sulfur containing compounds such as COS and H_2S, as well as other compounds that lower the surface energy of the iron catalyst. Temporary poisoning of the catalyst due to compounds such as O_2, CO_2, H_2O and CO can also occur [26]. These poisons can be removed from the surface of the catalyst and normal syngas activity will resume.

Purification of the syngas to remove contaminants is imperative for maintaining a high conversion rate of ammonia over time. The purification methods employed depend strongly on the feedstock used for syngas production; today, nearly all modern ammonia production facilities use fossil fuels though several processes are common throughout the industry. Typical purification processes for hydrocarbon feedstocks are carried out in several successive steps [1, 24-25]:

1. Desulfurization removes sulfur compounds from the feedstock and from the resulting syngas.
2. Shift conversion for the removal of carbon monoxide (CO) and the simultaneous production of hydrogen.
3. Absorption of carbon dioxide (CO_2) and any residual sulfur containing compounds.
4. Liquid nitrogen wash purification removes all traces of oxygen containing compounds.

An example of syngas quality is shown in Table 1 for the Kellogg Ammonia Process, which was developed in the mid 1960s [27]. The methane and the argon present in the Kellogg process are spectator compounds, but affect the reaction by accumulating in the synthesis loop and taking up volume.

Table 1 – The typical composition of syngas for the Kellogg Ammonia Process

Compound	Mol %
H_2	74.2
N_2	24.7
CH_4	0.8
Ar	0.3
Total	100

After the numerous purification processes the syngas sent to the ammonia converter often contains a CO content of less than 10 ppm and a CO_2 content of 15 ppm [25].

Because it is favored by the majority of ammonia plants, the steam reforming process will be described in greater detail in the following section.

2.1.1 Conventional Steam Reforming

There are several methods of obtaining the required syngas. The syngas must be a pure mixture of hydrogen and nitrogen in the stoichiometric ratio of approximately 3:1 regardless of the combination of methods used in the syngas production. Nearly all industrial ammonia plants in operation today use water, air and fossil fuels as the raw materials for the syngas.

Light hydrocarbons such as naphtha, liquefied petroleum gas or natural gas are used in the steam reforming process to produce hydrogen. The process is nearly identical for each of the different

feedstocks, though the following example will use methane – the primary constituent of natural gas – as the feedstock.

The steam reforming process uses a nickel catalyst that is sensitive to sulfur poisoning, therefore sulfur compounds present in the feedstock must be eliminated prior to reforming. This is achieved using hydrodesulfurization with a zinc oxide absorbent [27-28]. The initial step is to react hydrogen – which usually comes from the synthesis loop of the plant – with any sulfur compounds present in the feed gas to produce hydrogen sulfide (Equation 1). The "R" in the equation denotes any group that is covalently bonded to the SH, or the H. The second step uses a bed of zinc oxide particles for hydrogen sulfide removal, producing zinc sulfide in the process (Equation 2).

$$R - SH + H_2 \xrightarrow{yields} RH + H_2S$$ **Equation 1**

$$H_2S + ZnO \xrightarrow{yields} ZnS + H_2O$$ **Equation 2**

The primary reforming process uses a furnace containing a myriad of tubes that house the nickel based catalyst. The heat required for the reaction is transferred from the furnace to the tubes via radiation [28]. The primary reformer partially converts the desulphurized methane to carbon monoxide and hydrogen using the following reaction:

$$CH_4 + H_2O \xrightarrow{yields} CO + 3H_2 \ (\Delta H^o = 206 \ \frac{kJ}{mol})$$ **Equation 3**

The reaction is deliberately controlled to achieve a 60% conversion rate, based on the methane feed [29].

During the secondary reforming process the nitrogen required for the reaction is introduced as air and the feed gas conversion is completed. The process air is compressed and heated to 500-600°C such that the methane content is very low (see Table 2).

The carbon monoxide shift conversion uses carbon monoxide as a reducing agent for water to produce hydrogen and carbon dioxide. Thus, carbon monoxide – a temporary poison to the iron-containing catalysts – is removed from the syngas in favor of carbon dioxide and hydrogen according to the reaction:

$$\boldsymbol{CO + H_2O \xrightarrow{yields} CO_2 + H_2\ (\Delta H^o = -41.2\ \frac{kJ}{mol})} \qquad \textbf{Equation 4}$$

Carbon dioxide must be removed from the gas stream prior to its introduction to the ammonia synthesis unit because it is a temporary poison to the catalyst. While there are several processes for removing carbon dioxide from the gas stream, most of them are chemical-based scrubbing techniques. In recent years pressure swing adsorption (PSA) has been used in favor of the scrubbing techniques because it also replaces the methanation step. The typical composition of the gas following carbon dioxide removal is given in Table 2.

Table 2 – Gas composition following carbon dioxide removal [27]

Gas	Mol. %
H_2	74.6
N_2	24.4
CH_4	0.3
CO	0.3
CO_2	0.1
Ar	0.3

Methanation removes the last traces carbon oxides to below 10 parts-per-million levels by means of a nickel-containing catalyst at temperatures of 250-350 °C through the following reactions:

$$CO + 3H_2 \xrightarrow{yields} CH_4 + H_2O \ (\Delta H^o = -206 \ \frac{kJ}{mol}) \qquad \textbf{Equation 5}$$

$$CO_2 + 4H_2 \xrightarrow{yields} CH_4 + 2H_2O \ (\Delta H^o = -165 \frac{kJ}{mol}) \qquad \textbf{Equation 6}$$

A small amount of hydrogen is lost in this process, though the implementation of methanation prevents catalyst poisoning in the synthesis loop.

2.1.2 Partial Oxidation

The partial oxidation route is used for heavy hydrocarbon feedstocks such as naphtha, heavy fuel oil, crude oil, asphalt and tar [30]. The feedstock, in this process, is burned in the presence of steam with a limited supply of oxygen and is given by Equation 7.

$$C_xH_y + \left(\frac{x}{2}\right) O_2 \xrightarrow{yields} xCO + (\frac{y}{2})H_2 \qquad \textbf{Equation 7}$$

The main products of the reaction are carbon monoxide and hydrogen; however carbon dioxide, water, methane, sulfur compounds, and soot are also present. The soot is removed by cooling the exhaust gases from the partial oxidation and scrubbing them with water. The soot removal is followed by several steps to purify the syngas. The first step is the high temperature shift conversion given in Equation 4. Subsequent steps involve the removal of acid gases, carbon dioxide and hydrogen sulfide. The final purification of the gas is performed with a liquid nitrogen wash to nearly eliminate carbon monoxide, carbon dioxide, methane and argon. The liquid

nitrogen is obtained from an air separation unit which also provides oxygen for the partial oxidation reaction.

2.1.3 Electrolytic Ammonia

Electrolysis is the least common approach for the manufacture of ammonia, representing less that 0.5% of total worldwide production [10]. The only difference between electrolytic ammonia and steam reforming or partial oxidation is the production route for hydrogen and nitrogen. Figure 1 shows a block diagram of the process. The reactors and compressors used in the process are the same as those used in steam reforming or partial oxidation.

The nitrogen feed is derived from an air separation unit. Typically, large plants will use air liquefaction and separation to isolate nitrogen from the other major constituents of air. The liquid oxygen is sometimes expanded to provide cooling for separating ammonia from the syngas, or to provide auxiliary power [16].

The hydrogen feed is produced by water electrolysis, which uses electricity to split water into its two components – oxygen and hydrogen. Electrolysis of water consumes more energy per mole of hydrogen produced than steam reforming or partial oxidation. Thus, electrolytic ammonia is primarily used in conjunction with inexpensive hydroelectric power.

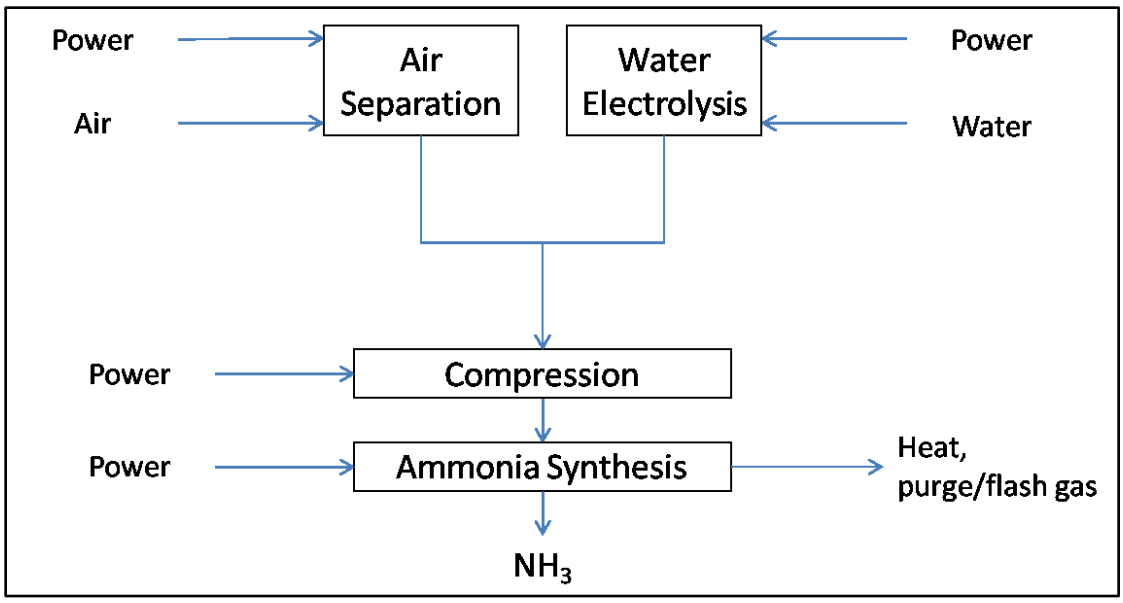

Figure 1 – Electrolytic ammonia process flow diagram

Once the hydrogen and nitrogen synthesis gases are generated, and any impurities removed, they are compressed and sent to the ammonia synthesis reactor.

Further discussion of air separation, water electrolysis, syngas compression, and ammonia synthesis are included in Chapter 4.

2.1.4 Syngas Compression

In the 1950s, ammonia plant capacities were only a few hundred tons per day. At that time, ammonia syngas was produced at atmospheric pressure and synthesis was carried out at pressures of 200-400 bar. Reciprocating compressors driven by synchronous motors or steam turbines were tasked with the syngas compression duties. While these compressors are efficient across a range of pressures and loads, they are limited by cost, size, upkeep, and potential contamination of the syngas from the lubricating oil [23]. In 1963 M.W. Kellogg introduced centrifugal compressors for syngas, process air, recycle gas and refrigeration [28] because the economics of the machines were more favorable due to higher plant throughputs. Centrifugal compressors have since become

state-of-the-art in all modern ammonia plants that produce more than 600 tons per day at pressures ranging from 150-250 bar [31].

The cost of reciprocating compressors is proportional to plant capacity while the cost of centrifugal compressors varies very little over a wide range of large plant sizes [32]. Therefore, when centrifugal compressors were first introduced, the threshold for switching from reciprocating compressors to centrifugal compressors was estimated to be between 550 and 600 tons per day [32]. Today with improved manufacturing techniques, improved catalysts and lower synthesis pressures in some plants, centrifugal compressors are economical down to 220 tons per day [1].

2.1.5 Synthesis of Ammonia

After the syngas is compressed it enters the ammonia synthesis loop. Equation 8 gives the reaction for the formation of ammonia from nitrogen and hydrogen. The negative value of enthalpy indicates that the reaction is exothermic, releasing approximately 2.7 gigajoules of heat per metric ton of ammonia produced. This is equivalent to about 8% of the energy input for the entire process [33].

$$N_2 + 3H_2 \xrightarrow{yields} NH_3 (\Delta H = -92.44 \frac{kJ}{mol}) \qquad \textbf{Equation 8}$$

Because of the thermodynamic and kinetic equilibrium positions of this reaction the syngas is only partially converted into ammonia; typical single pass conversions are between 25% and 35% [1, 31].

The ammonia synthesis loop always contains the following elements [23] which are shown in Figure 2:

- A reactor or series of reactors containing the catalysts, temperature control and heat recovery equipment.
- Cooling units for condensing the product ammonia and recovering heat.
- Separation units for ammonia recovery from the unreacted gas.
- Preheating units for the reactor feed that are often integrated with other heat recovery units.
- Purge gas removal equipment to prevent the buildup of inert gases such as argon and methane in the synthesis loop. Their presence will decrease the overall conversion efficiency.
- Recirculation equipment for moving the unreacted gas back to the synthesis reactor.

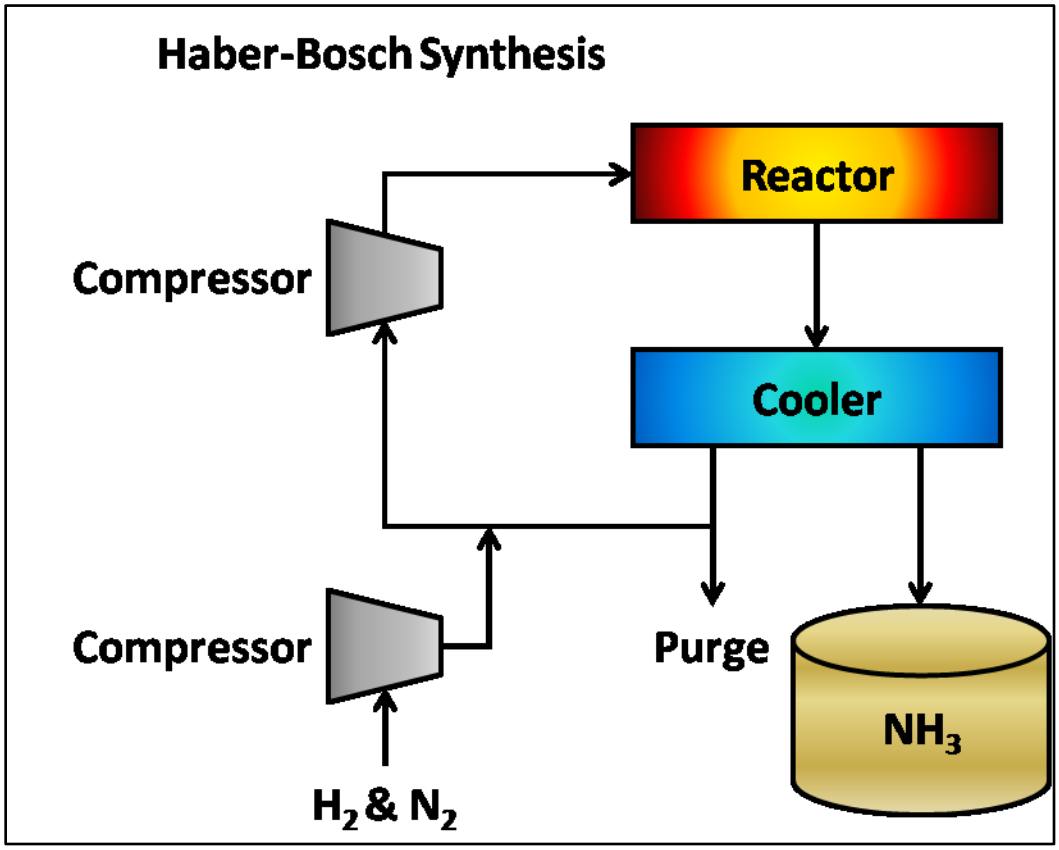

Figure 2 – Process flow of ammonia synthesis loop

Ammonia synthesis reactors are highly nonlinear and have numerous operating variables. Reactor models are prevalent in the literature [20, 23, 34-36] and involve solving partial differential equations for the mass and energy balance. The most relevant features of the model are listed below:

- Pressure: An increase in pressure will improve the conversion rate by increasing the reaction rate and improving the ammonia equilibrium.
- Inlet temperature: The temperature has conflicting effects since a higher temperature will increase the reaction rate while decreasing the equilibrium concentration.
- Space velocity (units are m^3 gas per hour per m^3 of catalyst): Increased space velocity increases the total ammonia production but decreases the outlet ammonia concentration.
- Inert level: Inert gases decrease the partial pressures of hydrogen and nitrogen forcing the equilibrium to change detrimentally.
- Nitrogen/Hydrogen ratio: The reaction rate exhibits a maximum at a particular nitrogen/hydrogen ratio. While the maximum depends in space velocity this ratio is generally between 2.0-3.0.
- Catalyst particle size: Smaller particles have higher conversion rates due to lower diffusion restrictions and larger surface area.

The manipulation of these six variables dictates the rate of ammonia production and how the reactor responds to disturbances such as changes in inlet temperature, feed concentration, or reactor pressure, among others [35].

To this end, nearly one hundred years of industrial ammonia production experience has made ammonia production a highly efficient, though energy intensive, process. The best current technology for ammonia synthesis consumes 28 gigajoules per ton of ammonia produced, based on the lower heating value of natural gas [37]. The ammonia production process is 66.4% efficient, with respect to the lower heating value (LHV) of ammonia, assumed to be 18.6 gigajoules per ton.

2.1.6 Technical Requirements

At present, most ammonia plants produce 1000-1500 tons per day (mtd) with some plants designed for 3000 tons per day [37]. Some smaller ammonia plants exist, with capacities of 250 tons/day being the smallest ammonia plant with a conventional design [38]. Heat transfer from the pipes and the reactor begin to dominate the design of ammonia plants that produce less than 250 tons/day. Smaller plants exist [39], but they are mainly for niche purposes.

As discussed above, ammonia production has specific technical requirements that must be met to achieve successful operation. Some of the requirements originate from the fragile nature of the catalyst: pressure and temperature cycling degrade the effectiveness, as do oxygen, sulfur and other elements. Other considerations are the result of economic factors: a continuous process enables more ammonia to be produced than a batch process, and in less time. As a result, ammonia plants are designed to run using pure reactants, at nearly constant pressure and temperature, almost continuously for their entire lifetime.

The ammonia plant requirements and specifications are as follows:

Hydrogen feed [14, 23, 28]:

Hydrogen – 99.999 Mol % Min

Oxygen – 0.001 Mol % Max

Nitrogen feed [14, 23, 28]:

Nitrogen – 99.99 Mol % Min

Oxygen 0.01 Mol % Max

Pressure of syngas: 150-250 atm

Catalyst heat rates [40]:

The catalyst cannot be heated faster than 38°C/hr up to 400°C; 19°C/h from 400-510°C.

Catalyst replacement for a 1500mtd plant is $10m^3/yr$ for the synthesis section.

Syngas Ratio [28]:

A ratio of hydrogen to nitrogen of 3:1 is commonly used to maintain a stoichiometric balance.

Compression [23, 27, 29-30, 32]:

The synthesis gas must be compressed to between 100 and 200 atmospheres prior to entering the reactor. The large range of pressures is due to different reactor types.

Temperature [23, 27-29, 31]:

The synthesis gas must be heated to between 350°C and 550°C prior to entering the reactor. The large range of temperatures is due to different reactor types.

Reactions [23, 27-29, 31]:

Only 20-30% of the synthesis gas is converted to ammonia per pass. This is due to unfavorable equilibrium conditions present in the reactor.

Ammonia Quality [29, 31, 40]:

Anhydrous ammonia with a purity of 99.5% is typically produced in industrial reactors [41]. The other 0.5% is composed of water and process machine oil. Higher purities of ammonia, required for refrigeration and semiconductors, are attainable through distillation.

Heat of Reaction [33, 42]:

The heat of reaction represents roughly 8% of the required energy input for a conventional ammonia plant. This energy is typically used to heat the incoming synthesis gas stream or to provide heat for boilers.

Startup/Shutdown [8, 29, 40]

Conventional ammonia plants are designed to be available for 330 days per year. Shutdowns due to technical failures occur, on average, 5.7 times per year [29]. The startup then takes several days.

It should be noted that these are the requirements and specifications for "generic" ammonia synthesis reactor. Other specifications are needed for the upstream processes in a conventional ammonia plant that uses steam reforming, partial oxidation or electrolysis.

2.1.7 Environmental Issues

Ammonia arises naturally in the life cycle from animal waste products and from the decay of plant and animal matter. It is also released into the environment directly from fertilizer use and, to a lesser extent, from industrial emissions. Thus, ammonia is ubiquitous in both groundwater and surface water in low concentrations where it is highly soluble. Ammonia manufacture releases some ammonia into the environment in addition to gases and some catalysts. Furthermore, ammonia spills are an environmental concern because ammonia is highly soluble in water and can be very toxic at high concentrations. The following two sections discuss the

emissions from the manufacture of ammonia as well as the environmental issues with ammonia itself.

2.1.7.1 Emissions from Ammonia Manufacturing

Conventional ammonia production is based mainly on fossil fuel reforming which must – according to a stoichiometric balance – emit some carbon-, and sulfur-based compounds. As the equations for steam reforming and partial oxidation show in the preceding sections, carbon dioxide, carbon monoxide and methane are produced during ammonia manufacture. Moreover, due to imperfect thermodynamic reactions in the reformers, some NOx and sulfur dioxides are also produced.

A large steam reforming plant producing 1200 metric tons of ammonia per day will emit more than 2000 metric tons of carbon dioxide per day when using natural gas. For a heavy hydrocarbon- or coal-based ammonia plant of the same size, 3000 metric tons and 4800 metric tons will be emitted, respectively [43]. Furthermore, depending on the technology being used, other gases such as NOx, carbon monoxide and sulfur dioxide and ammonia will be released in varying quantities.

Other emissions from ammonia plants include process condensates such as ammonia and methanol which may become effluents if handled improperly. Furthermore, the spent catalysts must be disposed of in landfills. The amount of catalyst that is discharged depends on plant capacity and configuration. Table 3 and Table 4 list the emissions of a medium sized ammonia plant in Europe.

The emissions for a plant based on electrolysis are vastly different. First, the electrolysis plant does not use a carbon-based feedstock such as natural gas, coal or heavy hydrocarbons. Thus, the synthesis gas in an electrolysis facility is free from impurities generated from reactors, reformers or boilers. The emissions would be limited to the synthesis reactions, the compressor section and

the process condensates. As a result, the only emissions would be ammonia from the process condensate and the synthesis sections, and the synthesis catalyst. Compared to a conventional ammonia plant the emissions are negligible.

Table 3 – Ammonia production emissions for a 1200 metric ton/d steam reforming plant [43]

Emission Sources	Pollutants	Emission Levels (t = metric tonnes)		
		Air	Water	Land
Desulphurisation	Catalyst			6 m^3/yr
Primary Reformer	NOx SO_2 CO_2 CO Particulates Catalyst	0.6 – 1.3 kg/t NH_3 <0.01 kg/t NH_3 500 kg/t NH_3 <0.03 kg/t NH_3 5 mg/Nm^3		5 m^3/yr
Secondary Reformer	Catalyst			4 m^3/yr
Shift Reactors	Catalyst			30 m^3/yr HT 10 m^3/
CO_2 removal	CO_2 Amines	1200 kg/t NH_3 5 mg/Nm^3		
Methanation	Catalyst			2 m^3/yr
Synthesis Section	NH_3 Catalyst	75 mg/Nm_3 <40 g/t NH_3		10 m^3/yr
Process Condensates	NH_3 CH_3OH All organics Others	0.4 - 2 kg/t NH_3 35 - 75 mg/Nm^3	0.4 - 1.5 kg/t NH_3 10 g/t NH_3 0.6 - 2 kg/t NH_3 20 mg/l BOD 50 g/t NH_3	

Table 4 – Ammonia production emissions for a 1200 metric ton/d partial oxidation plant [43]

Emission Sources	Pollutants	Emission Levels		
		Air	Water	Land
Gasifier	Carbon and slag		Traces	
Superheater	NOx SO_2 CO	200 - 450 mg/Nm^3 0.1 - 2 mg/Nm^3 10 ppmv		
Shift reactors	Catalyst			30 m^3/yr
CO_2 removal	CO_2 (heavy HCx) CO_2 (coal) Amines CH_3OH H_2S	2.5 t/t NH_3 4 t/t NH_3 5 mg/Nm_3 100 ppmv 0.3 ppmv		
Synthesis section	Catalyst			10 m^3/yr
Process condensate	NH_3 CH3OH All organics Others	0.4 – 2 kg/t NH_3 35 – 75 mg/Nm_3	0.4 - 1.5 kg/t NH_3 10 g/t NH_3 0.6 - kg/t NH_3 20 mg/l BOD 50 g/t NH_3	
Auxiliary boiler	NOx SO_2 CO Particulates	700 mg/Nm_3 1700 mg/Nm_3 10 ppmv traces		
Syngas compressor **Claus unit**	NH_3 SO_2	traces 2 % of the S-content in fuel		

2.1.7.2 Ammonia in the environment

Ammonia is miscible in water due to its highly polar nature and the ability to form hydrogen bonds. In aqueous solution ammonia forms a hydroxyl anion and an ammonium cation according to the equation:

$$OH^- + NH_4^+ \leftrightarrow NH_3 + H_2O$$ **Equation 9**

Ambient ammonia is a natural part of the lifecycle and is not an environmental concern at low concentrations. However, if high concentrations exist in the environment as a result of agricultural runoff or industrial spills environmental toxicity concerns arise. The unionized form of aqueous ammonia, NH_3, is considered much more toxic to fish and other aquatic animals than the ammonium cation (NH_4^+) , and can cause death or other central nervous system problems at elevated concentrations [44-45].

Humans are familiar with the acrid odor of ammonia. Ammonia is easily detectable in the air even at low concentration near 5 ppm. However, when concentrations increase above 100 ppm, humans begin to experience adverse reactions. Though rare, respiratory exposure can result in death, though instances of death seem to be rare [46]. Anhydrous and hydrated ammonia can also cause caustic burns to the skin, mouth throat and lungs. Case studies have reported that some individuals have died as a result of contact with ammonia [47]. Table 5 is provided as a guide for ammonia toxicity for humans [48].

Table 5 – Ammonia toxicity to humans [48]

Ammonia Concentration (ppm)	Health Effect
5	Threshold detection limit
50	Easily Detected
50-72	No impairment to respiration
100	Irritation to nose and throat;
	Burning sensation in eyes
200	Headache and nausea
>300	Irritation to respiration tract;
	Difficulty breathing
250 to 500	Rapid heart rate
>455	Respiratory and eye irritation;
	Corneal opacities
700	Immediate onset of burning sensation in eyes
1000	Immediate coughing
1700	Coughing with labored breathing
2500-4500	Fatal after short exposure
>5000	Death by respiratory arrest

CHAPTER 3

OFFSHORE WIND POWER

Offshore wind power refers to wind turbines placed in the ocean, lakes, or seas, subjected to hydrodynamic loading. The wind turbines are similar to those built on land; they differ primarily in the foundations and substructures. The technology is nascent: the first offshore turbine was installed in 1990 and the total offshore capacity is less than 2% of onshore capacity. As of November 2010, ninety five percent of all offshore wind capacity existed in European waters; the remaining 5% were installed in China and Japan [49].

Offshore wind energy will likely become an important contributor to the energy portfolio of the United States, as it currently is in Europe. The resource in the coastal waters of the United States is immense, accessible and wholly untapped. As shown in Figure 3, the National Renewable Energy Laboratory (NREL) estimates the resource to be in excess of 4 TW, with over one terawatt in water that is less than 30 meters deep [50]. Furthermore, the offshore resource is close to large load centers such as the Northeast, the Mid-Atlantic and the Gulf Coast regions. In Europe, the technology is growing rapidly with more than a fourfold increase in installed capacity from 2003 to 2009 [51]. The United States, as the world leader in installed onshore wind capacity, will surely turn to offshore wind power in the near future. The first offshore wind farm in the United States, Cape Wind, was approved in April of 2010 by Secretary of the Interior Ken Salazar [52].

Offshore wind power offers several advantages over onshore wind power. These include [53-54]

- Larger area for siting the turbines

- Lower visual and auditory impact
- Higher wind speeds with less intrinsic turbulence and lower wind shear than onshore

However, the disadvantages include:

- Higher overall project costs due to specialized equipment, vessel scheduling and logistics, and larger support structures.
- Significant wave loading influences the dynamic response of the structure.
- Designs must account for “50 year storms” or rogue waves
- Extreme loading situations caused by sea ice
- Varying sea levels may influence the power output
- Challenging working conditions
- Technically challenging installation
- Decreased ability for maintenance
- Corrosion prevention and weatherproofing of the structure

The design and equipment necessary for an offshore wind turbine differ from onshore installations. First, ships are required for offshore wind installations. Ships must be able to safely navigate the waters, making some sites inaccessible. Second, shorter towers can be used for offshore turbines because of the more uniform wind characteristics that exist. Moreover, the sea level varies, sometimes significantly, with tidal oscillations and waves. Thus, the turbine design must account for these factors.

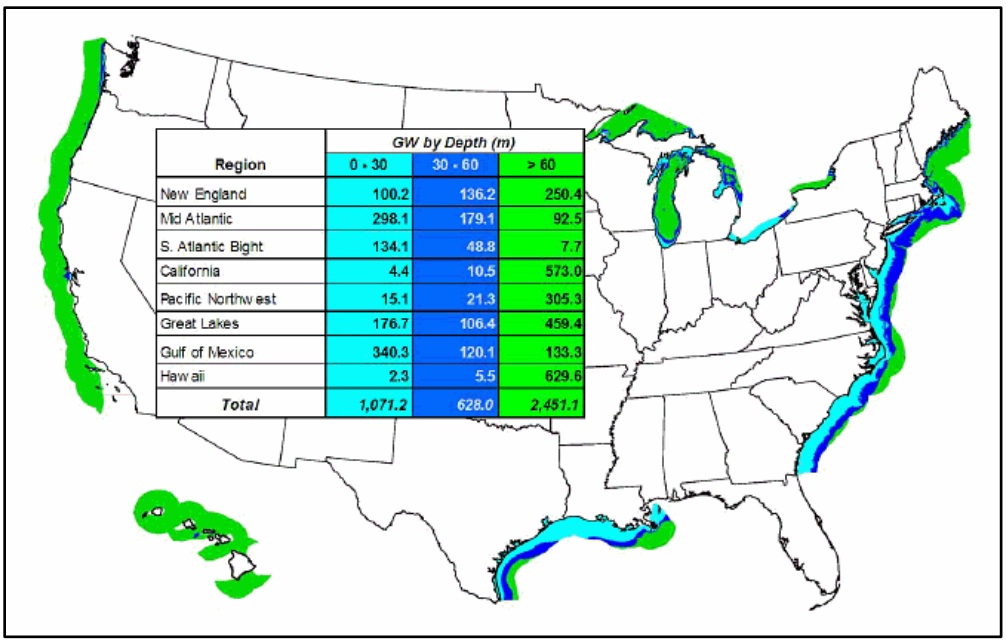

Figure 3 – The US offshore wind resource [50]

3.1 State-of-the-Art

An offshore wind turbine is similar in many ways to an onshore wind turbine. The main difference is the support structure which consists of the tower, the substructure and the foundation. For offshore wind farms, the support structure must be installed with ships, creating different constraints than onshore installations.

The rotor and nacelle assembly function in the same way as the onshore wind turbines, but includes "marinization" for the main components [55]. The substructure of the turbine begins at the bottom of the tower and extends beyond the ocean floor where the foundation is affixed. Figure 4 and Figure 5 show the main support structures used in the offshore industry. Table 6 summarizes the major substructures that are feasible for wind turbines [51]. Many of the fixed structures have been deployed in the wind industry, with the exception of the suction caisson.

Shallow water is defined by NREL for offshore wind turbines as less than 30 meters of depth; transitional water is 30-60 meters; and deep water is more than 60 meters of depth [56]. In general, the monopile and gravity base are used in shallow waters, while the tripod and jacket are used in deeper waters. The deepest monopile installation for an offshore wind turbine is the Princess Amalia farm in The Netherlands, at a depth of 24 meters [57-58]. (Refer to Table 7 for references in this section, and others). By contrast, the deepest jacket foundation resides in 40 meters of water at the Beatrice wind farm in the UK [57, 59].

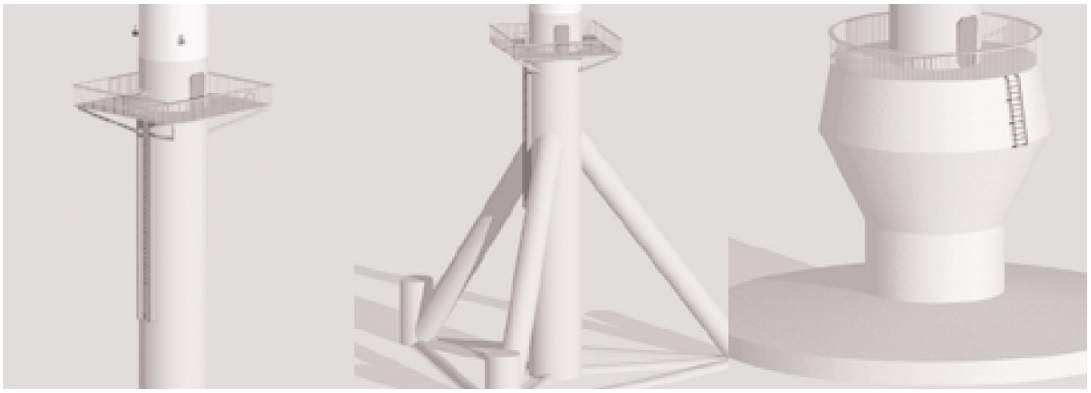

Figure 4 – Offshore wind turbine structures for shallow water. From L-R: monopile, tripod, and gravity foundations [60]

Figure 5 – The jacket type structure for offshore wind installations. [61]

Table 6 – Support structure types used in offshore wind farms [51]

Type of Structure	Design Depth	Description	Advantages	Limitations
Monopile	0-30m	One pillar	Easy to manufacture, experience with previous projects	Piling noise, drilling problems
Monopile with Concrete	0-40m	One pillar	Proven methods, cost effective, reduced piling noise over standard monopiles	Heavy to transport
Gravity Base	0-40m	Large concrete structure	Inexpensive, no noise	Heavy to transport, expensive to remove, requires seabed preparation
Suction Bucket	N/A	Inverted bucket pressed into seabed	No piling, simple removal	Seabed dependent
Tri/quad pod	0-40m	3/4 legged structure	Strong, suitable for large structures	Complex manufacturing, heavy to transport
Jacket	0-50m	Lattice structure	Reduced noise, suitable for large scale turbines	Expensive, wave loading and fatigue failure are problematic
Floating	>60m	Connected to seabed with cables	Deep water enables vast resources to be exploited	Weight and cost, dynamic instability, no precedent in wind industry
Spar Buoy	120-700m	Buoyant steel cylinder attached to seabed	Very deep water	Costly
Semi-Submersible	>100m	Buoyant steel cylinder attached to seabed	Very deep water	Costly

The monopile is a steel tube that is typically driven into the sea floor by a hammer, though some monopiles are inserted into predrilled holes. The monopile is the most popular shallow water structure used because it is a simple and mature technology. Of the 37 wind farms for which information is available, 20 of them employ monopiles, accounting for roughly 66% of all installed offshore wind turbines [49]. Little or no seabed preparation is required for a monopile installation, rather the seabed geology must be either sand or gravel so the pile can be easily driven. The depth that the monopile is driven depends largely on the seabed conditions, and, to a lesser extent, the wave and wind conditions. The monopile is susceptible to vibration which restricts the depth at which monopiles are viable.

The gravity base foundation consists of a large concrete or steel caisson that is fabricated on land and tugged to the site. Upon placement on the sea floor the caisson is filled with ballast to further increase its mass. The gravity base has found limited use where the monopile was deemed unacceptable, or too expensive. Most notably, the gravity base has been deployed in China's 100MW Donghai Bridge offshore farm as well as Thornton Bank and Nysted II. One advantage of the gravity base is that it can be totally removed from the site, upon project decommissioning.

The tripod is a support structure with three legs that supports a steel tube similar to a monopile. Each of the legs is anchored to the sea floor with steel tubes. The structure itself is more complex than a monopile, making it more expensive. It is generally used for deeper water owing to its stability and stiffness. Tripods are not common offshore foundations – the only installation is at the Alpha Ventus wind farm in Germany.

The jacket is a lattice-type, trussed structure, usually with three or four legs [61]. The piles for each leg are driven directly into the seabed, much like a tripod. The jacket structure is not

common in the offshore wind industry, with only two wind farms using the technology as of 2010. The jacket is, however, a common structure in the oil and gas industry.

Floating wind turbines are also possible: one floating wind turbine already exists in Norwegian waters, at a depth of 220 meters [62]. Floating platforms are common in the oil and gas industry. The Gulf of Mexico alone harbors nearly 4000 offshore oil and gas platforms, both fixed bottom and floating, the deepest being the NaKika platform at 1,932 meters (6,340 feet) [63]. While the offshore oil and gas industry uses several varieties of floating platforms, the wind industry has yet to do so on a commercial scale.

3.1.1 Electrical Connection

The electrical system for an offshore wind farm interconnects the turbines, and connects them to a central collection point. The collection point is usually an offshore substation for large wind farms. Most wind turbines operate between 690V and 1000V so transformers are used within the turbine to increase the voltage to the level of the collector, usually to between 11kV and 38kV [64]. The high voltages present within the farm reduce resistive losses at the expense of larger and costlier transformers.

The layout of the wind farm takes into consideration numerous factors such as seabed conditions, water depth, turbulence effects and turbine spacing. The spacing of the turbines influences how the turbines themselves are connected to a common collection station. The high voltage cables used for inter-turbine connection are generally rated at 33kV and 40 MVA [65]. Consequently, only 8 turbines rated at 5MW can be connected to the feeder cable. As a result of limited turbine

capacity per node, the possible layouts for the turbines are limited to three main designs: radial, star and octopus, as shown in Figure 6 [66].

The radial configuration is used in both the Nysted and Horns Rev offshore wind farms, as well as other major wind farms. Typically, the cable will taper as it moves to the outer turbines in this configuration, as shown in Figure 7. The cable is tapered because the amount of power being transmitted at the end of a string is lower than at the root, and thinner cables reduce capital costs. The downside to this approach is that if a fault occurs at the hub, the power in the entire string of turbines will be lost. The outages can be mitigated by using redundant cabling and switchgear, at the expense of higher capital costs as was done in the offshore wind farm Lillgrund, in Sweden [67].

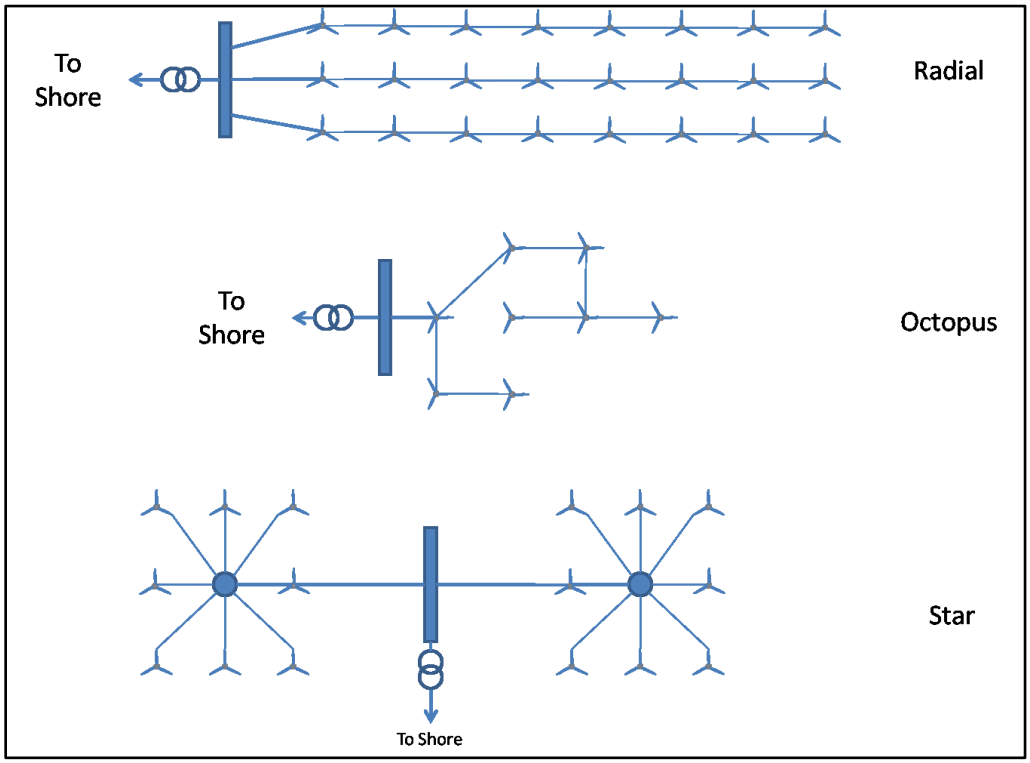

Figure 6 – Electrical layouts for offshore wind farms

Table 7 – Worldwide offshore wind farm data (references in table)

Project Name	Country	Online	Capacity (MW)	# Turbines	Turbine Size (MW)	Turbine Hub Height (m)	Average Water Depth (m)	Average Distance to Shore (km)	Foundation	Reference
Vindeby	Denmark	1991	4.95	11	0.45	38	4	2.5	Gravity	[57, 68]
Lely	Netherlands	1994	2	4	0.5	39	8	0.75	Monopile	[57, 69]
Tunø Knob	Denmark	1995	5	10	0.5	40.5	3	6	Gravity	[57, 68]
Irene Vorrink	Netherlands	1996	16.8	28	0.6	50	2	0.03	Monopile	[57, 70]
Bockstigen	Sweden	1998	2.75	5	0.55	41.5	7	3	Monopile	[57, 68]
Blyth Offshore	United Kingdom	2000	4	2	2	69	6	1	Monopile	[57, 71]
Middelgrunden	Denmark	2001	40	20	2	64	4	2	Gravity	[57, 72]
Utgruden I	Sweden	2001	10.5	7	1.5	65	7	7	Monopile	[57, 69]
Horns Rev 1	Denmark	2002	160	80	2	70	10	17	Jacket	[57, 73]
Yttre Stengrund	Sweden	2002	10	5	2	60	10	4	Monopile	[57, 69]
Nysted I	Denmark	2003	166	72	2.3	70	8	8	Gravity	[57, 74]
Samsø	Denmark	2003	23	10	2.3	63	10	3.5	Monopile	[57, 75]
North Hoyle	United Kingdom	2003	60	30	2	67	7	6	Monopile	[57, 76]
Arklow Bank	Ireland	2004	25.2	7	3.6	74	4	10	Monopile	[57, 77]
Setena	Japan	2004	1.2	2	0.6	40	13	0.7		[78]
Sakata	Japan	2004	10	2	2	60	4	1.3	Monopile	[79]
Scroby Sands	United Kingdom	2004	60	30	2	68	6	2.5	Monopile	[57-58]
Kentish Flats	United Kingdom	2005	90	30	3	70	5	8.8	Monopile	[57-58]
Barrow	United Kingdom	2006	90	30	3	75	22	7	Monopile	[57-58, 80]
Suizhong 36-1 Oil Field	China	2007	1.5	1	1.5			70	Jacket	[81]
Egmond aan Zee	Netherlands	2007	108	38	3	70	20	10	Monopile	[57-58]
Lillgrund	Sweden	2007	110.4	48	2.3	69	6	10	Gravity	[57, 82]

Table 7 – Worldwide offshore wind farm data (references in table)

Project Name	Country	Online	Capacity (MW)	# Turbines	Turbine Size (MW)	Turbine Hub Height (m)	Average Water Depth (m)	Average Distance to Shore (km)	Foundation	Reference
Beatrice	United Kingdom	2007	10	2	5	88	40	25	Jacket	[57, 59]
Burbo Bank	United Kingdom	2007	90	25	3.6	83.5	10	5.2	Monopile	[57, 83]
Thornton Bank phase 1	Belgium	2008	30	6	5	94	20	28	Gravity	[57, 84]
KemiAjos phases 1 & 2	Finland	2008	24	8	3	88	3	1	Gravity	[57, 85]
Prinsess Amalia	Netherlands	2008	120	60	2	59	20	23	Monopile	[57-58]
Lynn\Inner Dowsing	United Kingdom	2008	194	54	3.6	80	10	5.2	Monopile	[57, 86-87]
Horns Rev 2	Denmark	2009	209	91	2.3	68	13	30	Monopile	[57-58, 88]
Alpha Ventus-Borkum West	Germany	2009	60	12	5	90	28	45	Tripod	[57, 89]
Floating Hywind	Norway	2009	2.3	1	2.3		220	12	Floating	[62]
Rhyl Flats	United Kingdom	2009	90	25	3.6	80	10	8	Monopile	[57, 76, 90]
Robin Rigg	United Kingdom	2009	180	60	3	80	5	9.5	Monopile	[57, 91]
Gunfleet Sands 1 & 2	United Kingdom	2009	172	48	3.6	75.5	8	7	Monopile	[57, 92-93]
Donghai Bridge	China	2009	102	34	3	91	7	102	Gravity	[94]
Longyuan	China	2009	32	16	2			32	Monopile	[95]
Xiangshui	China	2009	2	1	2	84	4	2		[96]
Nysted II	Denmark	2010	207	90	3.6	68	10	207	Gravity	[97]
Kamisu	Japan	2010	14	7	2	60	5	14	Monopile	[98]
Dafeng	China	2010	2	1	2			2		[99]

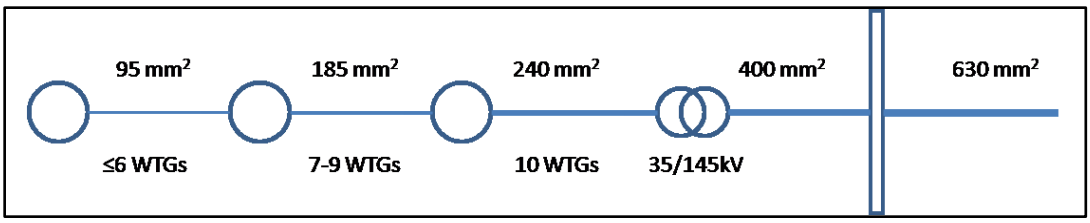

Figure 7 – Cabling specifications for the Lillgrund offshore wind farm [67]

The star configuration alleviates the possibility of losing an entire string of turbines due to a cable fault. However, if there is a node fault all the turbines will be offline. The benefits are that lower cable ratings can be used because the wind farm cables are tasked only with transmitting the power of each turbine to the node. However, some larger cables will be required to transmit the power from the node to the hub. In general, this method has low capital costs and offers a robust system.

3.1.2 Current Trends

The rise of offshore wind as a viable energy source has been exponential, as shown in Figure 8. In 1995, the total worldwide installed offshore wind capacity was about 12 MW. By 2000 it had tripled to about 36 MW; in 2010 it reached 2615MW – an increase of more than two orders of magnitude in 15 years. By the end of 2010 offshore wind farms were installed in eleven countries with northern Europe claiming 95% of the total capacity. The breakdown by country is given in Figure 9. At the same time, more than 2500MW was under construction worldwide – which almost doubles the worldwide capacity of offshore wind [49].

The first offshore wind turbine was installed in Nogersund, Sweden in 1990. The turbine was a 220 kW machine that was built in waters about 6 meters in depth and about 250 meters from the coast [100]. Shortly thereafter, the first wind farm was built in Denmark in 1991. The wind farm consisted of eleven turbines with a combined capacity of nearly 5 megawatts. The 1990s saw the erection of small offshore wind farms ranging in capacity from 2 MW to 16.8 MW. But it was not

until the Middelgrunden wind farm was built in Denmark in 2001 that large-scale offshore arrived. The following two years each saw offshore wind farms that quadrupled the capacity of Middelgrunden – Horns Rev I at 160 MW and Nysted I at 166 MW, both in Denmark.

Offshore wind technology is moving further from shore, into deeper waters and utilizing larger wind turbines. Figure 10 shows a scatter plot of water depth, distance to shore and wind farm capacity for European offshore installations (see Table 7 for references in this section). From this plot, it is clear that the larger installations have been mostly clustered at about 10 meters of depth or less and fewer than 10 kilometers from shore. However, Figure 11 shows that wind turbine rotor sizes and wind farms are getting larger with time. Furthermore, Figure 12 shows that since 2005 several offshore wind farms have been developed in waters exceeding 10 meters of depth, many being more than 15 kilometers from shore. These two trends point toward large turbines grouped in large farms in deep water to fully utilize economies of scale. Moreover, with the exception of research level offshore installations in Japan and China, all offshore turbines installed since 2002 have been 2 MW or larger. In Europe, the weighted average turbine size for all offshore installations since 2002 is about 2.7 MW, with the smallest turbine being a 2 MW machine and the largest being 5MW.

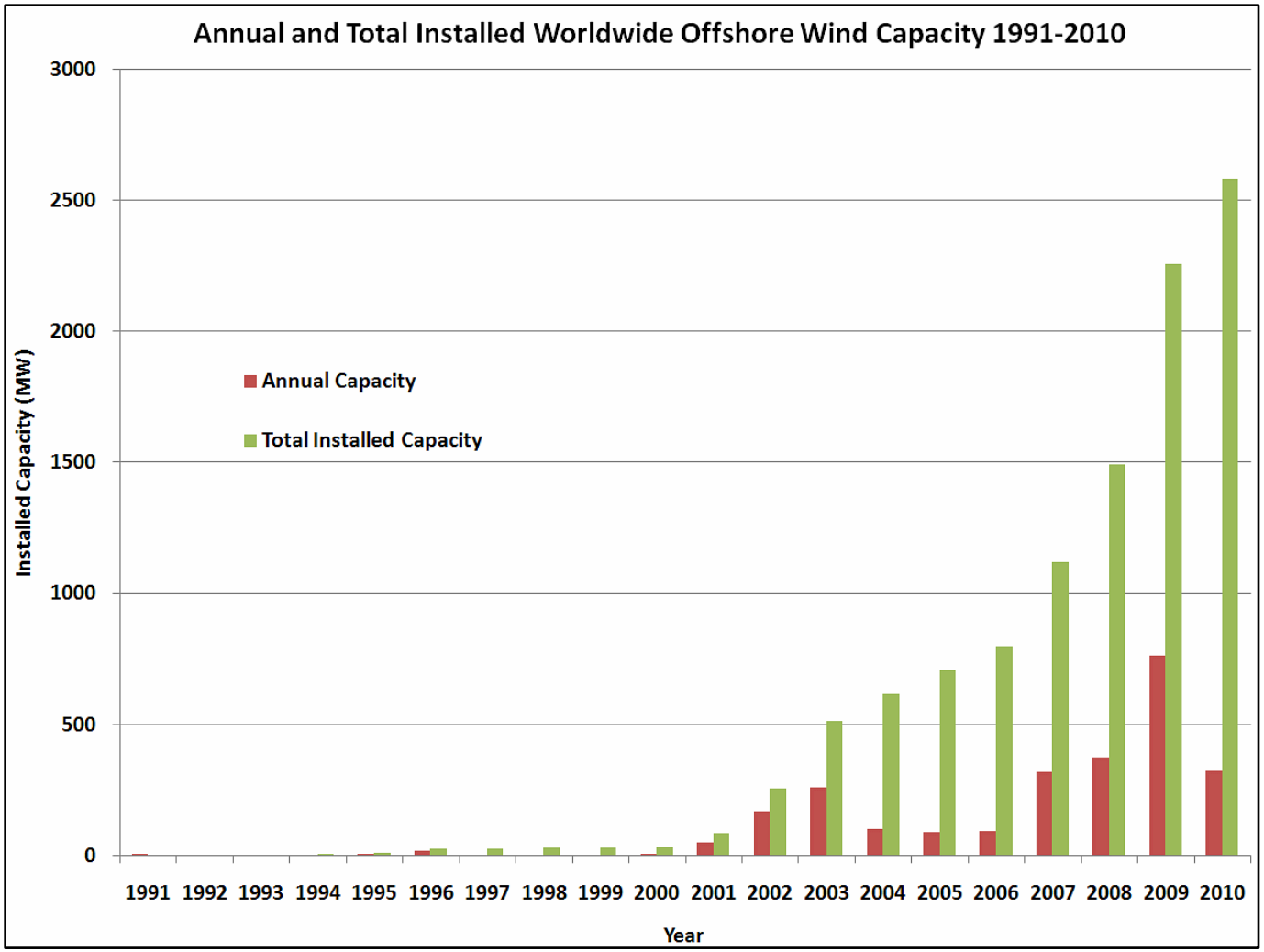

Figure 8 – Worldwide offshore wind power development 1991-2010 (References: see Table 7)

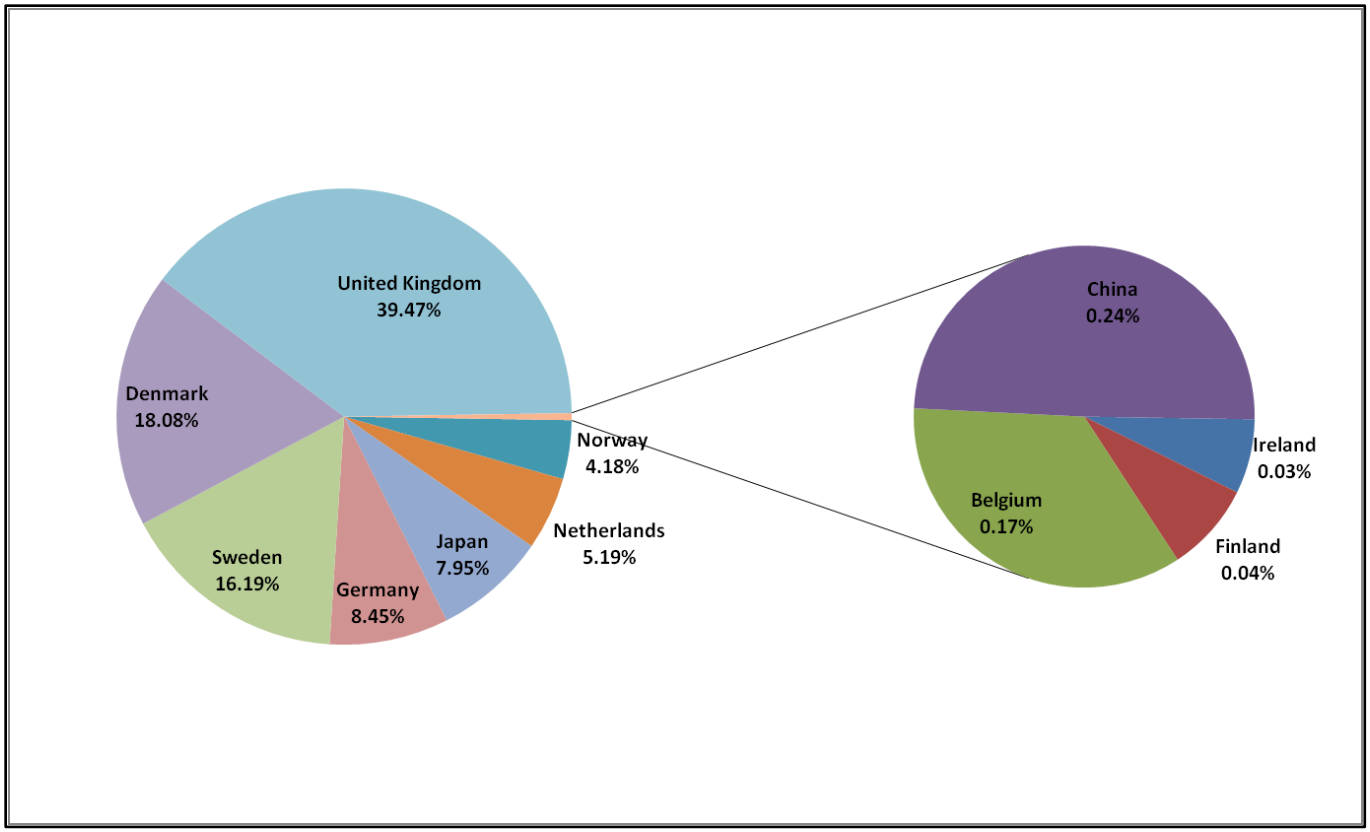

Figure 9 – Offshore wind capacity by country (November 2010) (References: see Table 7)

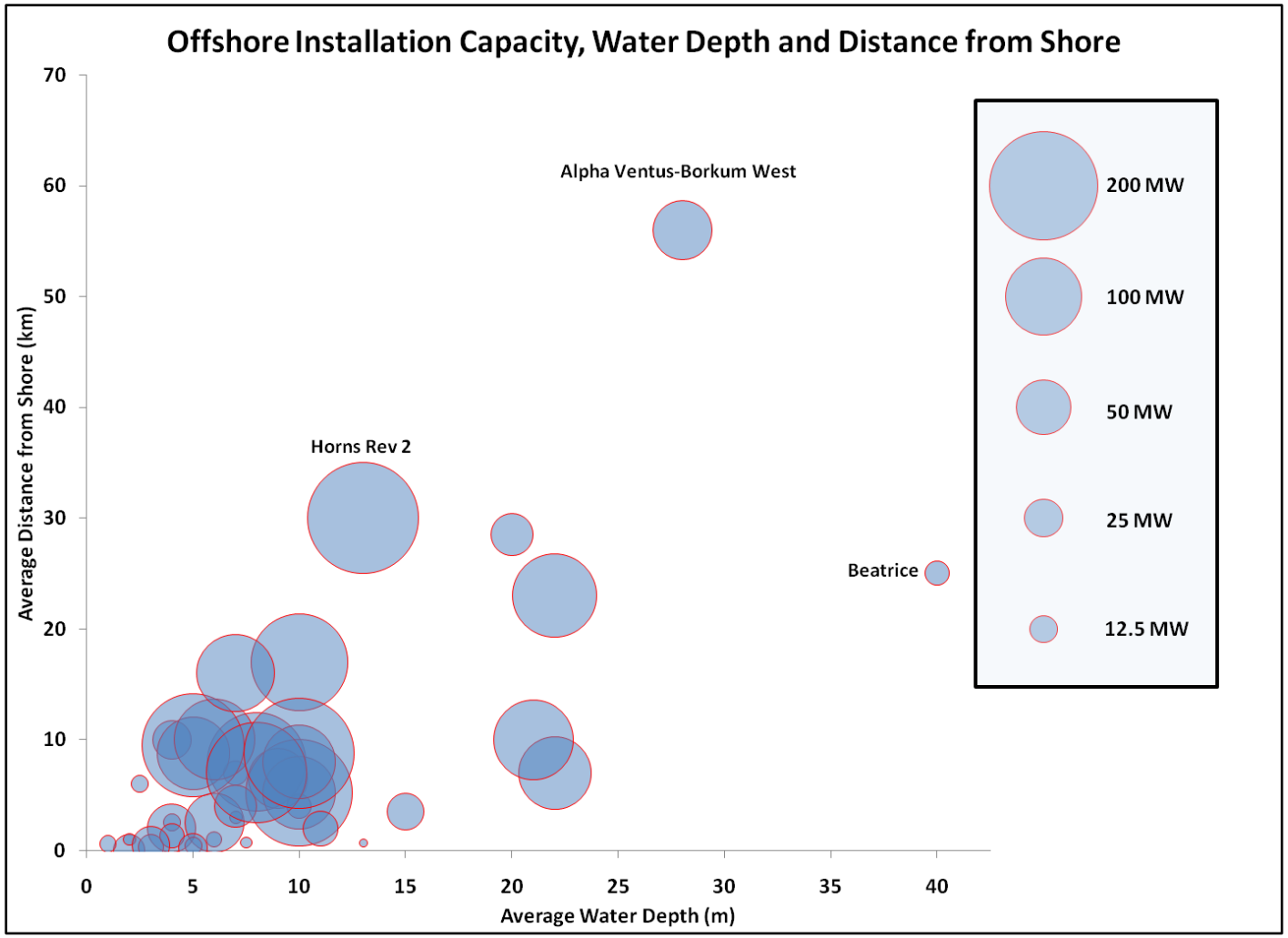

Figure 10 – Average distance from shore, water depth and wind farm size (References: see Table 7)

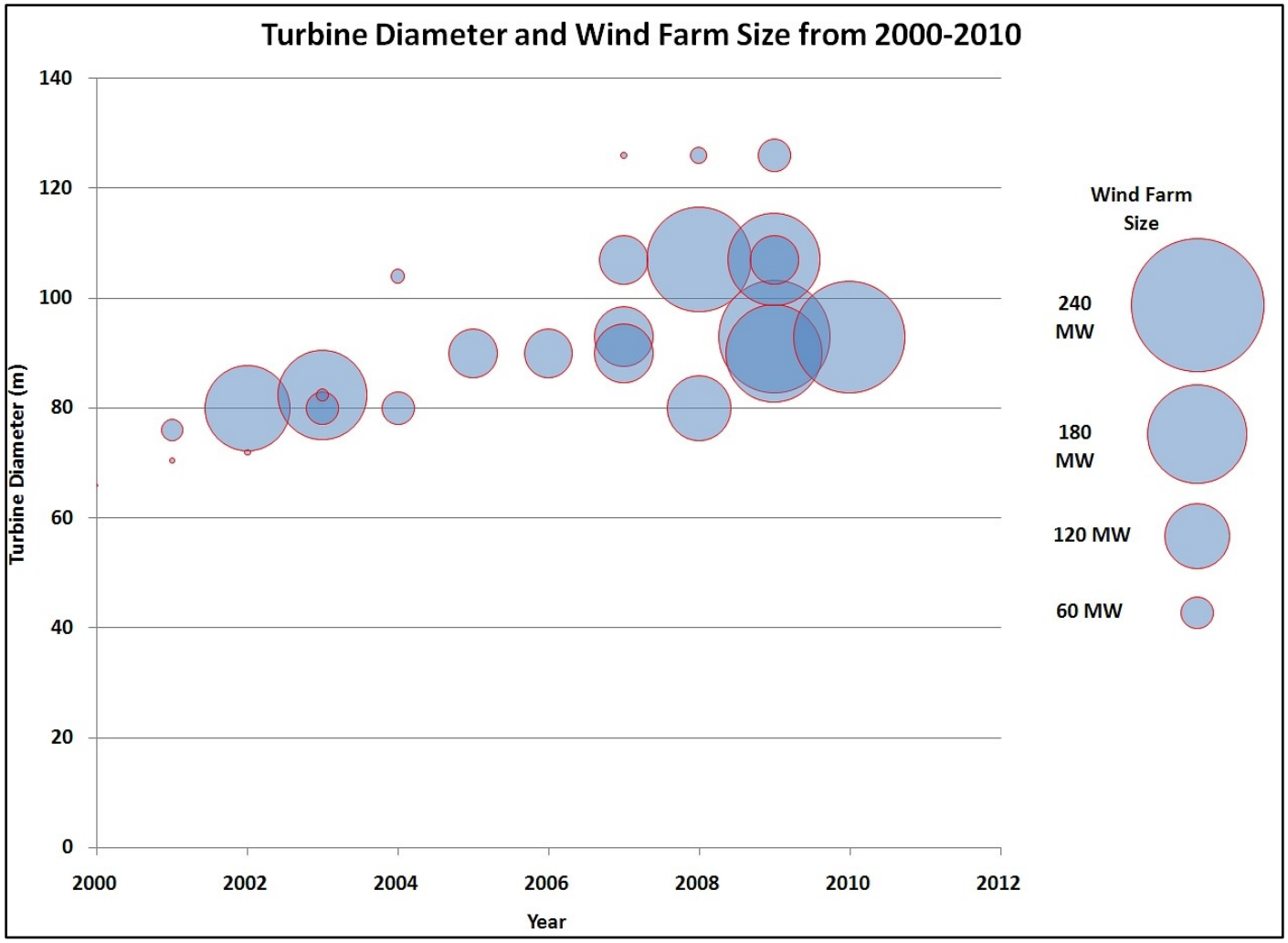

Figure 11 – Turbine rotor diameter and wind farm size trends in European waters, 2000-2010 (References: see Table 7)

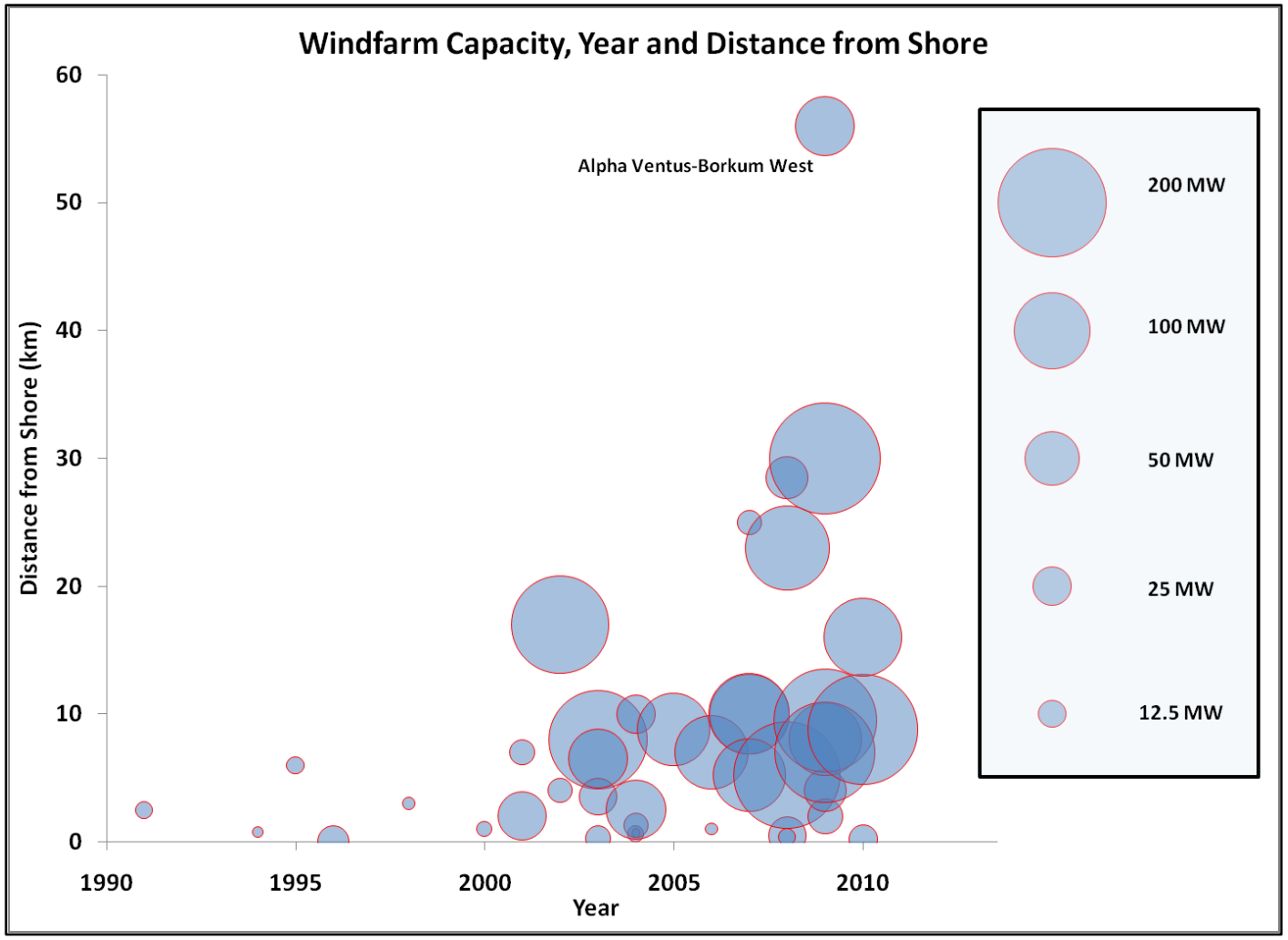

Figure 12 – The progression of offshore wind into deeper water further from shore (References: see Table 7)

3.2 Environmental

The impact of offshore wind turbines on the local habitat can either be due to their construction, their physical presence, or both. While the construction for each turbine may only last a few weeks, the turbines themselves are fixtures in the ocean for 20 years or more. The marine life will be impacted, albeit either positively or negatively. Quantifying the effect that the turbines have on the environment must be done to ensure that marine conditions are not adversely impacted. Extensive environmental impact studies on the Horns Rev and Nysted wind farms attempted to quantify environmental impacts by assessing the habitats both before and after the farms were built [101].

3.2.1 Birds

Bird collisions with wind turbines are a major environmental concern that must be addressed when selecting a site. Turbines can become obstacles to bird migration paths as well as feeding areas and nesting grounds. A well researched environmental impact study combined with good siting can help to minimize bird deaths.

Wind turbines can affect birds both directly and indirectly. The indirect effects of a wind farm include loss of habitat and loss of food resources around and under foundations; the direct effects are collisions with moving turbine blades. While bird collisions themselves are inherently negative, foundations could fundamentally alter the seabed in a positive way. The substrates and scour protection may present new feeding opportunities.

In a radar study at the Horns Rev and the Nysted offshore wind farms, it was found that between 71% and 86% of the bird flocks generally avoid the wind farms by altering flight paths well before arriving [101-102]. The bird tracks are shown in Figure 13. Based on thermal animal

detection and radar studies, as stochastic bird collision model was developed [101]. The model revealed that with 95% certainty that about 0.02% of birds would collide with all turbines during the fall season. Roughly 235,000 birds pass the wind turbines during that period of time, so about 48 of those would result in collisions.

Horns Rev and Nysted bird studies show that birds exhibit avoidance response to the turbines. Furthermore, the gross area of the seabed affected by the turbine foundation is negligible; habitat loss or disruption is unlikely. Still, further studies need to be performed, as site specific and species specific effects may be present.

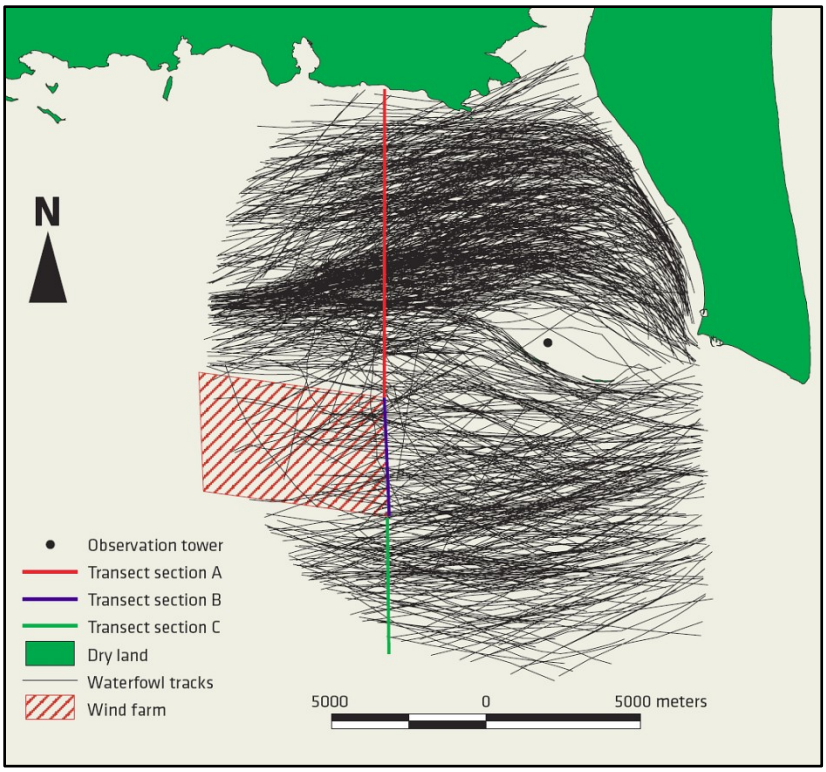

Figure 13 – Bird tracks derived from RADAR at the Nysted offshore wind farm [101]

3.2.2 Fish and Marine Mammals

The effects of wind turbines on fish and other aquatic animals are important because of potential impacts to local the local environment and to fisheries. Most of the impacts are due to the construction of the foundations, the foundations themselves, operation and maintenance of the wind farm, and electromagnetic fields generated by seafloor cables. Thus, a slight change in habitat for both the fish and sea animals is expected.

Studies at Horns Rev and Nysted revealed that scour protection and foundations act as an artificial habitat for mussels and barnacles [102]. This habitat, in turn, attracts fish and sea mammals such as seals and porpoises to the area. No significant effect on fish population was found during the studies. Mammal populations decreased during the construction of the wind farms due to noise and active deterrents to protect hearing. The porpoise population of Nysted has been slow to recover from the construction and operation of the farm. However, the populations of seals rebounded in both sites once construction ceased.

3.2.3 Benthos

The installation of foundations and the undersea cables causes a significant short-term, local disruption to benthic plants and animals. The seabed is directly altered causing the turbidity of the water to increase, limiting sunlight to vegetation. At both the Horns Rev and Nysted wind farms massive colonization of mussels were observed on the scour protection and on the upper foundations [101]. At Horns Rev species of benthic animals not previously seen in the area were detected; at Nysted the benthic communities returned to pre-wind farm levels.

3.3 Power Curves

When a turbine is purchased from the manufacturer, a power curve – a graph of the generated power versus the wind speed – is provided. Each power curve has the same general features:

- The power production is zero at low wind speeds until the cut-in wind speed is reached and the turbine begins to produce power.
- From the cut-in wind speed to the turbine's rated wind speed, the power increases with the cube of the velocity.
- Above the rated speed the turbine is controlled to maintain the rated power until the cut-out wind speed is reached.
- When the cut-out speed is reached the turbine is shut down and yawed out of the wind to avoid damage to the components.

As an example, the power curve for a GE 1.5sl wind turbine is shown in Figure 14 [103].

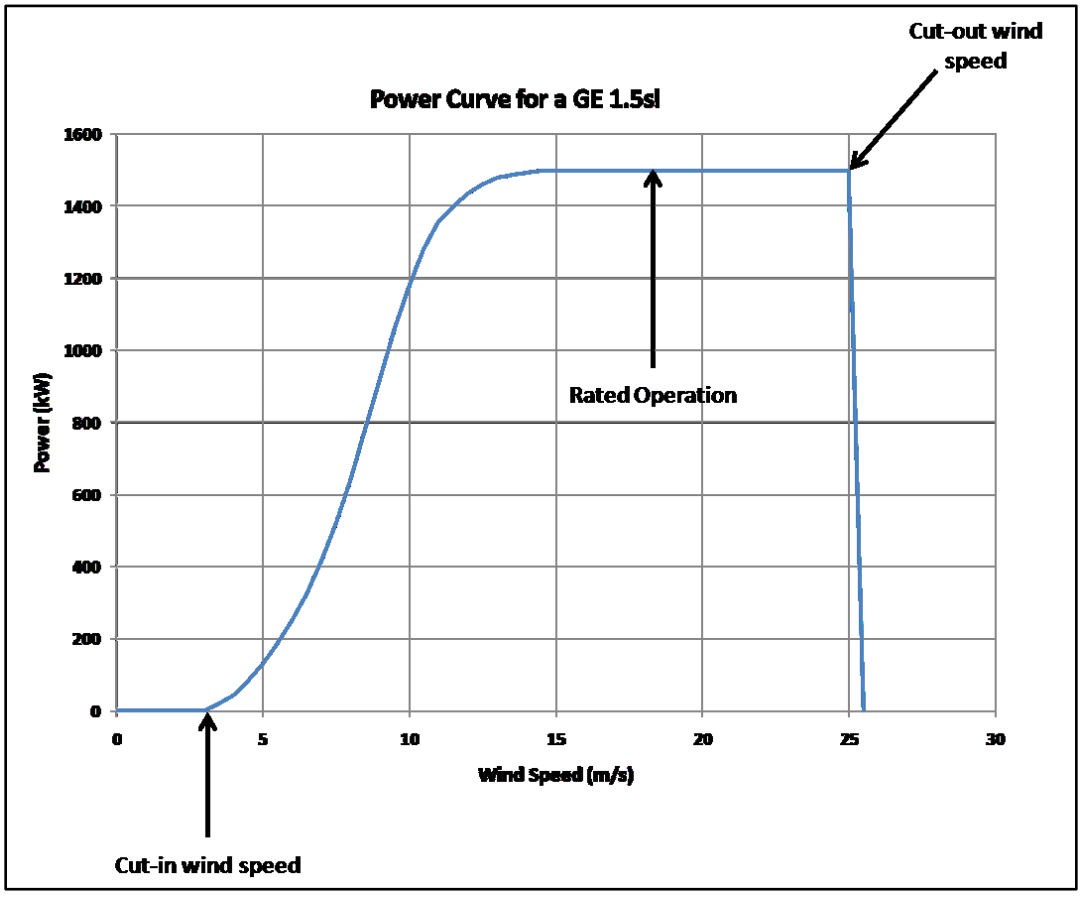

Figure 14 – The power curve for a GE 1.5sl wind turbine [103]

The power curve can be used to determine the amount of energy that a wind turbine produces over a given time interval. For example, the annual energy output from a single wind turbine is

$$E_y = 8760 \int_{v_{in}}^{v_{out}} P(V)\phi(V)dV \qquad \textbf{Equation 10}$$

where:

E_y is the annual energy yield in Watt-hours

$P(V)$ is the power curve of the wind turbine in watts

$\phi(V)$ is the wind speed distribution

v_{out} and v_{in} are the cut out and cut in wind speeds, respectively.

By definition a wind farm has multiple turbines. Thus, a simple way to determine the approximate energy output of a wind farm would be to multiply the energy produced from one turbine by the total number of turbines. In reality, the energy of the wind farm will be reduced by the availability of the wind turbines within the farm, the array losses within the wind farm, the electrical efficiency of transmission, and any soiling losses on the blades [104]. The annual energy yield for the wind farm taking these factors into account will be:

$$E_{y,farm} = N_T E_y \eta_{Avail} \eta_{Farm} \eta_{Elec} (1 - t_{soil}) \qquad \textbf{Equation 11}$$

where:

$E_{y,farm}$ is the annual energy yield of the entire farm in watt-hours

N_T is the number of wind turbines in the farm

E_y is the annual energy yield in watt-hours from a single turbine

η_{Avail} is the availability of the wind farm

η_{Farm} is the efficiency of the wind farm which accounts for array losses

η_{Elec} is the electrical efficiency, including cable losses, and transforming losses

t_{soil} is the loss due to soiling of the blades

The power curve used in this work is generic and is of the form:

$$\boldsymbol{P = {}^{1}/_{2}\,\rho A U^{3} C_p \eta_{RNA}} \qquad \textbf{Equation 12}$$

The air density, ρ, is assumed to be 1.225 $\frac{kg}{m^3}$, the average coefficient of performance, C_p, is taken to be 0.40, the efficiency of the rotor nacelle assembly, η_{RNA}, is 95%. The cut-in and cut-out wind speeds are assumed to be 4 m/s and 25 m/s respectively. The efficiency and losses external to the wind turbine are discussed in the following section.

A typical 3 MW wind turbine, based on a Vestas model [105], has a rotor diameter of 112 meters; a cut in speed of 3 m/s; a cut out speed of 25 m/s; and a rated speed of 12.5 m/s. The assumed power curve based is shown in Figure 15.

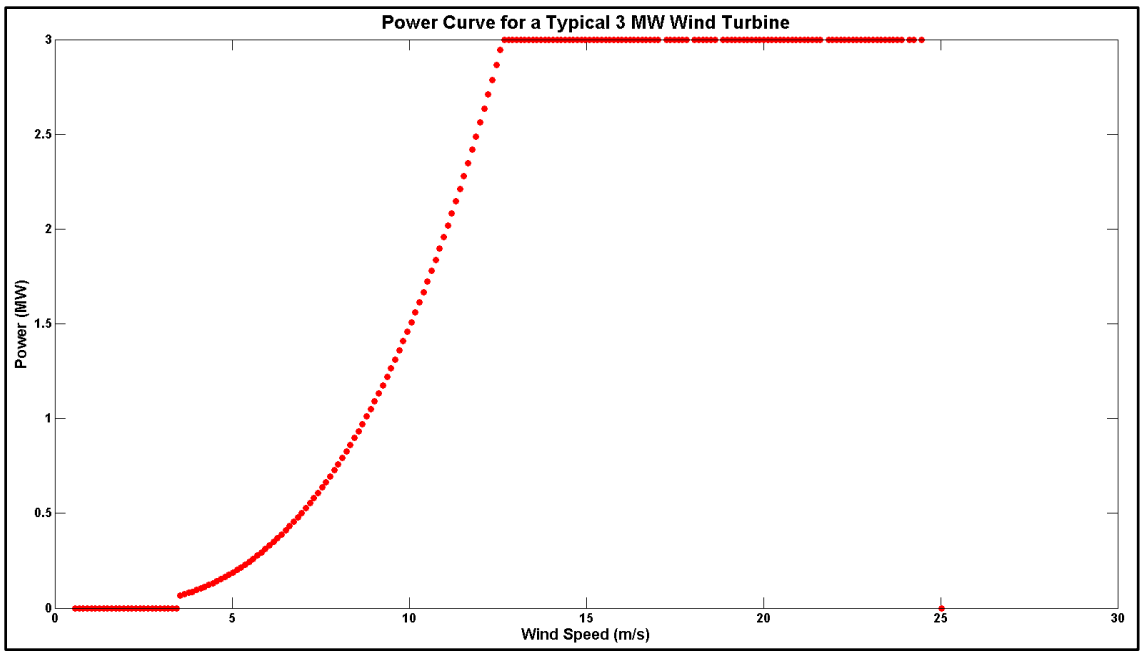

Figure 15 – A power curve for a generic 3 MW wind turbine

Clearly, the dimensions of the turbine make a difference both in the cost and the performance characteristics of the machine. This work utilizes only turbine dimensions and characteristics that have been used in the field. Doing so ensures that the Betz Limit is not violated, and provides insight into how an actual machine would function under the conditions placed upon it.

3.3.1 Wind Farm Power Curve

In practice, the power curve for a wind farm would not be the power curve of a single turbine multiplied by the number of turbines in the farm [106]. First, the wind speed is not uniform over the entire area of the farm. For wind speeds near the cut-in or cut-out speeds, some turbines may be operating and others may be stopped. The result is a power curve profile that has lower power before the cut-out speed, and non-zero power after the cutout speed [107]. Furthermore, the cut-in speed and the rated speed sections of the power curve would also be smoothed out. The overall effect is that multiple turbines in a wind farm each produce less power than a single isolated

turbine. Moreover, the kinetic energy in the wind is diminished as it passes through the blades because some of its energy goes into spinning the rotor. Downstream of the rotor, the wind velocity remains lower causing subsequent turbines to experience lower overall wind speeds. These effects are referred to as array losses. Their magnitude is determined by a number of factors including [54]:

1. Wind turbine spacing, including crosswind and downwind
2. Wind turbine operating characteristics
3. Number of turbines and wind farm size
4. Turbulence intensity
5. The wind rose for the site

For an offshore wind farm the effects are greater than for onshore because the intrinsic turbulence intensity is lower. The lower turbulence results in less air mixing and more pronounced downstream wakes. There are several models to predict array losses in turbines. These include surface roughness models, semi-empirical models, eddy viscosity models and computational fluid dynamics (Navier-Stokes) models [54]. Because the array loss models are highly uncertain, the values in Table 8 will be used to determine the array efficiency, as suggested in [104]. Nominally, a square or rectangular spacing of 10 turbine diameters will be used in this work. However, it is assumed that if fewer than 10 wind turbines exist in a wind farm, the array efficiency will be 97%. This is based on the fact that the turbines would likely be in a single row, facing the prevailing wind direction.

Other factors that decrease the total energy production are the availability, the electrical transmission, and any soiling losses that may occur. The annual availability of the entire wind farm is assumed to be 95%, based on information collected in [108]. The electrical efficiency of the wind farm is the product of the cable efficiency and the transformer efficiency. The electrical

efficiency is often very high, and a value of 97% is assumed [109]. The soiling loss is minimal and is taken to be 3.5% in this work [110]. Thus, combining the electrical efficiency, the availability, the soiling and the array losses yields an overall efficiency of 82.9%.

Table 8 – Array efficiencies based on turbine spacing [104]

Spacing of Turbines in Diameters	Efficiency (%)
8	90.00
9	91.60
10	93.20
11	94.10
12	95.00
13	95.60
14	96.20
15	96.60
16	97.00

Using the assumptions for losses, a wind farm power curve can be generated. The curve is simple: a power curve for a single 3 MW wind turbine is used, multiplied by the number of turbines in the farm, and finally multiplied by the overall efficiency.

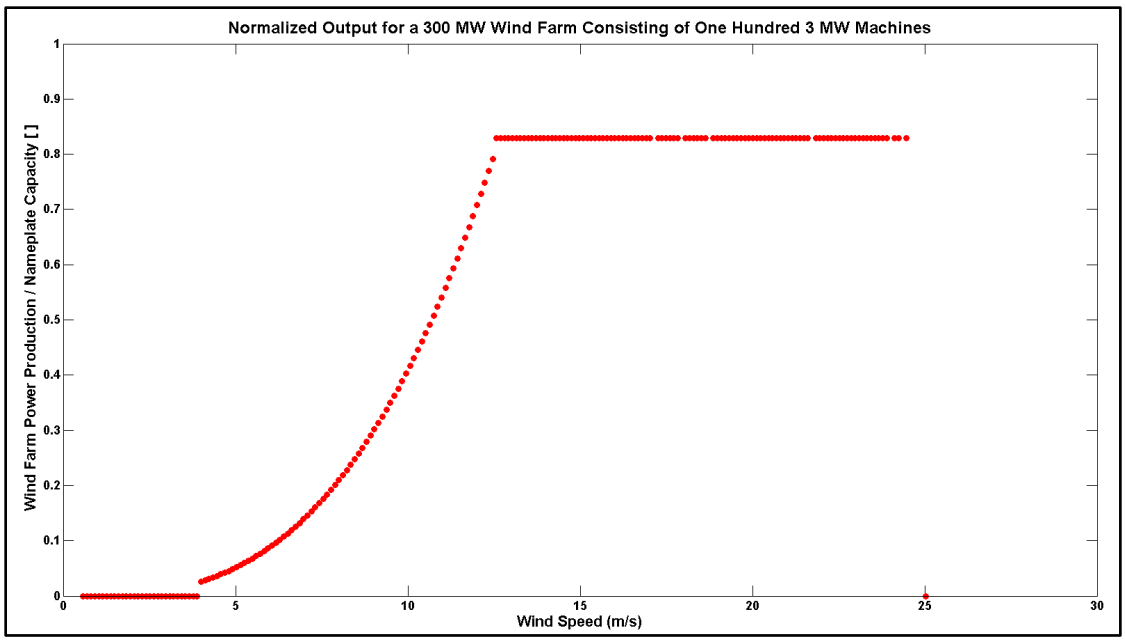

Figure 16 – A normalized composite power curve for a theoretical 300 MW wind farm

In general, the power curve for the entire wind farm would be different than simply adding all of the power curves together. Figure 17 shows a typical example of the power smoothing of an entire wind farm [111]. When the average wind speed for the farm is near either the cut-in or cut-out speed of the turbines some operate while others do not. Thus, the wind farm cut-in and cut-out speeds are different than that of a single turbine.

This work does not use the smoothed power approach for the entire wind farm. Instead, the power curve for a single wind turbine is used for each turbine in the farm and the total power output is multiplied by the overall efficiency of the farm, as discussed earlier.

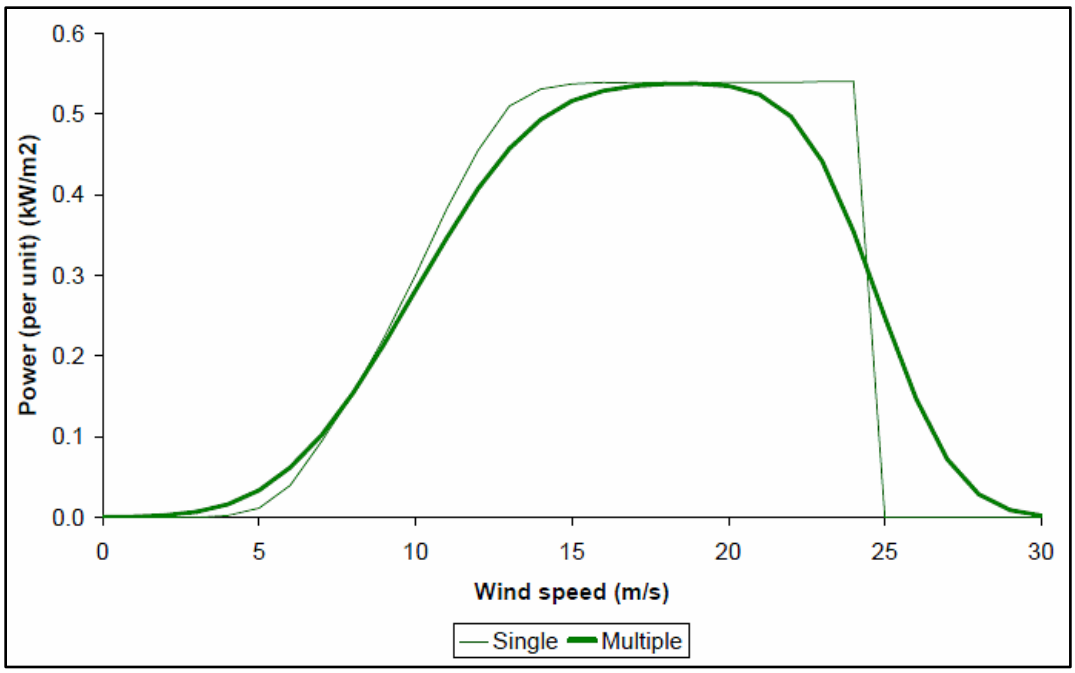

Figure 17 – Normalized power curves for a single turbine and a wind farm [111]

CHAPTER 4

REVIEW OF ALL-ELECTRIC AMMONIA SUBSYSTEM ANALOGUES

In order to determine the feasibility of an offshore wind powered ammonia plant, the operational requirements for industrial ammonia plants must be matched with the technical specifications of available industrial equipment. The following sections discuss electrically-driven analogs to the equipment used in industrial ammonia production. Not all equipment needs to be replaced: industrial ammonia typically used natural gas as a feedstock and therefore requires specialized processing which is unnecessary for electrolytic ammonia production. The hydrogen and nitrogen generation units are the most significant pieces of equipment that require replacement.

4.1 Hydrogen Production

Hydrogen is the most abundant element in the universe but it is generally bound to molecules such as water (H_2O) or organic compounds. Hydrogen is also the lightest element with a molecular weight of 1.008 grams per mole and a density of 0.0899 kilograms per cubic meter at STP. In ammonia synthesis the hydrogen is typically produced through steam reforming (Equation 4) which is not an option for an all-electric process. The following discussion focuses on electrolyzers which are inherently electrically driven processes.

4.1.1 Electrolyzers

An electrolyzer is an electrochemical device that uses an electric current to decompose water into hydrogen and oxygen. Electrolyzers are capable of producing ultrapure hydrogen with purities in excess of 99.998%. At present, there are three types of electrolyzers available: alkaline, proton

exchange membrane (PEM), and solid oxide. Both the alkaline and the PEM electrolyzers are mature technologies while the solid-oxide electrolyzer has yet to be proven [112]. Any of the three processes is governed by the theoretical energy requirement of 39.4 kWh per kilogram of hydrogen produced.

4.1.1.1 Alkaline Electrolyzer

Alkaline electrolyzers typically use an aqueous solution of water and 25-35% by weight potassium hydroxide (KOH) as an electrolyte, though other electrolytes such as sodium hydroxide (NaOH) and sodium chloride (NaCl) have also been used [113]. When an anode and a cathode are submerged in the aqueous solution and a direct current is applied, the electrolyte transports ions between the electrodes through a nickel-oxide diaphragm [114]. The electrolyte acts like a catalyst in that it is not consumed in the reaction, though it must be periodically replaced. Figure 18 shows a schematic of an alkaline electrolyzer. The reaction at the anode is given by Equation 13, the reaction at the cathode is given by Equation 14 and the overall reaction is given by Equation 15.

$$2OH^-(aq) \xrightarrow{yields} {}^1/_2\, O_2(g) + H_2O(l) + 2e^- \qquad \textbf{Equation 13}$$

$$2H_2O(l) + 2e^- \xrightarrow{yields} H_2(g) + 2OH^-(aq) \qquad \textbf{Equation 14}$$

$$H_2O(l) + electrical\ energy \xrightarrow{yields} H_2(g) + {}^1/_2\, O_2(g) \qquad \textbf{Equation 15}$$

Alkaline electrolyzers operate with current densities which typically range from 200-600 milliamps per square centimeter (mA/cm^2)[115]. The highest reported energy efficiency for

alkaline electrolyzers, based on the higher heating value of hydrogen, is reported to be 73% [116].

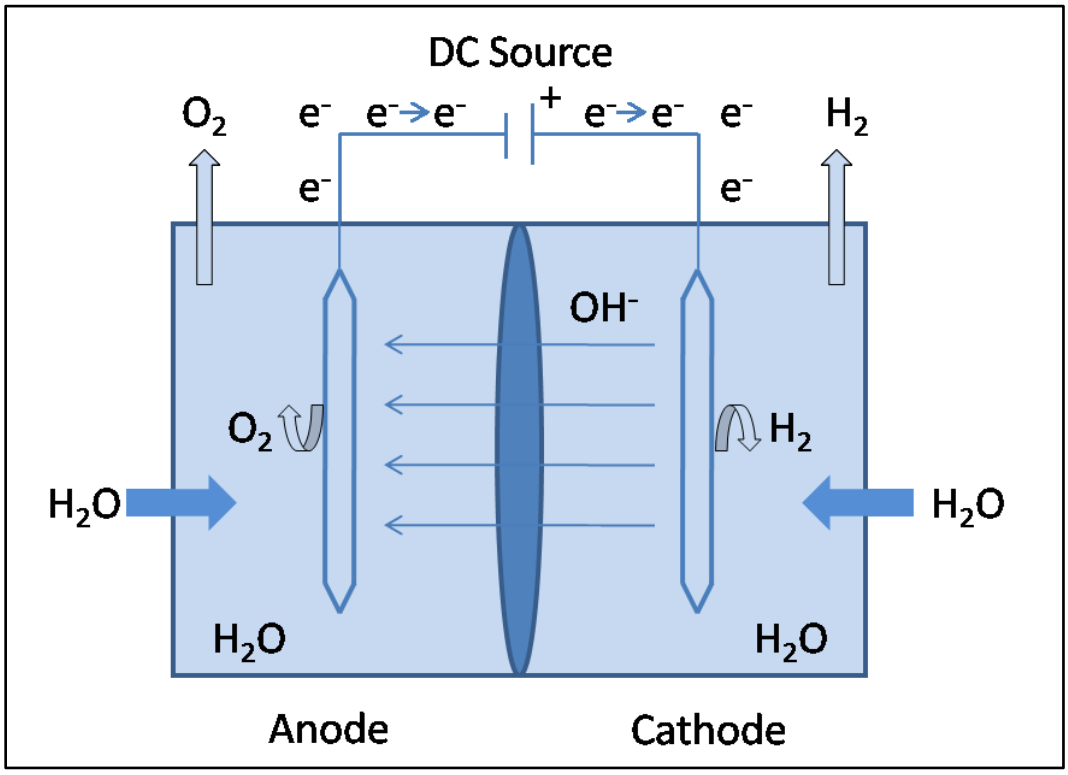

Figure 18 –Schematic of an alkaline electrolyzer

4.1.1.2 PEM Electrolyzer

A PEM electrolyzer fundamentally differs from an alkaline electrolyzer because it employs a solid proton-conducting membrane instead of a aqueous electrolyte. The membrane separates the anode and the cathode chambers and acts as a proton conductor. When deionized water is furnished to the anode and cathode under the presence of an electric field, protons are forced through the proton exhange membrane and then pair with electrons to form hydrogen gas. A schematic of a PEM electrolyzer is shown in Figure 19. The reactions at the anode and the cathode differ from those in an alkaline electrolyzer because protons (H^+) are transported rather than hydroxyl ions (OH^-). Equation 16 gives the equation for the reaction at the anode; Equation

17 gives the reaction at the cathode. The overall reaction remains the same and is given by Equation 15.

$$H_2O(l) \xrightarrow{yields} {}^1/_2\, O_2(g) + 2H^+ + 2e^- \qquad \textbf{Equation 16}$$

$$2H^+ + 2e^- \xrightarrow{yields} H_2(g) \qquad \textbf{Equation 17}$$

PEM electrolyzers operate at current densities in excess of 1500 mA/cm^2, nearly an order of magnitude higher than alkaline electrolyzers. The highest energy efficiency of PEM electrolyzers, based on the higher heating value of hydrogen, is reported by the manufacturer to be 53% [116].

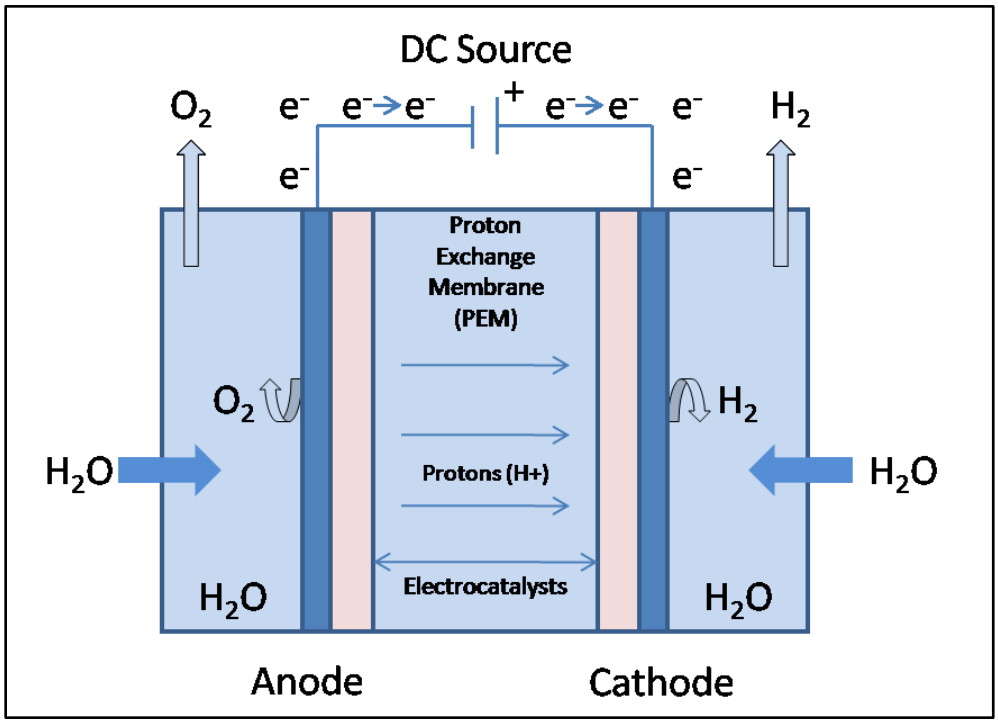

Figure 19 – Schematic of a Proton Exchange Membrane (PEM) electrolyzer

The advantages of a PEM electrolyzer include:

- Ultra-pure hydrogen product (>99.999%) without the need from drying and rinsing [117]

- Operation at high pressure reduces the need for compressor work
- The solid electrolyte avoids caustic aqueous potassium hydroxide
- At low production rates gases do not permeate the electrolytes as readily as in alkaline electrolyzers [118]
- The electrolyte is solid so circulating an aqueous medium is not required
- A wide operational window, typically 5-100% of rated capacity, as compared to 20-100% for alkaline electrolyzers [119]

The disadvantages include:

- Deionized water is required with at least a resistance of 1MΩcm [113]
- Stack lifetimes ranging from 3000 hours to 5 years, depending on operational current density [117]
- Smaller system sizes, with the largest units delivering only 0.9 kilograms per hour at a 63 kilowatts [116]

4.1.1.3 Chloro-Alkali Process

The electrolysis of aqueous sodium chloride (brine) is used to produce chlorine (Cl_2) and caustic soda (NaOH) which are both in the top ten industrially produced chemicals in the United States. The process also produces hydrogen gas (H_2) as a co-product so these cells must be considered. Moreover, since the ammonia plant discussed in this thesis uses sea water as a feedstock, chloro-alkali processes must be considered for hydrogen production.

There are three main cell processes that produce chlorine, sodium hydroxide and hydrogen: the mercury cell, the diaphragm cell and the membrane cell. Of these, the diaphragm cell and the membrane cell are most widely used, representing 86% of total U.S. capacity in 2006

[120]. The main difference in the three cell types is the method used to separate the product chlorine and the sodium hydroxide. Equation 18 gives the overall reaction for all of the processes.

$$2NaCl + 2H_2O \xrightarrow{yields} 2NaOH + Cl_2 + H_2 \ (\Delta H = 422.2 \frac{kJ}{molCl_2}) \qquad \textbf{Equation 18}$$

4.1.1.3.1 Mercury Cells

Mercury cells are made of an inclined steel base with flanged side walls lined with rubber [121]; metal anodes hang from the top of the cell while mercury flows through the bottom. A current passes from the steel bottom plate, through the mercury and electrolyzes the flowing brine at the anode, producing chlorine gas. The sodium ions are combined with mercury to form a sodium amalgam which is further reacted with water in a decomposer in the presence of a graphite catalyst to produce sodium hydroxide and hydrogen [122]. The reaction at the cathode in a mercury cell is given in Equation 19; the reaction in the decomposer is given in Equation 20; the overall cell reaction is given in Equation 21.

$$Na^+ + Hg + e^- \xrightarrow{yields} NaHg \qquad \textbf{Equation 19}$$

$$2Na(Hg) + 2H_2O \xrightarrow{yields} 2NaOH + 2(Hg) + H_2 \qquad \textbf{Equation 20}$$

$$2Cl^- + 2Na^+ + 2Hg \xrightarrow{yields} Cl_2 + 2Na(Hg) \qquad \textbf{Equation 21}$$

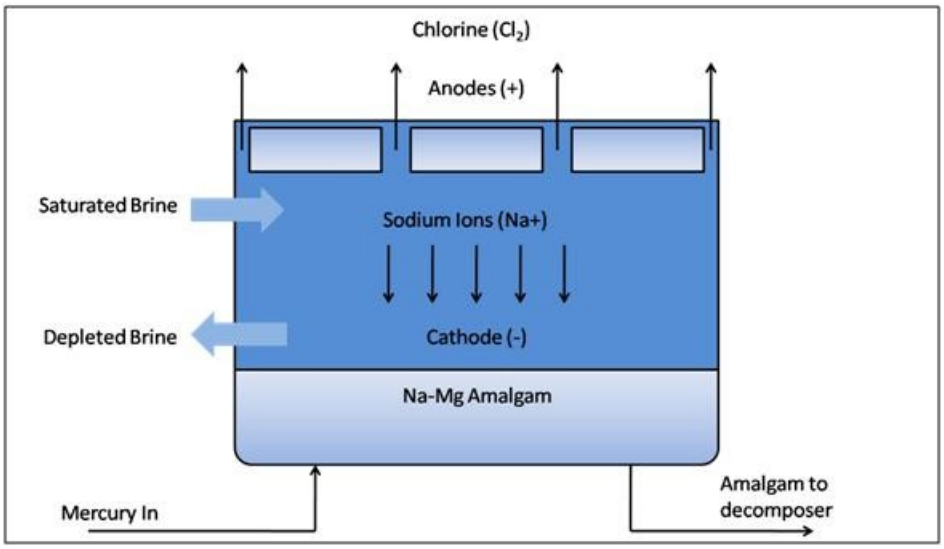

Figure 20 – Schematic of a Mercury Cell for chlorine and hydrogen production

The isolated mercury from the decomposer is then pumped back into the cell to complete the process. The mercury serves two purposes in the process: a cathode for the reaction and a separator between the chlorine gas and the sodium chloride.

The mercury cell has been supplanted by the membrane cell in recent years. New industrial mercury cell chlorine plants have not been built since the 1990s and new installations are unlikely in the foreseeable future [123].

4.1.1.3.2 Diaphragm Cells

A diaphragm cell uses a synthetic (plastic or asbestos) diaphragm to isolate the cathode from hydroxyl ions produced at the anode. Since hydroxyl ions are still prone to enter the anode chamber, hydrostatic pressure is used to force sodium chloride through the diaphragm and into the cathode chamber. Figure 21 shows a diagram of the process. Saturated brine is introduced to the anode chamber and is electrolyzed, releasing chlorine gas and sodium ions. The sodium ions migrate to the cathode chamber due to electromigration and hydrostatic pressure where they

combine with the hydroxyl ions formed from the electrolysis of water molecules to form sodium chloride. Hydrogen gas is consequently formed as a byproduct of the process.

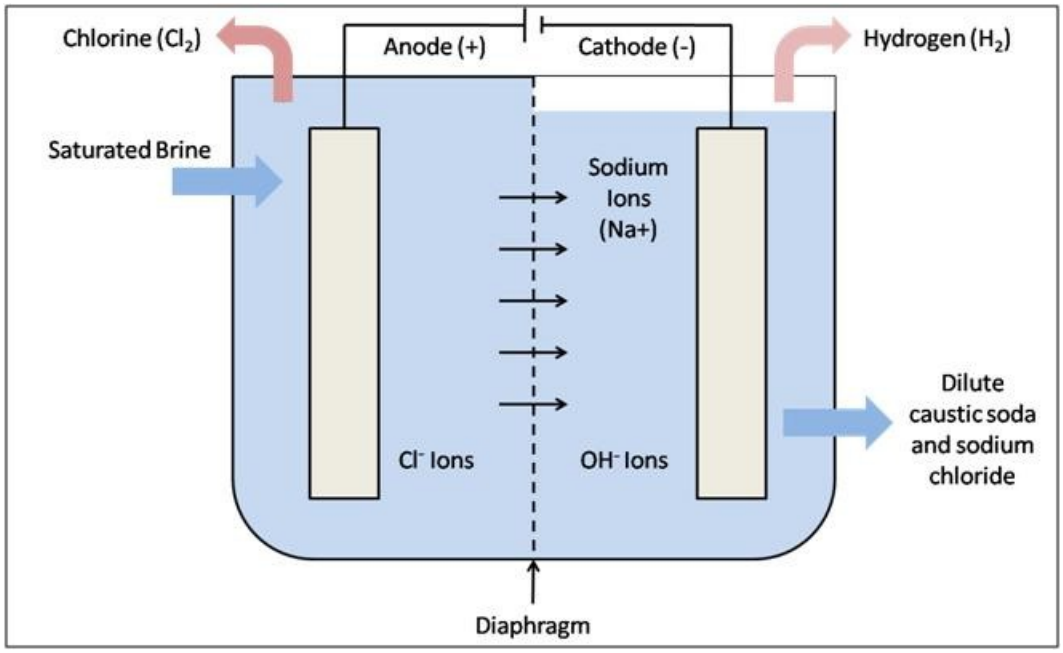

Figure 21 – Schematic of a diaphragm cell

Modern industrial diaphragm cells operate at a temperature of 90-95°C with a current density of 0.25A/cm^2 and a cell voltage of 3.5V [124].

4.1.1.3.3 Membrane Cell

A membrane cell employs a membrane composed of perfluorocarboxylic and perfluorosulfonic acid-based films that separates the anode and the cathode chambers. Similar to the diaphragm cell, the membrane cell introduces saturated brine into the anode chamber. The brine is electrolyzed into chlorine, which is drawn off as a product gas, and sodium, which migrates through the membrane to the cathode chamber. The process is shown in Figure 22. The membrane is more selective than the diaphragm cell so hydrostatic pressure is not needed to prevent the hydroxyl ions from migrating to the anode chamber. In the cathode chamber, 30-32% aqueous caustic soda is introduced so that the sodium ions react with the hydroxyl ions that were

liberated by the formation of hydrogen gas [120]. Hydrogen gas is drawn off as a byproduct and a more concentrated caustic soda solution is recovered in the product stream.

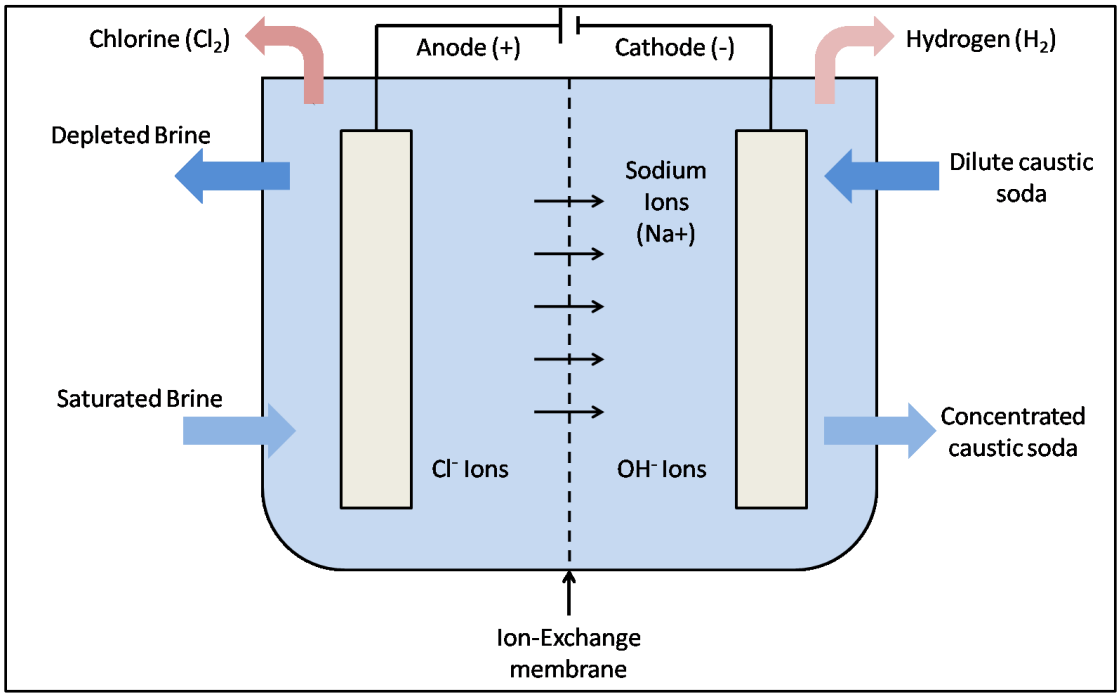

Figure 22 – Membrane cell for chlorine and hydrogen production.

4.1.2 Thermodynamics of electrolyzers

The total change in Gibbs energy for water electrolysis is given by Equation 22 where ΔH is the change in enthalpy of the products and the reactants; T is the temperature and ΔS is the change in entropy between the products and the reactants. Gibbs energy is the theoretical minimum amount of work needed to split water at constant temperature and pressure.

$$\Delta G = \Delta G_p - \Delta G_r = \Delta H - T\Delta S \qquad \textbf{Equation 22}$$

At standard temperature and pressure the value of Gibbs energy is $\Delta G° = 237 \frac{kJ}{mol}$. The electrical work done on the system equals Gibbs energy if the system is fully reversible. If the system has losses the change in Gibbs energy will be higher than the charge times the voltage – given by zF,

where z is the number of transferred electrons and F is the Faraday constant. Equation 23 gives the reversible cell voltage, U_{rev}, for electrolysis; at standard temperature and pressure U_{rev} has a value of 1.229V.

$$\boldsymbol{U_{rev} = \frac{\Delta G}{zF}} \qquad \textbf{Equation 23}$$

The actual work required to split the water into hydrogen and oxygen is given by the change in enthalpy between the products and the reactants. At standard temperature and pressure the enthalpy change for splitting water is $\Delta H° = 286 \frac{kJ}{mol}$. The thermoneutral voltage of the electrolyzer is the quotient of the enthalpy change and the charge flowing in the system, given by Equation 24.

$$\boldsymbol{U_{tn} = \frac{\Delta H}{zF}} \qquad \textbf{Equation 24}$$

In practice, the electrolyzers are often operated at conditions above ambient pressure and/or temperature. Deviations in cell voltage due to temperature and pressure can be calculated using the Nernst Equation, given in Equation 25. Other empirical equations such as Equation 26 and Equation 27 are also used, but they require knowledge of the working conditions of the electrolyzer [114].

$$\boldsymbol{U_{cell} = U_{rev} + \frac{RT}{zF} \ln\left(p_{H_2} {p_{O_2}}^{1/2}\right)} \qquad \textbf{Equation 25}$$

$$\boldsymbol{U_{cell} = U_{rev} + \frac{r}{A} I + s \log\left(\frac{t}{A} I + 1\right)} \qquad \textbf{Equation 26}$$

$$\boldsymbol{U_{cell} = U_{rev} + \frac{r_1 + r_2 T}{A} I + s \log\left(\frac{t_1 + t_2 T + t_3 T^2}{A} I + 1\right)} \qquad \textbf{Equation 27}$$

The current efficiency is given by the empirical relation $n_F = \frac{(I/A)^2}{f_1+(I/A)^2} f_2$ where f_1 and f_2 are constants, I is the current in the cell and A is the area of the electrodes. Finally, the hydrogen produced by the electrolyzer is given by:

$$\dot{n}_{H_2} = n_F \frac{n_c I}{zF} \qquad \textbf{Equation 28}$$

where n_c is the number of electrolyzer cells in series, I is the current through the cells, and zF are as before. The oxygen production is simply half of the hydrogen production on a molar basis due to the stoichiometry of the water molecule.

The nominal energy efficiency is the quotient of the changes in enthalpy and Gibbs free energy. In practice, because higher temperatures and pressures are used it is more convenient to calculate the efficiency using the thermoneutral voltage and the reversible cell voltage:

$$n_e = \frac{U_{tn}}{U_{cell}} \qquad \textbf{Equation 29}$$

The total power required for the electrolyzer is simply the overall current times the electrolyzer voltage:

$$P = n_c U_{cell} I \qquad \textbf{Equation 30}$$

The heat generated by the electrolyzers is the power that was not utilized for hydrogen production, namely:

$$\dot{Q}_{gen} = n_c UI(1 - n_e) \qquad \textbf{Equation 31}$$

Compression work for hydrogen can be done within the electrolyzer instead of by compressors. This approach simplifies the overall process and saves capital cost expenses for the compression

machinery including drivers and compressors. The compression work must be the same for both processes, and the derivation that appeared in Larminie and Dicks [125] is presented below:

$$\Delta W_{comp} = P_1 V_1 \ln\left(\frac{P_2}{P_1}\right) = nRT \ln\left(\frac{P_2}{P_1}\right)$$

$$\Delta U = \frac{RT}{zF} \ln\left(\frac{P_2}{P_1}\right)$$

$$\Delta W_{comp} = \Delta U \times Q$$

$$\Delta W_{comp} = \Delta U \times zF \times n$$

$$\Delta W_{comp} = \frac{RT}{zF} \ln\left(\frac{P_2}{P_1}\right) \times zF \times n = nRT \ln\left(\frac{P_2}{P_1}\right)$$

4.2 Nitrogen Production Methods

By volume, nitrogen represents over 78% of the Earth's atmosphere though it almost never exists in its pure atomic form. Rather, it usually exists as diatomic nitrogen (N_2) or nitrogen oxides because of the affinity of the nitrogen molecule for bonding. Diatomic nitrogen is chemically inert at standard temperature and pressure (STP) and is thus an important industrial chemical for preservatives and flame-retarding applications. The three main methods of obtaining pure nitrogen gas are cryogenic distillation, polymer membrane separation, and pressure swing adsorption. Of these, cryogenic nitrogen purification accounts for about 90% of all commercial production [126]. In addition, combustion can be used to eliminate oxygen from the air either in a reformer or in a combustor. This method yields a product stream that is oxygen deficient. As such, it produces a stream of mostly nitrogen, argon carbon dioxide and/or water vapor, depending on the fuel used.

Table 9 – Principle gases of dry air [127]

Constituent	Percent by Volume
Nitrogen (N_2)	78.084
Oxygen (O_2)	20.946
Argon (Ar)	0.934
Carbon Dioxide (CO_2)	0.034
Neon (Ne)	0.00182
Helium (He)	0.000524
Methane (CH_4)	0.00015
Krypton (Kr)	0.000114
Hydrogen (H_2)	0.00005

Table 10 – Application range of nitrogen separation processes [128]

Capacity (Nm^3/h)	Purities	Separation Method	Load Range (%)
1-1000	<99.5%	Membrane	30-100
5-5000	<99.99	Pressure Swing Adsorption	30-100
200-400000	ppb range	Cryogenic Rectification	60-100

The range for which the three main nitrogen production methods are economically competitive is shown in Figure 23. For completeness, delivered gaseous and liquid nitrogen are also shown. In

general, the nitrogen used for delivery comes from membranes, PSA or cryogenic distillation, and is available in small quantities.

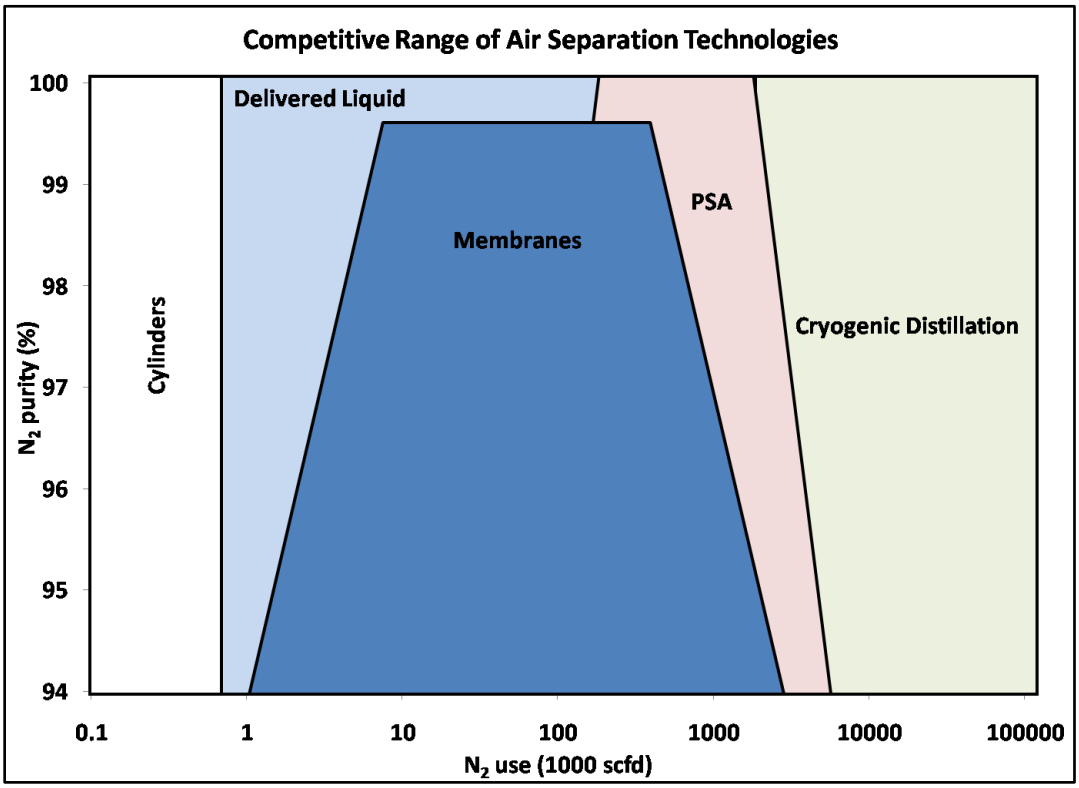

Figure 23 – Competitive range of air separation technologies [129]

4.2.1 Cryogenic Air Separation

Cryogenic air separation exploits the boiling point difference in the three main constituents of air – nitrogen, oxygen and argon whose boiling points are 77.4 K, 90.2 K, and 87.3 K, respectively. The process is highly nonlinear and tremendously complex and involves numerous fluid flows and components. Cryogenic air separation plants are divided into a warm section which is comprised of compression, drying, and purification, and a cold section that houses the heat exchanger and the distillation column. The general process design of a cryogenic air separation plant involves the following steps:

- Air is compressed and cooled with intercoolers to remove any water vapor
- The dry air stream is purified to remove contaminants such as carbon dioxide and residual water vapor
- The air is cooled using the waste product oxygen and purified nitrogen from the distillation column, further deducing contaminants
- The air is further cooled down to about 97 K (the dew point of air)
- The air is distilled into its components using a single distillation column

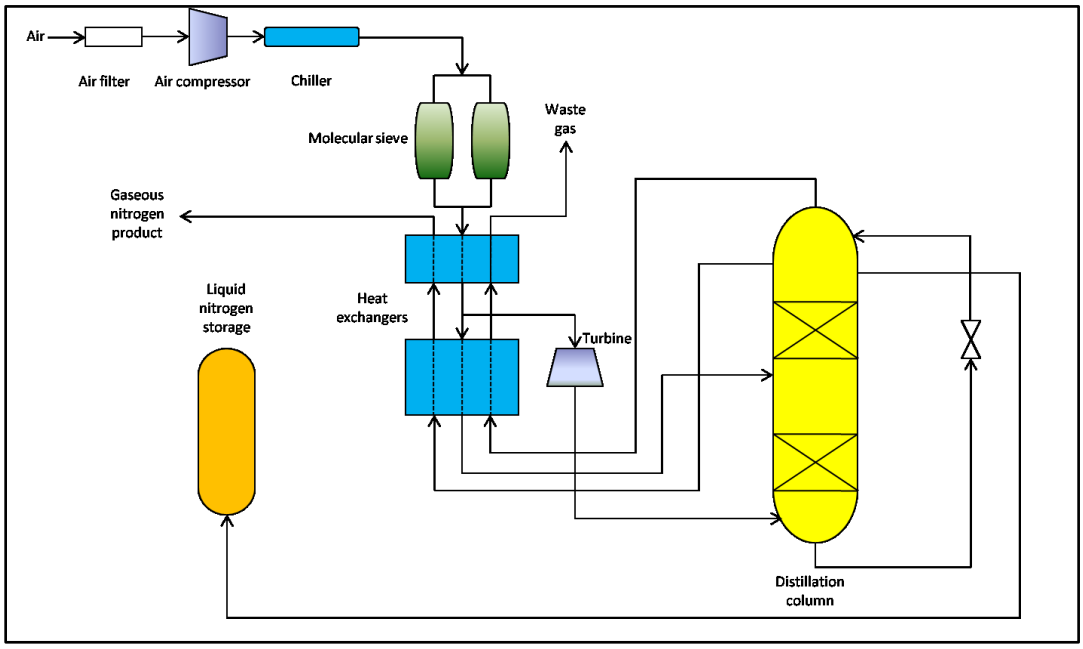

Figure 24 – A basic schematic of cryogenic air separation

4.2.2 Pressure Swing Adsorption (PSA)

A particle being attracted to an interface, like a gas molecule being attracted to a solid surface, is a phenomenon called adsorption [130]. Carbon molecular sieves contain pores and cavities into which nitrogen adsorbs more slowly than oxygen. Increased pressure accelerates adsorption because gas molecules will move faster and have added surface interactions. The reverse is also true: oxygen desorbs from the carbon molecular sieves more quickly as the pressure is reduced.

Using this principle, the pressure can be cycled from high, to remove oxygen from air and isolate nitrogen, to low, to remove oxygen from the adsorber. This process usually employs two adsorption tanks: one adsorber releases purified nitrogen into a holding tank; the second adsorber simultaneously pressurizes and generates nitrogen. A critical operating parameter is contact time, or the amount of time that the system is given to reach equilibrium [131]. A short contact time leads to low adsorption of oxygen; a long contact time enables the nitrogen to adsorb and reach equilibrium which eliminates selectivity.

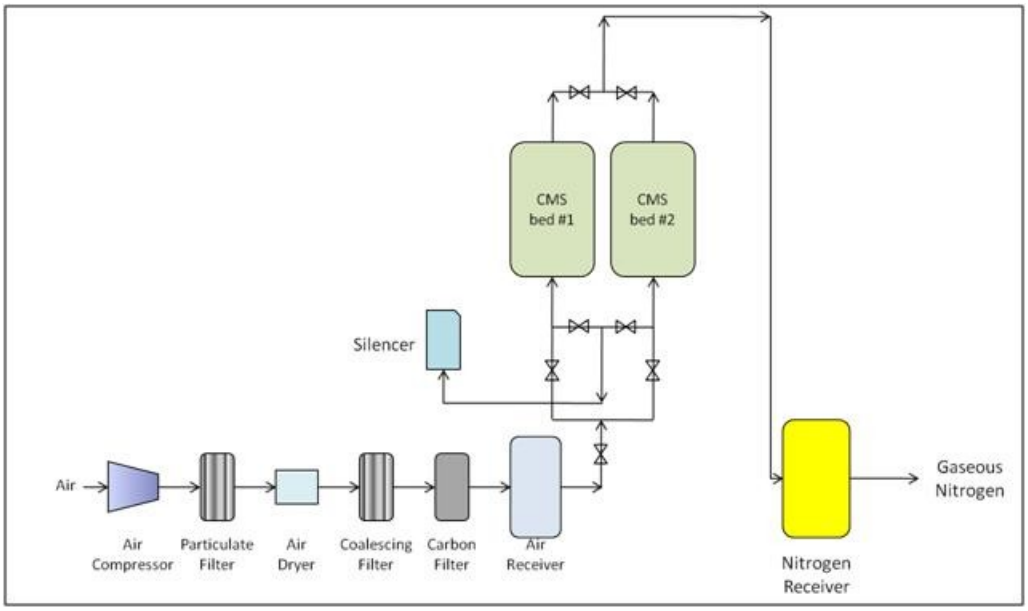

Figure 25 – Schematic of a PSA adsorption nitrogen generator [132]

PSA is capable of producing nitrogen with purities up to 99.99% and capacities of a few standard cubic meters to 5000 cubic meters per hour [128]. Higher production output is achieved with lower nitrogen purities but the residual oxygen content must be removed via a catalytic deoxygenation system for higher nitrogen purities.

4.2.3 Membrane Separation

A general definition for the macroscopic properties of a membrane is a *selective barrier between two phases* [133]. At the microscopic level, fluids absorb on the high pressure side, diffuse through the membrane and desorb on the low pressure side. The ability of the membrane to transfer the fluid from the high pressure side to the low pressure side is called permeability. The flow of the fluid through the membrane is the product of the permeability, the partial pressure gradient of the membrane and the ratio of the area to the thickness:

$$J_i = P_i \frac{A}{l} dp_i \qquad \textbf{Equation 32}$$

The selectivity describes the ability of a membrane to separate two components, *i* and *j*, of a fluid and is given by is the ratio of the permeability of the two components, $\alpha = Pi/Pj$. For air separation, oxygen gas, having a smaller radius than nitrogen, permeates most membranes much more readily. Thus, nitrogen is collected on the pressurized side as retenate.

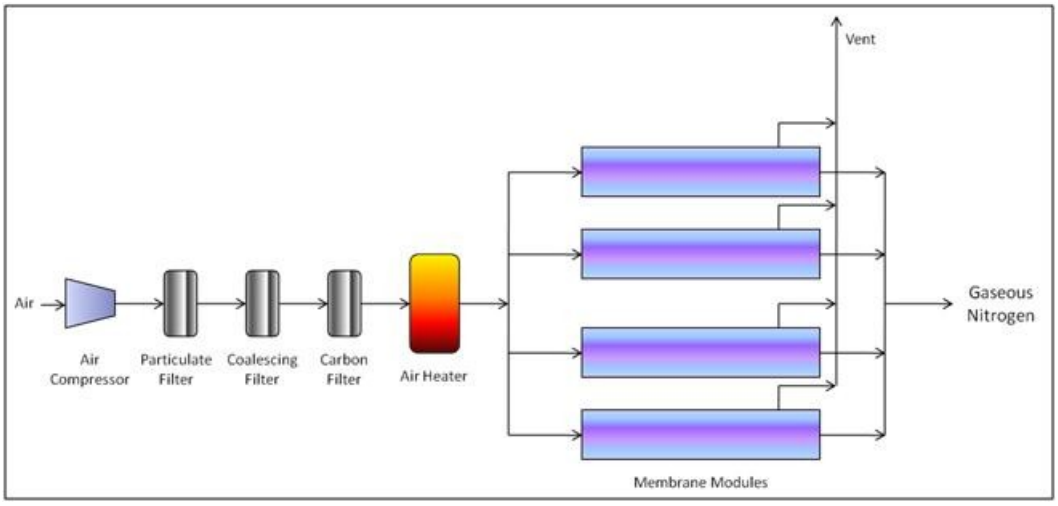

Figure 26 – Schematic of a membrane nitrogen generator

Nitrogen membrane separation is economically viable for nitrogen purities up to 99.5%; to produce nitrogen beyond that purity would require either catalytic deoxygenation or pressure swing adsorption [126]. The higher the purity of nitrogen, the lower the product yield. The available membrane systems have low to medium throughput rates ranging from 3-3000m^3/h, depending on the desired purity [132].

Because the fluid flow through a membrane is inversely proportional to the thickness, ultrathin membranes consisting of bundles of hollow fibers have been designed. These bundles are then arranged in modules so that large systems can easily be constructed [134].

4.2.4 Inert Gas Generators

Nitrogen can be produced by "inert gas generators" by burning a clean fuel, such as methane, propane or hydrogen, in a precise stoichiometric supply to eliminate oxygen gas from air [135]. In the product stream impurities will exist and depend on the fuel used for combustion. For example, methane and propane will produce carbon oxides, water vapor, sulfur compounds, hydrogen and nitrogen oxides while hydrogen may only produce water vapor and nitrogen oxides.

In order to react all of the oxygen present in the air the correct stoichiometric ratio of fuel to oxygen is required. The direct combustion of hydrogen produces very few byproducts because oxygen has such a high affinity for hydrogen. Equation 33 gives the reaction for the combustion of hydrogen in air.

$$2H_2 + O_2 \xrightarrow{yields} 2H_2O \ (\Delta H = -241.8 \ \frac{kJ}{mol}) \qquad \textbf{Equation 33}$$

However, hydrogen combustion does not eliminate other gases present in air such as argon, carbon dioxide, or other inert gases (see Table 9). The carbon dioxide would have to be further reduced to parts-per-million levels or the catalyst would be poisoned.

4.3 Gas Compressors

A compressor is a mechanical device that is used to increase the pressure of a gas. Compressors can be categorized into two general groups, intermittent flow and continuous flow, as shown in Figure 27. Intermittent flow compressors, also known as positive displacement compressors, intake a specific volume of gas, increase its pressure, and discharge it in a fluctuating cycle. A continuous compression mode entrains an uninterrupted stream of gas, converts the velocity of the gas into pressure, and moves it through the system.

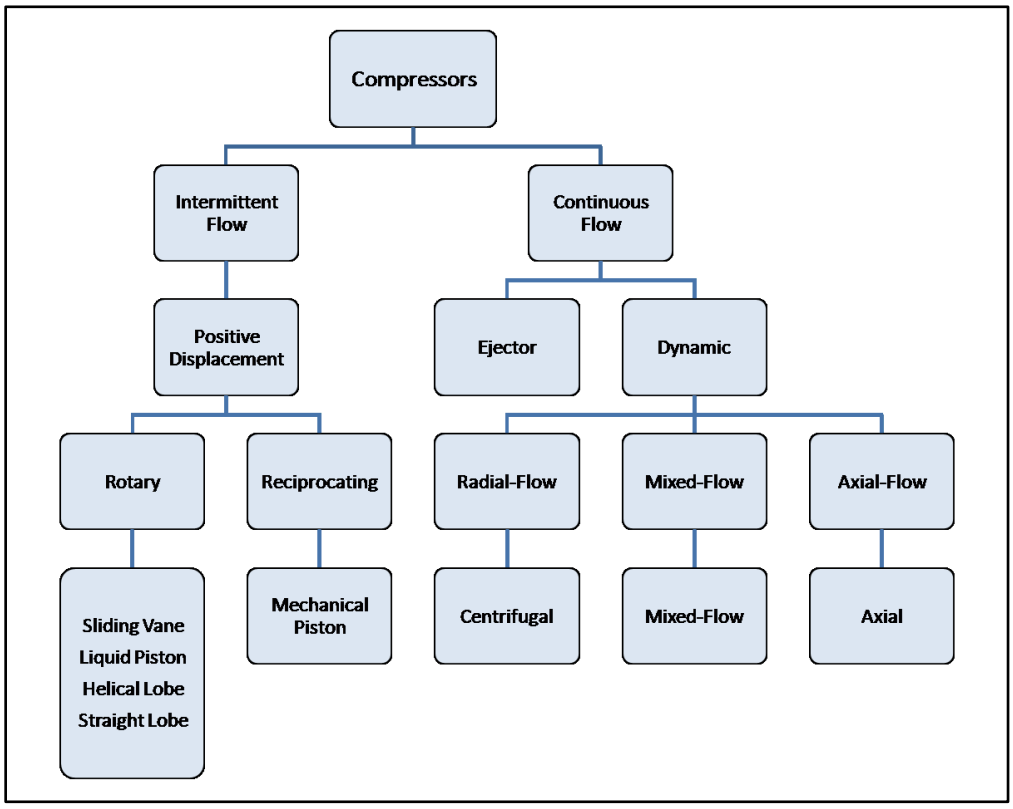

Figure 27 – Hierarchy of compressor types [136]

Positive displacement compressors are of two varieties: rotary compressors and reciprocating compressors. Rotary compressors utilize rotating elements that simultaneously displace and compress a gas. They can be further subdivided into the categories sliding vane, liquid piston,

helical lobe, and straight lobe. Reciprocating compressors use a cylinder and piston assembly to compress a specific volume of gas, similar to the action of an internal combustion engine.

Continuous flow compressors are classified as either ejectors or dynamic flow devices. Ejectors increase the pressure of a fluid by using a high velocity jet that is directed through a diffuser which converts the velocity of the fluid into pressure. Dynamic compressors make use of rotating components that transfer energy to the gas by accelerating it. The velocity is then converted into pressure both in a diffuser and in the rotating elements. These dynamic compressors can be centrifugal, mixed-flow or axial compressors. The names of the dynamic compressors describe the direction of flow for the gas: centrifugal compressors have radial flow; axial compressors have axial flow; and mixed flow compressors have elements of both radial and axial flow. The approximate competitive range for reciprocating, centrifugal and axial compressors is shown in Figure 28.

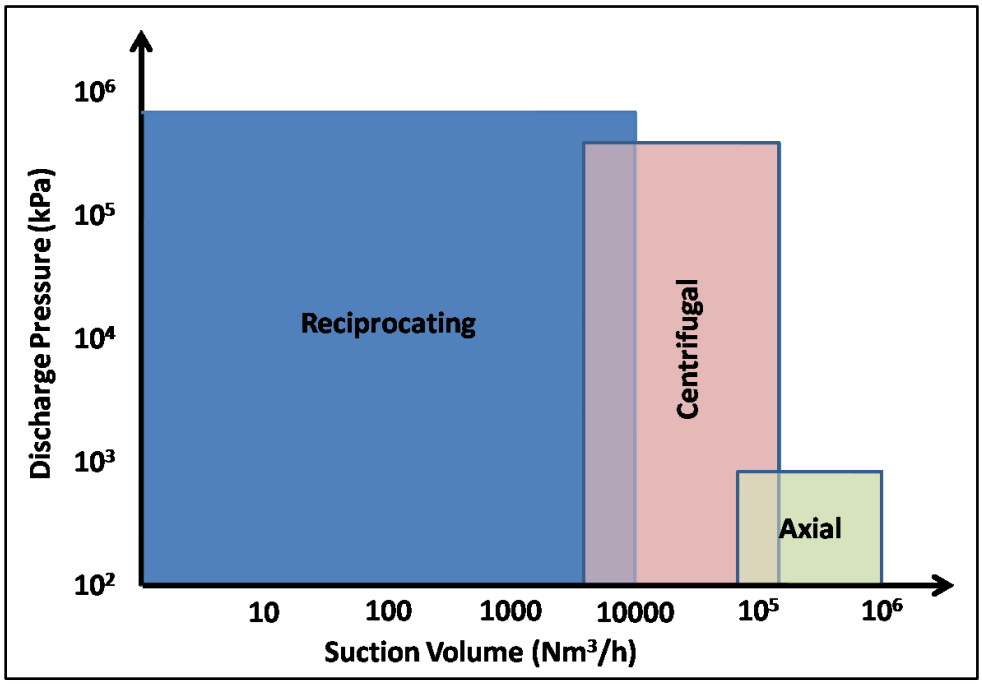

Figure 28 – Competitive ranges for compressors [137]

Nearly all contemporary ammonia plants use centrifugal compressors for syngas compression, though reciprocating compressors were used until the mid 1960s. The compressors utilize intercoolers to minimize the compression work and operate at constant throughput, delivering the syngas at constant pressure and temperature to the synthesis reactor. The synthesis loop operates adiabatically at constant pressure with a slight pressure drop across the reactor beds. The different subsystems of an ammonia plant – syngas production, syngas compression and the synthesis loop – all function at steady-state; cyclic operation exacerbates failure modes that already exist in ammonia plants [138]. For a wind-driven system the implication is that the syngas compression and synthesis loop must be supplied with constant power; variable power would damage the synthesis reactor.

Compressors are operated using drivers which provide a torque at either a constant speed or over a range of speeds. Drivers for compressors are one of three varieties: steam turbines, gas turbines and electric motors. In modern ammonia plants nearly all drivers are extraction steam turbines that power centrifugal compressors, though occasionally gas turbines are used [1]. Since both steam production and gas generation from a wind turbine for this purpose is extremely inefficient, only electric motor drivers will be considered in this section.

Electric motors are becoming increasingly more viable compressor drivers because of better technology which includes more compact designs and longer expected life. Both synchronous and induction motors can be employed, but their selection depends on the specific application, the power required and the angular velocity. For example, two pole induction motors should be used with 3600 rpm compressor drivers below about 3.7 megawatts (5000 horsepower) because of simple installation and high performance; synchronous motors are suited to drive large, low speed reciprocating compressors [136].

For coastal applications, the motors must be protected from the harsh climate of sand and ocean spray that can rapidly degrade machinery. Several enclosures exist for shielding the motors from outdoor conditions. The best option is probably the totally enclosed water-to-air cooler motor (TEWAC) which is completely sealed from the external environment [136].

4.4 Desalination of water

About 97% of all water on the Earth is in contained in the oceans. The remaining 3% is freshwater, of which about two-thirds is contained in glaciers and one-third is in lakes, ponds, rivers, streams and moisture [139]. A staggering 20% of all liquid freshwater is contained in Baykal Lake in Russia [140]. While ocean water is imperative for transportation and fishing, it is too salty for drinking or irrigation. Since at least Antiquity humans have recognized that the Earth's water cycle continuously renews fresh water supplies. Indeed, the concept of solar desalination was described as early as in the fourth century BCE by Aristotle [141].

Desalination refers to any of several processes that remove salts from water. The average salinity for seawater is about 35000 parts per million (ppm) of total dissolved solids (TDS) while brackish water has a salinity in the range of 1000 ppm TDS to 11000 ppm TDS [142].

Table 11 shows the typical concentrations of dissolved solids in seawater [143]. Desalination processes can be divided into two main categories:

- Distillation or phase-change processes that change the state of water through evaporation.
- Membrane processes that are based on filtration.

In general, distillation processes are capable of producing a water product with a salinity level at least an order of magnitude lower than membrane processes [144] and often attain levels in the 15-20 ppm TDS range [145]. Distillation processes utilize thermal energy to effect the separation of salts from the water. The thermal energy can come from any suitable source including

geothermal energy, nuclear power, solar energy, or fossil-fuels. Membrane processes exclusively use electricity: reverse osmosis requires high pressures which are provided by an electrically-driven pump; the ionization of the salts in the electrodialysis process is achieved using electricity. All desalination processes require some form of seawater pre-treatment to inhibit corrosion, scaling, foaming or biological growth.

The theoretical minimum energy for desalination is a function of freshwater recovery and the salt concentration [146]. For product water at 50% recovery and a typical ocean salt concentration of 35000 ppm TDS, the theoretical minimum work is just over 2 kJ/kg.

Table 11 – Typical composition of dissolved solids in seawater [143]

Element	Chemical Form	Concentration parts per million
Chlorine	Cl^-	18,980
Sodium	Na^+	10,561
Magnesium	Mg^{+2}	1,272
Sulfur	SO_4^{-2}	884
Calcium	Ca^{2+}	400
Potassium	K^+	380
Bromine	Br^-	65
Carbon (inorganic)	CO_3^{-2}; HCO_3^{-1}	28
Strontium	Sr^{+2}	13
Silicon	$HSiO_4^{-1}$	0.01-7.0
Boron	$H_2BO_3^{-1}$	4.6
Carbon (organic)	Complex	1.2-3.0
Aluminum	Al^{+3}	0.16-1.9
Fluorine	F^-	1.4

4.4.1 Thermal processes

About 40% of all desalted water in the world is produced by thermal processes to distill freshwater from seawater or brackish water [147]. Thermal desalination processes mimics the natural water cycle by evaporating saline water and condensing it to from freshwater. Processes based on this principle include multi-stage flash distillation (MSF), mulit-effect distillation (MED) and vapor compression (VC) which can be either mechanical (MVC) or thermal (TVC).

At standard conditions water boils at 100°C but by reducing the pressure the boiling point can be reduced. The variation in boiling point with reduction in pressure is shown in Figure 29. Using this principle, desalination plants based on distillation have been designed with several stages, each having a successively lower temperature and pressure. The lower pressure stages use the excess heat from previous stages to boil water and produce fresh water. This process also reduces scaling in which compounds precipitate out of the water and form hard scales on the mechanical equipment. The most notorious of the compounds is gypsum ($CaSO_4$), which leaves solution at about 95°C. Once scaling occurs, heat transfer and fluid flow are both adversely affected.

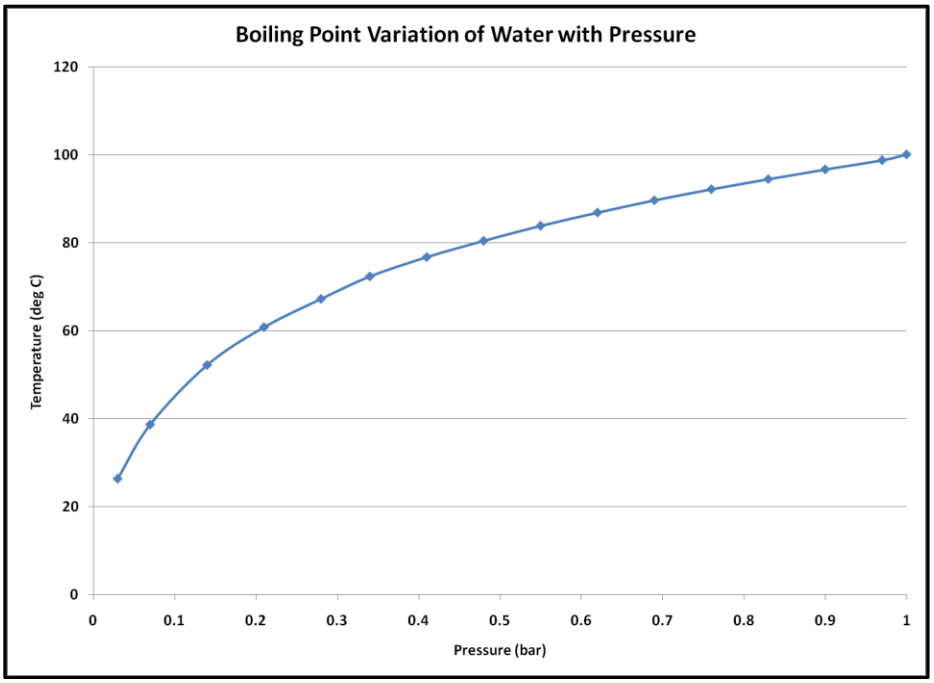

Figure 29 – Boiling point variation of water with pressure

4.4.1.1 Multi-Stage Flash

Of the installed thermal desalination systems worldwide, 93% are multi-stage flash (MSF) distillation [148]. MSF is capable of producing extremely pure water with low salt concentrations in the 15 ppm TDS range, even from water that has higher salinity than typical seawater. A series of stages is used to heat the seawater feed to its highest allowable temperature while rejecting the

brine and product at their lowest possible temperatures. The seawater feed is mixed with the recirculated brine and is further heated to achieve a temperature slightly below its saturation temperature at the maximum system pressure. The water is discharged to the first staged where it becomes superheated and flashes to steam. Some of the steam is stripped of brine droplets and condensed on cooling tubes, concurrently heating the seawater feed and increasing the thermal efficiency of the plant. The condensed distillate is rejected as freshwater while the remaining brine is sent to the subsequent stage which, again, is maintained at a pressure slightly lower than the saturation vapor pressure. The process continues through subsequent stages, each with lower pressures and temperatures.

MSF plants typically have 18 to 25 stages, though they may contain between 4 and 40 stages [147]. The smallest MSF plants produce roughly 10,000 m^3 per day and the largest plant – located in the UAE – is capable of 455,000 m^3 per day.

4.4.1.2 Multiple Effect Boiling (MEB) or Multi-Effect Distillation (MED)

Multiple effect boiling is similar to the MSF in that it reuses the heat of vaporization by placing the evaporators and condensers in series [147]. The steam in one effect transports heat to the next effect whereby evaporation occurs as the steam condenses. Thus, the water can go through several boilings without adding extra heat after the first effect. This process is possible because each effect has progressively lower pressure so that steam forms and carries energy to the next effect. All of the effects are used to preheat the feed water entering the system. The MEB plant is often configured as a once-through system which eliminates recirculating brine, and reduces pumping and scaling [141].

4.4.1.3 Vapor Compression (VC)

Vapor compression distillation is mostly used in small and medium installations. For VC units, the heat required for evaporating water is derived from the compression of vapor rather than heat from a boiler. A mechanical compressor or a steam jet can be used to condense vapor to produce enough heat to evaporate the feed water. The mechanical compressor is almost always electrically driven making this the only distillation process that can operate solely on electricity [149].

The VC process is very similar to the MEB system except that the vapor from the last effect is mechanically or thermally compressed, raising its saturation temperature before being recycled to the first effect.

4.4.2 Membrane Processes

There are two commercially viable processes that utilize a membrane to separate salt from water: electrodialysis and reverse osmosis. In each process the membrane acts to selectively separate the salts from the water. Each process arrives at the same result in two entirely different ways. Electrodialysis uses an electric potential to transport salts through a membrane, leaving fresh water. Reverse osmosis uses pressure to force the water through a membrane, leaving the salts behind. Both processes primarily use electricity as their primary power supply, though reverse osmosis can use mechanical power. Though both methods are very similar, electrodialysis is capable of desalting only brackish water while reverse osmosis can desalt both brackish and seawater.

4.4.2.1 Electrodialysis

Electrodialysis is an electromechanical method for desalting brackish water. The ED unit is composed of several hundred electric cell pairs with water channels and an anion-cation exchange

membrane stack between them. The feed water flows through the stack in three tubes each separated by a membrane. As the water flows the electric potential difference selectively attracts ions from the salts toward the electrodes with an opposite electric charge. The membranes permit the transport of the anions and cations to the outer tubes, leaving fresh water in the inner tube. Thus, the freshwater is produced continuously in parallel with the brine as the feed water flows through the stack. ED is not economical for water with a salinity above about 5000 ppm TDS [150].

4.4.2.2 Reverse Osmosis

Reverse osmosis (RO) uses a semi-permeable membrane to separate water from dissolved salts and particulate matter. The feed water is pressurized, forcing it through the membrane which is constructed such that particles, ions, and organic matter are excluded. The provided pressure must be greater than the substantial osmotic pressure that exists between the product and the brine. There is no heat required, as the energy required is for pressurizing the feed water. As the water passes through the membrane, the dissolved salts accumulate on the brine side, increasing the salinity. Membranes are capable of eliminating 99% of the latent mineral content in water in one pass [151]. A fraction of the highly saline brine is discharged without passing through the membrane.

RO systems consist of pretreatment, high pressure pump(s), a membrane array housed in pressure vessels, and post treatment. Pretreatment involves filtration to eliminate large particles that could clog the membranes, as well as chemical treatment to inhibit minerals precipitation and microbial growth.

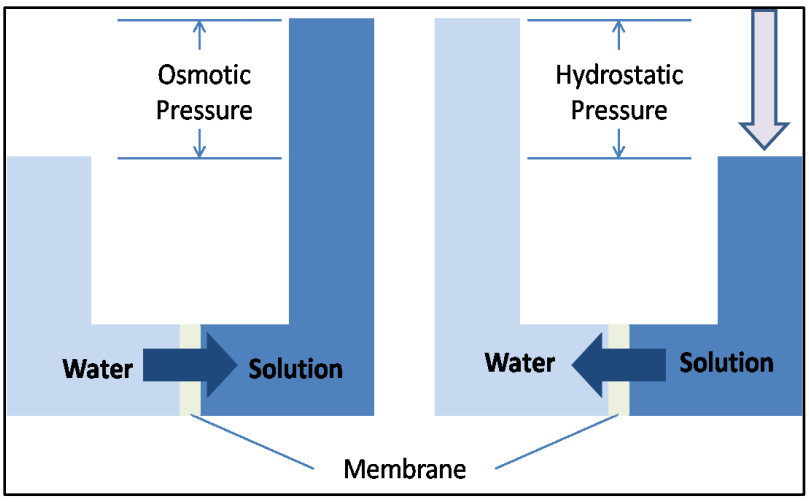

Figure 30 – The principle of reverse osmosis

4.4.3 Other desalination processes

A number of other processes have been used to desalt water, though none has achieved the commercial success enjoyed by distillation or membrane desalination. However, they may prove to be ideal or practical for certain situations.

4.4.3.1 Ion Exchange

Ion exchange (IX) methods utilize synthetic plastic resins integrated with hydrogen and hydroxide ions that pair with the anions and cations dissolved in water [151]. The hydrogen ions are exchanged for metal cations such as sodium, calcium and magnesium; the hydroxide ions are exchanged for chloride, sulfate or phosphate. The hydrogen and hydroxide ions are combined to form water. Ion exchange resins are eventually depleted of all hydrogen and hydroxide ions and must be regenerated using acids and bases. IX may be useful for small scale desalting of dilute brackish water with low salt concentrations [147].

4.4.3.2 Freezing

When water is frozen salts are not included in the formation of ice crystal lattice. Under controlled conditions, the slow freezing of water produces ice crystals before the bulk of the

water freezes solid. The ice crystals can be recovered, rinsed and melted to produce fresh water. While this process is simple, it presents difficulties in handling the solids and separating the ice from the brine. In addition the heat transfer to and from solid ice is vastly different than with liquids, which complicates the process. To date, freezing, has not found commercial success on an industrial scale.

Table 12 – Energy consumption of desalination systems assuming seawater with 35,000 ppm TDS [141] *calculated using parenthetical value in mechanical power column

Desalination Method	Heat input (kJ/kg of product)	Mechanical power input (kWh/m^3 of product)	Prime energy consumption (kJ/kg of product)*
Multi-Stage Flash	294	2.5–4 (3.7)	338.4
Multi-effect boiling	123	2.2	149.4
Vapor compression	–	8–16 (16)	192
Reverse osmosis	–	5–13 (10)	120
Reverse osmosis with energy recovery	–	4–6 (5)	60
Electrodialysis	–	12	144
Solar still	2330	0.3	2333.6

4.5 Product Storage

Chemical plants require storage in two main parts of the manufacturing process. First, day tanks store about 8 hours worth of reactants as a buffer within the process so that maintenance can be performed as needed without shutting down the entire facility [152]. Second, chemical plants generally require 30 days of storage for all products and reactants in case of supply chain disruption [153].

Several storage systems will be necessary for a wind-driven storage facility. First, several days worth of the liquid ammonia must be stored in large tanks for transport to world markets. Second, the subsystems – nitrogen generation, hydrogen and oxygen production, fresh water and

potentially chlorine and caustic – that comprise the ammonia plant must include storage for a standalone system. The size of the storage containers depends on the specific plant configuration and must account for lulls in electricity production. Hydrogen is to be used in an auxiliary power unit capable of powering the entire plant for several days.

There are three methods of product storage that will likely be used for a standalone ammonia plant. The first is ambient pressure and temperature storage which could be used for storing water. The second is pressure storage in which ambient temperatures in conjunction with high pressures are employed to store either a gas or a liquid. The third is cryogenic storage in which low temperatures are used in conjunction with ambient pressures.

4.5.1 Ammonia

Ammonia receives special treatment when being stored due to its inherent toxicity, its flammability, its ability to conduct electrons and its ability to cause stress corrosion cracking in carbon steels [154]. These problems have been overcome, but special attention must be given when designing ammonia storage tanks.

Though ammonia is toxic at high concentrations, it can be detected by humans at levels of around 5 ppm, well below levels that are considered dangerous. Often, windsocks are mounted atop outdoor ammonia tanks so that workers know which direction to evacuate during an emergency situation [154].

In ambient conditions, ammonia is a colorless gas with an acrid odor. It also exists as a colorless liquid either at high pressures and ambient temperature or at low temperatures and ambient pressure. Some relevant properties for anhydrous ammonia are shown in Table 13.

Most industrially produced ammonia is stored in refrigerated tanks at roughly atmospheric pressure and a temperature of -33 °C. Because the primary use of ammonia is for seasonal

fertilizers, large storage capacities are necessary. Insulated cylindrical steel tanks consisting of either single- or double-walled construction are used which have capacities up to 45,000 metric tons [154]. The ammonia that burns off due to heating is absorbed in water to form aqueous ammonia [31]. Up to 270 tons of ammonia may be stored at atmospheric temperature and a pressure of 18.25 bar [155]. This type of storage is generally used for balancing production fluctuations, loading and unloading other transported pressurized vessels, entrance to or exit from pipelines [28]. Table 14 summarizes the possible storage options for ammonia.

Table 13 – Properties of anhydrous ammonia [31]

Property	Value
molecular weight	17.03
boiling point, 8°C	-33.35
freezing point, 8°C	-77.7
critical temp, 8°C	133
critical pressure, kPa	11,425
specific heat, J/(kgK)	
0°C	2097.2
100°C	2226.2
200°C	2105.6
heat of formation of gas, ΔHf, kJ/mol	
0K	-39, 222
298 K	-46, 222
solubility in water, wt %	
0°C	42.8
20°C	33.1
40°C	23.4
60°C	14.1
specific gravity	
-40°C	0.69
0°C	0.639
40°C	0.58

The capital costs of ammonia storage tanks are related to the amount of steel required. For high pressure storage, about 2.8 tons of ammonia can be stored for every ton of steel, whereas for low temperature storage over 40 tons of ammonia can be stored per ton of steel.

Table 14 – Features of ammonia storage tanks [28]

Type	Pressure (bar)	Design Temperature (deg C)	Tons of Ammonia per Ton of Steel	Capacity, Tons of Ammonia	Refrigeration Compressor
Pressure Storage	16-18	Ambient	2.8	<270	None
Semi-Refrigerated Storage	3-5	0	10	450-2700	Single Stage
Low-Temperature Storage	1.1-1.2	-33.6	41-45	4500-45000	Two Stage

4.5.2 Hydrogen

Hydrogen energy storage can be achieved with several different methods including liquid storage, gaseous storage, and metal hydride storage [156]. Liquid storage of hydrogen is advantageous because the volumetric density is greatly increased compared to both gaseous hydrogen and metal hydrides. As a liquid, the density of hydrogen is 70.8 kg/m^3, compared to a density of 23.5 kg/m^3 for gaseous hydrogen at 350 bar. Heat transfer into the Dewar flashes liquid hydrogen to gaseous hydrogen which in turn creates high pressures within the vessel. To mitigate this, liquid hydrogen containers are fabricated as open systems so that hydrogen can boil off and not affect the pressure [157]. Boil-off occurs even with double walled, insulated tanks at a rate of about 0.4% per day for 50m^3 tanks, 0.2% for 100 m^3 tanks, and 0.06% for 20000 m^3 tanks [158]. Furthermore, liquid hydrogen production typically consumes a significant fraction of its HHV on liquefaction, depending on plant size. Estimates as high as 40% are reasonable [159].

Liquid hydrogen has a higher gravimetric energy density than gasoline but a lower volumetric energy density as shown in Figure 31. The low energy density of hydrogen, both when liquefied and at high pressure, presents a storage challenge for vehicular applications, as well as large scale hydrogen storage.

At present, there are three primary methods of storing hydrogen: compressed gaseous hydrogen storage, liquid hydrogen, storage in metal hydrides. Of these methods only gaseous storage and liquid storage are used for large-scale stationary applications. Compressed gaseous hydrogen storage includes metal tanks in addition to underground compressed gaseous hydrogen storage [160].While metal hydrides may be suitable for mobile applications [157, 161], they are not yet commercially viable for large systems [162].

Compressed gas hydrogen storage is a simple technology that is well developed and popular. The volumetric hydrogen density for gaseous storage is low: to store 4 kilograms of hydrogen at 200 bar requires a 225 liter tank. The energy required to compress hydrogen to 200 bar in a multistage compression system can be significant, consuming around 8% of the HHV of the hydrogen without considering electrical efficiencies in the machinery [159]. However, the advantage is that only a compressor train and a pressure vessel are required.

Hydrogen is compressed to pressures exceeding 600 bar and stored in carbon fiber reinforced tanks [163] for mobile applications. Storage systems for large-scale stationary applications use spherical or cylindrical storage tanks. Spherical tanks can hold as much as 1,300 kg of hydrogen at about 15 bar [156]; cylindrical containers with pressures of 50 bar are also used [162] All metal, thick walled cylinders and spheres are used almost exclusively in stationary applications, where volume and mass constraints are less stringent than for vehicular applications.

Underground hydrogen storage is used in both France and the UK to enable shutdowns and maintenance of hydrogen production facilities [164]. More recently, cavernous hydrogen storage has been developed in the Gulf Coast in the USA [165]. The technology is similar to the storage of natural gas in pressurized underground reservoirs. In 2004, the United States and Canada had over 116 billion standard cubic meters of natural gas storage capacity spread over 428 facilities [166]. Underground natural gas storage requires specific geological formations such as depleted

oil fields, salt caverns and aquifers which are also suitable for underground hydrogen storage [164].

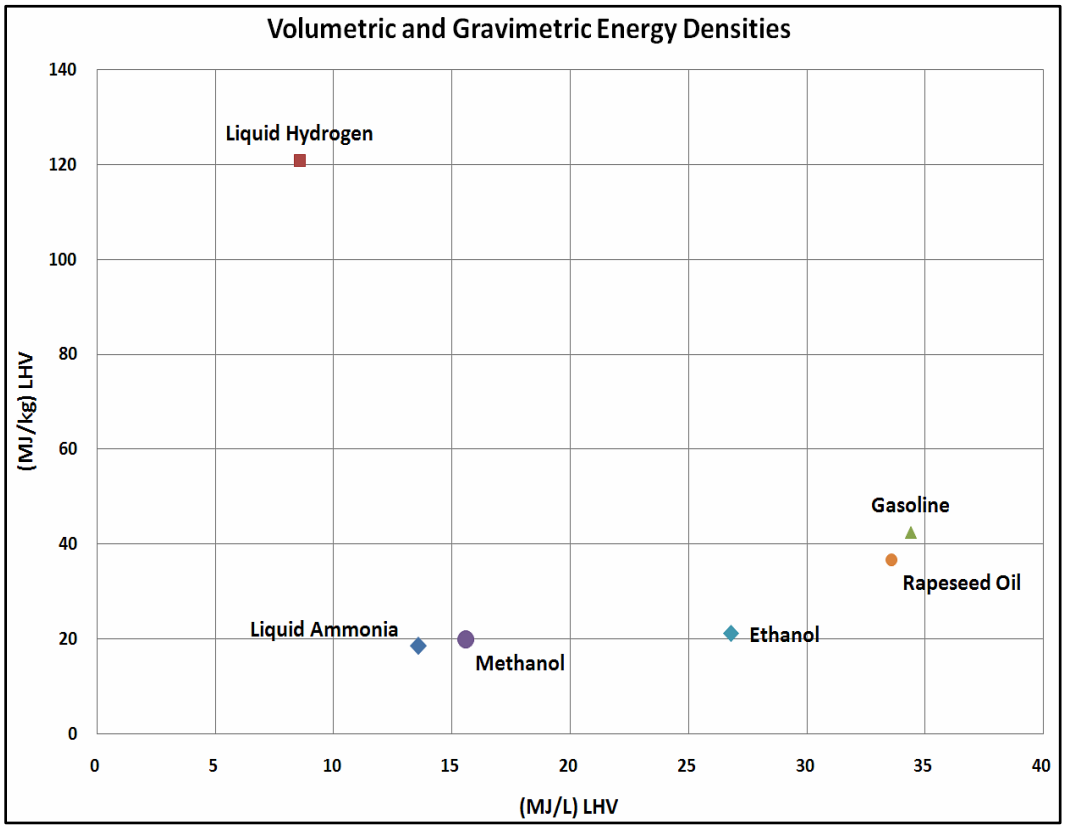

Figure 31 – Volumetric and gravimetric energy densities of some alternative fuels

Hydrogen can be stored as a liquid at ambient pressure and 21.2K. Liquefaction of hydrogen can be achieved through a combination of heat exchangers, compressors, expanders, and throttling valves. One peculiarity with hydrogen is that it warms when expanded at room temperature, due to its low inversion temperature of 202K. In order to reach the inversion temperature modern processes use liquid nitrogen to cool the hydrogen [156].

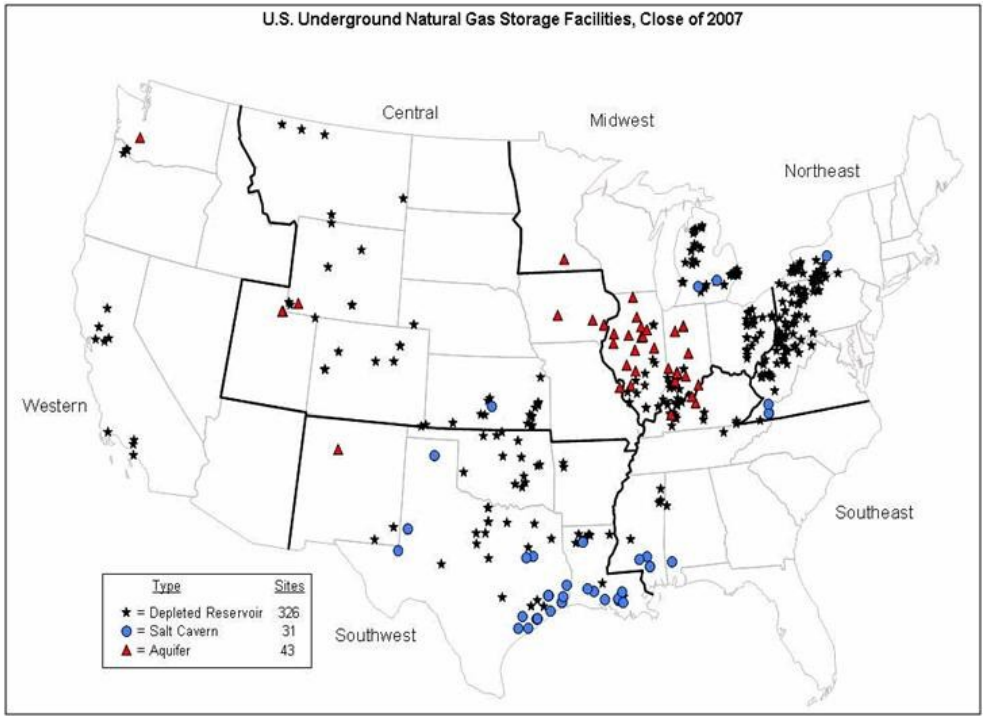

Figure 32 – Underground natural gas storage facilities in the United States [167]

Liquid storage of hydrogen is advantageous because the volumetric density is greatly increased compared to gaseous hydrogen. As a liquid, the density of hydrogen is 70.8 kg/m^3, compared to a density of 23.5 kg/m^3 for gaseous hydrogen at 350 bar. However, liquid hydrogen containers are open systems so that strong pressures do not develop due to heat transfer into the Dewar [157]. The open system configuration results in hydrogen boil off. Even with double walled, insulated tanks boil off still occurs at a rate of about 0.4% per day for 50 m^3 tanks, 0.2% for 100 m^3 tanks, and 0.06% for 20000 m^3 tanks [158]. Furthermore, liquid hydrogen production typically consumes a significant fraction of its HHV on liquefaction, depending on plant size. Estimates as high as 40% are reasonable [159] .

4.5.3 Nitrogen and Oxygen

Nitrogen and oxygen are the two most abundant elements in the earth's atmosphere (see Table 9). Because of nitrogen's strong triple bond it is an inert gas and is used as such in industry to prevent combustion or contamination of food. Oxygen is more reactive and participates in combustion so precautions must be taken to ensure its safe handling and use.

Nitrogen and oxygen are often produced using air fractionation (also known as cryogenic air separation) and are stored on site in liquid form with capacities ranging from 500-2000 m^3 [154]. Large quantities of nitrogen and oxygen are always stored in liquid form at modest pressures and low temperatures [154].

4.5.4 Purified Water

Water storage is relatively common throughout much of the world because it is essential for human life. Distilled water is nontoxic and is a liquid at STP so its storage and handling are relatively simple. Welded steel standpipes with capacities ranging from 190 m^3 to 190,000 m^3 can be constructed [168].

4.6 Energy Storage

A small standalone ammonia plant will require significant energy storage, probably in the 100 MWh range. The available technologies that are capable of storing that much energy are relatively few: pumped hydroelectric, compressed air energy storage (CAES), flow redox batteries (FRB), and sodium sulfur batteries (NaS) [169-171], as shown in Figure 33. Of these, pumped hydroelectric and CAES depend on local geology – pumped hydro requires a large body of water at a suitable elevation; CAES requires underground caverns in which air can be stored at high pressure. CAES also requires a fuel such as natural gas to be burned so that the pressurized

air can expand through a turbine. Furthermore, only two CAES facilities exist in the world. Thus, the only probable energy storage systems are redox flow batteries and sodium sulfur batteries.

The only commercially available battery is the sodium sulfur (NaS) battery which is installed sparingly in parts of the United States, Japan, Germany, France, and the United Arab Emirates [172]. As of late 2009 about 365 MW were installed worldwide.

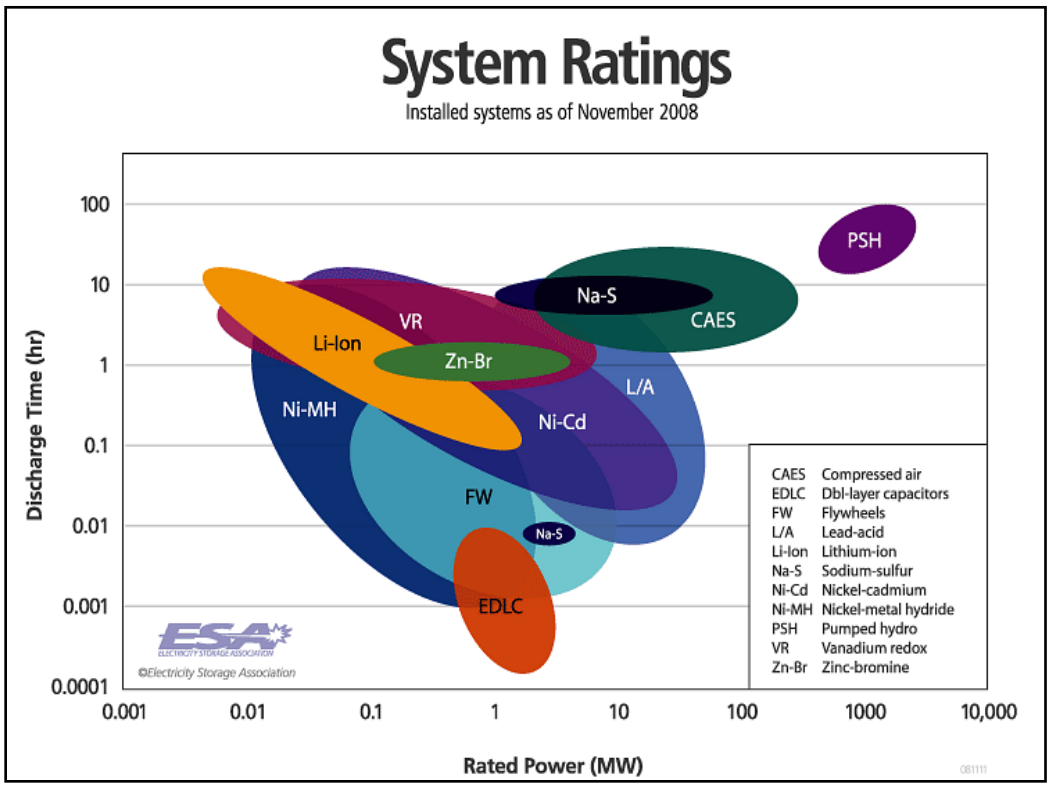

Figure 33 – Electricity storage options [171]

4.6.1 Sodium Sulfur

The sodium sulfur battery was developed by the Ford Motor Company for vehicular applications in the 1960s and 1970s [173]. The project was disbanded due to major technical hurdles and because of the rise in other, superior battery technologies such as lithium-ion and nickel-cadmium. However, the technology was adopted by Japan for utility-scale electrical storage. As

of 2009, there were 190 NaS battery systems in Japan, representing 270MW of storage, the largest being a 34 MW/245MWh installation [170]. In Presidio, Texas, an 8MW/32MWh NaS battery was installed for $25 million in 2010 to provide stability on a weak grid [174].

Sodium sulfur (NaS) batteries employ molten sulfur at the cathode, molten sodium at the anode and the solid electrolyte "beta-alumina" in between. At high temperatures of about 300-350°C, β-alumina conducts only sodium ions which combine with sulfur to produce sodium polysulfides when charging. During discharge, the sodium ions flow from the sodium polysulfides through the electrolyte and combine with the sodium anions to form elemental sodium. Sodium sulfur batteries fundamentally differ from conventional batteries because the electrodes are liquid and the electrolyte is a solid. The conceptual configuration of the sodium-sulfur battery is shown in Figure 34.

The reaction at the positive electrode is:

$$S_x^{-2} + 2Na^+ \leftrightarrow Na2S_x \qquad \textbf{Equation 34}$$

and the reaction at the negative electrode is:

$$2Na^+ - 2e^- \leftrightarrow 2Na \qquad \textbf{Equation 35}$$

with the overall reaction being:

$$2Na + xS \leftrightarrow Na_2S_x \qquad \textbf{Equation 36}$$

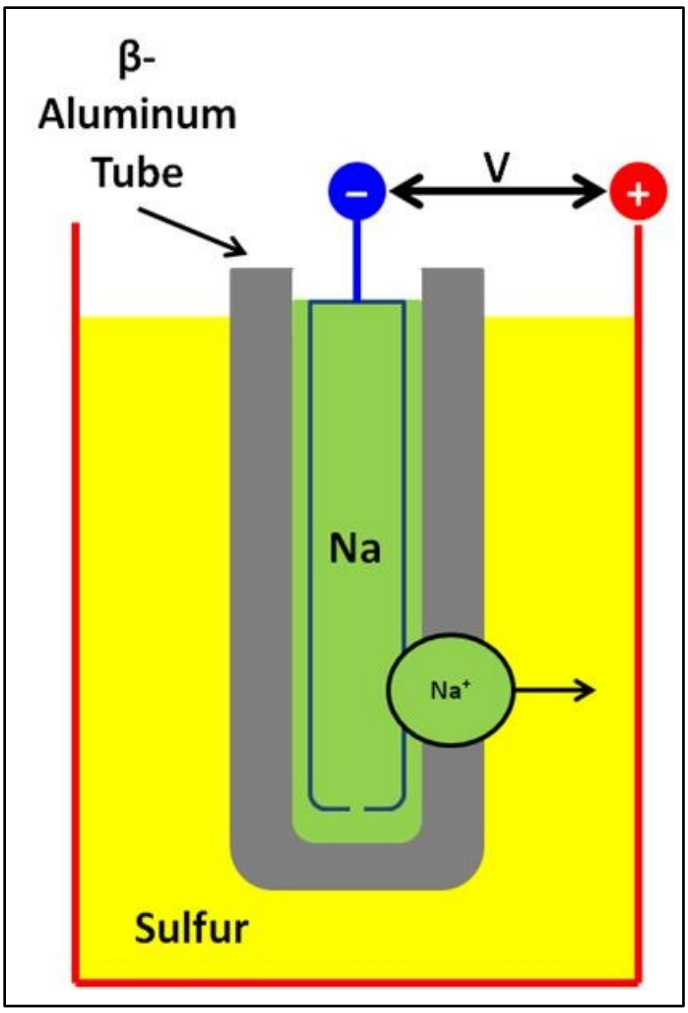

Figure 34 – Schematic of a sodium sulfur cell [175]

Sodium sulfur batteries have achieved efficiencies of over 90% with lifetimes of over 15 years and 4500 cycles at 90% depth of discharge [176]. Furthermore, their fast charging dynamics and high energy densities make them a good candidates for large stand-alone systems. However, the high operating temperature of the battery requires rigorous thermal management; the elevated temperature of the cell must be maintained, even during idle operation [176]. Moreover, sodium is reactive with both sulfur and water, causing highly exothermic reactions. Thus, the design of the cell must strictly control both the internal moisture content and the integrity of the solid electrolyte separating the sulfur and sodium.

4.7 Literature Review of Ammonia Subsystems

Ammonia production from renewable energy sources is scarce in the literature despite the fact that hydroelectric power was used in some of the earliest plants. There have been a few large scale electrolytic hydrogen facilities throughout the world since 1928 when hydrogen was first produced via hydroelectric power in Norway [7-9]. By the 1970s plants in India, Egypt, Zimbabwe, Peru, Iceland and Canada were also producing fertilizers from electrolytic hydrogen [10], the largest of these facilities being the 180 megawatt plant in Egypt. In 1998 there were thought to be seven hydroelectric ammonia facilities in the world, accounting for roughly 0.5% of total worldwide ammonia production [10]. There was also a proposal to produce hydrogen using Canadian hydropower and ship it to Europe using three storage media: methylcyclohexane, ammonia and liquid hydrogen [177]. The project reached the "demonstration phase" but was never realized [178].

Other renewable technologies have been considered for electrolytic ammonia production. A significant amount of work was done at The Johns Hopkins University in the 1970s and 1980s on ammonia production using ocean thermal energy conversion (OTEC). Various reports about OTEC were issued, discussing subjects ranging from liquid hydrogen and ammonia production [179], hydrogen, ammonia and aluminum production [180], ammonia production [181-182], ammonia, methanol, liquid methane and liquid hydrogen production [183], and ammonia and methanol [184]. The visionary approach to fossil-fuel free ammonia did not reach fruition and no OTEC plant ships were produced. While these articles offer useful glimpses of ammonia plantships, the power characteristics of OTEC align better with an ammonia plant than wind does. The OTEC power production is relatively constant over short time intervals, so ammonia is more easily made.

At least five articles and one report have touched on ammonia or fertilizer production using solar energy. Jourdan and Roguenant [185] propose using ammonia as a means of storing solar energy for isolated regions. The authors provide a detailed subsystem description of an actual 75 ton/day plant in operation in France. The facility produces ammonia from the off-gases of a chlorine plant that electrolyzes brine. The subsystem description is especially important because air separation units are discussed with respect to interrupted operation. To produce ammonia continuously during air separation unit shutdown, hydrogen is burned with air to eliminate the oxygen – a potential solution for isolated wind-powered ammonia production. The same authored argued that the cost of an air separation unit would be far less than a hydrogen combustor integrated with a catalytic deoxygenation process.

Abdel-Aal [186] assessed the manufacture of ammonia fertilizers from a central receiver solar system (CRSS) in Saudi Arabia and determined the economics of a 1000 ton/day plant. The results (from 1984) were unfavorable for solar ammonia production but were predicted to improve. The remaining three articles discussed atmospheric nitrogen being converted to nitrogen oxide by means of an electrical arc inside a metal tube [187-189]. This process is extremely energy intensive and has been almost non-existent since Fritz Haber and Carl Bosch invented modern ammonia synthesis. Because it is so energy intensive and natural gas – the primary source of fertilizer manufacturing – has been so inexpensive, these methods are unable to compete. A detailed report was issued to the US Department of Energy regarding a solar central receiver for supplying heat to the reformer system of an ammonia plant [190]. The solar central receiver was designed to operate at a maximum of 34.5 MW and provide energy for reforming of natural gas. Because the sun's position is continuously changing, the system never reaches steady state. A control system was proposed to vary the fossil-fuel reformer output as needed, reaching full production during the nighttime and minimum production at solar noon. It is unclear if the recommendations listed in the report were realized.

Several authors have studied the possibility of producing ammonia or nitrogen-based fertilizers from wind energy. The most prominent and comprehensive is the report commissioned by the National Science Foundation (NSF) and Lockheed California Company which illustrates methods of nitrogenous fertilizer production using wind power [14]. Two summaries of the report are also available [15-16]. The report outlines design criteria, gives a description of the system, sketches mass and energy flows through the system, and offers an economic analysis. The conclusion is that, while technical challenges exist, wind-powered fertilizer and ammonia plants are feasible and could be cost-competitive if the price of natural gas increases.

The NSF report is still the most comprehensive report issued on wind powered ammonia production. However, it treats the major subsystems such as electrolysis, water purification, and air separation, fleetingly. The report generally assumes that the subsystems, including the ammonia synthesis loop, can perform well under cyclic operation, which is not reasonable. Many of the technologies discussed in the report are now obsolete, including the electrolyzers and wind turbines. Furthermore, the report considers only standalone ammonia and ammonium nitrate systems, and does not consider using salt water as a feedstock.

There are some other minor articles tangentially related to wind powered ammonia production. One article mentions nitrogenous fertilizer in the context of storage [191] , two discuss using the antiquated electric arc process for fertilizer generation [192-193] and the last article offers a brief outline of a wind-fertilizer system [194]. These articles are mostly of historical interest, and offer little practical information.

In the early 1960s, ammonia was investigated as an energy storage medium by the United States Army for the Nuclear Power Energy Depot program [195]. The concept was to produce chemical fuels from nuclear power using only ubiquitous raw materials such as water and air. Three papers were presented at the same conference, as a series, in 1965. The first paper offered an overview of

a method for reducing the stress on the military's supply chain by manufacturing synthetic fuels in situ [13]. The second paper elucidated the processes and methods that could be used for the manufacture and storage of liquid hydrogen as well as ammonia [12]. The third paper evaluated ammonia as an internal combustion engine fuel and determined that modified engines could perform as well as conventional gasoline engines [11]. The Energy Depot program was eventually suspended in 1965 and no nuclear-powered autonomous ammonia production prototypes were built [195]. The Energy Depot program arrived at an important conclusion: ammonia is *the most practical* fuel that can be manufactured using abundant raw materials.

More recently, ammonia has been proposed as an energy vector for hydrogen storage [196]. The author of that study envisions ammonia production from the waste heat of nuclear plants which could then be used as a vehicle fuel, as a heating fuel or as a source for chemical fertilizers. Ammonia has been further explored as a replacement for hydrogen fuel in automobiles [197-198]. It was concluded that ammonia would be preferable because it costs less, can be stored at room temperature, and requires a smaller fuel tank. However, research conducted by the Department of Energy (DOE) found ammonia to be unsuitable for onboard vehicle energy storage for PEM fuel cells [199]. Ammonia was found to be a safety hazard upon tank ruptures or leaks; onboard ammonia crackers were found to be too large and cumbersome to be practical; and ammonia was found to be a poison to PEM fuel cells. In a rebuttal to the DOE report Feibelman and Stumpf [200]point out that instead of using a PEM fuel cell, ammonia should be burned directly in an internal combustion engine or direct ammonia fuel cells. Furthermore, ammoniated salts or specially engineered tanks that employ porous monoliths are suggested to diminish the safety hazard. Storage of ammonia in metal amine salts such as $Ca(NH_3)_8Cl_2$ and $Mg(NH_3)_6Cl_2$ is also suggested in [201] as a means of reducing toxicity to well below those of gasoline and methanol while simultaneously eliminating the threat of explosion.

Research regarding the feasibility of using ammonia in conjunction with compression-ignition engines for reducing CO_2 emissions has been conducted [202]. The authors found that ammonia can be used in diesel engines at various diesel/ammonia ratios and that carbon dioxide emissions are reduced. A recent article offers an extensive literature review for using ammonia as a fuel [203]. The same authors also suggest that ammonia can also be used as a refrigerant to cool the engine to recover about 11% of the engine's power while simultaneously simplifying the air conditioning system. Finally, a report was issued by the Iowa Energy Center in which ammonia and hydrogen were directly compared for production, storage and transportation [204]. The report concludes that ammonia is significantly more cost effective for long term storage; transportation is much less expensive with ammonia; and that the total production, storage and distribution cost of ammonia is less than one quarter that of hydrogen.

Electrolyzing seawater for hydrogen production was investigated during the oil crisis in the 1970s [143]. The study concluded that, while direct electrolysis is possible, it may prove unrealistic due to the discharge of harmful products into the environment. Nevertheless, using the chlor-alkali process for storing wind energy as chlorine and caustic soda was proposed shortly thereafter [205]. The hydrogen off-gas was to be used for generating electricity via a turbine to power the auxiliary components and instrumentation of the plant. Furthermore, the concept of a chlorine-hydrogen energy storage system has also been proposed in the past for electric utilities [206]. Hydrochloric acid was to be electrolyzed to produce hydrogen and chlorine which could be recombined in a hydrogen-chlorine cell to produce power.

More recently, a pair of papers by the same authors of [205] suggests using sodium as an energy storage medium for non-grid connected offshore wind power [207-208]. Hydrogen would be produced with the exothermic reaction of sodium and pure water, and thus the sodium would be an indirect form of hydrogen storage. Other co-products of the plant included: caustic soda, fresh water, magnesium, hydrochloric acid and sulfuric acid.

4.7.1 Survey of Ammonia Production Subsystems Powered by Renewable Energy

While ammonia synthesis using renewable energy is itself not discussed prominently in the literature, some of the required subsystems are covered thoroughly. The subsystems include the desalination technologies for water purification and the production of hydrogen from water (electrolytic hydrogen). The production of nitrogen via an air separation unit powered by renewable energy is absent from the literature. However, there is some discussion of variable production techniques for air separation units for increasing the agility of the plants [209-210]. Although it is standard practice to operate an air separation unit continuously, the load range can vary.

4.7.1.1 Hydrogen Production from Renewable Energy

Renewable energy based stand alone systems often have some form of storage so that power can be delivered during lulls in production. One option for storing energy is via electrolysis of water to produce hydrogen for chemical energy storage. The hydrogen can then be utilized in a fuel cell or burned directly in an engine to produce electricity when needed.

Several standalone renewable hydrogen systems exist throughout the world in various configurations ranging from wind power to solar power to hybrid systems.

4.7.1.1.1 Solar Systems

The Instituto Nacional de Técnica Aeroespacial (INTA) in Spain began a pilot project in 1989 to study solar hydrogen production as a storage medium for electricity and to assess its ability to be used in manned space missions [211]. The pilot project had three distinct phases: the first phase connected a photovoltaic panel to an electrolyzer for hydrogen production; the second phase included adding hydrogen storage in the form of metal hydrides and pressurized gas; the third phase integrated a phosphoric acid fuel cell and a proton exchange membrane fuel cell. The pilot plant had the following specifications:

- 8.5 kW photovoltaic array
- 5.2 kW alkaline electrolyzer
- 24 m^3 $TiMn_2$ metal hydride storage
- 8.8 m^3 of pressurized storage at 200 bar
- 10 kW PAFC
- One 2.5 kW PEMFC and one 5 kW PEMFC

The system operated continuously for three years, and was operated sporadically thereafter. The PV panels, the electrolyzer, the storage system, and the fuel cells all performed satisfactorily although the pneumatic feed water pump required yearly replacement.

Table 15 – Selected solar hydrogen plant installations.

Year	Location	Project name	Electrolyzer		Reference
			Type	Size (kW)	
1989	Spain	INTA	alkaline	5.2	[211]
1989	USA	SCHATZ	alkaline	6	[212]
1992	Germany	SWB	alkaline	100	[213]
1993	Germany	PHOEBUS	alkaline	26	[214-215]
1997	Italy	SAPHYS	alkaline	5	[211, 216]

The Stand-Alone Small Size Photovoltaic Hydrogen Energy System (SAPHYS) Project was created to assess the efficiency of solar electricity storage using hydrogen and to determine the feasibility of unattended system operation. The configuration of the plant consisted of the following:

- A 5.6kW PV array
- A 5.0 kW alkaline electrolyzer
- A pressurized steel tank with a capacity of 120 Nm^3 at 200 bar
- One 3.0 kW PEM fuel cell
- Lead-acid batteries with a 51 kWh energy capacity

This plant was in operation for about 1200 hours from September 2, 1997 – November 3, 1997. During that time the electrolyzer as well as the plant showed encouraging results. The alkaline electrolyzer had no major problems, but further testing under field conditions is necessary to determine possible deterioration. The main problem plaguing the plant was the auxiliary equipment which included the water demineralization unit, the compressed air unit and the inert gas. The plant required shutdowns to diagnose and correct the problems.

The PHOEBUS demonstration plant in Germany supplied the Central Library of Forschungszentrum Julich with autonomous solar generated electricity year-round for ten years. The project proved the technical feasibility of a stand-alone energy supply system based on solar, and hydrogen storage. The main components of the system were:

- A 43 kW PV array
- A 26 kW electrolyzer
- A pressurized steel tank with a capacity of 3000 Nm3 at 120 bar.
- A 5.6 kW PEM fuel cell
- Lead-acid batteries with a 304 kWh energy capacity

The electrolyzer was able to operate without any major problems for 10 years, though the efficiency decreased from 87% to 83%. The weak point in the system was continually the fuel cell. The initial 6.5 kW alkaline fuel cell was found to be unreliable so it was replaced by a 5 kW PEM fuel cell. When the 5 kW fuel cell did not meet the required power level it too was replaced by another PEM fuel cell which lasted until the end of testing. While no fuel cell data was reported the failure of the fuel cells is in itself telling.

The stated goal of the Schatz Solar Hydrogen Project was to demonstrate that hydrogen is a practical energy storage medium for solar energy and that solar hydrogen is a safe and reliable energy source for society [212]. Photovoltaic panels provided power to a 600 W when possible.

Excess energy was used to produce hydrogen with an alkaline electrolyzer so that a fuel cell could be used as an uninterruptible power supply during low insolation. The system consisted of:

- A 9.2 kW PV array
- A 6 kW alkaline electrolyzer
- A pressurized steel tank with a capacity of 60 Nm3 at 8 bar.
- A 1.5 kW PEM fuel cell
- Lead-acid batteries with a 5.3 kWh energy capacity

The system is designed to function automatically, with an operator only needed for periodic maintenance and startup. During 1995 the system was operational for 72% of the year, the remaining 28% being non-operational due to various problems [211]. The non-operational periods were caused by twenty distinct shutdowns, the two most frequent being a hood exhaust fan sensor and utility grid outage which accounted for 9 total shutdowns. The alkaline electrolyzer showed no noticeable signs of degradation after over 4000 hours of operation from 1992 to 1998 [115]. The PEM fuel cell showed serious signs of degradation and was removed from the system in 1996.

The Solar-Wasserstoff-Bayern (SWB) project demonstrated on an industrial scale that hydrogen could be produced by solar energy alone without emitting carbon dioxide [213]. The system was located in Neunburg vorm Wald, Germany and had the following configuration:

- Numerous photovoltaic arrays totaling 381.6 kW of power
- Three alkaline electrolyzers totaling 311 kW
    - A 100 kW alkaline electrolyzer operating at 32 bar
    - One 111 kW alkaline electrolyzer operating at 80 millibar
    - One PEM electrolyzer operating at 1.5 bar
- Hydrogen capacity of 5,000 Nm^3 in a steel vessel at 30 bar

- A 79.3 kW phosphoric acid fuel cell

The SWB project relied on prototypes of system components which resulted in poor overall performance: several electrolyzers required replacement; the alkaline fuel cell was eventually eliminated; the peripheral systems for the phosphoric acid fuel cell required extensive repair and maintenance [115]. The phosphoric acid fuel cell was cycled on and off about 450 times logging approximately 2600 hours of operating time. The cyclic operation resulted in a nearly 20% decrease in output power over its lifetime. After over 50,000 hours of stand-by time and 2,300 hours of operating time the PEM alkaline electrolyzer was decommissioned, mainly because of high oxygen content in the hydrogen gas [217]. The project was deemed successful because it provided insight into how a solar hydrogen production plant could function in the future. Many unexpected problems were encountered and solved leading to vast stores of knowledge.

4.7.1.1.1.1 Wind Systems

Wind systems for hydrogen production have been studied extensively in the literature for a number of years as either solely wind [117-119, 218-245] or hybrid systems [112, 246-254]. The major wind powered hydrogen generation systems that have been installed worldwide in the past decade [117, 119, 233-239, 250] are shown in Table 16. The research can be further divided into three groups: standalone systems [112, 117, 119, 218-219, 224, 232-236, 239-240, 246, 249-254], grid connected systems [220-221, 225, 227-231, 237-238, 241-242, 245, 248] and grid and standalone system comparisons [118, 222-223, 226, 243-244, 247].

There are some notable works that pertain to wind driven hydrogen production that cannot be adequately categorized due to their scope and breadth. The first is the pioneering work by Dutton, et al. [232] which details the intermittent operation of a wind powered water electrolyzer. The report provides insight into how an electrolyzer responds to variable operation and the control strategy that should be used to mitigate electrolyzer failure. The second is the Wind-to-Hydrogen

pilot project at the Basin Electric Power Cooperative [241] which chronicles the development of an electrolysis-based wind powered hydrogen production system. The report includes a feasibility study for the project, a system design and overview and operational results. The third is the report by the National Renewable Energy Laboratory (NREL) that relates the operational experience of the Wind-to-Hydrogen project in which numerous power configurations were tested and evaluated using an electrolyzer [238]. The report offers a system overview, installation details, testing and analysis and system optimization. The fourth is a report issued by the International Energy Agency [211] which presents ten case studies of installed solar-hydrogen systems throughout the world. It offers useful insight into system integration, performance and failure modes. Finally, the book entitled *Hydrogen-based Autonomous Power Systems* [255] is an exhaustive work that details several case studies, offers economic analysis and market potential of hydrogen systems, and provides a roadmap to commercialization.

The grid connected systems often utilize hydrogen as a means of balancing the fluctuations on the grid. Using this concept, an estimate has been made for the global hydrogen production potential from wind [225], though it is clear that this is the absolute maximum limit of production. One paper focused on much smaller systems that produce hydrogen from excess wind power for stationary energy or transportation purposes [226]. It was also shown that hydrogen production from idle generation capacity of wind is capable of stabilizing local grid imbalances [227] and that scheduling the production of electrolytic hydrogen from a grid-tied wind farm can help mitigate transmission constraints [245].

Table 16 – Major hydrogen systems that include wind power that have been installed since 2000.

Year	Location	Project Name /Description	Wind Turbine(s)	Electrolyzer			Ref
			Size (kW)	Size (kW)	Type	Pressure (bar)	
2000	ENEA Research Centre, Casaccia, Italy	Prototype wind-hydrogen system	5.2	2.25	Alkaline	20	[234]
2001	University of Quebec, Trois-Rivieres, Canada	Renewable energy systems based on hydrogen for remote applications	10	5	Alkaline	7	[250]
2004	Utsira Island, Norway	Demonstration of autonomous wind/hydrogen-systems for remote areas	600	50	Alkaline	12	[119, 235, 239]
2004	West Beacon Farm, Loughoroug h, UK	HARI	50	36	Alkaline	25	[236]
2005	Unst, Shetland Islands, UK	PURE	30	15	Alkaline	55	[117]
2005	Keratea, Greece	RES2H2	500	25	Alkaline	20	
2007	NREL, Golden, CO	Wind2H2	100	40	Alkaline	10	[237-238]
2007	NREL, Golden, CO	Wind2H2	10	6	PEM	14	[237-238]
2009	Patagonia, Argentina	Wind/hydrogen demonstration plant	2400	7	Alkaline	7	[233]

The economics of producing hydrogen from excess wind power in Denmark [242], Ireland [222] and Europe [230] have been addressed, though to date, there are no known commercial facilities that generate hydrogen from excess wind power. A Norwegian case study explored the economics of hydrogen production in both grid-connected and standalone systems [223]. The authors found that hydrogen produced from the stand-alone system is more than twice as expensive as a grid connected system. Another article compared the cost of hydrogen storage in a hybrid standalone system with battery storage in the Pacific Northwest [253] . The results showed a definite

economic advantage using the battery system. In an NREL study, the price of wind-produced hydrogen in the near-term, mid-term and long-term was considered in large-scale wind powered hydrogen production [243]. For a 50,000 kilogram/day facility it was shown that the price of hydrogen would decrease by more than half, from $5.69/kilogram in 2005 to $2.12/kilogram between 2015 and 2030. A second study, also funded by NREL, revealed that distributed wind generation and a central electrolyzer could produce hydrogen at $4.03/kilogram and $2.33/kilogram, in the near- and long-term, respectively [244]. Two articles have explored the economics of hydrogen production from offshore wind power. Kassem [228] showed that uncertainty plays a key role in determining the assessment of economic viability for offshore hydrogen production and that capacity factor is an integral parameter. Mathur, et al. [229] discussed the feasibility of offshore wind-driven hydrogen being used for the transportation sector. It was concluded that wind turbine cluster size is an important metric and that the technology will be feasible in the near future.

Modeling of wind/hydrogen systems was a focus of some research [112, 115, 240, 246, 248, 256-257] in recent years. A complete mathematical model of a generic stand-alone renewable energy system utilizing hydrogen storage was developed to study its behavior with a control strategy via simulation [246, 257]. Models to determine optimal power management strategies for generic renewable-hydrogen systems [218, 220, 256], wind systems [218] and for photovoltaic systems [258] were also reported. A detailed model of an electrolyzer and its ancillary systems for control purposes is given in [248]. At least two theses have been dedicated to distributed wind-based generation systems. The monumental work by Wang [112] (which is now part of a textbook [259]), covers topics from unit modeling of hybrid renewable energy systems to control of grid connected fuel cell systems to standalone fuel cell systems to simulations and optimal placement of said systems. The thesis by Korpås [247] focused on distributed grid-connected wind systems with hydrogen storage. Two other theses detailed solar-based hydrogen storage systems with one

focusing on component models [240] and the other focusing on the operational experience with a physical system in Norway [115]. For all of the articles that discuss modeling renewable energy hydrogen systems only a handful discuss their optimization. A literature review of optimization techniques for stand-alone renewable energy systems is given in [249]. The unit sizing of a hybrid stand-alone renewable energy system is determined using particle swarm formation in [224] while linear programming is used to optimize the energy management of a grid connected wind-hydrogen system in [218]. A multi-objective optimization that simultaneously minimized cost, carbon dioxide emissions and unmet load for a stand-alone hybrid system is given in [252] and a single-objective optimization of the control strategy that governs a stand-alone hydrogen based renewable energy system is given in [251].

4.7.1.2 Desalination using renewable energy

Renewable energy sources offer a practical approach to desalinate water in many areas of the world including the deserts of northern Africa, the arid Middle East and isolated island locations. As renewable energy technologies become more mature and well developed, exploiting stand-alone renewable systems for desalination will become more attractive. Figure 35 shows possible combinations of wind and solar energy resources with desalination technologies.

For many years, several of the wind- and solar-desalination combinations have been studied in the literature [141, 150, 260-263]. For standalone desalination systems, optimal matching between the renewable energy source and the freshwater demands is necessary to minimize costs. The selection of the proper combination depends on several factors: water demand, wind and solar resources, feed water salinity, grid connectivity, geographical conditions, capital and operational costs, and societal infrastructure. Since renewable energy power output is variable, standalone systems must employ an energy storage mechanism so that the desalination processes operate under optimal conditions. A standalone system without energy storage is subject to the

stochastic output, resulting in non-optimal operation. The tradeoff is the capital costs of the installation versus the output achieved.

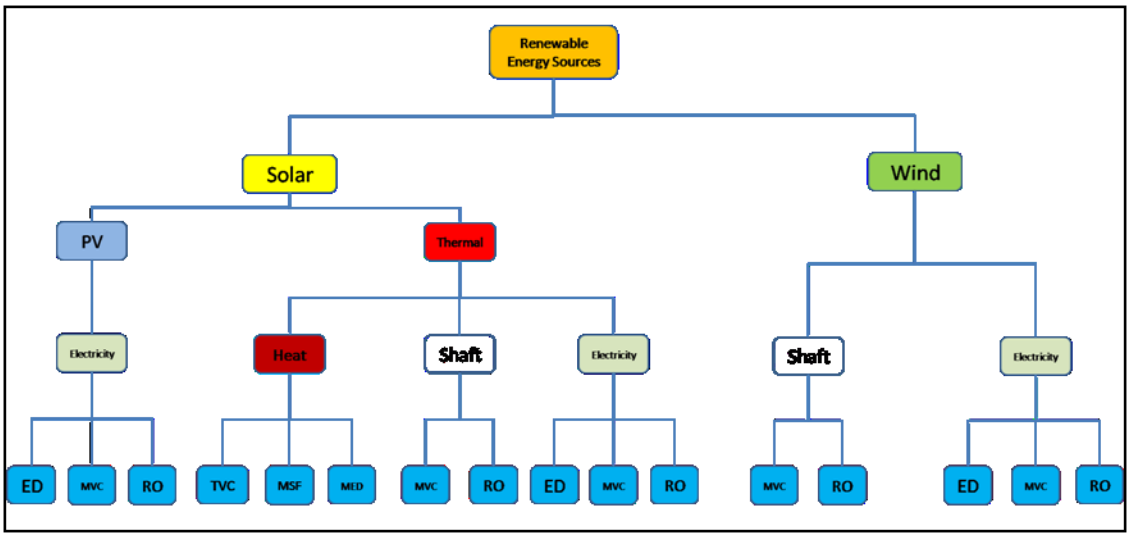

Figure 35 – Possible pairings of solar and wind energy systems with desalination technologies

4.7.1.2.1 Solar still

Solar stills take advantage of the earth's natural water cycle by allowing sunlight to evaporate saline water which is then condensed on a cool surface. The systems are simple, but are not capable of producing large quantities of water in a practical manner. The rule of thumb is that solar stills produce about 4 liters of water per square meter in one day [149]. The principle is simple: a tilted clear glass or plastic glazing covers a basin of saline water which is exposed to sunlight. The sun's radiation heats and evaporates the water which condenses on the cooler panels. The condensed water flows down to a trough and is collected for use. The most important component in this configuration is the glazing because it serves several critical functions: it prevents water vapors from escaping the envelope of the still; it acts as a condenser because it is simultaneously exposed to cooler ambient air and warmer inner air; it channels the evaporated distillate; it acts as an isolative barrier. This type of system is generally no more than about 45% efficient, due to reflection from the glazing and top losses [150].

4.7.1.2.2 Solar thermal desalination

Solar thermal desalination differs from a solar still in that a fluid is heated by the sun and circulated throughout the system. An example of this configuration is multi-effect distillation (MED). Recently, an economic comparison was made between a entirely solar, a solar-assisted and a traditional fossil- fuel stand-alone MED system [264]. The fully solar system collected thermal energy for evaporation with solar heat exchangers in addition to electricity for water pumping from PV panels; the solar-assisted scheme used solar heat exchangers to provide hot water to the evaporator; the traditional fossil-fuel system used steam and a diesel generator. The study found that solar systems could be competitive with traditional fossil-fuel systems if solar collectors came down in price and diesel fuel increased in price.

In general, solar-MED systems have high product outputs and necessarily have immense solar collector areas. The solar requirements imply that a large land area containing solar collectors is necessary to be economically viable.

At least two solar assisted mechanical vapor compression systems have been studied in the literature. A system simulation of a mechanical vapor compression desalination plant was performed in [265]. A parabolic trough collector provides the thermal energy for the entire system while the compressors, pumps and turbines are all powered by electricity. A detailed analysis of a solar assisted MVC system in the United Arab Emirates (UAE) was presented in [266]. The paper offered in-depth drawings of numerous components; detailed mathematical models; design optimization; and system parameters for a single effect MVC desalination plant.

4.7.1.2.3 Solar photovoltaic

PV panels can be connected to any desalination process that primarily uses electricity, such as electrodialysis, mechanical vapor compression and reverse osmosis. For example, a photovoltaic-

reverse osmosis demonstration plant was installed on the island Gran Canaria, in the Canary Islands off the coast of Morocco [267-268]. The stand-alone 4.8 kilowatt system is capable of producing up to three cubic meters of drinking water per day.

Excellent reviews of solar desalination systems are given in [141, 145, 260-263, 269-270] .

Table 17 -- Worldwide solar powered Reverse-Osmosis plants [262]

Plant location	Salt concentration	Plant capacity	PV system
Cituis West, Jawa, Indonesia	Brackish water	1.5 m^3 /h	25 kWp
Concepcion del Oro, Mexico	Brackish water	1.5 m^3 /day	2.5 kWp
Doha, Qatar	Seawater	5.7 m^3 /day	11.2 kWp
Eritrea	–	3 m^3 /day	2.4 kWp
Florida St. Lucie Inlet State Park, USA	Seawater	2 x 0.3 m^3/day	2.7 kWp + diesel generator
Hassi-Khebi, Argelie	Brackish water (3.2 g/l)	0.95 m^3/h	2.59 kWp
Heelat ar Rakah camp of Ministry of Water Resources, Oman	Brackish water	5 m^3 /day (5 h/day operation)	3250 kWp
INETI, Lisboa, Portugal	Brackish water about 5000	0.1–0.5 m^3/day	–
Jeddah, Saudi Arabia	42,800 ppm	3.2 m^3 /day	8 kWp
Lampedusa Island, Italy	Seawater	3 x 2 m^3/h	100 kWp
Lipari Island, Italy	Seawater	2 m^3 /h	63 kWp
North of Jawa, Indonesia	Brackish water	12 m^3/day	25.5 kWp
North west of Sicily, Italy	Seawater	–	9.8 kWp + 30 kW diesel generator
Perth, Australia	Brackish water	0.5–0.1 m^3/h	1.2 kWp
Pozo Izquierdo-ITC, Gran Canaria, Spain	Seawater	3 m^3 /day	4.8 kWp
Red Sea, Egypt	Brackish water (4.4 g/l)	50 m^3/day	19.84 kWp (pump) 0.64 kWp (control)
Thar desert, India	Brackish water	1 m^3 /day	0.45 kWp
University of Almeria, Almeria, Spain	Brackish water	2.5 m^3 /h	23.5 kWp
Vancouver, Canada	Seawater	0.5–1 m^3/day	4.8 kWp
Wanoo Roadhouse, Australia	Brackish water	–	6 kWp

Table 18 – Worldwide solar distillation plants [261]

Plant location	Desalination process	Desalted water output (m^3/d)	Solar collectors
La Desirade Island, French Caribbean	ME, 14 effects	40	Evacuated tube
Abu Dhabi, UAE	ME, 18 effects	120	Evacuated tube
Kuwait	MSF	25	Solar electricity generation
Kuwait	RO	20	system
Kuwait	MSF auto-regulated	100	Parabolic trough
La Paz, Mexico	MSF, 10 stages	10	Flat plate + parabolic trough
Arabian Gulf	ME	6000	Parabolic trough
Al-Ain, UAE	ME, 55 stages; MSF, 75 stages	500	Parabolic trough
Takami Island, Japan	ME, 16 effects	16	Flat plate
Margarita de Savoya, Italy	MSF	50-60	Solar pond
El Paso, Texas	MSF	19	Solar pond
Berken, Germany	MSF	20	-
Lampedusa Island, Italy	MSF	0.3	Low concentration
Islands of Cape Verde	Atlantis "Autoflash"	300	Solar pond
University of Ancona, Italy	ME, TC	30	Solar pond
PSA, Almeria, Spain	ME, heat pump	72	Parabolic trough
Gran Canaria, Spain	MSF	10	Low concentration
Area of Hzag, Tunisia	Distillation	0.1-0.35	Solar collector
Safat, Kuwait	MSF	10	Solar collector
Near Dead Sea	MED	3000	Solar pond

4.7.1.2.4 Wind driven desalination

Wind driven desalination facilities can be either electrically powered or shaft driven, as indicated in Figure 35. Only a couple of shaft powered wind desalinations have been reported in the literature, probably because electricity-generating wind turbines are ubiquitous whereas wind-driven desalting systems must be custom made [142, 271]. However, using a direct drive system eliminates two steps from the conventional process: converting wind power to electricity; converting electricity back to mechanical power.

Autonomous wind desalination systems were studied in the literature as early as the mid 1980s [272]. This pioneering work developed complex mathematical models of wind powered reverse osmosis desalination systems and simulated the physical and economic performance. The results suggested that RO-wind desalination could be economical in the future. This prediction proved accurate years later when other economic analysis were performed [273-275] that found RO-wind systems to be competitive with conventional desalination plants in specific locations.

Reverse osmosis plants are the most common variety wind powered desalination systems because they have inherently low specific energy requirements, they are robust, and they can deliver potable water from seawater as well as brackish water. However, there have been relatively few installations reported in the popular literature, some of which are pilot or research scale [249-250]. Perhaps the most significant installation is the SDAWES project on the island of Gran Canaria in the Canary Islands of Spain [276-277]. The system has two wind turbines with a combined output of 460 kW, a 100 kVA synchronous generator connected to a 1500 RPM flywheel assembly and a 10 kW uninterruptible power supply (UPS), forming a local mini-grid. The concept was to analyze three different autonomous desalination processes [278]:

- Eight RO modules capable of a total production of 200 m^3/day.
- A 50 m^3/day Vacuum Vapor Compression (VVC) unit.
- A Reversible Electrodialysis (EDR) system with 190 m^3/day production capacity.

The research resulted in a wealth of experimental knowledge for autonomous desalination processes. The main points are summarized in

Table 19. Further information on the wind-EDR plant can be found in [279].

Table 19 – Advantages and disadvantages for different autonomous desalination systems [278]

Desalination system	Advantages	Disadvantages
RO	Fast start-up and stop Absence of harmonics Low specific energy consumption	Discontinuous power consumption Pressure control in the feed water circuit
VVC	Variable continuous power consumption	Slow startup Scaling if discontinuous operation Harmonic distortion Specific stable temperature and pressure
EDR	Variable continuous power consumption Fast starting-up and stop	Only for brackish water High harmonic distortion (due to the conversions DC/AC/DC)

Other research has been performed on wind powered RO desalination plants, including a proposed hybrid wind/PV plant in Libya [253-254]. The 300 m^3/day plant was intended to provide drinking water to the village of Ras Ejder from seawater with a salinity of 45,000 ppm TDS. The performance of another smaller autonomous wind-RO plant was reported in [280]. The sensitivity of the system to three parameters – wind speed, battery storage and reverse osmosis operating pressure – was analyzed. A literature review of wind-RO systems and installations is given in [148] and a thorough examination of renewable energy powered desalination plants is given in [281].

Wind-driven mechanical vapor compression appears in the literature to a much lesser extent than reverse osmosis. An stand-alone installation on Ruegen Island in the Baltic Sea was reported in [282-283]. The plant produced 15m^3/hour of potable water by closely matching the compressor load with the wind power. When the wind power exceeded the required compressor power an electric heater acting as a dump load was used to heat the sea water in the evaporator-condenser unit. A very similar plant, also located on a German Island, this time in the North Sea, with a capacity of 2m^3/hour was reported as well [281].

Only one wind-driven electrodialysis plant has been reported [279] in which brackish water was desalted. The product flow rate varied from 3 to 8.5 m^3/h and was commensurate with the required power which ranged from 4 to 19 kW.

CHAPTER 5

SYSTEM SELECTION AND TECHNICAL FEASIBILITY

This section details the selection of equipment that will be used to configure the ammonia plant. First, the total flow rates of the distilled water and the synthesis gases – hydrogen and nitrogen – are calculated for a 300 metric ton per day plant. The technical requirements of the ammonia plant that were discussed in 2.1.6 will be used along with the flow rates to make the final system selection. Finally, the feasibility of a standalone ammonia production will be discussed.

5.1 Electric Ammonia Plant Flow Rates

For any given ammonia plant size, the flows of reactants and products throughout the plant can be easily calculated. The flow rates through the system are determined from the stoichiometry of ammonia. The chemical formula for ammonia is NH_3 so – using the Periodic Table of Elements – its molecular mass is 17.03 g/mol of which nitrogen is approximately 14 g/mol. Thus, ammonia is 82.25% nitrogen by mass; and 17.75% Hydrogen by mass. A 300 ton per day ammonia plant will require about 246.7 tons of nitrogen and 53.3 tons of hydrogen per day.

Air separation units are rated in terms of normal cubic meters per hour which is the volume of the gas at standard temperature and pressure. Using the ideal gas law (with the temperature assumed to be 293K and the pressure assumed to be 1 bar) to convert a mass of 246.7 tons of nitrogen to units of meters cubed gives a volume of 214,500 cubic meters per day or about 8,940 cubic meters per hour. A similar calculation can be done to convert the mass of hydrogen into units of normal cubic meters per hour. The daily amount of hydrogen is about 643,700 cubic meters per day which equates to almost 26,820 cubic meters per hour.

The total amount of pure water feed for the electrolyzers is also necessary. Again, the volume can be determined from the stoichiometry of the problem:

$$H_2O \rightarrow \frac{1}{2}O_2 + H_2 \qquad \textbf{Equation 37}$$

Equation 37 states that for each mole of hydrogen gas produced one mole of water is required. Since the number of moles of elemental hydrogen is known according to Equation 37 half of that value equals the moles of water required. The molecular mass of water is approximately 16 grams per mole and one gram of water equals one milliliter so the total volume of water required can be calculated. A 300 ton per day ammonia plant will require about 476,000 kg, or 476 tons of distilled water per day. The flow rates of nitrogen, hydrogen and water are summarized in Table 20.

Table 20 – The flow rates of nitrogen, hydrogen and water through an electric ammonia plant

Process	Product	Amount (tonnes/day)	Flow Rate (kg/h)
Air Separation	N_2	246.7	10,200
Electrolysis	H_2	53.3	2,220
Desalination	H_2O	476	19,830

The flow rates are a useful metric for screening equipment options for the all-electric ammonia plant. The following section details the final equipment selection for nitrogen, hydrogen and water.

5.2 All-Electric Ammonia Plant Equipment Selection

The major equipment in an all-electric process must meet or exceed all of the requirements listed in section 2.1.6, as well as the flow rates discussed in the previous section. The hydrogen and nitrogen generation must provide pure gases using only electric processes. The ammonia plant of interest produces 300 tons per day, which corresponds to roughly 55 tons of hydrogen and 245 tons of nitrogen. Furthermore, the gases need to be ultra-pure – 99.999% for hydrogen and nitrogen. The water required for the electrolyzers must be distilled with almost no dissolved solids.

5.2.1 Nitrogen Subsystem

The nitrogen purity is important in the production of ammonia, primarily because impurities lower the yield either temporarily or permanently. Taken alone, the purity of the nitrogen is not enough to eliminate any particular technology – membrane, PSA or cryogenic. Each technology can generate highly pure nitrogen that can be made suitable for synthesis with a deoxygenator. However, when the production volume of nitrogen is considered as a constraint, both membranes and PSA are eliminated. Neither technology is capable of sustained, economical production of nitrogen at this time.

For membrane air separation, the technology simply is not yet ready for ammonia synthesis. While the purity requirements are within the extreme lower bounds of what may be considered acceptable, the production volume is orders-of-magnitude too low [128]. Producing low volumes of impure nitrogen would require multiple membrane modules in addition to advanced catalytic deoxygenation processes to remove impurities. The deoxygenation processes require residual hydrogen to be present in order to generate water from the excess oxygen which implies that additional electrolyzers would be necessary, at a high capital cost [132]. A modular membrane air

separation plant would achieve no economy of scale and would likely be cost and space prohibitive. Therefore, membrane air separation for nitrogen feedstock is eliminated.

The pressure swing adsorption can achieve high levels of output, but nitrogen purity decreases as output volume increases [135, 284]. Thus, PSA can achieve both the ultra-pure nitrogen and the production volume required for ammonia synthesis, but not at the same time. While the PSA nitrogen generators would be ideal for micro-ammonia plants, they cannot realistically achieve the volume and purity requirements for a moderately sized, 300 ton per day ammonia plant. Several PSA air separation units would be required, limiting the scalability and the economics of the system. Moreover, high volume nitrogen production from PSAs would require deoxygenation and additional hydrogen production capacity, similar to the membranes discusses above. PSA is eliminated as a suitable candidate for large-scale ammonia synthesis, though improvements in the industry may make it viable in the near future.

Cryogenic air separation is a mature, electric process, with high product purity and high volumetric flow rates. From a technical standpoint, it meets all of the requirements of an ammonia synthesis loop. In fact, some Linde ammonia synthesis processes currently use cryogenic air separation to produce the required nitrogen [28]. Therefore, cryogenic air separation must be selected as the nitrogen generator for a wind driven ammonia plant.

5.2.2 Hydrogen Subsystem

Hydrogen subsystems have less competition than air separation: there are only 2 commercial choices for electrically driven hydrogen production – proton exchange membrane (PEM) and alkaline electrolyzers [285]. Both PEM and alkaline electrolyzers offer nearly indistinguishable end product hydrogen, with purities in the 99.99% range [116]. PEM electrolyzers offer fast response times and dynamic startup and shut down characteristics compared to alkaline electrolyzers [285]. While each technology is commercially mature, alkaline electrolysis has

existed for several decades longer than PEM. Consequently, commercial alkaline electrolyzers have more manufacturers and more options for system selections. Furthermore, PEMs are not as efficient as alkaline electrolyzers, and may become equivalent in the future.

The two technologies diverge primarily in the scale at which they operate. PEM electrolyzers are frequently small devices, capable of supplying relatively low outputs of pure hydrogen – in the 10-100 kg/day range [286]. The total volumetric flow rates available in commercial PEM electrolyzers are far too low to be practical for a 300 ton per day ammonia plant [286-287], which requires 55,000 kg per day. Moreover, the capital cost of PEMs per kilogram of hydrogen produced is still thought to be higher than alkaline electrolyzers [287].

The size and availability of PEMs preclude them from being considered serious contenders for large-scale ammonia synthesis. The purchase of 500 to 5000 standalone electrolyzers from manufacturers (depending on the output) is not realistic or cost effective. However, as PEMs mature into the future they should be considered for large-scale ammonia synthesis. They are already in use for small-scale ammonia synthesis in the Netherlands [39].

The decision to select alkaline electrolyzers over PEM electrolyzers for ammonia synthesis echoes the H2A program which also selected Norsk Hydro (now NEL Hydrogen) as the electrolyzer of choice [288]. The H2A program has perhaps the most complete publically-available catalogue of cost and technical information available regarding Norsk Hydro electrolyzers, making the selection more attractive. Alkaline electrolyzers are selected to be the source of hydrogen for the ammonia plant.

5.2.3 Water Desalination

The water desalination system must provide the alkaline electrolyzers with pure, distilled water [289]. While the electrolyzers themselves are equipped with purification equipment (RO

modules) they are not designed for desalination. The three main options for electrically-driven water desalination are: reverse osmosis, electrodialysis, and mechanical vapor compression. The defining characteristics for the three processes are shown in Table 21.

Table 21 – Characteristics of the three major electrical desalination processes [141, 145, 281]

Process	Mechanical power input (kWh/m3 of product)	Feed water quality (ppm TDS)	Product water purity (ppm TDS)
Vapor compression	8–16 (16)	Any	<20
Reverse osmosis	5–13 (10)	Any	250-700
Electrodialysis	12	3000-11000	20-700

It is assumed that the wind-ammonia plant will be operating near or on the ocean; sea water is assumed to be the feedstock for the electrolyzers. Two main factors influence the choice of the desalination process: the feed water quality and the product purity. The former is a measure of the maximum salt concentration that the desalination is capable of purifying; the latter is a measure the quality of the product.

First, the salt concentration of seawater ranges from 10,000 – 45,000 ppm TDS but averages 35000 ppm TDS; brackish water is considered to be between 1,500-10,000 ppm TDS [290]. Since seawater is assumed to be the feedstock, electrodialysis is immediately eliminated because it is primarily used for the desalination of brackish water. The remaining two desalination technologies – reverse osmosis and mechanical vapor compression – accept any type of feed water.

The product purity requirement for an alkaline electrolyzer is about 10 ppm TDS, which is essentially distilled water. Only thermal processes are capable of achieving such purities [145]. Therefore, RO cannot offer the water purity required by the electrolyzers, without the risk of damaging the electrolyzer stacks. Any damage that occurs simultaneously adds costs and lowers production.

By contrast, MVC can produce distilled water from seawater of any salinity [144]. Furthermore, the MVC units typically fall into the range of about 250-2000 tons of distillate per day [147] are highly flexible, robust, and cost effective. The possibility of heat integration with the electrolyzers makes MVC the best candidate to supply feed water to the electrolyzers.

5.2.4 Synthesis Loop

Ammonia synthesis loops are unique to particular plants, but all have the same general equipment: compressors, heat exchangers, and reactors. The actual design of the synthesis loop is beyond the scope of this thesis. Instead, state-of-the-art synthesis loop equipment is assumed for costing purposes. For example, the compressors are assumed to be centrifugal because they have become the industry standard in recent decades [28]. The next chapter will define the equipment in more detail.

5.2.5 Final Subsystem Selection

The final subsystem selection for the synthesis gas generation equipment is shown in

Table 22. At the time of this writing it is believed that this is the best equipment with which to produce the required mixture of gaseous hydrogen and nitrogen from air and seawater using only electricity.

Table 22 – Subsystem selection for an all-electric ammonia plant

Process	Selection	Reason(s)
Air Separation (N_2)	Cryogenic	High purity product; high volume output; mature technology
Electrolysis (H_2)	Alkaline	High output; good load range; mature technology
Water Desalination (H_2O)	Mechanical Vapor Compression	Thermal system with possibility of heat integration; flexible with good load range; little pretreating required; high purity product needed for electrolysis

5.3 Flexible Ammonia Production

The concept of a standalone ammonia production system was discussed thoroughly in a report issued by the Lockheed California Company in 1977 [14]. The conclusion was that standalone systems could be operated at steady state through the use of hydrogen or batteries to smooth the variations in wind power. Using this condition, small standalone system may be feasible, but expensive. However, larger 100 tonne per day systems require significant storage capacity to maintain operation at steady state. For example, a 100 tonne per day facility requires about 45MW of continuous power. A two day wind lull would require storage on the order of 2 GWh. According to Figure 33 only two energy storage options exist: compressed air energy storage (CAES) and pumped hydro. At present, there are only two CAES plants operating in the world and they are used primarily to provide back work to gas turbines [166]. Pumped hydro requires a specific geological terrain: a large hill near a large body of water. Neither CAES nor pumped hydro would be practical for ammonia production.

Historically, ammonia synthesis was a constant process that used abundant sources of fossil fuels as feedstocks [28]. Because the feedstocks could be supplied continuously, there was never an incentive to create a flexible or variable process. That is now changing. Price spikes in ammonia

fertilizers coupled with declining domestic production have created a demand for alternative ammonia production techniques [291-292], including flexible ammonia production processes such as solid state ammonia synthesis (SSAS) [293-294]. However, these processes are still in the research stages, and are likely years away from commercial production. Nonetheless, it is useful to consider flexible ammonia production processes to better understand the possible economic benefits that they can have.

If a wind-NH_3 plant were to be built using existing equipment and knowledge, it would probably have a low ramp rate and a high turndown ratio. Some of the wind-powered ammonia plant subsystems would handle the changes in load better than others. The electrolyzer, for example, is rated for a load range of 20%-100% [285, 289] while the cryogenic air separation unit has much slower dynamics, on the order of hours [209-210]. The mechanical vapor compression systems can be fairly agile, if properly designed [282] while the centrifugal compressors have a load range between 55% and 115% [136]. If the centrifugal compressors fall below the minimum load range, surge can occur within the compressor, possibly causing mechanical damage. When the compressors are operated higher than the maximum, choke can occur.

Perhaps the principal impediment to creating a flexible ammonia production process is the ammonia synthesis catalysts. Disturbances in the feed rate composition, the inlet temperature and/or temperature, result in oscillatory behavior in the output and permanently damage the catalyst [14, 295], resulting in lower ammonia yields.

The ammonia synthesis gas production (nitrogen and hydrogen) could be manipulated to facilitate a flexible ammonia process. Some electrolyzers could be turned off to achieve low hydrogen production levels. Several ASUs of differing sizes and types could be installed to attain the proper stoichiometric flow rates of nitrogen. Compressors could be outfitted with inlet vane guide control [136] so that the system achieves high compression ratios with low mass flow rates. The

design of such a facility would be novel, and would require analysis and control of each subsystem.

CHAPTER 6

THE ECONOMICS OF AMMONIA PLANTS

Estimating the total cost for an entire chemical plant can be done with knowledge of the capital costs of the major pieces of equipment. The total plant cost is the sum of the direct project costs, the indirect project costs, the contingencies and fees, and the auxiliary services [296-298]. Direct project costs include equipment costs at the manufacturer's site, all piping, insulation, controls and any other material associated with the equipment, and the installation labor for the equipment. The indirect costs are comprised of transportation costs for the equipment, construction overhead and engineering expenses. The contingencies and fees are variable from project to project, the contingencies being payment for any unforeseen circumstances, and the contractor's fee depending on many factors. The auxiliary services consist of the site development, any auxiliary buildings that may be necessary on the property, and off-site utilities such as wastewater treatment.

6.1 Capital Costs

The following discussion of bare module equipment cost is based on the analysis published in [296]. The text offers updated costs for a large number of equipment types and costing results compare favorably with commercially available software [299]. Furthermore, that text references numerous canonical chemical engineering costing guides that it uses to calculate costs and cost factors. These guides include [300] – a detailed economic examination of popular chemical engineering processes; [152, 297] two classic texts on the design and economics of chemical processes; [298] – a small tome that describes project development and economics; [301] – the

handbook for any chemical engineer. Taken together, these six textbooks provide enough information to accurately design and cost almost any major chemical process plant.

The bare module equipment cost is the sum of direct and indirect costs for equipment that is fabricated using a common material such as carbon steel, and is designed for near ambient pressures [296]. In general, the equipment depends on several factors including:

1. The specific type of equipment
2. The operating pressure
3. The materials used for construction

The average free-on-board (f.o.b.) costs of industrial chemical process engineering equipment were fitted to Equation 38, where A is the capacity or area of the process equipment and K_i are the constants specific to the equipment type.

$$\log_{10} C_p^o = K_1 + K_2 \log_{10} A + K_3 [\log_{10} A]^2 \qquad \textbf{Equation 38}$$

The constants *K1, K2 and K3* that are used in this study are listed in Table 23 for all of the major equipment required in the ammonia plant.

Often, equipment prices are given at a known inflation index from a previous year. To account for effects of inflation, Equation 39 will be required to inflate or deflate a piece of equipment from a known index to the year of interest. In the equation, I_i correspond to inflation indices. The information given in [296] is from 2001 which has Chemical Engineering Plant Cost Index (CEPCI) of 397; the CEPCI index for 2010 is 550.8. Consequently, all costs found in [296] will be multiplied by a factor of $\frac{550.8}{397}$ to bring the costs into 2010 dollars.

Table 23 – Cost parameters used in this study, from [296]

Equipment	K_1	K_2	K_3	Capacity, Units	Min Size	Max Size
Centrifugal Compressor	2.2897	1.3604	-0.1027	Fluid Power, kW	450	3000
Totally Enclosed Electric Drive	1.956	1.7142	-0.2282	Shaft Power, kW	75	2600
Floating Head Heat Exchanger	4.8306	-0.8509	0.3187	Area, m^2	10	1000
Reactor, Vertical	3.4974	0.4485	0.1074	Volume, m^3	0.3	520
Reciprocating Pump	3.8696	0.3161	0.122	Shaft Power, kW	0	200

$$C_{p,2}^{o} = C_{p,1}^{o}\left(\frac{I_2}{I_1}\right) \qquad \textbf{Equation 39}$$

Departures from the standard base conditions can be managed through the use of multiplying factors, as shown in Equation 40 and Equation 41. Here, F_{BM} is the bare module cost factor, which corrects for both material – F_M – and pressure – F_P – factors for the equipment. Multiplying the bare module cost by F_{BM} gives the bare module cost, C_{BM}, which includes both direct and indirect costs for the equipment.

$$F_{BM} = F_P F_M \qquad \textbf{Equation 40}$$

$$C_{BM} = C_p^o F_{BM} \qquad \textbf{Equation 41}$$

6.1.1 Pressure Factors

Above ambient operating pressures increase the cost of equipment simply because the thickness of the walls within the equipment must increase. Furthermore, higher operating pressures also increase failure rates in welds and exacerbate the corrosiveness of some substances. In such cases,

inert materials such as glass or graphite are used to line the equipment walls. In all, the relationship between cost and pressure of a single piece of equipment is not straightforward but it is roughly correlated with the amount of material present in the equipment.

The departure in bare module cost due to elevated operating pressures in equipment can be determined using a cost factor, $\boldsymbol{F_P}$. The form of the fitted data is given in Equation 42.

$$\boldsymbol{Log_{10}F_p = C_1 + C_2 log_{10}P + C_3(log_{10}P)^2} \qquad \textbf{Equation 42}$$

where P is in bar gauge and the C_i terms are constants. Standard equipment is listed in the lookup tables given in [296] so that the pressure factor can be easily determined.

Pressure vessels are treated differently than many other pieces of equipment because of the risk of injury upon failure. Equation 43 gives the pressure factor for a process vessel based on four parameters: the operating pressure, P; the vessel diameter D; the corrosion allowance, CA, taken to be 0.00315m; and t_{min}, the thickness of the vessel, taken to be 0.0063m.

$$\boldsymbol{F_{p,vessel} = \frac{\frac{(P+1)D}{2(850-0.6(P+1))} + CA}{t_{min}}} \qquad \textbf{Equation 43}$$

The $\boldsymbol{F_{p,vessel}}$ is used to determine the costs of the ammonia synthesis reactor and the flash drum.

6.1.2 Materials Factors

The materials factor, $\boldsymbol{F_M}$, is also used to cost equipment that is fabricated using materials that are more expensive than standard carbon steel. For example, sea water applications require that the process equipment be made of nickel- or titanium-based materials due to the corrosive nature of some salts with steel, aluminum and copper. Materials factors can range from unity to more than twelve, depending on the material, and they are available in lookup tables for specific equipment. Table 24 shows the cost factors for the equipment described in this paper [296].

$$C_{BM} = C_p^o F_{BM} = C_p^o(B_1 + B_2 F_m F_p)$$ **Equation 44**

Equation 44 is a general equation that accounts for both a material factor and a pressure factor. It also includes the equipment specific fitted constants B_1 and B_2 , which may be unity.

Table 24 – Bare module cost factors for ammonia synthesis equipment

Equipment	F_{BM}
Centrifugal Compressor	5.80
Totally Enclosed Electric Drive	1.50
Floating Head Heat Exchanger	8.56
Reactor, Vertical	118.18
Reactor, Flash	118.18
Reciprocating Pump	3.92

Equation 44 can be used, together with knowledge of operating temperatures and pressures, to determine the bare module cost of a single piece of equipment.

Finally, once all of the major equipment in the synthesis loop is costed using the Equation 45 which incorporates pressure factors, material factors, inflation and size scaling, the total grass roots cost can be found using Equation 46 and Equation 47. In Equation 46 the multiplying factor of 1.18 is to compensate for a contingency costs and other miscellaneous fees. The contingency costs are assumed to be 15% of the bare module cost; the fees are assumed to be 3%. Equation 47 contains a factor of 50% for auxiliary facilities costs, which are generally unaffected by the construction materials and pressures within the plant.

$$C_2 = C_1 \left(\frac{A_2}{A_1}\right)^n \left(\frac{I_2}{I_1}\right)(F_M F_P)$$ **Equation 45**

$$C_{TM} = \sum_{i=1}^{n} C_{TM,i} = 1.18 \sum_{i=1}^{n} C_{BM,i}$$ **Equation 46**

$$C_{GR} = C_{TM} + 0.50 \sum_{i=1}^{n} C_{BM,i}^{\circ}$$ **Equation 47**

6.2 Manufacturing Costs

The manufacturing costs of a chemical plant are integral when determining the economic feasibility of a process. The manufacturing costs are directly related to the process flow within the plant, the fixed capital invested, and the type of process. In general, the manufacturing costs can be divided into three categories: the direct costs including operating expenses related to labor, maintenance and repairs, and raw materials; the fixed costs such as depreciation, taxes, and insurance; and the general expenses such as overhead, and research and development. The cost of manufacture (COM) is the sum of the direct costs (DMC), the fixed costs (FMC) and the general expenses (GE):

$$\boldsymbol{COM = DMC + FMC + GE} \qquad \textbf{Equation 48}$$

The COM can be estimated with knowledge of the following [296]:

1. The fixed capital investment (*FCI*) (also known as Grass Roots Cost)
2. Cost of operating labor (C_{OL})
3. Cost of utilities (C_{UT})
4. Cost of waste treatment (C_{WT})
5. Cost of raw materials (C_{RM})

Each of these costs can be used together with a multiplication factor to determine elements of direct manufacturing costs, fixed manufacturing costs and general expenses. For example, the depreciation of chemical plant equipment, as well as the taxes and insurance are directly related to the fixed capital investment; the plant overhead costs are directly related to the labor and the fixed capital investment. Table 25 shows a summary of the assumed values for each of the manufacturing cost categories. The total cost of manufacture (COM) is found by solving Equation 48 and the total costs listed in Table 25 for the cost of manufacture, given in Equation 49.

$$COM = 0.180FCI + 2.73C_{OL} + 1.23(C_{UT} + C_{WT} + C_{RM}) \quad \textbf{Equation 49}$$

Since the depreciation is not considered in this analysis, the cost of manufacturing equation uses 18% of the fixed capital investment instead of the 28%, as suggested by Turton, et al. [296]

6.2.1 Raw materials

The raw materials often dominate the production costs of a chemical plant [297]. The amount of raw materials is related to the material balance of the chemical plant of interest and can be found using the process flow diagram. In the case of an all-electric ammonia facility there are almost no raw material costs required because air and ocean water are assumed to be free.

Table 25 – Direct manufacturing costs for chemical plants [296]

Direct Manufacturing Costs	**Typical Value**
Raw materials (C_{RM})	C_{RM}
Waste treatment (C_{WT})	C_{WT}
Utilities (C_{UT})	C_{UT}
Operating labor (C_{OL})	C_{OL}
Direct supervisory and clerical labor	$(0.18)C_{OL}$
Maintenance and repairs	(0.06)FCI
Operating supplies	(0.009)FCI
Laboratory charges	$(0.15)C_{OL}$
Patents and royalties	(0.03)COM
Total Direct Manufacturing Costs	**$C_{RM} + C_{WT} + C_{UT}$ +(1.33) C_{OL} + (0.069)FCI+(0.03)COM**
Fixed Manufacturing Costs	
Depreciation	MACRS
Local taxes and insurance	(0.032)FCI
Plant overhead costs	(0.78) C_{OL} + (0.036)FCI
Total Fixed Manufacturing Costs	**(0.78) C_{OL} +(0.068)FCI+MACRS**
General Manufacturing Expenses	
Administration costs	(0.177) C_{OL} + (0.009)FCI
Distribution and selling costs	(0.11)COM
Research and development	(0.05)COM
Total General Manufacturing Expenses	**(0.177) C_{OL} + (0.009)FCI + (0.16)COM**
Total Costs	**C_{RM}+C_{WT}+ C_{UT}+(2.287)C_{OL} + (0.146)FCI + (0.19)COM +MACRS**

6.2.2 Waste Treatment

Many chemical processes have waste streams that are gaseous, liquid or solid or slurries. Often federal regulations require the waste streams to be properly treated before entering the environment. The waste streams in an electric ammonia plant are negligible compared to the size and cost of the plant. The streams include small amounts of ammonia that may leak from the synthesis loop and enter the environment; the brine discharge from the mechanical vapor compression; the oxygen and argon streams that are generated from air separation and electrolysis. All waste streams except ammonia are assumed to be environmentally friendly. The waste treatment cost is assumed to be negligible.

6.2.3 Utilities

The utility requirements for a process plant can be easily obtained from material and energy balances around the major equipment. The utilities usually include the steam, electricity, cooling water, fuels, refrigeration and fuels. The price of utilities is correlated with the price of energy (fossil fuels), so it is inherently difficult to predict.

The price of utilities in this thesis will include the price of electricity and the cost of cooling water. All processes within the system are assumed to be electrically-driven. Thus, compressors, water desalination, air separation, electrolysis, pumps and blowers are all electric. The price of utilities will therefore be the electricity requirement multiplied by the price of electricity. The cooling water is required for intercooling the compressor trains and for cooling the electrolyzer stacks. The total amount of water required was calculated in previous sections.

The electrical utilities in this thesis are assumed to come from wind turbines, when the power is available. When the power is not available from the wind, the power will be purchased from the grid at the cost at that time. However, there will be times when the wind turbines produce excess

electricity. When this occurs, the power is assumed to be sold to the grid at the buying price of electricity. *Therefore, the utilities costs are offset when the wind turbines produce more power than is required by the ammonia plant.* This is the key difference between this wind-powered ammonia plant and traditional chemical plants.

The total cost of the electricity is the total cost of the power purchased from the grid less the power sold back to the grid and does not include the cost of the wind turbines. The economics of the wind turbines will be assessed separately.

6.2.4 Operating labor

Estimating operating labor is relatively straightforward. There are two main rules-of-thumb available to determine the number of personnel required for process plant operation. One can assume either that the labor is related to the major process equipment via Equation 50 [296]:

$$\boldsymbol{N_{OL} = \left(6.29 + 31.7P^2 + 0.23N_{np}\right)^{0.5}} \qquad \textbf{Equation 50}$$

where:

N_{OL} is the number of operators per shift,

P is the number of processing steps that include solids handling – zero for this application,

and N_{np} is the number of nonparticulate processing steps, including compressors, towers, heat exchangers, reactors and heaters, shown in Equation 51.

$$\boldsymbol{N_{np} = \sum Equipment} \qquad \textbf{Equation 51}$$

Or one can assume that the labor is related simply to plant capacity [301]:

$$\boldsymbol{\log Y = -0.783 \log X + 1.252 + B} \qquad \textbf{Equation 52}$$

where:

Y is the operating labor in units of hours/ton per processing step; X is the plant capacity per day;

B is a constant related to the process type (-0.167 for a continuous process).

Equation 50 and Equation 52 have units of operators per shift. As chemical plants are assumed to run every hour, all year, at three shifts per day, they require 1095 operating shifts. Since a single operator works for 49 weeks per year at 5 shifts per week, a chemical plant requires 4.5 operators for every working operator. To obtain a dollar value, the salary for the chemical plant operator is required. Salaries are available from the Bureau of Labor and Statistics [302].

Supervision for operations is required, and depends on the complexity of the process being considered. A reasonable assumption is 10-20% of operating labor [152]. Payroll charges, which includes workers' compensation, social security, unemployment taxes, paid vacations and holidays and medical and dental insurance, account for approximately 30-40% of operating labor [301].

6.3 Ammonia Synthesis Loop

An ammonia synthesis loop is a continuous cycle of gasses that travel at high temperature and pressure through an adiabatic reactor. The reactor converts a portion of the gases into ammonia gas which is then separated in a flash vessel and recovered for storage. The synthesis loop is maintained at steady state conditions with few interruptions, since interruptions can damage the catalysts present in the reactor and lower the conversion efficiency. The gases present in the feed to the synthesis loop are pure hydrogen and pure nitrogen; once the feed is mixed with the recycle gas some ammonia is also present because the separation of ammonia from the syngas is imperfect.

The synthesis loop is integrated into an overall ammonia synthesis process that typically employs natural gas as a feedstock. The resulting feed from the reforming section of the plant has inert

gases such as methane and argon present. While the feed gas production of a natural gas plant is similar to an all electric plant there are some notable differences. First, the feed gas in an all electric process will have far fewer inerts and fewer catalyst poisons such as oxygen-containing compounds. Because natural gas is used as the major feedstock in traditional (non-electric) ammonia plants, some of the impurities that exist in the gas cannot be removed fully before reaching the synthesis loop. An all electric plant derives the synthesis gas from air separation which produces high purity nitrogen and from water electrolysis which produces high purity nitrogen. Thus the characteristics of the synthesis loop are inherently different.

The specifications of temperatures and pressures throughout an ammonia synthesis loop are scarce in the literature. Perhaps the best treatment of a modern synthesis loop is given in [34] which incorporates a full Aspen Plus flow sheet. Other treatments are given in [303] and [304]. For this analysis, it is assumed that the temperatures and pressures are valid for any size ammonia plant. In practice this is an oversimplification, but it can be used as an order of magnitude estimate of an electric ammonia plant.

Thus, once the size of the plant is chosen the flow rates through the plant can be estimated and the equipment can be properly sized. Economic costing methods that were developed in several sources [152-153, 296-298, 301, 305-307] are incorporated into the model so that the overall grass roots cost can be determined.

The major process equipment in an ammonia synloop consists of compressors heat exchangers pumps and the reactor. The compressor sizing is straightforward and is primarily driven by the flow rates and pressure ratios. The heat exchangers are sized according to the required temperatures and flow rates and the reactor is sized according to Rase in the case study [308]. Smaller process equipment such as pumps, pipes, small heat exchangers and turbines are dealt with by using multiplication factors after the major process equipment is determined.

The cost of the process equipment dependents on three major factors: the size, the material of construction and the operating pressure. The material of construction depends solely on the composition of the fluids flowing through the equipment. A table found in [152] lists the compatibility of construction metals with numerous chemicals. Also, pressure affects the cost of a piece of process equipment because higher pressures often require more material and heavier frames.

While there are a myriad of ammonia synthesis loop configurations some basic assumptions enable an economic analysis which is valid for any synthesis loop. The assumptions are as follows:

1. A centrifugal compressor train takes the feed gas from 1 bar to operating pressure.
2. A recycle compressor is used to compensate for the pressure drops in the loop.
3. The operating pressures and temperatures are valid for any size ammonia plant.
4. The flow rate alone can be used to determine the approximate equipment sizing.
5. There are four major heat exchangers for heating the feed gas and cooling the product stream.

The synthesis loop of the ammonia plant converts the mixture of nitrogen and hydrogen into ammonia in a continuous cycle as shown in Figure 36. The associated stream table (Table 26) is also given to give a sense of the operating temperatures and pressures throughout the synthesis loop. The conversion process is done at high temperature and pressure within a fixed bed catalytic reactor [309], which also serves as a heat exchanger to remove the heat of reaction. The synthesis loop consists of a series of compressors, heat exchangers, pumps, a reactor, a flash drum. The ammonia conversion rate is low, and depends strongly on the operating parameters chosen for the system. The ammonia is separated from the synthesis gas stream in a flash vessel and is stored in

a cryogenic tank at atmospheric pressure. The synthesis gas is recycled and combined with the fresh feed.

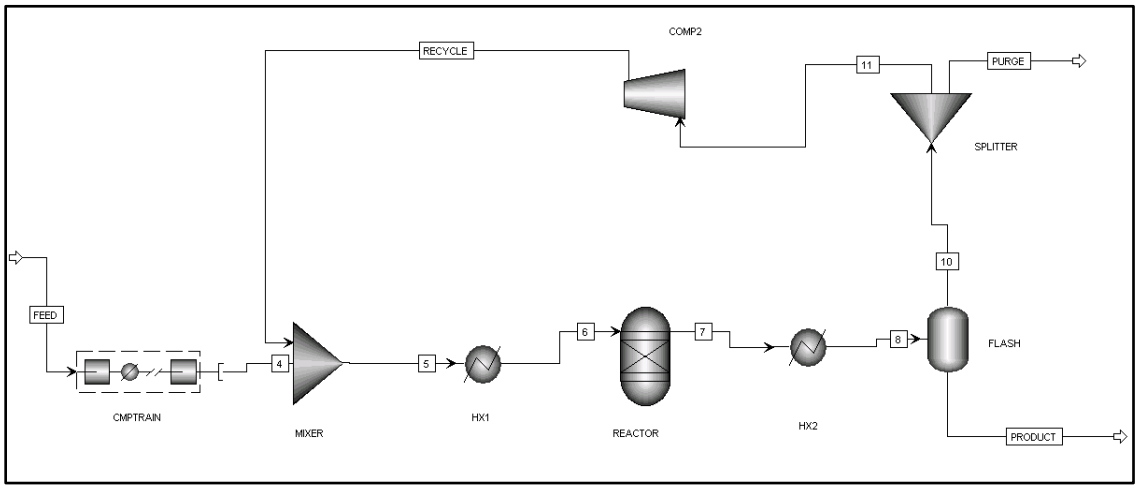

Figure 36 – A simple ammonia synthesis loop in Aspen Plus

Table 26 – Stream table for a simple ammonia synthesis loop

Stream	Units	Feed	4	5	6	7	8	Product	10	Purge	11	Recycle
Mass Flow	Ton/hr	12.5	12.5	88.03	88.03	88.03	88.03	12.49	75.54	0.01	75.53	75.53
Mass Flow	Ton/day	300.0	300.0	2112.7	2112.7	2112.7	2112.7	299.8	1813.0	0.2	1812.7	1812.7
Component Mass Flow												
H_2	Ton/hr	2.22	2.22	37.4	37.4	35.2	35.2	0.01	35.19	0	35.19	35.18
N_2	Ton/hr	10.28	10.28	27.76	27.76	17.58	17.58	0.1	17.48	0	17.48	17.48
NH_3	Ton/hr	0	0	22.87	22.87	35.25	35.25	12.38	22.88	0	22.87	22.87
Mole Flow	Kmol/s	0.41	0.41	5.8	5.8	5.6	5.6	0.2	5.4	0	5.39	5.39
Component Mole Flow												
H_2	Kmol /s	0.31	0.31	5.15	5.15	4.85	4.85	0	4.85	0	4.85	4.85
N_2	Kmol /s	0.1	0.1	0.28	0.28	0.17	0.17	0	0.17	0	0.17	0.17
NH_3	Kmol /s	0	0	0.37	0.37	0.57	0.57	0.2	0.37	0	0.37	0.37
Temp	K	299.82	400	308.06	755.37	755.37	299.82	299.82	299.82	299.82	299.82	301.16
Press	bar	1.01	151.9	151.9	151.9	149.9	149.9	149.9	149	149.9	149.9	151.99
Vapor Fraction		1	1	1	1	1	0.96	0	1	1	1	1
Molar Enthalpy	MJ/Kmol	0.05	2.96	-2.66	10.84	9.31	-5.37	-64.65	-3.13	-3.13	-3.13	-3.09
Mass Enthalpy	MJ/kg	0.01	0.35	-0.63	2.57	2.13	-1.23	-3.82	-0.8	-0.8	-0.8	-0.79
Enthalpy Flow	MW	0.03	1.22	-15.41	62.84	52.08	-30.08	-13.25	-16.79	0.00	-16.78	-16.57

6.3.1 Compression power for the feed stream

Centrifugal compressors are used to obtain the high operating pressures required within the synthesis loop. There are two sections within the synthesis loop that require compressors: the feed gas and the recycle stream. The feed gas must be compressed to the operating pressure of the synthesis loop - taken to be 150 bar in this analysis – while the recycle compressor must compensate for pressure drops around the entire synthesis loop. It is assumed that all of the compressors are driven by large electric motors. In conventional natural gas ammonia plants the drivers are steam turbines that utilize some of the heat of reaction in the ammonia reactor.

For the feed stream, it is assumed that the hydrogen is available at STP from the electrolyzer bank, nitrogen is at standard temperature and 8 bar from the ASU, and the mass fractions of both are given by their relative masses in the NH_3 molecule: 14/17 for N_2 and 3/17 for H_2. The fluid compression power required is given by Equation 53 where T_{in} is the temperature of the feed entering the compressor train in K; N is the number of stages in the compression train; n is the polytropic exponent; R is the specific gas constant in kJ/kgK; $\dot{m}$ is the mass flow rate in kg/s; P_2 is the final pressure in bar; P_1 is the initial pressure in bar. Note that the term $\left(\frac{P_2}{P_1}\right)^{\frac{1}{N}}$ gives the compression ratio across each compressor.

$$\dot{W}_{fluid} = T_{in} N \frac{n}{(n-1)} R\dot{m} \left[\left[\left(\frac{P_2}{P_1} \right)^{\frac{1}{N}} \right]^{\left(\frac{n-1}{n}\right)} - 1 \right] \qquad \textbf{Equation 53}$$

If isentropic compression assumed, the temperature is raised across each compressor according to Equation 54. Intercooling is utilized between the stages to minimize the compressor work. Thus, each intercooler must remove the heat imparted on the feed gas by the compressors. It is assumed

that the intercoolers cool the gas down to the inlet temperature of the compressor. In this case, each compressor has the same conditions and uses the same amount of power. The total cooling power – given by $\dot{Q}$ in Equation 55 – is used to size the heat exchangers (intercoolers) used in the compressor train. For the mixture of nitrogen and hydrogen, the total heat transferred out of the intercooler is the sum of the contributions of each component. The mass flow rates of the feed are given by the stoichiometric ratio of nitrogen and hydrogen in the ammonia molecule and the C_p values are given by Equation 56 with the coefficients listed in Table 27. The last compressor is not aftercooled because hot gases are required in the synthesis loop.

$$T_{out} = T_{in}\left[\left(\frac{P_2}{P_1}\right)^{\frac{1}{N}}\right]^{\left(\frac{n-1}{n}\right)} \quad \textbf{Equation 54}$$

$$\dot{Q} = \dot{m}(N-1)(T_{out} - T_{in})C_{p,mix} \quad \textbf{Equation 55}$$

$$C_p = a + bT + cT^2 + dT^3 \quad \textbf{Equation 56}$$

Table 27 –Coefficients used in calculating the specific heats of the gases present in the synloop [310]

Coefficients	N_2	H_2	NH_3
a	28.9	29.11	27.568
b	-0.1571e-2	-0.1916e-2	2.5630e-2
c	0.8081e-5	0.4003e-5	0.99072e-5
d	-2.873e-9	-0.8704e-9	-6.6909e-9

The specific heat of the mixture – $C_{p,mix}$ – is calculated using the mole fractions (x) and specific heats of each component as given in Equation 57.

$$C_{p,mix} = x_{N_2} C_{pN_2} + x_{H_2} C_{pH_2} + x_{NH_3} C_{pNH_3}$$ **Equation 57**

The hydrogen and nitrogen are available at the compressor inlet at two different pressures. The total compression power is still given by Equation 53 and is the sum of the compression for each component. The conditions for each component of the feed are given in Table 28.

Table 28 – Assumed operating conditions and parameters of the ammonia synthesis loop

T_{in} (K)	293
***N* (stages)**	5
P_{final} (bar)	150
P_{in} N_2 (bar)	8
mole fraction *(x)* N_2	0.8224
R_{N2} (kJ/kgK)	0.2968
P_{in} H_2(bar)	1
mole fraction (*x*) H_2	0.1776
R_{H2} (kJ/kgK)	4.124

Equation 53 shows that the relationship between the size of the ammonia plant and the compression power required is linear with the flow rate of feed gas, given any synloop operating pressure. This further implies that the size of the compressors and the drivers for the compressors is also linear with flow rate. Figure 37 shows the fluid compression power required for various ammonia plant capacities.

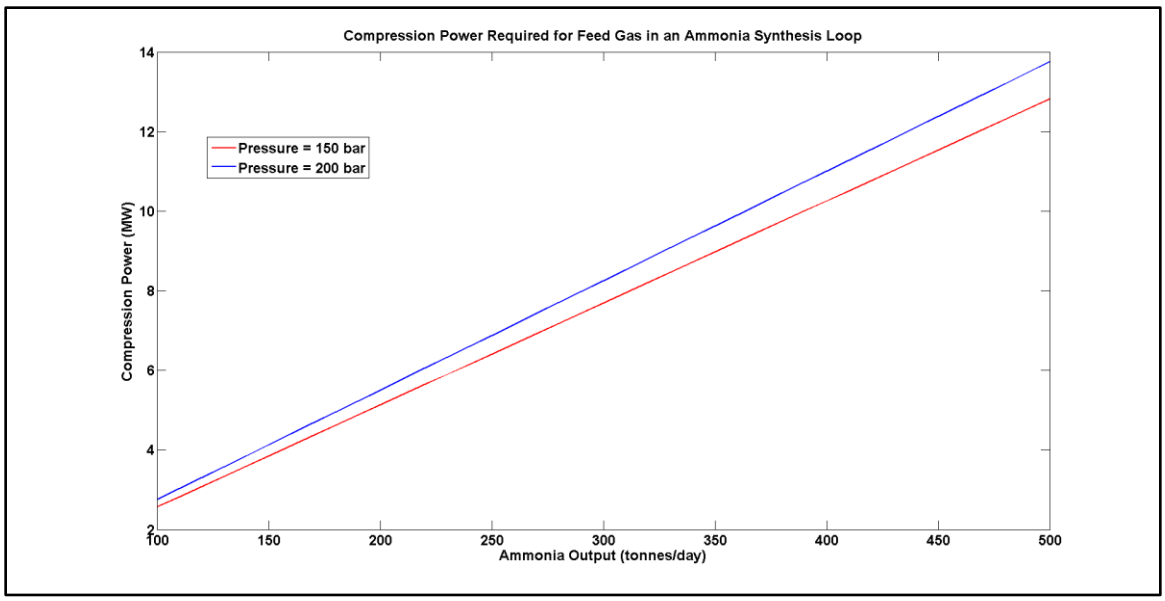

Figure 37 – Fluid compression power for the feed gas in an all-electric ammonia synthesis loop

The shaft power is typically used when determining the overall costs of compressors [296] and differs from the fluid power that was calculated in Equation 53. The power required to turn the compressor is the fluid power divided by the isentropic efficiency of the compressor, as shown in Equation 58. The isentropic efficiency is taken to be 75%, as given in [152], Table 4-9. Thus, the actual power needed at the shaft is about 25% higher than required by the fluid.

$$\dot{W}_{shaft} = \frac{\dot{W}_{fluid}}{\eta_i} \qquad \textbf{Equation 58}$$

6.3.2 Compression in the recycle stream

The recycle compressor is tasked with compressing more mass than the feed stream but with a smaller pressure ratio. Equation 59 shows that there is no accumulation within the synthesis loop. However, Equation 60 gives the mass flow rate through the recycle compressor for a given feed

and conversion efficiency. Using a simple mass balance, the mass flow rate in the synthesis loop is the mass flow rate of the feed divided by the conversion efficiency of the reactor.

$$\dot{m}_{feed} - \dot{m}_{purge} - \dot{m}_{product} = 0 \qquad \textbf{Equation 59}$$

$$\dot{m}_{loop} = \frac{\dot{m}_{feed}}{\eta_{Conv}} \qquad \textbf{Equation 60}$$

The conversion efficiency refers to the conversion rate of ammonia in the synthesis reactor and is generally around 15%. Therefore, the synloop has roughly 6 times the flow rate of the feed gas and contains ammonia as well as the hydrogen and nitrogen from the feed. The pressure drop around the synthesis loop varies with the configuration, and operating parameters of the entire plant. However, a total pressure drop of about 6% can be assumed as a baseline to determine the total compression power of the recycle compressor [34]. The number of stages is assumed to be 1 for the recycle compressor; Equation 53 and Equation 58 are both still valid.

6.3.3 Drivers

Each compressor is driven by its own electric motors ("drivers"). The power requirements for the compression are determined by dividing the shaft power of the compressor by the efficiency of the electric motor. The electric motor efficiency is generally greater than 90% and increases with the rated operating power and the turndown ratio [153]. Because the ammonia synthesis happens at steady state and the compression power required for small plants is in the MW range, an efficiency of 95% is assumed for this analysis. Equation 61 summarizes the power requirements for drivers. Here, $\dot{W}_{fluid}$is calculated from Equation 53, and the isentropic efficiency, η_i, is taken to be 75%, and the efficiency of the driver, η_{drv}, is taken to be 95%.

$$\dot{W}_{driver} = \frac{\dot{W}_{fluid}}{\eta_i \eta_{drv}}$$ **Equation 61**

6.3.4 Power Requirements for Compression

The total electric power required for the compression within the synthesis loop is now well defined. The electric power is provided to the drivers, which in turn provide the shaft power to the compressors which transfer the power to the gases. A summary of the power requirements for the compressors and the drivers is shown in Table 29.

Table 29 – The power requirements for the compressors and the drivers for various ammonia plants

Ammonia Plant Size (Tonnes/Day)	Total Fluid Power (MW)	Shaft Power (MW)	Driver Power (MW)
100	1.88	2.50	2.64
200	3.76	5.01	5.27
300	5.63	7.51	7.91
400	7.51	10.02	10.54
500	9.39	12.52	13.18

6.3.5 Ammonia Synthesis Reactor and Flash Drum

The size of the reactor is related to the amount of catalyst that is necessary to produce the required ammonia. The amount of catalyst can be found by using Temkin-Pyzhev kinetics [34, 309] shown in Equation 62 where f is a multiplier factor for catalyst activity with a value of 4.75 [34]; ρ_{cat} is the bulk density of the catalyst with a value of 2.65kg/L; p_i are the partial pressures in bar of the components; k_1 and k_2 are given by Equation 63 and Equation 64 where R is the universal gas constant (8.351 $\frac{J}{K \times mol}$) and T is the temperature in K. Once the reaction rate is calculated, the volume of the reactor can be found using quotient of the mass flow rate of product ammonia and the reaction rate times the bulk density of the catalyst given in Equation 65.

$$r_{NH_3} = 2f\left(k_1\frac{p_{N_2}p_{H_2}^{1.5}}{p_{NH_3}} - k_2\frac{p_{NH_3}}{p_{H_2}^{1.5}}\right)\frac{17}{3.6\times10^6}\left[\frac{kg\ NH_3}{\left(\frac{m^3\ cat}{s}\right)}\right]$$ **Equation 62**

$$k_1 = 1.79\times10^4 e^{\frac{-87090}{RT}}$$ **Equation 63**

$$k_2 = 2.75\times10^{16} e^{\frac{-198464}{RT}}$$ **Equation 64**

$$Vol = \frac{\dot{m}_{NH_3}}{1000r_{NH_3}}[m^3]$$ **Equation 65**

To find the approximate dimensions of the reactor for use with the reactor economics Equation 66 can be used in conjunction with Figure 38 to find the reactor length. Here the ΔP_2 is assumed to be 2% of the operating pressure of the reactor; ΔP_1 can be found by determining the space velocity and using Figure 38; the space velocity quotient is assumed to be unity; P_1 and T_1 are the reactor reference pressure and temperature in bar and Kelvin respectively; P_2 is the operating pressure of the reactor of interest in bar; T_2 is the operating temperature of interest in bar; M_1 is the reference molecular weight of the feed to the reactor, taken to be 11.61 g/mol and M_2 is the molecular weight of the feed mixture of interest; finally, Z_1 is the height of the catalyst bed in meters of the reference reactor. The diameter can now be calculated using the reactor volume and height.

$$Z_2 = Z_1\left(\frac{\Delta P_2}{\Delta P_1}\left(\frac{SV_1}{SV_2}\right)^{1.85}\frac{P_2}{P_1}\frac{T_1}{T_2}\left(\frac{M_1}{M_2}\right)^{0.85}\right)^{\left(\frac{1}{2.85}\right)}$$ **Equation 66**

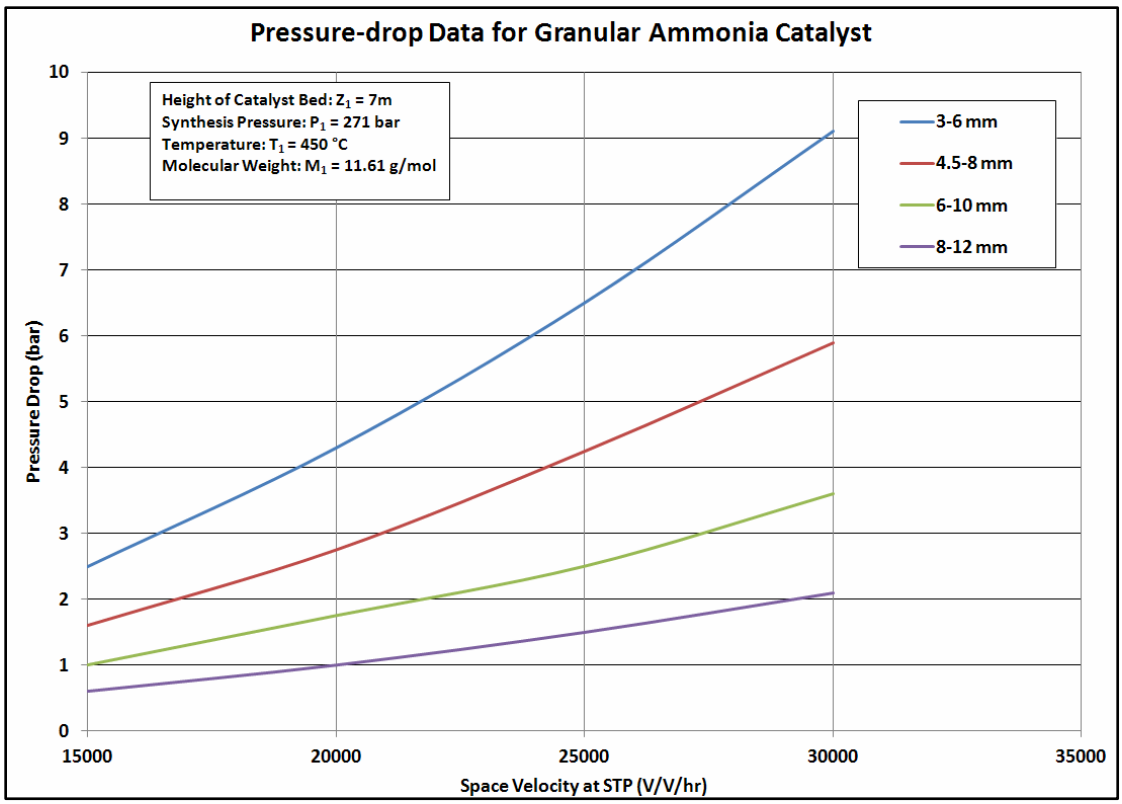

Figure 38 – Pressure drop as a function of space velocity for granular ammonia catalyst [308]

Figure 39 and Figure 40 show the changes in reactor size and shape with pressure and capacity. The diameter here is important because it is used to determine the thickness of the vessel, which influences the overall cost.

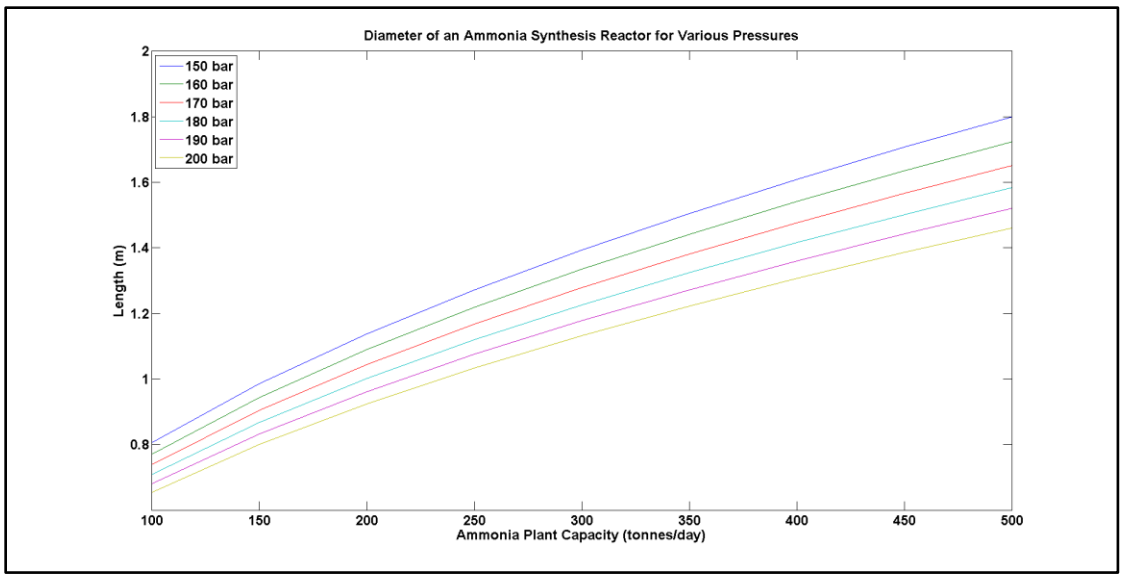

Figure 39 – Approximate diameters for an ammonia reactor for various ammonia capacities and operating pressures.

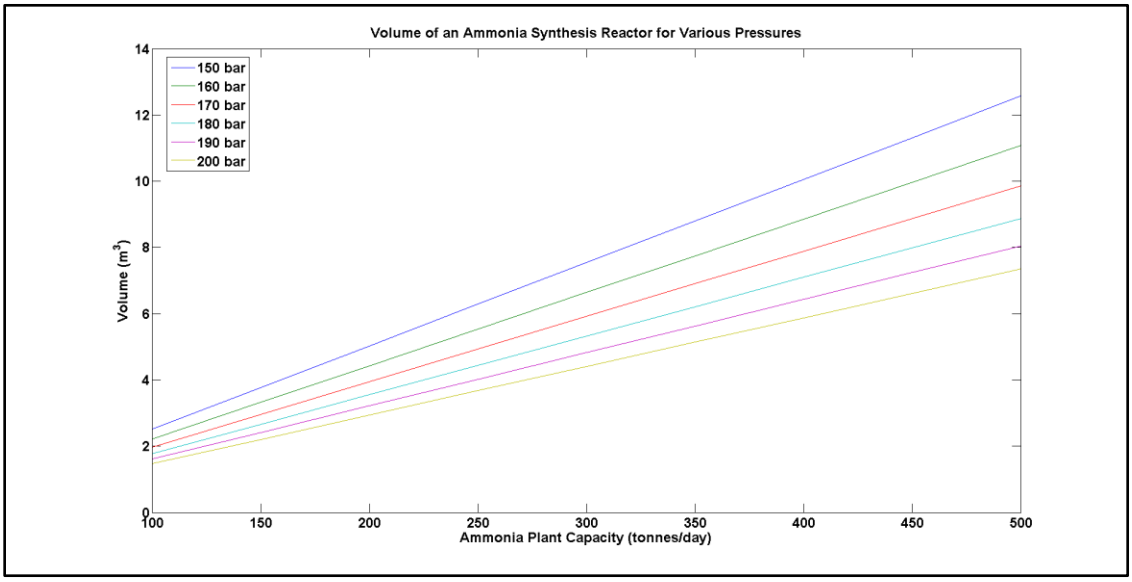

Figure 40 – The volume of ammonia synthesis reactors for various ammonia plant capacities and operating pressures.

6.3.6 Heat Exchangers

The heat exchangers are required to integrate the heat throughout the synthesis loop. There are assumed to be four major heat exchangers in the loop that are tasked with heating up the feed gases that enter the reactor and cooling down the product streams as they leave the reactor. There are also intercoolers that cool the gases between compression stages to minimize the compressor work. While other heat exchangers undoubtedly exist in actual ammonia plants they are assumed to be small relative to those described herein.

The size of the heat exchanger is related to its heat duty – how much heat must be transferred – and can be calculated with knowledge of the mass and composition of the components flowing through it and their temperatures. Determining the composition of the components flowing through the synthesis loop is nontrivial. Advanced computer models written in Aspen Plus or COCO must be used to simulate the process environment. A rigorous analysis of a synthesis loop was done in [34] and the values presented there will be used to size the heat exchangers. Figure 41 shows the schematic of the synthesis loop and shows the associated stream temperatures, pressures and compositions [34]. (A full Aspen Plus ammonia model is also available to accompany [34] at the following address: http://www.nt.ntnu.no/users/skoge/publications/2008/araujo_ammonia_cce/aspen.)

There are four major heat exchangers labeled HX-001, H-501, H-502, H-583 in Figure 41. Heat exchangers HX-001 and H-502 are used to preheat the reactor feed; heat exchanger H-583 is used to cool the synthesis gas so that it can be condensed in the knockout drum.

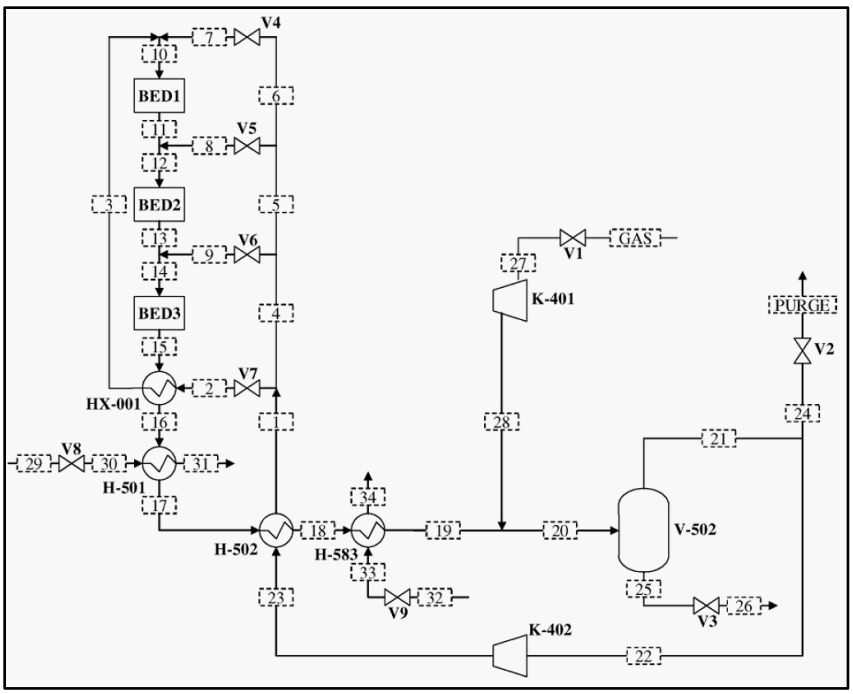

Figure 41 – An ammonia synthesis loop with a 3 bed reactor [34]

H-501 is supposed to generate low pressure steam from the ammonia synthesis reaction heat. It is assumed that low pressure steam is not required for an all-electric ammonia plant so the cooling water will remain liquid and a higher flow rate will be necessary. Furthermore, if steam is not raised then the pressures and temperatures of the streams will need to be augmented. For example, stream 30/31 was superheated as a high pressure steam. This will be changed in the model to be high temperature water. The temperature change of the water across the heat exchanger is assumed to be 50 °C to accommodate for the loss of heat exchange due to phase change. Also, a possible error exists in the given stream table: a temperature crossover occurs in heat exchanger H583. In this case it was assumed that the syngas stream was the correct temperature because it needs to be cool to condense and separate the ammonia. The cooling water temperatures were instead changed to an inlet temperature of 5°C and a temperature increase of 10°C. This ensures that no temperature crossover occurs within the heat exchanger. In Table 30 and Table 31 the asterisks have been placed next to those temperatures that were altered for this model.

Table 30 – Stream table for an ammonia synthesis loop [34]

		Mole Fractions					
Stream	**Temperature (°C)**	**Hydrogen**	**Nitrogen**	**Methane**	**Argon**	**Ammonia**	**Water**
1	231.7	0.624	0.183	0.033	0.023	0.136	0
2	231.8	0.624	0.183	0.033	0.023	0.136	0
3	340.1	0.624	0.183	0.033	0.023	0.136	0
4	231.7	0.624	0.183	0.033	0.023	0.136	0
5	231.7	0.624	0.183	0.033	0.023	0.136	0
6	231.7	0.624	0.183	0.033	0.023	0.136	0
7	231.8	0.624	0.183	0.033	0.023	0.136	0
8	231.8	0.624	0.183	0.033	0.023	0.136	0
9	231.8	0.624	0.183	0.033	0.023	0.136	0
10	306.3	0.624	0.183	0.033	0.023	0.136	0
11	456.2	0.536	0.151	0.036	0.026	0.251	0
12	420.1	0.551	0.157	0.036	0.025	0.231	0
13	452.1	0.531	0.149	0.037	0.026	0.258	0
14	423.9	0.544	0.154	0.036	0.025	0.241	0
15	449.3	0.527	0.148	0.037	0.026	0.262	0
16	394.4	0.527	0.148	0.037	0.026	0.262	0
17	296.9	0.527	0.148	0.037	0.026	0.262	0
18	107.6	0.527	0.148	0.037	0.026	0.262	0
19	27.1	0.527	0.148	0.037	0.026	0.262	0
20	40.5	0.567	0.167	0.031	0.022	0.214	0
21	40.4	0.624	0.183	0.033	0.023	0.136	0
22	40.4	0.624	0.183	0.033	0.023	0.136	0
23	48	0.624	0.183	0.033	0.023	0.136	0
24	40.4	0.624	0.183	0.033	0.023	0.136	0
25	40.4	0.014	0.005	0.006	0.006	0.969	0
26	40.5	0.014	0.005	0.006	0.006	0.969	0
27	17	0.745	0.249	0.003	0.003	0	0
28	304.2	0.745	0.249	0.003	0.003	0	0
29	15	0	0	0	0	0	1
30	15.1	0	0	0	0	0	1
31	144.7*	0	0	0	0	0	1
32	15	0	0	0	0	0	1
33	15.1*	0	0	0	0	0	1
34	82.9*	0	0	0	0	0	1
Feed	17	0.745	0.249	0.003	0.003	0	0
Purge	40.2	0.624	0.183	0.033	0.023	0.136	0

Table 31 – Heat exchanger temperature data from the synloop

Heat Exchanger	Cold inlet Temp (°C)	Hot inlet Temp (°C)	Cold outlet Temp (°C)	Hot outlet Temp (°C)	LMTD (°C)
HX001	231.8	449.3	340.1	394.4	134.1
H501	15.1	394.4	65.1*	296.9	304.9
H502	48	296.9	231.7	107.6	62.35
H583	5*	107.6	15*	27.1	49.2

Araujo and Skogestad [34] also list the mole fractions of each component flowing through the synthesis loop. Because the Aspen model is based on an industrial synthesis reactor inert gases such as argon and methane are present in the loop. It is assumed that the baseline electric ammonia plant does not contain inerts. As an approximation, the mass flow rate occupied by the inerts was replaced by hydrogen, nitrogen and ammonia in their relative proportions. That is, the inerts were assumed to be zero but their mass was redistributed to hydrogen, nitrogen and ammonia and the new flow rates were used. Since the Araujo and Skogestad (2008) paper [34] was based on a 1650 metric tonne per day plant and the present analysis is based on a 300 metric tonne per day plant, all flow rates were nominally scaled by 300/1650. Note also that the recycle stream has approximately 6 times the flow rate of the input stream. This is due to the poor conversion efficiency which usually is between 10% and 20% of the feed stream.

Table 32 – Summary of calculations for redistributed gases to displace inerts

	H_2	N_2	CH_4	Ar	NH_3	Total Flow (kg/s)
Molecular Weight (g/mol)	2.02	28.00	16.00	39.95	17.00	
Mass Flow (kg/s)	14.2	57.8	6.0	10.4	26.1	114.3
Inerts Flow (kg/hr)	0	0	16.4	16.4	0	16.4
Ratios of Component Mass to Total Mass of Reactives	0.14	0.59	0	0	0.27	
New Flow Rates (kg/s)	16.5	67.4	0	0	30.4	114.3
Scaled Flow (kg/s)	3.01	12.28	0	0	5.54	20.83

Equation 57 can be used to determine the overall specific heat of the mixture once the stream compositions throughout the plant are known. The amount of heat transferred from one stream to another can now be calculated with knowledge the mass flow rate, composition, and the inlet and

outlet temperatures as shown in Equation 67. However, the temperature profile of both streams is likely to be different so the log mean temperature difference – given in Equation 68 – is used for sizing purposes. It is assumed that one stream is "hot" and the other is "cold" with each having an inlet temperature and an outlet temperature. Then, using Equation 102 together with knowledge of the overall heat transfer coefficient, U, the area of the heat exchanger can be calculated directly.

$$\dot{Q} = C_p \dot{m} \Delta T \qquad \textbf{Equation 67}$$

$$LMTD = \frac{(T_{H,i} - T_{C,o}) - (T_{H,o} - T_{C,i})}{\ln\left[\frac{(T_{H,i} - T_{C,o})}{(T_{H,o} - T_{C,i})}\right]} \qquad \textbf{Equation 68}$$

$$A = \frac{Q}{U \times LMTD} \qquad \textbf{Equation 69}$$

The U-values depend strongly on the types of fluids flowing through the heat exchanger, and also on their phase changes during entrainment. While many ammonia plants raise process steam with the heat exchangers for use with gas turbines, an electric plant does not. Therefore it is assumed that the cooling water does not change phase. Without knowing the exact operating conditions for an ammonia plant, sizing the heat exchangers is difficult. However, the composition of the fluids, their temperatures, pressures and flow rates are similar enough that a meaningful analysis can be done.

Operational ammonia plants do not publish the sizes of the equipment used so simplifying assumptions must be made. There are several resources available to aid in determining the U-values of particular heat exchanger configurations. First, Ulrich [152] and Woods [306] presents tables (Table 15, and Table 3-9, respectively) which have numerous heat exchanger configurations and process fluids; second, a design project at West Virginia University offered by

Shaeiwitz and Turton – authors of [296] – a contains U-values to be used for sizing heat exchangers; finally, a report from the University of Saskatchewan [311] presents the sizing of a gas to gas heat exchanger and the U value associated with it. As summarized in Table 33, there is enough information to estimate the size of the four assumed heat exchangers.

Table 33 – Approximate U-values for the major heat exchangers present in an ammonia synloop

U-Value (W/m^2K)	Fluids exchanging heat
865	Condensing ammonia vapor, nitrogen gas, hydrogen gas
500	Condensing ammonia vapor, nitrogen gas, hydrogen gas, cooling water
56	Ammonia vapor, nitrogen gas, hydrogen gas, cooling water

The intercoolers in the compressor train are also considered in this section. To size them essentially the same procedure is used as before but the temperatures, pressures and compositions of the fluids flowing through are prescribed by the size and operating pressure of the ammonia plant. The intercoolers are assumed to be cooled by water that is available at 278K and has a temperature increase of 10K. The U-value for the heat exchange is assumed to be 56 $\frac{W}{m^2K}$ which is the same for the synthesis loop heat exchanger. Equation 54 is used to determine the temperature increase across a single compressor. For a five stage compressor train, the pressure ratio across each compressor is 2.72 bar; using a starting temperature of 293K the final temperature will be 390K – an increase of 97K. If perfect intercoolers are assumed then the final temperature of the synthesis gas before it reaches the next stage will be the starting temperature at the first stage – 293K. Thus, the LMTD is the same for each intercooler. Finally, the heat transferred to the fluid by the compressor – given by Equation 55 – must be removed by the intercoolers. Since the inlet

temperature and pressure ratio are assumed to be the same for each compressor, the size of each intercooler will also be the same. The results of the above discussions are summarized in Table 34.

Table 34 – The approximate surface area of each of the major heat exchangers within the compressor train and synloop

Unit	Duty (MW)	LMTD (°C)	U (W/m^2K)	Total Surface Area (m^2)	Fluids
Intercoolers	4.60	45.00	56	1690	N_2, H_2, $H_2O(l)$
Condensing Gas to Gas	3.31	134.00	865	28.5	$NH_3(g)$, $NH_3(l)$, N_2, H_2
Cooling Water/Gas	5.72	305.00	56	332.2	$NH_3(g)$, N_2, H_2, $H_2O(l)$
Condensing Gas to Gas	10.67	62.50	865	197.5	$NH_3(g)$, $NH_3(l)$, N_2, H_2
Cooling Water/Gas	4.35	49.20	500	177	$NH_3(g)$, $NH_3(l)$,N_2, H_2, $H_2O(l)$

The intercoolers are by far the largest heat exchangers required in the ammonia synthesis loop with each on being over 420 m^2. The reason for this is that the feed stream has a relatively low temperature relative to the cooling medium (water) that is used. The result is a low LMTD and a low U-value which creates the need for large heat exchange surfaces.

6.3.7 Pumps

Pumps are a necessity in the synthesis loop because they provide the cooling water for the intercoolers and for the heat exchangers. To determine the size for the pumps, it is first necessary to determine the cooling water requirements.

For the intercoolers, the cooling water must carry away all of the heat that is imparted on the gas by the compressors. Thus, the cooling required is given by Equation 55. The cooling water is assumed to increase in temperature from 278K to 288K in the intercoolers. Using the standard

specific heat of water of 4.18 $\frac{kJ}{kgK}$ it is possible to find the mass flow rate of water through one intercooler via Equation 70:

$$\boldsymbol{H_2O_{cool} = \frac{\dot{Q}}{Cp_{H_2O}(T_2 - T_1)} = 27.5\frac{kg}{s}} \qquad \textbf{Equation 70}$$

The result must be multiplied by four to get the total cooling water for all intercoolers. The same procedure is applied to the two other water-cooled heat exchangers in the synthesis loop and the result is an additional 48.25 $\frac{kg}{s}$ of cooling water. The total cooling water requirements are then about 160 $\frac{kg}{s}$. Heuristics can be used to approximately size the pumps [153]:

$$\boldsymbol{P_{pump} = \frac{1.67\dot{m}_{H_2O}\Delta P}{\eta_{pump}}\ (kW)} \qquad \textbf{Equation 71}$$

where $\dot{m}_{H_2O}$ is the mass flow rate of water in $\frac{m^3}{min}$; ΔP is the pressure drop in the piping in bar, and η_{pump} is the efficiency of the pump.

If the reciprocating pump is assumed to have a pressure drop of 6 bar with a pump efficiency of 85%, then the total pumping power is 112 kW.

6.3.8 Synthesis Loop Capital Costs

This section details the capital cost calculations for the synthesis loop based on the discussion in the previous section. The major equipment for the synthesis loop includes the compressor train, the recycle compressor, the electric drivers for the compressors, the heat exchangers for the compressors and the synthesis loop, the adiabatic ammonia synthesis reactor, the knockout drum and a reciprocating pump. The sizing of each component was discussed in previous sections; the specifications for each piece of equipment are listed in Table 35.

Table 35 – Summary of the sizes and costs of the equipment required for a synloop

Heat Exchangers				
Type	**Material**	**Area (m^2)**	**Heat Duty (MW)**	**Installed Cost (2010$)**
Floating head	Stainless Steel	1690	4.60	3,016,600
Floating head	Stainless Steel	28.5	3.31	219,610
Floating head	Stainless Steel	332.2	5.72	610,520
Floating head	Stainless Steel	197.5	10.67	427,770
Floating head	Stainless Steel	176.8	4.35	400,450
Totals		**2425**	**28.64**	**4,674,950**
Compressors				
Type	**Material**	**Fluid Rating (MW)**	**Number**	
Centrifugal	Stainless Steel	1.02	5	2,216,200
Centrifugal	Stainless Steel	0.52	1	1,420,200
Totals				**12,501,200**
Drivers				
Type		**Shaft Rating (MW)**	**Number**	
Totally Enclosed		1.54	5	283,010
Totally Enclosed		0.78	1	210,720
Totals				**1,625,770**
Reactors				
Type	**Material**	**Volume (m^3)**	**Pressure (bar)**	
Packed Bed	Stainless Steel	7.54	150	1,686,900
Flash Drum	Stainless Steel	6.1	150	1,477,900
Totals				**3,164,800**
Pumps				
Type	**Material**	**Rating (kW)**		
Reciprocating	Carbon Steel	112		581,840
Total				**$22,548,560**

The cost parameters from [296] will again be employed to determine the installed costs for the major equipment in the synthesis loop. The cost parameters to be used with Equation 38 are listed in Table 36.

The costs of these pieces of equipment are free-on-board and must be updated to include the effects of inflation and the material and pressure factors that affect the installed cost. The inflation

index that is used in this study is the CEPCI, with all equipment being inflated to 2010 dollars. A factor of $\frac{550.8}{397}$ is used to bring the costs from 2001 dollars to 2010 dollars for all of the equipment.

Table 36 – Cost parameters used in this study

Equipment	K_1	K_2	K_3	Capacity, Units	Min Size	Max Size
Centrifugal Compressor	2.2897	1.3604	-0.1027	Fluid Power, kW	450	3000
Totally Enclosed Electric Drive	1.956	1.7142	-0.2282	Shaft Power, kW	75	2600
Floating Head Heat Exchanger	4.8306	-0.8509	0.3187	Area, m^2	10	1000
Reactor, Vertical	3.4974	0.4485	0.1074	Volume, m^3	0.3	520
Reciprocating Pump	3.8696	0.3161	0.122	Shaft Power, kW	0	200

6.3.8.1 Compressors and Drives

The compressors are not sensitive to pressure factors because they are by definition pressure changers. Thus, the construction of the compressor already assumes high operating pressures. However, the composition of the materials that flow through the compressors is different for different applications. In this case, the compressor train will only have to raise the pressure of a mixture of nitrogen and hydrogen. The nitrogen is inert so almost any metal can be used for fabricating the compressor. Nonetheless, hydrogen can cause serious damage to compressors made of carbon steel. The recommended materials for compressors processing hydrogen at the temperatures and pressures required for ammonia synthesis are stainless steel, nickel, copper, aluminum, or titanium [152]. Since stainless steel is the least expensive option it is selected as the fabrication material. The bare module material factor is listed as 5.8 for compressors made of stainless steel [296]. A similar logic can be applied to the recycle compressor which must process hydrogen, nitrogen and ammonia. Stainless steel also tolerates ammonia under the conditions within the synthesis recycle stream, though nickel might be a better choice. Regardless, stainless steel is selected for simplicity.

The drives for the compressors experience neither pressure effects nor corrosion effects. The cost factor is therefore based solely on installation, which adds 50% to the overall cost.

6.3.8.2 Heat Exchangers

There are 8 main heat exchangers within the synthesis loop – four intercoolers and four floating head heat exchangers within the recycle stream. The intercoolers are also assumed to be floating head heat exchangers for simplicity. Equation 44 is required to calculate the overall cost factor for the heat exchangers; Equation 42 is necessary to determine the pressure factor. The material used for fabrication is stainless steel because the same logic that was used for compressors is still valid for heat exchangers. The material factor for stainless steel heat exchangers is listed as 2.75 in Turton, et al. [296] The pressure factor required three constants to be used with Equation 42 as well as an assumed operating pressure. While the pressure will undoubtedly be different depending on the stage of compression or the point in the synthesis loop, the operating pressure is assumed to be 150 bar for every heat exchanger. The constants are $C_1 = 0.03881, C_2 = -0.11272, C_3 = 0.08183$ and the pressure factor becomes 1.52. The two constants to be used with Equation 44 are $B_1 = 1.63, B_2 = 1.66.$ Thus, the total cost factor for the heat exchangers is 8.56.

6.3.8.3 Pressure Vessels

The reactor and the knockout drum are essentially large pressure vessels that process the ammonia and the synthesis gases. Pressure vessels have specific design criteria so that catastrophic rupture can be avoided. As discussed previously Equation 43 is used to determine the pressure factor for both the ammonia synthesis reactor and the knockout drum. The dimensions of the synthesis reactor for a 300 tonne per day ammonia plant are assumed to be 7 meters tall and 1.4 meters wide. At an operating pressure of 150 bar the pressure factor is calculated to be 22.5. The material factor for the reactor is taken to be 3.1 since it is made of stainless steel. Finally, the

constants to be used in Equation 44 are taken to be $B_1 = 2.25, B_2 = 1.82.$ The final cost factor for the synthesis reactor is then:

$$F_{BM} = (2.25 + 1.82 \times 22.5 \times 3.1) = 118.18$$

The flash drum has similar characteristics to the reactor. The flash is sized to have 10 minutes of residence time of the liquid (ammonia); the size is then doubled to account for expansion [153]. The volume under these conditions is calculated to be 6.1 m^3. Using an aspect ratio of length to diameter equal to 4 [152]the diameter is 1.5 meters and the height is 6.25 meters – similar specifications to the reactor. Therefore, the cost factor is assumed to be the same for the flash drum.

6.3.8.4 Pumps

The pumps are simply moving fresh water through the system. Since fresh water is not terribly corrosive and the pressures at which the pumps are operating are relatively low, the material and pressure factors are 1.5 and unity, respectively. Equation 44 must be used again to determine the overall cost factor for the pumps, using $B_1 = 1.89$ and $B_2 = 1.35$ the cost factor is calculated to be 3.92.

6.3.8.5 Grass Roots Cost

Table 35 lists all of the equipment, the sizes or capacities necessary, and the costs. The costs were derived using Equation 38 with the constants listed in Table 36 and the bare module cost factors listed in Table 37. All of the equipment for a 300 tonne per day ammonia synthesis loop will cost approximately $22.1M in 2010 dollars.

Equation 46 and Equation 47 are used to estimate the total grass roots cost of the ammonia synthesis loop. The total bare module cost of all of the equipment in the synthesis loop is

$3.928M in 2010 dollars; the actual installed cost of the equipment is $22.55M in 2010 dollars. The contingency fee is 18% of the actual equipment costs, or $4.09M; the auxiliary facilities are assumed to be 50% of the bare module costs, or $1.96M. Finally, the total grass roots cost for the entire 300 tonne per day ammonia synthesis loop facility is $55.24M. The normalized capital costs are shown in Figure 42.

Table 37 – The bare module cost factors for the synthesis loop equipment

Equipment	F_{BM}
Centrifugal Compressor	5.80
Totally Enclosed Electric Drive	1.50
Floating Head Heat Exchanger	8.56
Reactor, Vertical	118.18
Reactor, Flash	118.18
Reciprocating Pump	3.92

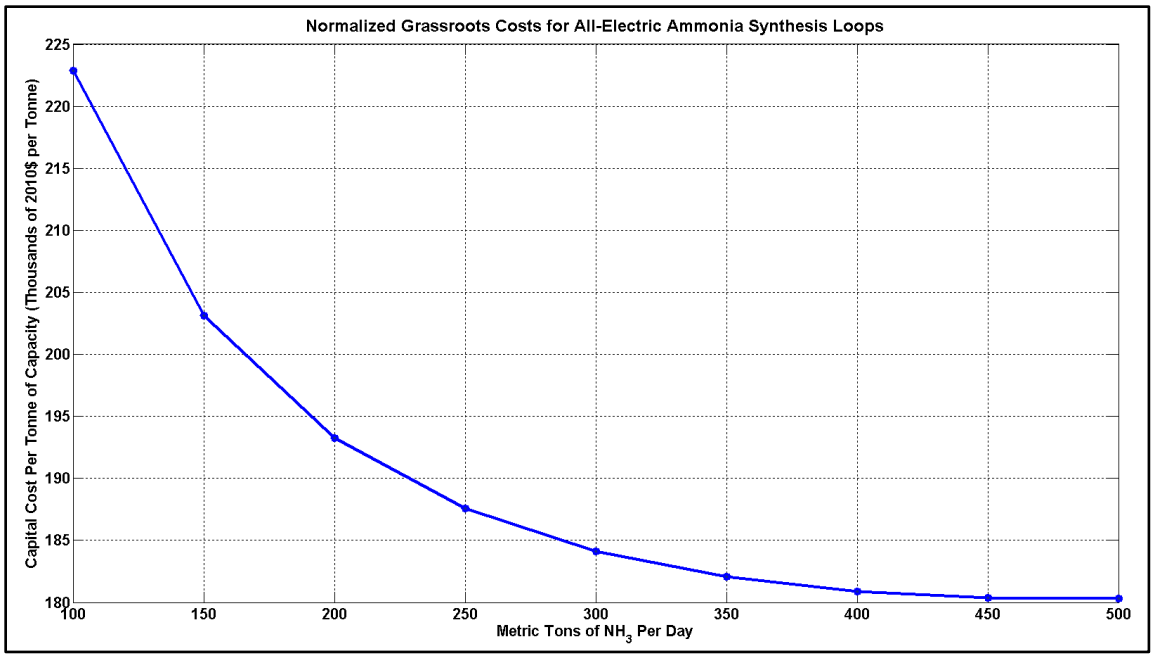

Figure 42 – A grassroots cost plot of small all-electric ammonia synthesis loops

The normalized grassroots costs for the synthesis loop decrease as the ammonia plant capacity increases. The decrease in cost is similar to traditional ammonia process plants which have been

getting larger to utilize economies of scale. In this case, the decrease in cost is mostly due to the economies of scale for the compressors, the reactor, and the heat exchangers.

6.3.9 Synthesis Loop Manufacturing Costs

The manufacturing costs in the synthesis loop involve the cost of the utilities and the cost of the labor, and can be calculated using Equation 49 and Equation 50, and Equation 51. Equation 52 will not be used, but is included for the interested reader. The raw materials and waste treatment costs for the synthesis loop are both assumed to be zero so Equation 49 becomes:

$$\boldsymbol{COM = 0.280FCI + 2.73C_{OL} + 1.23C_{UT}} \qquad \textbf{Equation 72}$$

The cost of the electrical utilities will be somewhat offset by the power produced by the wind turbines. The expected typical total cost must be assessed by means of an hourly simulation that considers the power produced by the wind, the cost of grid electricity and the selling price of electricity.

The labor for the synthesis loop is easily calculated using the data in

Table 35, with the handling steps for solids taken to be zero ($P = 0$). The number of heat exchangers is 8 (there are 4 intercoolers); there are 6 compressors (drivers are not included); and there are two reactors for a total of 16 pieces of equipment. Therefore:

$$N_{OL} = (6.29 + 31.7(0)^2 + \ 0.23 \times 16)^{0.5} = 3.16 \ \frac{Operators}{Shift}$$

The number of operators hired per one operator is assumed to be 4.5 [296] so the total operators per shift is taken to be:

$$3.16 \ \frac{Operators}{Shift} \times 4.5 \ Shifts = 14.2 \rightarrow 15 \ Operators$$

A basic chemical engineering worker made $28.32/hr in 2010 [312] which corresponds to a salary of $56,640/yr. The total labor cost is then $849,600/yr for the ammonia synthesis loop. The cost is assumed to be independent of the size of the synthesis loop in the range considered.

6.4 Hydrogen Production/Electrolyzers

Hydrogen production from electricity falls into three main processes: alkaline electrolysis (AE), proton exchange membrane (PEM) electrolysis, and solid oxide electrolysis (SOE). Of these processes, only AE and PEM are commercially viable, with SOE being relegated to the laboratory scale [285]. In general, PEM electrolysis systems have smaller capacities than their more mature alkaline counterparts. Furthermore, the normalized capital costs and the electricity requirements are both higher for PEM than for alkaline electrolyzers [313-314]. Thus, PEM electrolyzers are not yet technologically or economically viable for large scale production of hydrogen. Alkaline electrolyzers, by comparison, have the ability to produce more than a metric ton of hydrogen per day per unit [116, 285, 315-316]. The uninstalled costs of the unit are quoted as being $675 (in $2002) per uninstalled kW [288] for central hydrogen production from the grid.

Table 38 – State of the art hydrogen production technology from electrolysis of water [314]

Manufacturer	Technology	System Energy Requirement (kWh/kg)	Max H_2 Production Rate (kg/day)	Power Required for Max. H_2 Production Rate (kW)	H_2 Product Pressure (psig)
Avalence	Unipolar Alkaline	56.4 – 60.5	10	2-25	Up to 10,000
Proton	PEM	62.3 – 70.1	22	3-63	200
Teledyne	Bipolar Alkaline	59.0 – 67.9	90	17-240	60-115
Stuart	Bipolar Alkaline	53.4 – 54.5	195	15-360	360
Norsk Hydro	Bipolar Alkaline (high pressure)	53.4	129	48-290	230
Norsk Hydro	Bipolar Alkaline (atmospheric)	53.4	1041	240-2,300	0.3

6.4.1 Overview of Electrolysis Economics

The cost of hydrogen from an electrolyzer is dominated by the cost of electricity. This can be demonstrated using a simple economic model which considers capital costs, specific energy consumption, electricity costs and inflation and discount rates. Fixed operations and maintenance costs and variable costs are not considered in this analysis because they are a small fraction of the cost [286, 288]. The simple lifetime net present value of the system cost is the capital cost plus the cost of the electricity taken over a twenty year period, as shown in Equation 73.

$$C_{life} = C_{cap} + \frac{(k - k^{(1+life)})}{(1-k)}(OM_{cost}) \qquad \textbf{Equation 73}$$

$$k = \frac{(1+i)}{(1+d)} \qquad \textbf{Equation 74}$$

The variable *k* is equal to one plus the average inflation rate divided by one plus the average discount rate over the 20 year period. The capital costs are assumed to be paid in cash in year zero, so no loan is considered. The O&M cost is calculated by multiplying the number of operating hours by the electricity price by the operating power. Thus, the operating cost in year 1 is $931,000.

Using the data from Table 39 and Equation 73, the baseline plant has a lifetime NPV cost of about $14M over a 20 year period in 2010 dollars.

Table 39 – Baseline operating parameters for a Norsk Hydro 5040 Atmospheric electrolyzer [116, 288]

Cost Installed ($/kW)	$1,000
Operating Power (kW)	2330
Specific Energy (kWh/Nm^3)	4.8
Operating Capacity (Nm^3/hr)	485
Operating hours per year	8000
Electricity Price ($/kWh)	0.05
Discount Rate	7%
Inflation Rate	3%

The tornado chart in Figure 43 shows the sensitivity of the five parameters: capital costs, specific energy consumption, cost of electricity, discount rate and inflation rate. Clearly, the cost of electricity dominates the economics. When the electricity is $0.03/kWh, the cost is under $10M; when the cost is $0.15/kWh, the cost is nearly $40M. The inflation rate and the discount rate are also significant parameters because they dictate costs of the future payments.

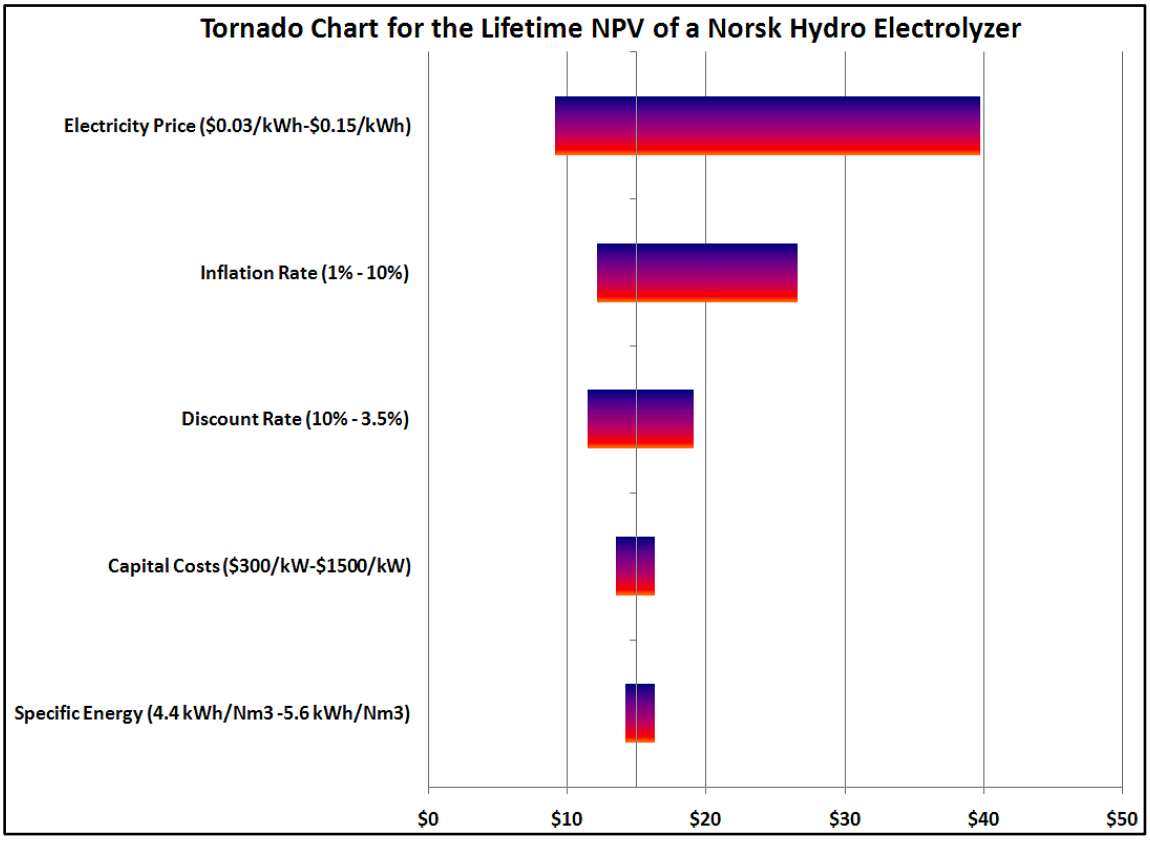

Figure 43 – Tornado chart for the simple lifetime cost of a Norsk Hydro 5040 electrolyzer

The best case scenario for the electrolyzer occurs when the left-hand values of the parameters on the y-axis of Figure 43 are used. Thus, the best case scenario is an electrolyzer that costs $5.4M in 2010 dollars. The worst case scenario occurs when the right-hand values are used in the same

figure. The cost is $132.8M in 2010 dollars – more than an order of magnitude difference over the lifetime of the electrolyzer.

6.4.2 Large Scale Electrolyzers

Large electrolyzer installations suffer from lack of economic economies of scale because they are frequently modular, prepackaged and arrive as a single unit [289]. Thus, the capital costs are assumed to be a function of the number of electrolyzers purchased, or the required hydrogen output [288]. Several reports and papers [243-244, 317] purport that future capital costs of electrolyzers will decrease based on the H2A analysis tool produced by the DOE [318] but no rationale is given for how the reduction will be accomplished. The present work offers a chemical engineering approach to capital cost reductions for large scale electrolyzer systems based on the H2A assumptions and information given in [288].

Scaling up chemical processing equipment common to each electrolyzer presents an opportunity to reduce the capital costs of large systems of electrolyzers. For example, rather than using multiple compressors or lye tanks, one central compressor train or one lye tank could be utilized. The ability to scale-up the size of the equipment rather than purchasing numerous smaller units results in significant cost savings.

6.4.2.1 Electrolyzer Cost Basis

Large electrolyzer installations are typically modular and do not exhibit economies of scale. This work offers an analysis using well-known chemical engineering scaling techniques to determine the capital costs associated with large-scale electrolytic hydrogen production. The major equipment common to Norsk Hydro electrolyzers is reviewed along with the associated scaling exponents. The equipment is then scaled up to meet the processing requirements of large electrolyzer systems. The costs of the scaled electrolyzer systems are calculated and compared to standard modular electrolyzer scaling. It is shown that scaling the compressors, the gas holding

tanks, the transformers and the balance of plant equipment can reduce the capital costs by as much as 60%.

The DOE's H2A program produced Excel spreadsheets that can be used to analyze the cost of producing hydrogen using electricity [288]. The capital costs for the electrolyzers are based on a quote of 11,620,000 Norwegian kroner by Norsk Hydro (now NEL Hydrogen) for a bipolar alkaline electrolyzer system (Atmospheric Type No.5040 - 5150 Amp DC) in 2002. The quote was exchanged to US dollars and inflated to 2005 prices for use in the spreadsheet. The final uninstalled capital cost was found to be $675/kW for a single 2330 kW electrolyzer.

However, when converting money from one currency to another across several years one needs to be mindful of the method used. For example, the H2A analysis tool exchanges Norwegian Kroner for US dollars in 2002 using the exchange rate listed in Table 40 [319]. The value is then inflated to dollars using the GDP deflator [320] for the United States from 2002 to 2005 (Table 41) to arrive at the total cost in dollars. If the Norwegian kroner are first inflated to 2005 kroner using the GDP deflator [321] then exchanged to dollars, the cost is nearly 35% higher, as shown in Table 42.

Table 40 – Exchange rates for Norwegian kroner and US dollars for 2002 and 2005 [319]

Year	Exchange Rates (NOK to USD)
2002	0.1261
2005	0.1553

Table 41 – General inflation for the US and Norway

Inflation, Norway (2002-2005)	Inflation, US (2002-2005)
1.188	1.085

Table 42 – The costs in 2005$ of a Norsk Hydro electrolyzer using two methods

Exchange First	Inflate First
$1,586,600 (2005 basis)	$2,139,500 (2005 basis)
$680/kW	$918/kW

To translate the costs across time and space another method has also been proposed: an average of every combination of inflating and exchanging [322]. This method mitigates the problem of using a single exchange rate for the conversion. The general formula for the averaging approach is given as:

$$C_n = C_1 \frac{\sum_{i=1}^{n} \left(\frac{I_n}{I_i}\right)\left(\frac{J_i}{J_1}\right) S_{k,i}}{n} \qquad \textbf{Equation 75}$$

Here, there are two price indicators, *I* and *J*, which refer to the inflation indices of the desired currency and the known currency, respectively; $S_{k,i}$ is the exchange rate to US dollars in year *i* for country *k*, and C_1 is the known cost in the foreign currency. The subscripts refer to the year with 1 being the first year and *n* being the last year of the time period. When *i* is equal to 1 in Equation 75, the term in the summation series represents exchange-inflate; when *i* is the last number in the summation series the term represents inflate-exchange.

To translate the electrolyzer costs to 2010 dollars, the original currency in the original year must be used – 11,620,000 Norwegian kroner. The GDP deflator for both Norway and the United States is used as a proxy for inflation; the average yearly exchange rates for each year translate the currencies. The full results are shown in Table 43 below. The average of all translated costs is $2,456,000 – almost a million dollars higher than the exchange-inflate value for 2002-2005. However, in this case, the exchange-inflate method yielded a value of $1,761,200 while the inflate-exchange method yielded $2,822,100 – two entirely different values from the 2002-2005 conversion.

The range of normalized costs is significant. The highest translated cost occurred in exchange year 7, when both the exchange rate and the inflation were at their maxima.

Table 43 – The averaging approach to currency conversion across time, as applied to electrolyzer costs

	GDP Deflator					
Year	**Norway**	**US**	**Exchange Rate**	**Exchange Year**	**Translated Cost (2010$)**	**Normalized Cost (2010$/kW)**
2002	84.2	92.19	0.1261	1	$1,761,200	$756
2003	86.7	94.13	0.1414	2	$1,991,600	$855
2004	91.8	96.78	0.1485	3	$2,154,000	$924
2005	100	100	0.1553	4	$2,374,900	$1,019
2006	108.7	103.24	0.1561	5	$2,513,400	$1,079
2007	112	106.23	0.171	6	$2,757,000	$1,183
2008	124.2	108.57	0.1796	7	$3,141,900	$1,348
2009	116.3	109.73	0.1597	8	$2,588,400	$1,111
2010	123.7	111	0.1656	9	$2,822,100	$1,211
				Averages	$2,456,000	$1,054

6.4.2.2 Electrolyzer Scaling

In 2007,the following cost breakdown was given for the Norsk Hydro Atmospheric Type No.5040 - 5150 Amp DC alkaline electrolyzer: electrolyzer unit – 32%; transformer/rectifier – 6%; compressor system – 29%; gas storage system – 15%; balance of the plant – 18%, which includes the lye tank, the H_2 scrubber, feed water purification, deoxidizer and the twin tank drier [288, 317]. The schematic of the electrolyzer is shown in Figure 44. It is assumed that the cost breakdown for the electrolyzer components is still valid. The costs for each subsystem are fractions of the translated 2010 dollar cost and are listed in Table 44 below.

Table 44 – Cost breakdown of a Norsk Hydro electrolyzer

Electrolyzer Subsystem	**Cost (2010$)**
1 Electrolyzer Stack	$786,000
1 Transformer/Rectifier Unit	$148,000
2 Compressor Units to 30 bar (435 psig)	$712,000
1 Gas Holder	$368,000
Balance of Plant, includes:	$442,000
- Gas Purifier (H_2 scrubber)	
- Feed Water Purifier/De-mineralizer	
- Lye Tank	
- Deoxidizer	
- Twin Tower Drier	
Totals	$2,456,000

The main scaling equation that will be employed is from classic chemical engineering texts [152-153, 301]:

$$\left(\frac{\boldsymbol{C_1}}{\boldsymbol{C_2}}\right) = \left(\frac{\boldsymbol{S_1}}{\boldsymbol{S_2}}\right)^{\boldsymbol{n}} \qquad \textbf{Equation 76}$$

The equation simply states that the ratio of the costs of two pieces of equipment – $\boldsymbol{C_1}$ and $\boldsymbol{C_2}$ – is related to the ratio of sizes of the same pieces of equipment – $\boldsymbol{S_1}$ and $\boldsymbol{S_2}$ in units of power, capacity, etc – by the exponent *n* – the scaling exponent. The scaling exponent changes for different equipment because some manufacturing processes utilize economies of scale better than others. In the case of pre-packaged electrolyzer plants, the scaling exponent for the facility is close to unity because the plant is modular.

In order to use Equation 76 to determine the scaled costs of equipment the sizes of the equipment, the original cost and the exponent need to be known. Fortunately, the fact that pre-packaged plants are modular simplifies the equation: *the equipment sizes for two plants is twice the size of a single plant*, three plants will require equipment that is three times a single plant, and so on. Then the term $\left(\frac{\boldsymbol{S_1}}{\boldsymbol{S_2}}\right)$ is equal to the number of pre-packaged electrolyzer plants of interest. Since the cost of the electrolyzer plant and the cost breakdown of the equipment are both known, the equipment scaling exponents are the only variables left to determine the scaled costs.

6.4.2.3 Selecting Scaling Exponents

Scaling exponents for equipment can be found in the literature (see [153, 297, 301, 307]) and are well known for compressors, tanks and the transformer/rectifier units. Together, these subsystems make up exactly half of the total cost.

The scaling exponent for a centrifugal compressor can be as low as 0.62 in terms of fluid power capacity [153], but electric drivers have scaling exponents of 0.75 in terms of shaft power. Taken together, a reasonable value of 0.7 is selected for scaling by the required power. Gas holders have extremely low scaling exponents, with values reaching as low as 0.43 for scaling with volume [307]. Transformers are an entirely different category than chemical engineering process equipment, though they do scale with rated capacity. The scaling exponent for the transformer/rectifier unit is taken to be 0.75 [323]. The balance of plant components could be scaled as well, though the exact cost breakdown is unknown. Often, in this situation the "six tenths rule" would be used as the scaling exponent. To be conservative, a value of 0.8 will be used. It can be assumed that the electrolyzer stacks do not scale well because they are essentially modular. The scaling exponents used as the baseline for this study are summarized in Table 45 below.

Table 45 – Assumed scaling exponents for the equipment analyzed in this study

Equipment, Capacity	Scaling Exponent
Compressor Scale, kW	0.7
Gas Holder Scale, Vol	0.5
Transformer/Rectifier, MVA	0.75
Balance of Plant, [ ]	0.8

6.4.2.4 Compressor scaling

Two compressors are used in the electrolyzer module, presumably in series, to pressurize the hydrogen to 30 bar for purification purposes [288]. While the size of the compressors is not given, it can be easily calculated using the specifications for the electrolyzer. The electrolyzers are rated at 1046 kg/day [289] which corresponds to a mass flow rate of 0.012 kg/s. Using a hydrogen gas constant of 4.124 $\frac{kJ}{kgK}$, and assuming an initial temperature of 293K and an initial pressure of 1 bar the fluid power requirement can be calculated using:

$$\dot{W}_{fluid} = T_{in} N \frac{n}{(n-1)} R\dot{m} \left[\left[\left(\frac{P_2}{P_1} \right)^{\frac{1}{N}} \right]^{\left(\frac{n-1}{n}\right)} - 1 \right] \qquad \textbf{Equation 77}$$

where N is the number of compressors (2), and n is the adiabatic exponent, taken to be 1.4. The fluid power required calculated to be 64 kW. It is assumed that the compression costs also include the compressor driver, which has a higher power rating according to the following equation:

$$\dot{W}_{driver} = \frac{\dot{W}_{fluid}}{\eta_i \eta_{drv}} \qquad \textbf{Equation 78}$$

where η_i is the isentropic efficiency of the compressor, taken to be 75%, and η_{drv} is the driver efficiency, taken to be 95%. Thus, the driver power requirement is 90 kW.

In order to scale the two compressors, an upper bound is needed for the practical size of the equipment. Since two compressors are to be used, the fluid power required per compressor is actually 32kW. If the electrolyzer plant is scaled to 50 times the base plant size, the compressor power will be 1600kW and the driver power will be 2250kW – well within the limits of compressors and drivers [296].

The scaling equation for the compressors takes the form:

$$C_{comp} = \$712(X)^n \qquad \textbf{Equation 79}$$

where C_{comp} is the scaled cost of the compressors in thousands of 2010 dollars, the original compressor cost is taken from Table 44, X is the number of electrolyzers of interest, and n is the scaling exponent with a value of 0.7.

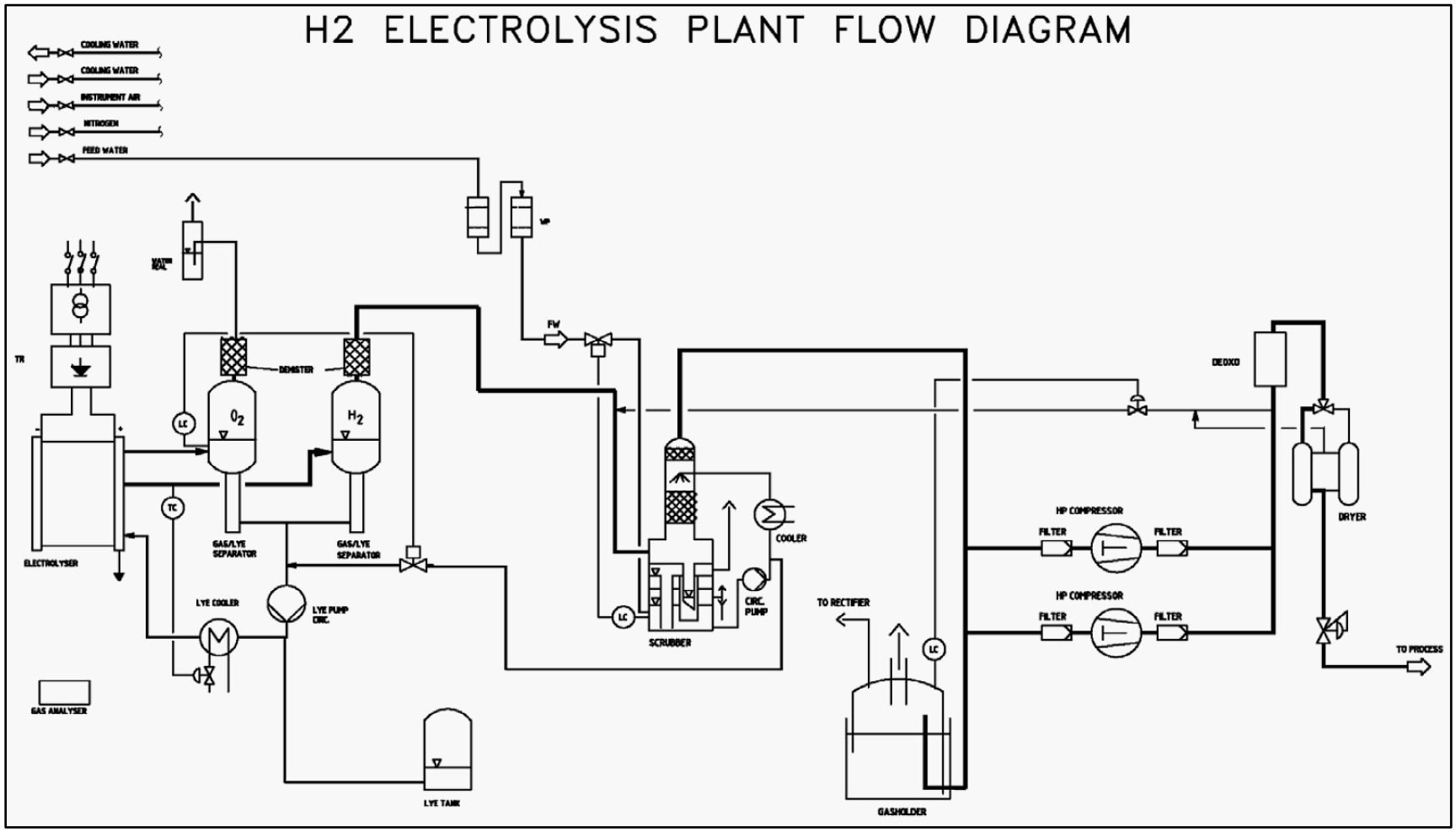

Figure 44 – The schematic of an electrolysis plant [317]

6.4.2.5 Gas holder scaling

The tank used in the electrolyzer plant is a "gas holder", which probably stores the hydrogen at atmospheric pressure, as seen in Figure 44. The actual size of the tank is unclear, but its high cost is probably related to the material used for construction. The price of tanks is related to the quantity of material which is proportional to the surface area. The following derivation is from [152], modified for cylindrical tanks. For a cylindrical tank the volume is:

$$V_{t,1} = \pi R_{t,1}^2 H \qquad \textbf{Equation 80}$$

The ratio of the volume of two tanks with the same height and different radii is:

$$\frac{V_{t,1}}{V_{t,2}} = \left(\frac{R_{t,1}}{R_{t,2}}\right)^2 \qquad \textbf{Equation 81}$$

For a cylindrical gas holder the ratio of length to diameter ranges from 1 to 2 [152]. If a mean value of 1.5 ($H = 1.5D = 3R$) is used then the ratio of volumes becomes

$$\frac{V_{t,1}}{V_{t,2}} = \frac{3\pi R_{t,1}^3}{3\pi R_{t,1}^3} = \left(\frac{R_{t,1}}{R_{t,2}}\right)^3 \qquad \textbf{Equation 82}$$

Since the cost is proportional to the surface area:

$$A_{t,1} = 2(\pi RH + \pi R^2) \qquad \textbf{Equation 83}$$

The ratio of the surface area of two tanks with an aspect ratio of 1.5 is

$$\frac{A_{t,1}}{A_{t,2}} = \left(\frac{R_{t,1}}{R_{t,2}}\right)^2 \qquad \textbf{Equation 84}$$

Since the total cost, C_t, depends on the cost per area, C_a, it is linearly proportional to the surface area:

$$C_{t,1} = A_{t,1} C_a \qquad \textbf{Equation 85}$$

which implies

$$C_{t,1} = C_{t,2}\left(\frac{R_{t,1}}{R_{t,2}}\right)^2 \qquad \textbf{Equation 86}$$

Finally, since Equation 82 implies

$$\left(\frac{R_{t,1}}{R_{t,2}}\right) = \sqrt[3]{\left(\frac{V_{t,1}}{V_{t,2}}\right)} \qquad \textbf{Equation 87}$$

Equation 86 becomes

$$C_{t,1} = C_{t,2}\left(\frac{V_{t,1}}{V_{t,2}}\right)^{2/3} \qquad \textbf{Equation 88}$$

Equation 88 predicts that the scaling exponent for a tank should be in the range of 0.66. Indeed, many tanks are in this range or lower. This study assumes a value of 0.5 for the gas holder since it operates at ambient pressure. The cost equation for scaling tanks becomes

$$C_{tank} = \$368X^{0.5} \qquad \textbf{Equation 89}$$

where C_{tank} is the cost of the tank in thousands of 2010 dollars, and X is the number of electrolyzers.

6.4.2.6 Transformer/Rectifier

The electrolyzer units operate at 2330 kW DC power at 5150 amperes. Each transformer unit must convert the incoming AC power into the DC power for use in the electrolyzer. If the efficiency of the transformer unit is taken to be 95% [324] and the rectifier efficiency is taken to be 95% [238], then the total efficiency is 90% for the unit. Then the transformer/rectifier rating will be 2589 kW.

A cost equation for large scale 100MVA+ transformers was developed using industry data [323]. The equation relates the rated power of the transformer in MVA to the cost in millions of 2004 euros:

$$C_{trans} = 0.03327P^{0.7513} \quad \textbf{Equation 90}$$

The currency has no influence over the scaling exponent since each cost in euros would simply be scaled by the same factor to convert to dollars. Accordingly, the scaling exponent for transformers is taken to be 0.75:

$$C_{trans} = \$148X^{0.75}$$

where C_{trans} is the transformer cost in thousands of 2010 dollars and X is the number of electrolyzers.

6.4.2.7 Balance of Plant

From Table 44, the balance of the plant consists of a hydrogen scrubber that purifies the hydrogen stream from the electrolyzer stack, a feed water purifier that consists of a reverse osmosis unit and a demineralizer , a "lye tank" for storing the potassium hydroxide solution; a deoxidizer and a twin tower drier. Together, this equipment costs $442,000.

There is some opportunity to scale the equipment, but an exact number cannot be determined without the cost contributions to the total balance of plant cost. The estimated scaling exponents for the equipment are listed in Table 46.

Table 46 – Scaling exponents for the balance of plant equipment

Equipment	Scaling Exponent	Reference
Gas Purifier (H_2 scrubber)	0.81	[325]
Feed Water Purifier/De-mineralizer (RO Unit)	1	[326]
Lye Tank	0.5	[152]
Deoxidizer (Burner)	0.82	[325]
Twin Tower Drier	0.38	[307]

An unweighted average of the scaling exponents gives a value of 0.75 for the balance of plant scaling factor. A scaling exponent value of 0.8 is selected to be conservative.

The scaling equation for the balance of plant components is:

$$\boldsymbol{C_{BoP} = \$442X^{0.8}} \qquad \textbf{Equation 91}$$

where C_{BoP} is the cost of the balance of plant in thousands of 2010 dollars and X is the number of electrolyzers.

6.4.3 Results

The above analysis was used to scale the electrolyzer hydrogen production plants. The number of equivalent electrolyzer plants is the total hydrogen generation capability divided by the maximum output for an electrolyzer. Each subsystem is scaled according to the corresponding scaling equation and the scaled costs for each subsystem are shown in Figure 45. The total cost for the equivalent electrolyzer plant is the sum of the costs for the scaled subsystems and the cost of the electrolyzer stacks required to produce the hydrogen. Thus, the total cost in thousands of 2010 dollars for X electrolyzers equivalent is:

$$\boldsymbol{C_{plant} = \$786X + \$712X^{0.7} + \$148X^{0.5} + \$368X^{0.75} + \$442X^{0.8}} \qquad \textbf{Equation 92}$$

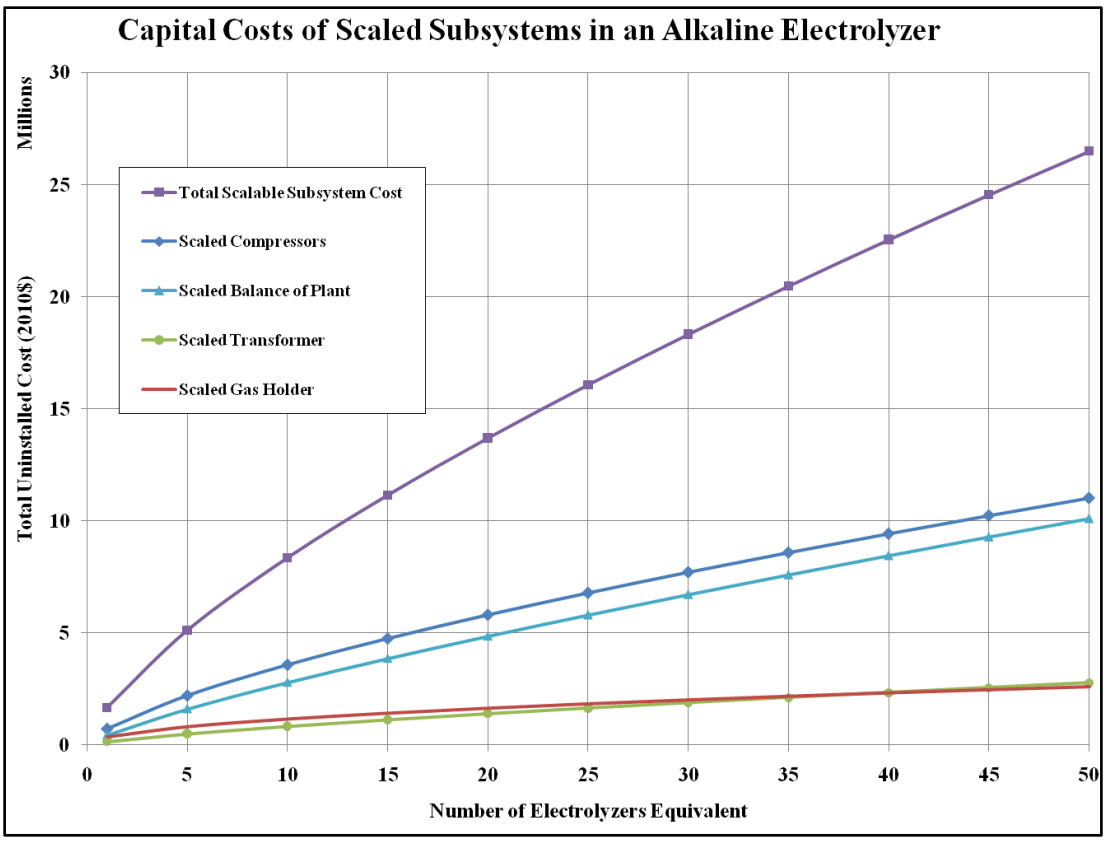

Figure 45 – The capital costs for scaled subsystems within a Norsk Hydro alkaline electrolyzer

Figure 46 shows the total uninstalled costs for an electrolyzer plant that utilizes scaling for all major subsystems with the exception of the modular electrolyzer banks. The results suggest that with scaling the equipment costs for a 50,000 kg/day plant could cost as much as 46% less than the modular plants.

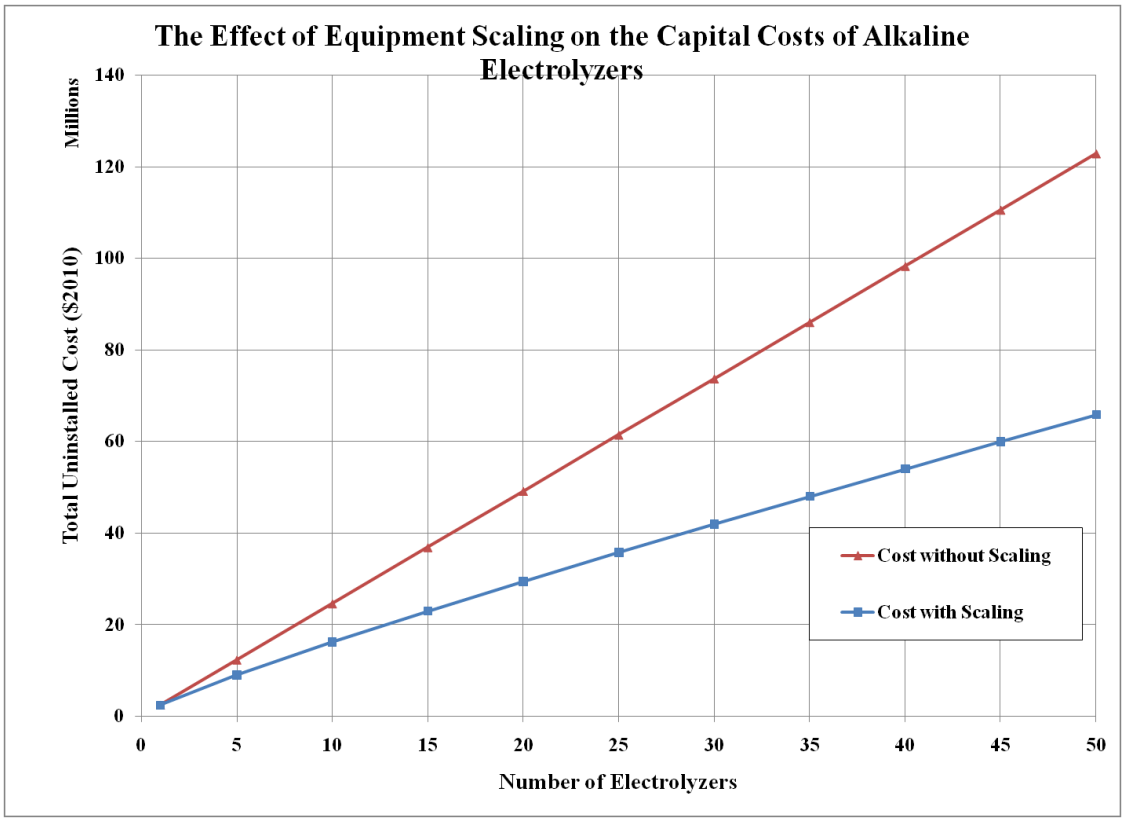

Figure 46 – The total uninstalled costs for scaled and unscaled electrolyzers

The results are significantly affected by the scaling exponents of each subsystem. Several scenarios were used to show the sensitivity to the scaling exponents. The best-, mid- and worst-case assumptions are shown in Table 47, along with the case of no scaling, where all exponents are unity. None of the systems should have scaling of unity or greater, and some, such as the gas holder may have values lower than the original assumption. The three scenarios attempt to give reasonable bounds for the scaling exponents of each of the subsystems.

Table 47 – The scenarios used for sensitivity analysis

Equipment	Best Case	Mid Case	Worst Case	No Scaling
Compressor	0.5	0.7	0.9	1
Tank	0.3	0.5	0.7	1
Transformer	0.5	0.7	0.9	1
Balance of Plant	0.5	0.7	0.9	1

The four cases are shown in Figure 47. All cases show significant cost reduction over the unscaled electrolyzer plant with the "best" scenario showing nearly 60% decrease in cost.

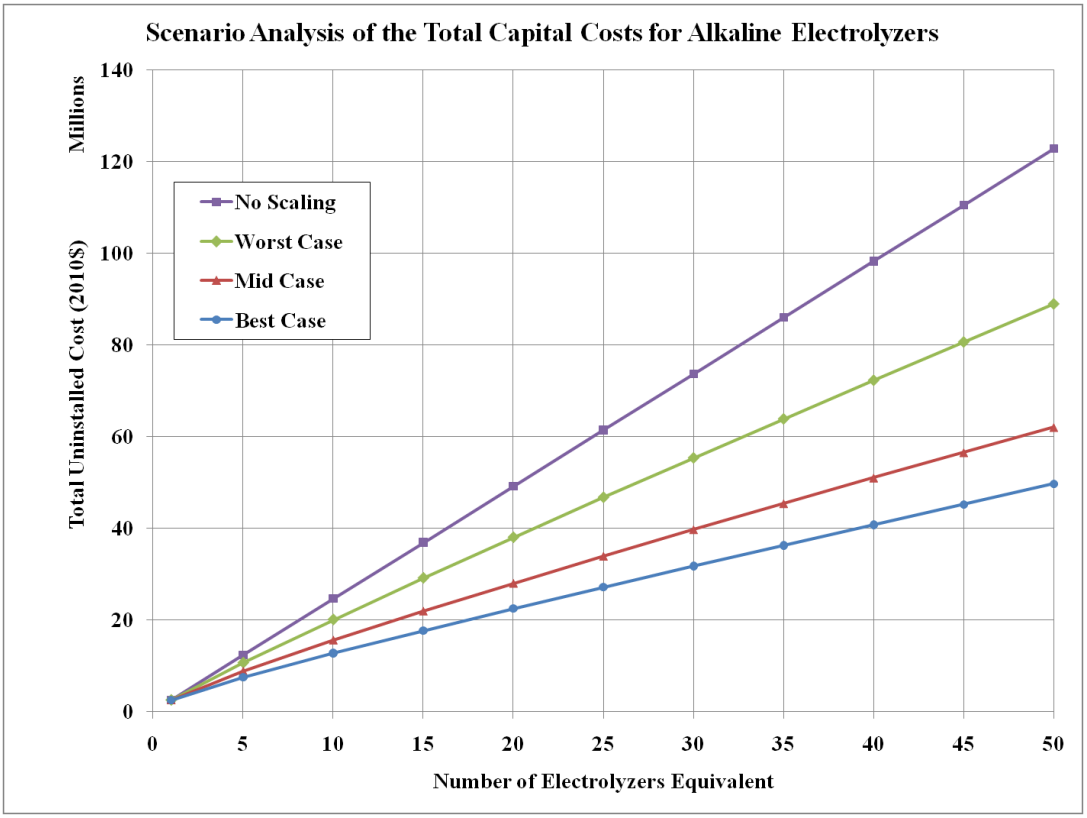

Figure 47 – The effect of different scaling exponents on the uninstalled costs of alkaline electrolyzers

The individual subsystems effect on the sensitivity is shown in a tornado chart in Figure 48. Clearly, the scaling exponent for the compressors has the largest influence on the capital cost. Changing the compressor scaling exponent from 0.5 to 0.9 results in a capital cost increase of nearly $10 million for the 50 electrolyzer equivalent plant.

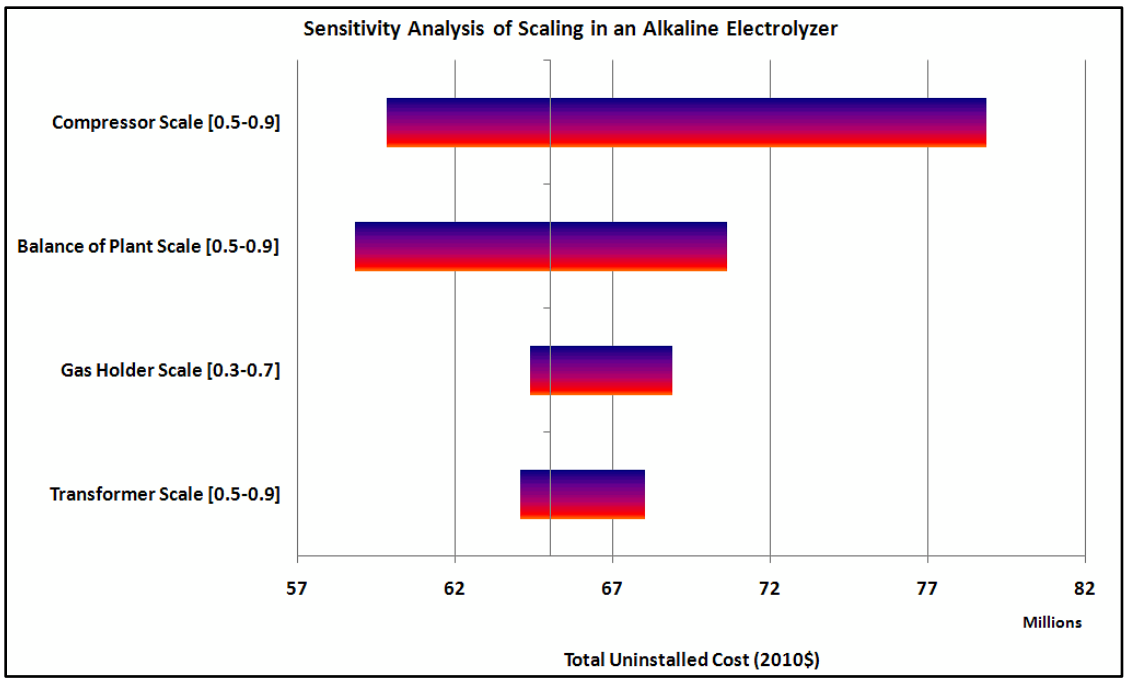

Figure 48 – Tornado chart for the scaling of equipment in an alkaline electrolyzer

6.4.4 Conclusions

Major capital cost reductions are possible for large scale electrolyzer systems if manufacturers use a chemical plant approach to electrolytic hydrogen production. It was shown that economies of scale are practical for electrolytic hydrogen plants, with capital cost reductions as high as 60%, based on the economics of a Norsk Hydro Atmospheric Type No.5040 electrolyzer. Furthermore, utilizing a single compressor train rather than numerous small compressors has the largest effect on capital cost reduction.

6.5 Air Separation

Air separation technologies isolate the three main constituents of air – nitrogen, oxygen and argon – into pure streams for industrial applications. Nitrogen, oxygen and argon are now used in a wide variety of industries ranging from metals production, electronics, welding and petroleum

refining [327]. The separation of air is a complex, energy intensive process that generally falls into three major categories: membrane separation, pressure swing adsorption and cryogenic air separation. The selection of the air separation process is driven by the required product, quantity of desired product and its purity. Large volumes of ultra-pure gaseous nitrogen can only economically and realistically be achieved using cryogenic air separation [129].

The capital cost of cryogenic air separation plants are not adequately discussed in the literature, probably because the designs are proprietary. However, the equipment that is used in a cryogenic air separation facility is available in standard chemical engineering textbooks, as well as in many academic papers [209-210, 301]. The entire process is well understood and can be modeled using standard simulation software such as Aspen or COCO. Once the process is simulated for a given product, purity and flow rate, the equipment used in the plant can be sized and costed to determine the capital cost of the entire facility. This section focuses on the framework for determining the capital costs for a cryogenic air separation facility for ultra-high purity gaseous nitrogen for volumetric flow rates of about 8900 Nm^3/hr. A typical ASU schematic is shown in Figure 49 [328].

Cryogenic air separation exploits the boiling point difference in the three main constituents of air – nitrogen, oxygen and argon whose boiling points are 77.4 K, 90.2 K, and 87.3 K, respectively. The process is highly nonlinear, tremendously complex and involves numerous fluid flows and components. Cryogenic air separation plants are divided into a warm section which is comprised of compression, drying, and purification, and a cold section that houses the heat exchanger and the distillation columns. The general process design of a cryogenic air separation plant involves the following steps:

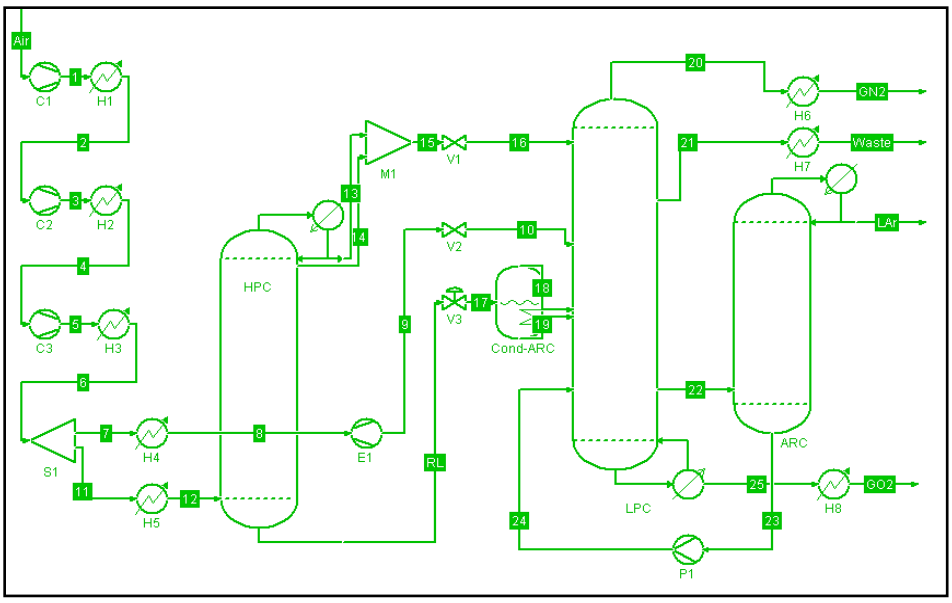

Figure 49 – A schematic on an air separation unit (ASU) for the production of nitrogen, oxygen and argon [328]

- Air is compressed and cooled with intercoolers to remove any water vapor
- The dry air stream is purified to remove contaminants such as carbon dioxide and residual water vapor
- The air is cooled using the waste product oxygen and purified nitrogen from the distillation column, further deducing contaminants
- The air is further cooled down using Joule-Thompson cooling in an expander
- The air is distilled into its components using a multiple distillation columns

A simplified version of a process for producing liquid argon, and gaseous nitrogen and oxygen is shown in Figure 50.

A simulation of an air separation plant using COCO software [329] showed that heat exchanger duty, compressor power, and expander size all scaled linearly with the air intake flow rate. The distillation tower sizes are valid over a broad range of plant outputs as shown in the simulation. In practice the towers would be scaled up or down to match the plant characteristics. However,

tower sizing is non-trivial and depends on several operating and performance parameters. The model used in this thesis adopts the tower dimensions used within the COCO ASU simulation [329]. The column dimensions for the high-pressure column (HPC), the low-pressure column (LPC) and the argon condenser (ARC) are summarized in Table 48.

Table 48 – Column dimensions for an ASU [328]

	HPC	LPC	ARC
Diameter (m)	2.44	2.25	0.62
Height (m)	28.84	44.09	74.59
Volume (m^3)	134.85	175.31	22.52

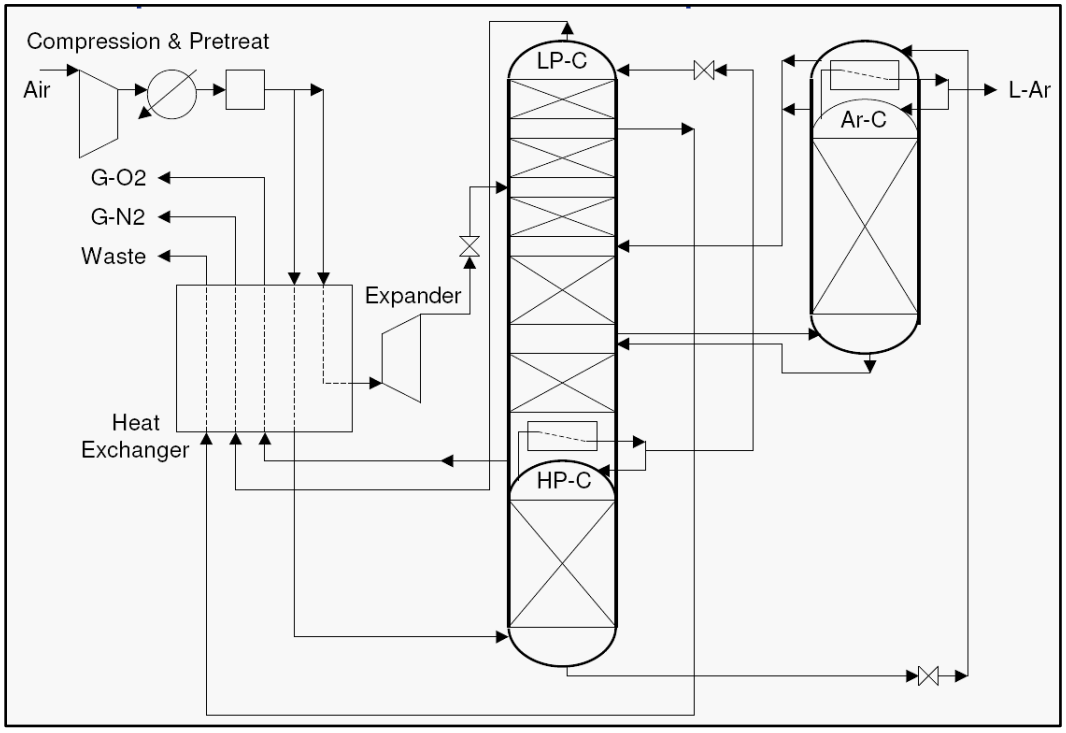

Figure 50 – A schematic of a cryogenic air separation facility [328]

6.5.1 Compression and expansion

The compression section of the cryogenic plant involves centrifugal compressors coupled with intercooling to raise the pressure to approximately 8 bar. The size of the compressors in the compressor train is then related to the flow rate and temperature of the air intake as shown in Equation 93.

$$\dot{W}_{fluid} = T_{in} N \frac{n}{(n-1)} R\dot{m} \left[\left[\left(\frac{P_2}{P_1} \right)^{\frac{1}{N}} \right]^{\left(\frac{n-1}{n}\right)} - 1 \right] \qquad \textbf{Equation 93}$$

The compression train often employs intercoolers to minimize the compression work required. Consequently, the heat exchangers are tasked with removing the heat imparted on the air by the heat compressors. The outlet air temperature will be raised – according to Equation 94 – commensurate with the pressure differential across the compressor. The heat duty of the heat exchanger will then be related to both the mass flow rate and the required temperature across the heat exchanger, as shown in Equation 95.

$$T_{out} = \left[\frac{P_2}{P_1} \right]^{\left(\frac{n-1}{n}\right)} \qquad \textbf{Equation 94}$$

$$\dot{Q} = \dot{m}(T_{out} - T_{in}) C_{p,mix} \qquad \textbf{Equation 95}$$

Because the total pressure change is 8 bar, using two compressors and two intercoolers is likely. The pressure across each compressor is equal to $\sqrt{8} = 2.83$ bar.

The shaft power is typically used when determining the overall costs of compressors [296] and differs from the fluid power that was calculated in Equation 93. The power required to turn the compressor is the fluid power divided by the isentropic efficiency of the compressor, as shown in

Equation 96. The isentropic efficiency is taken to be 75%, as given in [152], Table 4-9. Thus, the actual power needed at the shaft is about 25% higher than required by the fluid.

$$\dot{W}_{shaft} = \frac{\dot{W}_{fluid}}{\eta_i} \qquad \textbf{Equation 96}$$

The Joule-Thompson cooling is done via throttling and expansion throughout the process. The expander takes high pressure air and expands it through a turbine to create power. The energy recovered from the expander is assumed to be negligible.

Table 49 – The compressors for an ASU

	Compressors	
Type	**Material**	**Rating (kW)**
Centrifugal	Stainless Steel	379
Centrifugal	Stainless Steel	362.5
Centrifugal	Stainless Steel	413.5
Totals		**1155**

6.5.2 Drivers

Each compressor is driven by its own electric motor ("driver"). The power requirements for the drivers are determined by dividing the shaft power of the compressor by the efficiency of the electric motor. The electric motor efficiency is generally greater than 90% and increases with the rated operating power and the turndown ratio [153]. Because the ammonia synthesis happens at steady state and the compression power required for small plants is in the MW range, an efficiency of 95% is assumed for this analysis. Equation 97 summarizes the power requirements for the shafts of the drivers. Here, $\dot{W}_{fluid}$ is calculated from Equation 93, and the isentropic efficiency, η_i, is taken to be 75%. To determine the total input power requirements the right-hand side (RHS) of Equation 96 must be divided by the efficiency of the driver, η_{drv}, which is taken to

be 95%. The full equation for the input power required by the driver is given in Equation 97 below.

$$\dot{W}_{driver} = \frac{\dot{W}_{fluid}}{\eta_i \eta_{drv}} \qquad \textbf{Equation 97}$$

A summary of the driver ratings, the total number required and their costs is shown in Table 50.

Table 50 – Compressor drivers and ratings for an ASU

Drivers			
Type	**Rating (kW)**	**Number**	**Cost (2010$)**
Totally Enclosed	505.3	1	105,050
Totally Enclosed	483.1	1	103,360
Totally Enclosed	551.3	1	108,330
Totals	**1539.7**		**$316,740**

6.5.3 Heat Exchangers

The main heat exchanger in a cryogenic air separation facility is the "cold box" – a large multi-stream brazed aluminum heat exchanger that cools incoming warm air against the cooler waste and product streams [330]. The total volume, *V*, of the heat exchanger can be estimated for costing purposes from the heat duty and the average temperature difference between the streams, as shown in Equation 98 [128].

$$\boldsymbol{V = \frac{Q}{C \times dT}} \qquad \textbf{Equation 98}$$

$$\boldsymbol{A = V \times A_\rho = \frac{Q A_\rho}{C \times dT}} \qquad \textbf{Equation 99}$$

Here, *Q* is the total heat duty of the cold box in Watts; *C* is a constant, taken as 50,000 $\frac{W}{m^3 K}$; and *dT* is the average temperature difference of all the streams exchanging heat within the cold box,

taken as 5K. The area of the heat exchanger can then be found by assuming a value for the surface density (A_ρ) of the fins on the plate-fin exchanger. Values for air separation range from 500 – 1500 $\frac{m^2}{m^3}$ [128, 331] so a value of 1000 $\frac{m^2}{m^3}$ was selected for this analysis. It should be noted that the driving temperature difference here is assumed to be 5K. Since the heat exchanger is a multi stream exchanger the traditional equation for the log mean temperature difference is not valid. However, a lumped approach can be taken around the entire exchanger where the streams have an effective bulk outlet and inlet temperature [332]. Finally, the total heat exchanger area for the cold box is the product of the volume (Equation 98) and the surface density (A_ρ), as shown in Equation 99.

The intercoolers are standard, water cooled, liquid-gas heat exchangers. The process air stream is assumed to be cooled to the inlet temperature at each step, which is a function of the pressure increase across the compressor. Accordingly, the total heat duty for the heat exchangers is given by Equation 100 in which the C_p value for air is taken to be 1.3 $\frac{kJ}{kgK}$. If the cooling water temperature increase is assumed to be 10°C, the log mean temperature difference can be calculated using Equation 101 and the heat exchanger area can be calculated using Equation 102. The major heat exchanger sizes, materials, areas and heat duties are summarized in

Table 51.

$$\dot{Q} = C_p \dot{m} \Delta T \qquad \textbf{Equation 100}$$

$$LMTD = \frac{(T_{H,i} - T_{C,o}) - (T_{H,o} - T_{C,i})}{\ln\left[\frac{(T_{H,i} - T_{C,o})}{(T_{H,o} - T_{C,i})}\right]} \qquad \textbf{Equation 101}$$

$$A = \frac{Q}{U \times LMTD} \qquad \textbf{Equation 102}$$

Table 51 – Major heat exchangers, sizes and heat duties in an ASU

Heat Exchangers			
Type	**Material**	**Area (m^2)**	**Heat Duty (MW)**
Floating head	Stainless Steel	121.32	0.33
Floating head	Stainless Steel	127.56	0.364
Floating head	Stainless Steel	188.19	0.468
Plate-Fin	Brazed Aluminum	2855.69	1.29
Totals		**3292.76**	**2.452**

6.5.4 Towers

The distillation towers fractionate the air using several stages which are implemented as trays within the column. A temperature gradient exists within the column, usually with the bottom being hot and the top being colder. The trays within the column separate the vapor-liquid equilibrium, and the volatile mixture condenses on the tray. As the mixture rises through the temperature gradient, the more volatile component remains in the vapor state while the less volatile component flashes to liquid and returns to the bottom.

The size of the column can be determined through use of the Fenske Equation, Underwood's equations and the Gilliland correlation [152, 301], but the details of column sizing are beyond the scope of this work. See basic texts [301, 307] on chemical engineering and distillation for more information.

Instead, the simulation program COCO was used to determine the number of stages required, which is indifferent to the feed rate, but depends on the product purity. The number of trays, height and diameter for the low pressure, high pressure and argon columns are given in Table 52, for high purity (99.999 mol%) nitrogen. Kerry also states that the number of plates may be as high as 90 for ultra-pure nitrogen [126]. The assumption of 45 trays will be used for economic purposes.

The oxygen and argon products can also be distilled from the air at the additional cost of large columns many stories tall, additional compression power to compensate for the pressure drops and the necessary storage.

A simulation of an air separation plant using COCO software [329] showed that all of the heat exchangers, compressors, and expanders scaled linearly with the air intake flow rate. The distillation tower sizes are valid over a broad range of plant outputs as shown in the simulation. In practice the towers would be scaled up or down to match the plant characteristics.

Table 52 – Columns specifications for an air separation unit

Column	Trays	Height (m)	Diameter (m)	Volume (m^3)	Pressure (bar)
High Pressure Column	45	28.84	2.44	134.85	6
Low Pressure Column	70	44.09	2.25	175.3	1.8
Argon Column	120	74.59	0.62	22.5	1.3

6.5.5 Economics of Air Separation

As discussed in the previous section, a cryogenic air separation unit is a series of compressors, drivers, heat exchangers, distillation columns and expanders. The cost data for the equipment to be used in Equation 42 are presented in Table 53. Equation 39 will be needed to update the bare module costs from 2001 dollars to 2010 dollars. All costs quoted herein are in 2010 dollars.

Table 53 – The cost constants for the major pieces of equipment in an ASU

Cost Constants	K_1	K_2	K_3	Capacity, Units	Min Size	Max Size
Centrifugal compressor	2.2897	1.3604	-0.1027	Fluid Power, kW	450	3000
Floating Heat HX	4.8306	-0.8509	0.3187	Area, m^2	10	1000
Radial Gas	2.2476	1.4965	-0.1618	Fluid Power, kW	100	1500
Towers	3.4974	0.4485	0.1074	Volume, m^3	0.3	520
Drivers	2.9508	1.0688	-0.1315	Shaft Power, kW	75	2600

6.5.5.1 Heat Exchangers

The compact plate and fin heat exchanger that is used for the cold box was not included in the equipment list in Turton, et al. (2009). Cost data are available for compact heat exchangers, the cost of which can be approximated using Equation 103 (updated to \$2010) where A is the heat exchange area of the cold box in square feet. The equation is valid for stainless-steel compact plate and fin heat exchangers with areas of greater than 200 ft^2, and pressures of up to 10 bar [333].

$$\boldsymbol{Cost = 189A^{0.6907}} \qquad \textbf{Equation 103}$$

The installation costs for the compact heat exchanger are not included in the cost equation. If the heat exchanger data in Turton et al. is assumed to be valid for this case, then Equation 104 can be used to determine the bare module cost factor. A brazed aluminum heat exchanger is assumed so the materials constant is taken to be 1.5; since Equation 103 is valid for pressures up to 10 bar, no pressure factor is needed, i.e. $F_P = 1$.

$$\boldsymbol{F_{BM} = (B_1 + B_2 F_P F_M)} \qquad \textbf{Equation 104}$$

Table 54 – Coefficients for the bare module cost factor of heat exchangers and towers.

Coefficients for Equation 104		
	B1	B2
Heat Exchangers	0.96	1.21
Towers	2.25	1.82

Thus, the bare module cost equation becomes:

$$\boldsymbol{C_{BM} = C_p^o F_{BM} = C_p^o(0.96 + 1.21 \times 1.5) = 2.775\, C_p^o} \qquad \textbf{Equation 105}$$

All of the intercoolers are assumed to be made of carbon steel so both the materials factor and the pressure factor are equal to 1 and the total bare module factor is the sum of the coefficients B_1 and B_2, or $2.17C_p$.

6.5.5.2 Compressors

The compression train is tasked with increasing the pressure of the intake air, from ambient pressure to a final pressure of 8 bar. It is assumed that standard carbon steel, centrifugal compressors are used since air is relatively inert and non-corrosive. The cost of these machines is related to the fluid power required in the application, which can be calculated using Equation 93. The installation factor is taken from Figure A.19 in [296] to be 2.75. A summary of the compressors, their rating and costs in 2010 dollars is shown in Table 55.

Table 55 – Compressors used in an ASU

Compressors				
Type	**Material**	**Rating (kW)**	**Uninstalled Cost**	**Installed Cost**
Centrifugal	Stainless Steel	379	$180,720	$496,980
Centrifugal	Stainless Steel	362.3	$174,070	$478,690
Centrifugal	Stainless Steel	413.5	$194,210	$534,080
Totals		**1154.8**	**$549,000**	**$1,509,750**

6.5.5.3 Drivers

The drivers are required to turn the compressors. For costing purposes they are rated in shaft power, which is related to the compressor fluid power by the efficiency of both the driver motor and the compressor, as shown in Equation 97. They are assumed to be totally enclosed all-electric motors made of carbon steel. They are subjected only to ambient pressures and temperatures, and do not come into contact with any corrosive substances. The installation factor for drives is taken to be 1.5, as shown in Figure A.19 in [296]. The three drivers, their rating, and their associated costs in 2010 dollars are shown in Table 56.

Table 56 – The drives used in conjunction with the compressors in an ASU

Drivers			
Type	Rating (kW)	Uninstalled Cost	Installed Cost
Totally Enclosed	505.3	$105,050	$157,580
Totally Enclosed	483.1	$103,360	$155,040
Totally Enclosed	551.3	$108,330	$162,500
Totals	**1539.7**	**$316,740**	**$475,120**

6.5.5.4 Towers

The distillation towers in an ASU are used to separate the air; for an ammonia synthesis process only the low pressure distillation column is required. The high pressure column is used to separate the oxygen from the air and the side column is used for the remaining argon. The oxygen column and the argon column are optional, and add complexity to the system in terms of tight heat integration.

The bare module cost of the tower can be calculated using the data in Table 53, using Equation 38. Because the distillations towers are so large, the material and pressure factors have a major influence on the overall cost. The coefficients for the bare module cost factor for the towers are given in Table 54. Because the towers are used in cryogenic duty, stainless steel is assumed to be the material. The material cost factor for a stainless steel tower is assumed to be 3. The pressure factor for the towers can be calculated using Equation 43, using the data in Table 52. For the high pressure column the pressure factor is calculated to be 2.1; the low pressure column is 1.08; and the argon column is assumed to be unity. The results are presented in Table 57.

Table 57 – Total bare module cost factors for the distillation towers in an ASU

Column	Pressure Factor	Material Factor	Total Factor
High Pressure	2.1	3	13.72
Low Pressure	1.09	3	8.2
Argon	1	3	7.71

To be conservative, the cost factor for the low pressure column was applied to the argon column for the economic analysis.

Table 58 – Tower cost data for an ASU

Towers					
Type	**Material**	**Volume (m^3)**	**Pressure (bar)**	**Uninstalled Cost (2010$)**	**Installed Cost (2010$)**
High Pressure Distillation Column	Stainless Steel	134.9	6	120,800	1,658,670
Low Pressure Distillation Column	Stainless Steel	175.3	1.8	153,700	1,206,960
Argon Distillation Column	Stainless Steel	22.5	1.3	27,710	217,600
Totals				**$302,210**	**$3,083,230**

6.5.5.5 Expander turbine

A small expansion turbine is used both to recover power and to decrease the temperature of the air feed via the Joule-Thompson cooling. The turbine is assumed to be a stainless steel, radial gas turbine with a rating of 25kW for a 250 t/d GN_2 plant. The installed cost for such a turbine is roughly $90k [296]. The installed costs for all of the major equipment are given in Table 59. The total grass roots cost can be found using Equation 46 and Equation 47. In Equation 46 the multiplying factor of 1.18 is to compensate for a contingency costs and other miscellaneous fees. The contingency costs are assumed to be 15% of the bare module cost; the fees are assumed to be 3%. Equation 47 contains a factor of 50% for auxiliary facilities costs, which are generally unaffected by the construction materials and pressures within the plant. The costs of various air separation plant sizes can be found by applying the above analysis. The results are presented in Figure 51.

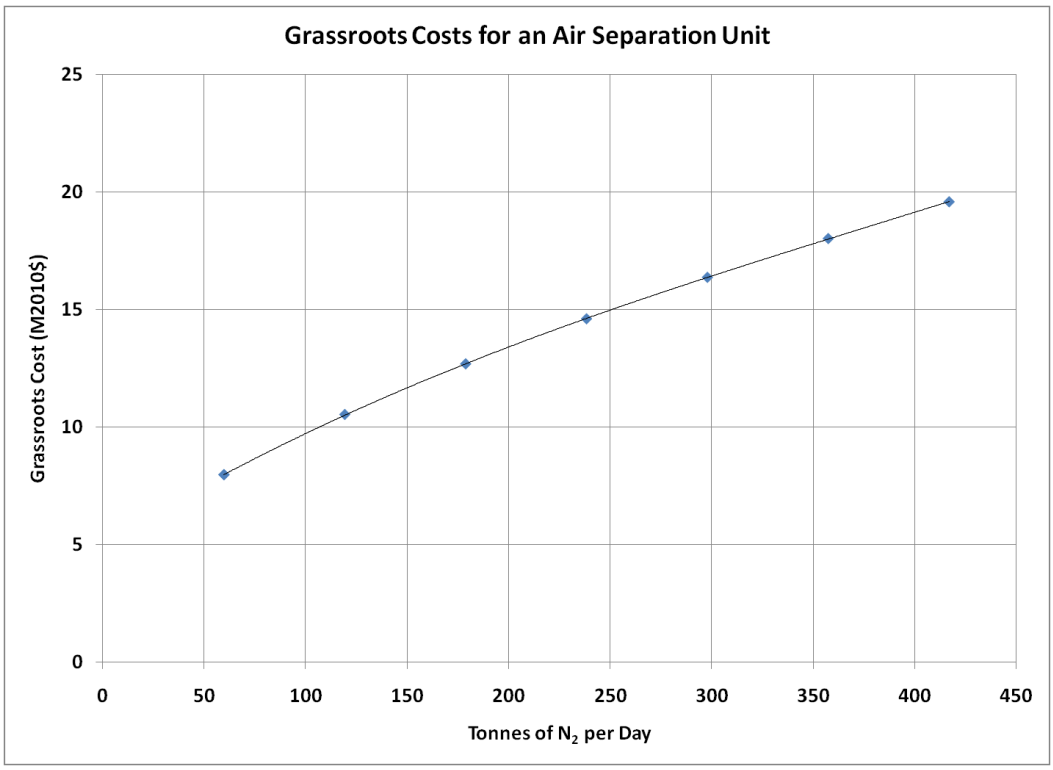

Figure 51 – Capital Costs of an ASU

The results are similar to a "ballpark figures" obtained from Universal Industrial Gases [334]. However, this analysis assumes that the main product is gaseous nitrogen; liquid products are not produced, as they would significantly increase the cost and the power requirements.

Table 59 – Equipment list and costs for a 250 tonne/day GN_2 ASU plant

Heat Exchangers					
Type	**Material**	**Area (m^2)**	**Pressure (bar)**	**Uninstalled Cost (2010$)**	**Installed Cost (2010$)**
Floating head	Stainless Steel	121.32	2	38,340	83,200
Floating head	Stainless Steel	127.56	4	39,280	85,240
Floating head	Stainless Steel	188.19	8	48,550	105,350
Plate-Fin	Brazed Aluminum	2855.69	8	514,910	1,428,880
TOTALS		**3292.76**		**641,080**	**1,702,670**
Compressors					
Type	**Material**	**Rating (kW)**	**Number**	**Uninstalled Cost**	**Installed Cost**
Centrifugal	Stainless Steel	379	1	180,720	496,980
Centrifugal	Stainless Steel	362.3	1	174,070	478,690
Centrifugal	Stainless Steel	413.5	1	194,210	534,080
TOTALS		**1154.8**		**549,000**	**1,509,750**
Drivers					
Type		**Rating (kW)**	**Number**		
Totally Enclosed		505.3	1	105,050	157,580
Totally Enclosed		483.1	1	103,360	155,040
Totally Enclosed		551.3	1	108,330	162,500
TOTALS		**1539.7**		**316,740**	**475,120**
Towers					
Type	**Material**	**Volume (m^3)**	**Pressure**		
High Pressure Distillation Column	Stainless Steel	134.9	6	120,800	1,658,670
Low Pressure Distillation Column	Stainless Steel	175.3	1.8	153,700	1,260,050
Argon Distillation Column	Stainless Steel	22.5	1.3	27,710	227,170
TOTALS				**302,210**	**3,145,890**
Turbine					
Type	**Material**	**Rating (kW)**			
Radial Gas	Carbon Steel	25		14,590	89,000
TOTALS				**14,590**	**89,000**
TOTAL				**$1,823,620**	**$6,922,430**

6.6 Mechanical Vapor Compression

Vapor compression (VC) distillation is mostly used in small and medium installations for capacities of under 2000 tons of distillate per day [145]. For VC units, the heat required for evaporating water is derived from the compression of vapor rather than heat from a boiler. A mechanical compressor or a steam jet can be used to condense vapor to produce enough heat to evaporate the feed water. The mechanical compressor is almost always electrically driven making this the only distillation process that can operate solely on electricity [149]. The process is also indifferent to the salt concentration [144] which makes it an attractive option for any sea water.

A full mathematical description of a single effect mechanical vapor compression system is available in the literature [335-336] and will be used here to size the major equipment necessary in the plant. The sizes of the major equipment can be used to determine the overall grass roots capital cost, just as in previous sections.

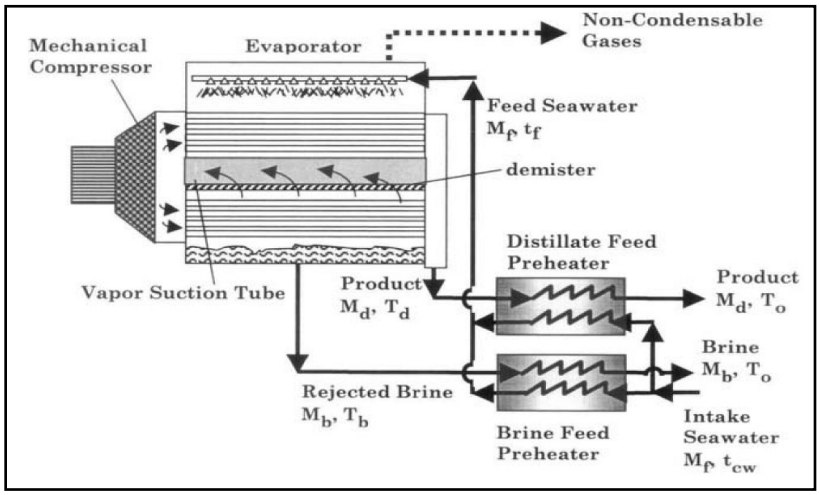

Figure 52 – A Schematic of a mechanical vapor compression (MVC) plant [335]

6.6.1 Mathematical model

The following mathematical model was taken from [335-336] and can be used to model a single-effect mechanical vapor compressor desalination plant.

An overall mass balance for the system involves the intake feed water, M_f, the brine, M_b, and the distillate product, M_d, as depicted in Figure 52 and shown in Equation 106.

$$\boldsymbol{M_b = M_f - M_d} \qquad \textbf{Equation 106}$$

A salt balance equation is also necessary since the mass of the salt must also be conserved. Thus, the total amount of salt in the feed water must equal the total mass of salt in the brine as shown in Equation 107.

$$\boldsymbol{M_f X_f = M_b X_b} \qquad \textbf{Equation 107}$$

Using energy balances around the preheaters and the evaporator it is possible to find the outlet temperature of the preheating streams, T_o, in terms of the salt concentrations, X_b and X_f, in the brine and the intake, and the temperatures of the seawater T_{cw}, brine water, T_b, and distillate water T_d as shown in Equation 108.

$$\boldsymbol{T_o = (T_{cw} - T_f) + \left(\frac{X_f}{X_b}\right) T_b + \left(\frac{X_b - X_f}{X_b}\right) T_d} \qquad \textbf{Equation 108}$$

The temperature of the water reaching the evaporator, T_f, is easily calculated using the salt concentrations of the brine and the feed, the temperatures of the compressed vapor temperature, T_s, taken to be 6 degrees Celsius higher than distillate temperature, and the specific heats of the water and water vapor. The latent heats of condensation and evaporation for the distillate and

brine respectively can be calculated using simple correlations given in Equation 110 and Equation 111.

$$T_f = \frac{(X_b - X_f)}{X_b}\left(\frac{\lambda_b - \lambda_d}{C_p} - \frac{C_{p_v}}{C_p}(T_s - T_d)\right) + T_b \quad \textbf{Equation 109}$$

$$\lambda_d = 2499.5698 - 2.204864T_d - 0.002304T_d^2 \quad \textbf{Equation 110}$$

$$\lambda_b = 2499.5698 - 2.204864T_b - 0.002304T_b^2 \quad \textbf{Equation 111}$$

The area of the evaporator can be calculated using Equation 112 by assuming an overall heat transfer coefficient of 2.4 $\frac{kW}{m^2C}$.

$$A_e = \frac{\left(M_d\lambda_d + M_dC_{p_v}(T_s - T_d)\right)}{U_e(T_s - T_d)} \quad \textbf{Equation 112}$$

To determine the heat exchange areas of the two preheaters the standard LMTD equations (Equation 113 and Equation 114) are used with the appropriate inlet and outlet temperatures which were previously calculated. Overall heat transfer coefficients for the brine and the distillate preheaters are assumed to be 1.5 and 1.8 $\frac{kW}{m^{2\circ}C}$ respectively. The heat exchanger areas are calculated using Equation 115 and Equation 116 for the distillate preheater and the brine preheater, respectively.

$$LMTD_d = \frac{\left[(T_d - T_f) - (T_o - T_{cw})\right]}{\ln\left(\frac{(T_d - T_f)}{(T_o - T_{cw})}\right)} \quad \textbf{Equation 113}$$

$$LMTD_b = \frac{\left[(T_b - T_f) - (T_o - T_{cw})\right]}{\ln\left(\frac{(T_b - T_f)}{(T_o - T_{cw})}\right)} \quad \textbf{Equation 114}$$

$$A_d = \frac{\left(M_dC_p(T_d - T_o)\right)}{U_dLMTD_d} \quad \textbf{Equation 115}$$

$$A_b = \frac{\left(M_b C_p (T_b - T_o)\right)}{U_b LMTD_b} \qquad \textbf{Equation 116}$$

The compression power is calculated using Equation 117 by first determining the inlet and outlet pressures using the correlations given in Equation 119 and Equation 120; the specific volume, V_i, is calculated using the correlation given in Equation 121. The total electrical power required for producing the distillate is the fluid power calculated in Equation 117 divided by the product of the efficiency of the compressor and the driver as shown in Equation 118.

$$\dot{W}_{comp} = \frac{\gamma}{(\gamma - 1)} P_i V_i \left(\left(\frac{P_o}{P_i} \right)^{\frac{\gamma - 1}{\gamma}} - 1 \right) \left(\frac{1000}{3600} \right) \left(\frac{\dot{m}_{perday}}{24} \right) \qquad \textbf{Equation 117}$$

$$\dot{W}_{Drive} = \frac{\dot{W}_{comp}}{\eta_i \eta_{Drive}} \qquad \textbf{Equation 118}$$

$$P_o = 10.17246 - 0.6167302 T_s + 0.01832249 T_s^2 - 0.000177376 T_s^3 + 0.00000147068 T_s^4 \qquad \textbf{Equation 119}$$

$$P_i = 10.17246 - 0.6167302 T_b + 0.01832249 T_b^2 - 0.000177376 T_b^3 + 0.00000147068 T_b^4 \qquad \textbf{Equation 120}$$

$$V_i = 163.3453 - 8.04142 T_b + 0.17102 T_b^2 - 0.00187812 T_b^3 + 1.03842 \times 10^{-5} T_b^4 - 2.28215 \times 10^{-8} T_b^5 \qquad \textbf{Equation 121}$$

Table 60 contains the assumptions used in the model as given in [335] pages 85-97. The base case model produces 500 tonnes of distillate water per day with an intake seawater temperature of 5 degrees Celsius. The distillate is assumed to enter the feed preheater at a temperature of 62 degrees and the vapor within the evaporator is assumed to be superheated to a temperature of 68 degrees. The results of the model give the approximate sizes of the necessary equipment. The equipment list for this system is comprised of the evaporator, two flat plate heat exchangers, the compressor and the compressor driver. All values are given in Table 61.

Table 60 – Parameters used in the MVC model [335]

Distillate (tonnes/day)	500
Distillate flow rate (kg/s)	5.79
$C_{pv}\left(\frac{kJ}{kg°C}\right)$	1.884
$C_p\left(\frac{kJ}{kg°C}\right)$	4.2
$U_e\left(\frac{kW}{m^2°C}\right)$	2.4
$U_b\left(\frac{kW}{m^2°C}\right)$	1.5
$U_d\left(\frac{kW}{m^2°C}\right)$	1.8
$T_{cw}(°C)$	25
$T_d(°C)$	62
$T_s(°C)$	68
$T_b(°C)$	60
$X_f(ppm)$	42000
$X_b(ppm)$	70000
η	0.75
γ	1.32
η_{drv}	0.95

Table 61 – The approximate sizes of the equipment in a MVC distillation plant

Equipment	Capacity	Units
Compressor	337.5	kW
Driver	475	kW
Evaporator	2850	m^2
Brine Flat Plate HX	862	m^2
Distillate Flat Plate HX	248	m^2

The calculated equipment sizes agree with the examples listed in [335] for a single-effect mechanical vapor compression desalination plant.

6.6.2 Economics of MVC

To determine the costs of the equipment required for the MVC desalination system, the procedure outlined in previous sections is used. The total cost for the desalination plant is based solely on

the costs of the compressor, driver, evaporator, and two heat exchangers. While other minor equipment exists, it will is considered herein.

The MVC distillation plant primarily processes raw seawater which is particularly corrosive to many metals. Corrosion charts for metals used to process seawater or brine can be found in standard chemical engineering texts [152, 337]. This thesis assumes that stainless steel alloys can be used to process the seawater, though generic "stainless steel" is not recommended by Ulrich. The cost difference between using stainless steel and nickel or titanium is on the order of ten million dollars. As such, the materials factors for the relevant equipment are simply assumed to be 3.

The cost constants to be used with Equation 38 are given in Table 62 for the evaporator, compressor, heat exchangers and the driver.

Table 62 – Cost constants for the MVC equipment [296]

Cost Constants	K1	K2	K3
Centrifugal compressor	2.2897	1.3604	-0.1027
Evaporator	4.642	0.3698	0.0025
Flat Plate HX	4.6656	-0.1557	0.1547
Drivers	2.9508	1.0688	-0.1315

The compressor transfers all of the energy to the water for distillation. It is located adjacent to the evaporator and comes into direct contact with the seawater vapors; corrosion resistance is paramount. The driver is tasked with spinning the compressor and does not come into direct contact with the seawater. The evaporator and two heat exchangers encounter both the seawater and brine and are therefore susceptible to corrosion.

The costs for each piece of equipment are calculated for a 500 cubic meter per day distillation plant, and are listed in Table 63 below.

Using Equation 46 and Equation 47 the total module cost and grass roots cost can be calculated for the MVC plant. The results for the grass roots capital costs are shown at the top of Figure 53. The capital cost values are an order of magnitude higher than other published capital costs found in the literature [145, 338]. The discrepancy is likely due to several factors. First, the costs here are given in 2010 dollars, while the costs listed in the references are from other years or

Table 63 – Equipment list for a 500 m^3/day distillation plant

Equipment	Capacity	Units	Uninstalled Cost ($)	Installed Cost ($)
Compressor	338	kW	164,050	492,150
Driver	475	kW	102,630	153,950
Evaporator	2850	m^2	1,235,220	3,705,670
Flat Plate HX (distillate)	248	m^2	454,940	1,364,810
Flat Plate HX (brine)	862	m^2	1,047,740	3,143,210
Totals			**3,004,580**	**8,859,790**

currencies. Second, the costs are given in terms of either investment or installed cubic meter of distillate capacity, or as investment per cubic meter delivered. It is unclear what assumptions were used to determine the unit product cost in the references. The bottom half of Figure 53 shows the per unit cost of MVC desalination. Here, the net present value is based on an interest rate of 4%; an inflation rate of 3%; a discount rate of 7%; a 20 year project life; and a 15 year loan period. The per unit cost decreases with capacity and falls within the appropriate unit cost range reported in [338].

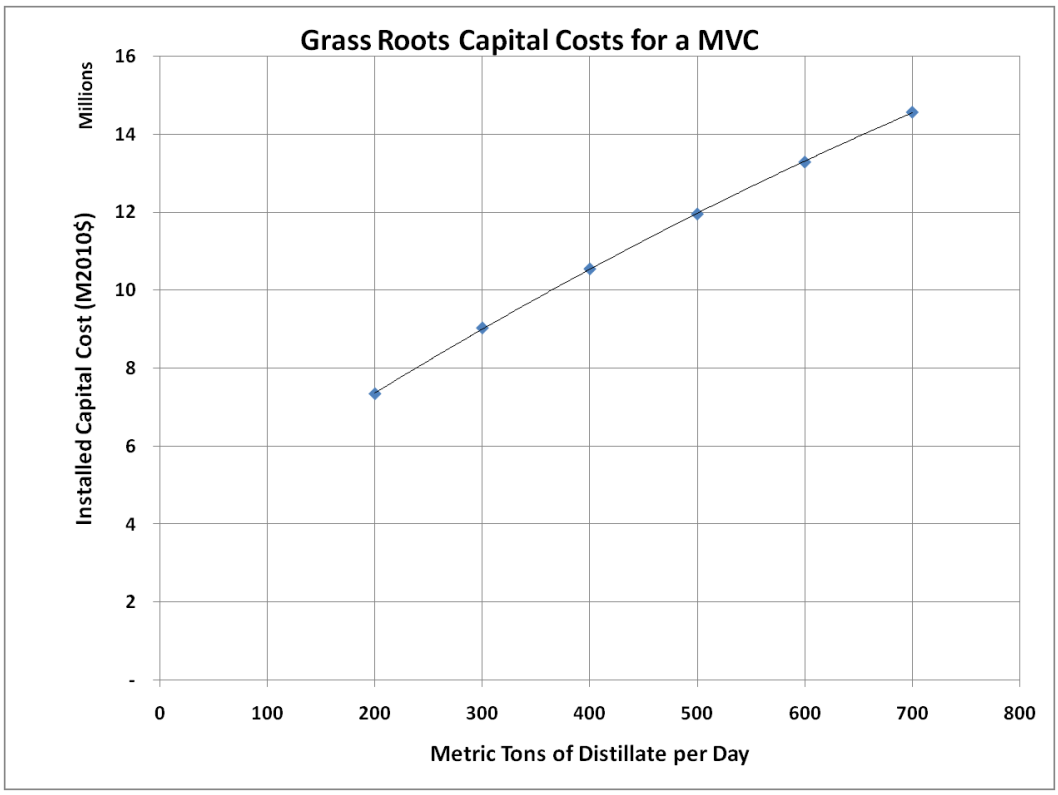

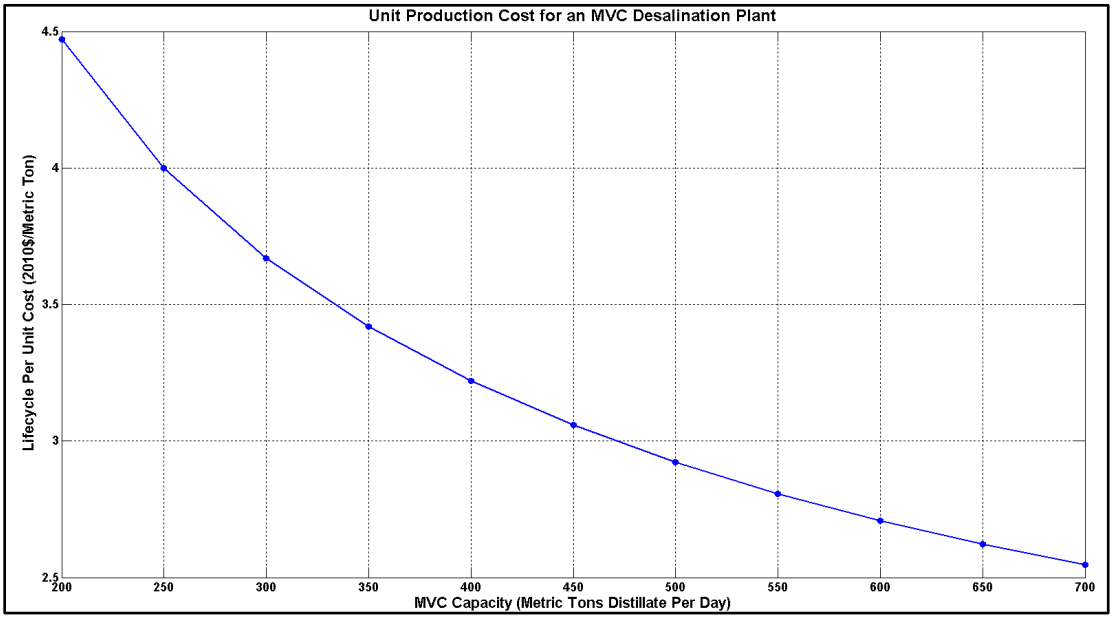

Figure 53 – Grass roots cost (top) and unit product cost (bottom) for MVC plants of various sizes

6.7 Ammonia Storage

Ammonia is typically stored in large quantities as a cryogenic liquid. The liquid is maintained at -33°C and atmospheric pressure in an insulated double containment tank. Due to heat transfer to the tank from the outside, some boil off of ammonia occurs. To recover escaping ammonia vapors from the storage tanks, a compression-refrigeration loop is created to condense the ammonia vapor and return it to the tank. Two intercooled compressors raise the pressure of the ammonia vapor to about 13 bar before sending it to the condenser. The ammonia is then condensed with a small evaporator or cooling tower before being flashed in an intercooler. A simplified ammonia refrigeration loop is shown in Figure 54; the stream table is shown in Table 64

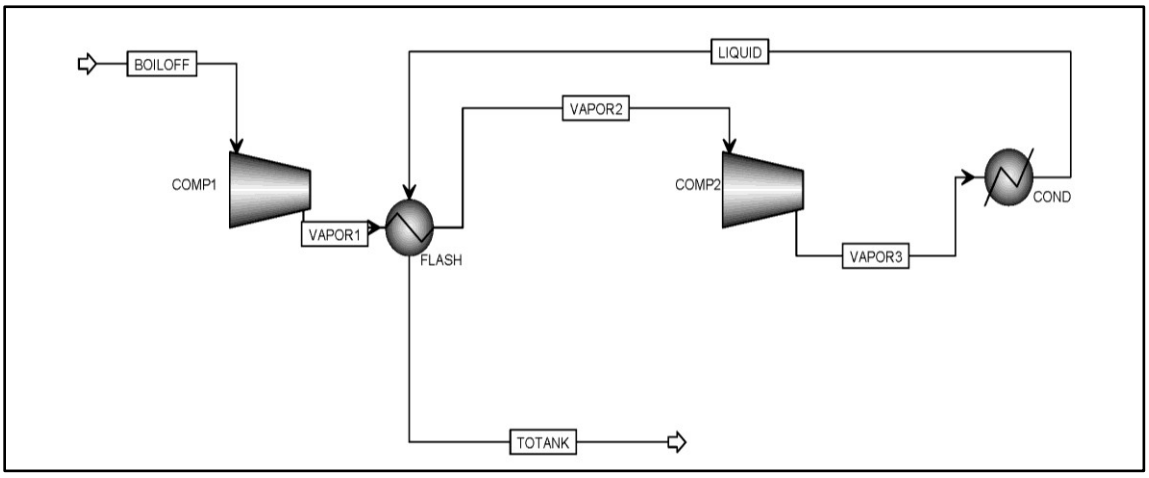

Figure 54 – A simplified ammonia storage compression loop

Generally about 30 days of storage are needed for a chemical plant [152]. Since ammonia is a continuous process with few disruptions, the product must be adequately stored on site. Thus, a 300 t/d ammonia plant will require at least a 9000 tonne storage container, which corresponds to about 13,200 m^3. An additional 10% freeboard is added [153], which increases the total volume of the container to 14,500 m^3. The storage tanks have a D/H ratio of about 0.75 [339], which implies that a tonne storage facility based on 9000 tonnes of storage will be about 21.7 meters high and 29.1 meters wide. The tanks are actually double containment vessels to ensure that

harmful vapors are not released in the case of a tank rupture. The outer tank is 1-2 meters away from the inner tank and is structurally designed to support the roof [340]. Taking a mean value of 1.5 meters as the distance between the two tanks yields an outer tank diameter of 32.1 meters; the height is assumed to be the same as the height of the inner tank.

The heat transfer into the ammonia tank is proportional to the surface area of the tank. The total heat transferred into the tank can be found using Equation 122 where $\dot{Q}$ is the heat transfer in W; U is the overall heat transfer coefficient for the tank, assumed to be 0.32 $\frac{W}{m^2K}$ [341]; and ΔT is the temperature difference between the tank and the outside air. The ambient temperature is assumed to be 10°C and the tank temperature is -33°, so $\Delta T = 43°C$. The surface area of a tank for a 300 t/d facility is 3315 m^3.

$$\dot{Q} = UA\Delta T \qquad \textbf{Equation 122}$$

To determine the total boil off, Equation 123 can be used. The heat of vaporization (ΔH_{Vap}) for liquid ammonia at -33°C is 1370 kJ/kg. Thus, the total boil off for the tank is given by Equation 124 where $NH_{3_{Evap}}$ is the mass of evaporated ammonia produced in a single day; $NH_{3_{Storage}}$ is the amount of available storage.

$$NH_{3_{Evap}} = \frac{\dot{Q}}{\Delta H_{Vap}} \qquad \textbf{Equation 123}$$

$$BoilOff = \frac{NH_{3_{Evap}}}{NH_{3_{Storage}}} \qquad \textbf{Equation 124}$$

Typical boil off values are about 0.04% or lower. Using the values given above the boil-off is 0.03% and the total ammonia entering the refrigeration loop is 2.88 tonnes per day. Using Table

64, the stream table for the simple refrigeration loop, the compressors, the flash and the condenser can all be sized.

Table 64 – A stream table for the ammonia refrigeration loop shown in Figure 54

	Unit	Boiloff	Vapor1	Vapor2	Vapor3	Liquid	To tank
NH_3	kg/sec	0.03	0.03	0.03	0.03	0.03	0.03
Pressure	bar	1.08	3.04	3.04	12.67	12.67	3.55
Temp.	K	241.07	333.45	291.97	442.62	283.65	268.17
Enthalpy flow	KW	-97.63	-90.98	-94.02	-82.43	-137.12	-140.17
Liquid fraction		0	0	0	0	1	1
Mass enthalpy	kj/kg	-2811.81	-2620.26	-2707.91	-2373.95	-3949.13	-4036.78

Equation 93 can again be used to size the compressors, this time with pure ammonia vapor flowing at 0.03 kg/s at a temperature of 241K. Intercooling is provided by flashing the ammonia liquid coming out of the condenser in a vessel that also contains the pressurized superheated ammonia vapor form the first compressor. The second compressor further raises the pressure to about 13 bar. At this stage it enters the condenser near its saturation point and leaves as a liquid. Using the values for temperature and pressure in the stream table Equation 93 can be applied once again to calculate the fluid power. If a value of 0.4882 $\frac{kJ}{kgK}$ is assumed for the gas constant of ammonia [310] then the fluid power for the first and second compressors is 4.75 kW and 8 kW, respectively. The flash drum is sized to have 10 minutes of liquid holdup due to both incoming streams, which corresponds to a volume of 0.055 m^3. The condenser area can be calculated using the following equation

$$\boldsymbol{Area = \frac{\dot{m}_{NH_3} H_{mass}}{U_{cond} T_{cond}}} \qquad \textbf{Equation 125}$$

where $\dot{m}_{NH_3}$ is the mass flow rate of the ammonia in kg/s, $H$is the specific mass enthalpy of the flowing ammonia, taken to be 1575 $\frac{kJ}{kg}$, $U_{cond}$is the overall heat transfer coefficient of the condenser, taken to be 15 $\frac{W}{kgK}$, and $T_{cond}$is the temperature at which the condenser operates, taken to be 284K. The condenser area is then calculated for an ammonia flow rate of 0.033 $\frac{kg}{s}$ (converted from tonnes per day) to be 12.3 m^3.

6.7.1 Economics of Ammonia Storage

The total cost of the storage can be estimated using the procedures outlined above. The capital cost for an ammonia storage system depends on the storage tank, the compressors, the flash drum and the condenser. The constants for each component to be used with Equation 38 are given in Table 65.

Table 65 – Cost constants to be used for ammonia storage [296]

	K_1	K_2	K_3
Storage Tank	4.8509	-0.3973	0.1445
Centrifugal compressor	2.2897	1.3604	-0.1027
Drivers	1.956	1.7142	-0.2282
Condenser	4.0336	0.2341	0.0497

The bare module cost of the inner storage tank with a volume of 14500 m^3 is calculated to be $696,000 in 2010 dollars. A stainless inner steel tank is assumed corresponding to a material factor of 4.5. Accordingly, the actual installed cost for the tank will be $3.13M in 2010 dollars. Similarly, for the outer tank a volume of 17,600 m^3 is assumed corresponding to a bare module cost of $814k in 2010 dollars. The outer tank is made of thick concrete so a material factor of 1.5 was selected with no pressure factor. Hence, the total actual cost of the outer tank is $1.22M in 2010 dollars.

The compressors are not large compared to the compressors used in the ammonia synthesis loop. They will be under similar conditions in that they will be tasked with processing ammonia, albeit

at lower overall pressures and flow rates. Since the size of the compressors is actually outside the suggested limits of the model the two compressors are lumped together into one large compressor with one large drive. The compressor bare module cost is roughly $7,000 in this scenario, with the installed cost being $31,100 in 2010 dollars. The drives operate with an actual power being about 25% higher than the fluid power as discussed in previous sections. The bare and actual costs for the lumped driver are assumed to be $8,000 and $11,700 respectively.

The condenser must cool all of the incoming ammonia vapor and condense it to liquid. The unit is not large but it is assumed to be an air cooler heat exchanger (as shown in the presentation by [342]), but must be constructed of stainless steel much like all of the other equipment that process ammonia. The bare module cost is $31k and the installed cost under these conditions is $92.7k in 2010 dollars.

It should be noted that other emergency equipment such as a flare, lightening and earthquake protection, backup generators and a wind vane would be necessary as well [154, 340]. A reasonable amount of $50,000 can be assumed for the emergency backups.

Again using the standard equations, the grass roots cost of a facility that stores 9000 tons of ammonia is taken to be $6.47M in 2010 dollars. These costs are similar to those published in [10].

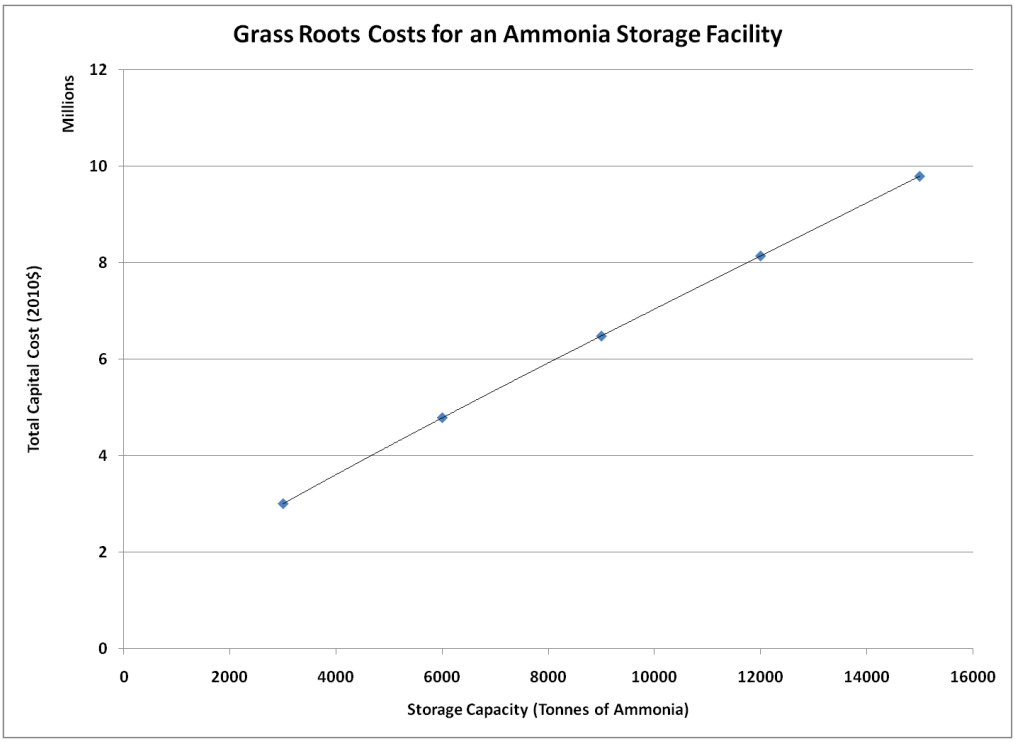

Figure 55 – Grass roots cost for an ammonia storage facility

6.8 Total Overall Costs

The total capital costs for the entire ammonia facility are simply the sum of the costs of the individual subsystems, including the electrolyzers, synthesis loop, air separation, water purification, and storage. The total cost curves for the cases of electrolyzer scaling and no scaling are shown in Figure 56.

When electrolyzer scaling is used, the electrolyzer stacks share common industrial equipment to reduce costs. The best case scenario is has a cost curve with a scaling factor of 0.5, and overall capital costs are drastically reduced. The capital cost breakdown for a 300 tonne per day all-electric ammonia facility that utilizes electrolyzer scaling is shown in Figure 57. Electrolyzers dominate the economics, totaling 65% of the overall capital costs. The synthesis loop is slightly over one-fifth of the capital costs. The remaining costs are for the ASU, MVC and the storage facility.

For the case of no electrolyzer scaling, the electrolyzers are purchased as modular units and installed in series to produce the required hydrogen. That scenario yields a cost curve with an overall scaling factor of 0.91. The slight economy of scale is solely from the ASU, MVC and the storage facility. Figure 58 shows the cost breakdown for a 300 tonne per day facility. The electrolyzers have a larger share (77%) in this scenario than they did in the case that used scaling. All other subsystem costs were held constant.

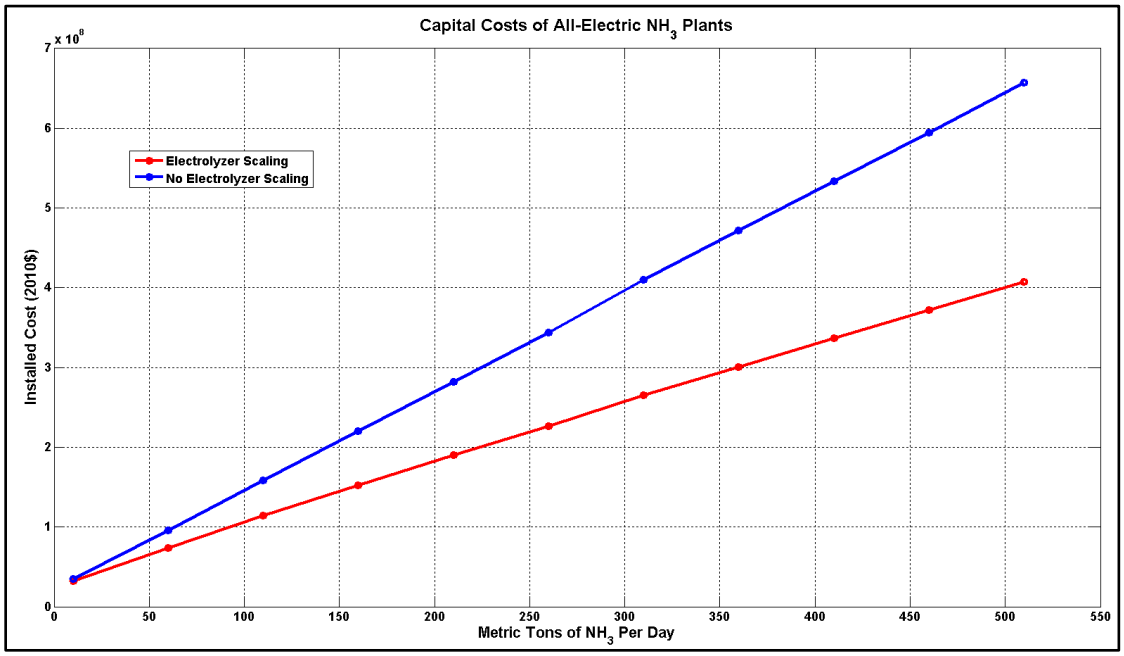

Figure 56 – Capital cost curve for an all-electric ammonia plant

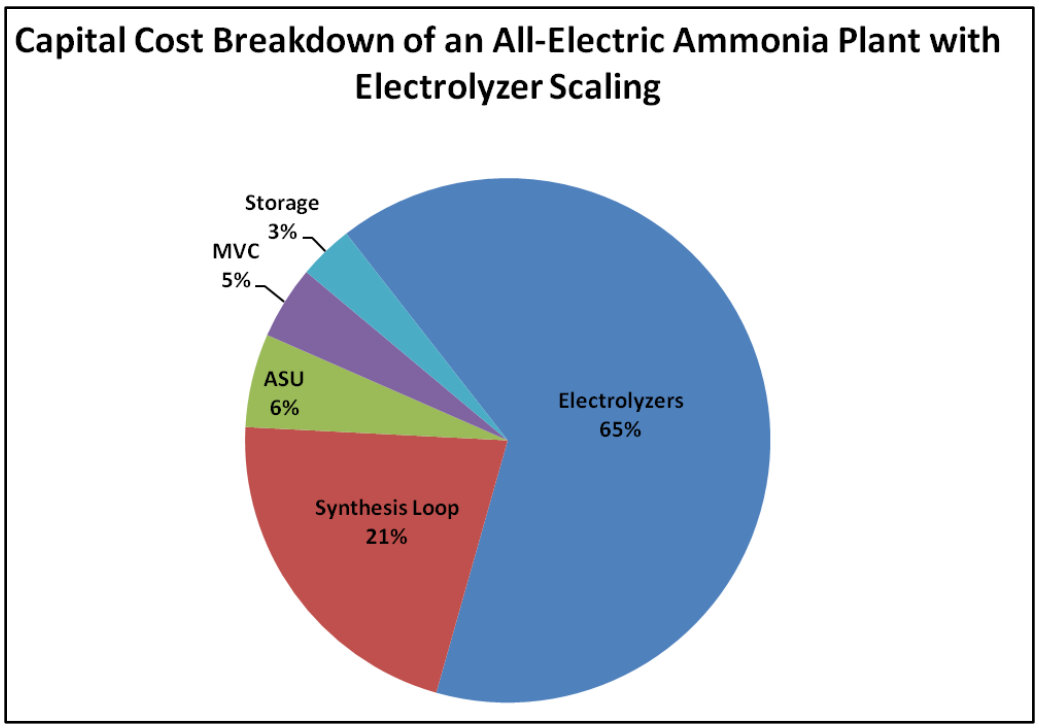

Figure 57 – Capital cost breakdown of a 300 t/d all-electric ammonia plant with electrolyzer scaling

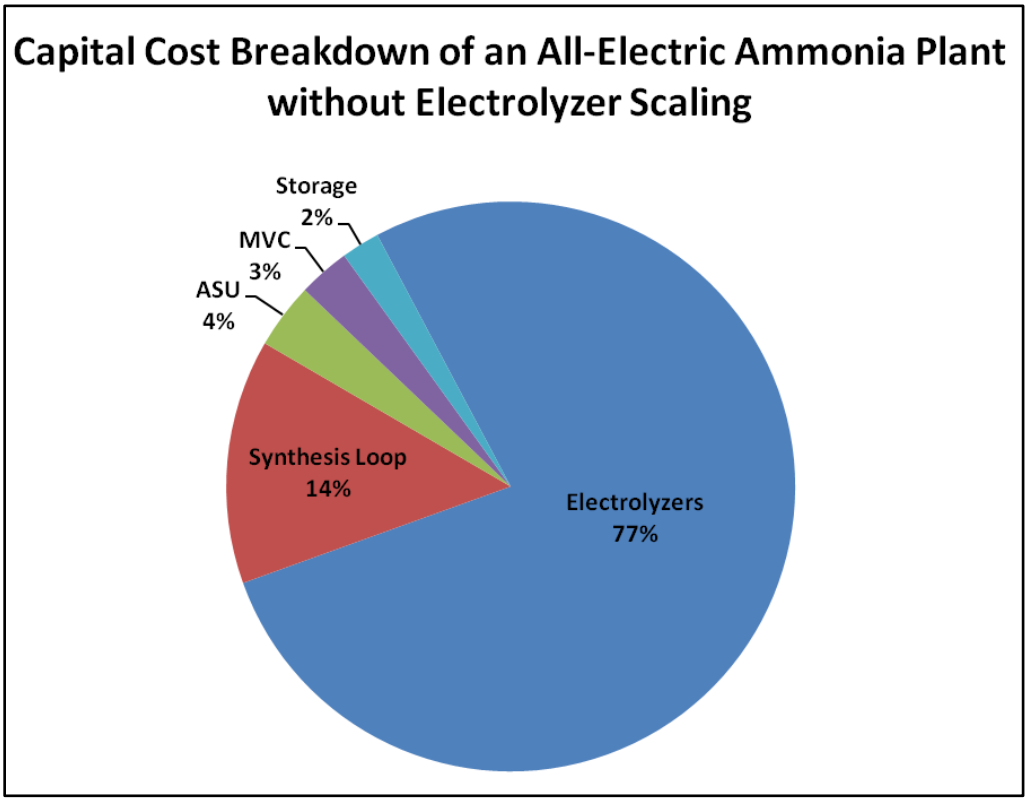

Figure 58 – Capital cost breakdown of a 300 t/d all-electric ammonia plant without electrolyzer scaling

When scaling is used, the electrolyzer stacks make up about 65% of the total cost of the installed system; without scaling electrolyzers represent over 75% of the cost.

6.9 Total Power Requirements in the Ammonia Synthesis Process

The issue of the power required for the all-electric ammonia plant was addressed tangentially in some of the capital cost sections. For example, the compression power in the synthesis loop was fully detailed in Section 6.3 which discussed the fluid power and driver power requirements. The total ammonia plant power requirements will be formally discussed here to supplement the previous discussion.

6.9.1 Synthesis Loop

The power in the synthesis loop is required almost exclusively by the compression train and the recycle compressor. To a much lesser extent pumping power is also required, but it is almost negligible. A 300 tonne per day ammonia synthesis plant that operates at 150 bar and 450 degrees Celsius requires 7.91 MW of electrical power, as described in Section 6.3.4. The pumping power is related to the cooling water requirements which equal 9.5 tons per minute as shown in Section 6.3.7. The total pumping power required is 112 kW bringing the total power required in the synthesis loop to 8.02 MW.

6.9.2 Air Separation Power

The power required for air separation is almost solely from the compression train used at the inlet and depends on the design of the plant. Thus, Equation 53 can be used to determine the fluid power required. The assumptions for the air separation plant are: the intake temperature is 294K; there are 3 stages of compression to raise the pressure to 8 bar; the polytropic exponent is 1.4; and the recovery ratio of the air separation plant – η_{ASU} – is 70% by volume [334]. The last

assumption is critical because the total volumetric flow rate of air into the compression train is the total nitrogen production capacity divided by the recovery ratio:

$$\dot{V}_{air} = \frac{\dot{V}_{N_2}}{\eta_{ASU}} \qquad \textbf{Equation 126}$$

A 300 tonne per day ammonia plant will require 247 tonnes per day or 8940 Nm^3/hr of nitrogen according to Section 5.1. Thus, the air intake into the first compressor of the ASU will be 352.8 tonnes per day of air, or 4.08 kg/s. Then, using Equation 53 with $R_{air} = 0.287\ \frac{kJ}{kgK}$, the fluid power required is 792 kW. If an adiabatic compressor efficiency of 75% is assumed together with a driver efficiency of 95%, the total power required will be 1.112MW. While some water would be required for compressor intercooling, the pump power is assumed to be negligible in this circumstance.

6.9.3 Mechanical Vapor Compression

The power required in the MVC was discussed in Section 6.6.2. The equations used in the analysis were:

$$\dot{W}_{comp} = \frac{\gamma}{(\gamma - 1)} P_i V_i \left(\left(\frac{P_o}{P_i} \right)^{\frac{\gamma-1}{\gamma}} - 1 \right) \left(\frac{1000}{3600} \right) \left(\frac{\dot{m}_{perday}}{24} \right) \qquad \textbf{Equation 117}$$

$$\dot{W}_{Drive} = \frac{\dot{W}_{comp}}{\eta_i \eta_{Drive}} \qquad \textbf{Equation 118}$$

A 300 tonne per day ammonia facility required about 500 tonnes of water for electrolysis, as discussed in Section 5.1. The total power required is found using Equation 117-Equation 121. The fluid power calculated from Equation 117 is 338 kW; the shaft power required by the driver assuming an adiabatic efficiency of 75% and a driver efficiency of 95% is 475 kW. The specific power for this system is 22.75 $\frac{kWh}{m^3}$.

6.9.4 Electrolyzers

The power requirements for electrolysis of water can easily be calculated using the manufacturer specifications for the specific power requirements. The specific power for Norsk Hydro Atmospheric Type 5040 electrolyzers is listed as 4.8kWh/Nm^3 of hydrogen, of which 4.3 kWh/Nm^3 is for electrolysis and the remaining 0.5 kWh/Nm^3 is for the balance of plant. From these figures, the calculation for the power requirements for a 300 tonne per day – 26,800 Nm3/hr of hydrogen – ammonia plant is straightforward:

$$P_{elec} = \left(4.8\frac{kWh}{Nm^3}\right)\left(26{,}800\frac{Nm^3}{hr}\right) = 128.65MW$$

This is the direct current (DC) power requirement for electrolysis. The alternating current (AC) power requirements are found by dividing the DC power requirement by a rectifier efficiency of 95% [238] to get 135.4 MW.

6.9.5 Ammonia Storage

The power for the ammonia storage facility is required by the compressors in the vapor compression loop. The power calculations were discussed in 6.3 and the power requirements are assumed to be about 15 kW for the drivers – a negligible amount in the facility.

6.9.6 Total Power Required

The total power required for the all-electric ammonia facility with an operating pressure of 150 bar is a sum of the power requirements for each of the subsystems; the power requirements are shown in Figure 59. A linear fit is used to describe the power requirements for ammonia plants of different sizes, as shown in Equation 127.

$$\boldsymbol{P_{NH_3} = 0.482 Size_{NH_3}} \qquad \textbf{Equation 127}$$

Here $Size_{NH_3}$ is the ammonia plant output capacity in tonnes per day and P_{NH_3} is the power required by the ammonia plant in megawatts.

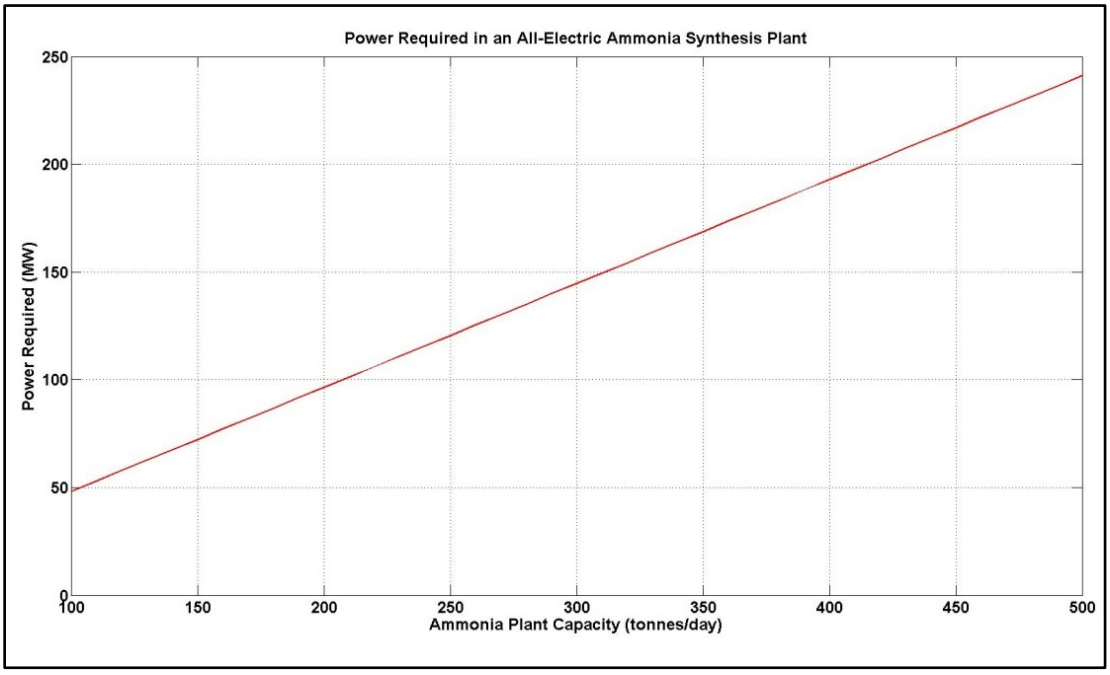

Figure 59 – Power requirements of all-electric ammonia facilities

The power requirements are almost entirely for the electrolysis of water. For a 300 ton per day plant, the power requirements are 145MW total with 135MW being required for the electrolysis – 93% of the total. The synthesis loop requires about 8MW of power, or about 5.5% of the total power requirements. The ASU and the MVC are not power intensive processes and together make up only 1% of the total power required – the ASU requires 1.05MW while the MVC requires 450 kW. The breakdown is shown in Figure 60.

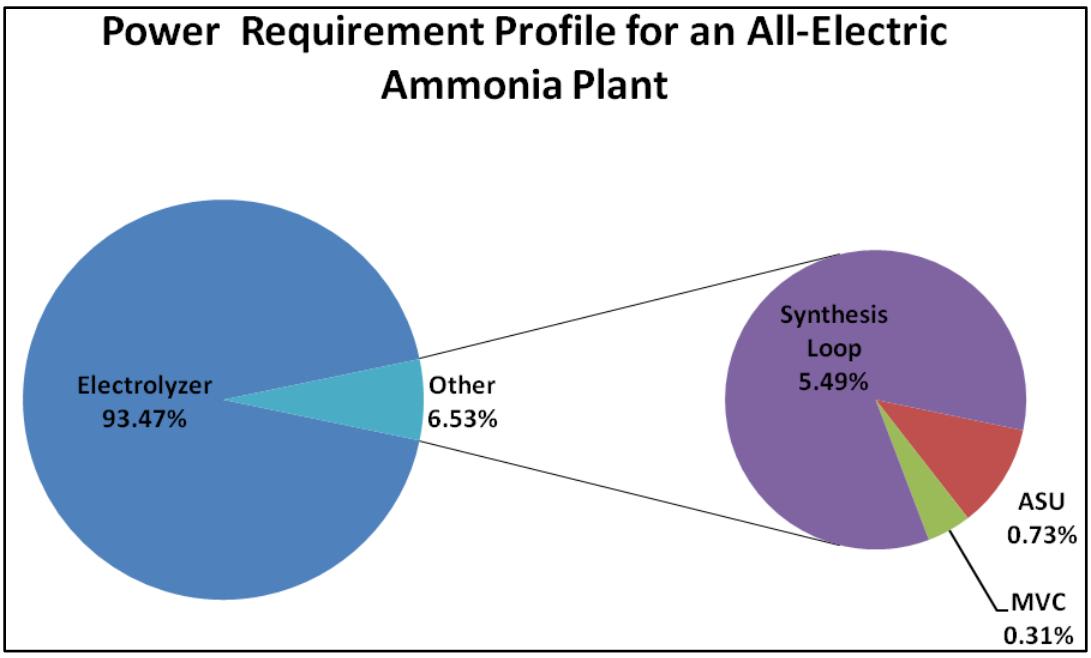

Figure 60 – The power requirement breakdown for an all-electric ammonia plant

The power requirements for the all-electric ammonia production correspond to about 41.76 GJ per metric ton of ammonia, with respect to the lower heating value. If the lower heating value of ammonia is taken to be 18.6 GJ/ton [28] , then the process is about 45% efficient. The energy requirements for the all-electric facility correspond with the state-of-the-art in ammonia synthesis from the 1960s and 1970s, and are close to the global average in the year 2000 [343].

6.10 Manufacturing Costs for Ammonia Synthesis

The procedure to estimate the costs of manufacturing were discussed in Section 6.2. The main equation used to estimate the COM is shown again in Equation 49.

$$COM = 0.280FCI + 2.73C_{OL} + 1.23C_{UT} \qquad \textbf{Equation 49}$$

It has already been assumed that raw materials and waste streams will be negligible factors in the overall costs because 1) the feedstocks are air and water 2) the waste streams are oxygen and salt water. The major ongoing costs will be labor and utilities which are both discussed in this section.

The operating labor can be approximated using Equation 50 where the N_{np} term is a sum of all of the individual compressors, heat exchangers, towers, reactors and heaters. It is assumed that the number of operators that are employed per working operator is 4.5 [296]. The total operators are the product of N_{OL} and the operators per operator rounded up to the nearest whole number. The salaries are computed with hourly wage data from the BLS, assuming 2000 paid hours per year [312].

Table 66 shows a summary of the required labor and the yearly cost. It should be noted that electrolyzers are designed for unattended operation; the H2A analysis tool suggests that 3 total operators are required for a 50 tonne per day electrolyzer facility [288].

$$\boldsymbol{N_{OL} = \left(6.2 + 0.23 N_{np}\right)^{0.5}} \qquad \textbf{Equation 50}$$

$$\boldsymbol{N_{np} = \sum Equipment} \qquad \textbf{Equation 51}$$

The utility requirements include the cooling water and the electricity needed to run the plant. It was shown in Section 6.3.7 that the synthesis loop required approximately 160 kg/s of cooling water for the compressors; the same procedure shows that the ASU will require approximately 10.5 kg/s of cooling water. The electrolyzers are self-cooled using the potassium hydroxide solution; the ammonia storage does not require cooling water; and the MVC system is the antithesis of cooling. The final value is taken to be 170 kg of cooling water per second which equates to 15,120 tonnes per day. The cost of cooling water includes the cost of the cooling tower and the electricity necessary electricity and is given as $\frac{\$0.50}{m^3}$ in 2005 dollars [311]. An updated cost of $\frac{\$0.58}{m^3}$ is found using the CEPCI values for 2005 (468.2) and 2010 (550.8), giving a total cost of $8,760 per day.

Table 66 – Summary of the operating labor required for an all-electric 300 tpd ammonia plant, based on Equation 50

Equipment	ASU	MVC	Storage	Synthesis Loop	Electrolyzers	Totals
Compressors	3	1	2	6	2	14
Heat Exchangers	4	3	1	8	0	16
Towers	4	0	1	0	0	5
Reactors	0	0	0	1	0	1
Heaters	0	0	0	0	0	0
N_{OL}	2.97	2.69	2.69	3.12	2.60	
Operators per Operator	4.5	4.5	4.5	4.5	1	
Total Operators	14	13	13	15	3	
Salary/year	$56,640	$56,640	$56,640	$56,640	$100,000	
Total Labor Cost	**$792,960**	**$736,320**	**$736,320**	**$849,600**	**$300,000**	**$3,415,200**

The cost of electricity is a major factor in the profitability of an electric ammonia plant. Section 6.9.6 detailed the power requirements for any all-electric ammonia facility in the neighborhood of 300 tonnes per day. In general, the "uptime" of a chemical plant is about 90%, giving about 330 operating days per year, or 7920 operating hours. Using Equation 127, the power required for a 300 tonne per day plant is about 145 MW. Thus, the plant will consume 1,148,400,000 kWh of energy annually. In 2010 the average price of industrial electricity in the United States was 6.81¢/kWh [344] which equates to a cost of over $78 million.

CHAPTER 7

WIND POWER ECONOMICS

The economics of offshore wind turbines in the United States is a matter of considerable ongoing debate. At the time of this writing (April 2012) there are still no wind turbines operating in US waters. Perhaps the closest comparison to offshore wind farms in the United States is the Fox Island wind project off the coast of Maine [345]. While the project was ultimately terrestrial, the turbines, towers, concrete, and all necessary heavy machinery had to be barged and trucked to the site [346]. The unusually high project costs were estimated to be over $3200/kW, with the added cost likely due to the transportation and project logistics [347]. This figure will likely be even higher for offshore wind farms.

The following discussion of offshore wind turbine costs draws heavily from the European experience. Published costs from various European sources are used throughout this work to estimate the costs of a US offshore wind project. Necessarily, the costs must be translated in both space and time: the costs from previous years must be brought to 2010; the costs from other currencies must be brought to US dollars. It will be shown that while this is a highly uncertain process, a standardized, transparent method can help legitimize the conclusions. The result is a simple but comprehensive method that can estimate the cost of a US offshore wind farm in shallow waters, close to shore.

7.1 Rotor Nacelle Assembly (RNA) and Tower

The Consumer Price Index (CPI) is often used to inflate costs of manufactured goods such as wind turbines. However, the CPI is designed to measure the buying power of consumers in an urban environment, not to escalate costs in the industrial manufacturing sector [348]. The

Producer Price Index (PPI) is a better option for inflating specific pieces of industrial equipment. The PPI measures the average change in selling prices received over time for specific products and services in the United States, as reported by domestic producers [302]. The PPI captures changes in production costs, labor rates and raw materials with a single number, specific to a particular product. Using the PPI, the cost of specific components within the turbine can be escalated or deescalated generating an accurate updated cost for the turbine. It will be shown here that the Consumer Price Index underestimates the cost by more than 15% compared to using the PPI.

While the PPI is typically listed for specific components, an effective PPI for a complex machine can be calculated if the cost contributions of the components are known. The effective PPI is simply the weighted average of the PPI of all of the components. In a National Renewable Energy Laboratory (NREL) technical report a framework was created in order to scale and cost wind turbines [110]. Part of the framework that they created allowed for the cost model to be updated by incorporating the Producer Price Index (PPI) for each turbine component. The result was a baseline turbine cost in 2002 dollars that could use the Producer Price Index (PPI) to update the costs to the desired year. Doing so requires looking up numerous codes within the Bureau of Labor Statistics and incorporating their indices into the cost model.

It can be assumed that most horizontal axis wind turbines are made of similar materials, have similar design characteristics, and scale with well-known empirical laws [54]. This was the basis for of the original wind turbine scaling models that were used to determine the capital costs associated with wind turbines [110]. Thus, the mass of a turbine component can be calculated given design characteristics such as radius, hub height and rated power. The cost of a turbine component is assumed to be proportional to its mass, so the empirical scaling laws can be used to determine the total cost. However, turbines are fabricated using various components and materials

which must all be considered when scaling the turbine. Accordingly, to accurately determine the cost of a scaled turbine, assumptions must be made regarding the scaling laws, the materials, and the time value of costs for each component.

7.1.1 Cost Escalation Method

In order to keep the model current the authors matched each major component in the wind turbine to the North American Industry Classification System (NAICS) number [349]. Each NAICS number has an associated Producer Price Index (PPI) to track the price escalation or de-escalation of the product or service over time. The authors also estimated the relative contribution of each of the products to the overall cost of each turbine component, making it possible to estimate the updated cost.

The PPI can be used to inflate and deflate the cost of materials and parts used in a turbine so that older costs can be brought into present value. Thus, with knowledge of the PPI from two specific years the cost of a product can be escalated or deescalated. The PPI for the component given in reference [110] was found in the database of the US Bureau of Labor Statistics [302] which maintains a website that includes the PPI index for each of the NAICS codes over a period of about 10 years. The PPI indices for 2002 and 2010 for each component are presented in Table 67 along with the NAICS codes used and the component cost contribution. Using the PPI for each component, together with the cost contribution of the component in the subsystem, results in the calculation of effective PPI for a complete system.

Table 67 – Wind turbine components and associated NAICS codes (*General inflation) [110]

Component	Sub-Component	NAICS Code	Component Cost (%)	PPI 2002	PPI 2010
Blades	Fiberglass fabric	3272123	61	99.5	83.3
	Vinyl type adhesives	32552044	27	145.6	189.1
	Urethane and other foam products	326150P	9	94.57	138.2
	Other externally threaded metal fasteners, including studs	332722489	3	98.9	103.4
Hub	Ductile iron castings	3315113	100	149.8	287.8
Pitch Mechanisms	Bearings	332991P	50	168.7	227.1
	Drive motors	3353123	20	149.9	216.2
	Speed reducer, i.e., gearing	333612P	20	165.4	222.3
	Controller and drive - industrial process control	334513	10	156.8	194
Low Speed Shaft	Cast carbon steel castings	3315131	100	143.3	223.2
Bearings	Bearings	332991P	100	168.7	227.1
Gearbox	Industrial high-speed drive and gear	333612P	100	165.4	222.3
Mechanical brake, high-speed coupling, etc.	Motor vehicle brake parts and assemblies	3363401	100	106.7	109.5
Generator (not permanent-magnet generator)	Motor and generator manufacturing	335312P	100	139.9	183.6
Variable-speed electronics	Relay and industrial control manufacturing	335314P	100	148.6	194.3
Yaw drive and bearing	Drive motors	3353123	50	149.9	216.2
	Ball and roller bearings	332991P	50	168.7	227.1
Main frame	Ductile iron castings	3315113	100	149.8	287.8
Electrical connections	Switchgear and apparatus	335313P	25	151	197.3
	Power wire and cable	3359291	60	109.7	227.1
	Assembly labor	GI*	15	100	120.4
Hydraulic system	Fluid power cylinder and actuators	339954	100	131.5	180
Nacelle cover	Fiberglass fabric	3272123	55	99.5	83.3
	Vinyl type adhesives	32552044	30	145.6	189.1
	Assembly labor	GI*	15	100	120.4
Control, safety system	Controller and drive - industrial process control	334513	100	162.5	202.2
Tower	Rolled steel shape manufacturing - primary products	331221	100	109.9	171.8

7.1.2 Application of the cost escalation method

The wind turbine dimensions used in this study are based on the Vestas V82 1.65MW model [350] and are listed in Table 68 below. It is assumed that the turbine has a "baseline" tower and blades – rather than an "advanced" tower and blades, as described in [110] – and a three stage helical/planetary generator. This initial analysis only focuses on the turbine and tower and omits transportation to the site, the foundation, installation, and permitting. Thus this is a "ground up" analysis of the turbine costs. The foundations and installation costs were not included in this model because the NAICS have been discontinued since the NREL report was issued [351]. The transportation of the turbine will be included in a later section to facilitate comparison with results obtained by LBNL.

Table 68 – Specifications for a Vestas V82 1.65MW wind turbine

Number of Blades	3
Radius (m)	41
Area (m^2)	5281
Hub Height (m)	70
Rating (kW)	1650

The cost and empirical mass equations presented in reference [110] were used exclusively to obtain estimated costs for the various components of the "baseline" turbine and tower. Using the percentages given for the relative contribution of each part in the assorted turbine components shown in Table 67 it is possible to resolve an effective PPI for each component. A simple weighted average is used of the form:

$$\boldsymbol{PPI_{Effective} = \sum \frac{PPI_i\,(2010)}{PPI_i\,(2002)} w_i \times 100} \qquad \textbf{Equation 128}$$

where PPI_i is the Producer Price Index of part *i* for each year and w_i is the fraction of the part in the overall component, i.e. the blades. Where the PPI was not available for the specified years, the GDP deflator [320] was used to escalate or deescalate the PPI to the required year. Some turbine components such as the platforms and railings did not have associated NAICS numbers. In these cases, the GDP deflator [320] was used to determine "general inflation" of the component from 2002 to 2010. As such, general inflation is taken to be 20.4% between 2002 and 2010, corresponding to an index of 120.4 in 2010 with a base index of 100 in 2002.

The effective PPIs are given in Table 69 for each of the components; the components that used the GDP deflator are marked with an asterisk (*). It can be seen that all components had effective PPIs over 100, but some components, such as the blades and the brake, had lower effective PPIs than general inflation over the same period. The new inflated cost of each component is then the original cost in 2002 dollars times the effective PPI for the component, divided by 100 – the index at the base year.

The updated cost of each component is then calculated by multiplying the effective PPIs by the original cost of the component to get the cost in 2010 dollars, as shown in Table 69.
The overall PPI for the entire wind turbine is calculated by summing the inflated component costs and dividing by the original cost of the turbine. The overall PPI for the turbine is simply the ratio of the inflated turbine cost to the baseline turbine cost from 2002:

$$\boldsymbol{PPI_{Overall} = \left(\frac{Turbine\ Cost_{2010}}{Turbine\ Cost_{2002}}\right) \times 100 = 139.1} \qquad \textbf{Equation 129}$$

The overall PPI for the turbine is substantially higher than the GDP deflator over the same time period, yielding costs that are nearly 20% higher. Moreover, the PPI is found to be almost indifferent to the turbine model – baseline or advanced, using any of the four generator types –

for any reasonable combination of rating, height and radius. The implications are that the PPI should be used regardless of the turbine model to escalate the costs, and that Equation 129) is an excellent approximation for all models over the period between 2002 and 2010.

Table 69 – The original and inflated costs of all the components

Component	Original Cost (2002$)	Inflated Cost (2010$)	Effective PPI (2002-2010) [2002 = 100]
Blades	235,670	253,450	107.5
Hub	53,820	103,400	192.1
Pitch System	58,600	79,350	135.4
Nose Cone*	5,550	6,680	120.4
Low Speed Shaft	33,510	52,190	155.7
Bearings	20,910	28,150	134.6
Gearbox	171,710	230,780	134.4
Brake	3,280	3,370	102.7
Generator	107,250	140,750	131.2
Variable Speed Electronics	130,350	170,440	130.8
Yaw Drive	31,900	44,470	139.4
Mainframe	51,870	99,650	192.1
Platforms, Railings*	13,270	15,980	120.4
Electrical Connections	66,000	115,460	174.9
Hydraulics	19,800	27,100	136.9
Nacelle	22,890	24,420	106.7
Industrial Process Control	35,000	43,300	123.7
Tower	218,180	341,070	156.3
Totals	**1,279,570**	**1,780,040**	**139.1**

The contribution to the overall cost for each component has changed over the period, primarily due to the changes in material costs. For example, the cost contribution of the blades decreased by over 4%, primarily due to the reduction in the cost of fiberglass. However, substantial cost contribution increases were observed in the hub (+1.6%) , the mainframe (+1.54%) , the electrical connections (+1.33) and the tower (+2.1%) due to the considerable costs spikes of steel and copper.

In order to differentiate the components (i.e. blades, pitch mechanisms, etc) from the parts (i.e. fiberglass, drive motors, etc) it is useful to look at the cost contributions as identified by their

NAICS codes. Doing so will help elucidate which particular materials most influence the overall cost. There are 17 unique NAICS codes used in the cost model for the turbine and tower; some codes, such as bearings (NAICS 332991P) or fiberglass (NAICS 3272123) were used with multiple components. In this case, each the cost contribution for each part was summed for the entire turbine. The cost contributions for all 17 NAICS codes are given Figure 61, sorted by relative cost contribution.

The results show that four principal parts of the wind turbine make up nearly 50% of its cost: rolled steel manufacturing, the speed reduction gearing, fiberglass fabric, and relay and industrial control manufacturing. Major price fluctuations in any of these categories will have a profound influence on the overall cost of a wind turbine.

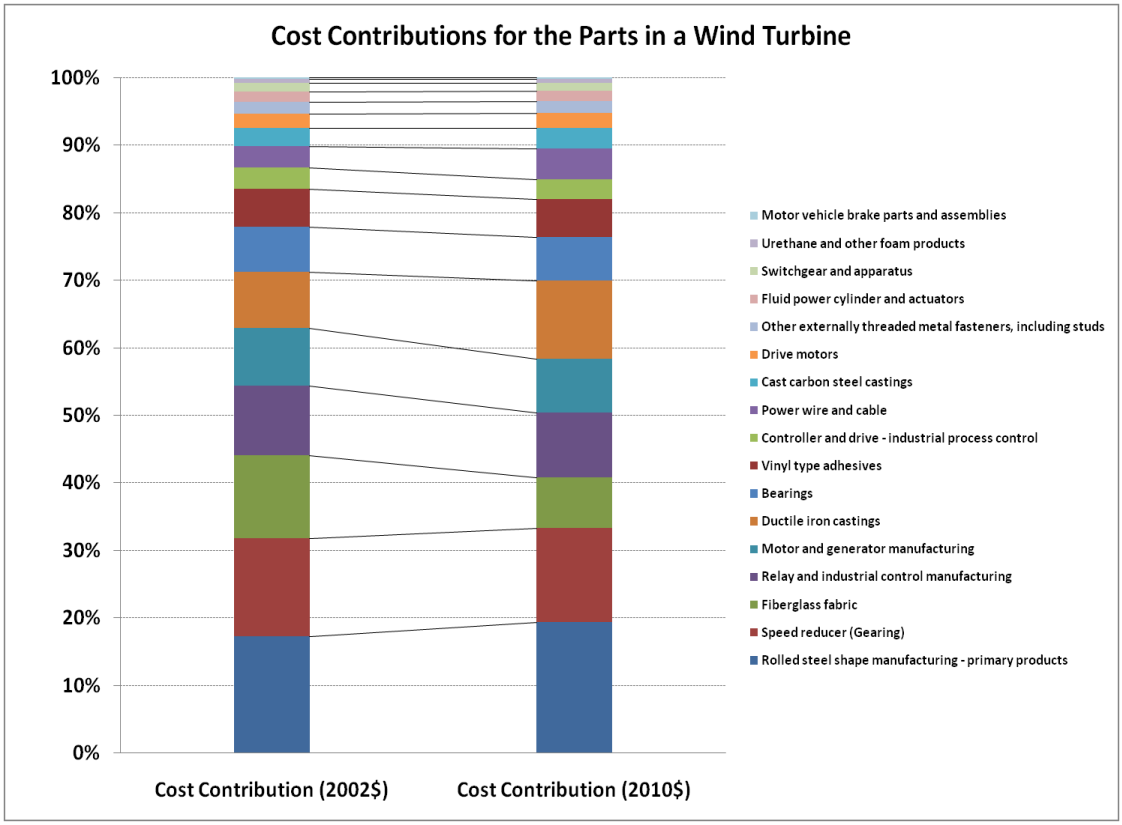

Figure 61 – Cost contributions for the parts in a wind turbine

7.1.3 Comparison with Wind Turbine Prices

The cost escalation method can be compared to a recent study carried out by Lawrence Berkeley National Laboratory (LBNL) in which the drivers of turbine prices were estimated [352]. A similar analysis is also published in the DOE 2010 Market Report [353]. The LBNL study focused on data gathered in the US wind turbine market from 1997 to early 2011. The price estimates include only the rotor-nacelle assembly (RNA), the tower and transportation to the site. The LBNL report indicated that normalized real wind turbine prices (2010$/kW) in the United States doubled from 2002 to 2008 – amidst a sixfold increase in installed wind turbine capacity – before decreasing in 2009 and 2010. The price trend contradicts traditional learning curve theories, which hold that as production increases, manufacturing costs decrease [69, 352]. The uncharacteristic price trend was explained with seven primary drivers: labor costs, warranty provisions, profit margins, turbine scaling, materials prices, energy prices and currency movements.

The present work assumes that the PPI can capture labor costs, materials, and energy but not currency movements, profit margins or warranty provisions. Furthermore, because the same wind turbine model (a generic model based on the dimensions of a Vestas V-82) is used throughout the analysis, wind turbine scaling is held constant at zero. The analysis done by LBNL included the effects of turbine scaling by holding PPI price levels constant and using the average turbine sizes for each year from 2001 through 2010 [352]. The cost of the turbines was found to increase by $234/kW over that time period.

By using the procedures discussed above, the cost escalation method can be extended to incorporate all years from 2002 to 2010. The turbine dimensions and nameplate capacity (Table 68) are still held constant, and the effective PPI is calculated for each component for each year. The effect is an “overall wind turbine PPI” for each year over the period 2002-2010. As a result,

the updated wind turbine costs are in nominal dollars for each year, rather than real 2010 dollars. In order to compare the cost escalation method presented here and the prices listed in the LBNL report, the results need to be inflated to 2010 US dollars using the GDP deflator. To obtain the real costs for each year in 2010 US dollars the GDP deflator is used, as shown in Equation 130):

$$\boldsymbol{C_{WT,2010} = C_{WT,2002}\left(\frac{GDP_{2010}}{GDP_j}\right)\left(\frac{PPI_j}{PPI_{2002}}\right)} \qquad \textbf{Equation 130}$$

Here, $C_{WT,2002}$ is the calculated wind turbine cost from the NREL model, in 2002 dollars; GDP_j is the GDP deflator for each year of interest, j; GDP_{2010} is the GDP deflator in 2010; PPI_{2002} is the effective PPI for the wind turbine base year; PPI_j is the PPI for the wind turbine in the year of interest, j. The calculation yields $C_{WT,2010}$ – the cost of the wind turbine in 2010 dollars. Therefore, if one wanted to determine the costs of a wind turbine in 2010 dollars for the year 2005 using this method, the effective PPI for 2005 would be used together with the GDP deflators for 2005 and 2010:

$$C_{WT,2010} = C_{WT,2002}\left(\frac{GDP_{2010}}{GDP_{2005}}\right)\left(\frac{PPI_{2005}}{PPI_{2002}}\right)$$

Figure 62 shows the full results of the wind turbine costs as well as the LBNL wind turbine prices. The costs in the figure include the transportation of the turbine and tower to the physical site, as outlined in reference [110]. The results show that the present cost escalation method overestimates the costs during 2002 and 2003, and then underestimates the costs throughout the latter part of the decade. The initial overestimation is likely due to the effects of turbine scaling, as discussed above. The effects of turbine scaling diminish until about 2007, when the average turbine size used in the LBNL study is roughly the same as the turbine used in this work. Between 2009 and 2010, the turbine sizes increase beyond 1.65MW indicating that the prices should be higher. However, at the same time, the profit margins, warranty provisions and currency movements decreased, causing a net reduction in turbine prices. The labor, materials and

energy can be isolated from the LBNL analysis and compared to the PPI cost update method. A summary of the cost changes is shown in Table 70. The results indicate that under the assumptions outlined above, the PPI is able to predict – almost exactly – the changes in labor, materials and energy costs for all three time periods. The actual turbine price for the generic 1.65 MW machine being analyzed can be calculated by adding the three drivers not captured by the cost escalation method: warranty provisions, profit margins, currency movements, and the costs of scaling from 2007 to 2010.

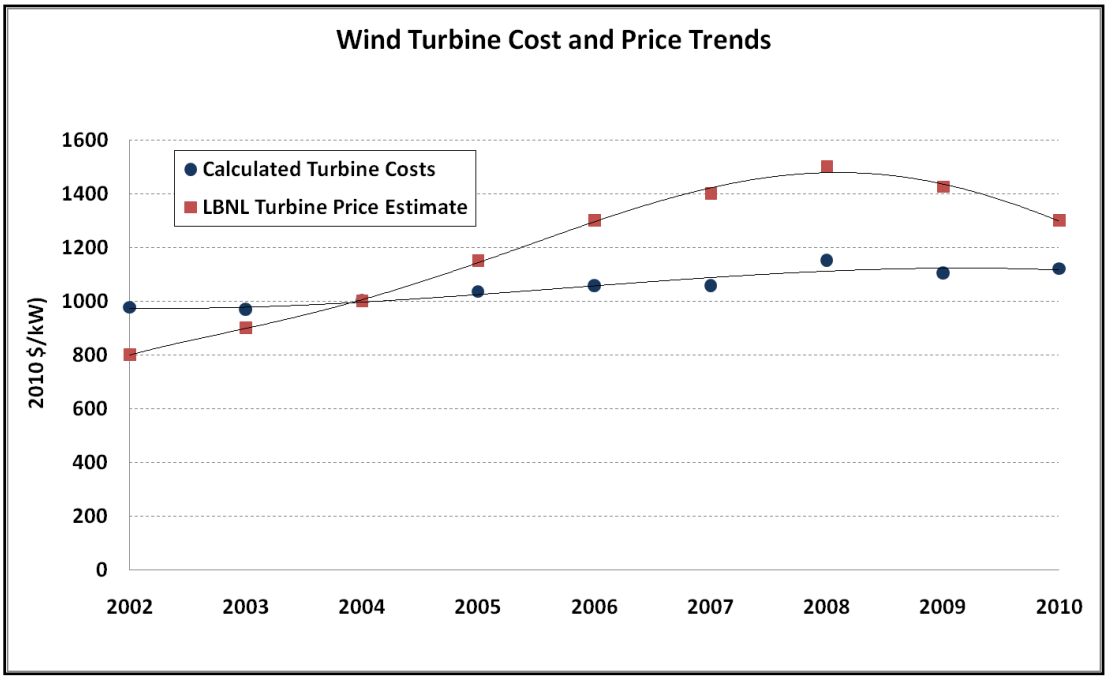

Figure 62 – Cost and price trends in wind turbines

Table 70 – A comparison of turbine cost changes for the LBNL analysis and the present work (2010$/kW)

	Drivers	2002-2008	2009-2010	2002-2010
LBNL Analysis	Labor	+91	+12	+103
	Materials	+71	-31	+40
	Energy	+12	-7	+5
	Totals	**+174**	**-26**	**+148**
PPI/GDP Method	**Labor, Materials, Energy**	**+175.3**	**-31.4**	**+143.9**

7.1.4 Conclusions

The results show that the PPI should be used instead of the CPI to update the costs given in [110]. The difference in the cost for the turbine and tower is using these two approaches on the order of 20%. Over the period between 2002 and 2010 the cost contributions for the various components have shifted slightly, probably due to the costs of raw materials, labor and energy. The products that have the most significant impact on the overall cost were identified as the gearing – NAICS code 333612P, the power electronics equipment – NAICS code 335314P, the rolled steel manufacturing – NAICS code 331221, and the relay and industrial control manufacturing – NAICS code 335314P. Together these four products make up nearly 50% of the total cost of the wind turbine.

The wind turbine cost update models were compared to wind turbine prices as reported by LBNL. It was shown that the PPI was able to accurately update turbine manufacturing costs by capturing the effects of labor rates, energy prices and materials prices. However, the PPI does not incorporate the effects of turbine scaling, exchange rates or profit margins – cumulatively equal to $357/kW from 2002-2010. The results suggest that the PPI can be used as a proxy to estimate the cumulative effects of materials, labor and energy over time. Further, the CPI should not be used to escalate wind turbine costs because it is not capable of representing sudden shifts in energy, materials or labor costs.

It should be noted that the calculated costs were based on terrestrial wind turbines rather than offshore turbines. The model was augmented to include crude estimates of offshore wind turbine costs, including transportation, installation and marinization. Costs for the substructure were also

presented in the NREL model but were not rigorous and considered only the machine rating as an input.

While the costs of a substructure are site dependent and depend on a host of parameters including soil characteristics, wave profiles and wind regimes. A review and implementation of monopile costs, gravity foundation costs and tripod costs beyond the scope of this work, but is given in [354]. Instead, this work assumes monopile substructures because they dominate the market to date.

7.2 European Cost Data

The European offshore wind power industry is often referred to when studying the economics of offshore wind in the United States. The historical costs of European wind farms and equipment are frequently translated from euros, British pounds or Danish kroner directly into US dollars by exchanging the currency and inflating to the desired year using the Consumer Price Index (CPI). However, exchanging and inflating are not commutative: the order of operations matters, especially for older values of the currency. Furthermore, as summarized in this section, there are several indices available for inflating currencies, some of which are not designed for large scale industrial projects. Thus, many European wind farm costs have been translated to US dollars using ambiguous methods with unclear inputs. While there is no "right way" to translate European costs to US dollars from one year to another, there should at least be a standard, transparent methodology used by researchers interested in the industry. This analysis offers a methodology that can be applied to any currency conversion, provided that proper indices and exchange rates are available. Three methods to translate European costs to US dollars are compared: exchange the currency in the original year, then inflate the US dollars using the GDP deflator (exchange-inflate); inflate the original currency, then exchange to US dollars in the final year (inflate-exchange); an average of all exchange-inflate combinations. The results show that

when euros are converted to US dollars using exchange-inflate and inflate-exchange over the period between 2000 and 2010 the values can vary by almost 40%.

To date, there has been significant uncertainty in understanding how to represent historical European offshore wind farm costs in real US dollars. As such, any European wind farm or equipment costs reported in US dollars should be carefully examined before being used in any reports, papers or presentations. While there is no "true" representation of the capital expenditure in another currency, some depictions misrepresent the situation. This article offers a framework for translating historical costs in foreign currencies into present US dollars (or *vice versa*) so that transparent economic comparisons can easily be made. The analysis will focus on the conversion of British pounds and European euros to 2010 US dollars, though the methodology is valid for any historical currency conversion, provided exchange rates, purchasing power parities and proper inflation indices exist.

The offshore wind industry is based mostly in Western Europe, with some modest installations in China and Japan. Accordingly, much of the public economic information on offshore wind turbines and offshore wind components is in terms of euros, Danish krones, Swedish krona, or British pounds. Some researchers have translated those figures into currencies such as US dollars or euros by using inflation and currency conversion [50, 77, 108, 355-356]. In addition, some authors point out that inflation and currency conversion are not commutative [61, 352]. That is, one will arrive at a different dollar value when exchanging from native currency then inflating in the desired currency; versus inflating in the native currency then exchanging to the desired currency. As a result, the costs should be considered a *range*, rather than a single number. This range must be considered when working with any currency that has been translated from another.

7.2.1 Variations in Inflation Indices

Comparing prices from year to year in a single currency is not an exact science. Indeed, many indicators exist that can be used to bring costs forward from one year to another: the Consumer Price Index [348] , the GDP deflator [320], the Big Mac index [357], or the Chemical Engineering Plant Cost Index [358]. These indicators prove to be useful for updating the costs of specific goods or services over time. However, one should not use the Chemical Engineering Plant Cost Index to determine the relative price of bread from one year to another; nor should the Big Mac index be used to compare the cost of a car in 2000 to one in 2010. Economic indices are developed for specific goods, services or "baskets" of both, and should only be used for their intended purpose.

In the United States a typical method for price comparisons uses the Consumer Price Index (CPI) which measures "changes in the prices paid by urban consumers for a representative basket of goods and services" [348]. The CPI is reported for almost all populations in the US including all urban consumers, consumers in large cities, consumers in the Northeast, etc. It also provides specific indices for a host of goods such as bread, housing, transportation and clothing. However, the CPI which is developed for urban consumers is frequently used as a proxy for general inflation, probably because it is simple, covers the entire country, and has easily accessible, quality data. The CPI is developed for urban consumers to understand their buying power over time, not for understanding the temporal cost shifts in construction projects or industrial equipment.

The Gross Domestic Product (GDP) tracks the relative value of all goods and services throughout the economy. The GDP is a better choice for offshore wind farm costs because they are large projects involving numerous industries working together [359]. The GDP deflator is the ratio of the nominal GDP to the real GDP multiplied by 100 and then normalized to the base year:

$$GDP\ deflator = \left(\frac{Nominal\ GDP}{Real\ GDP}\right) \times 100$$

The GDP deflator is maintained in the United States [320], the European Union [321] and the United Kingdom [360], among others [361], making it an obvious choice for determining the inflation rates in various countries, as they apply to large-scale construction projects.

While the GDP deflator can be used to inflate European project costs, the process is somewhat more complicated than in countries that have their own currency. Europe has several countries that use the same currency, but have different inflation rates. Also, there are countries within Europe such as Denmark, Sweden and the UK that have different currencies *and* inflation rates. However, since the GDP deflator index is available for the 17 country Eurozone [321] that index can be used in the home country of the wind farm to inflate the costs.

Figure 63 shows the variation in the GDP deflator for Denmark the United Kingdom, the United States and the 17 country Eurozone. The indices give different snapshots of how the economies are performing over the time interval. While the 17 member European GDP deflator was used here, other GDP deflator indices from specific countries could also be used. For example, the GDP deflator for Germany could be used for the Alpha-Ventus [89] wind farm instead of the 17 country Eurozone GDP deflator.

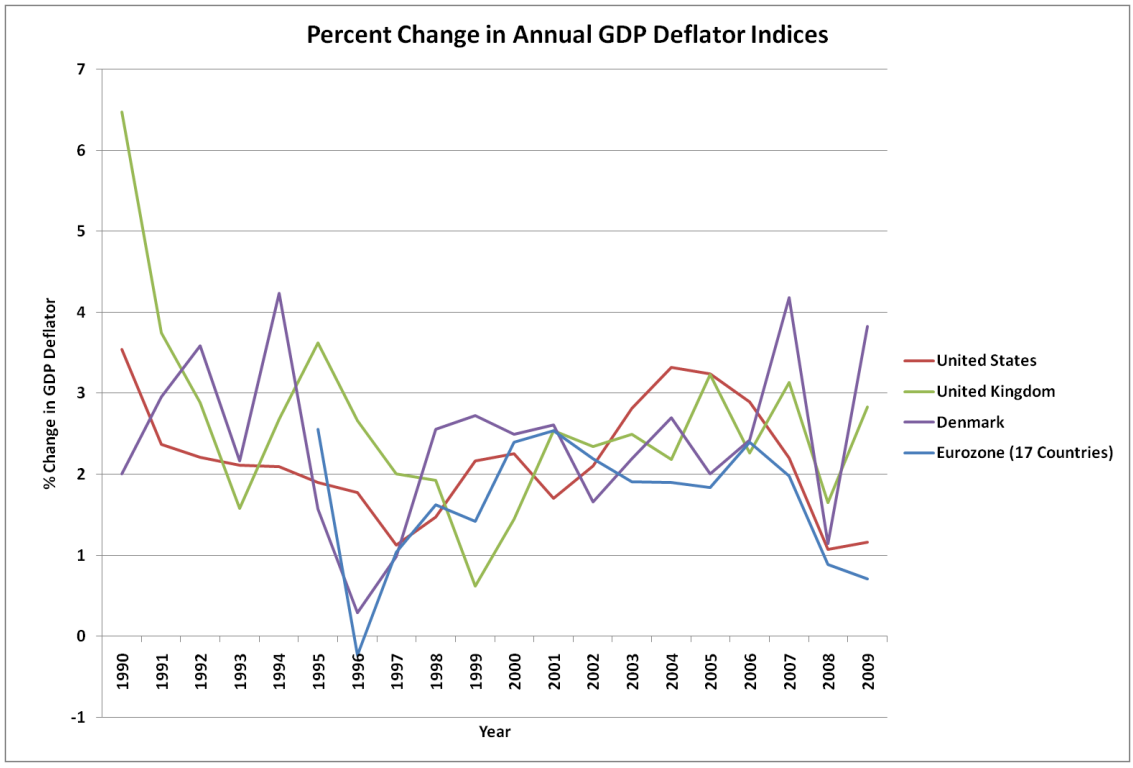

Figure 63 – Percent change in the GDP deflator indices in Europe, the UK and the US and Denmark over the period 1990 to 2010 [320-321, 360]

7.2.2 Currency Exchange and PPPs

Inflating the costs of the wind turbines is only part of the problem; the currency must also be exchanged. Exchange rates measure the value of one currency in terms of another currency so they can be used when converting from foreign currencies to the US dollar. Average annual values for three key European exchange rates are shown in Figure 64. (Note that the Danish krone has been officially pegged to the euro since January 1, 1999 so its exchange rate varies very little [362]. The peg does not directly affect krone to USD conversions using PPPs). Using these exchange rates it is possible to convert one currency to another, but only in a particular year. Thus, one could convert Danish krones in 2000 to US dollars in 2000, but not to any other year. An inflation correction must be used for that purpose.

Purchasing Power Parities (PPP) can be employed instead exchange rates to convert money between currencies [363]. The PPP is a special deflator for currency conversion that levelizes

prices across countries, allowing meaningful comparisons of goods and services [364]. Thus, PPPs act like implicit currency converters, with the common currency taken to be US dollars at a price level of unity. While PPPs function exactly like exchange rates in the conversion process, they may diverge significantly in value, as shown in Figure 64.

The underlying assumption for the PPP exchange rate is that international prices hold for all economies – a unit of currency has the same buying power across countries. While tariffs, transportation, taxes and other barriers may invalidate the theory of PPP to a certain extent [365], this work assumes that the theory of PPP exchange rates holds for the economies of interest – the United States, and Western European countries.

Since the PPP per GDP for US dollars is always unity, the PPP exchange rate S_k, for a particular country, *k*, is given by:

$$\frac{\mathbf{1}}{\boldsymbol{PPP_k}} = \boldsymbol{S_k} \qquad \textbf{Equation 131}$$

There are several data sets available for PPPs: one maintained by the Organization for Economic Co-operation and Development (OECD) [364], one maintained by the International Monetary Fund (IMF) [361], and another maintained by the Center for International Comparisons of Production, Income and Prices at the University of Pennsylvania [366] . Slight differences occur between the datasets simply due to the methodologies used to compile and compute the data. For this analysis, the PPP for GDP data are sourced from the OECD.

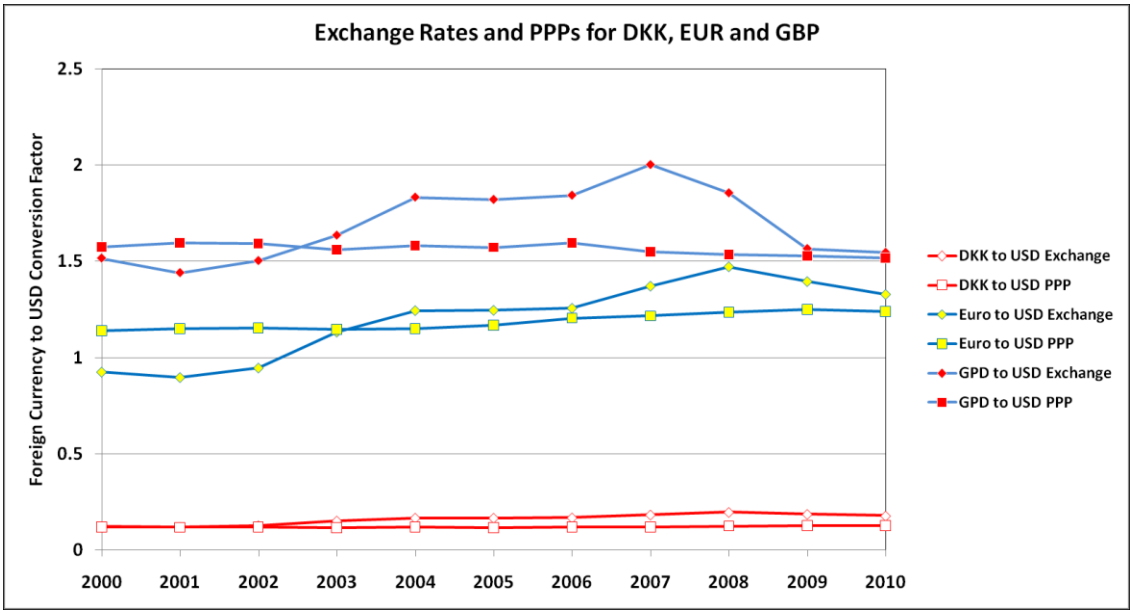

Figure 64 – Exchange rates and PPPs for several countries with offshore wind farms [319, 361, 367]

The equation for converting a foreign currency, C_k, to US dollars, C_{US}, using the exchange rate S_k for a country, k, is given below:

$$\boldsymbol{C_{US} = C_k S_k} \qquad \textbf{Equation 132}$$

The value, $\boldsymbol{C_{US}}$, calculated using Equation 132 is either in nominal US dollars if the foreign currency was exchanged in year 1 (exchange-inflate) or in real dollars if the foreign currency was inflated first (inflate-exchange).

7.2.3 Translating Historical Foreign Costs to Real US Dollars

As already mentioned, the currency can be exchanged first then inflated ("exchange-inflate"), or inflated then exchanged ("inflate-exchange"), or some other combination of inflate-exchange. The exchange-inflate method exchanges all of the foreign currency in year 1 to US dollars and then inflates the value in US dollars to year n to determine the cost. This can be done using either the exchange rate or the PPP for GDP:

$$C_n = C_1 \left(\frac{I_n}{I_1}\right) S_{k,1} \qquad \textbf{Equation 133}$$

Here, the *I* values are the inflation index in the United States in years 1 and *n*, and the $S_{k,1}$ value is the exchange rate to US dollars or the PPP for GDP in year 1 for country *k*; C_1 and C_n refer to the nominal cost in the foreign currency and real cost in the new currency (assumed here to be US dollars), respectively.

Another method could be to inflate the original currency to year n, and then use the exchange rate in year *n* to convert to US dollars (inflate-exchange). The general form of the equation is:

$$C_n = C_1 \left(\frac{J_n}{J_1}\right) S_{k,n} \qquad \textbf{Equation 134}$$

Here, the *J* value is the inflation index of the foreign currency in years 1 and *n*; $S_{k,n}$ is the exchange rate to US dollars, or the PPP per GDP in year *n* for country *k*. When using this method the currency is typically inflated in the foreign currency and only exchanged in the year of interest. However, this need not be the case. The foreign currency can be exchanged in any year during the interval, and the year in which the exchange takes place has a dramatic effect on the result [322].

In order to represent the range of numbers with a single value, one suggested method uses an average of all the possible combinations of inflate and exchange to determine the updated cost [322]. This approach gives equal weight to all of the currency exchanges and the inflation rates:

$$C_n = C_1 \frac{\sum_{i=1}^{n} \left(\frac{I_n}{I_i}\right)\left(\frac{J_i}{J_1}\right) S_{k,i}}{n} \qquad \textbf{Equation 135}$$

Here, there are two price indicators, *I* and *J*, which refer to the inflation indices of the desired currency and the known currency, respectively; $S_{k,i}$ is the average yearly exchange rate to US dollars or PPP per GDP in year *i* for country *k*, and C_1 is the known cost in the foreign currency.

The subscripts refer to the year with 1 being the first year and *n* being the last year of the time period. When *i* is equal to 1 in Equation 75 the term in the summation series represents exchange-inflate; when *i* is the last number in the summation series the term represents inflate-exchange.

7.2.4 Example Cost Conversion Calculations

Table 71 presents data for offshore wind farms built in UK waters. The UK wind farms were chosen because the UK has always used the pound sterling as a currency. Thus, currency ambiguities that arise from the switch to a common currency in continental Europe do not occur.

The costs of each wind farm are given in British pounds and the costs are assumed to be incurred during the first year of operation. In order to represent the costs of these wind farms in 2010 US dollars some combination of inflating and exchanging must be utilized.

The Blyth Offshore wind farm is used to illustrate the concepts discussed above. Data from Figure 64 and Table 71 are used together with the exchange-inflate method (Equation 133) to calculate the cost of the Blyth wind farm:

$$\boldsymbol{C_1 = £4\left(\frac{111}{88.65}\right) \times 1.5162 = \$7.59\ Million}$$

Here, C_1 is the translated cost of an offshore wind farm with the original currency exchanged in year 1. However, if the inflate-exchange method is used (Equation 134) the cost in 2010 US dollars becomes:

$$\boldsymbol{C_{11} = £4\left(\frac{100}{78.771}\right) \times 1.5458 = \$7.85\ Million}$$

Table 71 – Wind farms built in the UK with reliable capital cost information [49]

Wind Farm	Cost (Million £)	Size (MW)	Year
Blyth Offshore	4	4	2000
North Hoyle	80	60	2003
Scroby Sands	75.54	60	2004
Kentish Flats	105	90	2005
Barrow	139.5	90	2006
Beatrice	35	10	2007
Lynn	300	97	2008
Inner Dowsing	300	97	2008
Rhyl Flats	198	90	2009
Robin Rigg	396	180	2009
Gunfleet Sands 1 & 2	420	172	2009
Thanet	900	300	2010

In this case the original currency was exchanged in 2010, or year 11. Finally, if every combination of exchange and inflate is calculated and averaged the "real value" of the Blyth Offshore wind project could be taken to be $8.39 million dollars in 2010, as shown in Table 72. The data in Table 72 includes the three calculations that were already discussed – marked in the middle column according to the equation used – as well as the additional calculations. The results clearly differ depending on the year of the exchange: for traditional exchange rates, the second year has the lowest value; the eighth year has the highest. Thus, the range of values is $7.15 million to $9.84 million, depending on the year of exchange, with the average being $8.39 million.

The PPP for GDP figures could also be used to perform the calculation using the same procedure as above. Those results are also shown in the right-hand column of Table 72 along with the pure exchange rate cost update figures. The costs of Blyth Offshore are much more consistent – and lower – when using the PPPs to exchange the currency. The average value is more than a half a million dollars lower than the pure exchange rate method. The high is $7.98 million, occurring in year 3; the low is $7.63 million, occurring in years 8-10, and the average is $7.80 million.

Table 72 – Example calculations for representing the cost of Blyth Offshore wind farm in 2010 US dollars

Exchange Year	Cost of Blyth Offshore using exchange rate (Millions $2010)	Cost of Blyth Offshore using PPP GDP (Millions $2010)
1	7.58	7.88
2	7.15	7.93
3	7.51	7.98
4	8.20	7.83
5	9.17	7.91
6	9.00	7.78
7	9.11	7.90
8	9.84	7.63
9	9.13	7.63
10	7.78	7.63
11	7.85	7.70
	$8.39 Million	**$7.80 Million**

Using the pure exchange rate method, Equation 73 and Equation 75 are applied to the entire set of UK offshore wind farm costs listed in Table 71, then normalized with the nameplate capacity. The full results are shown in Figure 65. Instead of reporting the inflate-exchange and exchange-inflate values, only the high and low values of the range will be reported along with the average value of the entire interval. The range represents all possible values using this method. In addition, the *de facto* industry standard CPI-based exchange-inflate results are included for comparison.

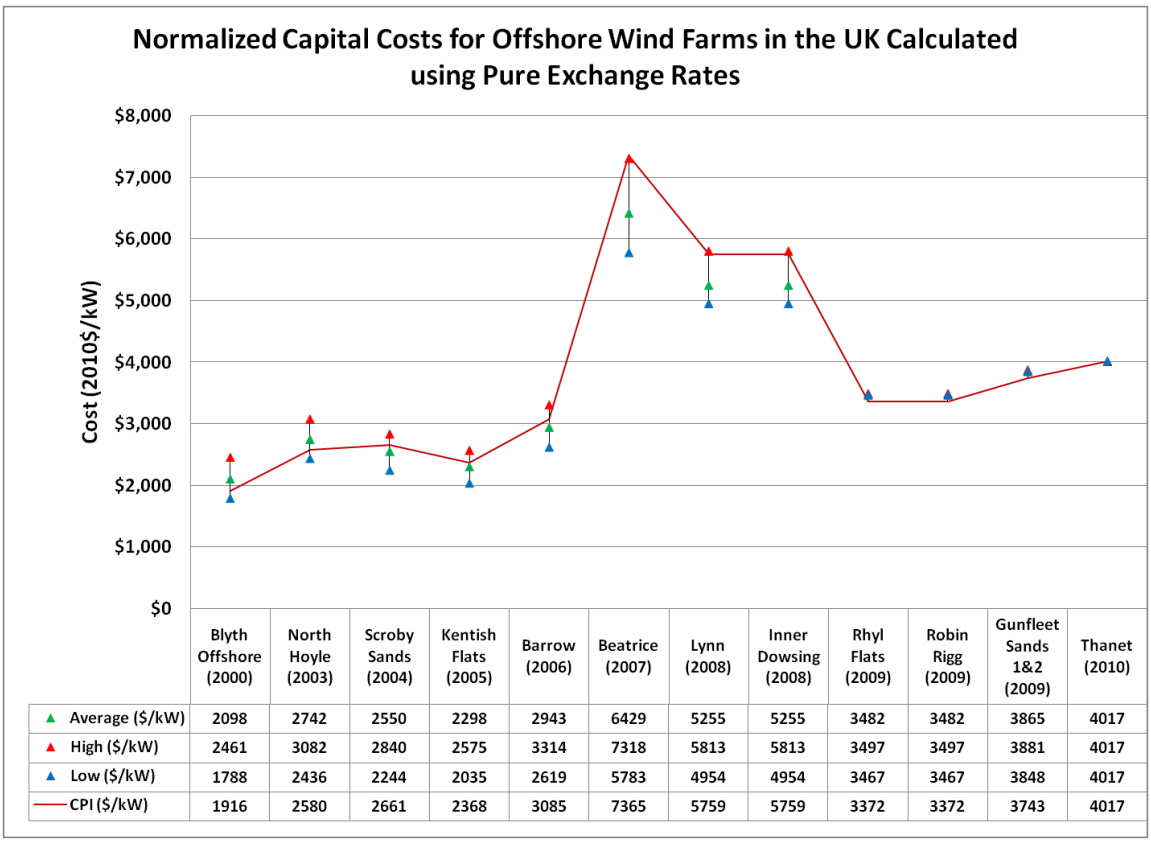

	Blyth Offshore (2000)	North Hoyle (2003)	Scroby Sands (2004)	Kentish Flats (2005)	Barrow (2006)	Beatrice (2007)	Lynn (2008)	Inner Dowsing (2008)	Rhyl Flats (2009)	Robin Rigg (2009)	Gunfleet Sands 1&2 (2009)	Thanet (2010)
Average ($/kW)	2098	2742	2550	2298	2943	6429	5255	5255	3482	3482	3865	4017
High ($/kW)	2461	3082	2840	2575	3314	7318	5813	5813	3497	3497	3881	4017
Low ($/kW)	1788	2436	2244	2035	2619	5783	4954	4954	3467	3467	3848	4017
CPI ($/kW)	1916	2580	2661	2368	3085	7365	5759	5759	3372	3372	3743	4017

Figure 65 – The capital costs for offshore wind farms in the UK, calculated using pure exchange rates

In general, the older wind farms have greater variance between the three calculated values than the newer farms. This is reasonable because as the time interval approaches zero the exchange-inflate and the inflate-exchange scenarios become equal, which is the case for the Thanet wind farm. The Beatrice wind farm has the greatest variance because the exchange rate increased significantly in 2007, when the wind farm was built. The CPI method uses these high exchange rates and then inflates in US dollars. Thus the CPI method captures fluctuations in exchange rates and reports results that are on the high end of the range, as with Beatrice, and Lynn/Inner Dowsing.

The same procedure is applied to the UK dataset using the PPPs for GDP instead of the pure exchange rates. Those results are shown in Figure 66, along with CPI-based exchange-inflate

method. It is easily seen that the PPPs levelized the costs and significantly decreased the variance in the reported range. The CPI method is higher than many of the values calculated using the PPP method.

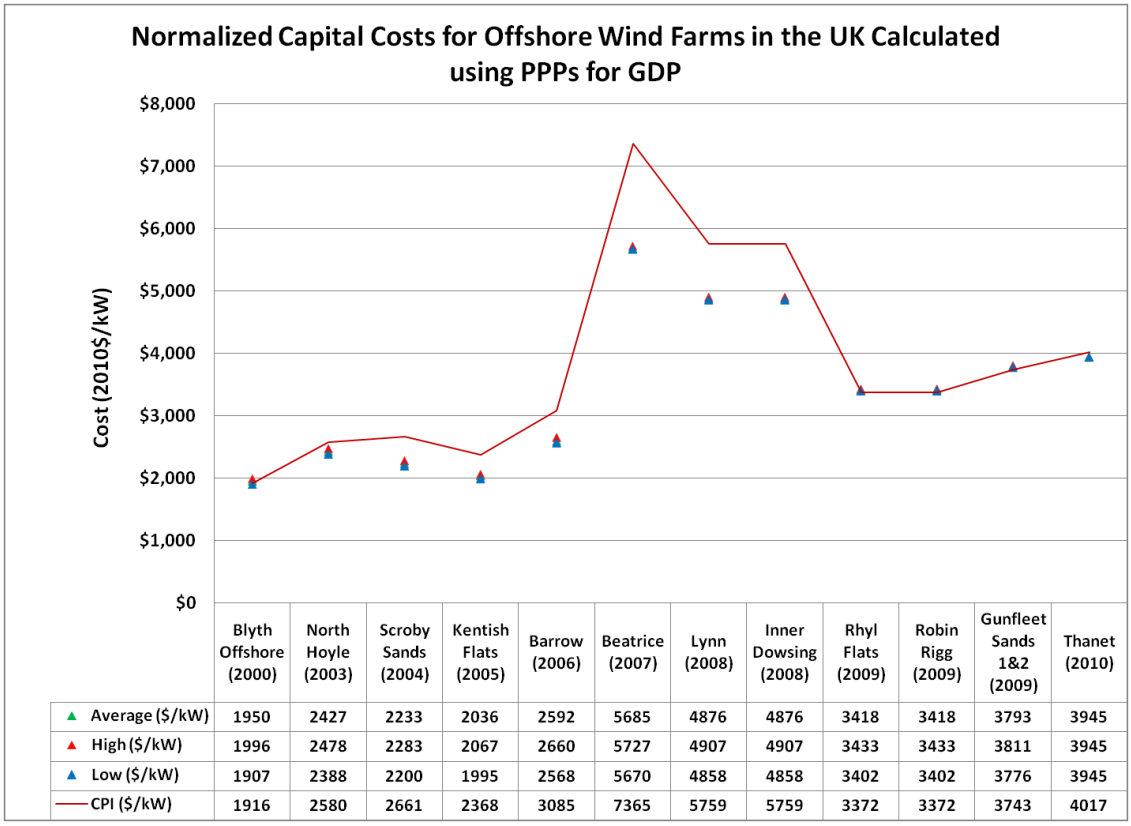

	Blyth Offshore (2000)	North Hoyle (2003)	Scroby Sands (2004)	Kentish Flats (2005)	Barrow (2006)	Beatrice (2007)	Lynn (2008)	Inner Dowsing (2008)	Rhyl Flats (2009)	Robin Rigg (2009)	Gunfleet Sands 1&2 (2009)	Thanet (2010)
Average ($/kW)	1950	2427	2233	2036	2592	5685	4876	4876	3418	3418	3793	3945
High ($/kW)	1996	2478	2283	2067	2660	5727	4907	4907	3433	3433	3811	3945
Low ($/kW)	1907	2388	2200	1995	2568	5670	4858	4858	3402	3402	3776	3945
CPI ($/kW)	1916	2580	2661	2368	3085	7365	5759	5759	3372	3372	3743	4017

Figure 66 – The capital costs for offshore wind farms in the UK calculated using PPPs

7.2.5 Discussion of Conversion Results

The conversion factors for translating the costs are unique for a particular time period and currency. That is, the ratio of translated US dollar cost to the original cost is a constant, as can be seen in Equation 31-Equation 75. The factors for converting British pounds to 2010 US dollars are tabulated and graphed for each year, method, and type of exchange rate as shown in Figure 67.

For the pure exchange rate method, the results show that the average of the entire possible range is higher than either the exchange-inflate or the inflate-exchange methods for the first four time intervals. This further implies that several values in the range exceed all three methods. The Blyth example above illustrates this point. Furthermore, the exchange-inflate and inflate-exchange are close in value in the first four time intervals, before diverging for the following six time intervals. The inflate-exchange and the averaging methods are both smooth functions whereas the exchange-inflate is not. This is primarily because inflation rates are relatively stable compared to exchange rates. The inflate-exchange uses only one static exchange rate – the exchange rate between pounds and dollars in 2010; the exchange-inflate uses a different exchange rate for each time interval.

When the same inflation indices are employed in conjunction with PPPs instead of traditional exchange rates the results are much different. First, the variance in the conversion methods nearly disappears, and is much more stable than when using traditional exchange rates. Second, the trend line essentially follows the same path as the inflate-exchange method in the top graph in Figure 67. These phenomena make intuitive sense: the PPPs levelized the variations in exchange rates across countries so that goods and services could be meaningfully compared. Thus, the results shown in the PPP graph should be similar to the inflate-exchange method in the top graph because inflate-exchange uses only the exchange rate in 2010, which is indeed the case.
The same procedure can be used to produce indices to convert from euros to 2010 US dollars. In this case the three methods generate wildly different results in the first three intervals. The exchange-inflate method results in a conversion factor that is a great deal lower than either the inflate-exchange method or the average over all combinations. Nevertheless, the exchange-inflate method practically converges to the other two methods in the middle part of the decade before becoming higher than both the inflate-exchange method and the average method in the later intervals.

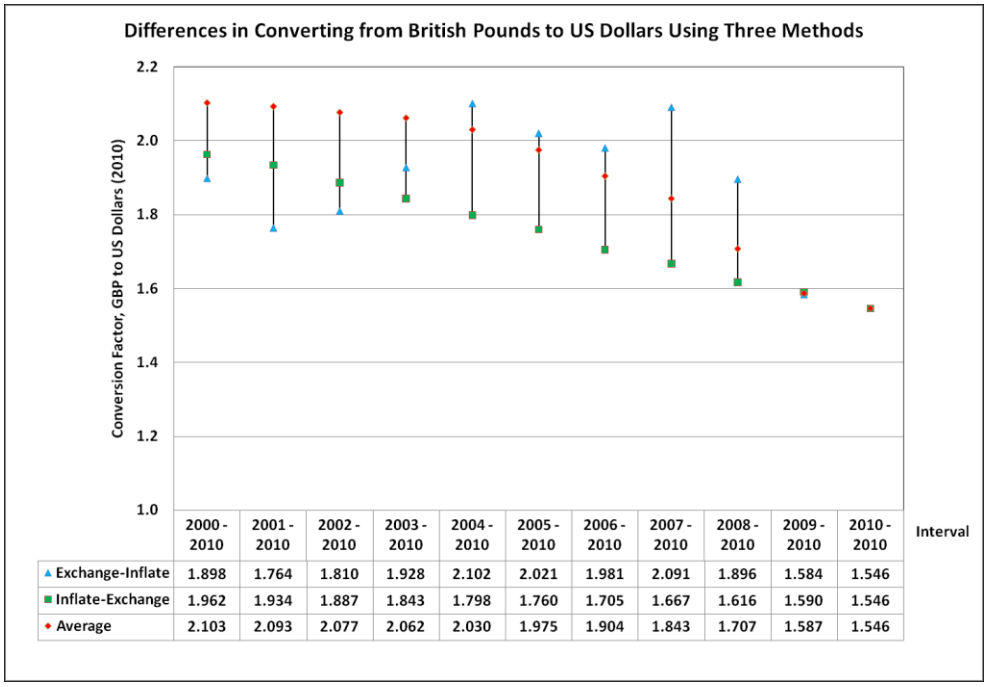

	2000 - 2010	2001 - 2010	2002 - 2010	2003 - 2010	2004 - 2010	2005 - 2010	2006 - 2010	2007 - 2010	2008 - 2010	2009 - 2010	2010 - 2010
Exchange-Inflate	1.898	1.764	1.810	1.928	2.102	2.021	1.981	2.091	1.896	1.584	1.546
Inflate-Exchange	1.962	1.934	1.887	1.843	1.798	1.760	1.705	1.667	1.616	1.590	1.546
Average	2.103	2.093	2.077	2.062	2.030	1.975	1.904	1.843	1.707	1.587	1.546

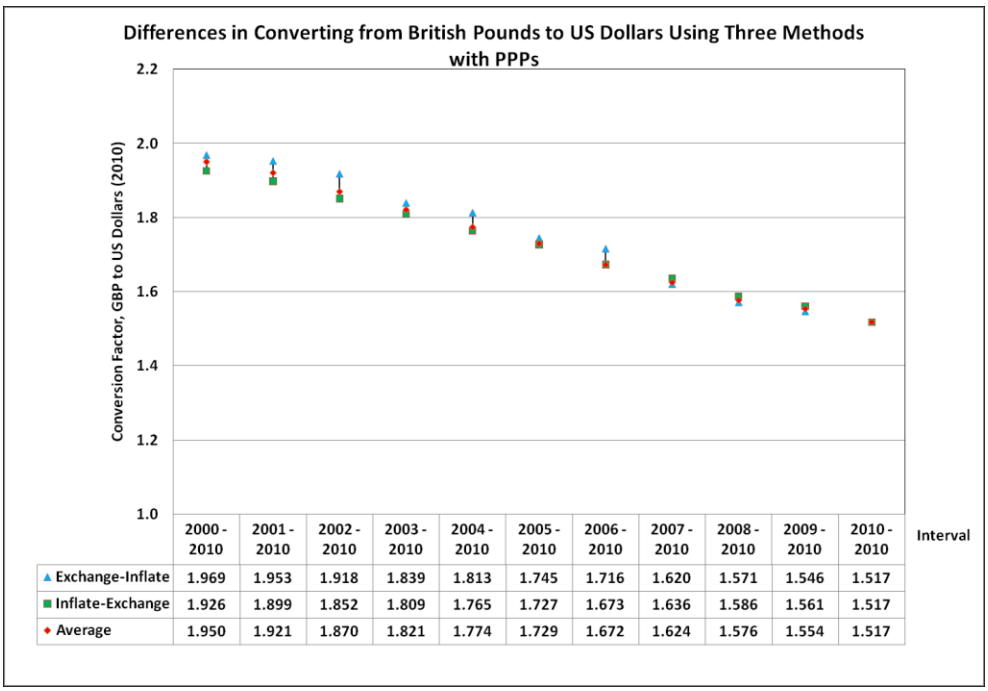

	2000 - 2010	2001 - 2010	2002 - 2010	2003 - 2010	2004 - 2010	2005 - 2010	2006 - 2010	2007 - 2010	2008 - 2010	2009 - 2010	2010 - 2010
Exchange-Inflate	1.969	1.953	1.918	1.839	1.813	1.745	1.716	1.620	1.571	1.546	1.517
Inflate-Exchange	1.926	1.899	1.852	1.809	1.765	1.727	1.673	1.636	1.586	1.561	1.517
Average	1.950	1.921	1.870	1.821	1.774	1.729	1.672	1.624	1.576	1.554	1.517

Figure 67 – The conversion factors for GBP to 2010 USD using exchange-inflate, inflate-exchange, and the average over all combinations for the period 2000-2010 with traditional exchange rates (top) and PPPs (bottom)

The euro to US dollar conversion exhibits similar behavior to the British pound to US dollar conversion. The average and the inflate-exchange methods are smooth functions while the

exchange-inflate is not, again due to fluctuations in the exchange rate. Moreover, the value for the average method exceeds both the exchange-inflate and the inflate-exchange in the middle part of the decade – just as it did in the early part of the decade for the GBP to USD conversion.

If PPPs are used instead of traditional exchange rates, again the variance decreases significantly. However, the results are not as consistent as the GDP to USD results using PPPs, probably because Europe is a much more diverse economy than the UK, and was still adapting to a new national currency. Nonetheless, the euro to USD conversion using PPPs shows a similar trend to the inflate-exchange method using traditional exchange rates, just as it did in the GDP to USD conversion. The similarities are beholden to the 2010 exchange rate, which was not guaranteed to fit the trend.

All of the results show that translating costs across time and space is not a trivial procedure. The answer should be considered a range, rather than a single number. If a single value is used, large fluctuations in inflation or exchange rates could have skewed the final result and misrepresented the situation. Clearly, the PPPs are capable of levelizing exchange rate fluctuations, but do little to mitigate inflation effects. The averaging approach should be used for that purpose because it flattens the spikes than may occur in inflation rates as well as exchange rates. Therefore, a good, consistent representation of translated costs should at least use the averaging approach that is being advocated here. The PPPs should be employed as well if large swings in exchange rates have occurred during the interval of interest.

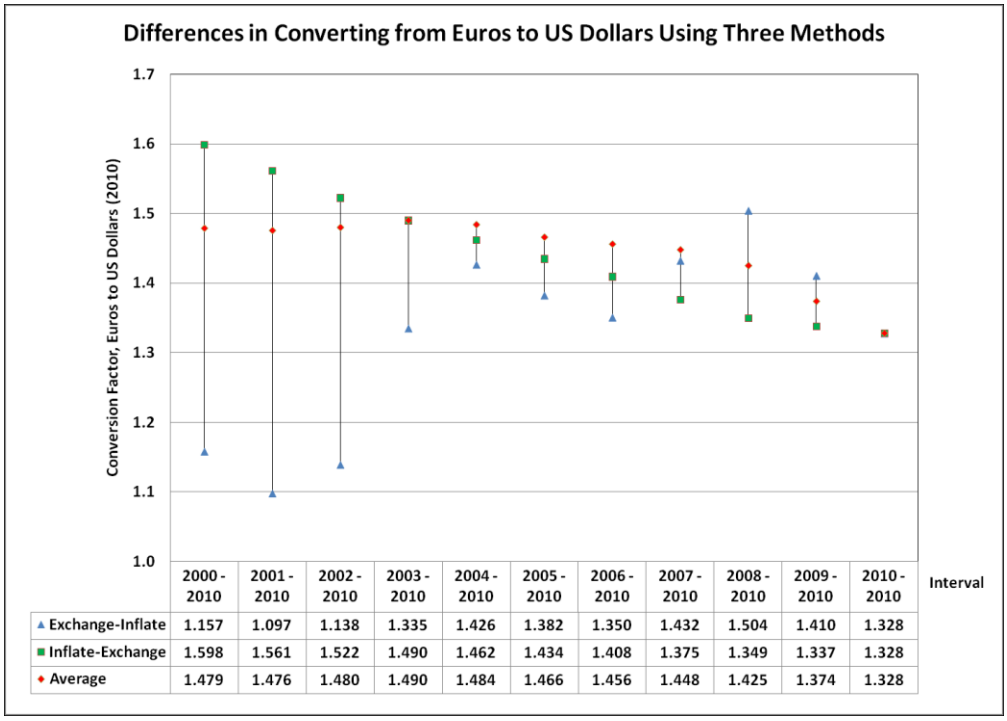

	2000 - 2010	2001 - 2010	2002 - 2010	2003 - 2010	2004 - 2010	2005 - 2010	2006 - 2010	2007 - 2010	2008 - 2010	2009 - 2010	2010 - 2010
Exchange-Inflate	1.157	1.097	1.138	1.335	1.426	1.382	1.350	1.432	1.504	1.410	1.328
Inflate-Exchange	1.598	1.561	1.522	1.490	1.462	1.434	1.408	1.375	1.349	1.337	1.328
Average	1.479	1.476	1.480	1.490	1.484	1.466	1.456	1.448	1.425	1.374	1.328

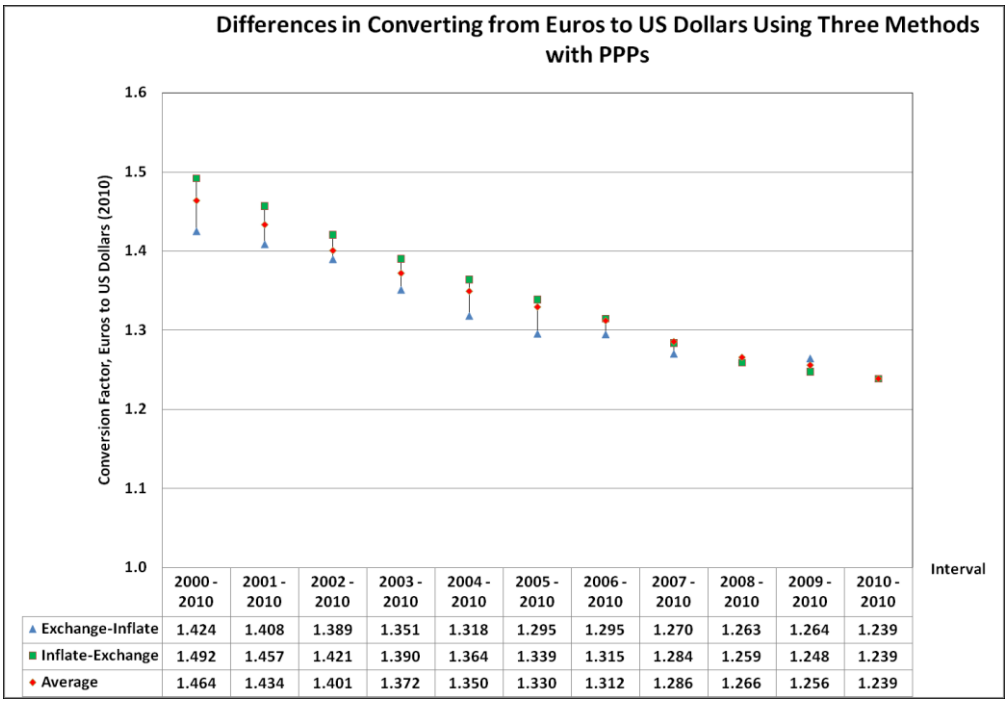

	2000 - 2010	2001 - 2010	2002 - 2010	2003 - 2010	2004 - 2010	2005 - 2010	2006 - 2010	2007 - 2010	2008 - 2010	2009 - 2010	2010 - 2010
Exchange-Inflate	1.424	1.408	1.389	1.351	1.318	1.295	1.295	1.270	1.263	1.264	1.239
Inflate-Exchange	1.492	1.457	1.421	1.390	1.364	1.339	1.315	1.284	1.259	1.248	1.239
Average	1.464	1.434	1.401	1.372	1.350	1.330	1.312	1.286	1.266	1.256	1.239

Figure 68 – The conversion factors for EUR to 2010 USD using exchange-inflate, inflate-exchange, and the average over all combinations for the period 2000-2010 with traditional exchange rates (top) and PPPs (bottom)

The methods discussed heretofore are not unique to US dollar conversion – they could be used to convert U.S. dollars to other currencies, or any currency to another, provided that the exchange rate data or PPPs and inflation indices exist for each currency. Furthermore, the methods propounded above are technology-agnostic: they are not unique to large scale offshore wind construction projects, and could easily be adapted to offshore wind equipment cost data, solar PV data or any other similar data set.

When cost data are translated into real US dollars for specific target year, the data are valid only for target year that they are representing. If researchers seek to use the translated costs in a different target year, the data should be retranslated from the original currency and year to the desired currency and year. Doing so ensures that consistent methods are employed to translate costs across time and space. If the translated currency is simply inflated in US dollars then the exchange rates and foreign inflation are ignored.

The inflation rate advocated in this work is the GDP deflator which is a measure of the overall health of the economy. It is assumed that the GDP deflator is a good indicator for a large construction project like an offshore wind farm because it requires many industries working collectively to erect the wind farm. If, however, one is interested in a small project, or a piece of equipment, other economic indices may be more relevant. For example, the Producer Price Index (PPI) is available in the United States for numerous industries and pieces of equipment [302]. The PPI measures the average change in selling prices received over time for specific products and services in the United States, as reported by domestic producers [302]. The PPI captures changes in production costs, labor rates and raw materials with a single number, specific to a particular product. Using the PPI, the cost of specific equipment can be escalated or deescalated generating accurate updated costs. Thus, an index like the PPI can be used for small projects or equipment instead of the GDP deflator to better encapsulate the specific inflation rate over time.

7.2.6 Conclusions

This analysis offered an economic model that levelizes costs of construction projects or large-scale equipment so that meaningful comparisons can be made across space and time. Historical costs in foreign currencies are brought into present-day US dollars using a combination of exchange rates and inflation indices. Three primary methods for converting historical foreign currencies to current US dollars were discussed: exchange-inflate, inflate-exchange and the average over all possible combinations. Each method could be used to convert foreign currencies to real US dollars, or any currency to another, provided that the exchange rate data and inflation indices exist for each currency. The three methods yield a range of translated project costs, all of which are valid. While each method is suitable for representing historical foreign currencies in real US dollars, there are some marked differences. First, the exchange-inflate method depends on the inflation index for the US dollar over the time period and the exchange rate or PPP at the beginning of the time interval. The inflate-exchange method is dependent on the inflation rate for the foreign currency, and the exchange rate or PPP at the end of the time interval. Thus, both the inflate-exchange and the exchange inflate depend linearly on the value of the exchange rate or the PPP, but at different times.

The maximum and minimum of the translated cost range need not include the exchange-inflate or the inflate-exchange. The average over all possibilities attempts to correct ephemeral instabilities in the exchange rates or PPPs as well as the inflation rates by using a simple averaging approach. The averaging approach considers each exchange year to be equally valid. Thus, large aberrations in exchange and inflation rates are smoothed out and give a better understanding of the "real value" of the project in question.

It is imperative that any costs found in the literature are verified as either being US dollar costs originally, or suitably translated to US dollars from a foreign currency. Furthermore, it is essential

that when the translated costs are discussed, the method used, the exchange rate, and the inflation indices should be disclosed. With this knowledge, the costs in the original currency can be properly recovered.

7.3 European Equipment Costs

It was already shown that the PPI is a good metric for escalating costs of wind turbine components and encapsulating price movements in labor rates, materials and energy. It was also shown that representing European costs in US dollars can be accomplished using several approaches, each with its own drawbacks. The inflate-exchange and exchange-inflate both capture instantaneous exchange rates at the expense of fluctuation in inflation rates. The average-over-all-values attempts to levelize the exchange rate and the inflation rate fluctuations to give a better representation of costs. A combined approach that uses the PPI and the average-over-all-values will be utilized to estimate European equipment costs in present US dollars. First, the costs will be converted from the base currency to US dollars using the averaging approach. Second, the costs will be further escalated (or de-escalated) using the PPI. Since the PPI already assumes some level of inherent inflation, the "general inflation" as calculated by the GDP deflator will first be subtracted from the PPI. The result is a model that simultaneously translates European costs to 2010 US dollars and then further escalates the dollars according to the PPI – or PPIs – for the equipment. Accordingly, the NAICS codes need to be assumed for the equipment. Simplifying assumptions will be used to reduce the dimensionality of the problem.

The cost model developed in this thesis is meant to be a generic model that uses a top-down approach. Optimization and high-level design are not employed in favor of general system configurations common to wind farms and the equipment therein. The model can be applied to any wind farm that utilizes monopile foundations, standard cables, and conventional wind turbines. There are several meaningful parameters that are incorporated into the model such as

turbine size, water depth, distance from shore, turbine spacing – all of which influence the capital costs. The results are reported in 2010 US dollars and are thought to be decent approximations of the total capital costs, akin to a "factored estimate" in chemical engineering.

7.3.1 Foundation/Substructure

The following is a short discussion of the forces and the moments due to wind and water that act on the monopile. However, the design of monopile substructures is beyond the scope of this thesis.

Offshore wind turbine foundations and substructures are sized largely according to the forces that are expected to impinge upon them. The forces are the combined results of gravity, waves, wind, currents, tides and sea ice [368] and must be opposed by the foundation, substructure and, subsequently, the soil. The lateral strength of the soil resists the horizontal wind and water forces while the vertical gravitational force is mainly opposed by friction between the soil and the monopile [354].

A simplified, two-dimensional view of an offshore wind turbine is depicted in Figure 69. Here, the force of the wind is acting on the rotor, and the combined force of the water – including waves, currents, and tides – acts on the monopile. The gravitational force on the rotor nacelle assembly (RNA) usually produces a moment because the center of mass is not directly above the center of the tower. The moment due to the monopile and soil interaction resists the combined moment of gravity, wind and water. Finally, the friction force between the monopile and the soil balances most of the weight of the entire structure including the RNA, the tower, and the monopile. Some of the gravitational force is countered by the rim of the monopile pushing on the seabed as well as the soil plug that forms within the monopile [368].

The forces acting on the turbine could originate from several directions. For example, the wind and the waves could come from the west, while the tides come from the east and the currents from the south. Thus, it is useful to resolve the forces into individual contributions from wind and water to facilitate analysis.

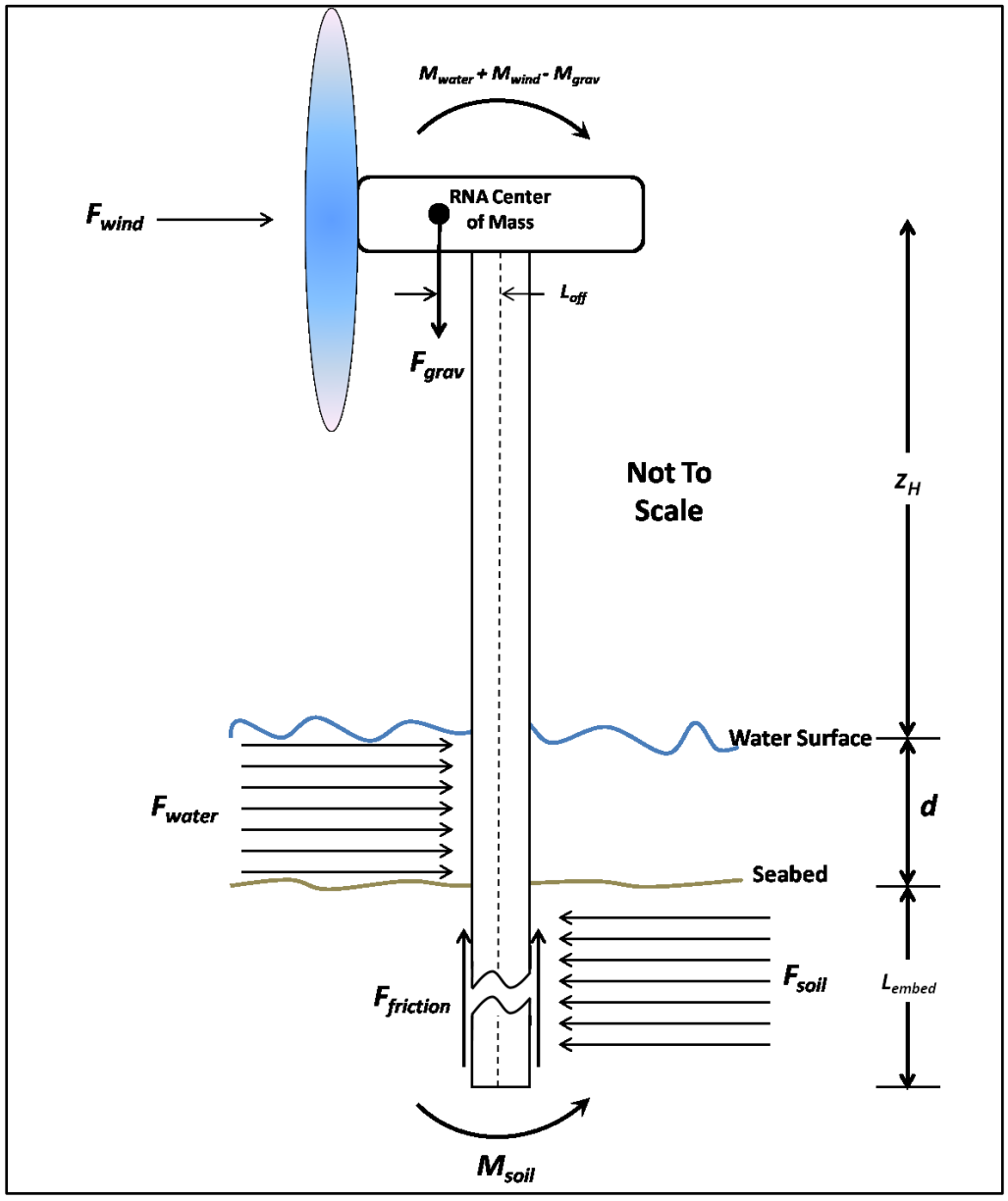

Figure 69 – Forces acting on an offshore wind turbine with a monopile substructure

The thrust on the rotor acts at the hub height, z_H, and produces an overturning moment, M_{wind}. The overturning moment on an ideal turbine due to the wind is a product of the hub height, z_H, and the thrust acting on the rotor disk:

$$\boldsymbol{M_{wind} = \left(\frac{1}{2}\right)\left(\frac{8}{9}\right)\rho\pi R^2 U^2 z_H} \qquad \textbf{Equation 136}$$

The inertial and drag forces of the waves also induce a moment on the structure. The forces due to waves on a monopile can be calculated directly using the Morison Equation, which relates the wave forces to the velocity and acceleration of the water [54]. It is easiest to view the Morison Equation as the sum of the inertial force, F_I, and the drag force, F_D:

$$\boldsymbol{F_I = \frac{1}{2} C_m \rho g \left(\frac{\pi D^2}{4}\right)\hat{\zeta}\tanh(kd)} \qquad \textbf{Equation 137}$$

$$\boldsymbol{F_D = \frac{1}{2} C_D \rho g \left(\frac{D}{2}\right)\hat{\zeta}^2\left[\frac{1}{2} + \frac{kd}{\sinh(2kd)}\right]} \qquad \textbf{Equation 138}$$

where:

F_I	Inertial force due to waves [N]
F_Dl	Drag force due to waves [N]
C_m	Inertia coefficient [-]
C_D	Drag coefficient [-]
ρ	Density of water [$\frac{km}{m^3}$]
g	Gravity [$\frac{m}{s^2}$]
D	Diameter of the monopile [m]
$\hat{\zeta}$	Wave amplitude ($\frac{1}{2}$ peak to trough) [m]
k	Wave number ($\frac{2\pi}{L}$) where L is the wavelength [$1/m$]
d	Water depth [m]

The moments at the seafloor that result from the inertial and drag forces are:

$$\boldsymbol{M_I = \frac{1}{2} C_m \rho g \left(\frac{\pi D^2}{4}\right)\hat{\zeta} d\left[\tanh(kd) + \frac{1}{kd}\left(\frac{1}{\cosh(kd)} - 1\right)\right]} \qquad \textbf{Equation 139}$$

$$\boldsymbol{M_D = \frac{1}{2} C_D \rho g \left(\frac{D}{2}\right) \hat{\zeta}^2 \left[\frac{d}{2} + \frac{2(kd)^2 - \cosh(2kd) + 1}{4k \sinh(2kd)}\right]} \qquad \textbf{Equation 140}$$

The moment due to the mass of the RNA, m_{RNA}, is simply the product of the weight of the RNA and the length, L_{off}, which it is offset from the center of the tower:

$$\boldsymbol{M_{grav} = m_{RNA} \times g \times L_{Off}} \qquad \textbf{Equation 141}$$

The moments that result from wind, water and gravity must all be opposed by the soil. The soil-monopile interactions are often modeled using a series of springs which provide the lateral resistance [368]. The spring stiffnesses are tuned to match the soil characteristics which must be measured directly at a particular site. A full discussion of the analytical methods used to determine the monopile-soil interaction is beyond the scope of this thesis. The interested reader is referred to [354, 368-369] for more in depth information.

Since monopiles are a well established technology and are fabricated with common steel – a simple top-down approach was chosen for the cost. The four-parameter equation depends primarily on the depth of water – a driver for the overall length; the turbine power which determines the thrust and the moment due to the wind; a "load factor" equivalent to the height times the radius squared is also used as a factor in the cost, as shown in Equation 142 [370]. The equation is a proxy for the required mass of steel. The nominal cost of 320k€/kW instead was given as the basis at 8 meters of depth. The cost was escalated to $477/kW in 2010 US dollars using Figure 68. The PPI for rolled steel – NAICS number 331221 – escalated faster than the GDP deflator between the years 2003 and 2010. Consequently, the nominal cost was further increased by 25% to $595/kW.

$$\boldsymbol{C_f = \$595 P_{WT}(1 + 0.02(Depth - 8))\left(1 + 0.8 \times 10^{-6}\left(H\left(\frac{D}{2}\right)^2 - 10^5\right)\right)} \qquad \textbf{Equation 142}$$

An additional £96,000 per turbine was added for the installation of the foundation [371]. That cost was updated to 2010 US dollars using the 2006-2010 pounds to dollars conversion factor listed in Figure 67.

This equation does not directly address the forces of the water on the monopile, which would influence both the diameter and the thickness. It also does not address the soil characteristics which also have a bearing on the monopile dimensions. However, the equation is able to give an estimate of the nominal mass of steel required under typical conditions.

7.3.2 Wind Farm Cables

Wind farm power cables fall into two categories for the purposes of this model: medium voltage and high voltage. The medium voltage cables are used for inter-turbine connections and usually fall in the 30-40kV range. High voltage cables are assumed to connect the wind farm transformer to the grid, usually operating around 150kV. While the cables are similar, the costs are slightly different for each [355] . Consequently, the medium- and high-voltage cables will use slightly different cost models.

7.3.2.1 Medium-Voltage Cables

Undersea inter-turbine cables are sized based on the XLPE users guide [372] and data taken from [355]. The cables are not assumed to be constant diameter for the entire wind farm. For example, the wind farm at Lillgrund uses cables with different cross-sectional areas: higher currents near the transformer require larger cables, while those at the end of the strings require less ampacity [373]. This cable design is shown in Figure 70.

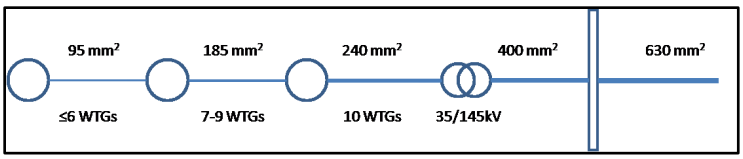

Figure 70 – An example of tapered cables used in the Lillgrund wind farm

There are myriads of possible cable configurations for the wind farm, but this work assumes a square or rectangular setup, with any extra turbines inhabiting a separate string. (Herein, string will refer to a number of turbines connected on one set of cables.) Other works optimize the design of the layout subject to several constraints [354], but optimization is beyond the scope of this thesis.

The cost of cables is related to the mass of copper or aluminum that is used for fabrication. The mass is related to the length as well as the cross sectional area of the cables. Since the cross sectional area is also proportional to the ampacity, the cable costs can be related to the inter-turbine voltage and the turbine sizes.

To calculate the overall inter-turbine cable cost, the operational voltage and the wind farm layout are required. Using this information, the cables can be properly sized to determine the uninstalled cost per unit length. The maximum power that can be carried through the three cables is given by:

$$\boldsymbol{P_{max} = I_{max} V_{max} \cos \Phi} \qquad \textbf{Equation 143}$$

It is assumed here that P_{max} is the real power of the wind turbines connected to the cable, in watts; V_{max} is the rated cable voltage in volts; I_{max} is the rated current in amps; and the term $\cos \Phi$ is the power factor, taken to be 0.707.

The overall length of the cables is directly related to the spacing of the turbines, as shown in Figure 71. Thus, if the spacing of the turbines is 10D, the total cable length will be approximately

twice as long as a 5D setup, requiring higher capital costs. However, longer spacing results in increased energy capture due to reduced wake interactions between turbines.

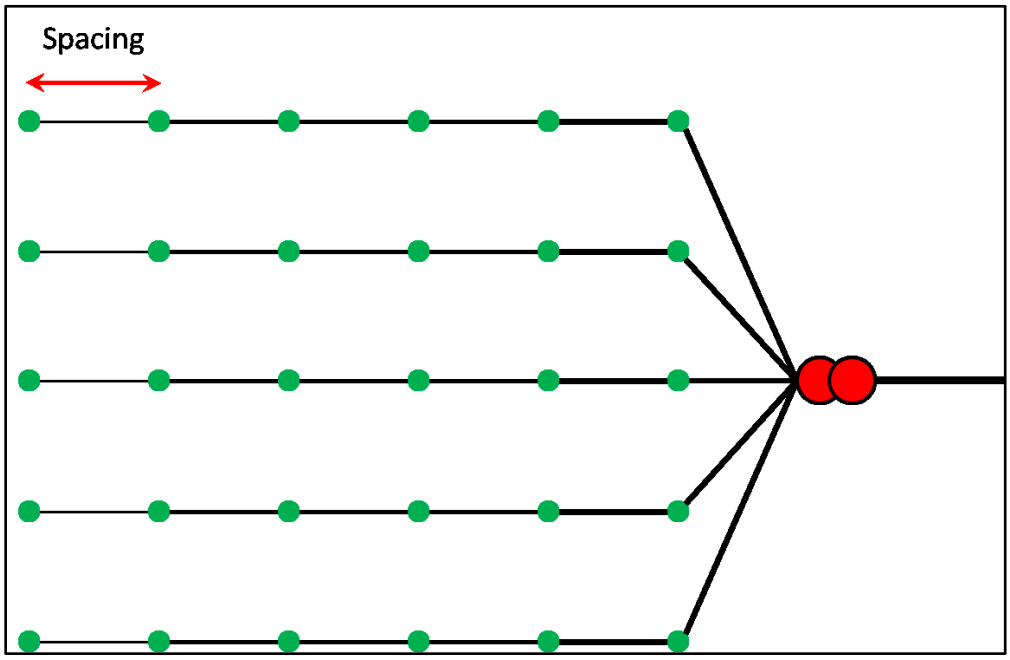

Figure 71 – Rectangular offshore wind farm setup showing the influence of spacing on the inter-turbine cable length

The model is only capable of describing uniform turbine spacing, i.e. a rectangular or square grid layout. Many actual wind farms, such as Thanet in the UK, utilize different spacings that depend on the prevailing wind direction, with cross-wind spacing being shorter [374]. To accommodate for this, the average of the two spacings is used to calculate the total cable length.

The model first establishes the wind farm configuration using the cables sizing chart and three inputs: the number of wind turbines in the farm, the rated power of each, and the inter-turbine voltage. The cables are assumed to be copper placed in the seabed, so 935 amps is chosen as the maximum amperage. The model then establishes the maximum number of wind turbines that a single large cable can hold and, subsequently, how many are required for the farm. Frequently, there will be extra turbines that inhabit a shorter string, with lower ampacity. The remaining

turbines are attached to this one short string, which is sized using the same method as the longer strings.

The cable model was run on six case studies – Thanet, Horns Rev, Lillgrund, Princess Amalia, Nysted, and Gunfleet Sands – to determine how well it could predict the array cable length. The assumptions used in the model as well as the actual and calculated cable lengths are presented in Table 73 below. The model predicted, almost exactly, the array cable lengths for Nysted and Gunfleet Sands; it underestimated the lengths of the four other case studies by between 6.8 and 12%.

The discrepancy between the model and the actual layout is likely due to how the strings of turbines connect to the substation. The results, however, are reasonable given the uncertainties that exist in the reported lengths, and spacing.

Table 73 – Actual and calculated array cable lengths

	Thanet	Horns Rev	Lillgrund	Princess Amalia	Nysted	Gunfleet Sands I and II
Turbine Size (MW)	3	2	2.3	2	2.3	3.6
Number	100	80	48	60	72	45
Voltage (kV)	32	36000	33	22	33	33
Row Dist (m)	800	560	400	550	848.72	890
Along Rows (m)	600	560	307	550	477.92	435
	700	560	353.4	550	663.32	662.5
Rotor Diameter	90		93		82.4	107
Cable Dist Act	75	63	22	45	48	34
Cable Dist Calc	66.3	55.9	20.5	39.6	47.7	33.81
Error	11.6%	11.3%	6.8%	12.0%	0.6%	0.6%
	-11.6%	-11.3%	-6.8%	-12.0%	-0.6%	-0.6%
References	[374-375]	[73, 376-377]	[373]	[378]	[49, 379]	[92, 380-381]

The cross sectional areas of the large 220 kV XLPE cables are shown in Table 74 and were taken from Table 1 in [372]. The original cost was in 2009k€/km, but was updated to $2010/km using

the value in Figure 68. The cost was further escalated because the price of power cables increased by 20% over the period from 2009-2010 [302] while inflation was relatively low.

$$C_c = 768S + 159,000 \qquad \textbf{Equation 144}$$

Here, S is the cross sectional area of the cable in mm^2 and C_c is the cost in 2010 dollars per kilometer. The cables must also be put into trenches on the sea floor using specialized equipment. The model assumes that the cable installation costs $372,000 per kilometer which is based on information given in [371] and [382]. The total installed costs for the inter-turbine cables in 2010 dollars per kilometer are therefore:

$$C_{C,total} = 768S + 531,000 \qquad \textbf{Equation 145}$$

Table 74 – XLPE AC Cable Data

Current Rating for Three-Core Cables, Amps								
Rated voltage up to 220 kV								
	Aluminum Conductor				Copper conductor			
Cross section mm^2	In ground		In air		In ground		In air	
	65°C	90°C	65°C	90°C	65°C	90°C	65°C	90°C
16	74	89	60	82	96	115	78	105
25	95	115	80	110	120	145	105	140
35	115	135	97	130	145	175	125	170
50	135	160	120	165	175	210	155	210
70	165	195	145	195	210	250	185	250
95	195	230	170	230	250	300	220	290
120	220	265	200	270	285	340	255	345
150	245	295	225	300	315	380	285	390
185	280	335	255	345	355	430	325	440
240	320	385	300	400	410	495	380	515
300	365	435	335	455	460	555	430	580
400	410	490	385	525	515	625	490	680
500	465	560	445	610	580	700	560	780
630	525	635	510	705	640	785	635	890
800	585	715	585	810	705	865	715	1000
1000	645	785	655	915	755	935	785	1100

7.3.2.2 High-Voltage Cables – Offshore and Onshore

The high voltage cables connect the offshore substation to the mainland. The voltage is generally much higher on these lines than on the inter-turbine cables, often in the 130kV to 250kV range. Accordingly, the costs for these cables are higher for a given conductor size. The following expression was given for the capital cost of high voltage undersea cables [382].

$$C_{c,HV} = \frac{1.7\left(A_p + B_p \exp\left(\frac{C_p S_n}{10^8}\right)\right)}{6.45} \qquad \textbf{Equation 146}$$

$$S_n = \sqrt{3 U_R I_R} \qquad \textbf{Equation 147}$$

Here, A_p, B_p and C_p are cost constants, listed in Table 75; S_n is the rated power of the cable in VA; U_R and I_R are the rated line-to-line voltage in volts, and the rated current of the cable in amps, respectively.

Equation 146 was converted to \$2010 from 2003 SEK using a factor of $1/6.45 \frac{\$}{SEK}$. The conversion factor was found using the methods discussed above with Swedish Harmonized Index of Consumer Prices (HICP) data from [383] and exchange rate data from [319].

The costs of the copper cables were also escalated in US dollars using the producer price index for power cables. In 2003 the PPI for power cables was 114.7 while in 2010 the PPI was 227.1 [302]. However, over the same time period, inflation was about 13% in Sweden and 18% in the United States. Accordingly, a cost correction factor of 1.7 was chosen to account for the increased costs as well as the differences in inflation between the two countries.

Table 75 – Cost constants to be used with Equation 146

Rated voltage [kV]	A_p	B_p	C_p
22	284,000	583,000	6.15
33	411,000	596,000	4.1
45	516,000	612,000	3
66	688,000	625,000	2.05
132	1,971,000	209,000	1.66
220	3,181,000	110,000	1.16

This work assumes that installation of the cable is insensitive to the number of cables installed. That is, it is assumed that one bundle of cables is placed in one trench, rather than several cables placed in separate trenches. Therefore, the installation cost is simply the distance between the offshore transformer and the landing point times the installation cost per length. An installation cost of $990,000/km was chosen, in accordance with published costs for the transportation and installation of high voltage seabed cables [355].

In the United States the developer is responsible for connecting to the wind farm to the local utility grid via the transformer station ; in much of Europe utilities must connect to the offshore platform [384]. Thus, there is a slight difference in modeling an offshore wind farm in the US and one in Europe. This work assumes the US approach, so the costs may be slightly higher for high voltage transmission to the grid.

The high voltage transmission lines from the substation must connect to the local utility grid. These lines can either be above ground, underground or some combination thereof. The costs of the transmission lines are taken from the Regional Energy Deployment System (ReEDS) optimization model developed by NREL [385]. Because the inflation rate was just over 1% for the period 2009-2010, the costs are assumed to be roughly the same in 2010 dollars, and within any errors that are present in the data.

The following cost structure is assumed for an offshore wind power facility in Maine:

Transmission Costs (2010$)	
765 kV line	$746/MW-km
Line cost multiplier	3.56
Substation Cost	$20/kW
AC-DC-AC intertie cost	$230/kW

7.3.2.3 Transformer

Fundamentally, transformers are used to convert one voltage to another. In an offshore wind farm a transformer is required to change the voltage from the inter-turbine cabling (usually at 36kV) to the voltage of the local grid (usually more than 130kV). Transformers use the principle described by Faraday's Law of Induction whence the voltage is changed according to:

$$\boldsymbol{E = -N\frac{d\Phi_B}{dt}} \qquad \textbf{Equation 148}$$

where E is the voltage, N is the number of windings, and $\frac{d\Phi_B}{dt}$ is the change in the magnetic flux through one turn in the coil per time. In a transformer there are two windings, both of which have the same magnetic flux. Thus, Equation 148 states that the voltage, *E*, is proportional to the number of windings, *N*, in an ideal transformer. In order to step the voltage up or down only the number of windings in the coil must be changed. For an ideal transformer connected to a load the input power must be the same as the output power. The relation between the voltage, number of windings and the current is given by [386]:

$$\boldsymbol{\frac{E_p}{E_s} = \frac{N_p}{N_s} = \frac{I_s}{I_p}} \qquad \textbf{Equation 149}$$

The cost of a transformer is related to the physical size of the device, which in turn, is related to the apparent power capacity. Transformer costs were found in [323] and converted to thousands of 2010 dollars from 2004 euros using the methods listed above.

$$\boldsymbol{C_{trans} = 1.5 \times 49.5P^{0.7513}} \qquad \textbf{Equation 150}$$

Here *P* is the rated capacity of the transformer in MVA. The PPI for transformers (NAICS 335311) over the period 2004-2010 increased by 66% – about fifty percentage points more than

inflation in the US. Therefore, a correction factor of 1.5 is included to further escalate the costs of the transformer.

The apparent power is the product of the line voltage and the line current, or

$$\boldsymbol{S = \sqrt{3} V_{LL} I_L} \qquad \textbf{Equation 151}$$

The apparent power, *S*, is measured in volt-amperes. The apparent power is related to the real power by the power factor, which is the cosine of the phase angle:

$$\boldsymbol{P = \sqrt{3} V_{LL} I_L \cos\phi} \qquad \textbf{Equation 152}$$

The phase angle is not readily calculated for a generic offshore wind system like the one described herein. The simplifying assumption used in this work is that the phase angle is 45 degrees, corresponding to a power factor of 0.707. Hence, the rating of the transformer is about 42% higher than the rated capacity of the wind farm.

7.3.2.4 Switchgear

The switchgear is used to connect and disconnect the wind turbine from the larger system, which includes the inter-turbine cables and the grid. Switchgear are standard in the industry and typically represent a small fraction of the overall costs. One purpose of the switchgear is to isolate either single turbines or strings of turbines when failure occurs. A simple approach is to use switchgear sparingly to disconnect strings of turbines when failure occurs. The single power switch is inexpensive, but results in greater idle turbine hours. A more complex approach uses numerous switches to isolate single turbines from the rest of the wind farm. This approach is more expensive, but enables higher availability of the turbines. Intricate schemes that are used to isolate turbines from the wind farm, such as those discussed in [387], are not considered in the present work.

Instead, this work assumes that the array voltage and the switchgear costs are linearly related: the equation for the switchgear costs depends solely on the nominal system voltage, V_n. The switchgear costs are taken from [382] and updated from 2003 Swedish krona to 2010 US dollars using the averaging method detailed above. The voltage is typically 36kV, but depends on the system architecture.

The switchgear costs are also escalated using the PPI. The PPI values for switchgear (NAICS 33513) were 197.3 in 2010 and 152.2 in 2003 – an increase of nearly 30%. Over the same interval the inflation rate in the United States was about 18% using the GDP deflator, and 13% using the CPI in Sweden. Given these numbers, a value of 15% is chosen to escalate the costs of switchgear beyond general inflation. The final expression for switchgear costs in 2010 USD is given as:

$$\boldsymbol{C_{switch} = 1.15 \times (100330 + 2.8726 V_n) \times 0.155} \qquad \textbf{Equation 153}$$

where $V_n$is the inter-turbine voltage and C_{switch} is the cost of the switchgear for one string of turbines. The total cost of the switchgear for the entire wind farm is the number of turbine strings connected to transformers multiplied by C_{switch} [355].

7.3.2.5 Substation

A substation structure is required to house the switchgear, the transformers and any other auxiliary equipment that is necessary to operate the wind farm. This work assumes an offshore substation such as the one shown in Figure 72.

Figure 72 – The offshore substation installed at Lillgrund [373]

Equation 154 shows the cost for the substation which is taken from [382] and updated to 2010 US dollars.

$$C_{ss} = (20,000,000 + 0.7 n_{wt} P_{WT}) \times 0.155 \qquad \text{Equation 154}$$

Here, C_{ss} is the cost of the substation and the foundation required to support it, n_{wt}, is the number of wind turbines, and P_{WT} is the rated power of each turbine in watts.

7.3.2.6 Supervisory Control and Data Acquisition System, Project Development and Permitting

The supervisory control and data acquisition (SCADA) system is the master control system for the entire wind farm. The system connects each turbine to a master computer via fiber optic cables so that operators can diagnose any problems with individual turbines as well as the wind farm as a whole. Furthermore, the meteorological conditions are monitored concurrently with the turbines so that turbine performance can be evaluated, predicted, or even scheduled on small time scales. The SCADA system generates several outputs which are of interest to the operator

including the instantaneous power generation, the energy output, and any errors that might have occurred.

The SCADA cost is generally given as a per-turbine cost, and frequently is included with turbines by the manufacturer. However, additional SCADA functionality such as meteorological towers is typically installed in larger projects to better understand the system performance [60].

In 2003, the Nysted wind farm reportedly had a SCADA cost of €10 million for the 72 turbine farm [379]. This value will be used as a baseline cost for SCADA systems. The cost has been updated to 2010 US dollars per turbine using the methods discussed in previous sections.

$$C_{scada} = \$114,000/turbine \qquad \textbf{Equation 155}$$

Project development costs are often given as a fixed percentage of the total capital investment. Some authors suggest that project development costs should be between 2 and 4% [355, 388] of the total fixed capital investment. As such, this work assumes that project development is 3% of the total fixed investment. In addition to all of the capital costs and project development associated with building the wind farm, there will also be costs for testing and commissioning the facility, as well as costs for permitting and engineering and any unforeseen costs that may occur. The total costs for permitting, engineering, testing and commissioning are taken to be 11% of the total fixed investment and project development [371]. For the nascent offshore wind industry in the United States, this value is probably conservative.

7.4 Results and Validation

The purpose of the offshore wind farm cost model is to give a general idea of the required investment for nearly any reasonably-sized wind farm. The model is capable of determining capital costs for wind farms with different turbine spacings, turbine sizes, turbine heights, number of turbines, depths, transmission distances and voltages. Altogether, the model has eleven

parameters: number of wind turbines, turbine power, turbine height, turbine diameter, average wind farm depth, average spacing, the offshore transmission distance, the onshore transmission distance, the array and transmission voltages, and the type of substation. Any of these parameters can be varied to give an overall investment cost. The model was written in Matlab and consists of several files. All files are included in **Error! Reference source not found.**. The four files that are called from the main file (WindCost.m) are tasked with computing the array setup and the cost of the array (ParkSetup.m and CableCost.m); determining the cost of a given length of high-voltage cable from the transformer to the shore (SubmarineCost.m); and determining the cost of the turbine itself (TurbineCost.m). All other costs estimates, such as those for the foundation and consenting, are computed in the WindCost.m file. Finally, all costs are collected and summed to determine the overall capital cost of the wind project. A schematic of the wind farm inputs and their influences on the capital costs is shown in Figure 73. The schematic also shows the influence of the wind farm parameters on the power production model.

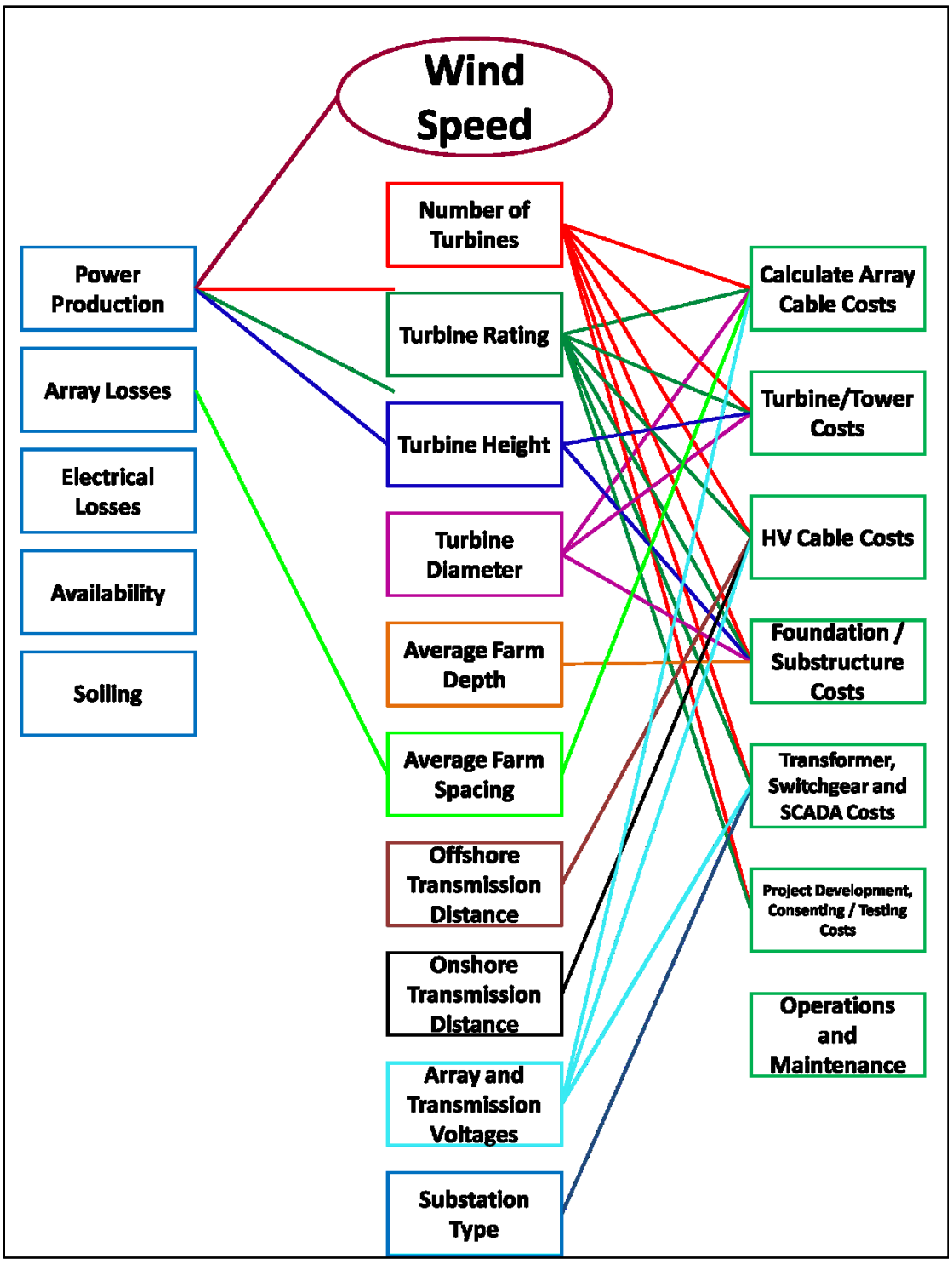

Figure 73 – Inputs to the power production and cost models

The model takes the inputs, computes the array cable length and cost, the transformer power and cost, the turbine cost – assuming an 'advanced', 'three stage' turbine as outlined in [110]; the

foundation cost based on the turbine size, power and the depth; the switchgear cost based on the array voltage and the number of turbines; the substation cost based on the total power; the submarine transmission cable sizing and cost; the onshore transmission cost; the SCADA cost; the integration system cost; the project development cost; and the consenting and other costs.

The full economic model for a generic offshore wind farm of any size uses the capital cost framework discussed in the preceding sections. The model is capable of handling turbine sizes ranging from 1MW to 5MW in accordance with the NREL cost and scaling model [110]. The turbines costs include the RNA as well as the tower. The model does not consider complex turbine layouts or optimized configurations thereof. Instead, the model relies on creating a rectangular array using the desired number of wind turbines. Clearly, rectangular grids cannot be formed with an arbitrary number of turbines, so the model produces a rectangle with the largest possible number of turbines and adds the remaining turbines to an extra string. The cost is then determined using the defined turbine spacing, the cable cross section and the cable costs per unit length.

The model was tested on a generic wind farm with the following characteristics: 100 3MW wind turbines with a hub height of 105 meters, a undersea transmission distance of 10 km, located in 10 meters of water, a spacing of 10 diameters, array and transmission voltages of 33kV and 150kV, respectively; 20 kilometers of onshore transmission. The total cost of the generic offshore wind farm was found to be about $1.125 billion dollars, equating to about $3750/kW. The cost breakdown of the farm – shown in Figure 74 – was found to be similar to those shown in [371] or [50].

In the pie chart, the onshore transmission system includes the underground high voltage cables that connect the wind farm transformer (if any) to the utility grid transformer; it also includes the intertie and the substation connection cost. The consenting and testing consists of environmental

statements, negotiation of contracts, preliminary and detailed geotechnical and bathymetric surveys, commissioning the turbines, legal fees, and any other contingency costs that may occur.

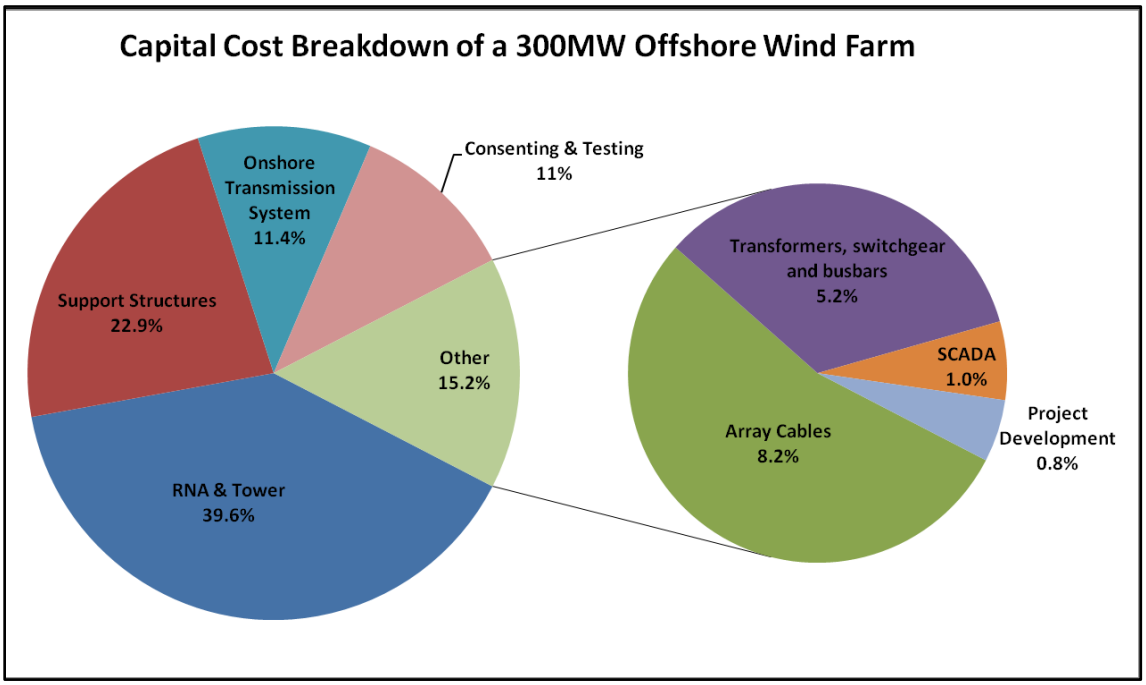

Figure 74 – Calculated capital cost breakdown of the baseline offshore wind farm

The model was also tested on eight actual European wind farms spanning three countries and eight years. The eight wind farms chosen relied on monopile support structures, had reliable, and complete technical descriptions for each of the eleven model parameters and had credible cost information which was consistent across several sources. Furthermore, all of the farms were built within the last 10 years and include modern turbine designs and experienced installation crews. The eight wind farms, the associated technical details, the actual and model costs, and references are included in Table 76 below.

It was found that the model compared favorably with the more recent costs from 2008-2010 while it diverged slightly from costs for the period 2002-2006. For the farms built between 2008 and 2010, the model estimates the costs within 20% for all five farms, the best being Princess Amalia which it underestimates by 5%. The model did not perform as well when applied to the Horns

Rev and Egmond aan Zee, overestimating the costs by 43% and 36% respectively; the model only overestimated the cost of Scroby Sands by 17% which is similar to the wind farms built between 2008 and 2010.

The differences in the present model cost estimation and the actual costs probably stem from several factors. First, some of the costs used by the model have all been translated across space and time. For example, some costs were translated from 2003 Swedish krona to 2010 US dollars; some were translated from Danish krone. The translation was done in some cases using the GDP deflator and exchange rates, in other cases the GDP deflator and exchange rates were combined with the PPI to further update costs. Other equipment costs were translated only across time – the estimates of turbine costs from 2006 were updated using the PPI. The net effect of translating costs likely influences the accuracy of the model estimates. Second, while every effort was taken to determine the capital costs of the wind farms in their native currency with estimates given by knowledgeable parties, the stated costs cannot be taken as facts. Moreover, the costs were also translated across space and presented in 2010 US dollars – another possible source of error.

The eleven parameters in the model are not all absolute. For example, the depth of a wind farm is not a single value, but a range of values. The reported depths often give a minimum and maximum depth; the average value need not be the average of the minimum and maximum. The average depth was used in the model for simplicity, and directly influences the cost of the foundation. Since support structure costs are difficult to precisely determine for a given wind project, it is difficult to validate the support structure model that was used in this work. Instead, the cost breakdown was compared to other published costs.

The distance from shore was used as a proxy for the offshore transmission distance in the model. In reality, the reported distance from shore is the minimum distance from shore to the closest turbine. The closest point to shore and the closest turbine do not necessarily represent the

endpoints for the transmission lines. Thus, one would expect the model to underestimate the costs of the high voltage lines.

The array spacing is usually not uniform throughout the wind farm; turbines are generally spaced differently across and along rows. Additionally, rectangular array configurations are used infrequently – radial or octopus configurations imply longer array distances than simple rectangular layouts. The model dealt with differing spacings by taking the average of the spacing across and along rows.

Finally, the precise electrical configuration for any particular wind farm is usually unknown. The high voltage switchgear, the busbars, the transformers and other power electronics are generally not published in the literature. Altogether, these have little influence on the total cost – turbines, support structures, and cables constitute the vast majority of the costs – but may account for some error.

The model developed here is deemed accurate as an "order-of-magnitude" estimate, suitable for preliminary analysis. It was designed to be robust, simple and accurate, using updated cost models from significant, respected sources. The sole purpose of the wind farm cost model was to inform the ammonia plant model. The wind farm model is a significant factor in the determination of the levelized cost of ammonia. Furthermore, because the OWF model can be applied across wind farm sizes, depths, distances, etc, it is useful for finding suitable wind-ammonia size pairings.

Table 76 – Eight wind farms used in the offshore wind farm validation

	Horns Rev	Scroby Sands	Egmond aan Zee	Princess Amelia	Gunfleet Sands I and II	Horns Rev II	Robin Rigg	Thanet
Year	2002	2004	2006	2008	2009	2009	2010	2010
# Turbines	80	30	36	60	48	91	60	100
Power/Turbine (MW)	2	2	3	2	3.6	2.3	3	3
Rotor Diameter (m)	80	80	90	80	107	93	90	90
Height (m)	70	60	70	59	75	68	80	70
Depth (m)	10	4	17.5	21.5	8.5	13	10	18.5
Average Spacing (Turbine Dia)	7	7	6.7	6.875	6.2	7.35	7.8	7.2
Transmission Distance (km)	21	2.5	15	28	9.3	42	25	52.6
Array Voltage (kV)	36	33	34	22	33	33	33	32
Transmission Voltage (kV)	150	33	150	150	132	150	132	132
Offshore Substation	off	on	on	off	off	off	off	off
Onshore Transmission (km)	34	0.5	7	7	3.8	57.7	2	14.4
Actual Cost (M2010$)	410	162	290	506.8	667	728	628	1391
Model Cost (M2010$)	588	190	393	479	710	872	669	1140
Error	43%	17%	36%	-5%	6%	20%	7%	-18%
References	[49, 379]	[49, 379]	[49, 379]	[49, 378]	[49, 380-381]	[49, 61, 377]	[49, 389]	[49, 374-375]

The economic model was used to calculate the total capital costs and the normalized capital costs for offshore wind farms comprised of between one and one hundred 3 MW wind turbines. The total capital costs are plotted on a semi-log plot in Figure 76. The curve shows that the costs vary linearly with the number of turbines installed.

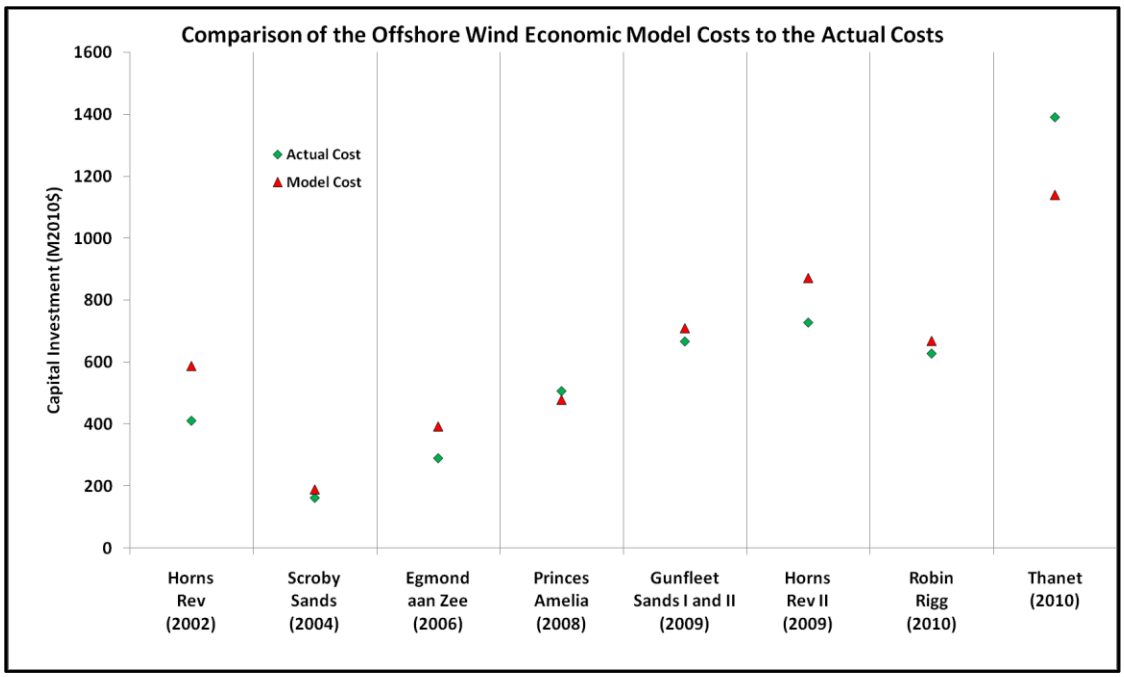

Figure 75 – A visual comparison of the offshore wind economic model and the actual costs

The normalized costs are shown in Figure 77. There are noticeable aberrations in the normalized cost graph, primarily between about eight and thirty turbines. These are a result of the way the program selects the array configuration. Since the layout is assumed to be rectangular, the program generates strings of turbines; new turbine strings are more costly and result in the humps. The cost spikes are smoothed out after about 30 turbines. In reality, the layout would be optimized, and the cost function would generally fit the curve produced below. Regardless, economies of scale are clearly present in wind farms that have fewer than 10 turbines – the normalized cost of one turbine is greater than $10000/kW; the normalized cost for 10 turbines is near $4000/kW.

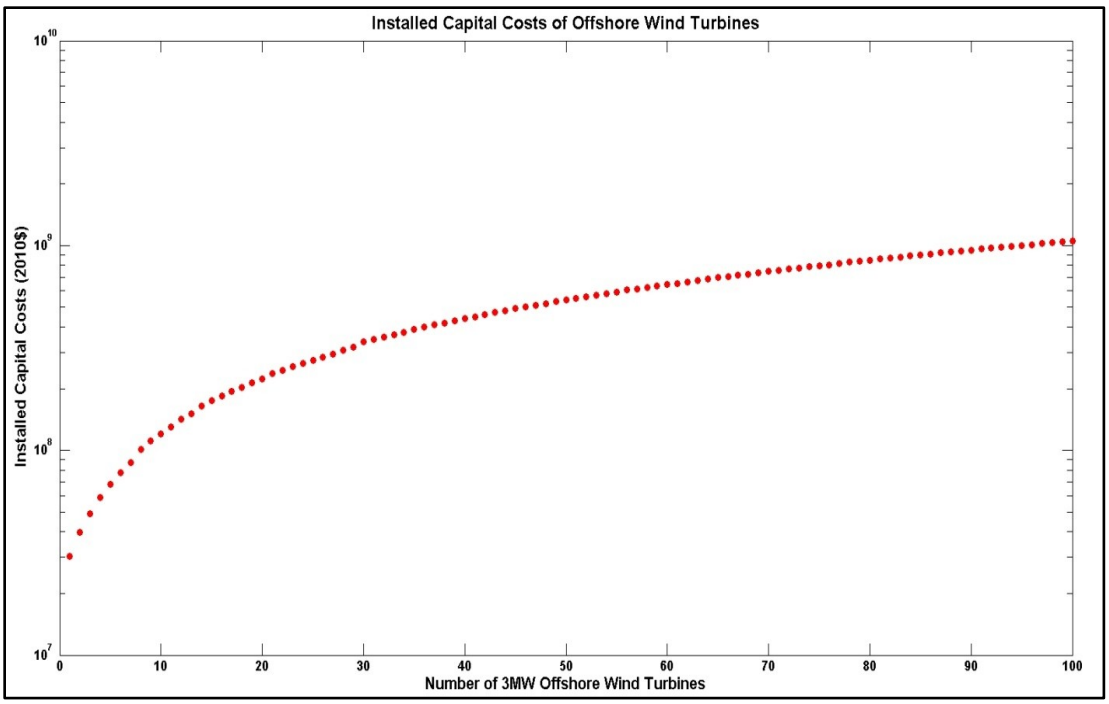

Figure 76 – Calculated installed capital costs of offshore wind farms in the United States.

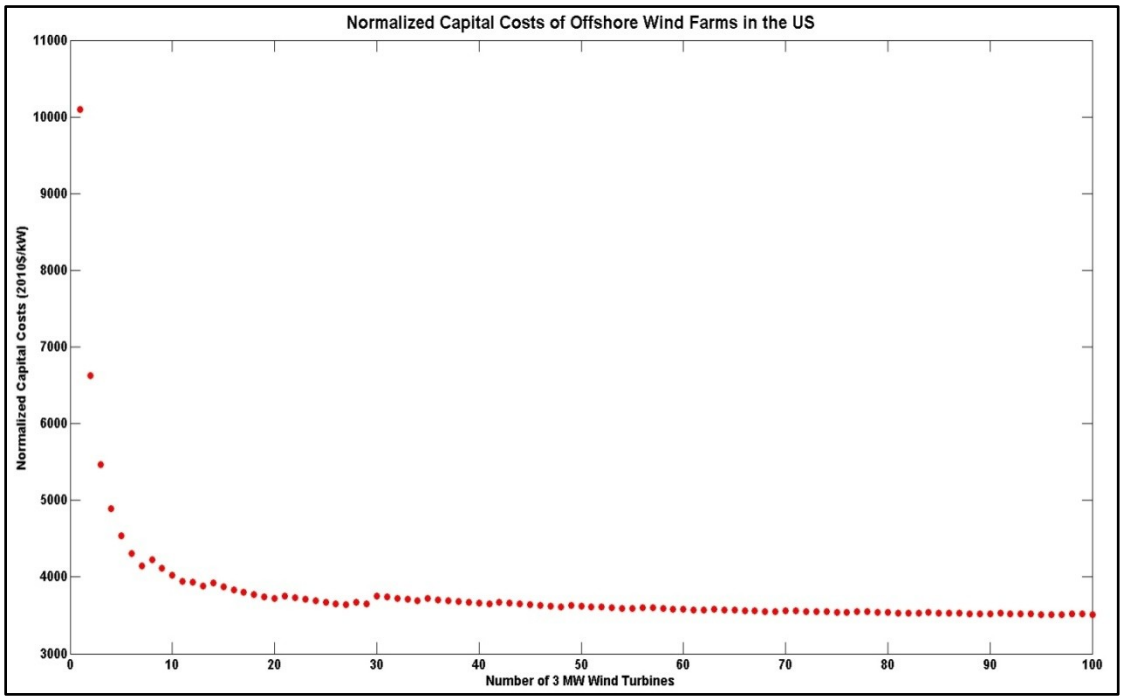

Figure 77 – Calculated normalized capital costs for offshore wind farms in the United States

CHAPTER 8

BASELINE NH_3 – OFFSHORE WIND PLANT

The first seven chapters detailed ammonia subsystem technologies, the basics of offshore wind and cost models for ammonia plants and wind farms. This chapter incorporates the power generation model for offshore wind, the power requirement model for the ammonia facility, the cost model for offshore wind farms and the cost model for all-electric ammonia plants. The model is applied to a hypothetical ammonia facility located in the Gulf of Maine, where there has been active interest in wind-ammonia [390].

8.1 Gulf of Maine Wind Resource

The Gulf of Maine offers a significant offshore wind resource. Unfortunately, the bathymetry of the Gulf is fairly deep – even close to shore as shown in Figure 78. Nonetheless, there are some opportunities for offshore wind development near islands that dot the shoreline as well as on George's Bank.

There are several sites with reliable wind information including Matinicus Rock and Mount Desert Rock, shown on the map in Figure 78. The two sites are roughly 62 kilometers apart. The National Data Buoy Center provides free ten-minute time series wind data at both Matinicus Rock and Mount Desert Rock for the period 1996-2011 [391] as well as averaged weather data from 1984-2008. The anemometer heights at the sites are listed at 22.9 and 22.6 meters, respectively, making them good candidates for estimating wind at higher elevations . However,

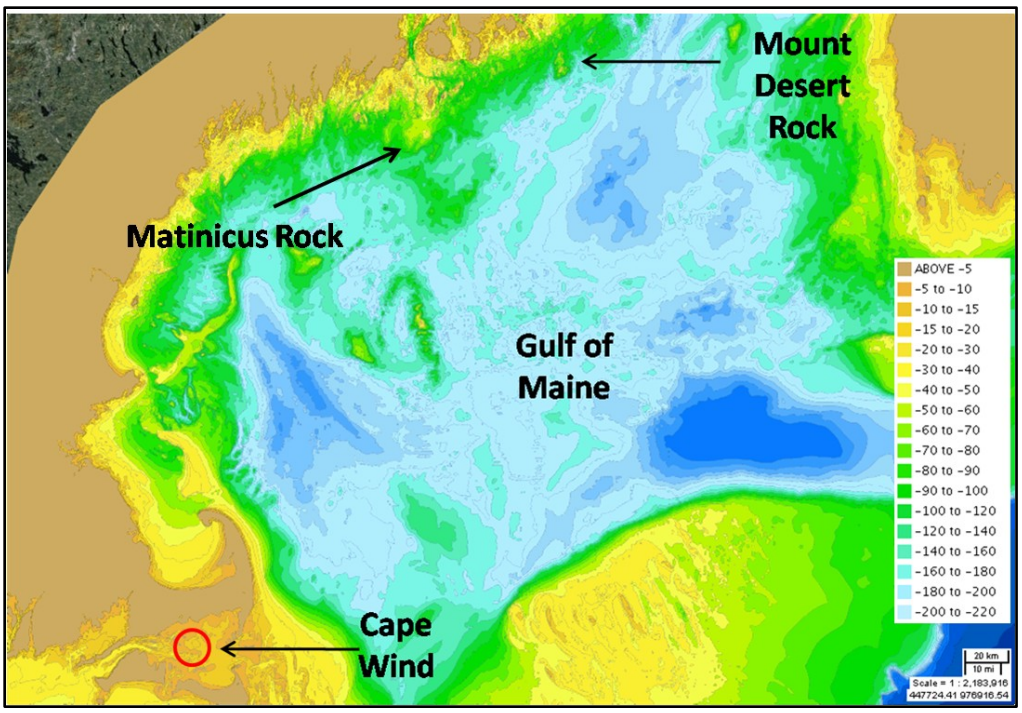

Figure 78 – Gulf of Maine Bathymetry [392]

the Matinicus Rock site is actually 16.2 meters above mean sea level and the Mount Desert Rock site is 9.1 meters above sea level. In order to make a direct comparison between the two sites, the log-law (Equation 156) is used to translate the Desert Rock anemometer readings to 39.1m AMSL.

$$U_{new} = \frac{\ln\left(\frac{H_{new}}{z_o}\right)}{\ln\left(\frac{H_{ref}}{z_o}\right)} \qquad \textbf{Equation 156}$$

Here, U_{new} is the wind speed at the desired height, H_{new}; the reference height, H_{ref}, is the height of the anemometer, and $z_o$is the surface roughness, taken to be 0.0005m for blown ocean conditions [54]. While the surface roughness on an ocean is continuously changing [54], a bulk value is used over the three year period for simplicity. The full results are shown in Figure 79.

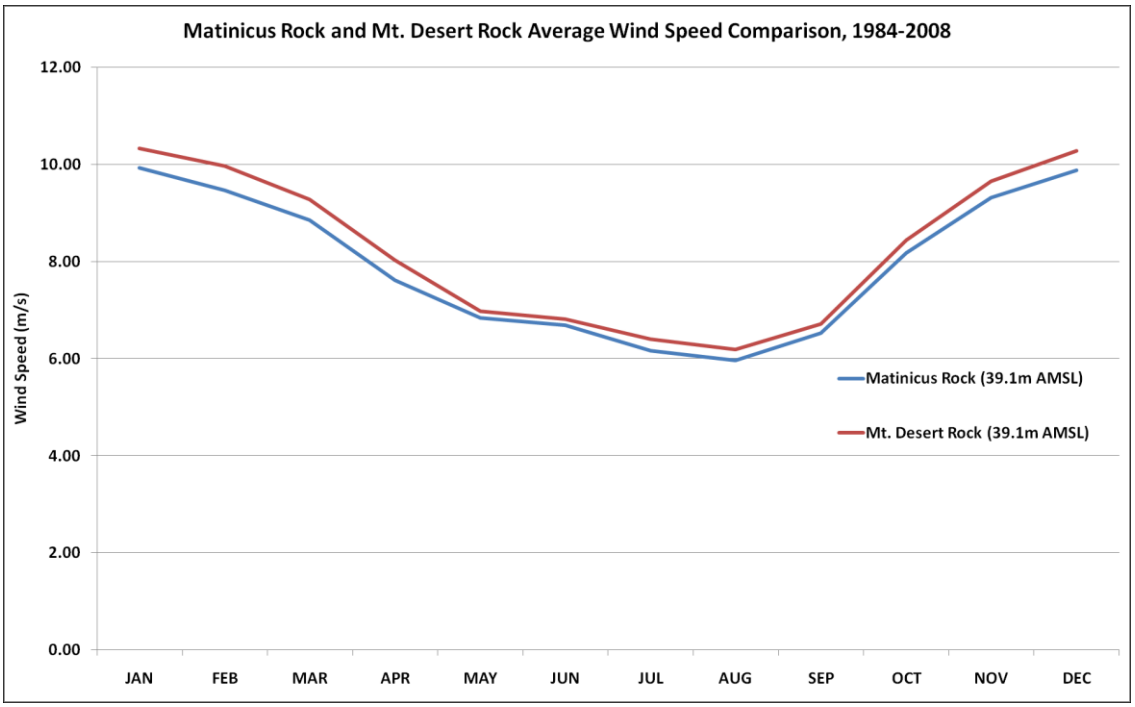

Figure 79 – Comparison of averaged wind data from 1984-2008 for Matinicus Rock and Mt. Desert Rock

The averages wind speeds from Mount Desert Rock are higher, with the annual average wind speed being greater by 0.26 meters per second. The difference in average wind speed translates into a nearly 10% difference in wind power. The results suggest that the wind speeds at the two sites and the resulting wind turbine power differ significantly, but are strongly correlated over long time intervals.

The Mount Desert Rock site exhibits relatively constant annual average wind speeds. From 1985 to 2008 the range of the average annual speed was 7.72 m/s to 8.54 m/s. The monthly averages are less consistent: February, March and April all have maxima and minima that are statistical outliers within the time period. However the average values appear to be relatively consistent. The average, maximum and minimum monthly and annual wind speeds are shown in Figure 80. The average wind speeds for 2005-2007 – 8.39, 8.44 and 8.44 m/s, respectively – is slightly higher than the average annual speed from 1985 to 2008.

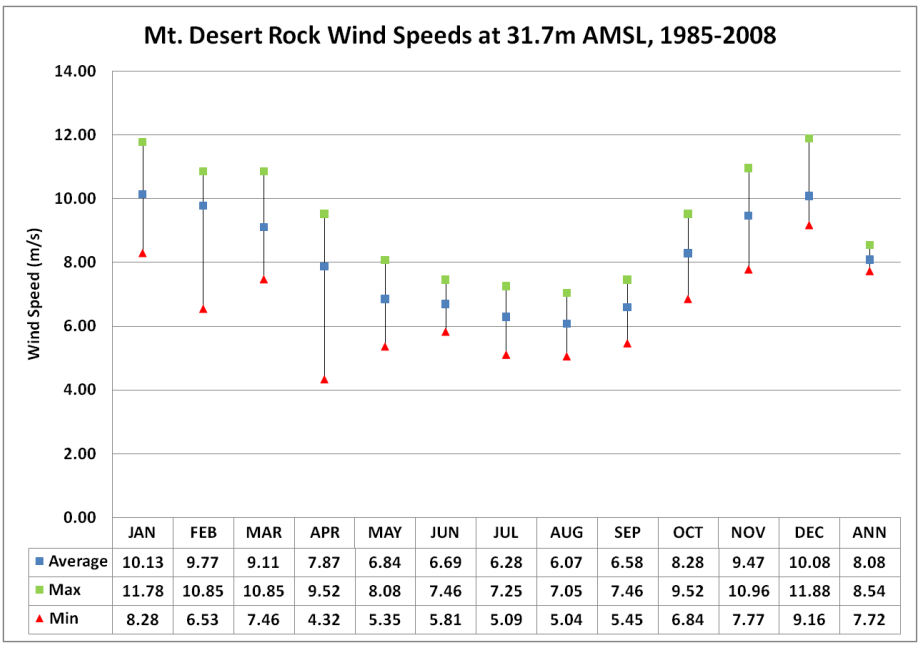

	JAN	FEB	MAR	APR	MAY	JUN	JUL	AUG	SEP	OCT	NOV	DEC	ANN
Average	10.13	9.77	9.11	7.87	6.84	6.69	6.28	6.07	6.58	8.28	9.47	10.08	8.08
Max	11.78	10.85	10.85	9.52	8.08	7.46	7.25	7.05	7.46	9.52	10.96	11.88	8.54
Min	8.28	6.53	7.46	4.32	5.35	5.81	5.09	5.04	5.45	6.84	7.77	9.16	7.72

Figure 80 – Range of average monthly wind speeds at Mt. Desert Rock, 1985-2008

Beyond wind speed, the wind direction is also an important parameter in wind farm designs. Wind farms are oriented so as to minimize wake effects and maximize power production. Ten-minute wind data taken between 2005-2007 at Mt. Desert Rock were used to determine the prevailing wind directions and magnitudes [391]. The wind direction and speed are both plotted on a wind rose (Figure 81). At Mount Desert Rock, the wind generally comes from the westerly direction, though the strongest winds come from the northeast, likely the result of "nor'easters", strong storm systems common in the region.

Any offshore wind farm that is to be built in the vicinity of Mount Desert Rock would need to be oriented with longer rows being perpendicular to the westerly winds. However, a discussion of the specific layout and design of the wind farm are beyond the scope of this thesis, and the interested reader should consult [354].

.

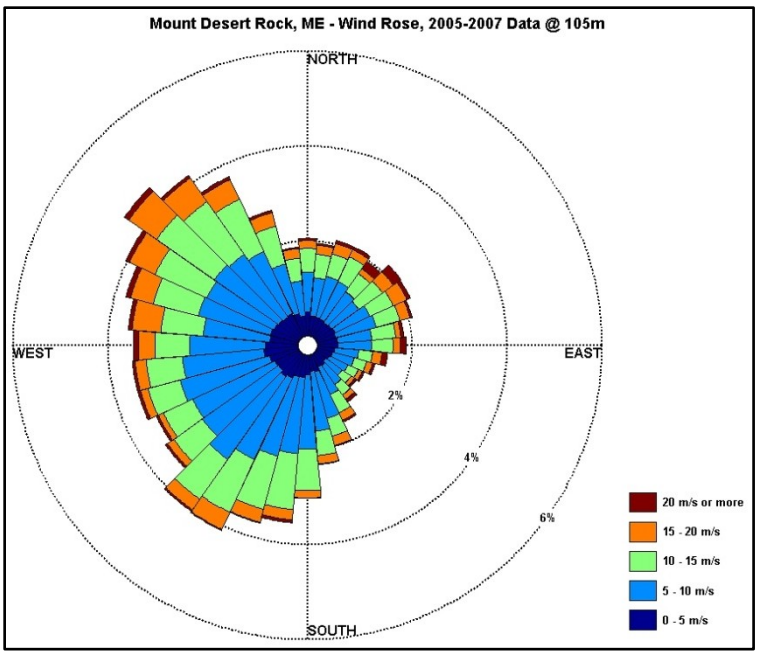

Figure 81 – Wind rose for the Mt. Desert Rock site in the Gulf of Maine.

8.2 Baseline Wind Farm Specifications

A baseline wind farm will be used to assess the viability of offshore ammonia production. The characteristics of the farm are derived from those already in operation; the turbine characteristics are based on machines that have been built. It is unclear that this particular farm could be built in the Gulf of Maine; more than likely it could not. In later sections sensitivity analysis will be used to determine how factors such as depth and distance from shore influence the overall costs. This baseline wind farm should be considered a best case scenario for the Gulf of Maine.

The full assumptions for the wind farm are shown in Table 77. The total installed capacity is assumed to be 300 MW which includes 100 3MW machines. The turbine size, diameter, rated speed and hub height are based on the design specifications of a Vestas 3MW turbine and a WinWinD 3MW turbine [105, 393]. The depth, distance from shore and the spacing were chosen to be 10km, 10m, and 10D, respectively. The depth and the distance are in typical for wind farms, as illustrated in Figure 10; a 10D spacing is used in both directions (across and down the prevailing wind) to be conservative. The inter-turbine voltage and the transmission voltage are

common among many of the existing operational wind farms. The onshore transmission distance was chosen to be 20 km, though this value can be much longer, as was the case with Horns Rev II.

Table 77 – Baseline wind farm specifications

Parameter	Value
Number of Turbines	100
Turbine Size	3MW
Diameter	100 m
Rated Speed	12.5 m/s
Distance from Shore	10 km
Depth	10 m
Spacing	10 D
Hub Height	105 m
Inter Turbine Voltage	33 kV
Transmission Voltage	136 kV
Onshore Transmission Distance	20 km

8.3 Power Production

A time series of the estimated power production can be produced by coupling the wind farm power production model – discussed in Section 3.3.1 – with the 10-minute wind speed data from Mt. Desert Rock. However, since plotting 10-minute data for three years is difficult to represent on a graph, the data was averaged into 156 one-week periods and presented in Figure 82. Over this time frame the capacity factor was calculated to be 40.9%; the energy generated was calculated to be 3,223,100MWh.

The results show that the wind exhibits strong seasonal variability, just as the historical 25 year data indicated. Additionally, the inter-week data also shows significant variability, especially in the spring. The average power generation over the lifetime of the farm is likely to be lower because the wind speeds during 2005-2007 were significantly higher than the 23 year average. Moreover, the power production at the Matinicus Rock site may be lower than Mount Desert Rock by about 10% due to the lower overall wind speeds. More data would be required for an in-depth comparison of the two sites.

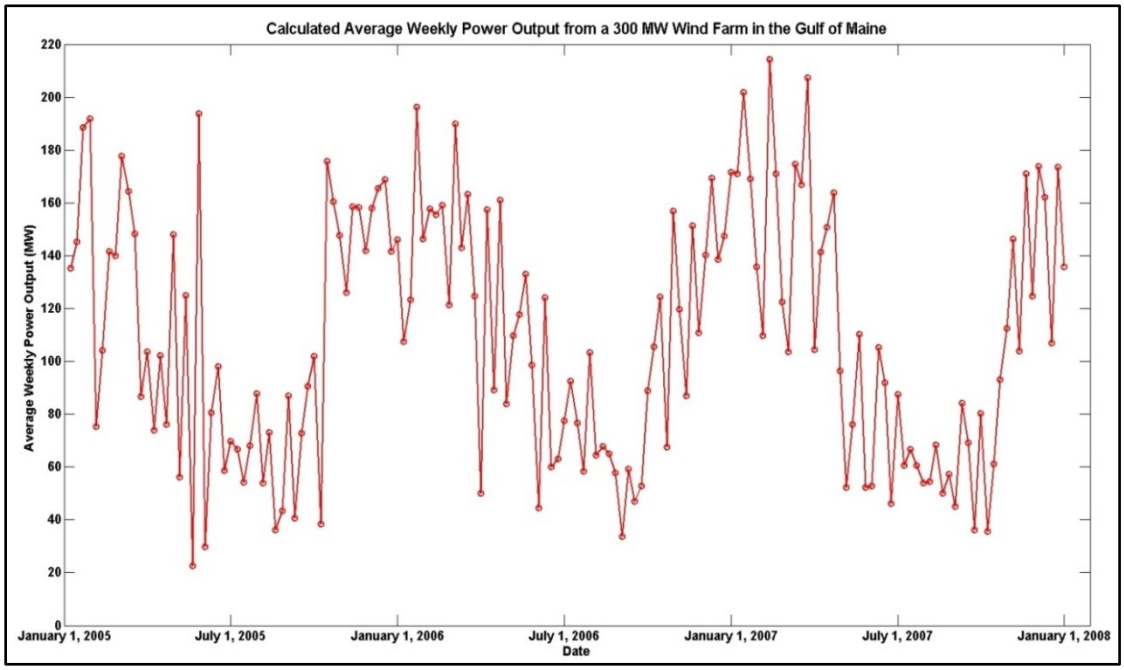

Figure 82 – Calculated average weekly power output from a fictitious 300 MW wind farm in the Gulf of Maine

8.4 Levelized Costs

The concept of *levelized costs* is introduced so that alternative technologies that operate on different scales, across different time periods and different forms of investment can be compared [394]. While levelized costs are frequently used to compare alternative forms of energy generation, the concept is extended here to include the production of ammonia. The central concept of the levelized cost is that each unit generated over the lifetime of the system must have an associated cost. That is, the present value of all of the capital costs, operations and maintenance costs, and costs of capital are considered over the lifetime of the system, summed, and divided by the total production. The levelized cost method ranks the alternatives on a unit production basis so that the alternatives can be compared.

8.4.1 Levelized Cost of Energy

Levelized costs are frequently applied to alternative forms of energy generation as a convenient method to rank the alternatives and remove biases [395-396]. When the concept of levelized cost is applied to energy, it is referred to as either levelized production cost (LPC), or levelized cost of energy (LCOE). The term LCOE will be used in this thesis. The levelized cost of energy (LCOE) is a measure of how much a unit of energy costs over the project lifetime. For a wind farm, the LCOE incorporates the capital costs, operations and maintenance costs, and the future payments for interest on the loan and the power production model. The LCOE is frequently expressed as \$/kWh or \$/MWh for electricity production. The equation for the levelized cost of energy is [54]:

$$\boldsymbol{LCOE = \frac{P_d + P_a\left(\frac{\left(\frac{1}{1+r}\right) - \left(\frac{1}{1+r}\right)^{(n_{loan}+1)}}{1-\left(\frac{1}{1+r}\right)}\right) + Wind_{O\&M}\left(\frac{\left(\frac{1+i}{1+r}\right) - \left(\frac{1+i}{1+r}\right)^{(n_{life}+1)}}{1-\left(\frac{1+i}{1+r}\right)}\right)}{Total\ Lifetime\ Energy\ Production}} \qquad \textbf{Equation 157}$$

Here P_d is the down payment on the entire wind farm, P_a is the annual payment on the loan, n_{loan} is the length of the loan period in years, n_{life} is the project lifetime, $Wind_{O\&M}$ is the yearly operations and maintenance cost, i is the inflation rate, and r is the nominal discount rate.

To determine the annual payment on the loan, the capital recovery factor is used:

$$\boldsymbol{P_a = (C_c - P_d)CRF = (C_c - P_d)\left[\frac{b}{(1-(1+b)^{-n_{loan}})}\right]} \qquad \textbf{Equation 158}$$

Here, C_c is the total capital cost of the wind farm, and b is the interest rate of the loan. Using both Equation 157 and Equation 158 the net present value of any wind farm can be calculated and used to determine the LCOE.

To simplify the LCOE calculation, the down payment on the wind farm is assumed to be 10% of the total capital costs. The project lifetime is taken to be 20 years while the life of the loan is 15

years. The inflation rate, interest rate and discount rate are assumed to be 3%, 4%, and 7% respectively. Finally, the operations and maintentance for the wind farm is assumed to be 3% of the fixed capital investment.

The economic assumptions used to compute the LCOE with Equation 157 are summarized in Table 78 below.

Table 78 – Assumptions for calculating the LCOE using Equation 157

Parameter	Value
Discount Rate	7%
Inflation Rate	3%
Interest Rate	4%
Loan Life	15 Years
Project Life	20 Years
O & M Fraction for Wind	3% of Capital Expenditure
Down Payment	10% of total Capital Cost

The expected lifetime energy production of the wind farm can be calculated directly using the wind data from Mt. Desert Rock and the wind farm power production estimates in the previous section. The total energy production is found by averaging the annual energy production for the three years and multiplying by the project lifetime, assumed to be 20 years:

$$\boldsymbol{E_{life} = n_{life}\frac{\sum E_{a_i}}{3}} \qquad \textbf{Equation 159}$$

where $E_{life}$is the expected lifetime energy, n_{life} is the lifetime of the wind project, E_{a_i} is the annual energy production in year *i*.

The NPV and the lifetime energy production were determined for wind farms comprised of one turbine through one hundred turbines. The plot for the LCOE is shown in Figure 83. The results are given in 2010 dollars per MWh and show the value of utilizing economies of scale for offshore wind farms. A one turbine offshore installation requires a single cable connection to shore and to the utility grid; one hundred turbines require exactly the same infrastructure. The economies of scale are significant for the first fifty turbines, with costs going from over

$2000/MWh to about $100/MWh. A 300 MW wind farm composed of one hundred 3 MW turbines has a levelized cost of roughly $70/MWh. The values here are representative of values found in the published literature and collected in the Transparent Cost Database, published by NREL [396].

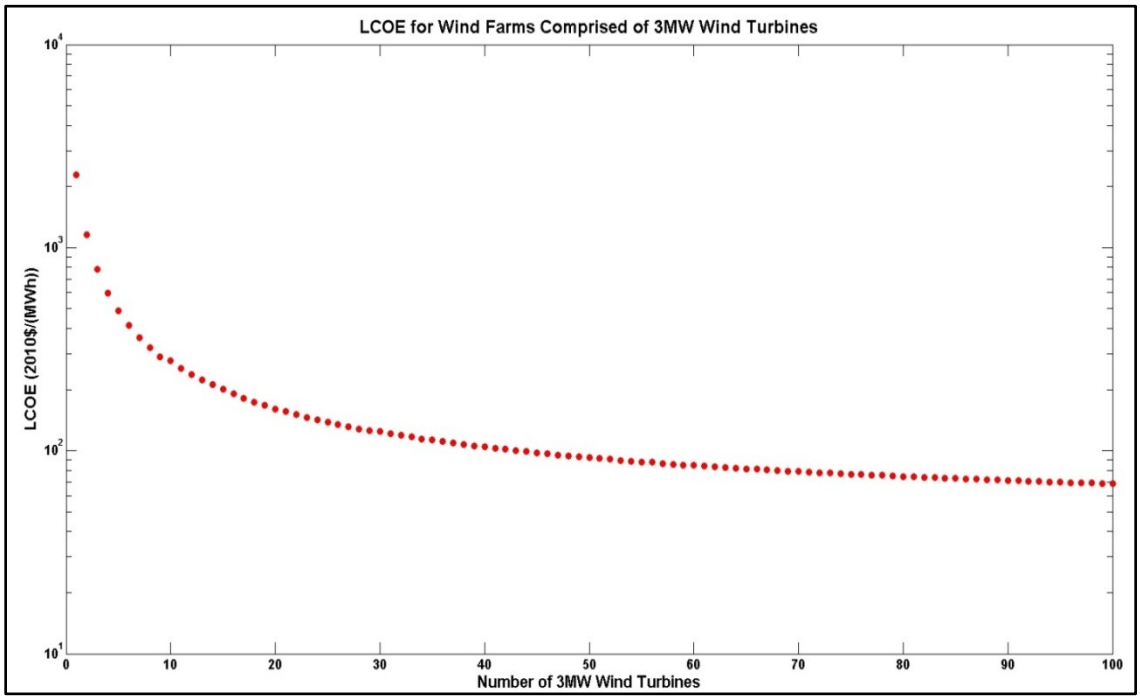

Figure 83 – LCOE for offshore wind farms ranging from 3 MW to 300 MW

8.4.2 Levelized Cost of Ammonia

Much like the levelized cost of energy, the costs to produce ammonia over the lifetime of the plant can be calculated, and normalized per ton of ammonia. The concept is defined as the Levelized Cost of Ammonia (LCOA), which is the sum of the present value of the capital costs and the operations and maintenance costs over the lifetime of the system, divided by the total ammonia production. If a wind farm is used to drive the facility, the capital costs and operations and maintenance costs can also be incorporated:

$$LCOA = \frac{P_d + P_a\left(\frac{\left(\frac{1}{1+r}\right) - \left(\frac{1}{1+r}\right)^{(n_{loan}+1)}}{1-\left(\frac{1}{1+r}\right)}\right) + \left(Wind_{O\&M} + NH_{3_{O\&M}}\right)\left(\frac{\left(\frac{1+i}{1+r}\right) - \left(\frac{1+i}{1+r}\right)^{(n_{life}+1)}}{1-\left(\frac{1+i}{1+r}\right)}\right)}{Total\ Lifetime\ NH_3 Production} \quad \textbf{Equation 160}$$

Here P_d is the down payment on the entire plant (wind farm and the ammonia facility), P_a is the annual payment – calculated with Equation 158, as before, n_{loan} is the length of the loan period in years, n_{life} is the project lifetime, $Wind_{O\&M}$ and $NH_{3_{O\&M}}$ are the required annual operations and maintenance for the wind farm and the ammonia plant, respectively, i is the inflation rate, and r is the discount rate.

The definition for the levelized cost generally assumes a single revenue stream such as selling electricity, or ammonia. The analysis for the wind/NH_3 plant is different: there are two product streams – electricity and ammonia – that must be considered. To accommodate both revenue streams, it is assumed here that ammonia is the primary product that the wind farm is producing, while electricity is secondary. Structuring the economic model to produce only ammonia is advantageous because it allows the levelized costs to easily be calculated for a single product.

The electricity revenue is incorporated directly into the operations and maintenance of the NH_3 plant. That is, purchasing electricity from the utility grid results in positive operations and maintenance costs; these costs can be offset with electricity revenue when selling power back to the utility grid. When calculating the operations and maintenance for the NH_3 plant, the sum of the yearly electricity revenue is used. Since it is assumed that the power will be both bought from the utility grid and sold to the utility grid, the revenue could be either positive or negative.

8.4.2.1 Wind Farm Revenue

A simple method to predict the potential revenue from an offshore wind farm is to use the generated power and the price that the power is worth in local markets. A proxy for the selling

price of electricity is locational marginal pricing (LMP) which is used by system operators to determine the optimal generational dispatch in addition to the locational and transmission congestion prices [397]. Complex algorithms and bidding processes are used to establish which generators can cover the load, and how much will be paid per unit of energy delivered. Thus, the LMP is the marginal cost of generation, plus the congestion cost, plus the cost of the line losses.

The hourly LMP data are sourced from ISO New England (ISO-NE) [398] and are used as a proxy for the selling price of electricity. Because the data is hourly, and the wind data is 10-minute, either the wind data would have to be averaged in one-hour blocks, or the hourly grid data would have to be extended to 10-minute data by duplicating entries. The latter approach was chosen so that the wind data could be kept granular and spikes and troughs in wind power production could be preserved. A graph of the average weekly LMP for the period 2005-2007 is shown in Figure 84.

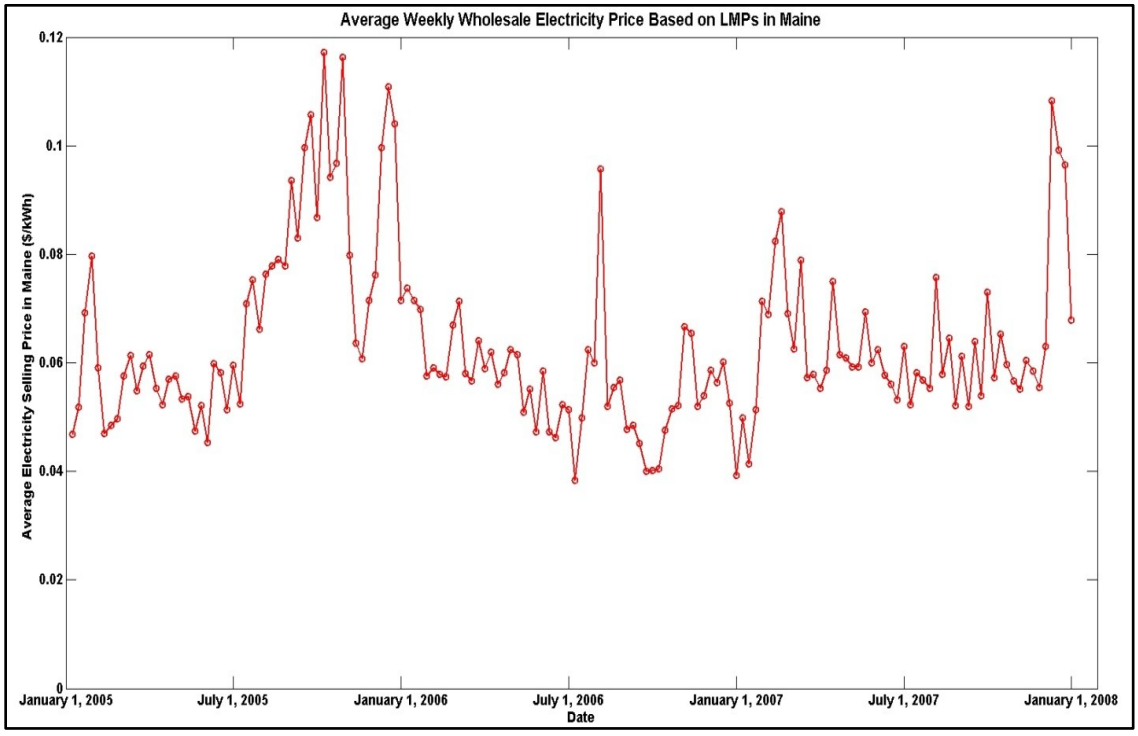

Figure 84 – Average Weekly Electricity Price Based on LMPs

Once all of the wind and LMP data are formatted properly, the result is a large database containing 157,680 lines for a three year period, between 2005 and 2007. Each line contains the date and time stamp, the wind speed, the wind direction, and the selling price of grid electricity. Therefore, at each timestep the simulation reads a line of data into the program, generates a plausible wind power output from the wind farm, and estimates the revenue stream over the interval. The revenue stream is given as:

$$\boldsymbol{Revenue = E_W C_{Grid}} \qquad \textbf{Equation 161}$$

where E_W is the energy generated by the wind turbine, in MWh and C_{Grid} is the selling price of electricity in $\frac{\$}{MWh}$. The full results are shown in Figure 85 below:

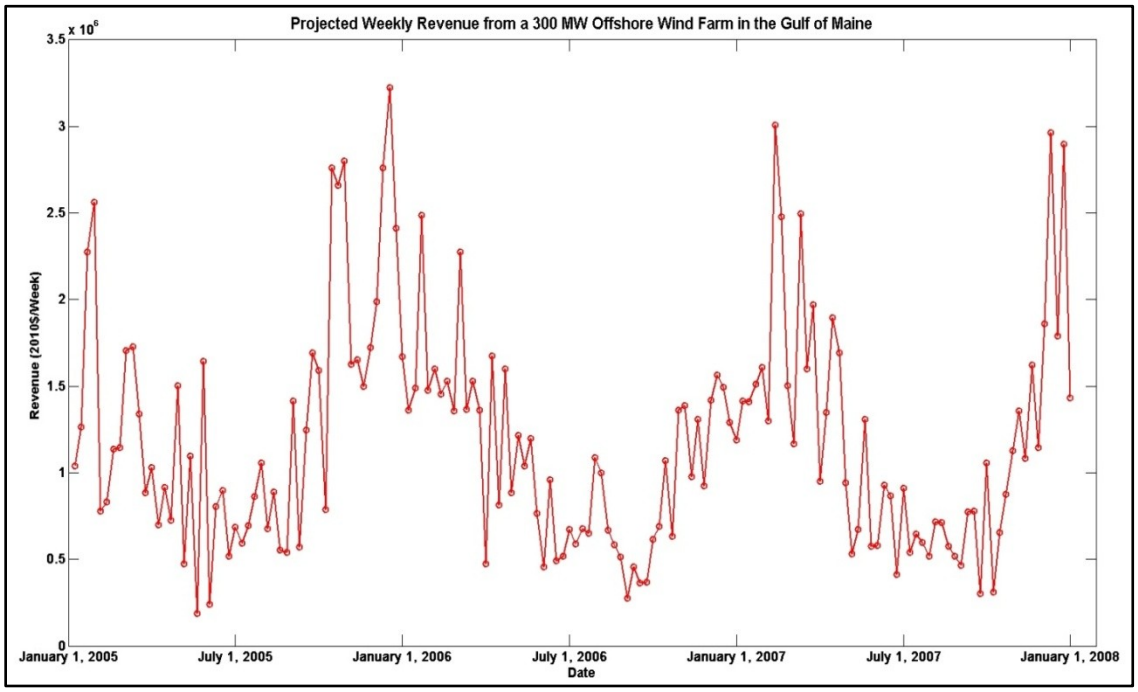

Figure 85 – The projected weekly revenue from the baseline wind farm

The sum of the revenue for the three years is projected to be $187.7 million. The results are valid only for the Gulf of Maine, since the wind data and the LMP data were both specific to the region.

In the following sections, the ammonia plant will be incorporated into the wind farm revenue model. Thus, some of the electricity will be used to produce ammonia, rather than being sold to the utility grid. The revenue for the wind-NH_3 plant is then split into two streams: electricity and ammonia.

8.4.2.2 Conventional Natural Gas Ammonia Production

The LCOA for a conventional steam reforming plant will be calculated using Equation 160. This enables comparison to an all-electric wind powered ammonia production plant. Reasonable assumptions are made regarding the size of the ammonia facility, the operating costs and the fuel requirements. A state-of-the-art plant is assumed as the baseline ammonia production facility.

The cost of a conventional NH_3 plant is given in [307] as \$180M for a 453,592 metric ton per year plant in 2004 dollars, corresponding to about \$250M in 2010 dollars. The labor costs, waste processing costs and utilities can be estimated using data in [296] for a nitric acid plant. The labor is estimated to be \$300,000 per year for a 92,000 metric ton per year plant. Using a scaling factor of 0.65 as suggested in [297] together with inflation, the yearly labor costs are roughly \$1.2M per annum in 2010 dollars. Using a similar analysis, the waste treatment and utilities are assumed to be \$4M and \$1.4M per year, respectively.

The total natural gas feedstock cost can be estimated with knowledge of the energy requirements of an ammonia plant and the price of natural gas. An ammonia plant is assumed to require 29.34 gigajoules of NG per ton of NH_3, based on various estimates found in [28, 43]. Assuming that the density of natural gas is 0.8 kg/m^3 and the lower heating value is 47.14 MJ/kg [399] a volumetric density of 37.712 MJ/m^3 is calculated. The average nominal price of natural gas over the period between 2002 and 2010 was found to be \$6.78 per thousand cubic feet [400]. The nominal price was converted to 2010 US dollars by using the Producer Price Index (PPI) [302] and found to be

$7.48 per thousand cubic feet. Using these values the approximate cost of natural gas is $94M per year. (The less common $/m^3 is used in the following graph. 1000 ft^3 = 28.31 m^3.) However, it is interesting to note that the price of natural gas is expected to drop over the next several years due to natural gas extraction from shale. Therefore, the estimated costs are expected to be an overestimate.

If the interest rate, discount rate, and inflation are taken to be 5%, 7%, and 3%, respectively then the net present value of the ammonia plant is about $2.94B. Using an uptime of 90% – the low end for industrial ammonia plants [29] – the levelized cost of one metric ton of ammonia is $360 in 2010 dollars. Consequently, the price for anhydrous ammonia for the end-user averaged over $660 per metric ton between 2008 and 2012 [401].

The levelized cost of ammonia is highly sensitive to the cost of natural gas – its main feedstock. The tornado chart in Figure 86 shows the variation in the levelized cost of producing ammonia for a range of natural gas prices spanning an order of magnitude from ten cents per cubic meter to one dollar per cubic meter. (This corresponds to $2.8 per 1000 ft^3 to $28 per 1000 ft^3.) The discount rate was also found to be important because it significantly affects the future payments on the investment.

The levelized cost of ammonia for a wind powered ammonia plant is the subject of the next section. The key difference between a conventional ammonia plant and a wind-powered ammonia plant is a wind-powered ammonia plant generates revenue by selling power to the grid, effectively offsetting some operations and maintenance cost. While larger wind farms would cost more to purchase and operate, they also offset the costs of manufacturing ammonia. The interplay between wind farms and ammonia production will be explored in detail.

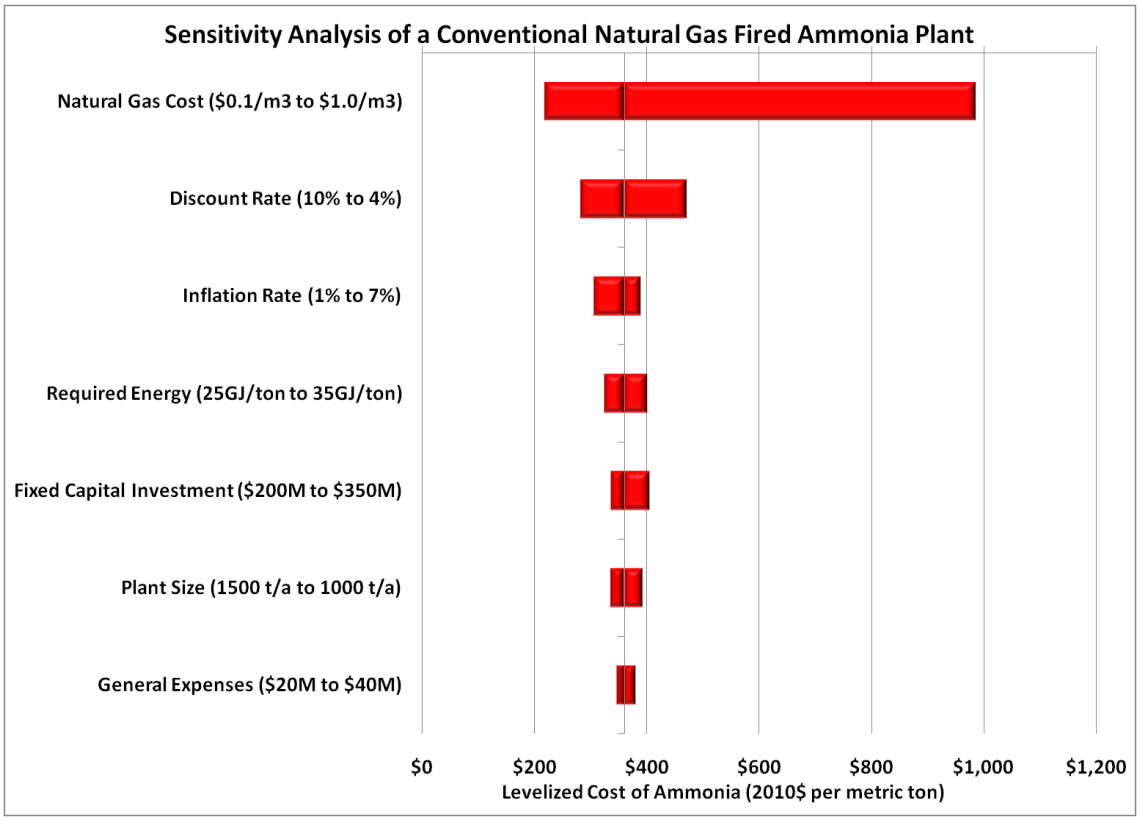

Figure 86 – Tornado chart for a conventional natural gas fired ammonia plant

8.4.2.3 LCOA for a Wind-Powered Ammonia Plant

The LCOA for an offshore wind powered ammonia plant can be calculated using the capital cost inputs that were discussed in Chapter 6 and Chapter 7 as well as any operations and maintenance costs. The operations and maintenance costs for an offshore wind farm are typically given as a percentage of the capital expenditure while the operations and maintenance costs for an ammonia plant are more complex. The simulation informs the total operations and maintenance costs for the net present value (NPV) calculation by determining the sales of electricity. In order to simplify the NPV calculation, the electricity revenues help offset some of the operations and maintenance costs.

8.4.2.3.1 Simulation Logic for a Simple Wind Driven Ammonia Plant

The wind-driven ammonia production process can be simulated using the power requirement of the ammonia plant, the wind farm characteristics, and the corresponding grid and wind data. The most basic design is to run the ammonia plant using electricity generated by the wind turbines and from the grid: wind turbines provide the power to the ammonia plant when available. When wind power is insufficient, the deficit must be purchased from the grid. When the wind power is exceeds the ammonia plant power requirements, the excess power is sold to the grid. The overall energy balance is:

$$\boldsymbol{P_{wind} + P_{grid} - P_{NH_3} = 0} \qquad \textbf{Equation 162}$$

Once again, the selling price of electricity is sourced from ISO New England (ISO-NE) [398]; the purchase price for electricity is sourced from Electric Power Monthly [344]. The Electric Power Monthly data is coarse: it is monthly data that is extended to 10 minute data to match the wind speed data.

8.4.2.4 Baseline Ammonia and Wind Facility

The baseline offshore wind powered ammonia plant was simulated using the wind data from the Gulf of Maine discussed at the beginning of this chapter. The simulation was done for a three year period using wind and grid from 2005-2007. The results are averaged over the three year period to get one representative year of system outputs which are presented in Table 79 below. The 300 MW plant, which includes the NH_3 facility and the offshore wind farm, had a total capital cost of $1.39 billion 2010 dollars. Figure 87 shows the complete breakdown of capital costs for the facility.

The wind farm achieved a capacity factor of over 40% and required more than 534 GWh of electricity from the grid to sustain the ammonia production process. At the same time, a substantial amount of energy could be sold back to the grid, totaling more than 268 GWh. The

total ammonia production was based on a facility with 100% uptime – an unrealistic value. However, the uptime for an all-electric ammonia facility is likely to be greater than a conventional ammonia plant due to the simplicity of the design. The uptime was chosen to be 100% but will be varied in the sensitivity analysis in later sections to determine the effect that it has on the LCOA.

Table 79 – Results from the simulation of the baseline wind-ammonia plant

Metric	Value
Average Wind Speed (105m)	9.62 (m/s)
Capacity Factor	40.92%
Average Power	122.75 MW
Annual Electricity Sold	296,300 MWh
Annual Electricity Purchased	492,000 MWh
NH_3 Sold	109,500 metric tons
Overall NH_3 Conversion Efficiency	50%
Total Costs	$1.39 billion

The LCOA calculation requires several economic assumptions be made about the loan and the interest rates associated with the investment. The levelized cost calculation has several parts. First, the down payment on the investment is assumed to be in year 0 and is already in present value. For simplicity, the down payment is assumed to be 10% of the capital expenditure, or $139 million for the base case. The second term in the equation calculates the present value of the payments on the loan. Four parameters are required: the total value of the in present dollars, the interest rate on the loan, the inflation rate over the lifetime of the system, and the lifetime of the loan. The total amount of the loan is simply the total capital expenditure minus the down payment, or $1.251 billion dollars. The interest rate is assumed to be 4% with the inflation rate at 3%; the discount rate – a measure of the opportunity cost of money – is assumed to be 7%. The lifetime of the project is assumed to be 20 years, which is typical for wind farms and chemical processing plants. The loan life is 15 years.

The third term in the LCOA equation calculates the present value the operations and maintenance costs for the lifetime of the system – 20 years in this case. Recently, the operations and

maintenance cost for onshore wind farms was found to be $10/MWh, corresponding to about 2.4% of the capital expenditure [353]. Because the wind farms are offshore rather than onshore, a higher value of 3% of the capital expenditure is assumed for this analysis. A summary of the assumed values is given in Table 80.

Table 80 – Economic assumptions for the LCOA calculation

Parameter	Value
Discount Rate	7%
Inflation Rate	3%
Interest Rate	4%
Loan Life	15 Years
Project Life	20 Years
O & M Fraction for Wind	3% of Capital Expenditure
Down Payment	10% of total Capital Cost

The cost of manufacture for the ammonia facility is of paramount importance: a large fraction of the overall costs will come from purchasing electricity, assumed to be the "utility" cost. The cost of manufacture is the sum of waste disposal, labor costs, utilities, general expenses, raw materials, taxes, maintenance costs as well as other minor costs. The waste disposal is assumed to be negligible: the waste is oxygen or brine – both of which can be discharged safely into the environment with little or no processing. The raw materials expenses are low: air from the atmosphere and salt water from the ocean are assumed to be free. Thus, the raw material costs come mostly from the lye that is required for normal electrolyzer operation, equal to $17,500 per electrolyzer per year [288]. While the cost of manufacture equation suggests 18% of the fixed capital investment be used for cost of manufacture, this work deviates

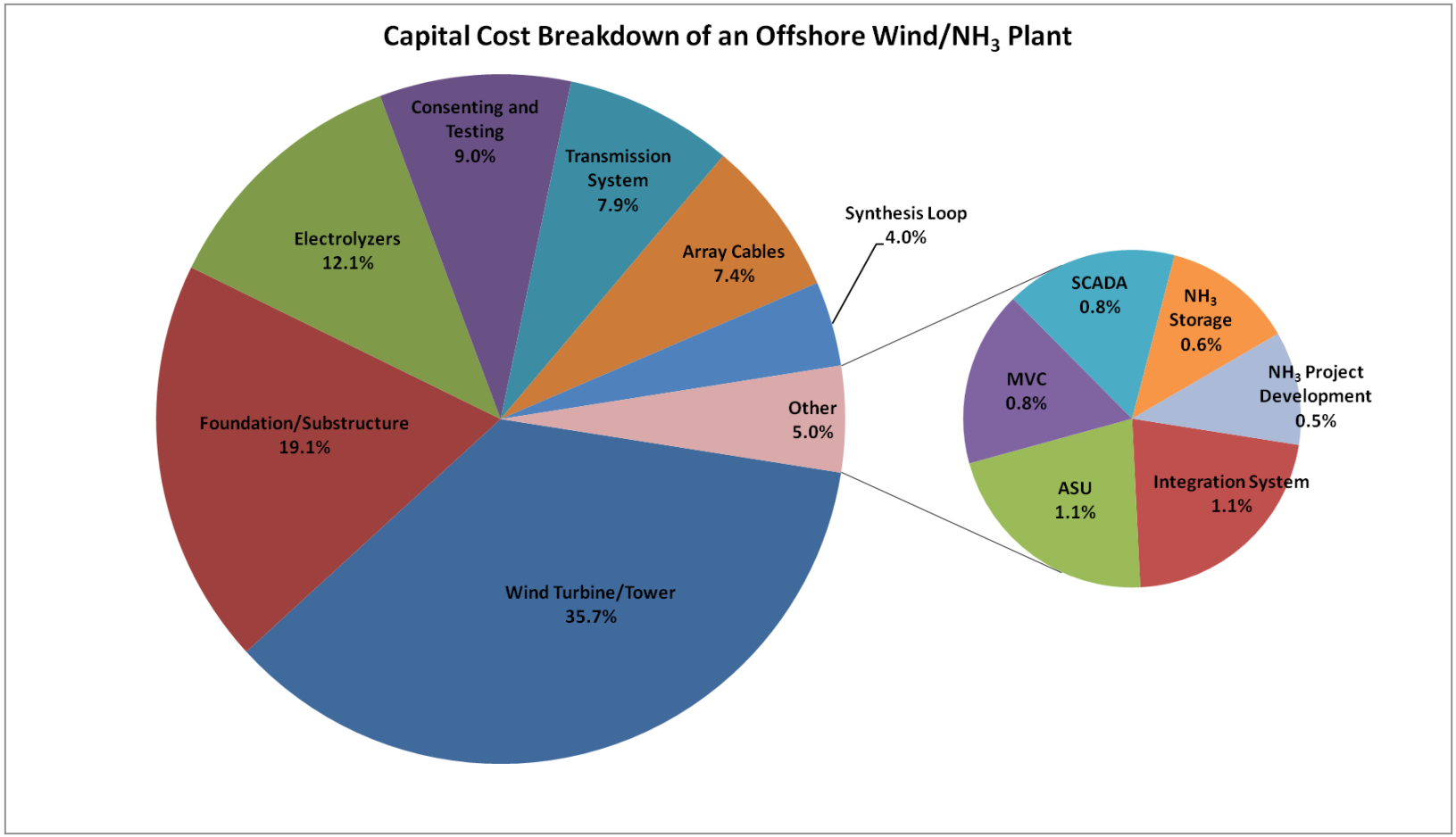

Figure 87 – Capital cost breakdown of an offshore wind/NH_3 plant

slightly from that figure. The Norsk Hydro electrolyzers were designed for continuous, unattended operation [289] so the maintenance costs are low relative to other chemical processes. As such, the cost of manufacture is much lower for electrolyzers; a value of 5% of the fixed capital investment was selected. The labor costs are based on Equation 50, Equation 51, and Equation 52 which estimate labor costs according to the equipment within the plant. A multiplier of 2.73 is used for the labor cost, as suggested in [296]. The utility costs are the sum of the electricity costs and the raw material costs multiplied by 1.23. The utility costs include all of the purchased electricity costs *minus the revenue from the electricity*. Thus, if the electricity revenue is higher than the costs, the cost of manufacture decreases.

The general expenses include administration, research and development, and distribution and marketing costs. Since the electrolyzers offer unattended, continuous operation, the multiplier for the determining the general expenses from the labor costs was reduced from 19% to 10%. The multipliers for the fixed capital investment and the cost of manufacture were held at 0.9% and 16%, respectively.

The LCOA for the baseline ammonia facility is calculated to be $1224 per metric ton – substantially higher than ammonia produced from a conventional natural gas fired ammonia plant. However, the LCOA for the wind-ammonia facility varies primarily with the cost of electricity, rather than with the cost of natural gas.

8.5 Deviations from the Base Case

Thus far, only a simple wind-NH3 plant was analyzed. The ammonia facility was assumed to run at steady state with no energy or reactant storage. This section details how the LCOA is affected by storage systems, flexibility, and renewable energy credits and investment strategies.

8.5.1 Hydrogen Storage Systems versus Battery Systems

Two main energy storage systems for large-scale ammonia production will be explored in this section: hydrogen storage and battery storage. As shown in Figure 33, megawatt-hour scale storage is restricted to certain varieties of batteries, pumped hydro and compressed air; hydrogen storage is not considered in the figure. Since pumped hydro and compressed air storage are geology specific, they will not be considered herein. Hydrogen storage –liquid, gaseous and metal hydride – will be explored, and compared to battery storage.

Hydrogen storage is a natural fit for an ammonia plant since the majority of the plant energy required is due to the production of hydrogen. At present, there are three primary methods of storing hydrogen: compressed gaseous hydrogen storage, liquid hydrogen, storage in metal hydrides [402]. Of these methods only gaseous storage and liquid storage are used for large-scale stationary applications. While metal hydrides may be suitable for mobile applications [157, 161] , they are not yet commercially viable for large systems [162]. Compressed gaseous hydrogen storage includes metal tanks in addition to underground compressed gaseous hydrogen storage [160].

Liquid storage of hydrogen is advantageous because the volumetric density is greatly increased compared to gaseous hydrogen. As a liquid, the density of hydrogen is 70.8 kg/m^3, compared to a density of 23.5 kg/m^3 for gaseous hydrogen at 350 bar. However, liquid hydrogen containers are open systems so that strong pressures do not develop due to heat transfer into the Dewar [157]. The open system configuration results in hydrogen boil off. Even with double walled, insulated tanks boil off still occurs at a rate of about 0.4% per day for 50m^3 tanks, 0.2% for 100 m^3 tanks, and 0.06% for 20000 m^3 tanks [158]. Furthermore, liquid hydrogen production typically consumes a significant fraction of its HHV on liquefaction, depending on plant size. Estimates as high as 40% are reasonable [159] . Because liquid hydrogen storage has significant energy requirements in addition to high capital costs, it will not be considered here.

Hydrogen can be stored in large tubular containers at pressures exceeding 400 bar and used when necessary. The conversion losses are minimal because the energy expended for compression offsets – to a certain extent – the compression work required in the synthesis loop. This is similar to Compressed Air Energy Storage mitigating the back work of gas turbines (see [403] for an analysis of CAES).

In order to estimates which storage option would be better – batteries or hydrogen – the economics of each system should be considered. Hydrogen storage involves several subsystems all working together to produce, compress, and store the hydrogen. Batteries are essentially packaged plants that can be purchased. They have relatively simple cost structures which generally depend on the discharge power and the energy storage potential [404].

The costs of hydrogen storage are primarily due to three subsystems: electrolysis, compression, and storage containers. The H2A program initiated and funded by the Department of Energy (DOE) has detailed cost estimates for gaseous hydrogen storage [315]. The analysis herein will utilize the cost functions developed by H2A which will be updated using the CEPCI.

The electrolysis modules, like batteries, are package plants. Thus, their costs are typically given in $/kW. See section 6.4 for more information on this topic. Hydrogen storage inherently assumes that the total number of electrolyzers exceeds the number needed to meet the daily hydrogen demand. That is, when there is additional wind power that could be sold to the grid, it instead generates hydrogen using the extra electrolyzers. This work assumes that two extra electrolyzers are available for hydrogen production. Each electrolyzer is capable of producing 1050 kg of hydrogen per day, with a power consumption of 2330 kW. The capital cost is assumed to be $1000/kW in 2005 dollars [288]. The compressor is sized using an equation similar to the Ideal Gas Law, except that a compressibility factor, *Z*, is used and taken to be 1.028:

$$\dot{W}_{fluid} = ZT_{in}N\frac{n}{(n-1)}R\dot{m}\left[\left[\left(\frac{P_2}{P_1}\right)\right]^{\left(\frac{n-1}{Nn}\right)} - 1\right] \qquad \textbf{Equation 163}$$

Assuming an inlet temperature of 300K, two stages, an adiabatic exponent of 1.4, an initial pressure of 1 bar, a final pressure of 425 bar, and a flow rate equal to the output of the two electrolyzers – 2100 kg/day – the fluid power is roughly 250 kW. If an isentropic efficiency of 88% and a driver efficiency of 95% are assumed, the required power delivered to the driver is about 302kW. The uninstalled cost function for the hydrogen compressor system is given by H2A in 2005 dollars as [288]:

$$C_{H_2Comp} = \$23,050(Driver\ Rating)^{0.6089} \qquad \textbf{Equation 164}$$

The installation factor is assumed to be 2 for the compression system. The storage tubes are assumed to be $1170 per kilogram of storage capacity in 2005 dollars. Finally, if a 20% contingency fee is assumed, and all costs are updated to 2010 dollars using the CEPCI, the total cost is $10.6 million. The entire hydrogen storage system uses 4600kW for the electrolyzers and 302 kW for the driver/compression system, the effective power is about 4300 kW.

The storage tanks are sized to store the equivalent of one day of hydrogen production – 2100 kg. So far the costs do not include the incremental increase in MVC capacity, or the water storage that would be necessary to support the hydrogen storage. The additional water required would be roughly 3 tons per day, with an additional cost for the MVC system of about $195,000. The water tank is assumed to be negligible since it is a steel drum with no special materials or pressure considerations. Using this information, the normalized cost per kilowatt and per kilowatt-hour can be calculated for simple comparison with battery systems. The normalized costs are: $2475/kW and $105/kWh in 2010 dollars.

The hydrogen storage option compares favorably to the batteries shown in Table 81. The only commercially available battery is the sodium sulfur (NaS) battery which is installed sparingly in parts of the United States, Japan, Germany, France, and the United Arab Emirates [172]. As of late 2009 about 365 MW were installed worldwide.

Table 81 – Energy storage characteristics and costs for batteries [405]

Technology option	Maturity	Capacity (MWh)	Power (MW)	% Efficiency (total cycles)	Total cost ($/kW)	Cost ($/kWh)
Advanced Pb-Acid	Demo	3.2–48	1–12	75–90 (~4500)	2000–4600	625–1150
Na/S	Comm.	7.2	1	75 (~4500)	3200–4000	445–555
Zn/Br flow	Demo	5–50	1–10	60–65 (>10,000)	1670–2015	340–1350
V redox	Demo	4–40	1–10	65–70 (>10,000)	3000–3310	750–830
Fe/Cr flow	R&D	4	1	75 (>10,000)	1200–1600	300–400
Zn/air	R&D	5.4	1	75 (~4500)	1750–1900	325–350
Li-ion	Demo	4–24	1–10	90–94 (~4500)	1800–4100	900–1700

Using a large-scale battery could be more beneficial than pure hydrogen storage because it has the ability to power all systems simultaneously, whereas a hydrogen storage system cannot. However, hydrogen must always be produced to synthesize ammonia. If it is assumed that some can be stored and used later, then the cycle efficiency for the hydrogen is higher than any battery system – 95% where even the "losses" are used to displace compression work. Moreover, the total storage capacity is higher – 105 MWh versus 50 MWh for the best batteries – and the total cost per kilowatt and per kilowatt hour are lower. In conclusion, hydrogen dominates all of the possible batteries. Hence, only gaseous hydrogen storage will be considered as a possible scenario.

8.5.1.1 Simulation with H_2 Storage

The simulation for an ammonia plant that incorporates gaseous H_2 storage proceeds in much the same way as the baseline wind-NH_3 simulation. However, in this case, when excess electricity exists, the electricity could be converted to gaseous H_2 and stored. There are several differences between the baseline analysis and the H_2 storage analysis. First, extra electrolyzers are required to provide hydrogen when there is excess electricity. Second, the simulation must keep track of the state of the storage tank and make decisions based on how much excess electricity is available and how much H_2 is in storage.

When the storage tanks are not full and there is excess electricity then the electricity is converted into H_2, compressed, and stored in the tanks. Moreover, if there is a deficit of electricity, and there is H_2 in the storage tanks, then it is used to supplement the required synthesis gas. The logic for the H_2 storage system is shown in Figure 88.

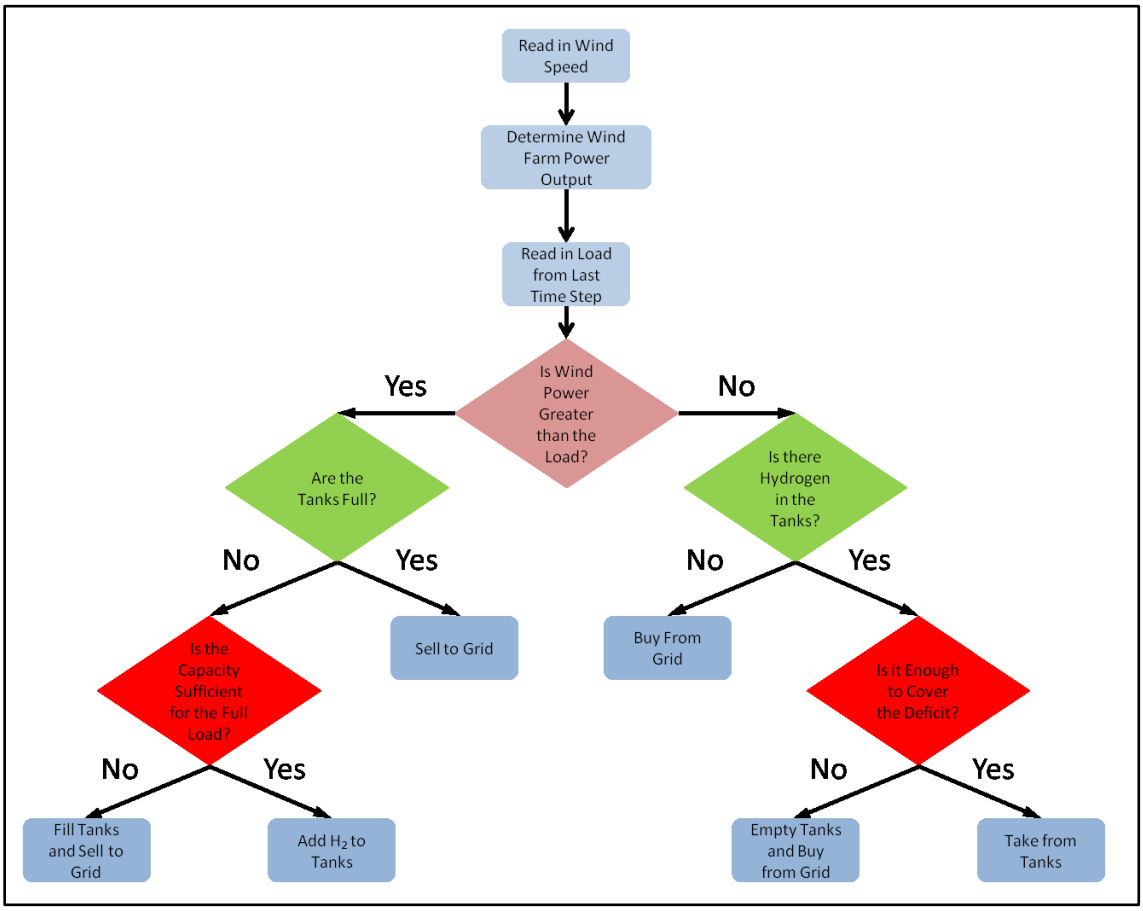

Figure 88 – Simulation logic for H_2 storage

The simulation was run on a series of cases to help elucidate which scenario would be the most beneficial to the overall system. The total storage capacity was chosen to be 1,000Nm_3, 5,000Nm_3 and 10,000Nm_3 for the 300 metric ton per day system. For each storage system, up to 5 extra electrolyzers were implemented. The outputs of the electrolyzers are assumed to be 485 Nm_3 per hour. The simulation incorporated the extra costs for the storage, compression, and the electrolyzers, as detailed above. The

simulation also calculated the offset electricity costs using three electricity utility grid purchase prices: the baseline price; twice the baseline price; and 5 times the baseline price. The results are presented in a dimensionless graph which shows the hourly electrolyzer output divided by the H_2 storage capacity on the abscissa, and the baseline LCOA divided by the calculated LCOA in the ordinate. The full results are shown in Figure 89.

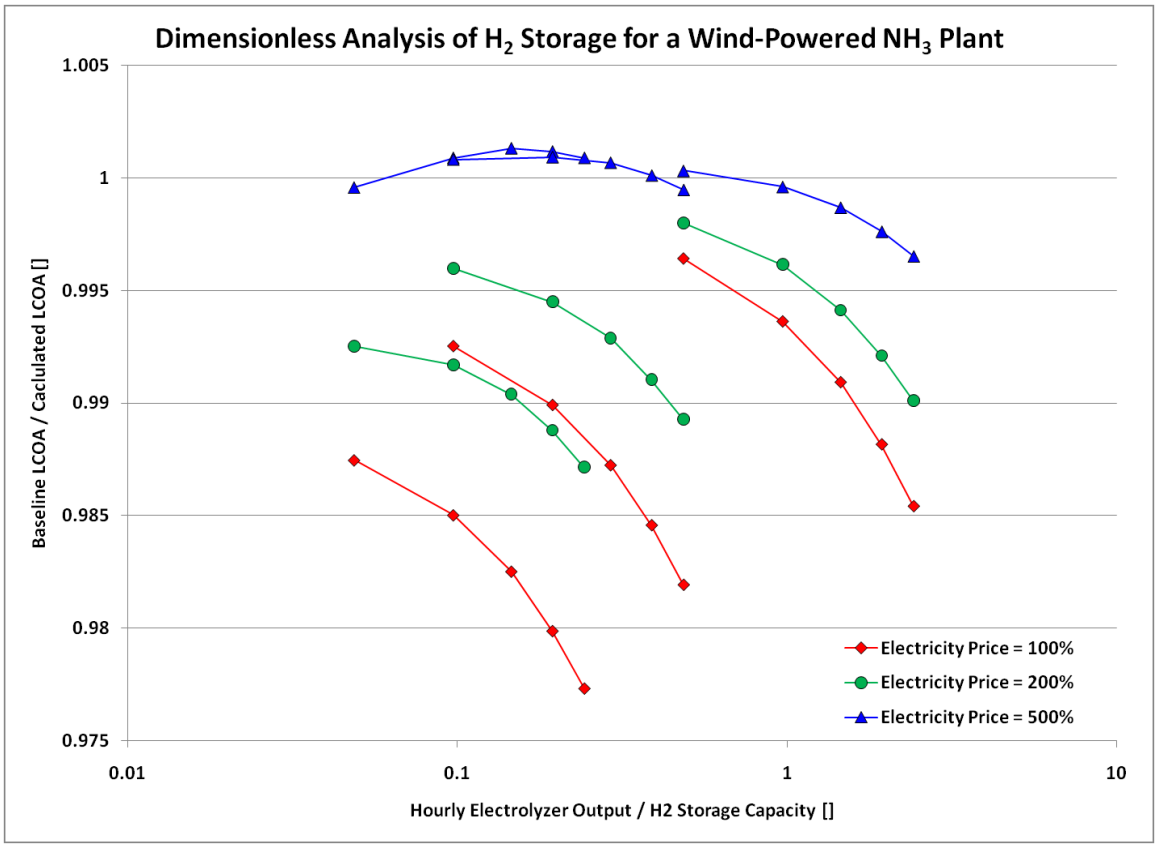

Figure 89 – Dimensionless analysis of H_2 storage for a wind-driven ammonia plant

The results show that having more hourly H_2 output per unit of storage capacity is beneficial, but only slightly. For example, when the electricity price is held at its baseline (red plot) the normalized LCOA changes by less than one percent when the abscissa values change by an order of magnitude. The electricity price also has a weak effect on the overall LCOA, with H_2 storage becoming more beneficial for higher electricity prices.

Overall, the H_2 storage for large-scale ammonia systems has limited utility. However, its usefulness would likely be more pronounced for smaller ammonia systems.

8.5.1.2 Flexible Ammonia Assumptions

The value in creating the flexible ammonia process need not be reducing the levelized cost. The value is being able to generate a fuel in a remote location such as an ocean, or a sparsely inhabited stretch of land. Flexible ammonia offers the potential to produce a synthetic fuel with only air and water, thus enabling revenues to be generated in places previously thought to be undesirable. However, this section details the LCOA calculation for a flexible ammonia plant.

There are two parameters that help define how flexible a chemical process can be: the turndown ratio and the ramp rate. The turndown ratio is the quotient of the lowest output to the highest output. In the case where there is an infinitely flexible ammonia process the turndown ratio is zero; a time-invariant, steady-state system would have a turndown ratio of unity. The ramp rate is a measure of how much the system load can change per unit of time. High ramp rates imply flexible plants.

Modeling the turndown ratio is straightforward: simply limit the power delivered to the plant which is directly related to the flow rates in the synthesis loop. The limited flow will result in less ammonia production and ultimately less ammonia product. The flexibility is handled by assuming that some fraction of the plant power can be changed at each time step. In its most basic form, the plant power operates in an "envelope" for each time step. In this case the time steps are 10 minutes so it is assumed that the dynamics of the electrolyzers, compressors, etc. are much faster than that.

A graphical depiction of the inter-timestep decision process is shown in Figure 90. Here, the red dot depicts the current load; the blue dots represent the future load possibilities which depend on the system flexibility; the green arrows represent possible wind production outputs. Greater flexibility is shown toward the right side of the figure where the blue dots are farthest apart. Thus, if the incoming wind

power is high or low, the most flexible plant could be changed to meet the requirements. The least-flexible plant – depicted as the blue dot on the left-side – does not change position no matter what the wind power output is. The entire scheme is also governed by the turndown, which could be high and prohibit any system flexibility; or low which promotes flexibility. Thus, there is a non-trivial interaction between the inter-timestep flexibility and the system flexibility which will be explored in the simulation.

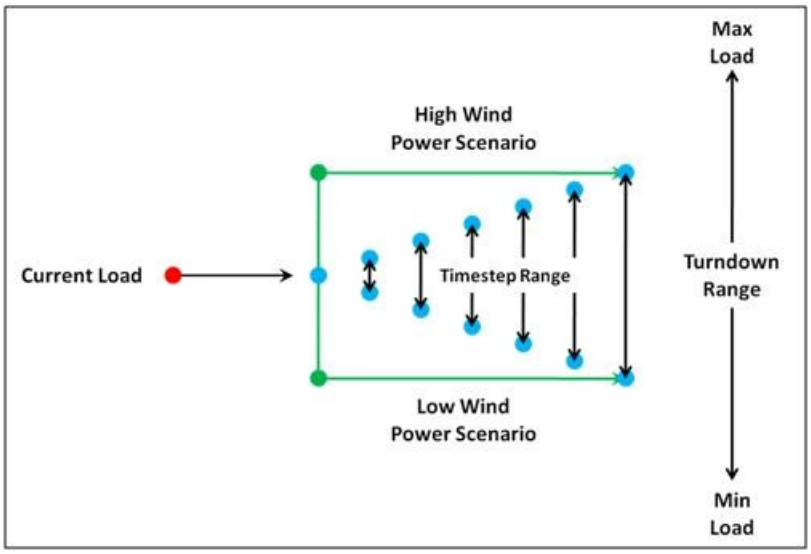

Figure 90 – The inter-timestep decision process.

At each 10-minute interval the simulation program reads in a line of information containing the wind speed, the buy and sell price for the grid, and the load from the previous step. The load from the previous timestep is compared to the wind power for the current timestep. The logic of the program maintains that if the wind is insufficient, then the load could decrease; if the wind is more than sufficient that the load could increase. In this way, the load will follow the wind power output to a certain extent. If the ramp rate is high and the turndown ratio is low then this system behaves exactly as a load following ammonia plant. If the ramp rate is zero and the turndown ratio is unity, then there is no opportunity to modify the load to match the wind power output. The flow chart for the decision process is given in Figure 91. The figure does not depict the situation when the load and the wind power are exactly equal. In that case, there is no grid or storage interaction, and the load is passed on to the next timestep.

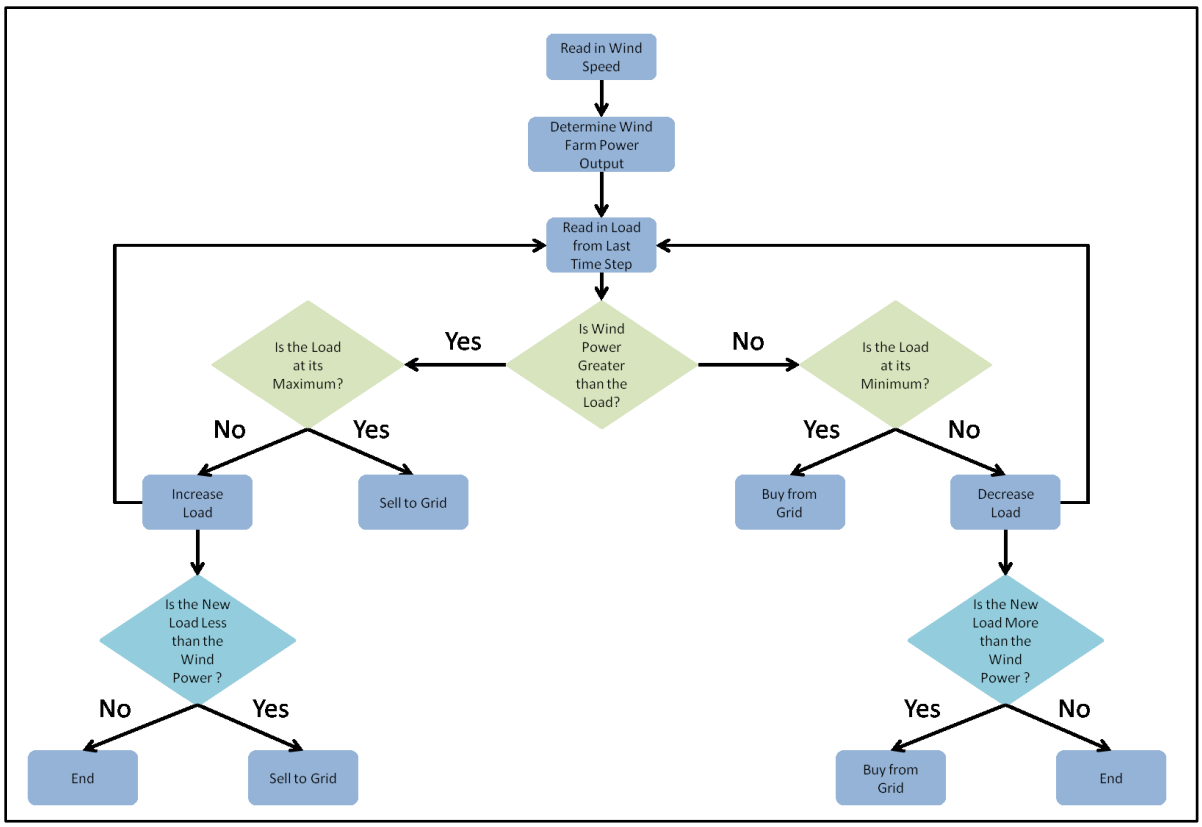

Figure 91 – Logic scheme for the flexible ammonia plant

The turndown ratio and the inter-timestep flexibility also alter the way the ammonia plant behaves. They are inherently tied together: if the turndown ratio is zero, then there can be no flexibility; the system is always at steady state. On the other hand, if the turndown ratio is unity and there is no inter-time step flexibility, then the system is also at steady state. When the two parameters take on intermediate values, the LCOA can change dramatically. The interplay between the two parameters is shown in a contour plot in Figure 92. While the plot is coarse, it still elucidates how the two parameters interact. First, the NPV is at a minimum when the plant is the least flexible. This is clearly due to inexpensive grid electricity to run the facility. Second, the NPV clearly increases as the turndown becomes more flexible. As the plant ramps up and down with the varying power from the wind, it produces less ammonia and translates into a higher overall LCOA. Third, the LCOA changes rapidly when the inter-timestep flexibility increases, but only at low values. The LCOA is essentially constant when the inter-timestep flexibility is between 20%

and 100%. Finally, when the facility is infinitely flexible (top right hand side) then the plant makes ammonia only when there is power available from the wind farm. The excess electricity is all sold to the grid, reducing the overall LCOA.

The results are contingent on the price of electricity which was taken to be $0.082/kWh over the period 2005-2007. If the electricity price doubles to $0.165/kWh the contour plot changes significantly, as shown in Figure 93. Here, the minimum shifts to the "most flexible" scenario, where the turndown ratio between 0 and ½ and the inter-timestep flexibility is greatest. In this case, it is advantageous to produce ammonia only when the wind is blowing: the cost of electricity from the grid is prohibitively expensive.

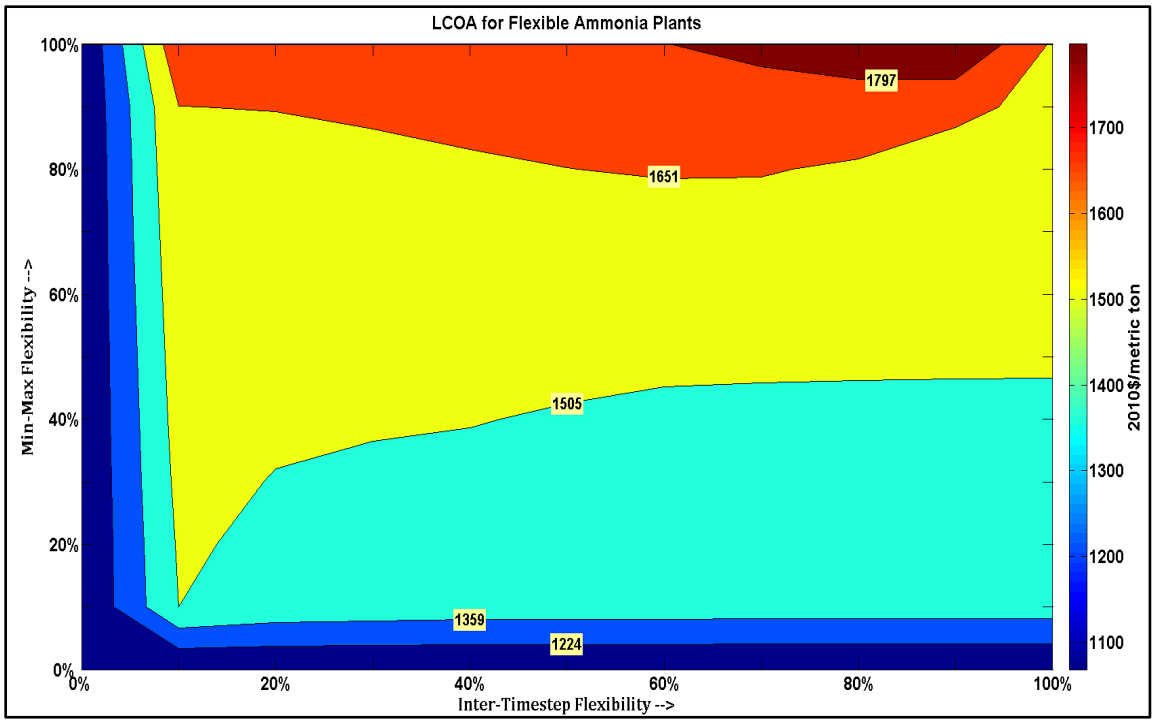

Figure 92 – Contour plot of the LCOA NPV for various plant configurations

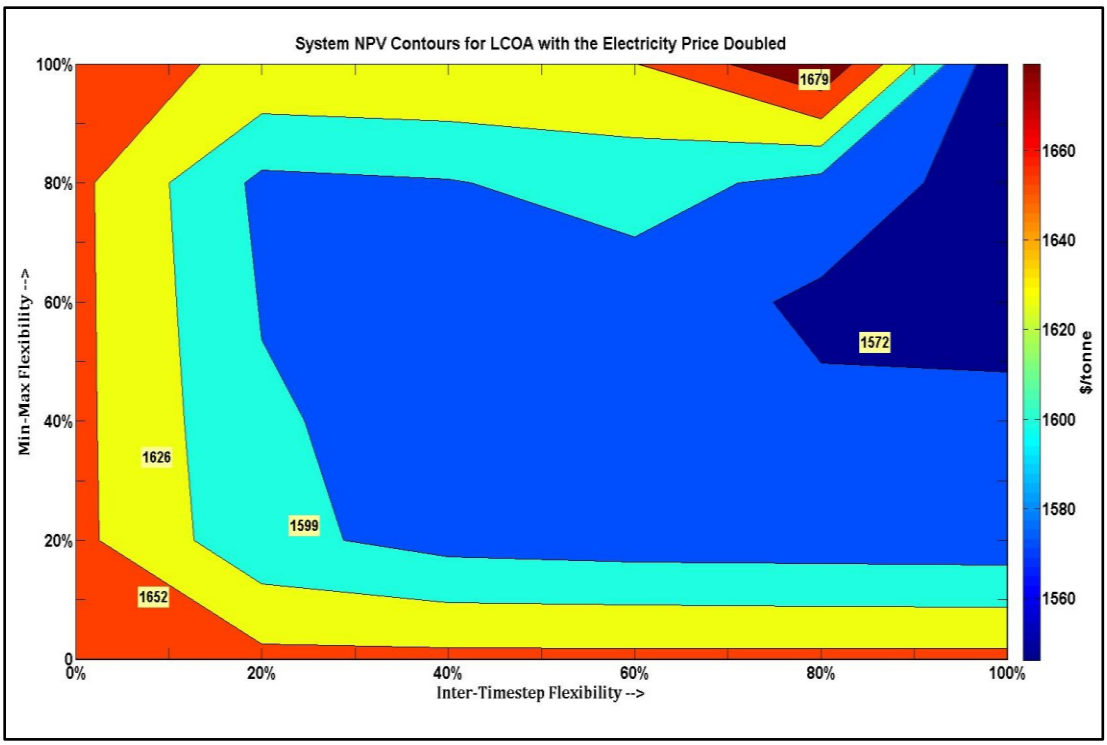

Figure 93 – Contour plot for the LCOA with the cost of electricity doubled

8.5.2 Tax Incentives and Investment Strategies

In practice, if a wind powered ammonia plant were to be built, there would likely be two companies: one to operate the ammonia plant and one to operate the offshore wind facility. Thus, one company owns the offshore wind farm and holds all or most of the associated risk. The other company owns the ammonia plant and enters into a power purchase agreement with the offshore wind farm. In this scenario, there is no "behind the meter" situation and all transactions are apparent. This enables the owners and financiers of the wind farm to lower their risk and utilize federal and state incentives. Such incentives include the Renewable Energy Certificates (RECS) [406-407] at the state level and Production Tax Credits (PTCs) [408] at the federal level that help reduce the overall cost of the wind farm.

It remains unclear what benefit the RECs would have for "behind the meter" applications. RECs are valid for wind project of all types, and "non-energy attributes" also qualify [407]. The non-energy attributes would be anything that offsets emissions, as a wind-NH_3 plant clearly does. Maine offers unbundled

RECs [409] which means that they can be sold separately from the electricity – a good indication that RECs are valid for a wind/NH_3 facility. The Production Tax Credit is set to expire on December 31, 2012 [410], so its fate is unknown at the time of this writing.

An Alternative Fuel Excise Tax Credit also exists but is not available for ammonia because it is not a federally recognized fuel [411].

Several innovative financial structures such as the "Strategic Investor Flip", "Institutional Investor Flip" or "Corporate" are available to finance wind farms [412] and would need to be investigated for the direct use of an ammonia plant. There are some ethanol plants that have been integrated with wind power (see [413] for Google search results), though the details of the Power Purchase Agreements (PPAs) are unknown.

This work assumes that both the wind farm and the ammonia plant are owned by the same entity, or entities and utilizes the Corporate finance structure. The Corporate structure was found to yield the highest levelized cost of energy of any financial structure [414], but no specific cost reduction occurs when other financing structures are employed. Thus, all tax incentives can be utilized by this entity, but it is unclear if the RECs could be utilized. This thesis assumes that the PTC cannot be utilized, since they are set to expire. It also assumes that RECs could be utilized in some states.

8.5.3 Sensitivity Calculations

The sensitivity of the LCOA to various inputs is of paramount importance. Sensitivity analysis enables one to identify the most meaningful parameters related to the system cost. There are several varieties of inputs that can be explored: direct costs such as that of the wind farm; LCOA parameters such as discount rate; indirect benefits from the wind speed; financial incentives such as RECs; and the ammonia plant parameters, such as turndown.

To better understand how some of the parameters affect the LCOA, a spider chart was constructed. The spider chart shows the percent change in the LCOA versus the percent change in the parameter of interest. That is, eight separate parameters – wind farm cost, NH_3 plant cost, wind speed, discount rate, COM, GE, NH_3 size, and electricity cost – will be varied from 25% to 200% of their baseline value, in steps of 25%. The resulting LCOA will be normalized with the baseline LCOA of $1224 per ton of ammonia to estimates the ordinate value. The full results are presented in Figure 94.

The sensitivity shows that the most meaningful parameters (those with the greatest slope) are the discount rate, the wind speed, the cost of the wind farm, and the cost of manufacturing. The LCOA varies linearly with many of the parameters, but several induce non-linear behavior. For example, the variation of the LCOA with wind speed resembles a sine wave because the power generated by the turbines is related to the cube of the velocity. Furthermore, if the wind speeds exceed critical values then the turbines "cut out" and no power is produced. This accounts for the increase in LCOA when the wind speed is doubled (200%).

Several other factors contribute to the LCOA, however these factors are best illustrated on a tornado chart like the one presented in Figure 95. The tornado chart is centered on $1224/ton of ammonia and shows the LCOA variations for nineteen parameters, discussed herein.

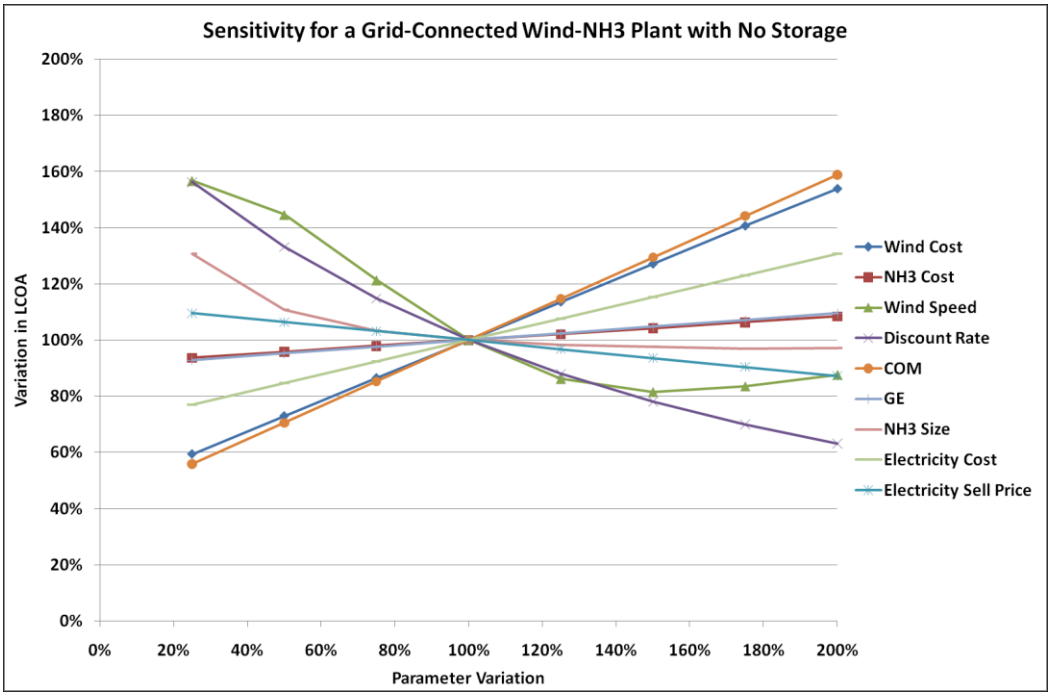

Figure 94 – Sensitivity analysis of an offshore wind powered ammonia plant. Baseline = $1224/tonne

The lifetime of the system has a major influence on the cost of producing ammonia: if the system life is low, then it will produce less ammonia for the same cost, raising the LCOA. Conversely, if the system life is long, the system will produce more ammonia over its lifetime at the same cost, reducing the LCOA. Renewable energy credits (RECs) can help reduce the overall LCOA because they can help offset some of the operations and maintenance costs – much like excess electricity. The RECs typically are sold in terms of $/MWh; the maximum price for a REC in the United States is about $50/MWh, though the prices are highly variable [415]. The operations and maintenance cost for the offshore wind farm is a matter of debate, but typical values are assumed to be 3% of the capital expenditure [354]. The impact of the O&M cost is significant, primarily because it represents ongoing costs for the lifetime of the project. Once the ammonia is produced, it must be freighted to its final destination, either by ship, train or truck. Furthermore, insurance is required in case of spills, or other catastrophic situations. The freight and insurance are roughly $60/metric ton, and does not depend on the total ammonia production. The uptime of the NH_3 plant has a dramatic influence on the LCOA because it directly impacts the total ammonia

production. A low uptime implies that the wind farm is selling electricity but not producing ammonia. The power required for the plant is related to the power for electrolysis, the compression of the syngas, the power for the ASU and the power for the MVC water desalination. Of these, the electrolyzer power dominates the demand. The power variation was selected to be between 95% and 110% of the baseline power requirements – 145MW for a 300 ton per day plant. The results are expected, but show that the power plays an important role in the LCOA.

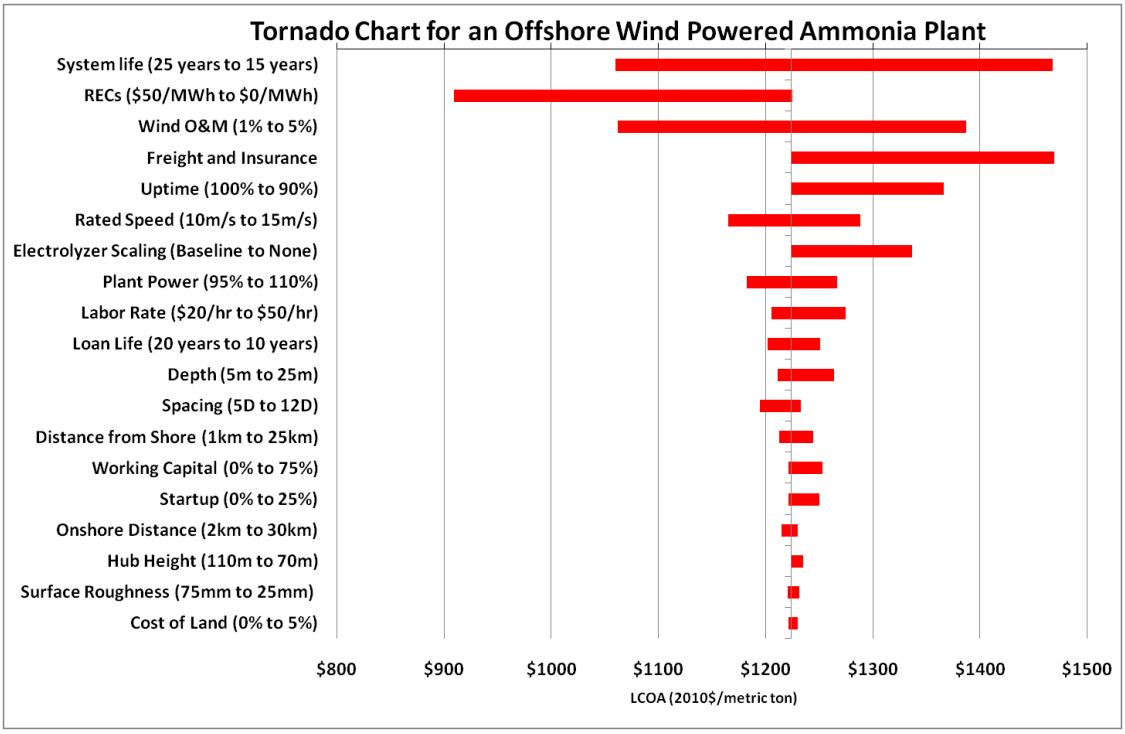

Figure 95 – Tornado chart for an offshore wind powered ammonia plant

The labor rate for chemical engineering plants is given by the Bureau of Labor Statistics as $28.32/hr in 2010[312]. If the labor rate range is taken as $20/hr to $50/hr the LCOA changes by nearly $70 per ton. It is assumed that the labor rate will remain at the 2010 levels or higher in accordance with other skilled labor rates.

The rated speed of the turbine is potentially significant: if the turbine is able to capture a larger swath of wind speeds at rated power then the power produced will be greater. Clearly, this is constrained by physics and the physical size of the turbine but the range of values for this parameter is turbine specific. By varying the rated speed from 10m/s to 13m/s while keeping everything else constant, the range of LCOA values was found to be about $63/ton.

The depth, distance from shore, and spacing of the wind turbines are all related to the cost of materials used in the construction. Greater depths require larger monopiles and therefore greater amounts of steel. Locating the turbines at a greater distance from shore requires more cables to be extended to the turbines form the connection point, increasing the capital costs due to the copper and the installation; the spacing of the turbines has two effects: first, greater spacing requires more copper cables to be strung between the turbines; second the spacing relates to the overall power generated by the turbines due to wake effects. The results of varying the three parameters show that the depth increases the LCOA by $53/MWh when varied between 5m and 25 m of depth. The spacing has a moderate influence, but it is masked by purchasing inexpensive grid power. The spacing would have a larger effect on the LCOA if no grid power were purchased.

Other factors are of minor importance: the working capital, the startup costs, the surface roughness, which is used to estimates the wind speed at elevation, the distance of the onshore electrical lines, the hub height and the cost of land.

The best case scenario for the LCOA would be to have a wind-ammonia facility with a long lifetime and no major disruptions in production. The facility would further lower its LCOA by selling RECs while paying low operations and maintenance rates, with no freight or insurance. This “perfect storm” would yield a levelized cost of ammonia of $583/ton which could be considered an absolute minimum levelized cost under the conditions outlined in this thesis.

CHAPTER 9

SUMMARY AND FUTURE WORK

This thesis showed that ammonia production with offshore wind power is technically feasible with current technologies and that it can be cost-competitive compared to conventional ammonia production if natural gas prices increase significantly in the coming years. The conventional ammonia production subsystems were thoroughly reviewed and analogous electrically driven state-of-the-art technologies were chosen as replacements. The hypothetical all-electric ammonia plant which included the synthesis gas production, water purification, synthesis loop, and ammonia storage was designed and costed using standard chemical engineering techniques. Wind power theory was discussed as it applies to the offshore wind industry in Europe. The economics of offshore wind were reviewed and a new cost-updating method was applied to published European equipment costs. An NREL turbine cost model was also updated so that the cost in 2010 dollars of any large wind turbine could easily be estimated. The translated and updated European equipment costs were coupled with the updated NREL cost model to produce a new offshore wind cost model that depends only on 11 wind farm parameters. A simulation program that incorporates the ammonia cost model and the wind cost model was applied to a generic site in the Gulf of Maine to estimates the levelized cost. The simulation program used actual utility grid pricing data, and real offshore wind data from the Gulf of Maine to calculate the levelized cost of ammonia. The levelized cost for an offshore wind powered ammonia plant was found to be about three and a half times higher than the equivalent natural gas-fired ammonia plant. The levelized cost was found to be most sensitive to the wind speed, the cost of the wind power, the cost of manufacturing for the synthesis gases and the lifetime of the system.

Summary of the work:

- An all electric ammonia synthesis production plant is feasible as conceived, though the actual equipment changes with the output of the plant. Micro ammonia plants (5 tonnes per day or less) could use a proton exchange membrane electrolyzer and a pressure swing adsorption nitrogen generator; larger facilities require alkaline electrolyzers and cryogenic air separation units. All configurations use the standard ammonia synthesis loop, mechanical vapor compression water purification, and ammonia storage.
- The ammonia plant was built "from the ground up" and included standard, commercially available equipment. The costs of the equipment were summed and cost curves were developed for the ammonia synthesis subsystems and for the entire ammonia plant.
- An economic model for large-scale alkaline electrolyzers based on standard chemical engineering equipment scaling principles was developed for this thesis. The results showed that significant capital cost savings can be achieved if the electrolyzers utilize common equipment such as compressors or gas holding tanks.
- An economic model developed at NREL was updated using the Producer Price Index as a proxy for inflation. The results showed that the PPI reflects changes in the cost of wind turbines that are due to materials, energy, and labor. A single inflation index for the turbine and tower was calculated to be 139.1 over the period between 2002 and 2010.
- A framework for translating wind farm and equipment capital costs across space and time was developed so that costs listed in foreign currencies could be incorporated into the economic models. The framework utilized the GDP deflator as a measure of general inflation instead of the Consumer Price Index. While the translated costs were found to be a range of possible values, the average of the range was selected as the best single metric for updating costs.
- A capital cost model for offshore wind farms in the United States was developed. The model incorporated the updated NREL cost model for the turbine and tower and translated European

costs for the cables, foundation and power electronics. The model showed good agreement with existing offshore wind farm capital cost data.

- The levelized cost of ammonia was calculated using the ammonia capital cost model, the wind farm cost model and the power production model. The LCOA estimate for ammonia produced with electricity from both the utility grid and wind turbines is $1224 per metric ton.
- A sensitivity analysis was performed on the LCOA and it was found that wind speed, the cost of manufacture and the wind farm cost were the three most influential design-side drivers of the cost.
- A separate sensitivity analysis that used secondary drivers found that the system life, the Renewable Energy Credits, the operations and maintenance, and the system uptime all had significant influence on the levelized cost.
- It was found that the minimum levelized cost of ammonia for an offshore wind powered facility is about $580 per metric ton.

9.1 Future Work

The work in this thesis could be improved upon in future projects. First, the ammonia reactor model assumes a steady-state operation for most of the thesis; flexible ammonia processes are assumed in a few limited instances. Ammonia synthesis loops are tremendously complex and to truly understand their capabilities and limitations, a dynamic model should be developed. Moreover, each of the subsystems were assumed to be steady state chemical plants. The steady-state assumption is valid for each of the plants – hydrogen, nitrogen, water, storage – but clearly system-level dynamics could occur on numerous occasions.

As an example, electrolyzers, compressors and the ammonia synthesis loop all produce heat which could be integrated into either the ammonia process or another process entirely to increase efficiencies. Heat integration was not considered for any of the subsystems.

Air separation units are an integral part of the overall ammonia system: they provide 82% of the mass of ammonia. However, the ASUs are nearly as complex as the ammonia plant, and require strict control in the heat exchangers and the distillation columns, as well as tight heat integration for efficiency.

Electrolyzers are the most expensive part of the synthesis gas processing, yet the modeling is kept relatively simple. The consequence of the simple model is that the heating and cooling dynamics are left in great uncertainty: electrolyzers operate at full output only when they are already "hot". This thesis assumes that the electrolyzers are instantly hot when called upon.

The cost models for the subsystems are approximations based on the expected major equipment lists; the minor equipment requirements are neglected. To compensate for the simplicity, extra costs in the form of a percentage of the major equipment, were added. More detailed, full economic models could be developed that may be more accurate and precise.

The Gulf of Maine was selected for offshore ammonia production simply because there was active, serious interest in the subject. The generic offshore wind site that was selected is probably not feasible because the Gulf of Maine has fairly deep waters close to shore. Some areas may be "shallow" but are near islands in waters that exceed 10 meters in depth. Furthermore, the wave and soil characteristics were not considered during the offshore wind farm design phase. Thus, a more suitable location with wind, wave and soil data would be a more meaningful case study than the Gulf of Maine. Iceland, the Faroe Islands, Hawaii, or any other archipelago might make for an interesting analysis.

Validation for many of the models developed in this thesis could not be performed. There are a few reasons for this. First, the all-electric ammonia plant does not yet exist so no cost estimates exist either. Some references to the cost of a synthesis loop exist, but only as fractions of the overall ammonia plant cost. Since there are literally dozens of synthesis loop configurations, the costs are highly uncertain. Second, air separation units are not discussed extensively in the literature and the information and costs are often proprietary. There is almost no mention of the cost for a large-scale nitrogen generator. Costs

that do exist are for oxygen generators that are an order-of-magnitude larger than the nitrogen generators required for the ammonia plant discussed heretofore.

Offshore wind farms do not yet exist in the United States, making the validation of the offshore wind cost model difficult to validate. The validation was performed on the translated costs of several European offshore wind farms, and showed good agreement. Ideally, the model would have been validated in the European currency and then adopted into present US dollars. That approach was not done because the ideas for translating and updating wind costs evolved independently over many years. Once the translation and cost updating structure was complete it was already interwoven within the overall cost model. In retrospect, the models should have been modular and built with a European currency platform and a US dollar supplement.

APPENDIX

MATLAB SIMULATION CODE

This appendix contains all of the Matlab files required for duplicating the analysis of the proposed offshore wind powered ammonia plant. The files listed below are ordered as they are called in the main (first) file in section A.1. For each file that is called by the main file, all subfiles are resolved before returning to the main file.

In order to run this program, all files must either be in the current working directory in Matlab, or in a defined path.

A.1 – The Main File that Calls All Other Files

```
% This is the engine that runs all other files to determine the LCOA of an ammonia plant.

clear all; close all;

global PerDay XTraElec

Scenario = 1; % 2 for storage, 1 for no storage;

PerDay = 144; % Ten minute data = 6 points per hour times 24 hours.
H_ref = 22.6; % The height of the anemometers at Desert Rock (check height
% - should be above sea level since it's an island)

% The 3MW turbine specifications are based on the Vestas 3MW machine

H_Hub = 105; % The assumed hub height for the 3MW wind turbines.
% Note that hub height here does not necessarily include the transition
% piece. See Snyder pgs 191-192. The range is about 6m to 25m.

TurbineSize = 3000000; % Watts
Pwt = TurbineSize; % Dummy variable
R_Spd = 12.5; % Global rated speed (m/s)

% Diameter should be based on turbine power!
dia = 100;
nwt = 100; % No. of wind turbines
Space = 10; % Spacing (diameters)
Cut_in = 4; % Cut in speed (m/s)
Cut_out = 25; % Cut out speed

NH3Size = 300; % Plant size in metric t/day
T = 450; % Operating Temp (C)
P = 150; % Operating pressure (bar)
```

```
% Wind Section
Voltage = 36000; % Inter turbine voltage
Dep = 10; % Depth of 10m
Dwf = 10; % Distance from shore of 10 km
h = H_Hub; % Hub height dummy
S = Space; % Dummy (from legacy code)
Vn = 33000; % Inter turbine voltage
HV = 136000; % High voltage
num_HV = 2; % HV lines
BB = 2; % Bus bars
TransDist = Dwf; % Transmission distance is the distance from shore
OnOff = 'Off'; % On/Offshore substation
Onshore_Dist = 20; % Onshore transmission distance (km)
nHV = 1; % # of HV on land lines

% Wind data from Mt Desert Rock
% http://www.ndbc.noaa.gov/station_page.php?station=mdrm1
% Height of anemometer is 22.6 meters above mean sea level.

if Scenario == 1

%{
Note that WindPriceComplete is a 10 column matrix containing the: Year; Month; Day; Hour; Minute; Wind
Speed; Wind Direction;
Electricity Sell Price; Electricity Buy Price; and NH3 Price
It is not included in this Appendix (~150,000 lines)
%}
   load WindPriceComplete.txt;
   WindSpeed = WindPriceComplete(:,6);
   Buy = WindPriceComplete(:,9); % Buy price in Wh
   Sell = WindPriceComplete(:,8); % Sell price in Wh
   NH3Price = WindPriceComplete(:,10); % Price of ammonia in $/metric ton
   WindSpd = ShearUp(WindSpeed,H_ref,H_Hub); % The wind speed sheared up to the hub height.


   % This section is the No storage section. It was verified and used to
   % produce the spider plot for the LCOA for the no storage situation

   % Set up vectors for faster processing
   Chunks = length(WindSpd);
   Rev = zeros(Chunks,1);
   RevNH3 = zeros(Chunks,1);
   NH3 = zeros(Chunks,1);
   RevElec = zeros(Chunks,1);
   Grid = zeros(Chunks,1);
   BuyElec = zeros(Chunks,1);
   SellElec = zeros(Chunks,1);
   Balance = zeros(Chunks,1);
   GridPwrAvail = zeros(Chunks,1);
   InitH2State = 0;
   % End vectors
  % The hydrogen storage component. Units of Nm3
   H2Max = [0:5000:10000];
    XTraElec = 0; % The number of extra electrolyzers for storage.
   delPlant = 1; % The plant's inter-timestep flexibility
   Turndown = 1; % The plant's global flexibility
```

```
   % Some statistics
   [mean stdev TI Pwr CapFac] = WindStats(WindSpd,TurbineSize,R_Spd,dia,Cut_in,Cut_out);

   PwrAvail = TotalWindPwr(nwt,Pwt,dia,WindSpd,Space,R_Spd,Cut_in,Cut_out);
   ActCapFac = nanmean(PwrAvail)/(nwt*TurbineSize);
   % Some NH3 specs
   [Plant_Pwr NumElec] = PlantPwr(P,NH3Size);
   [Strings Power TurbPerStrng SString ShortPwr TurbPerShStrng TotalPwr]...
      = ParkSetup(nwt,TurbineSize/1e6,Voltage);
   if Strings == 0
      ncl = 1;
   else
      % The number of long strings plus the short strings
      ncl = Strings+SString;
   end

   [Rev(1) RevNH3(1) NH3(1) RevElec(1) Grid(1) BuyElec(1) SellElec(1) GridPwrAvail(1) Balance(1)] =
TotalNH3Engine(PwrAvail(1),Plant_Pwr,Buy(1),Sell(1),NH3Price(1),InitH2State,H2Max,delPlant,Turndown
,Plant_Pwr,NH3Size,Scenario);
   for i = 2:length(WindSpd)
      if isnan(WindPriceComplete(i,6)) == 1 | isnan(WindPriceComplete(i,7))==1 |
isnan(WindPriceComplete(i,8))==1 | isnan(WindPriceComplete(i,9))==1
         Rev(i) = Rev(i-1);
         RevNH3(i) = RevNH3(i-1);
         NH3(i) = NH3(i-1);
         RevElec(i) = RevElec(i-1);
         Grid(i) = Grid(i-1);
         BuyElec(i) = BuyElec(i-1);
         SellElec(i) = SellElec(i-1);
         PwrAvail(i) = PwrAvail(i-1);

      else
         [Rev(i) RevNH3(i) NH3(i) RevElec(i) Grid(i) BuyElec(i) SellElec(i) GridPwrAvail(i) Balance(i)] =
TotalNH3Engine(PwrAvail(i),Plant_Pwr,Buy(i),Sell(i),NH3Price(i),InitH2State,H2Max,delPlant,Turndown,P
lant_Pwr,NH3Size,Scenario);
      end
   end

   [CC_Wind CWT CF Cc CIS CTS CSE CPD]  =
WindCost(nwt,Pwt/1e6,dia,R_Spd,h,Dep,Dwf,Space,TransDist,Vn,HV,BB,OnOff,Onshore_Dist,nHV);
   C_Other = ((CWT + CF + Cc + CIS + CTS + CSE + CPD)/(0.89))*0.11;

   [ElecCapCost ASUCapCost MVCGrassRts SynGrassRts StoreGrassRts TotalNH3Cost RawMatl
Labor_Cost] = NH3Cost(T,P,NH3Size,0,0);
   OM_Wind = 0.03;
   totalcost = CC_Wind+TotalNH3Cost;
   d_pay = 0.1;
   interest = 0.04;
   inflate = 0.03;
   discount = 0.07;
   life = 20;
   loan_life = 15;
   O_M = OM_Wind*CC_Wind;
   COM = 0.18*(ASUCapCost + MVCGrassRts + SynGrassRts + StoreGrassRts)+0.05*ElecCapCost +
2.73*Labor_Cost+1.23*(-sum(RevElec)/3 + RawMatl) + O_M;
```

```
    % General expenses, Turton page 224.
    % Unattended operation of electrolyzers warrants less GE (H2A tool)
    GE = 0.1 * Labor_Cost + 0.009 * TotalNH3Cost + 0.16 * COM;
    % The renewable energy credits that are possible in Maine (assumed 0)
    RECs = nansum(PwrAvail)/(3*6e6)*0;
    NPV_Costs = NPVCosts(totalcost,d_pay,interest,inflate,discount,life,loan_life,COM+GE-RECs);
    LCOA = NPV_Costs./((sum(NH3)/3)*life)

elseif Scenario == 2

    load WindPriceComplete.txt;
    WindSpeed = WindPriceComplete(:,6);
    Buy = WindPriceComplete(:,9); % Price in Wh
    Sell = WindPriceComplete(:,8); % Price in Wh
    NH3Price = WindPriceComplete(:,10); % Price of ammonia in $/metric ton
    WindSpd = ShearUp(WindSpeed,H_ref,H_Hub); % The wind speed sheared up to the hub height.

    H2Max = [0:5000:10000];
    XTraElec = 3; % The number of extra electrolyzers for storage.

    % Set up vectors for faster processing
    Chunks = length(WindSpd);
    Rev = zeros(Chunks,length(H2Max));
    RevNH3 = zeros(Chunks,length(H2Max));
    NH3 = zeros(Chunks,length(H2Max));
    RevElec = zeros(Chunks,length(H2Max));
    Grid = zeros(Chunks,length(H2Max));
    BuyElec = zeros(Chunks,length(H2Max));
    SellElec = zeros(Chunks,length(H2Max));
    ModLoad = zeros(Chunks,length(H2Max));
    H2State = zeros(Chunks,length(H2Max));
    PwrAvail = zeros(Chunks,length(H2Max));
    Addl_Pwr = zeros(Chunks,length(H2Max));
    Balance = zeros(Chunks,1);
    ReactPwr = zeros(Chunks,length(H2Max));
    % End vectors

    [mean stdev TI Pwr CapFac] = WindStats(WindSpd,TurbineSize,R_Spd,dia,Cut_in,Cut_out);

    PwrAvail = TotalWindPwr(nwt,Pwt,dia,WindSpd,Space,R_Spd,Cut_in,Cut_out);
    ActCapFac = nanmean(PwrAvail)/(nwt*TurbineSize);
    % Some NH3 specs
    [Plant_Pwr NumElec] = PlantPwr(P,NH3Size);

    [Strings Power TurbPerStrng SString ShortPwr TurbPerShStrng TotalPwr]...
       = ParkSetup(nwt,TurbineSize/1e6,Voltage);
    if Strings == 0
       ncl = 1;
    else
       % The number of long strings plus the short strings
       ncl = Strings+SString;
    end

    delPlant = 1;
    Turndown = 1;
    InitH2State = 0;
```

```
   for k = 1:length(H2Max)
      [Rev(1,k) RevNH3(1,k) NH3(1,k) RevElec(1,k) Grid(1,k) ModLoad(1,k) H2State(1,k) ReactPwr(1,k)
Addl_Pwr(1,k) Balance(1,k)]...
         =
TotalNH3Engine(PwrAvail(1),Plant_Pwr,Buy(1),Sell(1),NH3Price(1),InitH2State,H2Max(k),delPlant,Turndo
wn,Plant_Pwr,NH3Size,Scenario);
      for i = 2:length(WindSpd)
         if isnan(WindPriceComplete(i,6)) == 1 | isnan(WindPriceComplete(i,7))==1 |
isnan(WindPriceComplete(i,8))==1 |...
               isnan(WindPriceComplete(i,9))==1
            Rev(i,k) = Rev(i-1,k);
            RevNH3(i,k) = RevNH3(i-1,k);
            NH3(i,k) = NH3(i-1,k);
            RevElec(i,k) = RevElec(i-1,k);
            Grid(i,k) = Grid(i-1,k);
            ModLoad(i,k) = ModLoad(i-1,k);
            H2State(i,k) = H2State(i-1,k);
            ReactPwr(i,k) = ReactPwr(i-1,k);
            Addl_Pwr(i,k) = Addl_Pwr(i-1,k);
         else
            [Rev(i,k) RevNH3(i,k) NH3(i,k) RevElec(i,k) Grid(i,k) ModLoad(i,k) H2State(i,k) ReactPwr(i,k)
Addl_Pwr(i,k) Balance(i,k)]...
               = TotalNH3Engine(PwrAvail(i),ModLoad(i-1,k),Buy(i),Sell(i),NH3Price(i),H2State(i-
1,k),H2Max(k),delPlant,Turndown,Plant_Pwr,NH3Size,Scenario);
         end
      end

   end


   % The sum of the capital costs
   [CC_Wind CWT CF Cc CIS CTS CSE CPD]  =
WindCost(nwt,Pwt/1e6,dia,R_Spd,h,Dep,Dwf,Space,TransDist,Vn,HV,BB,OnOff,Onshore_Dist,nHV);
   [ElecCapCost ASUCapCost MVCGrassRts SynGrassRts StoreGrassRts TotalNH3Cost RawMatl
Labor_Cost] = NH3Cost(T,P,NH3Size,XTraElec,H2Max);

   OM_Wind = 0.03;
   totalcost = CC_Wind+TotalNH3Cost;
   d_pay = 0.1;
   interest = 0.04;
   inflate = 0.03;
   discount = 0.07;
   life = 20;
   loan_life = 15;
   O_M = OM_Wind*CC_Wind;


   % From Timmerhaus, page 176. Land is 1-2% of total capital cost
   Land = 0.01*TotalNH3Cost;
   startup = 0.00; % This is the percent of the totalNH3cost req'd for startup
   workingcap = 0.5; % 50% of total COM is required for working capital
   sales = sum(RevElec(RevElec>0))/3 + sum(RevNH3)/3; % Total electricity and nh3 sales based on 3 year
period
   COM = 0.18*(ASUCapCost + MVCGrassRts + SynGrassRts + StoreGrassRts)+0.05*ElecCapCost +
2.73*Labor_Cost+1.23*(-sum(RevElec)/3 + RawMatl) + O_M;
```

```
    % General expenses, turton page 224.
    % Unattended operation of electrolyzers warrants less GE (H2A tool)
    GE = 0.1 * Labor_Cost + 0.009 * TotalNH3Cost + 0.16 * COM;
    TaxRate = 0.3;
    Years = 20;
    IRR = 0.1;
    NPV_Costs = NPVCosts(totalcost,d_pay,interest,inflate,discount,life,loan_life,COM+GE);
    LCOA = NPV_Costs./((sum(NH3)/3)*life)
end
```

A.2 Wind Statistics

```
function [mean stdev TI Pwr CapFac] = WindStats(WindData,NamePlate,R_Spd,d,cut_in,cut_out)

mean = nanmean(WindData); % Mean speed of the wind
stdev = nanstd(WindData); % Std dev of the wind
TI = stdev/mean;
u = 0:35; % Wind speeds for the plot
p = (1/(stdev*(2*pi)^0.5))*exp(-(u-mean).^2./(2*stdev^2))

% Weibull calcs

k = (stdev/mean)^-1.086;
c = mean*(0.568+0.433/k)^(-1/k);
% Use the u from above...
Weibull = (k./c).*(u./c).^(k-1).*exp(-(u./c).^k);
plot(u,Weibull);
Pwr = nanmean(TurbinePower(NamePlate,d,WindData,R_Spd,cut_in,cut_out));
CapFac = Pwr/NamePlate;
```

A.3 Wind Shear Function

```
function ShearedWind = ShearUp(WindData,H_ref,H)

% Takes three inputs: ShearUp(WindData,H_ref,H)
% WindData is a vector of wind data, H_ref is the height that the wind data
% was taken at, and H is the height at which the wind speed is desired. The
% function returns a vector of the wind data.

zo = 0.5E-3; % surface roughness for a blown ocean.

% Using the Log Law from page 46 of Wind Energy Explained.
ShearedWind = WindData.*log(H/zo)/log(H_ref/zo);
```

A.4 Total Offshore Wind Farm Power Output

```
function TotalPwr = TotalWindPwr(NumTurb,TurbSize,Dia,WindSpd,Space,Rated,C_in,C_out)

% Usage TotalPwr = TotalWindPwr(NumTurb,TurbSize,Dia,WindSpd,Space)
% NumTurb is the number of turbines
% Turbsize is the size of the turbine in W
```

```
% Dia is the diameter of the turbine in meters
% WindSpd is a vector of wind speeds
% Space is the spacing of the farm in turbine diameters.


% The farm efficiencies are from Ozkan
if NumTurb < 10
   % Assume that the interaction is minimal, if properly designed.
   Farm_Eff = 0.97;
else
   F_Space = [8:16];
   F_Eff = [90 91.6 93.2 94.1 95 95.6 96.2 96.6 97];
   Farm_Eff = interp1(F_Space,F_Eff,Space,'nearest','extrap')/100;
end
ElecEff = 0.97; % Electrical efficiency
Avail = 0.95; % Availability
Soil = 0.035; % Soiling loss

TotalPwr = NumTurb*TurbinePower(TurbSize,Dia,WindSpd,Rated,C_in,C_out)...
   *ElecEff*Farm_Eff*(1-Soil)*Avail;
```

A.5 Simple Turbine Power Curve Model

```
function PowerCurve = TurbinePower(NamePlate,Dia,U,Rated,CutIn,CutOut)
% Simple turbine model
% Returns power in Watts
% Inputs: NamePlate power for the turbine in W, the rotor diameter in
% meters, the wind speed U in m/s, the rated wind speed
% in m/s, the cut in wind speed in m/s and the cut out wind speed in m/s

Area = pi / 4 * Dia^2; % (m^2)
Cp = 0.4; % power coefficient
Rho = 1.225; % Air density in kg/m^3
Eff = 0.90; % total overall efficiency for the RNA
PowerCurve = 1/2 * Rho * Area * U.^3 * Cp * Eff; %  Power out in (W)
for i = 1 : length(U)
   if U(i) >= CutOut | U(i) < CutIn
      PowerCurve(i) = 0;
   elseif PowerCurve(i) > NamePlate
      PowerCurve(i) = NamePlate;
   end
end
```

A.6 Ammonia Plant Power Requirements

```
function [Plant_Pwr NumElec] = PlantPwr(P,Size)

% This function aggregates several other functions to determine the power
% requirements for an ammonia plant. The usage is:
% [Plant_Pwr NumElec] = PlantPwr(P,Size) where the P is the operating
% pressure (150 bar) and size is in metric tons per day. The Ammonia energy
%function computes the flow rates of the water,
% nitrogen and the hydrogen required to run the plant. Those values are fed
% into other functions that compute the power required for electrolysis
% (ElecPower.m), air separation (ASUPower2.m), mechanical vapor
% compression (MVCPower.m). The size of the plant also determines the total
```

```
% compression power required for the plant. That is computed in CompPwr.m.
% The total is summed up and given as output along with the number of
% electrolyzers required.
% The power is given in Watts and the number of electrolyzers is a whole,
% positive number.
if Size == 0
   Plant_Pwr = 0;
   NumElec = 0;
else
% The raw material requirements for the operation of the plant.
[H20 N2 H2] = AmmoniaEnergy(Size);

% The power required by the synthesis of ammonia.
[FeedComp FluidWork Stages RECompTotal HeatOut Cool_H2O HX1Area HX2Area HX3Area HX4Area
HXArea_int] = CompPwr2(P,Size);

% The power required by the electrolyzers.
[Elec_Pwr NumElec] = ElecPower(H2);

% The power required for the air separation unit.
% Divide by the recovery of the unit to get the input of air required
[ASUCompPwr SheetPwr SpecPwr] = ASUPower2(N2/0.7);

% The power for mechanical vapor compression
[CompPwr MVC_Pwr] = MVCPower(H20);

% The total power.
Elec_Pwr
ASUCompPwr
MVC_Pwr
(FeedComp+RECompTotal)
Plant_Pwr = Elec_Pwr+ASUCompPwr+MVC_Pwr+(FeedComp+RECompTotal)
end
```

A.7 Raw Material Requirements

```
function [WaterReqdVol VN2h VH2h] = AmmoniaEnergy(Size)

if Size == 0
   WaterReqdVol = 0;
   VN2h = 0;
   VH2h = 0;
else
AmmoniaOut = Size; % Metric tons of ammonia
Tons2Kg = 1000; %
Kg2G = 1000;
% Input is in metric tons (t) per day
% Energy flow calculation for an ammonia plant
% Input needed is the ammonia plant capacity
% The program calculates the amount of hydrogen, nitrogen, and electricity
% needed for the process. It also gives the heat released by the reaction
% which can be used in the desalting process.

%Data needed for calculations
R = 8.314472E-5; % m^3*bar/K*mol
T = 293; % K standard temp
```

```
P = 1; % (bar) Standard pressure
H = 1.00794; % Hydrogen in grams/mol
O = 15.9994; % Oxygen in g/mol
N = 14.0067; % Nitrogen in g/mol

H2 = 2*H; % Hydrogen gas in g/mol
N2 = 2*N; % Nitrogen in g/mol
O2 = 2*O; % Oxygen in g/mol
H2O = 2*H + O; % Water in g/mol
NH3 = N + 3*H; % Ammonia in g/mol

% Reactions data
% Hydrogen
dHH2 = 0; % J/mol
dHH = 217000; % J/mol
dGH2 = 0; % J/mol
dGH = 203000; % J/mol

% Oxygen
dHO2 = 0; % J/mol
dHO = 249000; % J/mol
dGO2 = 0; % J/mol
dGO = 232000; % J/mol
H2OdH = -286000; % Reaction in J/mol H2O

% Nitrogen
dHN2 = 0; % J/mol
dGN2 = 0; % J/mol
dHNH3 = -46000; % J/mol
dGNH3 = -17000; % J/mol

% Water
dHH2Ol = -286000; % J/mol
dGH2Ol = -237000; % J/mol

% Reactions needed
% H2O (g) --> H2 + 1/2O2

dHElec = dHH2 + 1/2*dHO2 - (dHH2Ol); % Enthalpy change for electrolysis

%3H2 + N2 --> 2NH3
dHAmm = 2*dHNH3 - (3*dHH2 + dHN2); % The enthalpy change for 2 MOLES of NH3

% So with an desired ammonia output we need to figure out the water and
% nitrogen requirements

% Find the number of moles for all constituents
AmmoniaMoles = AmmoniaOut*Tons2Kg*Kg2G/NH3; % Moles of NH3
NitrogenMoles = AmmoniaMoles; % Moles of N!
HydrogenMoles = AmmoniaMoles*3; % Moles of H!

N2MH = NitrogenMoles/(2*24); % The flow rate of moles of N2 on a per hour basis
% The factor of 2 is from the conversion from moles of N to moles of N2
% which is half as many.

% For nitrogen required, get into standard units of Nm^3/h
```

```
% PV=nRT
VN2 = NitrogenMoles*R*T/(2*P); % Volume of N2 per day
VN2h = VN2/24; % Per hour basis

% Same for hydrogen
VH2 = HydrogenMoles*R*T/(2*P);
VH2h = VH2/24;

% Water Required
% The reaction is
% H2O (g) --> H2 + 1/2O2
% so 2 moles of hydrogen are produced for every mole of water

WaterReqdMoles = HydrogenMoles/2; % Moles of water required for reaction
WaterReqdMass = WaterReqdMoles*H2O; % Grams of water needed
WaterReqdVol = WaterReqdMass/1E6; % Cubic meters of water
NitrogenReqdMass = NitrogenMoles*N; % Grams of nitrogen required
HydrogenReqdMass = HydrogenMoles*H; %

N2MT = NitrogenReqdMass*1E-6; % Metric tons of N2 required
H2MT = HydrogenReqdMass*1E-6; % Metric tons of H2 required
```

A.8 Compressor and Heat Exchanger Calculations

```
function [FeedComp FluidWork Stages RECompTotal HeatOut Cool_H2O HX1Area HX2Area HX3Area
HX4Area HXArea_int] = CompPwr2(P2,Size)

% This function assumes that the operating conditions in the reactor are
% the same for any sized reactor. In practice this is not true, but this
% gives an estimate. It is best when used for ammonia plants in the 300
% tonne/day range, as the conditions were calculated for that specific
% plant.
if Size == 0;
   FeedComp = 0;
   FluidWork = 0;
   Stages = 0;
   RECompTotal = 0;
   HeatOut = 0;
   Cool_H2O = 0;
   HX1Area = 0;
   HX2Area = 0;
   HX3Area = 0;
   HX4Area = 0;
   HXArea_int = 0;
else
%Data needed for calculations
R = 8.314472E-5; % m^3*bar/K*mol
T = 293; % K standard temp
P = 1; % (bar) Standard pressure
H = 1.00794; % Hydrogen in grams/mol
O = 15.9994; % Oxygen in g/mol
N = 14.0067; % Nitrogen in g/mol

H2 = 2*H; % Hydrogen gas in g/mol
```

```
N2 = 2*N; % Nitrogen in g/mol
O2 = 2*O; % Oxygen in g/mol
H2O = 2*H + O; % Water in g/mol
NH3 = N + 3*H; % Ammonia in g/mol

P1 = 1; % Ambient pressure as reference (bar)
P1N2 = 8; % The pressure from the GN2 plant is 8 bar.
P1H2 = 1; % Atmospheric pressure from the H2 plant (bar)
% P2 = 150; % Final pressure (bar)
n = 1.4; % Thermodynamic exponent []

T1 = 293; % Ambient temp (K)

RN2 = 0.2968; % Gas constant kJ/kgK
RH2 = 4.124; % Gas constant for H2 kJ/kgK
Stages = 5;
mdotN2 = Size*1000*(N/NH3)/(24*3600); % kg/s of N2
mdotH2 = Size*1000*(3*H/NH3)/(24*3600); % kg/s of H2
CpN2 = RN2*(n/(n-1));
CpH2 = RH2*(n/(n-1));
CpH2O = 4.184; % kJ/kgK
IsenEff = 0.75; % Isentropic efficiency for the compressors
MechEff = 0.95; % Mechanical Efficiency

% Feed compressor fluid work (kW)
CWorkN2F = T1*Stages*n*RN2/(n-1)*mdotN2*(((P2/P1N2)^(1/Stages))^((n-1)/n)-1);
CWorkH2F = T1*Stages*n*RH2/(n-1)*mdotH2*(((P2/P1H2)^(1/Stages))^((n-1)/n)-1);
FluidWork = CWorkN2F + CWorkH2F;
% Feed compressor shaft work (kw)

% Amount of power required by each compressor (kW)
CWorkN2S = CWorkN2F/(IsenEff*MechEff);
CWorkH2S = CWorkH2F/(IsenEff*MechEff);

% Total compression power for feed comp train (W)
FeedComp = (CWorkN2S + CWorkH2S)*1000;
Tout = T1*((P2/P1)^(1/Stages))^((n-1)/n);

% The rejected heat in the intercoolers kW
HeatOut = 1000*((Stages-1)*(mdotN2)*(Tout-T1)*CpN2 + (Stages-1)*(mdotH2)*(Tout-T1)*CpH2);

T_w1 = 273+5;
T_w2 = 273+15;
U_int = 60;
LMTD_int = LMTD(abs(Tout-T_w2),abs(T1-T_w1));
% The area for the intercoolers.
HXArea_int = HeatOut/(U_int*LMTD_int);
% Specific heat
CpH20 = 4.18; % specific heat of water kJ/kgK
IntH2O = abs(HeatOut/(CpH2O*1000*(T_w2-T_w1))); % kg/s!

% The recycle stream has about 6 times more mass than the feed stream
% By mass the recycle stream has:
% H2: 0.1446; N2: 0.589; NH3: 0.266
% The new flow rates are:
```

```
mdotRCN2 = Size*6*1000*0.589/(24*3600); % kg/s of N2
mdotRCH2 = Size*6*1000*0.1446/(24*3600); % kg/s of H2
mdotRCNH3 = Size*6*1000*0.266/(24*3600); % kg/s of NH3
NumComp = 1; % number of compressors

% From the paper: “Control structure design for the ammonia synthesis
% process”, the pressure drop around the loop was (1-195.28/207.96) = 6.1%
% That is used here as well. (It also implies that the compression power is
% the same for any configuration!)

Pi = P2*0.94; % Starting pressure in bar
Po = P2; % outlet pressure, bar
T_RC = 273+40.4; % Recirculation temperature from Control Structure paper (K)
RNH3 = 0.4882; % Specific gas constant for ammonia (kJ/kgK)
% Work (kJ/hr) per kg of compressed ammonia
RECompWorkNH3 = T_RC*NumComp*n/(n-1)*RNH3*mdotRCNH3*((Po/Pi)^((n-1)/n)-1);
RECompWorkN2 =  T_RC*NumComp*n/(n-1)*RN2 *mdotRCN2*((Po/Pi)^((n-1)/n)-1);
RECompWorkNH3 = T_RC*NumComp*n/(n-1)*RH2 *mdotRCH2*((Po/Pi)^((n-1)/n)-1);
IsenEff = 0.75; % Isentropic efficiency for the compressors
MechEff = 0.95; % Mechanical Efficiency

% Total recompression power (W)
RECompTotal = 1000*(RECompWorkNH3 + RECompWorkN2 + RECompWorkNH3)/(IsenEff*MechEff) ;

%%%%%%%%%%%%%%%%%%%%%%%%%%%%%%%%
% Heat Exchanger Calculations
%%%%%%%%%%%%%%%%%%%%%%%%%%%%%%%%

RefSize = 1650;

% The heat exchange is given in Mcal/hr which is converted to W in this
% analysis

% The inputs to the LMTD are the temperature differences across the two
% streams. For example, for the first heat exchanger (HX-001) the
% temperatures are from streams 15-16 (449.3-394.4) and 2-3 (231.8-340.1)
% so the temperatures are ~450-340=110 and ~395-232 = 163;

% All streams we have:
del_T_CW = 50;
T1 = 231.7;
T2 = 231.8;
T3 = 340.1;
T15 = 449.3;
T16 = 394.4;
T17 = 296.9;
T18 = 107.6;
T19 = 27.1;
T23 = 48;
T30 = 15.1;
T31 = T30+del_T_CW;
% This stream is exchanging heat with the T18/T19, thus we can't have a
% temperature crossover, so T34 must be less than T19.
T33 = 5;
T34 = T33+10;
```

```
% Now the LMTD for each HX
HX1_delT = LMTD(abs(T15-T3),abs(T16-T2)); % HX001
HX2_delT = LMTD(abs(T16-T31),abs(T17-T30)); % H501
HX3_delT = LMTD(abs(T23-T18),abs(T1-T17)); % H502
HX4_delT = LMTD(abs(T18-T34),abs(T33-T19)); % H583

% The computed effectiveness for each HX
Eff_HX1 = (T15-T16)/(T15-T2);
Eff_HX2 = (T16-T17)/(T16-T30);
Eff_HX3 = (T17-T18)/(T17-T23);
Eff_HX4 = (T18-T19)/(T18-T33);



% Molar flow rates

% Stream 15 to 16
MF15_16H = 19266.5*(Size/RefSize); % kmol/h
MF15_16N = 5411.25*(Size/RefSize);
MF15_16NH3 = 9568.82*(Size/RefSize);
TMF15_16 = MF15_16H + MF15_16N + MF15_16NH3; %kmol/h
Cp15_16 = MF15_16H/TMF15_16*C_p('H2',(T15+T16)/2) +
MF15_16N/TMF15_16*C_p('N2',(T15+T16)/2)...
   + MF15_16NH3/TMF15_16*C_p('NH3',(T15+T16)/2); % kJ/kmolK
CpHX1_1 = -Cp15_16*TMF15_16*(T16-T15); % kJ/(hr) "first stream"

% Stream 2-3
MF2_3H = 12766.2*(Size/RefSize);
MF2_3N = 3745.89*(Size/RefSize);
MF2_3NH3 = 2785.42*(Size/RefSize);
TMF2_3 = MF2_3H + MF2_3N + MF2_3NH3;
Cp2_3 = MF2_3H/TMF2_3*C_p('H2',(T2+T3)/2) + MF2_3N/TMF2_3*C_p('N2',(T2+T3)/2) +
MF2_3NH3/TMF2_3*C_p('NH3',(T2+T3)/2);
CpHX1_2 = -Cp2_3*TMF2_3*(T3-T2); % kJ/hr, "second stream"

% Stream 16-17 (same as 15-16 and 18-19)
MF16_17H = 19266.5*(Size/RefSize); % kmol/h
MF16_17N = 5411.25*(Size/RefSize);
MF16_17NH3 = 9568.82*(Size/RefSize);
% For Cp the composition data for 15-16 was used and the temp data for 16-17 was
% used
Cp16_17 = MF15_16H/TMF15_16*C_p('H2',(T17+T16)/2) +
MF15_16N/TMF15_16*C_p('N2',(T17+T16)/2)...
   + MF15_16NH3/TMF15_16*C_p('NH3',(T17+T16)/2);
CpHX2_1 = -Cp16_17*TMF15_16*(T17-T16);

% Cooling water: streams 30-31 and 33-34

CpHX2_2 = CpHX2_1;
% Solve for the cooling water requirements
MFH2030_31 = -CpHX2_2/(CpH20*del_T_CW); % kg/h


% Stream 17-18
MF17_18H = 19266.5*Size/RefSize;
MF17_18N = 5411.23*Size/RefSize;
```

```
MF17_18NH3 = 9568.82*Size/RefSize;
Cp17_18 = MF15_16H/TMF15_16*C_p('H2',(T17+T18)/2) +
MF15_16N/TMF15_16*C_p('N2',(T17+T18)/2)...
   + MF15_16NH3/TMF15_16*C_p('NH3',(T17+T18)/2);
CpHX3_1 = -Cp17_18*TMF15_16*(T18-T17);

% Stream 23-1
MF23_1H = 25329.8*(Size/RefSize);
MF23_1N = 7432.32*(Size/RefSize);
MF23_1NH3 = 5526.53*(Size/RefSize);
TMF23_1 = MF23_1H + MF23_1N + MF23_1NH3;
Cp23_1 = MF23_1H/TMF23_1*C_p('H2',(T1+T23)/2) + MF23_1N/TMF23_1*C_p('N2',(T1+T23)/2)...
   + MF23_1NH3/TMF23_1*C_p('NH3',(T1+T23)/2);
CpHX3_2 = -Cp23_1*TMF23_1*(T1-T23);

% Streams 18-19 same as 15-16, etc
MF18_19H = 19266.5*(Size/RefSize); % kmol/h
MF18_19N = 5411.25*(Size/RefSize);
MF18_19NH3 = 9568.82*(Size/RefSize);
% Used data from other streams for this as well
Cp18_19 = MF15_16H/TMF15_16*C_p('H2',(T18+T19)/2) +
MF15_16N/TMF15_16*C_p('N2',(T18+T19)/2)...
   + MF15_16NH3/TMF15_16*C_p('NH3',(T18+T19)/2);
CpHX4_1 = -Cp18_19*TMF15_16*(T19-T18);

CpHX4_2 = CpHX4_1
MFH2033_34 = -CpHX4_2/(CpH20*del_T_CW); %kg/h

% Now get the total cooling water requirements
Cool_H2O = abs((MFH2033_34 + MFH2030_31)/60) + abs(IntH2O*60); %kg/min

% From Ammonia Synthesis with Alternate Feedstock by Deobalt et al. (2007)
% A gas to gas heat exchanger has a U = 865 W/m^2K. The U value was
% calculated using data on pages 47 and 110 (feed streams 114, 115, 109, 110): LMTD = 31.5C; Area = 2420
and
% the heat duty, Q = 65.86MW. Then U is calculated: U = Q/(AT) =
% 65.86e6W/(2420m^2*31.5) = 863; QED


UtotalHX1 = 865; %W/m^2K
HX1Area = CpHX1_1*1000/(3600*(HX1_delT*UtotalHX1));

% The following h values are taken from ammonia12.pdf from WVU
h_inHX2 = 1000; % W/m^2K
h_outHX2 = 60;

UtotalHX2 = 1/((1/h_inHX2)+(1/h_outHX2));
HX2Area = CpHX2_1*1000/(3600*(HX2_delT*UtotalHX2));

UtotalHX3 = 865; %W/m^2K
HX3Area = CpHX3_1*1000/(3600*(HX3_delT*UtotalHX3));

% Assume that the process stream partially condenses, as in the flowsheet
h_inHX4 = 1000; % W/m^2K
h_outHX4 = 1000;
```

```
UtotalHX4 = 1/((1/h_inHX4)+(1/h_outHX4));

% This is an approximation. Intercoolers + heat exchangers. They are
% essentially the same thing: S&T exchangers using water.
HX4Area = CpHX4_1*1000/(3600*(HX4_delT*UtotalHX4));


end
```

A.9 Specific Heats Function

```
function SH = C_p(Gas,T)

% Function usage:
% function SH = C_p(Gas,T) where Gas is a string of either 'N2', 'H2', or
% 'NH3' and T is the temperature in C. The function uses data from Cengel,
% page 887 for the ideal gas specific heat and it returns the specific heat
% in kJ/kmol*K
T = T+273;
% N2
if strcmp(Gas,'N2') == 1
a = 28.9; b = -0.1571e-2; c = 0.8081e-5; d = -2.873e-9;
elseif strcmp(Gas,'H2') == 1
% H2
a = 29.11; b = -0.1916e-2; c = 0.4003e-5; d = -0.8704e-9;
elseif strcmp(Gas,'NH3') == 1
%NH3
a = 27.568; b = 2.5630e-2; c = 0.99072e-5; d = -6.6909e-9;
else
   a = 0; b = 0; c = 0; d = 0;
end

SH = a+b*T+c*T^2+d*T^3;
```

A.10 Log Mean Temperature Difference Function

```
function LogT = LMTD(T1,T2)

LogT = (T1-T2)/log(T1/T2);
```

A.11 Electrolyzer Power

This computes the power required for the electrolyzers

```
function [Power NumElec] = ElecPower(Flow)

% This function computes the required AC power needed for electrolysis based
% on the flow rate. The electrolyzer specifications come from the Statoil
% website:
% http://www3.statoil.com/hydrogentechnologies/svg03816.nsf?OpenDatabase
% The flow rate is in Nm^3/hr.
% The rectifier efficiency is assumed to be 95% based on:
% The Wind-to-Hydrogen Project: Operational Experience, Performance
```

```
% Testing, and Systems Integration page 42
if Flow == 0
   Power = 0;
   NumElec = 0;
else
ElecEng = 4.8; % This is the system energy required in kWh/Nm^3. The
% value of 4.3 is only for the electrolysis. The balance of plant is 0.5kWh
% per Nm^3. Note that the value is actually given as a range or 4.7-4.9.

% The efficiency of the rectifier for converting from AC to DC.
Eff = 0.95;

Power = ElecEng*Flow*1000/Eff; % This is the power required.

% This section is also in the ElecCost.m file. The answers should be identical
DesignCap = 485; % Design capacity per electrolyzer (Nm^3/hr)
Capacity = 0.97;  % The capacity factor of the electrolyzer, based on Norsk quote
UpTime = 0.86;    % Actual running time on a yearly basis

% Total number of electrolyzers required
NumElec = ceil(Flow/(DesignCap*Capacity*UpTime));
end
```

A.12 ASU Power Requirements

```
function [CompPwr SheetPwr SpecPwr] = ASUPower2(Flow)
% Inputs: flow in Nm^3/hr of AIR;
% Note that the flow rate is the total flow rate in of the moist air. Some
% of this will be water and condensed out; some will not be recovered; the
% rest is nitrogen. Typically about 66% is recovered.
if Flow == 0
   CompPwr = 0;
   SheetPwr = 0;
   SpecPwr = 0;
else
% Constants
R = 8.314472E-5; % m^3*bar/K*mol
% Standard inputs (can change some later, if necessary)
P = 101325; % Standard pressure in pascals from NIST
T = 294; % Standard temp in K from NIST
rho = 1.225; % kg/m^3
WtAir = 28.964; % g/mol
SHeat = 1.4017; % Ratio of specific heats
n = 1.4017; % polytropic exponent
Rair = 0.287; % Specific gas constant for air, J/(g*K)
Recovery = 0.679; % recovery percentage (product/air)
Stages = 3;
CoolingTwr = 1;
Gam = 1.4; % Specific heat ratio for air
AuxPwr = 10; % kW from sheet
Pdrop = 3447; % pressure drop in the cooler (Pa).
TH2O = 294.25; % (K) temperature of water feed.
MMassH2O = 18.015; % Molecular mass of water g/mol

% Temperatures
```

```
TDb = 295; % Kelvin average dry bulb temperature over time of interest.
TWb = 289; % (K) Average wet bulb temp over time period of interest.

% From sheet M37
AdEffAir = 0.73;

% Stage 1 inlet data
Ts1 = 294.25; % Temperature into first stage
Pinlet1 = 99974; % Inlet pressure to first stage, Pa
PP_Wvapor1 = Carrier(TDb,TWb,Pinlet1); % Pa
SatPress1 = WaterSaturation(TDb); % Pa
RH = PP_Wvapor1/SatPress1; % Relative Humidity
MixMolWt1 = WtAir*(1-PP_Wvapor1/(Pinlet1))+ MMassH2O*PP_Wvapor1/(Pinlet1);
MolAir = Flow*(Pinlet1/(P*(R*Ts1*3600))); % (mol/s) conversion from Pa to bar and from /hr to /s
MolH2Oin1 = MolAir*PP_Wvapor1/(P-PP_Wvapor1); % mol of h2o in
NM3in1 = (MolAir+MolH2Oin1)*R*T/(P*1E-5); % Convert from Pa to bar for the gas constant
AM3in1 = NM3in1*(P/Pinlet1)*Ts1/T; % Actual volume in, m^3
PR1 = 1.91; % Pressure ratio across each stage

% Stage 1 outlet data
Poutlet1 = Pinlet1*PR1; % Pressure at the outlet of the first stage.
Tcout = 302.6; % K, temperature out from cooler
H2OSatP1 = WaterSaturation(Tcout); % Saturation vapor pressure of water at outlet
MolHout1 = MolAir*H2OSatP1/(Poutlet1-Pdrop-H2OSatP1); % Mol of H2O out of cooler


if(MolHout1>MolH2Oin1)
   MolH2OCond1 = 0;
else
   MolH2OCond1 = MolH2Oin1-MolHout1; % Moles of condensate out
end

H2OoutV1 = MolH2Oin1-MolH2OCond1; % Outlet water in mol/s

if(MolAir == 0)
   MWtOutV1 = 0;
else
   MWtOutV1 = WtAir*MolAir+18.02*H2OoutV1/(MolAir+H2OoutV1); % Mol wt of output vapor
end

Pwr1 = n*Rair*Ts1/(n-1)*(PR1^((n-1)/n)-1); % energy in J/g
Ptest = n*AM3in1*Pinlet1/(n-1)*(PR1^((n-1)/n)-1); % power in J/s

% Stage 2 inlet data

Ts2 = Tcout; % inlet temperature for stage 2 of the compression, from sheet, K
Pinlet2 = Pinlet1*PR1-Pdrop; % Pressure at the outlet of the intercooler
SatPress2 = WaterSaturation(Ts2); % Pa
PP_Wvapor2 = Pinlet2*(MolHout1/(MolHout1+MolAir));
MixMolWt2 = WtAir*(1-PP_Wvapor2/(Pinlet2))+ MMassH2O*PP_Wvapor2/(Pinlet2);
MolH2Oin2 = MolAir*PP_Wvapor2/(P-PP_Wvapor2); % mol of h2o in

%%%%Check this. Seems that SCFM and ACFM are wrong
NM3in2 = (MolAir+MolH2Oin2)*R*T/(P*1E-5); % Convert from Pa to bar for the gas constant
AM3in2 = NM3in2*(P/Pinlet2)*Ts2/T; % Actual volume in
PR2 = 1.89; %
```

```
% Stage 2 Outlet data
Poutlet2 = Pinlet2*PR2; % Pressure at the outlet of the first stage.
Tcout = 302.6; % K, temperature out from cooler
H2OSatP2 = WaterSaturation(Tcout); % Saturation vapor pressure of water at outlet
MolHout2 = MolAir*H2OSatP2/(Poutlet2-Pdrop-H2OSatP2); % Mol of H2O out of cooler

if(MolHout2>MolH2Oin2)
   MolH2OCond2 = 0;
else
   MolH2OCond2 = MolH2Oin2-MolHout2; % Moles of condensate out
end

H2OoutV2 = MolH2Oin2-MolH2OCond2; % Outlet water in mol/s

if(MolAir == 0)
   MWtOutV2 = 0;
else
   MWtOutV2 = WtAir*MolAir+18.02*H2OoutV2/(MolAir+H2OoutV2); % Molwt of output vapor
end

Pwr2 = n*Rair*Ts2/(n-1)*(PR2^((n-1)/n)-1); % energy in J/g of air
Ptest2 = n*AM3in2*Pinlet2/(n-1)*(PR2^((n-1)/n)-1); % power in J/s

% Stage 3 inlet data

Ts3 = Ts2; % This inlet temp is a function of the cooling water
Pinlet3 = Pinlet2*PR2-Pdrop; % Pressure at the outlet of the intercooler
SatPress2 = WaterSaturation(Ts2); % Pa
PP_Wvapor3 = Pinlet3*(MolHout2/(MolHout2+MolAir));
MixMolWt3 = WtAir*(1-PP_Wvapor3/(Pinlet3))+ MMassH2O*PP_Wvapor3/(Pinlet3);
MolH2Oin3 = MolAir*PP_Wvapor2/(P-PP_Wvapor2); % mol of h2o in
NM3in3 = (MolAir+MolH2Oin2)*R*T/(P*1E-5); % Convert from Pa to bar for the gas constant
AM3in3 = NM3in3*(P/Pinlet3)*Ts3/T; % Actual volume in
PR3 = 1.88; %

% Stage 3 Outlet data
Poutlet3 = Pinlet3*PR3; % Pressure at the outlet of the third stage.
H2OSatP3 = WaterSaturation(Tcout); % Saturation vapor pressure of water at outlet
MolHout3 = MolAir*H2OSatP3/(Poutlet3-Pdrop-H2OSatP3); % Mol of H2O out of cooler

PRTot = Poutlet3/Pinlet1;
if(MolHout3>MolH2Oin3)
   MolH2OCond3 = 0;
else
   MolH2OCond3 = MolH2Oin3-MolHout3; % Moles of condensate out
end

H2OoutV3 = MolH2Oin3-MolH2OCond3; % Outlet water in mol/s

if(MolAir == 0)
   MWtOutV3 = 0;
else
   MWtOutV3 = WtAir*MolAir+18.02*H2OoutV3/(MolAir+H2OoutV3); % Molwt of output vapor
end
```

```
Pwr3 = n*Rair*Ts3/(n-1)*(PR3^((n-1)/n)-1); % energy in J/g
Ptest3 = n*AM3in3*Pinlet3/(n-1)*(PR3^((n-1)/n)-1); % power in J/s

% The following equation gives the specific work for the compressors, in
% J/g. Multiply by the flow rate to get the total power.
% Note this is three stages: three terms.

% Efficiencies
EffAd = 0.73; % Adiabatic efficiency from sheet

% The following converts from a flow rate of /hr to /s. Thus, the power is
% constant throughout the hour and the energy is given in Wh over that time
% period.

CompPwr =
(Pwr1*(MolAir*MixMolWt1)+Pwr2*(MolAir*MixMolWt2)+Pwr3*(MolAir*MixMolWt3))/(EffAd);

%% Compare to the easy way: 1-16-2011 (maybe i'll do it!)

% CompPwrEZ = Stages*T*(n/(n-1))*Rair*
EffMot = LookupEff(CompPwr); % motor efficiency from sheet

CompPwr = CompPwr/EffMot;
SheetPwr = (Ptest+Ptest2+Ptest3)/(EffAd*EffMot);

SpecPwr = (60000+CompPwr)./(Flow*Recovery*1000);
% Ideal Conditions
% Ideal conditions for air separation, as a comparison
%
R2 = 8.314472; % Gas constant in different units (J/mol*K)
MWtAir = 28.96; % Mol weight of air, g/mol
MfN2 = 0.78; % Mole fraction of nitrogen in atmosphere
MfO2 = 0.21; % Mol frac of oxygen
MfAr = 0.009; % Mol frac of argon
Wideal = -MolAir*R2*T*(MfN2*log(MfN2)+MfO2*log(MfO2)+MfAr*log(MfAr));

end
```

A.13 MVC Power Requirements

```
This computes the power required for an MVC

function [CompSize DrvSize] = MVCPower(Flow)

% Usage: [Power] = MVCPower(Flow)
% Flow is in m^3/d
% This function calculates the power required for the MVC unit. The energy
% consumption is taken from several sources including

% Joule-Thermie Programme (1998). Desalination Guide Using Renewable
% Energies, Center for Renewable Energy Sources.
% Fiorenza, G., V. K. Sharma, et al. (2003). "Techno-economic evaluation
% of a solar powered water desalination plant." Energy conversion and
% management . 44 (Compendex): 2217-2240.

%{
```

```
MVCEnergy = 7; % kWh/m^3 of product. This is actually a range depending
% on plant configuration, etc. But 7 is a good starting point.

Power = MVCEnergy*Flow*1000/24; % Power in W.
%}

if Flow == 0
   CompSize = 0;
   DrvSize = 0;
else
Md = Flow*1000/(3600*24); % Flow rate of the distillate
Cpv = 1.884; % Specific heat of Saturated vapor above demister at constant pressure, (kJ/kgC)
Cp = 4.2; % Heat capacity of al liquid streams (kJ/kgC)
Ue = 2.4; % Heat transfer coefficient of the evaporator (kJ/(s*m^2*C))
Ub = 1.5; % Brine preheater heat transfer coefficient (kJ/(s*m^2*C)) (HX2)
Ud = 1.8; % Overall heat transfer coefficient for preheater (kJ/(s*m^2*C)) (HX1)
Tcw = 25; % Intake water temp (C)
Td = 62; % Condensed water temp (C)
Ts = Td + 6; % Compressed vapor temp (C)
Tb = Td-2; % Evaporation temperature (C)
Xf = 42000; % Feed water salinity in ppm
Xb = 70000; % Salinity of rejected brine in ppm
Eff = .75; % Compressor efficiency
Gam = 1.32; % Compression ratio
DrvEff = 0.95;

Mf = Md*(Xb/(Xb-Xf))
Mb = Mf-Md
Lam_d = 2499.5698-2.204864*Td-2.304e-3*Td
Lam_b = 2499.5698-2.204864*Tb-2.304e-3*Tb

Tf = ((Xb-Xf)/Xb)*((Lam_b-Lam_d)/Cp-(Cpv/Cp)*(Ts-Td))+Tb

To = (Tcw-Tf)+(Xf/Xb)*Tb+((Xb-Xf)/Xb)*Td

Ae = (Md*Lam_d+Md*Cpv*(Ts-Td))/(Ue*(Td-Tb))

LMTDd = ((Td-Tf)-(To-Tcw))/(log((Td-Tf)/(To-Tcw)))
LMTDb = ((Tb-Tf)-(To-Tcw))/(log((Tb-Tf)/(To-Tcw)))

Ad = (Md*Cp*(Td-To))/(Ud*LMTDb)
Ab = (Mb*Cp*(Tb-To))/(Ub*LMTDb)

Po =10.17246-0.6167302*Ts+1.832249e-2*Ts^2-1.77373e-4*Ts^3+1.47068e-6*Ts^4
Pi =10.17246-0.6167302*Tb+1.832249e-2*Tb^2-1.77373e-4*Tb^3+1.47068e-6*Tb^4

Vi =163.3453-8.04142*Tb+0.17102*Tb^2-1.87812e-3*Tb^3+1.03842e-5*Tb^4-2.28215e-8*Tb^5

W = (Gam/(Eff*(Gam-1)))*(Pi*Vi)*((Po/Pi)^((Gam-1)/Gam)-1)*(1000/3600);
CompSize = W*Flow/24; % Comp pwr (not fluid pwr)
DrvSize = CompSize/DrvEff*1000;

end
```

A.14 Offshore Wind Farm Setup Function

This function approximates the setup of a square offshore wind farm

```
function [Strings Power TurbPerStrng SString ShortPwr TurbPerShStrng TotalPwr] =
ParkSetup(nwt,Pwt,V)

% [Strings Power TurbPerStrng SString ShortPwr TurbPerShStrng TotalPwr] =
% ParkSetup(nwt,Pwt,V)
% nwt is the number of wind turbines
% Pwt is the power of the turbines in MW
% V is the inter-turbine voltage in volts
% This function finds the number of strings required for an offshore
% wind park and the power flow through them. A 935A max for the cable
% is assumed. 36kV is a standard value for voltage ; the 935A
% is from a handbook on cables by one of the manufacturers. A short string
% is also needed in some cases. The number of turbines and the power on the
% string are also returned

Max_Pwr = sin(pi/4)*935*V/1E6; % Maximum power for a string
String_Max = floor(Max_Pwr/Pwt); % Maximum # of turbines on a string


if nwt == 0 || Pwt == 0
   Strings = 0;
   Power = 0;
   TurbPerStrng = 0;
   SString = 0;
   ShortPwr = 0;
   TurbPerShStrng = 0;
   TotalPwr = 0;
elseif nwt*Pwt <= String_Max*Pwt % If true, one string is needed
   Strings = 0;
   Power = 0;
   TurbPerStrng = 0;
   SString = 1;
   ShortPwr = nwt*Pwt;
   TurbPerShStrng = nwt;
   TotalPwr = SString*Power;
else
   if nwt < floor(Max_Pwr/Pwt)
      Strings = 0;
      SString = 1;
      SString = nwt-Strings*TurbPerStrng;
      ShortPwr = (nwt*Pwt-Strings*Power);
      TurbPerShStrng = ShortPwr/Pwt;
      TotalPwr = Strings*Power + ShortPwr
   else
      Strings = floor(nwt/String_Max);
      if Strings > 0
         TurbPerStrng = String_Max;
      else
         TurbPerStrng = 0;
      end
      Power = TurbPerStrng*Pwt;
      if Strings*TurbPerStrng < nwt
         SString = nwt-Strings*TurbPerStrng;
```

```
        else
            SString = 0;
        end
        ShortPwr = (nwt*Pwt-Strings*Power);
        TurbPerShStrng = ShortPwr/Pwt;
        TotalPwr = Strings*Power + ShortPwr;
    end
end
```

A.15 The Engine for the Simulation

```
function [Revenue RevenueNH3 NH3 RevenueElec GridPwr ModLoad H2State ReactPwr Grid Balance]...
    = NH3Engine(PwrAvail, Load, Buy, Sell, NH3Price, H2State, H2Max, delPlant, Turndown,
NH3FullLoad,NH3Size,SysType)

global PerDay

% Wind data in m/s
% Per day is how many data points per day are in the wind data
% NumTurb is the number of wind turbines
% Load is the load required for the NH3 plant
% Buy is how much the electricity purchasing price is in $/kWh
% Sell is how much the electricity is sold for in $/kWh
% NH3Size is the amount of NH3 produced per day in metric tons.
% NH3Price is the selling price of the NH3 at the time.
% The H2State, etc are the state of charge of the gaseous storage systems.
% If there is no storage then these get set to 0. If there is some storage
% then the State is the amount of the gas (in Nm^3) in the tank. If there
% is a deficit of power in the system then the gas production processes can
% be shut down and the gas is taken from the tanks.
% The new state of the system is passed back to the user.


if SysType == 1
    % No storage, no modload

    Grid = PwrAvail - Load; % This is in Watts!
    ModLoad = Load;
    if Grid > 0
        % Have to divide by 1000 to convert from $/MWh to $/kWh
        % Also divide by 1000 to convert from W to kW
        % The result is divide by 1E6
        RevenueElec = Sell*(24/PerDay)*Grid/1E6; % Positive revenue ($)
        SellElec = Grid/1000*(24/PerDay); % This is in kWh
        BuyElec = 0;
        NH3Elec = Load;
        GridPwr = 0;
    elseif Grid < 0
        RevenueElec = Buy*(24/PerDay)*Grid/1E6; % Negative revenue ($)
        BuyElec = Grid/1000*(24/PerDay); % This is in kWh
        SellElec = 0;
        NH3Elec = -Grid+PwrAvail;
    else
        RevenueElec = 0;
```

```
        BuyElec = 0;
        SellElec = 0;
    end
    GridPwr=Grid;
    ReactPwr = 0;
Balance = Grid-PwrAvail+Load;
elseif SysType == 2
    % No storage, modload
    ModLoad = PwrEnv(PwrAvail,Load,delPlant,NH3FullLoad*Turndown,NH3FullLoad); % Modified Load
if Grid > 0
    Grid = PwrAvail - ModLoad; % This is in Watts!

    if Grid > 0
        RevenueElec = Sell*(24/PerDay)*Grid/1E6; % Positive revenue ($)
        SellElec = Grid/1000*(24/PerDay); % This is in kWh
        BuyElec = 0;
        NH3Elec = Load;
        % Have to divide by 1000 to convert from $/MWh to $/kWh
        % Also divide by 1000 to convert from W to kW
        % The result is divide by 1E6
    elseif Grid < 0
        RevenueElec = Buy*(24/PerDay)*Grid/1E6; % Negative revenue ($)
        BuyElec = Grid/1000*(24/PerDay); % This is in kWh
        SellElec = 0;
        NH3Elec = -Grid+PwrAvail;
    else
        RevenueElec = 0;
        BuyElec = 0;
        SellElec = 0;
    end
    GridPwr=Grid;
    ReactPwr = 0;
Balance = Grid-PwrAvail+ModLoad;
elseif SysType == 3
    % Storage and modload

   ModLoad = PwrEnv(PwrAvail,Load,delPlant,NH3FullLoad*Turndown,NH3FullLoad); % Modified Load
   %ModLoad = Load;
    Grid = PwrAvail-ModLoad ;% This is in Watts!

    % Additional power is what the wind cannot supply
    % Grid power is what must be supplied to the grid and is evaluated after
    % the stored reactants are assessed.

    % Need the max power absorbed by the electrolyzers so that we're not
    % producing phantom hydrogen with no electrolyzer capacity available!

    if Grid < 0 % Case: not enough power
        % Assume ASU and reactor @ steady state
        if H2State > 0 % Case: not enough power, H2 available in storage
            if React2Pwr('H2',H2State,24/PerDay) >= abs(Grid) % Case: not enough power, H2 storage sufficient
                H2State1 = H2State; % Dummy variable
                H2State = H2State - Pwr2React('H2',-1*Grid,24/PerDay);
                ReactPwr = -1*React2Pwr('H2',H2State1-H2State,24/PerDay);
                GridPwr = Grid-ReactPwr;
                RevenueElec = Buy*(24/PerDay)*(GridPwr/1e6);
```

```
        elseif abs(Grid) > React2Pwr('H2',H2State,24/PerDay) % Case: not enough power, H2 storage
insufficient
            H2State;
            ReactPwr = -1*React2Pwr('H2',H2State,24/PerDay);
            GridPwr = Grid - ReactPwr; % Because Grid is negative (W)
            H2State = 0;
            RevenueElec = Buy*(24/PerDay)*(GridPwr/1e6); % Negative revenue
        end
      elseif H2State == 0
        GridPwr = Grid;
        H2State = H2State;
        ReactPwr = 0;
        RevenueElec = Buy*(24/PerDay)*(GridPwr/1e6); % Negative revenue
      end
   elseif Grid > 0 % Case: too much power
      if H2State == H2Max % Case: too much power, H2 tank full
        RevenueElec = Sell*(24/PerDay)*Grid/1E6; % Positive revenue ($)
        SellElec = Grid/1000*(24/PerDay); % This is in kWh
        BuyElec = 0;
        NH3Elec = Load;
        GridPwr = Grid; % Forced to sell here; positive grid power --> pos revenue
        H2State = H2State; % Tank still full
        ReactPwr = 0;
      elseif H2State < H2Max % Case: too much power, H2 tank not full
        [RxEquiv Pwr4Elec GridXTra] = Pwr2React('H2',Grid,24/PerDay);
        if  RxEquiv <= H2Max-H2State % Case: too much power, ammount of power left won't fill tank
completely
            ReactPwr = Pwr4Elec; % Convention is that the power going in is positive.
            H2State = H2State + RxEquiv;
            GridPwr = Grid - ReactPwr;
            RevenueElec = Sell*(24/PerDay)*(GridPwr/1e6);
        elseif RxEquiv > H2Max-H2State % Case: too much power, leftover power fills tank and still has
extra power

            % This next line is the power required to make the exact amount
            % of H2 to fill the tank completely.
            [RxEquiv Pwr4Elec GridXTra] = Pwr2React('H2',React2Pwr('H2',(H2Max-
H2State),24/PerDay),24/PerDay);
            %[RxEquiv Pwr4Elec GridXTra] = Pwr2React('H2',(H2Max-H2State),24/PerDay);
            ReactPwr = Pwr4Elec;
            GridPwr = Grid-ReactPwr;
            H2State = H2Max;
            RevenueElec = Sell*(24/PerDay)*(GridPwr/1e6);
        end
      end
   elseif Grid == 0
      RevenueElec = 0;
      SellElec = 0;
      H2State=H2State;
      GridPwr = 0;
      ReactPwr = 0;

   end
   Balance = GridPwr-Grid+ReactPwr;

end
```

```
NH3 = NH3Size*(ModLoad/(PerDay*NH3FullLoad));
RevenueNH3 = NH3Price*NH3Size/PerDay*(ModLoad/NH3FullLoad);
Revenue = RevenueElec+RevenueNH3;
```

A.16 The Power Envelope Function

This function was written to allow a change in NH3 plant power in a single timestep.

```
function Load = PwrEnv(CurrentPwr,CurrentLoad,delLoad,MinLoad,MaxLoad)

% CurrentPwr in same units as load, minload and maxload
% The change in the load is the fractional change in the required power
% over the time interval (usually 10 min or 1 hour)
% For example, if the
% currentpwr = 100
% load = 150
% delLoad = 1.05
% MinLoad = 0
% Maxload = 150
% Then the power is 142.5 since it scales the power back to be closer to
% the produced power.
% If the delLoad = 1; then the currentpower and the load would be equal.
% Usage: ModLoad = PwrEnv(CurrentPwr,CurrentLoad,.05,Plant_Pwr*Turndown,Plant_Pwr);
pwr = CurrentPwr;
cload = floor(CurrentLoad);
mini = floor(MinLoad);
maxi = MaxLoad;
delta = delLoad*cload;

if cload == 0

   delta = MaxLoad;
   if delta < mini
      delta = mini;
   end
end

if delLoad == 0
   Load = cload;
elseif delLoad == 1 & mini == 0
   if pwr > maxi
      Load = maxi;
   elseif pwr<= maxi
      Load = pwr;
   end
elseif MinLoad == MaxLoad
   Load = MaxLoad;
elseif cload <= mini & pwr > 0
   if delta+cload >= pwr
      Load = pwr;
   elseif delta+cload < pwr
      Load = delta+cload;
   end
```

```
elseif cload > maxi
   Load = maxi;
elseif pwr >= cload
   if maxi == pwr & pwr == (cload + delta)
      Load = pwr;
   elseif maxi > pwr & pwr == (cload + delta)
      Load = pwr;
   elseif maxi < pwr & pwr == (cload + delta)
      Load = (cload + delta);
   elseif maxi < pwr & pwr < (cload + delta)
      Load = maxi;
   elseif maxi > pwr & pwr < (cload + delta)
      Load = pwr;
   elseif maxi == pwr & pwr > (cload + delta)
      Load = (cload + delta);
   elseif maxi == pwr & pwr < (cload + delta)
      Load = pwr;
   elseif maxi > pwr & pwr > (cload + delta)
      % Need to avoid the "0" trap!
      if (cload + delta) == 0
         % Turn it back on. Slowly.
         Load = pwr*delLoad;
      else
      Load = (cload + delta);
      end
   elseif maxi < pwr & pwr > (cload + delta)
      if (cload+delta) > maxi
         Load = maxi;
      elseif (cload+delta) <= maxi
         Load = (cload + delta);
      end
   end
elseif pwr < cload
   if mini == pwr & pwr == (cload - delta)
      Load = pwr;
   elseif mini > pwr & pwr == (cload - delta)
      Load = mini;
   elseif mini < pwr & pwr == (cload - delta)
      Load = (cload - delta);
   elseif mini < pwr & pwr < (cload - delta)
      Load = (cload - delta);
   elseif mini > pwr & pwr < (cload - delta)
      if (cload - delta) < mini
         Load = mini;
      elseif (cload - delta) >= mini
         Load = (cload - delta);
      end
   elseif mini == pwr & pwr > (cload - delta)
      Load = mini;
   elseif mini == pwr & pwr < (cload - delta)
      Load = cload - delta;
   elseif mini > pwr & pwr > (cload - delta)
      Load = mini;
   elseif mini < pwr & pwr > (cload - delta)
      if (cload - delta) <= mini
```

```
        Load = pwr;
      elseif (cload - delta) > mini
        Load = (cload - delta);
      end
    end
end
```

A.17 Equivalent Power of a Stored Gas

This function computes the equivalent power for an amount of (eg H2) produced

```
function PwrEquiv = React2Pwr(React,Vol,time)

% React is one of three reactants used in this study
% Vol is in normal meters cubed
% time is in hours
% PwrEquiv is in units of W
% An extra 0.1 kWh/Nm^3 was added for compression to compensate for
% storage for N2 and H2.


if strcmp(React,'H2') == 1
    SpecEng = 4.9E3; % specific energy for H2 (Wh/Nm^3)
elseif strcmp(React,'N2') == 1
   SpecEng = 0.3E3; % Specific energy for N2 in (Wh/Nm^3)
elseif strcmp(React,'H2O') == 1
   SpecEng = 0.7E3; % Specific energy for H2O in Wh/m^3
end

PwrEquiv = Vol*SpecEng/time;
```

A.18 Equivalent Power Required for the Required Volume of Gas

```
function [RxEquiv Pwr4Elec GridPwr] = Pwr2React(React,Power,time)

global XTraElec

% RxEquiv is in units of Nm^3
% Power is in W
% Time is in hours
%
% The XTraElec is the additional capacity of electrolyzers, each able to
% produce 485 Nm^3/h at about 2330kW or 4.9kwh/Nm^3

if strcmp(React,'H2') == 1
   % This includes compression
    SpecEng = 4.9E3; % specific energy for H2 (Wh/Nm^3)
elseif strcmp(React,'N2') == 1
   SpecEng = 0.2E3; % Specific energy for N2 in (Wh/Nm^3)
elseif strcmp(React,'H2O') == 1
   SpecEng = 0.7E3; % Specific energy for H2O in Wh/m^3
end

Pwr4Elec = SpecEng*XTraElec*485; % Watts available for electrolyzers
```

```
if Power >= Pwr4Elec
   RxEquiv = Pwr4Elec*time/SpecEng; % Use the available power for the H2
   % Positive grid power = positive revenue
   GridPwr = Power - Pwr4Elec; % Sell the remaining power on the grid
elseif Power < Pwr4Elec
   RxEquiv = Power*time/SpecEng; % All power into H2;
   Pwr4Elec = Power; % The actual power to the elec
   GridPwr = 0;
else
   RxEquiv = 0;
   GridPwr = 0;
   Pwr4Elec = 0;
end
```

A.19 Wind Farm Cost – Main Driver

```
function [C_Plant CWT CF Cc CIS CTS CSE CPD]  =
WindCost(nwt,Pwt,dia,R_Spd,h,Dep,Dwf,Space,TransDist,Vn,HV,BB,OnOff,Onshore_Dist,nHV)


% [C_Plant CWT CF Cc CIS CTS CSE CPD] =
% WindCost(nwt,Pwt,dia,Rated,h,Dep,Dwf,Space,TransDist,Vn,HV,BB,OnOff,Onshore_Dist,nHV)
% The inputs are the number of wind turbines (nwt), the power of each
% turbine (Pwt) in MW, the turbine diameter ,the rated speed of the turbine(m/s),
% The hub height (m), the depth (Dep) in meters, the distance offshore
% (Dwf) in km, the spacing between the turbines
% (assumed to be a square), S, in turbine diameters, the transformer
% distance to shore (TransDist)
% the voltage in the local (interturbine) network (Vn) in volts, the voltage in the
% high voltage lines to shore in volts, the number of breaker bars(BB), if there's an offshore
% substation (On/Off), the length of the onshore transmission (Onshore_Dist) in km,
% the number of HV lines to shore (nHV)

S=Space;
match = strcmp(OnOff,lower('Off'));
% Initialize other variables
% dia = Diameter(Pwt*1e6,Rated) % Diameter of a wind turbine with rated power
A = (dia^2/4)*3.1415926;

% The transformer is rated in MVA which implied apparent power, not real
% power. The power factor is sin of 45 degrees or 0.707. Thus the apparent
% power is higher than the real power by a factor of 1/0.707
Atr = nwt*Pwt/sin(pi/4);

% The number of transformers is assumed to be one.
nTR = 1;

% This is taken from Fingersh et al. (2006)
[Cowt Cwt RotorCost DriveCost] = TurbCost(dia,h,Pwt,nwt,'advanced','three stage');

% The following is the cost of a monopile foundation
% This is found in Offshore Wind Energy Projects Feasibility Study Guidelines
% The cost of 320euro/kW was updated to $477/kW (2010) then increased by
% 25% because the PPI over the period was 171/114 and the GDP deflator was
```

```
% about 120/100. Thus, 25% was added: 1.5/1.2 = 1.25 to get $595/kW
Cf = (595*Pwt*(1+0.02*(Dep-8))*(1+0.8E-6*(h*(dia/2)^2-1E5))); % [$2010/turbine]

% An entire function was written to handle the costs of the inter turbine
% grid for any size wind farm.
[Cc ncl] = CableCost(nwt,Pwt,dia,S,Vn,R_Spd);

% This is the cost of the transformer, but it is dependent on the size of
% the transformer, in MVA
if Atr<=50
   % This is from Lundberg (2003) and needs to be updated to $2010
   % This expression is valid for transformers up to 150 MVA [Euro]
   Ctr = 1.5*(-153.05 + 131.1*Atr^0.4473);
   %Where Atr is the rated power of the transformer
else
   % For transformers that are larger (50-800 MVA) the following is used:
   % This was updated already!
   % Factor of 1.5 is used because the PPI for transformers was 239.5/144
   % from 2004 to 2010. General inflation was about 15% in the US.
   Ctr = 1.5*(49.5*Atr.^0.7513).*1000; % $2010
end

% Cost of switchgear
% The factor of 1.15 is due to the PPI for switchgear being 1.3 over the
% interval. Since general inflation was low, 15% was added.
Csg = 1.15*(100330+2.8726*Vn)*0.155; % Switch gear cost [$2010]. Vn is the nominal voltage in V

% This is the cost of the busbar
% The gas insulated systems (GIS) are assumed, rather than air insulated

% This is a reproduction of the data from Table 5 in the paper.
% All costs in $2010
% Factor of 1.15 is applied here as well
SBB = [2650 2900]*1000*1.374;
DBB = [3280 3450]*1000*1.374;
CsgSB = [920 1250]*1000*1.374*1.15;
CsgDB = [950 1300]*1000*1.374*1.15;

if Vn < 230 & BB == 1
   Cbb = SBB(1);
   CsgHV = CsgSB(1);
elseif Vn < 230 & BB == 2
   Cbb = DBB(1);
   CsgHV = CsgDB(1);
elseif Vn > 230 & BB == 1
   Cbb = SBB(2);
   CsgHV = CsgSB(2);
elseif Vn > 230 & BB == 2
   Cbb = DBB(1);
   CsgHV = CsgDB(1);
else
   Cbb = SBB(1);
   CsgHV = CsgSB(1);
end
```

```
% Cost of a diesel generator backup
% Based on RS Means from Gabriel in the New England Islands study
% Ancillary services require 20kW/MW (the 0.02) and then the cost for the
% generator is $200/kW for large machines
Cdg = (0.02*Pwt*nwt)*200;

% Substation cost
% Updated from 2003 SEK (0.155)
Css = (20000000+0.7*nwt*Pwt*1e6)*0.155; % [$2010]
CmHV = SubmarineCost(nwt,Pwt,TransDist,HV); % This includes the installation costs

% The following are from ReEDS (NREL Optimization model)
Cost_Onshore_Trans = 745; % $2010/MW-km
Cost_Mult = 3.56;
Onshore_Substation = 20; % $20/kW for onshore substation required for transmission to grid
Intertie = 230; % $230/kW for intertie

% The following are no longer used in favor of US costs from NREL
%{
% Cost of overhead lines - single circuit ($/km)
ColSC = [270 350]*1.707*1000;
% Cost of overhead lines, double circuit
ColDC = [410 450]*1.707*1000;
% Cost of underground lines
Cug   = [1600 1950]*1.707*1000;
%}

CTS = Cost_Mult*Cost_Onshore_Trans*(nwt*Pwt)*Onshore_Dist...
   + (Onshore_Substation + Intertie)*(nwt*Pwt)*1e3...
   + CmHV*nHV;

% CIS is integration system cost
if match == 0
   % Onshore substation
   CIS = (nTR*Ctr+(ncl+nTR)*(Csg)+nHV*(2*CsgHV + Cbb));
   % CTS = (nHV*Cug(1)*(1-aol)*dps + nolHV*ColDC(1)*aol*dps + nHV*CsgHV);
elseif match == 1
   % Offshore substation
   CIS = (nTR*Ctr+(ncl+nTR)*(Csg)+nHV*(2*CsgHV + Cbb)+(Cdg+Css));
   %CTS = (nHV*CmHV + nHV*Cug(1)*(1-aol)*dps + nolHV*ColDC(1)*aol*dps...
    %   + nHV*CsgHV);
else
   CIS = (nTR*Ctr+(ncl+nTR)*(Csg)+nHV*(2*CsgHV + Cbb));
   % CTS = (nHV*Cug(1)*(1-aol)*dps + nolHV*ColDC(1)*aol*dps + nHV*CsgHV);
end

CWT = (Cowt*nwt); % Cost of the wind turbines
CSE = 114000*nwt; % Scada cost ($2010)

% The 96000 pounds is from Figure 11: use the total cost of 1.6 million
% pounds times the 6% installation!
CF = (Cf*nwt*1000) + 96000*1.904*nwt*Pwt; % Cost of the foundation
CPD = 0.03*(Cowt+Cf+Cc+CIS+CTS+CmHV); % Project development is 3% of total fixed investment

% The 0.89 factor is from page 51 of "Study of the costs of offshore wind
% generation" - Consenting - 7%, other - 2%, testing 2% = 11%.
```

```
C_Other = ((CWT + CF + Cc + CIS + CTS + CSE + CPD)/(0.89))*0.11;
C_Plant = (CWT + CF + Cc + CIS + CTS + CSE + CPD + C_Other)
pie([CWT  CF  Cc  CIS  CTS  CSE  CPD
C_Other],{'Turbine','Foundation','Cables','Integration','Transmission','Scada','Project Dev','Consenting &
Testing');
figure;
pie([CWT  CF  Cc  CIS  CTS  CSE  CPD C_Other]);
```

A.20 RNA and Tower Cost

```
function [Offshore_Total_Cost TotalCost RotorCost DriveCost] =
TurbCost(Dia,Height,Pwt,nwt,type,gentype)

% This is based on the analysis by Fingersh et al (2006).

% The Producer price indices are calculated in an Excel sheet. All data was
% taken from www.bls.gov/data. Each component of the turbine had an
% associated NAICS number which was used to calculate the PPI for the
% component. Often, large components (blades, gearbox, etc) are composed of
% other smaller components. The Fingersh analysis gave percentages of the
% final product cost. Thus an "effective" PPI for a blade could be
% calculated based on weighted PPIs. The results are in the array titled
% PPI below.

% Dollar basis is 2002 the PPIs are for 2010. Any inflation from 2002-2010
% is assumed to be 1.21 from the CPI inflation calculator
% http://data.bls.gov/cgi-bin/cpicalc.pl

NumBlades = 3;
Rad = Dia/2;
Area = (Dia/2)^2*pi;
Rate = Pwt*1000;  % Rating in kW

switch lower(type)
   case 'advanced'
      BladeMass = (.4948*(Dia/2)^2.53)*NumBlades;
      BladeCost = (((0.4019*Rad^3-21051)+2.7445*Rad^2.5025)/(1-0.28))*NumBlades;
      TowerMass = 0.2694*Area*Height+1779;
      TowerCost = TowerMass*1.5;
      HubMass = .954*BladeMass/3+5680.3;
      HubCost = HubMass*4.25;
   case 'baseline'
      BladeMass = (0.1452*Rad^2.9158)*NumBlades;
      BladeCost = (((0.4019*Rad^3-955.24)+2.7445*Rad^2.5025)/(1-0.28))*NumBlades;
      TowerMass = 0.3973*Area*Height-1414;
      TowerCost = TowerMass*1.5;
      HubMass = .954*BladeMass/3+5680.3;
      HubCost = HubMass*4.25;
   otherwise % Default to advanced
      BladeMass = (.4948*(Dia/2)^2.53)*NumBlades;
      BladeCost = (((0.4019*Rad^3-21051)+2.7445*Rad^2.5025)/(1-0.28))*NumBlades;
      TowerMass = 0.2694*Area*Height+1779;
      TowerCost = TowerMass*1.5;
      HubMass = .954*BladeMass/3+5680.3;
```

```
        HubCost = HubMass*4.25;
end

switch lower(gentype)
   case 'three stage'
        GearCost = 16.45*Rate^1.249;
        GenMass = 6.47*Rate^0.9223;
        GenCost = Rate*65;
        MFrameMass = 2.233*(2*Rad)^1.953;
        MFrameCost = 9.489*(2*Rad)^1.953;
   case 'single stage'
        GearCost = 74.1*Rate;
        GenMass = 10.51*Rate^0.9223;
        GenCost = Rate*54.73;
        MFrameMass = 1.295*(2*Rad)^1.953;
        MFrameCost = 303.96*(2*Rad)^1.067;
   case 'multi path'
        GearCost = 15.26*Rate^1.249;
        GenMass = 5.34*Rate^0.9223;
        GenCost = Rate*48.03;
        MFrameMass = 1.721*(2*Rad)^1.953;
        MFrameCost = 17.92*(2*Rad)^1.672;
   case 'direct'
        GearCost = 0;
        GenMass = 661.25*10^0.606;
        GenCost = Rate*219.33;
        MFrameMass = 1.228*(2*Rad)^1.953;
        MFrameCost = 627.28*(2*Rad)^0.85;
   otherwise % single stage by default
        GearCost = 74.1*Rate;
        GenMass = 10.51*Rate^0.9223;
        GenCost = Rate*54.73;
        MFrameMass = 1.295*(2*Rad)^1.953;
        MFrameCost = 303.96*(2*Rad)^1.067;
end


PitchBMass = .1295 * BladeMass + 491.31;
PitchSysMass = (PitchBMass*1.328)+555;
PitchCost = 2.28*(0.2106*(Dia)^2.6578);
NoseMass = 18.5*(2*Rad)-520.5;
NoseCost = 5.57*NoseMass;
LShaftMass = 0.0142*(2*Rad)^2.888;
LShaftCost = 0.1*(2*Rad)^2.887;
BearMass = ((2*Rad)*8/600-0.033)*0.0092*(2*Rad)^2.5;
BearCost = 2*BearMass*17.6;
BrakeCost = 1.9894*Rate-0.1141;
BrakeMass = BrakeCost/10;
VSElecCost = Rate*79;
YawMass = 1.6*(0.0009*(2*Rad)^3.314);
YawCost = 2*(0.0339*(2*Rad)^2.964);
RailsMass = 0.125*MFrameMass;
RailsCost = RailsMass*8.7;
ElecConnect = 40*Rate;
HydraulicMass = 0.08*Rate;
HydraulicCost = 12*Rate;
```

```
NacelleCost = 11.537*Rate+3849.7;
NacelleMass = NacelleCost/10;
ControlCost = 35000;

% Weighted PPIs for the turbine components.
PPI.blades = 1.076;
PPI.hub = 1.922;
PPI.pitch = 1.355;
PPI.lsShaft = 1.558;
PPI.bearing = 1.344;
PPI.gearbox = 1.344;
PPI.brake = 1.03;
PPI.gen = 1.312;
PPI.VSElec = 1.307;
PPI.yaw = 1.395;
PPI.mainframe = 1.921;
PPI.elecConnect = 1.75;
PPI.hydraulic = 1.202;
PPI.nacelle = 1.066;
PPI.control = 1.246
PPI.tower = 1.563;
PPI.trans = 1.171;
PPI.inf = 1.204;

Transport = Rate*(1.581e-5*Rate^2-0.0375*Rate+54.7)*PPI.trans;

RotorCost = BladeCost*PPI.blades + HubCost*PPI.hub + NoseCost*PPI.inf ...
   + PitchCost*PPI.pitch;

DriveCost = GearCost*PPI.gearbox + GenCost*PPI.gen + ...
   MFrameCost*PPI.mainframe + LShaftCost*PPI.lsShaft + ...
   BearCost*PPI.bearing + BrakeCost*PPI.brake + YawCost*PPI.yaw + ...
   RailsCost*PPI.inf + ElecConnect*PPI.elecConnect + ...
   HydraulicCost*PPI.hydraulic + NacelleCost*PPI.nacelle + ...
   VSElecCost*PPI.VSElec;

TotalCost = BladeCost*PPI.blades + TowerCost*PPI.tower + HubCost*PPI.hub...
   + GearCost*PPI.gearbox + GenCost*PPI.gen + MFrameCost*PPI.mainframe ...
   + PitchCost*PPI.pitch + NoseCost*PPI.inf + LShaftCost*PPI.lsShaft + ...
   BearCost*PPI.bearing + BrakeCost*PPI.brake + YawCost*PPI.yaw ...
   + RailsCost*PPI.inf + ElecConnect*PPI.elecConnect + ...
   HydraulicCost*PPI.hydraulic + NacelleCost*PPI.nacelle + ...
   VSElecCost*PPI.VSElec + ControlCost*PPI.control + Transport;

% Total cost escalated using the PPI, per my article.
MarineCost = TotalCost*0.135;

% WIND GENERATION, page 27
Offshore_Total_Cost = (TotalCost + MarineCost + Transport)*1.25; % + Port + Install + Permits + Access +
Scour;
```

A.21 Array Cable Cost

```
function [Cable_Cost num_string] = CableCost(nwt,Pwt,D,D_num,V,R_Spd)

% CableCost(nwt,Pwt,D,D_num,V)
```

```
% nwt is the number of wind turbines
% Pwt is the power for each turbine in MW
% D_num is the number of diameters spacing (assumed square) [m/turb]
% V is the intercabling voltage in Volts
% Pwt = Pwt*1000000
% First check to see what we have. For Lillgrund the feeders were either 9
% or 10 turbines. Horns Rev had 16 in 2 groups of 8.

% Data is from the XLPE Cable Systems User's guide by ABB
% Updated costs 4/2/2012 using the GDP deflator scheme
% The original 0.4818S+99... became 640S+132000

Cross = [0 16 25 32 50 70 95 120 150 185 240 300 400 500 630 800 1000];
Amps =  [0 115 145 175 210 250 300 340 360 430 495 555 625 700 785 865 935];


%{
Max_Pwr = Amps(end)*36000  % max W for one string root
if Pwt > Max_Pwr/10

   num_string = floor(Max_Pwr/Pwt)
   sht_string = mod(Max_Pwr/Pwt)
else
% First, strings of 10 turbines are assumed
num_string = floor(nwt/10)  % number of 10 stringers
sht_string = mod(nwt,10)  % This is a short string

[Strings Power TurbPerStrng SString ShortPwr TurbPerShStrng TotalPwr]
%}

[num_string Root_Pwr TurbPStrng sht_string sht_pwr TurbPerShStrng TotPwr] = ParkSetup(nwt,Pwt,V);
% Root_Strings = 1  % Assume that at least one root string is necessary
C_Root = 0;  % Initialize the cost of the root
C_Mid1 = 0;
C_Lst1 = 0;


if num_string > 0
   % For dimensioning the cables, see "Cost estimation of wind farms
   % internal grids" by Erika Nord, page 31
   Root_Amp = Root_Pwr*1e6/(V*sin(pi/4));
   %if Root_Amp > 935 % This is more than one cable can handle
   %    Root_Strings = ceil(Root_Amp/935)
   %end
   C_Sec_R = interp1(Amps,Cross,Root_Amp,'nearest','extrap');  % Cross sec @ root
   % Also need the cross section for the tapers toward the end. For this
   % Lillgrund is used as a model for design: 1-6 turbines on the last
   % string, 7-9 on the second string, and 10 on the root string.
   Mid_Pwr = (Root_Pwr-Pwt); %Assume 1 turbines on the root
   Mid_Amp = Mid_Pwr*1e6/(V*sin(pi/4)) ;
   C_Sec_S = interp1(Amps,Cross,Mid_Amp,'nearest','extrap') ;
   Lst_Pwr = Pwt*6;
   Lst_Amp = Lst_Pwr*1e6/(V*sin(pi/4));
   C_Sec_L = interp1(Amps,Cross,Lst_Amp,'nearest','extrap') ;

   % The length at the root (between the transformer and the first turbine is
```

```
    % simply the spacing. The length for turbines 7-9 is 2D and the length for
    % the remaining cable is 5D.
    Root_Lgt = D*D_num/1000*num_string;  % The length of all the roots [km]
    C_Root = (640*C_Sec_R + 132000)*Root_Lgt;  % The total cost of said root

    % Cost of the mid section
    % The "-5" is from the algebra for the number of cables: 19 requires 14 mid
    % sec lengths - three inter turbine and 1 from the last turbine to the xfmr
    % the same holds for 8 and 7. Six and under are simply equal to the number
    % of wind turbines.

    C_Mid1 = (D*D_num/1000*num_string*(TurbPStrng-1-5))*(640*C_Sec_S+132000);
    C_Lst1 = (D*D_num/1000)*num_string*5*(640*C_Sec_L+132000);

end

if sht_string > 0 & sht_string <= 6
    Lst_Pwr_S = Pwt*sht_string;  % Last power with a short section
    Lst_Amp_S = Lst_Pwr_S/(V*sin(pi/4));  % Last amps
    Lst_Sec_S = interp1(Amps,Cross,Lst_Amp_S,'nearest','extrap');  % Last cross sec
elseif sht_string > 6 & sht_string < 10
    Lst_Pwr_S = Pwt*6;  % Last power with a short section
    Lst_Amp_S = Lst_Pwr_S/(V*sin(pi/4));  % Last amps
    Lst_Sec_S = interp1(Amps,Cross,Lst_Amp_S,'nearest','extrap');  % Last cross sec
    Mid_Pwr_S = Pwt*sht_string;  % Short root power
    Mid_Amp_S = Mid_Pwr_S/(V*sin(pi/4));  % Short root amps
    Mid_Sec_S = interp1(Amps,Cross,Mid_Amp_S,'nearest','extrap');  % Short cross sec
end

% Now the lengths at each cross section are required to compute the total
% cost using the equation in Dicorato, et al. (2011)


% The short string is not always present
if sht_string > 0 & sht_string <= 6
    C_Lst2 = (D*D_num/1000)*sht_string*(640*Lst_Sec_S+132000);
    if num_string > 0
        C_Lst = C_Lst1+C_Lst2;
        C_Mid = C_Mid1;
    else
        C_Lst = C_Lst2;
        C_Mid = C_Mid1;
    end
elseif sht_string > 6 & sht_string < 10
    C_Mid2 = (D*D_num/1000*(sht_string-5))*(640*Mid_Sec_S+132000);
    C_Lst2 = (D*D_num/1000)*5*(640*Lst_Sec_S+132000);
    if num_string > 0
        C_Mid = C_Mid1 + C_Mid2;
        C_Lst = C_Lst1+C_Lst2;
    else
        C_Mid = C_Mid1;
        C_Lst = C_Lst2;
    end
else
    C_Mid = C_Mid1;
    C_Lst = C_Lst1;
```

```
end

InstCost = 372000; % Installation cost in $2010/km;
% Since the price of copper has increased significantly from 2003 to 2010
% I'll escalate with the PPI for US costs

% The price of power cables increased by 20% over the interval 2009-2010.
% Inflation was low (.7% in Europe, 1.1% in the US) so a cost multiplier of
% 1.2 was chosen. (227.1/114.7 for the PPI)

Cable_Cost = (C_Root+C_Mid+C_Lst)*1.2+nwt*D_num*D/1000*InstCost;
```

A.22 HV Cable Cost

```
function Cost = SubmarineCost(nwt,Pwt,Dist,U_rate)

In = (nwt*Pwt*1E6)/(U_rate*cos(pi/4)); % Total necessary current

Cross = [0 16 25 32 50 70 95 120 150 185 240 300 400 500 630 800 1000];
Amps =  [0 115 145 175 210 250 300 340 360 430 495 555 625 700 785 865 935];

% Largest cable is 935 amps. After that a smaller cable is necessary. Note
% that this is sub-optimal: two medium cables is probably preferable to a
% large and a small
if In > Amps(end)
   Num_Cables = floor(In/Amps(end));
   In2 = mod(In,Amps(end));
   if In2 <= 0 % Just to be cautious!
      Num_Sht_Cables = 0;
      Num_Cables = 0;
   else
      Num_Sht_Cables = 1;
      Num_Cables = 0;
   end
else
   In2 = 0;
   Num_Cables = 1;
   Num_Sht_Cables = 0;
end

Matrix = [22 284 583 .00615;
   33 411 596 0.0041;
   45 516 612 0.003;
   66 688 625 0.00205;
   132 1971 209 0.00166;
   220 3181 110 0.00116]*1000;

Volts = Matrix(:,1);
Alpha = Matrix(:,2);
Beta = Matrix(:,3);
Gamma = Matrix(:,4);

% First find the index
for i=1:length(Volts)
   if  Volts(i)>=U_rate
      a = Alpha(i);
```

```
        b = Beta(i);
        c = Gamma(i);
        break
    end
end

% The costs of the HV cables are from Lundberg, 2003.

if In2 == 0
    Sn = sqrt(3)*U_rate*In;
    Cost = ((a+b*exp(c*Sn/10e8))/6.36)*Num_Sht_Cables*Dist;
elseif In2 > 0
    Sn1 = sqrt(3)*U_rate*In;
    Sn2 = sqrt(3)*U_rate*In2;
    Cost = ((a+b*exp(c*Sn1/10e8))/6.36)*Num_Cables*Dist + ((a+b*exp(c*Sn2/10e8))/6.36)*Dist;
end

% This is the cost of the cables plus the installation of the submarine
% cables at 720,000 euro per km. The results were converted to 2010 USD
% Since the price of copper has increased significantly from 2003 to 2010
% I'll escalate with the PPI for US costs

% The price of power cables nearly doubled over the interval 2003-2010.
% Inflation was low (13% in Sweden, 18% in the US) so a cost multiplier of
% 1.7 was chosen. (227.1/114.7 for the PPI)

Cost = Cost*1.7 + 720000*1.374*Dist;%*(Num_Cables+Num_Sht_Cables);
```

A.23 Ammonia Plant Cost

```
function [ElecCapCost ASUCapCost MVCGrassRts SynGrassRts StoreGrassRts TotalNH3Cost RawMatl
LaborCost] = NH3Cost(T,P,Size,Extra,Store)

% Usage: [TotalNH3Cost OMCost] = NH3Cost(P,T,Size) where
% P is the operating pressure in bar
% T is the operating temperature in C and
% Size is in metric tons per day of ammonia production

% These numbers are needed for calculations: Water vol per day in [m^3] the
% volume of nitrogen in Nm^3/day and the volume of hydrogen in Nm^3/day
[WaterReqdVol VN2 VH2] = NH3Reactants(Size);

H = 1.00794; % Hydrogen in grams/mol
N = 14.0067; % Nitrogen in g/mol
NH3 = N + 3*H; % Ammonia in g/mol

NFrac = N/NH3;
HFrac = 3*H/NH3;

TonsN = NFrac*Size;
TonsH = HFrac*Size;

% Electrolyzer section
[NumElec ElecContFee ElecCapCost ElecLaborCost ElecRawMatl]...
    = ElecCost(TonsH,Extra,Store); % The function requires kg/day
```

```
% ASU section

[ASUCapCost ASULaborCost ASURawMatl] = ASUCost(Size);


% MVC Section

[MVCBareCost MVCActCost MVCGrassRts MVCLaborCosts MVCRawMatl]...
   = Evaporator(WaterReqdVol);
MVCRawMatl
% Synloop section

[SynBareCost SynActCost SynContFee SynGrassRts SynLabor SynMatl ActCompCost ActDrvCost
ActHXCost ActReactCost ActFlashCost ActPumpCost] = SynCost2(T,P,Size)

% Storage Section

[StoreBareCost StoreActCost StoreContFee StoreGrassRts] = StorageCost(Size);

% Total Capital Investment
TotalNH3Cost = ElecCapCost + ASUCapCost + SynGrassRts + MVCGrassRts + StoreGrassRts;

% Total O&M cost

LaborCost = ElecLaborCost + ASULaborCost + MVCLaborCosts + SynLabor;

RawMatl = ElecRawMatl + ASURawMatl + MVCRawMatl + SynMatl
ElecRawMatl
ASURawMatl
MVCRawMatl
SynMatl
OMCost = LaborCost + RawMatl;
```

A.24 Electrolyzer Cost

```
function [NumElec ContFee GrassRts LaborCost RawMatl] = ElecCost(Size,Extra,Store)

% Based on the Atmospheric Type No.5040 - 5150 Amp DC Electrolyzer
% available from Statoil (formerly Hydro)
% Inputs: Size of the plant in tons/d
% Extra is the extra electrolyzers required
% Store is the H2 storage in kg
% Since the design capacity of one electrolyzer is 1050 kg/d this is the
% base case.
% The following are the cost inflation factors
CEPCI2001 = 397;
CEPCI2002 = 468;

CEPCI2010 = 550.8; % CEPCI for 2010
SizeKg = Size*1000; % Convert to kg/d

EReqdSys = 4.8;   % System energy required for Electrolyzer plus system (kWh/Nm^3)
EReqElec = 4.3;   % Energy required per electrolyzer w/o system (kWh/Nm^3)
EReqSysKg = 53.4; % System energy per kilogram of H2 produced (kWh/kg)
```

```
H2Prod = 485;     % Hydrogen Product in Nm^3 per electrolyzer (Nm^3/hr)
PReqdElec = 2330; % Power Required per electrolyzer in (kW)
H2OReq = 1;       % Water required in L/Nm^3 of H2 produced.
H2OCool = 100;    % Cooling water required in L/Nm^3
DesignCap = 1046; % Design capacity per electrolyzer (kgH2/day)
Capacity = 0.97;  % The capacity factor of the electrolyzer, based on Norsk quote
% See pre-investigation of water electrolysis, pages 145-6
UpTime = 0.86;    % Actual running time on a yearly basis
H2MolKg = 1000/2.016; % The number of moles of H2 per kg of H2
R = 8.314472E-5; % m^3*bar/K*mol
T = 293; % Ambient temp
P = 1; % Pressure of 1 bar
VolH2 = H2MolKg*R*T/P; % Vol of H2 per kg of H2
CoolH2OReqd = VolH2*SizeKg*H2OCool/1000; % Cooling water in m^3/day
CoolH2OFlow = CoolH2OReqd/(24*60); % in m^3 per minute

%%%% Pumps section
P_drop = 3; % Losses from the pumping, vertical, etc (bar)
Eff = 0.75; % Efficiency of pump
PumpPwr = 1.67*CoolH2OFlow*P_drop/Eff; % in kW

NumElec = ceil(SizeKg/(DesignCap*Capacity*UpTime))+Extra; % Total number of electrolyzers required

K1P = 3.3892;
K2P = 0.0536;
K3P = 0.1538;

PumpCost = ChemCost(K1P,K2P,K3P,PumpPwr)*(CEPCI2010/CEPCI2001);

B1P = 1.89;
B2P = 1.35;
FM = 2.5;
FP = 1;

ActModCost = PumpCost*(B1P+B2P*FM*FP);
ContPump = 1.18*ActModCost;
PumpGrassRts = 1.5*PumpCost + ContPump;


% Financial section
% Uninstalled Costs for a single electrolyzer unit

% The following are from curve fits...
%% For scaling select the second line
%UninstCost = (786*NumElec + 712*NumElec^1 + 148*NumElec^1 + 368*NumElec^1 +
442*NumElec^1)*1000;
UninstCost = (786*NumElec + 712*NumElec^0.7 + 148*NumElec^0.5 + 368*NumElec^0.75 +
442*NumElec^0.8)*1000;
%NormCost = UnitCost/2330;


InstFac = 1.2;    % Installation factor for the plant

ActCost = UninstCost*InstFac; % Actual Equipment cost (Assuming bare module =
% actual cost since this is a per unit quote)
```

```
% From H2A tool, 1170/kg installed storage of H2
StoreCost = 1170*CEPCI2010/CEPCI2002*Store;

% Extra Compressor Cost
%%%%%%%%%%%%%%%%%%%%%%%%%%%%%%%%%%%%
% Extra compressors are required to elevate the total possible extra H2 to
% storage pressure
if Store == 0
   ActDrvCost = 0;
   ActCompCost = 0;
else
%Data needed for calculations
R = 8.314472E-5; % m^3*bar/K*mol
T = 293; % K standard temp
P = 1; % (bar) Standard pressure
H = 1.00794; % Hydrogen in grams/mol
O = 15.9994; % Oxygen in g/mol

H2 = 2*H; % Hydrogen gas in g/mol
P1 = 1; % Ambient pressure as reference (bar)
P1H2 = 1; % Atmospheric pressure from the H2 plant (bar)
P2 = 450; % Final pressure (bar)
n = 1.4; % Thermodynamic exponent []

T1 = 293; % Ambient temp (K)

RH2 = 4.124; % Gas constant for H2 kJ/kgK
Stages = 5;
M_Per_Day = 1046; % Maximum output per day per electrolyzer (kg)
mdotH2 = Extra*M_Per_Day/(24*3600); % kg/s of H2
CpH2 = RH2*(n/(n-1));
IsenEff = 0.75; % Isentropic efficiency for the compressors
MechEff = 0.95; % Mechanical Efficiency

% w [=] Acentric factor = -0.219 for hydrogen
% Tc for H2 is 33.19 K
% Pc for H2 is 13.13 bar

% Feed compressor fluid work (kW)
CWorkH2F = T1*Stages*n*RH2/(n-1)*mdotH2*(((P2/P1H2)^(1/Stages))^((n-1)/n)-1);
% Feed compressor shaft work (kw)

% Amount of power required by each compressor (kW)
CWorkH2S = CWorkH2F/(IsenEff*MechEff);

% This index takes the costs from 2001 to any other reasonable CEPCI index
% (usually +/- 15 years)
CEPCI = 397; % from 2001
Idx = 550.8; % 2010 from Chemical Engineering April 2011

% Compressors: 450-3000kW
K1Comp = 2.2897;
K2Comp = 1.3604;
K3Comp = -0.1027;

% Electric Drivers: Totally enclosed 75-2600kW
```

```
K1Drv = 1.956;
K2Drv = 1.7142;
K3Drv = -0.2282;

% The bare module factor for the compressors is from the corrosion guide on
% pages 254-255 in Ulrich and from Table A6, figure A.19 and Table A5 in
% Turton, et alli
% The bare module factor for the drives is from the tables and figures in
% Turton et alli
FBM_C = 5.8;
FBM_D = 1.5;

% Bare Module Cost has the index for the inflation but no pressure or
% material costs associated with the equipment.
if CWorkH2F/(1000*Stages)> 3000
   NumMaxC = floor((CWorkH2F)/(3000));
   SmallC = rem(CWorkH2F,3000);
   Comp1_Cost = NumMaxC*ChemCost(K1Comp,K2Comp,K3Comp,3000)...
      + ChemCost(K1Comp,K2Comp,K3Comp,SmallC);
else
Comp1_Cost = Stages * ChemCost(K1Comp,K2Comp,K3Comp,CWorkH2F/(Stages));
end

BareCompCost = (Idx/CEPCI)*(Comp1_Cost);
A = (Idx/CEPCI)*Comp1_Cost*FBM_C/Stages;
ActCompCost = BareCompCost*FBM_C;

%%%%%%%%%%%%%%%%%%%%%%%%%%%%%%%%
%%% Drivers for compressors

Drv1_Cost = Stages*ChemCost(K1Drv,K2Drv,K3Drv,CWorkH2S/(Stages*1000));
BareDrvCost = (Idx/CEPCI)*(Drv1_Cost);
ActDrvCost = BareDrvCost*FBM_D;
end

ContFee = 1.18*(ActCost+ActCompCost+ActDrvCost+StoreCost) + ContPump;
GrassRts = 0.5*ActCost + ContFee + PumpGrassRts;

TotalCapInvest = GrassRts;


% O&M Section of the module
Days = 365;

% Labor rate from http://www.bls.gov/oes/current/naics4_325100.htm for a
% Basic Chemical Manufacturing worker
Rate = 28.32; % $2010/hr

% This is the cost of lye per unit per year. From H2A sheet.
RawMatl = 17500*NumElec;

% Labor costs
% Since the electrolyzers are designed for continuous unattended operation,
% the total number of processing steps (num of electrolyzers) is quartered.
% H2A has labor = 0!
% Includes supervisor and clerical
```

```
LaborCost = Labor(Size,NumElec*0.25,Rate,Days);
```

A.25 Air Separation Unit Cost

```
function [Cost LaborCost RawMatl] = ASUCost(Size)

% Size is in tons of ammonia per day. The function returns the installed cost, the
% capital investment and the total O&M costs.

% This index takes the costs from 2001 to any other reasonable CEPCI index
% (usually +/- 15 years)
CEPCI = 397; % from 2001
Idx = 550.8; % 2010 from Chemical Engineering April 2011

% Updated July 25, 2012 to include the fitted curve from Excel
Cost = (0.0593.*(Size.*0.8224).^3-68.725.*(Size.*0.8224).^2+53319.*(Size.*0.8224)+5e6);
% For more information on the actual process see: Process Synthesis
% Optimization and Flexibility Evaluation of Air Separation Cycles

% Data for a bottom up analysis is from http://www.uigi.com/cryodist.html
% Major process equipment: compressors, molecular sieves, heat exchanger,
% one distillation column, and one expander (turbine)

% Axial compressors are assumed
% The ASUPower2 function computes the total power required using the input
% flow of air. The recovery rate is assumed to be 66%. Thus, the flow is
% the output desired divided by 0.66:

%{
[CompPwr SheetPwr SpecPwr] = ASUPower2(Size/0.66);

% The compressor power is actually the power to the driver. The fluid power
% is roughly 95% of the CompPwr value.

% From Turton, Table A.1
K1C = 2.2897;
K2C = 1.3604;
K3C = -0.1027;
F_BM_C = 3.8;
BareCompCost = ChemCost(K1C,K2C,K3C,CompPwr*0.95/1000)...
   *(Idx/CEPCI); % Div by 1000 for kW
ActCost = BareCompCost*F_BM_C;

%%%%%%%% Drives

% Electric Drivers: Totally enclosed 75-2600kW
K1Drv = 1.956;
K2Drv = 1.7142;
K3Drv = -0.2282;

FBM_D = 1.5;
Drv1_Cost = ChemCost(K1Drv,K2Drv,K3Drv,CompPwr);
BareDrvCost = (Idx/CEPCI)*(Drv1_Cost);
ActDrvCost = BareDrvCost*FBM_D;

%}
```

```
%Data needed for labor calculations
R = 8.314472E-5; % m^3*bar/K*mol
T = 293; % K standard temp
P = 1; % (bar) Standard pressure
N = 14.0067; % Nitrogen in g/mol
N2 = 2*N; % Nitrogen in g/mol

TonsN2 = (P*Size*.8226/(R*T))*N2*24/1E6;

% Labor rate from http://www.bls.gov/oes/current/naics4_325100.htm for a
% Basic Chemical Manufacturing worker
Rate = 28.32; % $2010/hr

% O&M Section of the module
Days = 365;

LaborCost = Labor(TonsN2,3,Rate,Days);

RawMatl = 0;
%{
IRR = 0.1; % Internal rate of return
Dep = 15; % Deprecation schedule (years)
Life = 20; % Lifetime of liquefier in years
Analysis = 20; % Period of analysis
Inflation = 0.019; % Inflation
StateTax = 0.06; %
FedTax = 0.35; %
TotTax = FedTax+(1-StateTax);

Land = 2500; % Assumes 2500m.^2 for a 30 ton plant and scales with a 0.6 factor;
LandCost = Land.*12.50; % This is the going rate for land in an urban environment, based on $400,000./acre
SitePrep = 0.04; % Site Preparation (percent of CapCost)
EngDesign = 0.10; % Engineering design
Cont = 0.10; % Project Contingency
Permit = 0.03; % Permiting
Owners = 0.12; % Owners cost
SitePrepCost = SitePrep*UnCost;
EngDesignCost = EngDesign*UnCost;
ContCost = Cont*UnCost;
PermitCost = Permit*UnCost;
OwnersCost = Owners*UnCost;
LandOtherCap = LandCost+SitePrepCost+EngDesignCost+ContCost+PermitCost+OwnersCost;
TotalCapInvest = LandOtherCap+UnCost;

%{
% O&M
Labor = 200.*(Demand./300000).^0.25; % 2 days per month for a 300000 facility
LaborPrice = 19.25; % Labor cost per hour
LaborCost = LaborPrice.*Labor;
% TotalCost = CapCost+LandCost+OwnersCost+LaborCost;
InsRate = 0.01; % Insurance Rate
Insurance = InsRate.*TotalCapInvest; % Total insurance
PropTaxRate = 0.015; % Property taxes
PropTax = PropTaxRate.*TotalCapInvest;
LicPermRate = 0.01; % Permits and Licensing
```

```
LicPerm = LicPermRate.*TotalCapInvest;
OMRepairRate = 0.005; % Operations, maintenance and repairs
OMRepairs = OMRepairRate.*TotalCapInvest;
OverheadRate = 0.50; %
Overhead = OverheadRate.*LaborCost;
FixedCost = Insurance+PropTax+LicPerm+OMRepairs+Overhead;
TotalOM = FixedCost+LaborCost;
%}
%}
```

A.26 Mechanical Vapor Compression Cost

```
function [MVCBareCost MVCActCost GrassRts LaborCosts RawMatl] = Evaporator(Size)

% Input here is in m^3/day of water
% Output is Evaporator area (m^2); distillate preheater area (m^2); ...
% Brine heater area (m^2); and the size of the compressor in W
% This was replaced by the excel fitted curve from MVCEvaporator1-11-12 on
% July 25.
MVCBareCost = 0.00167*Size^3 - 3.53*Size^2 + 5.67e+003*Size + 8.42e+005
MVCActCost = 0.00482*Size^3 - 10.2*Size^2 + 1.66e+004*Size + 2.48e+006;
GrassRts = 0.00652*Size^3 - 13.8*Size^2 + 2.25e+004*Size + 3.35e6;
% Calculates the evaporator area
% Ts = Compressed vapor temp (C)
% Tb = Brine temp (C)
% Tf = seawater feed
% Ue = Evaporator heat transfer coeff (kW/m^2C)
% Cp = heat capacity (Kj/kgC)
% Mf = mass flow rate of the feed (kg/s)
% Lamv = latent heat of vapor (kJ/kg)
% Md = Mass flow rate of distillate vapor (kg/s)

% References for this script
% ANALYSIS OF MECHANICAL VAPOUR COMPRESSION DESALINATION PROCESS Ettouney
% et al. 1999
% Design of single-effect mechanical vapor compression Ettouney, 2005
% Plastic/compact heat exchangers for single-effect desalination systems 1999
% Visual basic computer package for thermal and membrane desalination
% processes (2004)
% Design of single-effect mechanical vapor compression. Ettouney (2006)
% Fundamentals of Water Desalination (Ettouney)

%{
Md = Size*1000/(3600*24); % Flow rate of the distillate
Cpv = 1.884; % Specific heat of Saturated vapor above demister at constant pressure, (kJ/kgC)
Cp = 4.2; % Heat capacity of al liquid streams (kJ/kgC)
Ue = 3.94; % Heat transfer coefficient of the evaporator (kJ/(s*m^2*C))
Ub = 2; % Brine preheater heat transfer coefficient (kJ/(s*m^2*C)) (HX2)
Ud = 4.5; % Overall heat transfer coefficient for preheater (kJ/(s*m^2*C)) (HX1)
Tcw = 25; % Intake water temp (C)
Td = 62; % Condensed water temp (C)
Ts = Td + 6; % Compressed vapor temp (C)
Tb = Td-2; % Evaporation temperature (C)
Xf = 42000; % Feed water salinity in ppm
Xb = 70000; % Salinity of rejected brine in ppm
Eff = .589; % Compressor efficiency
```

```
Gam = 1.32; % Compression ratio

Mf = Md*(Xb/(Xb-Xf))
Mb = Mf-Md
Lam_d = 2499.5698-2.204864*Td-2.304e-3*Td
Lam_b = 2499.5698-2.204864*Tb-2.304e-3*Tb

Tf = ((Xb-Xf)/Xb)*((Lam_b-Lam_d)/Cp-(Cpv/Cp)*(Ts-Td))+Tb

To = (Tcw-Tf)+(Xf/Xb)*Tb+((Xb-Xf)/Xb)*Td

Ae = (Md*Lam_d+Md*Cpv*(Ts-Td))/(Ue*(Td-Tb))

LMTDd = ((Td-Tf)-(To-Tcw))/(log((Td-Tf)/(To-Tcw)))
LMTDb = ((Tb-Tf)-(To-Tcw))/(log((Tb-Tf)/(To-Tcw)))

Ad = (Md*Cp*(Td-To))/(Ud*LMTDb)
Ab = (Mb*Cp*(Tb-To))/(Ub*LMTDb)

Po =10.17246-0.6167302*Ts+1.832249e-2*Ts^2-1.77373e-4*Ts^3+1.47068e-6*Ts^4
Pi =10.17246-0.6167302*Tb+1.832249e-2*Tb^2-1.77373e-4*Tb^3+1.47068e-6*Tb^4

Vi =163.3453-8.04142*Tb+0.17102*Tb^2-1.87812e-3*Tb^3+1.03842e-5*Tb^4-2.28215e-8*Tb^5

% W is supposed to be in kWh/m^3 but I can't get the units to work yet.
W = (Gam/((Gam-1)))*(Pi*Vi)*((Po/Pi)^((Gam-1)/Gam)-1)*(1000/3600);
CompSize = W*Size/24

% Indices for adjusting the listed price from 2001 to 2010. From the
% Chemical Engineering Index.

CEPCI2001 = 397; % CEPCI price index for Sept 2001
CEPCI2010 = 550.8; % 2010 from Chemical Engineering April 2011

% Costs for the major components in the system
% A centrifugal compressor is assumed
% Ulrich indicates that for seawater either nickel or titanium can be used
% From Turton Figure A.19:

F_BM_Comp = 11.5; % Nickel
K1C = 2.2897;
K2C = 1.3604;
K3C = -0.1027;
BareComp = ChemCost(K1C,K2C,K3C,CompSize/Eff)*(CEPCI2010/CEPCI2001);
ActComp = BareComp*F_BM_Comp;
% The power required for the compressor driver is CpComp and the power
% required of the compressor (fluid power) is CompSize*Eff.

% The compressor driver selection followed the methodology from
% "Compressors: Selection and Sizing" by Royce Brown. Pg 315 for enclosure
% selection
% A open/drip proof driver was selected
F_BM_Drv = 1.5;
K1D = 2.9508;
K2D = 1.0688;
K3D = -0.1315;
```

```
BareDrive = ChemCost(K1D,K2D,K3D,CompSize)*(CEPCI2010/CEPCI2001);
ActDrive = BareDrive*F_BM_Drv;

% Evaporator
% Data taken from Analysis, Synthesis and Design of Chemical Processes
% Falling Film assumed (Max size is supposed to be 500 m^2 but this is
% neglected for the moment)
% Data also assumed carbon steel construction
% CEPCI = 397 (from Sept 2001)
K1_Ev = 4.642;
K2_Ev = .3698;
K3_Ev = .0025;
F_BM_Ev = 9.5; % Nickel alloy assumed
Num = floor(Ae/500)
Rem = mod(Ae,500);

if(Num == 0)
   BareEvap = ChemCost(K1_Ev,K2_Ev,K3_Ev,Ae)*(CEPCI2010/CEPCI2001);
   ActEvap = BareEvap*F_BM_Ev;
elseif(Rem == 0)
   BareEvap = ChemCost(K1_Ev,K2_Ev,K3_Ev,500)*Num*(CEPCI2010/CEPCI2001);
   ActEvap = BareEvap*F_BM_Ev;
else
   BareEvap = ChemCost(K1_Ev,K2_Ev,K3_Ev,500)*(CEPCI2010/CEPCI2001);
   BareEvapRem = ChemCost(K1_Ev,K2_Ev,K3_Ev,Rem)*(CEPCI2010/CEPCI2001);
   ActEvap = (BareEvap+BareEvapRem)*F_BM_Ev;
end

% For the flat plate heat exchangers
HXK1 = 4.6656;
HXK2 = -0.1557;
HXK3 = 0.1547;

B1 = 0.96;
B2 = 1.21;
Fm = 4.5;
Fp = 1;
F_BM_HX = (B1+B2*Fm*Fp);

NumHX1 = floor(Ad/1000)
RemHX1 = mod(Ad,1000);

if(NumHX1 == 0)
   logCHX1 = HXK1+HXK2*log10(Ad)+HXK3*(log10(Ad))^2;
   BareCpHX1 = (10^logCHX1)*(CEPCI2010/CEPCI2001);
   ActCpHX1 = BareCpHX1*F_BM_HX;
elseif(HX1Rem == 0)
   logCHX1 = HXK1+HXK2*log10(1000)+K3*(log10(1000))^2;
   BareCpHX1 = (10^logCHX1)*NumHX1*(CEPCI2010/CEPCI2001);
   ActCpHX1 = BareCpHX1*F_BM_HX;
else
   logCHX1 = HXK1+HXK2*log10(1000)+HXK3*(log10(1000))^2;
   logCHX1Rem = HXK1+HXK2*log10(RemHX1)+HXK3*(log10(RemHX1))^2;
   BareCpHX1 = ((10^logCHX1)*NumHX1+10^(logCHX1Rem))*(CEPCI2010/CEPCI2001);
   ActCpHX1 = BareCpHX1*F_BM_HX;
end
```

```
NumHX2 = floor(Ab/1000);
RemHX2 = mod(Ab,1000);

if(NumHX2 == 0)
   logCHX2 = HXK1+HXK2*log10(Ab)+HXK3*(log10(Ab))^2;
   BareCpHX2 = (10^logCHX2)*(CEPCI2010/CEPCI2001);
   ActCpHX2 = BareCpHX2*F_BM_HX;
elseif(RemHX2 == 0)
   logCHX2 = HXK1+HXK2*log10(1000)+HXK3*(log10(1000))^2;
   BareCpHX2 = (10^logCHX2)*NumHX2*(CEPCI2010/CEPCI2001);
   ActCpHX2 = BareCpHX2*F_BM_HX;
else
   logCHX2 = HXK1+HXK2*log10(1000)+HXK3*(log10(1000))^2;
   logCHX2Rem = HXK1+HXK2*log10(RemHX2)+HXK3*(log10(RemHX2))^2;
   BareCpHX2 = ((10^logCHX2)*NumHX2+10^(logCHX2Rem))*(CEPCI2010/CEPCI2001);
   ActCpHX2 = BareCpHX2*F_BM_HX;
end

BareCost = BareComp + BareDrive + BareEvap + BareCpHX1 + BareCpHX2;
ActCost = ActComp + ActDrive + ActEvap + ActCpHX1 + ActCpHX2;

ContFee = 1.18*ActCost;
GrassRts = 0.5*BareCost + ContFee;
%}

CEPCI2001 = 397; % CEPCI price index for Sept 2001
CEPCI2010 = 550.8; % 2010 from Chemical Engineering April 2011
% Labor rate from http://www.bls.gov/oes/current/naics4_325100.htm for a
% Basic Chemical Manufacturing worker
Rate = 28.32; % $2010/hr

% The number of processing steps is 2: compression and heat exchange.
Steps = 2;

% Timestep is 365 days

Days = 365;

LaborCosts = Labor(Size,Steps,Rate,Days);

%%%%%%%%%%%%
% Raw materials section

% From "Evaluating the Economics of Desalination" by Ettouney et al.
% The following are chemicals for desalination: sulfuric acid, Caustic
% Soda, Antiscalant, Chlorine.
RawMatl = (0.0122 + 0.0098 + 0.0095 + 0.00193)*Size*Days*...
   (CEPCI2010/CEPCI2001);

% Total cost for entire fluid processing plant.
% Lang factor for a Fluid Processing Plant is from pg 192 of the "Analysis,
% synthesis and design of chemical processes"
% Lang = 4.74;

% TotalCap = Lang*(CapComp+CapDrive+CapEvap+CapHX1+CapHX2);
```

```
% Total cost for the two flat plate heat exchangers is the sum of CapHX1BM
% and CapHX2BM

%{
Tcw = 20; % Temperature of intake seawater (C)
Td = 80; % Temperature of distillate (C)
Tb = 40; % Temperature of Brine (C)

eff = .5; % Efficiency of the vapor compressor
Deo = 0.01587; % Equivalent outer diameter of plate preheater, m
Dei = Deo - 0.7e-3; % Equivalent inner diameter of plate preheater, m from "Plastic/compact heat
exchangers for single-effect desalination systems"
Rfe = 0.1; % Fouling resistance, m2C/kW of evaporator
kwe = 0.042; % thermal conductivity (kW/mC)
delbp = 0.005; % Thickness of brine demister tube
deldp =  .2; % Thickness of distillate demister
kwb = 0.042; % thermal conductivity (kW/mC)
kwd = 0.042; % thermal conductivity (kW/mC)
Rfb = 0.1; % Fouling resistance, m2C/kW of Brine preheater
Rfd = 0.1; % Fouling resistance, m2C/kW of distillate preheater
Le = 5; % Evaporator length
vp = 5; % Demister velocity (m/s)
PT = 1.3; % Tube pitch
effvl = 0.9;  % Venting line efficiency
xvl = 0.02; % Mass fraction of venting line

Dor = 0.05; % Venting orifice diameter (m) from Design of single-effect mechanical vapor compression
Dvl = 0.1; % Venting line diameter (m) from Design of single-effect mechanical vapor compression

xm = % Salt fraction
% The following three values are from "Plastic/compact heat exchangers for
% single-effect desalination systems"

wbp = 0.5;  % Width of plate for brine preheater (m)
dbp = 0.003; % Plate spacing of brine preheater (m)
wdp = 0.7e-3; % Width of plate for distillate preheater (m)
rhop =
Lp = % Demister length
T = 25;

X = 35000E-6; % Salt mass fraction
S = 35; % Water salinity in g/kg

Bb = 10^-3*(6.71+T*6.34E-2+T^2*9.74e-5);
Cc = 10^-8*(22.238+T*9.59e-3+T^2*9.42E-2);
% Boiling point elevation
BPE = X*(Bb+Cc*X)*10^-3;

A = 4206.8 - 6.6197*S + 1.2288e-2*S^2;
B = -1.1262 + 5.4178e-2*S-2.2719e-4*S^2;
C = 1.2026e-2-5.3566e-4*S+1.8906E-6*S^2;
D = 6.8777e-7+1.1517e-6*S-4.4268e-9*S^2;

Cp = (A+B*T+C*T^2+D*T^3)*10^-3;
Lamv = 2501.897149-2.407064037*T + 1.192217*10^-3*T^2-1.5863*10^-5*T^3;
```

```
Mf = Md + Mb;
Mb = Mf*Xf/Xb;



Tb = Tv+BPE;
Md =
A = (Md*Lamv+Mf*Cp*(Tb-Tf))/(Ue*(Ts-Tb));

Ue = 1.9695+(1.2057E-2)*Tb-8.5989E-5*Tb^2+2.565E-7*Tb^3; % From Al-Juwayhel et al (1997)
%}
```

A.27 Synthesis Loop Cost

```
function [BareCost ActCost ContFee GrassRts LaborCost RawMatl ActCompCost ActDrvCost ActHXCost
ActReactCost ActFlashCost ActPumpCost] = SynCost2(T,P,Size)


% Size is in metric tons per day.
% Usage is [BareCost ActCost ContFee GrassRts LaborCost RawMatl] =
% SynCost2(Size)
% BareModuleCost is the installed cost
% CEPCI = 397

% The compression required for the plant.
% [TotRePwr TotSynPwr CoolPwr TotPwr] = CompPwr(Size);
[TotSynPwr FluidWork Stages TotRePwr HeatOut Cooling HXArea1 HXArea2 HXArea3 HXArea4
HXArea_int] = CompPwr2(P,Size);

% This index takes the costs from 2001 to any other reasonable CEPCI index
% (usually +/- 15 years)
CEPCI = 397; % from 2001
Idx = 550.8; % 2010 from Chemical Engineering April 2011

% Compressors: 450-3000kW
K1Comp = 2.2897;
K2Comp = 1.3604;
K3Comp = -0.1027;

% Electric Drivers: Totally enclosed 75-2600kW
K1Drv = 1.956;
K2Drv = 1.7142;
K3Drv = -0.2282;
% Electric drivers are 90% efficient (Ulrich, pg 87)
% Also assume compressors are 70% efficient converting shaft power to fluid
% power.

% The bare module factor for the compressors is from the corrosion guide on
% pages 254-255 in Ulrich and from Table A6, figure A.19 and Table A5 in
% Turton, et alli
% The bare module factor for the drives is from the tables and figures in
% Turton et alli
FBM_C = 5.8;
FBM_D = 1.5;
```

```
% Bare Module Cost has the index for the inflation but no pressure or
% material costs associated with the equipment.
if FluidWork/(1000*Stages)> 3000
   NumMaxC = floor((FluidWork)/(3000));
   SmallC = rem(FluidWork,3000);
   Comp1_Cost = NumMaxC*ChemCost(K1Comp,K2Comp,K3Comp,3000)...
      + ChemCost(K1Comp,K2Comp,K3Comp,SmallC);
else
Comp1_Cost = Stages * ChemCost(K1Comp,K2Comp,K3Comp,FluidWork/(Stages));
end
Comp2_Cost = ChemCost(K1Comp,K2Comp,K3Comp,(TotRePwr*0.7*0.95)/(1000));

BareCompCost = (Idx/CEPCI)*(Comp1_Cost + Comp2_Cost);
A = (Idx/CEPCI)*Comp1_Cost*FBM_C/Stages;
B = (Idx/CEPCI)*Comp2_Cost*FBM_C;
ActCompCost = BareCompCost*FBM_C;

%%%%%%%%%%%%%%%%%%%%%%%%%%%%%
%%% Drivers for compressors

Drv1_Cost = Stages*ChemCost(K1Drv,K2Drv,K3Drv,TotSynPwr/(Stages*1000));
Drv2_Cost = ChemCost(K1Drv,K2Drv,K3Drv,TotRePwr/(1000));
BareDrvCost = (Idx/CEPCI)*(Drv1_Cost + Drv2_Cost);
ActDrvCost = BareDrvCost*FBM_D;

%%%%%%%%%%%%%%%%%%%%%%%%%%%%%
% Major heat exchangers
% From 1250 TPD Ammonia Plant Equipment (International Process Plants)
% From 10-1000m^2


% Heat exchanger constants from Turton, et al. page 927. Floating head heat
% exchangers are assumed.

K1HX = 4.8306;
K2HX = -0.8509;
K3HX = 0.3187;

% Returns the heat exchanger areas in square meters

% The four major heat exchangers for an ammonia synloop;
HX1Cost = ChemCost(K1HX,K2HX,K3HX,HXArea1);
HX2Cost = ChemCost(K1HX,K2HX,K3HX,HXArea2);
HX3Cost = ChemCost(K1HX,K2HX,K3HX,HXArea3);
HX4Cost = ChemCost(K1HX,K2HX,K3HX,HXArea4);
HXintCost = ChemCost(K1HX,K2HX,K3HX,HXArea_int);

FM_HX = 2.75; %From Turton et al. Figure A.18; Table A.3

%% Equation A.3 in Turton et al. The 150 is the operating pressure in bar
C1 = 0.03881;
C2 = -0.11272;
C3 = 0.08183;
Fp = C1 + C2*log10(P) + C3*log10(P)^2;
Fp_HX = 10^Fp;
% From Table A.4: Bare module factor constants
```

```
B1 = 1.63;
B2 = 1.66;
FBM_HX = (B1 + B2*Fp_HX*FM_HX);

% The final price of the heat exchangers in 2010 dollars.
% Bare module cost - see page 197 of Turton.For a HX the bare module factor
% is when FP = 1 and FM = 1
BareHXCost = (HX1Cost+HX2Cost+HX3Cost+HX4Cost+HXintCost)*(Idx/CEPCI)*(B1 + B2);

ActHXCost = BareHXCost*FBM_HX;

%%%%%%%%%%%%%%%%%
% Reactor and Flash section
% %%%%%%%%%%%%%%%%%

% Data is from Chemical Reactor Analysis and Design by Bischoff page 510
P_op = P; % Operating pressure in bar
c = 0.25; % The mass fraction of NH3 in the feed
rho = 2.65; % Bulk density of catalyst in kg/L

[r CatMass React_Vol SV Length_R D_react] = ReactorVol(T,P,c,rho,Size);
K1RV = 3.4974;
K2RV = 0.4485;
K3RV = 0.1074;

% From table A.4 in Turton et al.
B1_t = 2.25;
B2_t = 1.82;

React_Cost = ChemCost(K1RV,K2RV,K3RV,React_Vol);

% From Turton, page 200 (modified for simplicity)
Fp_react = (((P_op+1)*D_react)/(2*(850-0.6*(P_op+1)))+0.00315)/0.0063;
FM_M = 3.1; % For a reactor made of stainless steel. From Turton, Fig A 18

FBM_RX = (B1_t +B2_t*Fp_react*FM_M);
BareReactCost = React_Cost*(Idx/CEPCI)*(B1_t +B2_t);
ActReactCost = BareReactCost*FBM_RX;

%%%% Flash vessel section
% The actual liquid product from the vessel is used to size it. The liquid
% product is ammonia.

% "ammonia-c.pdf" (a design project from UWV) use: 10 minute residence time
% and the vessel is doubled in size to allow for expansion. Finally, assume
% that it is vertical.

[WaterReqdVol VN2h VH2h] = AmmoniaEnergy(Size);

rho_nh3 = 682; % density of ammonia as a liquid (kg/m^3)

FlashVol = 2*(Size*1000)/(rho_nh3*24*6);
AR_Flash = 4;

K1_f = 3.4974;
K2_f = 0.4485;
```

```
K3_f = 0.1074;

Flash_Cost = ChemCost(K1_f,K2_f,K3_f,FlashVol);
BareFlashCost = (Idx/CEPCI)*Flash_Cost*(B1_t +B2_t);
ActFlashCost = BareFlashCost*FBM_RX;

% Using the same pressure and material factors for this and the reactor.

%%%%%%%%%%%%%%%%%%%
% Pump Section
% Assume one water pump. The cooling water was calculated based on the heat
% flows in the plant
% From "Control structure design..." which uses a 1650 MTD plant
P_Flow1 = Cooling/1000; % Originally in kg/min, converted to m^3/min

%% Efficiency
Eff_P = 0.85; % Assume a reciprocating pump

% Pressure drop (bar)
P_drop = 6;

% The heuristics of pumps (page 379, Table 11.9 of Turton et al.)
% These calculate the power requirement in kW
P_Pwr1 = 1.67*P_Flow1*P_drop/Eff_P;

K1_p = 3.8696;
K2_p = 0.3161;
K3_p = 0.1220;

FM_p = 1.5; % Materials factor for pumps
FP_p = 1; % Pressure less than 10 bar so all constants are 0
B1_p = 1.89; % From table A.4 in Turton
B2_p = 1.35;

Pump1_Cost = ChemCost(K1_p,K2_p,K3_p,P_Pwr1);

BarePumpCost = (Pump1_Cost)*(Idx/CEPCI)*(B1_p+B2_p);
ActPumpCost = BarePumpCost*(B1_p+B2_p*FM_p*FP_p);


BareCost = BareCompCost+BareDrvCost+BareHXCost+BareReactCost+...
   BarePumpCost+BareFlashCost;

ActCost = ActCompCost+ActDrvCost+ActHXCost+ActReactCost+...
   ActPumpCost+ActFlashCost;

ContFee = 1.18*ActCost;
GrassRts = 0.5*BareCost + ContFee;

% O&M Section of the module
Days = 365;

% Labor rate from http://www.bls.gov/oes/current/naics4_325100.htm for a
% Basic Chemical Manufacturing worker
Rate = 28.32; % $2010/hr
```

```
% Process steps: compression, reaction, refrigeration
P_step = 3;

LaborCost = Labor(Size,P_step,Rate,Days);

RawMatl = 0;

% Fractions for each of the equipment sections

ActCompCost/ActCost;
ActDrvCost/ActCost;
ActHXCost/ActCost;
ActReactCost/ActCost;
ActFlashCost/ActCost;
ActPumpCost/ActCost;
%{
A Vector for Excel

Vec = ['Compressor1' ChemCost(K1Comp,K2Comp,K3Comp,TotSynPwr/(0.75*Stages*1000));
'Compressor2' ChemCost(K1Comp,K2Comp,K3Comp,TotRePwr/(0.75*1000))]
%}
```

A.28 Reactor Volume Calculation

```
function [r Cat Vol SV Z2 D] = ReactorVol(T,p,c,rho,Size)

% Cat is the mass of the catalyst in kg
% Vol is the volume of the catalyst in m^3
% SV is the space velocity in m^3 feed / m^3 catalyst / hour
% Z2 is the length of the reactor
% D is the diameter of the reactor
% T - temperature [C]
% p is the pressure in bar
% c - mass fraction NH3 [-] Generally about 0.25, from the Aspen output
% rho is the catalyst bulk density (about 2.65 kg/L)
% Size is the plant size in metric tons/day
% Tempkin-Pyzhev kinetics; see Froment and Bischoff p. 511
% Assumes no inerts and stochiometric mixtures of N2 and H2

% This file is based on Skogestad which is available on the web:

% http://www.nt.ntnu.no/users/skoge/ammonia/

% The conditions that I have chosen for the dissertation:
%{

T = 755K = 482C
p = 150 bar
c = 0.25
rho = 2.65
Size = 300 t/d

%}

%%%% WARNING %%%%
```

```
% This is sensitive to the temperature used. For example, using the data
% and results in Froment and Bischoff pgs 510-511 calculates the catalyst
% volume to be low. Using the average temperature in the reactor (330C)
% gives a reasonable result. The top temperature gives the wrong result.
% A temperature of 250C gives an imaginary result!!

mNH3=c;  % mass fraction ammonia
mH2=(1-c)*6/34;
mN2=(1-c)*28/34;
nNH3=mNH3/17;
nH2=mH2/2;
nN2=mN2/28;
x=nNH3/(nNH3+nH2+nN2)*1;  % mole fraction ammonia
xH2 = nH2/(nNH3+nH2+nN2)*1; % mole fraction H2
xN2 = nN2/(nNH3+nH2+nN2)*1; % mole fraction N2

MWt = x*17 + xH2*2.008 + xN2*28;

R=8.31;
k1=1.79e+4*exp(-87090/(R*(T+273)));
k2=2.57e+16*exp(-198464/(R*(T+273)));
pnh3=x*p ;     % partial pressure (bar)
pn=(1-x)*0.25*p;
ph=(1-x)*0.75*p;
rN2=k1*pn*ph^1.5/pnh3 - k2*pnh3/ph^1.5;  % [kmol N2/ m3 cat, h]
rNH3 = rN2*2*17/(1000*3600*rho);        % [kg NH3/ kg cat, s]
r=4.75*rNH3;  % Multiply by 4.75 to match industrial instability

NH3_flow = Size*1000/(24*3600); % Required NH3 product (kg/s)

Cat = NH3_flow/r; % The mass of catalyst (kg)

Vol = Cat/(rho*1000); % The volume in cubic meters

ReactorVol = Vol/0.7; % The effectiveness factor used in Rase, page 72

% Using the design procedure on page 77 of Rase we have:
% delP2/delP1 = (Z2/Z1)^2.85*(SV2/SV1)^1.85*(P1/P2)(T1/T2)
% where all terms refer to the
% chart: Z1 = 7m; T1 = 450C; P1 = 271 atm; M2/M1 = 1;

% The space velocity calculation is straightforward: PV = nRT
R_SV = 8.314e-5;
T_SV = 293;
P_SV = 1;

% space velocity in m^3 of feed per m^3 of catalyst per hour
% Note that the denominator contains a 0.15 factor because the catalyst
% sees the recycle stream, not the feed stream. I'm assuming a conversion
% of 14%.

SV = 3600*(NH3_flow*mNH3*(1000/17)*R_SV*T_SV/P_SV +
NH3_flow*mH2*(1000/2.016)*R_SV*T_SV/P_SV...
   + NH3_flow*mN2*(1000/28)*R_SV*T_SV/P_SV)/(ReactorVol*0.14);
```

```
% Assume a particle size of 6-10 mm
% Then we have a matrix of pairs from the chart (also in Appl)
Space_V = [15000 20000 25000 30000];
Pressure_D = [1 1.7 2.6 3.55];

delP1 = interp1(Space_V,Pressure_D,SV,'linear','extrap');

delP2 = p*0.02; % Assumed pressure drop through the entire reactor = 2%

Z1 = 7; % From chart (m)
T1 = 450+273; % Also from chart (K)
P1 = 271; % Atm, from chart
M1 = 11.16; % Molecular weight of the mixture used in 225 atm bed 2 in Rase
% Now solve for Z2 and D:

Z2 = Z1*(delP2/delP1*(p/P1)*(T1/(T+273))*(M1/MWt)^0.85)^(1/2.85);
D = (ReactorVol*4/(Z2*pi))^0.5;
```

A.29 Storage Cost

```
function [BareCost ActCost ContFee GrassRts] = StorageCost(Size)

% Compare this value to page 200, Figure 7.2
% Fertilizer Manual By United Nations Industrial Development Organization,
% Int'l Fertilizer Development Center

CEPCI1990 = 356; % From Peters Timmerhaus
CEPCI2001 = 397; % 2001 from Turton
CEPCI2003 = 402; % From Crouper et al.
Idx = 550.8; % CEPCI for 2010

rho = 0.682; % Density of liquid ammonia (tons/m^3)
% From Walas: storage is 30 day capacity
Days = 30;
TotalStorage = Days*Size; % Total storage in tons
Volume = TotalStorage/rho % Total storage capacity in cubic meters
Gallons = Volume*264.17; % most storage vessels are rated in gallons
% Tanks = 2; % The ammonia tank is actually two tanks (double containment)



% Heat transfer section %
% See the book Foamglas Industrial Insulation Handbook By Pittsburgh Corning
% Page 82 has actual heat loss values!
% For tank specifications see:
% http://www.mannvit.com/Industry/AmmoniaStorage/
% 5000 t tank: H = 18.5; D = 24.8; Roof is a sphere shaped dome with a
% radius of 24.8m
%{
5000 t atmospheric ammonia storage tank in Sweden

Owner:  Akzo Nobel
The project included a complete new ammonia terminal and included new
refrigerated ammonia storage tank, refrigerating system, ship unloading
facilities, pumping and heating system for the ammonia from the tank. The
```

```
tank was commissioned in 1997 and is in operation without problems. The
project was completed in 19 months.
Tank details:  The ammonia storage tank is of the refrigerated atmospheric
type, with a nominal capacity of 5000 tons. The tank has 18.5 m high
sidewall and a diameter of 24.8 m. The roof is a sphere shaped dome with a
radius of 24.8 m. The foundation is built on elevated concrete walls so
that free air can circulate under the tank bottom, thus avoiding a heating
system. The tank is double integrity, with a single steel wall built into
rock, where the rock and concrete wall form the outer tank. The tank is
standing in a rock bund of nominal diameter of 30 m. To even out the
difference in the level on the top of the rock bund, concrete walls were
built. The opening into the rock bund used during construction was closed
with a concrete wall when the construction was finished, prior to
commissioning of the tank. The sidewall and the bottom of the tank are
insulated on the outside, but the roof insulation is suspended from the
tank roof.  The water vapor barrier is especially import to prevent damages
to the insulation due to ice build-up.
The design pressure is 140 mbar and the operating pressure is in the range
of 40-70 mbar. The design temperature is minus 40C and the operating
temperature is in the range of minus 32-33C.
%}
H_D = 18.5/24.8; % An aspect ratio of about 0.75
D = (16/(3*pi)*Volume)^(1/3);
H = D*H_D;

Surface = H*D*pi + 2*pi*(D/2)^2; % Ignore the domed roof
U = 0.32; % W/m^2K from Foamglass book
delT = (10+33); % Also from foamglass book. The ammonia is at -33C and ambient temp is 10C;

% From Boil off in Refrigerated Ammonia Tanks 92% goes into the ammonia,
% but assume 100%
Q = U*Surface*delT;

TonsRef = (Q/1000)*0.28435; % Convert to tons of refrigeration

EvapTemp = 0; % Temperature of the evaporator


H_vap = 1370; % Heat of vaporization in J/g at -33C

NH3_Evap = Q*3600*24/(1e6*H_vap); % The total daily energy transfer (3600s
% 24 hours, divided by the heat of vaporization times one million g/ton)

Boil_Off = 100*NH3_Evap/TotalStorage

NH3Loop = NH3_Evap*1000/(24*3600) % The flow rate of ammonia in kg/s

DrumSize = NH3Loop*10*60/(rho*1000); % 10 minutes of holding time.

% The thermodynamic states for calculation
n = 1.4;
N = 2;
T1 = 240; % Temp in K. This is the boiling point
P1 = 1; % The pressure in bar

P2 = 3;
```

```
T2 = T1*(P2/P1)^((n-1)/n);

T3 = 293; % From Aspen Plus analysis
P3 = P2;

P4 = 12.7;
T4 = T3*(P4/P3)^((n-1)/n);

T5 = 284;
P5 = P4;

P6 = 3.55;
T6 = 268;

% Constants from Turton for use with fixed roof storage tanks

K1t = 4.8509;
K2t = -0.3973;
K3t = 0.1445;
% From Ammonia Storage: Selection and Safety Issues, Lele, page 88 the
% outer tank is 1-2 meters away from the inner cup. Take 1.5m and multiply
% by two and add it to the diameter of the inner cup.
D_outer = D+3;
Vol_outer = D_outer^2*pi/4*H;

BareTankCost = ChemCost(K1t,K2t,K3t,Volume)*(Idx/CEPCI2001)+...
   ChemCost(K1t,K2t,K3t,Vol_outer)*(Idx/CEPCI2001);

P_fac = 1;
FBM = 4.5; % Materials factor from Ulrich, page 316, figure 5-61
ActTankCost = BareTankCost*FBM;

%%%%%%%
% Compressor Section

% Compressors: 450-3000kW
K1Comp = 2.2897;
K2Comp = 1.3604;
K3Comp = -0.1027;

% Electric Drivers: Totally enclosed 75-2600kW
K1Drv = 1.956;
K2Drv = 1.7142;
K3Drv = -0.2282;
% Electric drivers are 90% efficient (Ulrich, pg 87)
% Also assume compressors are 70% efficient converting shaft power to fluid
% power.

% The bare module factor for the compressors is from the corrosion guide on
% pages 254-255 in Ulrich and from Table A6, figure A.19 and Table A5 in
% Turton, et alli
% The bare module factor for the drives is from the tables and figures in
% Turton et alli
FBM_C = 5.8;
FBM_D = 1.5;
```

```
% Bare Module Cost has the index for the inflation but no pressure or
% material costs associated with the equipment.
RNH3 = 0.4882; % Specific gas constant for ammonia (kJ/kgK)
NumComp = 1;
% Worst case scenario for compression
CompWorkNH3_1 = T1*n/(n-1)*RNH3*NH3Loop*((P2/P1)^((n-1)/n)-1)
Comp1_Cost = ChemCost(K1Comp,K2Comp,K3Comp,CompWorkNH3_1)
CompWorkNH3_2 = T3*n/(n-1)*RNH3*NH3Loop*((P4/P3)^((n-1)/n)-1)
Comp2_Cost = ChemCost(K1Comp,K2Comp,K3Comp,CompWorkNH3_2)
BareCompCost = (Idx/CEPCI2001)*(Comp1_Cost+Comp2_Cost)

ActCompCost = BareCompCost*FBM_C

%%%%%%%%%%%%%%%%%%%%%%%%%%%%
%%% Drivers for compressors

Drv1_Cost = ChemCost(K1Drv,K2Drv,K3Drv,CompWorkNH3_1/(0.75*0.9));
Drv2_Cost = ChemCost(K1Drv,K2Drv,K3Drv,CompWorkNH3_2/(0.75*0.9));
BareDrvCost = (Idx/CEPCI2001)*(Drv1_Cost+Drv2_Cost);

ActDrvCost = BareDrvCost*FBM_D;

%%%%%%%%%%%%%%%%%%%%%%%%%%%%
%%% Condenser (assume air cooled b/c of picture in Webb)
K1Ev = 4.0336;
K2Ev = 0.2341;
K3Ev = 0.0497;

U = 15; % From Crouper, pg 187 converted from [Btu/(hr)(ft2)(F) to (W/m2K)

% The following is from Crouper, pages 189-90. It is assumed
% that the evaporator area increases linearly with the flow rate.
% Using approach temp of 442K and a cooling range of 442-284K the specific
% area is found to be 40 sq ft/[Btu/(hr)(F)]
Area = 40*.093; % Converted to sq m
CondArea = Area*(Size/300);
BaseCondCost = ChemCost(K1Ev,K2Ev,K3Ev,CondArea)*(Idx/CEPCI2001);

% Condensers are designed for 17 barg pressure
PEv = 17;
C1Ev = 0.1578;
C2Ev = -0.2992;
C3Ev = 0.1413;
Fp = C1Ev + C2Ev*log10(PEv) + C3Ev*log10(PEv)^2;
Fp_Ev = 10^Fp
ActCondCost = BaseCondCost*Fp_Ev;

BareCost = BareTankCost + BareCompCost + BareDrvCost + BaseCondCost;

ActCost = ActTankCost + ActCompCost + ActDrvCost + ActCondCost;

ContFee = 1.25*ActCost; % Normally at 18%, I'm increasing it to 25 due to insulation
% Timmerhaus et al. page 172;
GrassRts = 0.5*BareCost + ContFee;
```

A.30 NPV Cost Calculation

```
function npv = NPVCosts(totalcost,d_pay,interest,inflate,discount,life,loan_life,O_M)

% Usage:
% npv = NPVCosts(totalcost,d_pay,interest,inflate,discount,life,loan_life,O_Mfrac)
% total cost in $
% d_pay as a fraction of the total costs paid up front (year 0)
% interest on loan (0-1)
% inflation (0-1)
% discount rate (0-1)
% life is the project lifetime in years
% loan_life is the time of the loan in years
% O_M is paid per year in O&M costs

down_pay = totalcost*d_pay;
loan = totalcost-down_pay;
CRF = interest/(1-(1+interest)^-loan_life);

Ap = CRF*loan;
k_ap = 1/(1+discount);

NPV_loan = Ap*(k_ap-k_ap^(loan_life+1))/(1-k_ap);

k_OM = (1+inflate)/(1+discount);

if k_OM == 1
   NPV_OM = O_M*life;
else
   NPV_OM = O_M*(k_OM-k_OM^(1+life))/(1-k_OM);
end

npv = NPV_OM + NPV_loan + down_pay;
```

A.31 Labor Rate Calculation

```
function LaborCost = Labor(Size,Steps,Cost,Time)

% Based on PLANT DESIGN AND ECONOMICS FOR CHEMICAL ENGINEERS 2/e , page 198
% Usage: LaborCost = Labor(Size,Steps,Cost,Time) where
% Size is in tons/day; steps is the number of operating steps, defined as "
% any unit operation, unit process, or combination thereof, which takes
% place in one or more units of integrated equipment on a repetitive cycle
% or continuously (page 200); cost is in $/hr of labor; Time is in days
%
% For electrolyzers, use curve A. Ulrich suggests that the CEPCI can be
% used for labor as well
% This function returns the total labor - which inludes clerical and
% supervisory - for the given time frame ($2010).

CEPCI1990 = 356;
CEPCI2010 = 550.8;

% Timmerhaus et alli page 188
NE_Labor_Rt = 1.14; % Relative labor rate for New England
Prod_fac = 0.95; % Productivity factor
```

```
% The equation is of the form y = x^m + 10^b;

% From the graph, b = 1.0764, m = 0.2236;

b = 1.0764;
m = 0.2236;

OpLabor = Size^m + 10^b; % units of employee op hours/day/operating step

% The factor of 1.15 below accounts for clerical and supervisor labor
LaborCost = 1.15*Cost*OpLabor*Steps*NE_Labor_Rt*Time*...
   (CEPCI1990/CEPCI2010)/Prod_fac;
```

A.32 Cost Curve Fit Function

```
function Cost = ChemCost(K1,K2,K3,Size);

C = K1 + K2.*log10(Size) + K3.*log10(Size).^2;
Cost = 10.^C;
```

REFERENCES

[1] Appl M. Ammonia. Ullmann's Agrochemicals. Weinheim: Wiley-VCH Verlag GmbH & Co.; 2007. p. 143-297.

[2] Kelly TD, Matos GR. Historical Statistics for Mineral and Material Commodities in the United States. In: U.S. Geological Survey, editor. Washington, D.C.: U.S. Geological Survey; 2010.

[3] Kramer DA, "Mineral Commodity Profiles - Nitrogen," U.S. DEPARTMENT OF THE INTERIOR. Report: 2004-1290, 2004.

[4] U.S. Census Bureau. (Accessed: 2/17/2010, 2010). *US & World Population Clock*. Available: http://www.census.gov/main/www/popclock.html

[5] United Nations, "WORLD POPULATION TO 2300," United Nations, Department of Economic and Social Affairs, Population Division, New York. Report: ST/ESA/SER.A/236, 2004.

[6] Energy Information Administration, "Annual Energy Outlook 2009 with Projections to 2030," U.S. Department of Energy, Washington, DC. Report: DOE/EIA-0383(2009), 2009.

[7] Da Rosa AV. Fundamentals of Renewable Energy Processes. 1st ed. Boston: Elsevier Academic Press; 2005.

[8] Grundt T, Christiansen K. Hydrogen by water electrolysis as basis for small scale ammonia production. A comparison with hydrocarbon based technologies. International Journal of Hydrogen Energy. 1982;Vol. 7:247-57.

[9] Christiansen K, Andreassen K, Midjo M, "Industrial Electrolytic Hydrogen Production," presented at the Hydrogen Energy Progress V: proceedings of the 5th World Hydrogen Energy Conference, Toronto, Canada, pgs. 715-26. July 15-20, 1984: Pergamon Press

[10] United Nations Industrial Development Organization, International Fertilizer Development Center. Fertilizer Manual. 3rd ed. Norwell, MA: Kluwer Academic Publishers; 1998.

[11] Cornelius W, Huellmantel LW, Mitchell HR, "Ammonia as an engine fuel," presented at the International Automotive Conference, pgs. 300-26. January 11-15, 1965: Society of Automotive Engineers, Inc.

[12] Grimes PG, "Energy Depot Fuel Production and Utilization," presented at the International Automotive Congress, pgs. 281-99. 1965: Society of Automotive Engineers, Inc.

[13] Rosenthal AB, "Energy Depot - A concept for reducing the military supply burden," presented at the International Automotive Conference, pgs. 274-80. January 11-15, 1965: Society of Automotive Engineers

[14] Dubey M, Young F, Hlavin R, Johnson K, "Conversion and Storage of Wind Energy as Nitrogenous Fertilizer," National Science Foundation, Burbank, CA Report: LR 28338, July 1977.

[15] Dubey M, "Conversion and storage of wind energy as nitrogenous fertilizer," presented at the Intersociety Energy Conversion Engineering Conference, Washington, D.C., pgs. 525-32. August 28 - September 2, 1977: American Nuclear Society, Inc.

[16] Dubey M, "Technical and Economic Feasibility of Making Fertilizer from Wind Energy, Water, and Air," presented at the Sun, Mankind's Future Source of Energy, New Delhi, India, pgs. 1812-21. January 16-21, 1978: Pergamon Press

[17] Heronemus WE, "Pollution-Free Energy from Offshore Winds," presented at the 8th Annual Conference and Exposition, Washington, DC, 1972: Marine Technology Society

[18] National Renewable Energy Laboratory. (Accessed: June 5, 2009). *Wind Systems Integration Transmission Planning and Analysis*. Available: http://www.nrel.gov/wind/systemsintegration/capabilities_transmission.html

[19] Zumdahl SS, Zumdahl SA. Chemistry. 6th ed. Boston: Houghton Mifflin Company; 2003.

[20] Reddy KV, Husain A. Modeling and Simulation of an Ammonia Synthesis Loop. Industrial & Engineering Chemistry, Process Design and Development. 1982;Vol. 21:359-67.

[21] Badische Anlin- und Soda-Fabrik. Verfahren zur synthetischen Darstellung von Ammoniak aus den Elementen. In: Kaiserliches Patentamt, editor. http://v3.espacenet.com/publicationDetails/originalDocument?CC=DE&NR=235421C&KC=C&FT=D&date=&DB=EPODOC&locale=en_V3. Prussia: Badische Anlin- und Soda-Fabrik, ; 1908.

[22] Haber DF. Verfahren zur Darstellung von Ammoniak aus den Elementen durch Katalyse unter Druck bei erhohter Temperatur. In: Kaiserliches Patentamt, editor. Prussia: Haber, Fritz; 1909.

[23] Dybkjaer I. Ammonia Production Processes. In: Nielsen A, editor. Ammonia Catalysis and Manufacture. New York: Springer-Verlag; 1995. p. 199-328.

[24] Vancini CA. Synthesis of Ammonia. 1st ed. London: The Macmillan Press; 1971.

[25] Noyes R. Ammonia and Synthesis Gas. 2nd ed. Park Ridge, New Jersey: Noyes Development Corporation; 1967.

[26] Nielsen P, Højlund E. Poisoning of Ammonia Synthesis Catalysts. In: Nielsen A, editor. Ammonia Catalysis and Manufacture. Heidelberg: Springer-Verlag; 1995. p. 191-8.

[27] Cooper CW. Ammonia Synthesis: Commercial Practice. In: Jennings JR, editor. Catalytic ammonia synthesis: fundamentals and practice. New York: Plenum Press; 1991. p. 253-84.

[28] Appl M. Ammonia: Principles and Industrial Practice. 1st ed. New York: Wiley-VCH; 1999.

[29] European Commission, "Reference Document on Best Available Techniques for the Manufacture of Large Volume Inorganic Chemicals - Ammonia, Acids and Fertilisers." Report: 2007.

[30] Jennings JR. Catalytic ammonia synthesis: fundamentals and practice. New York: Plenum Press; 1991.

[31] Eggeman T. Ammonia. In: Kroschwitz JI, Howe-Grant M, editors. Kirk-Othmer Encyclopedia of Chemical Technology: John Wiley and Sons; 2001. p. 678-710.

[32] Borgars DJ. Advances in Ammonia Plant Technology. In: Borgars DJ, editor. Synthesis of Ammonia. London: The Macmillan Press Ltd.; 1971. p. 261-91.

[33] Ruddock J, Short TD, Brudenell K. Energy integration in ammonia production. Energy and the Environment. 2003;Vol. 7:267-76.

[34] Araujo A, Skogestad S. Control structure design for the ammonia synthesis process. Computers and Chemical Engineering. 2008;Vol. 32:2920–32.

[35] Holter E. Feedforward for Stabilization of an Ammonia Synthesis Reactor [Master's]. Trondheim, Norway: Norwegian University of Science and Technology; 2010.

[36] Brian PLT, Baddour RF, Eymery JP. Transient behaviour of an ammonia synthesis reactor. Chemical Engineering Science. 1965;Vol. 20:297-310.

[37] Rafiqul I, Weber C, Lehmann B, Voss A. Energy efficiency improvements in ammonia production—perspectives and uncertainties. Energy. 2005;Vol. 30:2487-504.

[38] Brown F. Small Ammonia Plants. Chemical Engineering World. 1988;Vol. 23:75-7.

[39] Proton Ventures. (Accessed: December 8, 2011). *Proton Ventures*. Available: http://www.protonchemie.com/NFUEL.html

[40] European Fertilizer Manufacturers' Association (EFMA), "Best Available Techniques for Pollution Prevention and Control in the European Fertilizer Industry," Brussells, Belgium. Report: April 2000.

[41] Maxwell GR. Synthetic nitrogen products: a practical guide to the products and processes. 1st ed. New York: Springer; 2004.

[42] Hooper CW. Ammonia Synthesis: Commercial Practice. In: Jennings JR, editor. Catalytic ammonia synthesis: fundamentals and practice. New York: Plenum Press; 1991. p. 253-84.

[43] European Commission, "Draft Reference Document on Best Available Techniques in the Large Volume Inorganic Chemicals, Ammonia, Acids and Fertilisers Industries " Technologies for Sustainable Development, Seville, Spain. Report: 2003.

[44] Randall RJ, Tsui TKN. Ammonia toxicity in fish. Marine Pollution Bulletin. 2002;Vol. 45:17-23.

[45] Miller DC, "Ambient aquatic life water quality criteria for ammonia (saltwater)," U.S. Environmental Protection Agency, Narragansett, RI. Report: EPA 440/5-88-004, 1989.

[46] Major Hazards Assessment Panel. Ammonia toxicity monograph: second report of the Toxicity Working Party. Rugby, UK: Institution of Chemical Engineers; 1988.

[47] U.S. Department of Health EaW, "Criteria for a Recommended Standard: Occupational Exposure to Ammonia," National Institute for Occupational Safety and Health, Washington, DC. Report: 74-136, 1974.

[48] Maxwell GR. Synthetic Nitrogen Products A Practical Guide to the Products and Processes. Boston: Kluwer Academic Publishers; 2005.

[49] 4C Offshore Limited. (Accessed: November 18, 2010). *Global Offshore Wind Farms Database*. Available: http://www.4coffshore.com/offshorewind/

[50] Musial W, Ram B, "Large-Scale Offshore Wind Power in the United States," National Renewable Energy Laboratory, Golden, CO. Report: NREL/TP-500-40745, 2010.

[51] European Wind Energy Association, "Oceans of Opportunity: Harnessing Europe's largest domestic energy resource," European Wind Energy Association, Brussels, Belgium. Report: 2009.

[52] Seelye KQ. Regulators Approve First Offshore Wind Farm in U.S. The New York Times. New York, NY: ; 2010.

[53] Hau E. Wind Turbines: Fundamentals, Technologies, Applications, Economics. 2nd ed. Berlin: Springer-Verlag; 2006.

[54] Manwell JF, McGowan JG, Rogers AL. Wind Energy Explained: Theory, Design and Application. 2nd ed. Hoboken, NJ: John Wiley & Sons Ltd.; 2010.

[55] Grarrad Hassan & Partners, Tractebel Energy Engineering, Risø National Laboratory, Kvaerner Oil & Gas, Energi & Miljoe Undersoegelser, "Offshore Wind Energy Ready to Power a Sustainable Europe," Delft University of Technology, Delft, The Netherlands. Report: 2001.

[56] Schwartz M, Heimiller D, Haymes S, Musial W, "Assessment of Offshore Wind Energy Resources for the United States," National Renewable Energy Laboratory, Golden, CO. Report: NREL/TP-500-45889, 2010.

[57] European Wind Energy Association. (Accessed: June 23, 2010). *Operational offshore wind farms in Europe, end 2009* [Electronic]. Available: http://www.ewea.org/fileadmin/ewea_documents/documents/statistics/OperationalOffshoreFarms2009.pdf

[58] www.offshorewindenergy.org. (Accessed: November 4, 2008). *Offshore Wind Energy - Information for Professionals*. Available: www.offshorewindenergy.org

[59] Talisman Energy Ltd. (Accessed: November 4, 2010). *Beatrice Wind Farm Demonstrator Project - Welcome*. Available: http://www.beatricewind.co.uk/home/

[60] Gardner P, Garrad A, Hansen LF, Jamieson P, Morgan C, Murray F, et al., "Wind energy - the facts: a guide to the technology, economics and future of wind power, Part I - Technology," European Wind Energy Association, Brussels, Belgium. Report: 2009.

[61] Kaiser MJ, Snyder B, "Offshore Wind Energy Installation and Decommissioning Cost Estimation in the U.S. Outer Continental Shelf," U.S. Dept. of the Interior, Bureau of Ocean Energy Management, Regulation and Enforcement, Herndon, VA. Report: TA&R 648, 2010.

[62] 4C Offshore. (Accessed: November 4, 2010). *Hywind Offshore Wind Farm*. Available: http://www.4coffshore.com/windfarms/windfarms.aspx?windfarmId=NO04

[63] Boland G. (Accessed: January 4, 2010). *NOAA Ocean Explorer: Expedition to the Deep Sea*. Available: http://oceanexplorer.noaa.gov/explorations/06mexico/background/oil/oil.html

[64] Ackermann T. Windfarm Power Connection. In: Twidell J, Gaudiosi G, editors. Offshore Wind Power. Brentwood, UK: Multi-Science Publishing Co. Ltd; 2009.

[65] Brakelmann H. Loss determination for long three-phase high-voltage submarine cables. European Transactions on Electrical Power. 2003;Vol. 13:193-7.

[66] Pierik JTG, Pavlovsky M, Bozelie J, Bauer P, de Hann SWH, "DOWEC Electrical System Baseline Design," Energy Research Centre of the Netherlands, Petten, The Netherlands. Report: DOWEC 045 rev. 2, 2002.

[67] Unosson O, "Offshore Cable Installation - Lillgrund," Vattenfall Vindkraft AB, Stockholm, Sweden. Report: 21858-1, January 2009.

[68] Beurskens LWM, de Noord M, "Offshore wind power developments: An overview of realisations and planned projects," Energy Research Center of the Netherlands. Report: ECN-C--03-058, 2003.

[69] Lako P, "Learning and Diffusion for Wind and Solar Power Technologies," Energy Research Center of the Netherlands (ECN), Petten, Netherlands. Report: ECN-C--02-001, April 2002.

[70] 4C Offshore. (Accessed: November 4, 2010). *Irene Vorrink Offshore*. Available: http://www.4coffshore.com/windfarms/irene-vorrink-netherlands-nl28.html

[71] Offshore Center Denmark. (Accessed: November 4, 2010). *Blyth Offshore*. Available: http://www.offshorecenter.dk/offshorewindfarms_detail.asp?id=37094&t=Blyth%20Offshore

[72] Net Resources International. (Accessed: November 4, 2010). *Specifications: Middlegrunden Offshore Wind Farm - Power Technology* Available: http://www.power-technology.com/projects/middelgrunden/specs.html

[73] Net Resources International. (Accessed: November 4, 2010). *Specifications: Horns Rev Offshore Wind Farm, Denmark - Power Technology*. Available: http://www.power-technology.com/projects/hornsreefwind/

[74] Volund P, Pederson PH, Ter-Borsh PE, "165 MW Nysted Offshore Wind Farm: First year of operation - performance as planned," presented at the European Wind Energy Conference, London, UK, 2004:

[75] Danish Energy Agency. (Accessed: November 4, 2010). *Samsø Renewable Energy Island*. Available: http://www.ens.dk/en-US/Info/news/Factsheet/Documents/samsoe170709.pdf%20engelsk.pdf

[76] May J. (Accessed: November 4, 2009). *North Hoyle and Rhyl Flats Offshore Wind Farms: Review of good practice in monitoring, construction and operation*. Available: http://www.snh.org.uk/pdfs/sgp/A303575.pdf

[77] Snyder B, Kaiser MJ. Ecological and economic cost-benefit analysis of offshore wind energy. Renewable Energy. 2009;Vol. 34:1567–78.

[78] Offshore Center Denmark. (Accessed: November 4, 2010). *Setena*. Available: http://www.offshorecenter.dk/offshorewindfarms_detail.asp?id=37021&t=Setana

[79] 4C Offshore. (Accessed: November 4, 2010). *Sakata Offshore Wind Farm*. Available: http://www.4coffshore.com/windfarms/windfarms.aspx?windfarmId=JP04

[80] Barrow Offshore Wind Limited. (Accessed: November 4, 2008). *Barrow Offshore Wind: Key Facts*. Available: http://www.bowind.co.uk/keyfacts.shtml

[81] Offshore Center Danmark. (Accessed: November 4, 2010). *Bohai Suizhong*. Available: http://www.offshorecenter.dk/offshorewindfarms_detail.asp?id=36953&t=Bohai%20Suizhong

[82] Offshore Center Danmark. (Accessed: November 4, 2010). *Lillgrund*. Available: http://www.offshorecenter.dk/offshorewindfarms_detail.asp?id=37057&t=Lillgrund

[83] Net Resources International. (Accessed: November 4, 2010). *Specifications: Burbo Offshore Wind Farm - Power Technology*. Available: http://www.power-technology.com/projects/burbowind/specs.html

[84] C Power NV. (Accessed: November 4, 2010). *C-Power offshore windfarm on the Thornton bank*. Available: http://www.c-power.be/applet_mernu_en/index01_en.htm

[85] Terramare. (Accessed: November 4, 2010). *Project Bulletin: Kemi Ajos 30 MW Offshore Wind Farm*. Available: http://www.terramare.fi/?download=TM_Project_Kemi_Ajos_web.pdf

[86] Centrica Energy Ltd. (Accessed: November 4, 2010). *Lynn & Inner Dowsing Wind Farms Fact Sheet*. Available: http://www.centricaenergy.com/files/pdf/lynn_factsheet.pdf

[87] Net Resources International. (Accessed: November 4, 2010). *Specifications: Lynn and Inner Dowsing Offshore Wind Farms - Power Technology*. Available: http://www.power-technology.com/projects/lynnandinnerdowsing/specs.html

[88] Offshore Center Danmark. (Accessed: November 4, 2010). *Horns Rev II*. Available: http://www.offshorecenter.dk/offshorewindfarms_detail.asp?id=36971&t=Horns%20Rev%20II

[89] 4C Offshore. (Accessed: November 4, 2010). *Alpha Ventus Offshore Wind Farm*. Available: http://www.4coffshore.com/windfarms/alpha-ventus-germany-de01.html

[90] RWE Npower Renewables Limited. (Accessed: November 4, 2010). *RWE Npower Renewables - Rhyl Flats Offshore Wind Farm*. Available: http://www.rwe.com/web/cms/en/310584/rwe-npower-renewables/sites/projects-in-operation/wind/rhyl-flats/summary/

[91] Net Resources International. (Accessed: November 4, 2010). *Robbin Rigg Offshore Wind Farm, United Kingdom*. Available: http://www.power-technology.com/projects/robinriggwind/

[92] Danish Energy Agency. (Accessed: November 4, 2010). *Gunfleet Sands*. Available: http://www.offshorecenter.dk/offshorewindfarms_detail.asp?id=37098&t=Gunfleet%20Sands

[93] Staff Writers. (Accessed: November 4, August 14, 2009). *First German offshore wind farm online*. Available: http://www.winddaily.com/reports/First_German_offshore_wind_farm_online_999.html

[94] 4C Offshore. (Accessed: November 4, 2010). *Donghai Bridge 100 MW offshore wind power demonstration project Offshore Wind Farm*. Available: http://www.4coffshore.com/windfarms/donghai-bridge-100mw-offshore-wind-power-demonstration-project-china-cn01.html

[95] 4C Offshore. (Accessed: November 4, 2010). *Longyuan Rudong Intertidal Demonstration Project Offshore Wind Farm*. Available: http://www.4coffshore.com/windfarms/windfarms.aspx?windfarmId=CN07

[96] 4C Offshore. (Accessed: November 4, 2010). *Xiangshui Intertidal Pilot Project- Shanghai Electric Offshore Wind Farm*. Available: http://www.4coffshore.com/windfarms/xianshui-intertidal-project-china-cn14.html

[97] Net Resources International. (Accessed: November 4, 2010). *Specifications: Rodsand II Windfarm, Denmark - Power Technology*. Available: http://www.power-technology.com/projects/rodsand/specs.html

[98] 4C Offshore. (Accessed: November 4, 2010). *Kamisu Offshore Wind Farm*. Available: http://www.4coffshore.com/windfarms/windfarms.aspx?windfarmId=JP05

[99] 4C Offshore. (Accessed: November 4, 2010). *Dafeng Intertidal Demonstration Offshore Wind Farm*. Available: http://www.4coffshore.com/windfarms/windfarms.aspx?windfarmId=CN29

[100] Ackermann T. Transmission systems for offshore wind farms. In: Ackermann T, editor. Wind power in power systems. Hoboken, NJ: John Wiley and Sons; 2005. p. 479-504.

[101] Dong Energy, Vattenfall, Danish Energy Authority, Danish Forest and Nature Agency, "Danish Offshore Wind: Key Environmental Issues." Report: 2006.

[102] Danish Energy Authority, "Offshore Wind Farms and the Environment: Danish Experiences from Horns Rev and Nysted," Danish Energy Authority, Copenhagen, DK. Report: 2006.

[103] General Electric Company. 1.5sl/1.5s wind turbine. In: General Electric, editor.: http://www.gepower.com/prod_serv/products/wind_turbines/en/downloads/ge_15brochure.pdf; 2003.

[104] Ozkan D. Financial Analysis and Cost Optimization of Offshore Wind Energy under Uncertainty and in Deregulated Power Markets [PhD]. Washington, DC: The George Washington University; 2011.

[105] Vestas Wind Systems. (Accessed: July 15, 2012). *V90-3.0 MW. Offshore. Wind. It means the world to us. | Vestas*. Available: http://www.vestas.com/en/wind-power-plants/procurement/turbine-overview/v90-3.0-mw-offshore.aspx#/vestas-univers

[106] Kusiak A, Zheng H, Song Z. Models for monitoring wind farm power. Renewable Energy. 2009;Vol. 34:583–90.

[107] Sørensen P, Pinson P, Cutululis NA, Madsen H, Jensen LE, Hjerrild J, et al., "Power fluctuations from large wind farms - final report," Risø National Laboratory for Sustainable Energy, Roskilde, Denmark. Report: Risø-R-1711(EN), 2009.

[108] Levitt AC, Kempton W, Smith AP, Musial W, Firestone J. Pricing Offshore Wind Power. Energy Policy. 2011;Vol. 39:6408-21.

[109] Negra NB, Todorovic J, Ackermann T. Loss evaluation of HVAC and HVDC transmission solutions for large offshore wind farms. Electric Power Systems Research. 2006;Vol. 76:916-27.

[110] Fingersh L, Hand M, Laxson A, "Wind Turbine Design Cost and Scaling Model," National Renewable Energy Laboratory, Golden, CO. Report: NREL/TP-500-40566, December 2006.

[111] Norgaard P, Holtinnen H, "A Multi-Turbine Power Curve Approach," presented at the Nordic Wind Power Conference, Chalmers University of Technology, March 1-2, 2004: Nordic Wind Power Conference

[112] Wang C. Modeling and Control of Hybrid Wind/Photovoltaic/Fuel Cell Distributed Generation Systems [PhD]. Bozeman, Montana: Montana State University; 2006.

[113] Turner J, Sverdrup G, Mann MK, Maness P-C, Ben Kroposki, Ghirardi M, et al. Renewable hydrogen production. International Journal of Energy Research. 2008;Vol. 32:379–407.

[114] Ulleberg O. Modeling of advanced alkaline electrolyzers: A system simulation approach. International Journal of Hydrogen Energy. 2003;Vol. 28:21-33.

[115] Miland H. Operational Experience and Control Strategies for a Stand-Alone Power System based on Renewable Energy and Hydrogen [Doktor ingeniør]. Trondheim, Norway: Norwegian University of Science and Technology; 2005.

[116] Ivy J, "Summary of Electrolytic Hydrogen Production," National Renewable Energy Laboratory, Golden, CO. Report: NREL/MP-560-36734, 2004.

[117] Gazey R, Salman S, Aklildhalluin D. A field application experience of integrating hydrogen technology with wind power in a remote island location. Journal of Power Sources. 2006;Vol. 157:841-7.

[118] Sherif S, Barbir F, Veziroglu T. Wind energy and the hydrogen economy-review of the technology. Solar Energy. 2005;Vol. 78:647-60.

[119] Ulleberg O, Nakken T, Ete A. The wind/hydrogen demonstration system at Utsira in Norway: Evaluation of system performance using operational data and updated hydrogen energy system modeling tools. International Journal of Hydrogen Energy. 2010;Vol. 35:1841-52.

[120] Bommaraju TV, Orosz PJ, Sokol EA. (Accessed: April 14, 2007). *Brine Electrolysis*. Available: http://electrochem.cwru.edu/encycl/art-b01-brine.htm

[121] Schmittinger P. Chlorine: principles and industrial practice. Weinheim, Germany: Wiley-VCH Verlag; 2000.

[122] Bommaraju TV, Luke B, O'Brien TF, Blackburn MC. Chlorine. In: Kroschwitz JI, Howe-Grant M, editors. Kirk-Othmer Encyclopedia of Chemical Technology. 4th ed: John Wiley & Sons, Inc.; 2001. p. 130-211.

[123] Kelham S. Chlor-alkali Products. In: Heaton CA, editor. An Introduction to Industrial Chemistry. Third ed. Glasgow, UK: Blackie Academic and Professional; 1996. p. 289-308.

[124] Hamann CH, Hamnett A, Vielstich W. Electrochemistry. 1st ed. Weinheim, Germany: Wiley-VCH; 1998.

[125] Larminie J, Dicks A. Fuel Cell Systems Explained. 2nd ed. Chichester, West Sussex PO19 8SQ, England: John Wiley & Sons Ltd.; 2003.

[126] Kerry FG. Industrial gas handbook : gas separation and purification. 1st ed. Boca Raton, FL: CRC Press; 2007.

[127] Lutgens FK, Tarbuck EJ. The Atmosphere: An Introduction to Meteorology. 4th ed. Englewood Cliffs, New Jersey: Prentice-Hall, Inc.; 1989.

[128] Heinz-Wolfgang H. Industrial Gases Processing. 1st ed. Weinheim: Wiley-VCH; 2008. p. 296.

[129] Baker RW. Membrane technology and applications. 2nd ed. Hoboken, NJ: John Wiley and Sons, Ltd.; 2004.

[130] Israelachvili J. Intermolecular and Surface Forces. 2nd ed. Burlington, MA: Academic Press; 1991.

[131] Ruthven DM, Farooq S, Knaebel KS. Pressure Swing Adsorption. 1st ed. New York, NY: VCH Publishers, Inc.; 1994.

[132] Hardenburger TL, Ennis M. Nitrogen. In: Kroschwitz JI, Howe-Grant M, editors. Kirk-Othmer Encyclopedia of Chemical Technology: John Wiley & Sons, Inc; 2005. p. 1-23.

[133] Mulder M. Basic principles of membrane technology. 2nd ed. Norwell, MA: Kluwer Academic Publishers; 1996.

[134] Baker RW. Membrane Technology. In: Kroschwitz JI, Howe-Grant M, editors. Kirk-Othmer Encyclopedia of Chemical Technology: John Wiley & Sons, Inc; 2005. p. 1-66.

[135] Downie NA. Industrial Gases. 1st ed. Boston: Kluwer Academic Publishers 1996.

[136] Brown RN. Compessors: Selection and Sizing. 3rd ed. Boston: Gulf Professional Publishing; 2005.

[137] Isalski WH. Separation of Gases. Oxford, UK: Clarendon Press; 1989.

[138] Gosnell J. Email Exchange with the author March 2-3, 2010. 2010.

[139] Pidwirny M. (Accessed: March 31, 2006). *Fundamentals of Physical Geography (Second ed.)*. Available: http://www.physicalgeography.net/fundamentals/8b.html

[140] Wetzel RG. Limnology. 2nd ed. Montreal, Quebec: Saunders College Publishing; 1983.

[141] Kalogirou S. Seawater desalination using renewable energy sources. Progress in Energy and Combustion Science. 2005;Vol. 31:242-81.

[142] Liu C, Migita R. Experiments of a prototype wind-driven reverse osmosis desalination system with feedback control. Desalination. 2002;Vol. 150:277-87.

[143] Williams LO, "Electrolysis of Seawater," presented at the Hydrogen Econ Miami Energy (THEME) Conference, Miami Beach, FL, USA, pgs. 417-24. March 18, 1974 - March 20, 1974, 1975: Plenum Press

[144] Fiorenza G, Sharma VK, Braccio G. Techno-economic evaluation of a solar powered water desalination plant. Energy conversion and management. 2003;Vol. 44:2217-40.

[145] Regional Energy Agency of Dodecanese S.A., Region of Crete - Regional Energy Agency, Punto Energia Provincia di Sassari - Multi S.P.A., GERLING Sustainable Development Project Gmbh, "RES Desalination Coupling Schemes: A technological database," European Commission Directorate-General for Energy and Transport. Report: 2001.

[146] Cerci Y, Cengel Y, Wood B, Kahraman N, Karakas ES, "Improving the Thermodynamic and Economic Efficiencies of Desalination Plants: Minimum Work Required for Desalination and Case Studies of Four Working Plants," University of Nevada, Revo, NV. Report: 99-FC-81-0183, 2003.

[147] Cooley H, Gleick PH, Wolff G, "Desalination with a grain of salt: A California Perspective," The Pacific Institute, Oakland, California. Report: 2006.

[148] García-Rodríguez L. Desalination by Wind Power. Wind Engineering. 2004;Vol. 28:453-63.

[149] Buros OK. The ABCs of Desalting. 2nd ed. Topsfield, MA: International Desalination Association; 2000.

[150] Al-Karaghouli A, Renne D, Kazmerski LL. Solar and wind opportunities for water desalination in the Arab regions. Renewable and Sustainable Energy Reviews. 2009;Vol. 13:2397-407.

[151] Pitter GA. The Economics of Desalination Processes. In: Amjad Z, editor. Reverse Osmosis: Membrane Technology, Water Chemistry, and Industrial Applications. New York, NY: Van Nostrand Reinhold; 1993. p. 77-103.

[152] Ulrich GD. A Guide to Chemical Engineering Process Design and Economics. 1st ed. New York, NY: John Wiley and Sons; 1984.

[153] Walas SM. Chemical Process Equipment: Selection and Design. 1st ed. Newton, MA: Butterworth-Heinemann; 1990.

[154] Long B, Garner B. Guide to Storage Tanks and Equipment. First ed. London, UK: Professional Engineering Publishing; 2004.

[155] Nielsen A. Ammonia Storage and Transportation Safety. In: Nielsen A, editor. Ammonia Catalysis and Manufacture. New York: Springer-Verlag Berlin Heidelberg; 1995. p. 329-46.

[156] Amos WA, "Costs of Storing and Transporting Hydrogen," National Renewable Energy Laboratory, Golden, CO. Report: NREL/TP-570-25106, 1998.

[157] Schlapbach L, Züttel A. Hydrogen-storage materials for mobile applications. Nature. 2001;Vol. 414:353-8.

[158] Zuttel A. Materials for hydrogen storage. Materials Today. 2003;Vol. 6:24-33.

[159] Bossel O, Eliasson B, Taylor G. (Accessed: 2005). *The Future of the Hydrogen Economy: Bright or Bleak?* Available: http://www.efcf.com/reports/E08.pdf

[160] Forsberg CW, "Assessment of Nuclear-Hydrogen Synergies with Renewable Energy Systems and Coal Liquefaction Processes," Oak Ridge National Laboratory. Report: ORNL/TM-2006/114, 2006.

[161] Jensen J, Vestbo a, Li Q, Bjerrum N. The energy efficiency of onboard hydrogen storage. Journal of Alloys and Compounds. 2007;Vol. 446-447:723-8.

[162] Tzimas E, Filiou C, Peteves SD, Veyret JB, "Hydrogen Storage: State-of-the-Art and Future Perspective," European Commission, Petten, The Netherlands. Report: EUR 20995 EN, 2003.

[163] U.S. Department of Energy. (Accessed: February 20, 2008). *FCT Hydrogen Storage: Gaseous and Liquid Hydrogen Storage*. Available: http://www1.eere.energy.gov/hydrogenandfuelcells/storage/hydrogen_storage.html#compressed

[164] Foh S, Novil M, Rockar E, Randolph P, "Underground Hydrogen Storage Final Report," Brookhaven National Laboratory, Upton, NY. Report: BNL 51275, 1979.

[165] Praxair Technology I. (Accessed: February 21, 2011). *Hydrogen Storage*. Available: http://www.praxair.com/praxair.nsf/AllContent/3A0AB529A089B473852571F0006398A3?OpenDocument&URLMenuBranch=19B4D941A5B182EE852571FC005510B2

[166] Succar S, Williams RH, "Compressed Air Energy Storage: Theory, Resources, and Applications for Wind Power," Princeton University, Princeton, NJ. Report: 2008.

[167] Energy Information Administration. (Accessed: May 15, 2008). *EIA - Natural Gas Pipeline Network - Underground Natural Gas Storage Facilities Map*. Available: http://www.eia.doe.gov/pub/oil_gas/natural_gas/analysis_publications/ngpipeline/undrgrndstor_map.html

[168] Meier S. Steel Water Storage Tanks: Design, Construction, Maintenence and Repair. New York, NY: McGraw Hill Professional; 2010.

[169] Ibrahim H, Ilinca A, Perron J. Energy storage systems—Characteristics and comparisons. Renewable and Sustainable Energy Reviews. 2008;Vol. 12:1221-50.

[170] Roberts B. Capturing Grid Power. IEEE Power & Energy Magazine. Piscataway, New Jersey: Institute of Electrical and Electronics Engineers; 2009. p. 32-41.

[171] Electricity Storage Association. (Accessed: February 9, 2009). *Power Quality, Power Supply*. Available: http://www.electricitystorage.org/ESA/technologies/

[172] Doughty DH, Butler PC, Akhil AA, Clark NH, Boyes JD. Batteries for Large-Scale Stationary Electrical Energy Storage. The Electrochemical Society Interface. 2010;Vol.:49-53.

[173] Sudworth JL, Tilley AR. The Sodium Sulfur Battery. New York: Springer; 1985.

[174] Wertheimer L. In Texas, One Really Big Battery. In: All Things Considered, editor.: National Public Radio; 2010.

[175] Huggins RA. Energy Storage. 1st ed. New York: Springer; 2010.

[176] Yang Z, Liu J, Baskaran S, Imhoff CH, Holladay JD. Enabling Renewable Energy and the Future Grid with Advanced Electricity Storage. JOM Journal of the Minerals, Metals and Materials Society. 2010;Vol. 62:14-23.

[177] Gretz J, Baselt JP, Ullmann O, Wendt H. The 100 MW Euro-Quebec Hydro-Hydrogen Pilot Project. International Journal of Hydrogen Energy. 1990;Vol. 15:419-24.

[178] Drolet B, Gretz J, Kluyskens D, Sandmann F, Wurster R. Euro-Quebec hydro-hydrogen pilot project [EQHHPP]: demonstration phase. International Journal of Hydrogen Energy. 1996;Vol. 21:305-16.

[179] Dugger GL, Olsen HL, Shippen WB, Francis EJ, Avery WH, "Tropical Ocean Thermal Power Plants and Potential Products," presented at the AIAA/AAS (American Astronaut Society) Solar Energy for Earth Conference Los Angeles, CA, USA, April 21-24, 1975: AIAA

[180] Avery WA, Blevins RW, Dugger GL, Francis EJ, "Maritime and Construction Aspects of Ocean Thermal Energy Conversion (OTEC) Plantships," The Johns Hopkins University Applied Physics Laboratory. Report: SR 76-1A, April 1976 1976.

[181] Richards D, Francis EJ, Dugger GL. Conceptual Designs for Commercial OTEC-Ammonia Production Plantships. Alternative Energy Sources. 1983;Vol. 4:185-99.

[182] Dugger GL, Francis EJ. Design of an Ocean Thermal Energy Plant Ship to Produce Ammonia via Hydrogen. International Journal of Hydrogen Energy. 1977;Vol. 2:231-49.

[183] Dugger GL, Henderson RW, Francis EJ, Avery WH. Projected Costs for Electricity and Products from OTEC Facilities and Plantships. Proceedings of the Intersociety Energy Conversion Engineering Conference. 1980;Vol. 2:1347-54.

[184] Avery WH, Richards D, Dugger GL. Hydrogen Generation by OTEC Electrolysis, and Economical Energy Transfer to World Markets via Ammonia and Methanol. International Journal of Hydrogen Energy. 1985;Vol. 10:727-36.

[185] Jourdan JP, Roguenant R, "Small Scale Ammonia Production as a Means for Hydrogen Storage," presented at the Second World Hydrogen Energy Conference, Zurich, Switzerland, pgs. 1401-29. 1978: Pergamon Press

[186] Abdel-Aal HK, "From Solar Hydrogen to Ammonium Fertilizer: An Assessment of Large-Scale Production in Saudi Arabia," presented at the Hydrogen Energy Progress V, Proceedings of the 5th World Hydrogen Energy Conference, Toronto, Ont, Can, pgs. 1803-17. 1984: Pergamon Press

[187] Treharne RW, Moles DR, Bruce MR, Rein BK, "Nitrogen Fertilizer Production by Solar Energy," presented at the Silver Jubilee Congress, Atlanta, GA, pgs. 2-5. 1979: Pergamon Press, Inc.

[188] Martin CW, Heber AJ, "Solar powered nitrogen fixation," presented at the Miami international conference on alternative energy sources, Miami Beach, FL, USA, pgs. 121-3. 1983: University of Nebraska, Lincoln

[189] Rein BK, Sullivan NW, Eisenbach PE, "Nitrogen fertilizer from solar energy," presented at the American Society of Mechanical Engineers, ASME Paper 80-3545, Chicago, Il, 1980: ASME

[190] Rozeman T, PFR Engineering Systems Inc., "Solar central receiver reformer system for ammonia plants," US Department of Energy, Marina Del Rey, CA. Report: DE-AC03-79SF10735, 1980.

[191] Ramakumar R, "Energy Storage Options for Harnessing Wind Energy," presented at the International Wind Energy Symposium Presented at 5th Annual Energy-Sources Technology Conference and Exhibition, New Orleans, LA, USA, pgs. 257-64. March 7 - March 10, 1982: ASME

[192] Heber AJ, Martin CW, Rein BK, "Nitrogen Fertilizer from Wind Energy," presented at the Winter Meeting American Society of Agricultural Engineers, Chicago, Illinois, 1982: ASAE

[193] NI-Lectra Corporation, "Wind-Electric Production of Nitrogen Fertilizer," U. S. Department of Energy. Report: DE83 009264, 1983.

[194] Ramakumar R, "Production of Hydrogen and Nitrogenous Fertilizer from Wind Energy," presented at the 2nd ASME Wind Energy Symposium Presented at 6th Annual Energy-Sources Technology Conference and Exhibition, Houston, TX, USA, pgs. 281-94. January 30 - February 3, 1983: ASME

[195] Suid LH. The Army's nuclear power program: the evolution of a support agency. Westport, Connecticut: Greenwood Publishing Group; 1990.

[196] Green Jr L. Ammonia Energy Vector for the Hydrogen Economy. International Journal of Hydrogen Energy. 1982;Vol. 7:355-9.

[197] MacKenzie JJ, Avery WH, "Ammonia fuel: The key to hydrogen-based transportation," presented at the Energy Conversion Engineering Conference, Washington, DC, USA, pgs. 1761-6. 1996: IEEE

[198] Avery WH. A Role for Ammonia in the Hydrogen Economy. International Journal of Hydrogen Energy. 1988;Vol. 13:761-73.

[199] Thomas G, Parks G, "Potential Roles of Ammonia in a Hydrogen Economy: A Study of Issues Related to the Use of Ammonia for On-Board Vehicular Hydrogen Storage," U.S. Department of Energy. Report: 2006.

[200] Feibelman PJ, Stumpf R. (Accessed: *Comments on Potential Roles of Ammonia in a Hydrogen Economy – A Study of Issues Related to the Use of Ammonia for On-Board Vehicular Hydrogen Storage*. Available: http://www.sandia.gov/surface_science/pjf/On_NH3_roles_in_H2_economy.pdf

[201] Klerke A, Christensen CH, Nrskov JK, Vegge T. Ammonia for hydrogen storage: Challenges and opportunities. Journal of Materials Chemistry. 2008;Vol. 18:2304-10.

[202] Reiter AJ, Kong S-C. Demonstration of compression-ignition engine combustion using ammonia in reducing greenhouse gas emissions. Energy and Fuels. 2008;Vol. 22:2963-71.

[203] Zamfirescu C, Dincer I. Ammonia as a green fuel and hydrogen source for vehicular applications. Fuel Processing Technology. 2009;Vol. 90:729-37.

[204] Bartels JR, Pate MB, "A feasibility study of implementing an ammonia economy," Iowa State University. Report: 2008.

[205] Kobylarz T, Al-Shehri A, "The application of wind energy to a system with an inherent energy storage medium," presented at the Intersociety Energy Conversion Engineering Conference, Boston, MA, pgs. 312-8. 1979: Americal Chemical Society

[206] Gileadi E, Srinivasan S, Salzano FJ, Braun C, Beaufrere A, Gottesfeld S. An Electrochemically Regenerative Hydrogen-Chlorine Storage System for Electric Utilities. Journal of Power Sources. 1979;Vol. 2:191-200.

[207] Murahara M, Seki K, "On site sodium manufacturing for energy storage with offshore wind power and seawater," presented at the 1st World Non-Grid-Connected Wind Power and Energy Conference, Nanjing, China, pgs. 407-11. September 24-26, 2009: IEEE Computer Society

[208] Murahara M, Seki K, "On-site sodium production with seawater electrolysis as alternative energy for oil by offshore wind power generation," presented at the 2008 IEEE Energy 2030 Conference, ENERGY 2008, Atlanta, GA, United States, November 17-18, 2008: Inst. of Elec. and Elec. Eng. Computer Society

[209] Miller J, Luyben WL, Belanger P, Blouin S, Megan L. Improving Agility of Cryogenic Air Separation Plants. Industrial & Engineering Chemistry Research. 2008;Vol. 47:394-404.

[210] Miller J, Luyben WL, Blouin S. Economic Incentive for Intermittent Operation of Air Separation Plants with Variable Power Costs. Industrial & Engineering Chemistry Research. 2008;Vol. 47:1132-9.

[211] Schucan T, "Case Studies of Integrated Hydrogen Systems," International Energy Agency Hydrogen Implementing Agreement. Report: 1999.

[212] Lehman PA, Chamberlin CE, Pauletto G, Rocheleau MA. Operating experience with a photovoltaic-hydrogen energy system. International Journal of Hydrogen Energy. 1997;Vol. 22:465–70.

[213] Szyszka A. Ten years of solar hydrogen demonstration project at Neunburg vorm Wald, Germany. International Journal of Hydrogen Energy. 1998;Vol. 23:849–60.

[214] Meurer C, Barthels H, Brocke WA, Emonts B, Groehn HG. PHOEBUS - an autonomous supply system with renewable energy: Six years of operational experience and advanced concepts. Solar Energy. 1999;Vol. 67:131-8.

[215] Ghosh PC, Emonts B, Janßen H, Mergel J, Stolten D. Ten years of operational experience with a hydrogen-based renewable energy supply system. Solar Energy. 2003;Vol. 75:469–78.

[216] Galli S, Stefanoni M. Development of a solar-hydrogen cycle in Italy. International Journal of Hydrogen Energy. 1997;Vol. 22:453–8.

[217] Stucki S, Scherer GG, Schlagowski S, Fischer E. PEM water electrolysers: Evidence for membrane failure in 100 kW demonstration plants. Journal of Applied Electrochemistry. 1998;Vol. 28:1041-9.

[218] Aguado M, Ayerbe E, Azcárate C, Blanco R, Garde R, Mallor F, et al. Economical assessment of a wind–hydrogen energy system using WindHyGen® software. International Journal of Hydrogen Energy. 2009;Vol. 34:2845-54.

[219] Bechrakis DA, McKeogh EJ, Gallagher PD. Simulation and operational assessment for a small autonomous wind-hydrogen energy system. Energy conversion and management. 2006;Vol. 47:46-59.

[220] Bernal-Agustin JL, Dufo-Lopez R. Hourly energy management for grid-connected wind–hydrogen systems. International Journal of Hydrogen Energy. 2008;Vol. 33:6401-13.

[221] Geer T, Manwell JF, McGowan JG, "A Feasibility Study of a Wind/Hydrogen System for Martha's Vineyard, Massachusetts," presented at the American Wind Energy Association Windpower 2005 Conference, Washington, D.C., USA, pgs. 27. 2005: American Wind Energy Association

[222] González A, McKeogh E, Gallochoir BO. The role of hydrogen in high wind energy penetration electricity systems: The Irish case. Renewable Energy. 2004;Vol. 29:471-89.

[223] Greiner C, Korpas M, Holen a. A Norwegian case study on the production of hydrogen from wind power. International Journal of Hydrogen Energy. 2007;Vol. 32:1500-7.

[224] Hakimi M, Tafreshi SMM, Rajati MR. Unit Sizing of a Stand-Alone Hybrid Power System Using Model-Free Optimization. 2007 IEEE International Conference on Granular Computing (GRC 2007). 2007;Vol.:751-6.

[225] Honnery D, Moriarty P. Estimating global hydrogen production from wind. International Journal of Hydrogen Energy. 2009;Vol. 34:727-36.

[226] Korpas M, Greiner C. Opportunities for hydrogen production in connection with wind power in weak grids. Renewable Energy. 2008;Vol. 33:1199-208.

[227] Mantz RJ, De Battista H. Hydrogen production from idle generation capacity of wind turbines. International Journal of Hydrogen Energy. 2008;Vol. 33:4291-300.

[228] Kassem N, "Offshore Wind Farms for Hydrogen Production Subject to Uncertainties," presented at the International Joint Power Generation Conference, Atlanta, GA, USA, pgs. 857-64. June 16-19, 2003: ASME

[229] Mathur J, Agarwal N, Swaroop R, Shah N. Economics of producing hydrogen as transportation fuel using offshore wind energy systems. Energy Policy. 2008;Vol. 36:1212-22.

[230] Shaw S, Peteves E. Exploiting synergies in European wind and hydrogen sectors: A cost-benefit assessment. International Journal of Hydrogen Energy. 2008;Vol. 33:3249-63.

[231] Short W, Blair N, Heimiller D, "Modeling the Market Potential of Hydrogen from Wind and Competing Sources," National Renewable Energy Laboratory, Denver, CO. Report: NREL/CP-620-38138, May 2005.

[232] Dutton AG, Ruddell AJ, Falchetta M, Prischich D, Dienhart H, Hug W, et al., "Hydrogen Generation from Stand-Alone Wind-Powered Electrolysis Systems," THE EUROPEAN COMMISSION. Report: JOU2-CT93-0413, 1996.

[233] Aprea JL. Hydrogen energy demonstration plant in Patagonia: Description and safety issues. International Journal of Hydrogen Energy. 2009;Vol. 34:4684-91.

[234] Dutton AG, Bleijs JAM, Dienhart H, Falchetta M, Hug W, Prischich D, et al. Experience in the design, sizing, economics, and implementation of autonomous wind-powered hydrogen production systems. International Journal of Hydrogen Energy. 2000;Vol. 25:705-22.

[235] Eide PO, Hagen EF, Kuhlmann M, Rohden R, "Construction and Commissioning of the Utsira Wind / Hydrogen Stand-Alone Power System," presented at the European Wind Energy Conference and Exhibtion (EWEC), London, UK, pgs. 1-4. November 22-25, 2004: EWEC

[236] Gammon R, Roy A, Barton J, Little M, "Hydrogen and Renewables Integration (HARI)," IEA Hydrogen Implementing Agreement. Report: 2006.

[237] Harrison KW, Martin GD, "Renewable Hydrogen: Integration, Validation, and Demonstration," Sacramento, CA. Report: NREL/CP-581-43114, July 2008.

[238] Harrison KW, Martin GD, Ramsden TG, Kramer WE, "The Wind-to-Hydrogen Project: Operational Experience, Performance Testing, and Systems Integration," National Renewable Energy Laboratory. Report: NREL/TP-550-44082, March 2009.

[239] Nakken T, Strand LR, Frantzen E, Rohden R, Eide PO, "The Utsira wind-hydrogen system - operational experience," presented at the European Wind Energy Conference and Exhibition (EWEC), Athens, Greece, 2006: EWEC

[240] Ulleberg Ø. Stand-alone power systems for the future: optimal design, operation & control of solar-hydrogen energy systems [Doktor Ingenior]. Trodheim, Norway: Norwegian University of Science and Technology; 1998.

[241] Rebenitsch R, Bush R, Boushee A, Woeste J, Basin Electric Power Cooperative, Brad G. Stevens PE, et al., "Wind-to-Hydrogen Energy Pilot Project: Basin Electric Power Cooperative," U.S. Department of Energy. Report: 2009-EERC-06-11, 2009.

[242] Jorgensen C, Ropenus S. Production price of hydrogen from grid connected electrolysis in a power market with high wind penetration. International Journal of Hydrogen Energy. 2008;Vol. 33:5335-44.

[243] Levene JI, "Economic Analysis of Hydrogen Production from Wind," Denver, CO. Report: NREL/CP-560-38210, May 2005.

[244] Levene J, Kroposki B, Sverdrup G, "Wind Energy and Production of Hydrogen and Electricity — Opportunities for Renewable Hydrogen," presented at the 2006 POWER-GEN Renewable Energy and Fuels Technical Conference, Las Vegas, NV, April 10-12, 2006:

[245] Peters RR, Stevens B, Mann MD, Salehfar H, "Dynamic scheduling of wind energy for hydrogen production by electrolysis," presented at the IEEE Power Engineering Society General Meeting, PES, Montreal, QC, Canada, June 18 - June 22, 2006: Inst. of Elec. and Elec. Eng. Computer Society

[246] Bilodeau A, Agbossou K. Control analysis of renewable energy system with hydrogen storage for residential applications. Journal of Power Sources. 2006;Vol. 162:757-64.

[247] Korpas M. Distributed Energy Systems with Wind Power and Energy Storage [Doktor ingeniør]. Trondheim, Norway: Norwegian University of Science and Technology; 2004.

[248] Zhou T, Francois B. Modeling and control design of hydrogen production process for an active hydrogen/wind hybrid power system. International Journal of Hydrogen Energy. 2009;Vol. 34:21-30.

[249] Bernal-Agustín JL, Dufo-López R. Simulation and optimization of stand-alone hybrid renewable energy systems. Renewable and Sustainable Energy Reviews. 2009;Vol. 13:2111-8.

[250] Agbossou K, Chahine R, Hamelin J, Laurencelle F, Anouar A, St-Arnaud J, et al. Renewable energy systems based on hydrogen for remote applications. Journal of Power Sources. 2001;Vol. 96:168-72.

[251] Dufo-Lopez R, Bernal-Agustın JL, Contreras J. Optimization of control strategies for stand-alone renewable energy systems with hydrogen storage. Renewable Energy. 2007;Vol. 32:1102–26.

[252] Dufo-Lopez R, Bernal-Agustın JL. Multi-objective design of PV– wind– diesel– hydrogen– battery systems. Renewable Energy. 2008;Vol. 33:2559– 72.

[253] Nelson DB, Nehrir MH, Wang C. Unit sizing and cost analysis of stand-alone hybrid wind/PV/fuel cell power generation systems. Renewable Energy. 2006;Vol. 31:1641-56.

[254] Kolhe M, Agbossou K, Hamelin J, Bose T. Analytical model for predicting the performance of photovoltaic array coupled with a wind turbine in a stand-alone renewable energy system based on hydrogen. Renewable Energy. 2003;Vol. 28:727-42.

[255] Zoulias EI, Lymberopoulos N. Hydrogen-based Autonomous Power Systems: techno-economic analysis of the integration of hydrogen in autonomous power systems. London: Springer-Verlag; 2008.

[256] Ipsakis D, Voutetakis S, Seferlis P, Stergiopoulos F, Elmasides C. Power management strategies for a stand-alone power system using renewable energy sources and hydrogen storage. International Journal of Hydrogen Energy. 2009;Vol. 34:7081-95.

[257] Khan MJ, Iqbal MT. Analysis of a small wind-hydrogen stand-alone hybrid energy system. Applied Energy. 2009;Vol. 86:2429-42.

[258] Zhou K, Ferreira JA, de Haan SWH. Optimal energy management strategy and system sizing method for stand-alone photovoltaic-hydrogen systems. International Journal of Hydrogen Energy. 2008;Vol. 33:477-89.

[259] Nehrir DMH, Wang C. Modeling and Control of Fuel Cells: Distributed Generation Applications: John Wiley and Sons 2009.

[260] Mathioulakis E, Belessiotis V, Delyannis E. Desalination by using alternative energy: Review and state-of-the-art. Desalination. 2007;Vol. 203:346-65.

[261] Garcia-Rodriguez L. Seawater desalination driven by renewable energies: a review. Desalination. 2002;Vol. 143:103-13.

[262] García-Rodríguez L. Renewable energy applications in desalination: state of the art. Solar Energy. 2003;Vol. 75:381-93.

[263] Tzen E, Morris R. Renewable energy sources for desalination. Solar Energy. 2003;Vol. 75:375-9.

[264] Elnashar a. The economic feasibility of small solar MED seawater desalination plants for remote arid areas. Desalination. 2001;Vol. 134:173-86.

[265] Fathalah KA, Darwish MA, Aly SE. Simulation of a solar powered vapor compression desalination system (SPRVCD). J Eng Appl Sci. 1983;Vol. 2:11-24.

[266] Helal AM, Al-Malek SA. Design of a solar-assisted mechanical vapor compression (MVC) desalination unit for remote areas in the UAE. Desalination. 2006;Vol. 197:273-300.

[267] Herold D, Horstmann V, Neskakis A, Plettner-Marliani J, Piernavieja G, Calero R. Small scale photovoltaic desalination for rural water supply - demonstration plant in Gran Canaria. Renewable Energy. 1998;Vol. 14:293-8.

[268] Herold D, Neskakis A. A small PV-driven reverse osmosis desalination plant on the island of Gran Canaria. Desalination. 2001;Vol. 137:285-92.

[269] Eltawil MA, Zhengming Z, Yuan L. A review of renewable energy technologies integrated with desalination systems. Renewable and Sustainable Energy Reviews. 2009;Vol. 13:2245-62.

[270] Kalogirou S. Survey of solar desalination systems and system selection. Energy. 1997;Vol. 22:69-81.

[271] Witte T, Siegfriedsen S, El-Allawy M. WindDeSalter Technology: Direct use of wind energy for seawater desalination by vapour compression or reverse osmosis. Desalination. 2003;Vol. 156:275-9.

[272] Feron P. Use of Windpower in Autonomous Reverse Osmosis Seawater Desalination. Wind Engineering. 1985;Vol. 9:180-99.

[273] Garcia-Rodriguez L, Romero-Ternero V, Gomez-Camacho C. Economic analysis of wind-powered desalination. Desalination. 2001;Vol. 137:259-65.

[274] Kiranoudis CT, Voros NG, Maroulis ZB. Wind energy exploitation for reverse osmosis desalination plants. Desalination. 1997;Vol. 109:195-209.

[275] Habali SM, Saleh IA. Design of stand-alone brackish water desalination wind energy system for Jordan. Solar Energy. 1994;Vol. 52:525-32.

[276] Carta JA, Gonzalez J, Subiela V. Operational analysis of an innovative wind powered reverse osmosis system installed in the Canary Islands. Solar Energy. 2003;Vol. 75:153-68.

[277] Carta JA, Gonzalez J, Subiela V. The SDAWES project: An ambitious R and D prototype for wind-powered desalination. Desalination. 2004;Vol. 161:33-48.

[278] Subiela VJ, Carta JA, Gonzalez J. The SDAWES project: Lessons learnt from an innovative project. Desalination. 2004;Vol. 168:39-47.

[279] Veza J, Penate B, Castellano F. Electrodialysis desalination designed for off-grid wind energy. Desalination. 2004;Vol. 160:211-21.

[280] Infield D. Performance Analysis of a Small Wind Powered Reverse Osmosis Plant. Solar Energy. 1997;Vol. 61:415-21.

[281] Joule-Thermie Programme, "Desalination Guide Using Renewable Energies," Center for Renewable Energy Sources. Report: 1998.

[282] Plantikow U. Wind-powered MVC seawater desalination — operational results. Desalination. 1999;Vol. 122:291-9.

[283] Gaiser P, Plantikow U, "Seawater Desalination by Wind-Powered Mechanical Vapour Compression Plants," presented at the International Desalination Association World Congress on Desalination and Water Sciences, Abu Dhabi, pgs. 411-24. 1995: International Desalination Association

[284] Waelti H, Cavalieri RP. Matching Nitrogen Equipment to Your Needs. Tree Fruit Postharvest Journal 1990;Vol. 1:3-13.

[285] Jansen JO, Bandur V, Bjerrum NJ, Jensen SH, Ebbesen S, Mogensen M, et al., "Pre-Investigation of Water Electrolysis," Energinet.dk, Fredericia, Denmark. Report: PSO-F&U 2006-1-6287, 2008.

[286] Genovese J, Harg K, Paster M, Turner J, "Current (2009) State-of-the-Art Hydrogen Production Cost Estimate Using Water Electrolysis," National Renewable Energy Laboratory, Golden, CO. Report: NREL/BK-6A1-46676, 2009.

[287] Stolten D, Krieg D, Weber M. (Accessed: September 4, 2010). *An Overview on Water Electrolysis*. Available: http://www.ifi.unicamp.br/ceneh/WICaC2010/PDF/24-DetlefStolten.pdf

[288] Ramsden T. Current (2005) Hydogen Production from Central Grid Electrolysis. Golden, CO: NREL; 2008.

[289] Hydrogen Technologies. (Accessed: March 3, 2010). *Hydrogen Technologies*. Available: http://www3.statoil.com/hydrogentechnologies/svg03816.nsf?OpenDatabase

[290] Cipollina A, Micale G, Rizzuti L. Seawater Desalination for Freshwater Production. In: Cipollina A, Micale G, Rizzuti L, editors. Seawater Desalination: Conventional and Renewable Energy Processes. Heidelberg, Germany: Springer-Verlag; 2009.

[291] Huang W-Y, "Impact of Rising Natural Gas Prices on U.S. Ammonia Supply," United States Department of Agriculture, Washington, D.C. Report: WRS-0702, 2007.

[292] Reese M. (Accessed: June 6, 2007). *Wind to Hydrogen to Ammonia*. Available: http://renewables.morris.umn.edu/wind/conferences/2007/Reese-WindToAmmonia.pdf

[293] Ganley JC, Holbrook JH, McKinley DE. (Accessed: January 10, 2007). *Solid State Ammonia Synthesis*. Available: http://www.energy.iastate.edu/Renewable/ammonia/ammonia/2007/SSAS_Oct2007_Final.pdf

[294] Holbrook JH, Ganley JC. Method and apparatus for anhydrous ammonia production. In: United States Patent and Trademark Office (USPTO), editor. United States: NH Three LLC; 2010.

[295] Morud J, Skogestad S. Analysis of Instability in an Industrial Ammonia Reactor. AIChE Journal. 1998;Vol. 44:888-95.

[296] Turton R, Bailie RC, Whiting WB, Shaeiwitz JA. Analysis, Synthesis and Design of Chemical Processes. 3rd ed. Boston, MA: Prentice Hall; 2009.

[297] Peters MS, Timmerhaus KD. Plant Design and Economics for Chemical Engineers. 5th ed. New York, NY: McGraw-Hill; 2003.

[298] Navarrete PF, Cole WC. Planning, Estimating, and Control of Chemical Construction Projects. 2nd ed. New York, NY: Marcel Dekker, Inc.; 2001.

[299] Feng Y, Rangaiah GP. Evaluating Capital Cost Estimation Programs. Chemical Engineering. 2011;Vol. 118:22-9.

[300] Guthrie KM. Process Plant Estimating Evaluation and Control. 1st ed. Solana Beach, CA: Craftsman Book Company of America; 1974.

[301] Green DW, Perry RH. Perry's Chemical Engineers' Handbook. 8th ed. New York, NY: McGraw-Hill; 2008.

[302] U.S. Bureau of Labor Statistics. (Accessed: January 3, 2011). *Producer Price Index (PPI)*. Available: http://www.bls.gov/ppi/home.htm

[303] Cremer H. Thermodynamic Balance and Analysis of a Synthesis Gas and Ammonia Plant. In: Gaggioli RA, editor. Thermodynamics: Second Law Analysis: American Chemical Society; 1980. p. 111-27.

[304] Kirova-Yordanova Z. Exergy analysis of industrial ammonia synthesis. Energy. 2004;Vol. 29:2373–84.

[305] Couper JR, Hertz DW, Smith FL. Process Economics. In: Green DW, Perry RH, editors. Perry's Chemical Engineers' Handbook. 8th ed. New York, NY: McGraw-Hill; 2008. p. (9-1) - (9-56).

[306] Woods DR. Process Design and Engineering Practice. Englewood Cliffs, NJ: Prentice Hall, Inc.; 1995.

[307] Seider WD, Seader JD, Lewin DR. Product and Process Design Principles: Synthesis, Analysis, and Evaluation. 2nd ed. New York, NY: John Wiley and Sons, Inc.; 2004.

[308] Rase HF. Chemical Reactor Design for Process Plants. New York, NY: John Wiley & Sons Inc; 1977.

[309] Froment GF, Bischoff KB. Chemical Reactor Analysis and Design. 1st ed. New York, NY: John Wiley & Sons; 1979.

[310] Cengel YA, Boles MA. Thermodynamics: An Engineering Approach. 6th ed. New York, NY: McGraw-Hill; 2006.

[311] Deobald R, Hayes J, Sigurdson S. Ammonia Synthesis with Alternate Feedstock. Saskatoon, Saskatchewan, Canada: University of Saskatchewan; 2007.

[312] U.S. Bureau of Labor Statistics. (Accessed: January 11, 2012). *Basic Chemical Manufacturing - May 2010 National Industry-Specific Occupational Employment and Wage Estimates*. Available: http://www.bls.gov/oes/current/naics4_325100.htm

[313] Menanteau P, Quéméré MM, Le Duigou A, Le Bastard S. An economic analysis of the production of hydrogen from wind-generated electricity for use in transport applications. Energy Policy. 2011;Vol. 39:2957-65.

[314] National Renewable Energy Laboratory. Technology Brief: Analysis of Current-Day Commercial Electrolyzers. Golden, CO: National Renewable Energy Laboratory,; 2004.

[315] Ringer M, "H2A Delivery Components Model Version 1.1: Users Guide," National Renewable Energy Laboratory, Golden, CO. Report: 2006.

[316] Mintz M, Elgowainy A, Gillette G, "H2A Delivery Scenario Analysis Model Version 2.0 (HDSAM 2.0) User's Manual," Argonne National Laboratory, Argonne, IL. Report: 2008.

[317] Ramsden TG, Steward D, Zuboy J, "Analyzing the Levelized Cost of Centralized and Distributed Hydrogen Production Using the H2A Production Model, Version 2," National Renewable Energy Laboratory, Golden, CO. Report: NREL/TP-560-46267, 2009.

[318] U.S. Department of Energy. (Accessed: January 5, 2012). *DOE Hydrogen and Fuel Cells Program: DOE H2A Analysis*. Available: http://www.hydrogen.energy.gov/h2a_analysis.html

[319] OANDA Corporation. (Accessed: January 5, 2012). *Historical Exchange Rates | OANDA*. Available: http://www.oanda.com/currency/historical-rates/

[320] U.S. Department of Commerce. (Accessed: January 20, 2012). *BEA National Economic Analysis*. Available: http://www.bea.gov/iTable/iTableHtml.cfm?reqid=9&step=3&isuri=1&910=X&911=0&903=4&904=2000&905=2010&906=A

[321] European Union. (Accessed: June 24, 2012). *Eurostat - Data Explorer*. Available: http://appsso.eurostat.ec.europa.eu/nui/show.do

[322] Officer LH, Williamson SH. (Accessed: January 21, 2011). *Computing 'Real Value' Over Time With a Conversion Between U.K. Pounds and U.S. Dollars, 1830 to Present*. Available: http://www.measuringworth.com/exchange/

[323] Lazaridis LP. Economic Comparison of HVAC and HVDC Solutions for Large Offshore Wind Farms under Special Consideration of Reliability [Master's]. Stockholm, Sweden: Royal Institute of Technology; 2005.

[324] Gonen T. Electrical Machines With Matlab. 2nd ed. Boca Raton, FL: CRC Press; 2012.

[325] Matche.com. (Accessed: January 8, 2003). *Matches provides 275 process equipment conceptual capital cost estimates* Available: http://matche.com/EquipCost/index.htm

[326] El-Halwagi MM. Sustainable Design Through Process Integration: Fundamentals and Applications to Industrial Pollution Prevention, Resource Conservation, and Profitability Enhancement. Waltham, MA: Elsevier Science; 2011.

[327] Air Products and Chemicals. (Accessed: December 16, 2011). *Gas Facts*. Available: http://www.airproducts.com/en/products/gases/gas-facts.aspx

[328] Taylor R, Kooijman H. (Accessed: 2006). *Simulation of an Air Separation Unit*. Available: http://www.chemsep.com/downloads/data/CScasebook_ASU.pdf

[329] van Baten J, Baur R. Cape Open to Cape Open Simulator Environment (COCO). http://www.cocosimulator.org/; 2011.

[330] Sirdeshpande AR, Ierapetritou MG, Andrecovich MJ, Naumovitz JP. Process Synthesis Optimization and Flexibility Evaluation of Air Separation Cycles. AIChE Journal. 2005;Vol. 51:1190-200.

[331] Linde AG. (Accessed: November 15, 2011). *Aluminum Plate-Fin Heat Exchangers*. Available: http://www.linde-engineering.com/en/images/P_3_2_e_10_150dpi19-5772.pdf

[332] Kohil AA, Farag HA, Ossman ME. Mathematical Modeling of a Multi-Stream Brazed Aluminum Plate Fin Heat Exchanger. Thermal Science. 2010;Vol. 14:103-14.

[333] Haslego C, Laval A, Polley G. Designing Plate and Frame Heat Exchangers. Chemical Engineering Progress. 2002;Vol. 98:32-7.

[334] Dwarnick W. Email Exchange Regarding Nitrogen Plants. Personal Communication; April 13, 2010.

[335] El-Dessouky HT, Ettouney HM. Fundamentals of Salt Water Desalination. 1st ed. New York: Elsevier 2002.

[336] Ettouney H. Design of single-effect mechanical vapor compression. Desalination. 2006;Vol. 190:1-15.

[337] Towler G, Sinnott R. Chemical Engineering Design: Principles, Practice and Economics of Plant and Process Design. Boston, MA: Butterworth-Heinemann; 2008.

[338] Ettouney HM, El-Dessouky HT, Faibish RS, Gowin PJ. Evaluating the economics of desalination. Chemical Engineering Progress. 2002;Vol. 98:32-9.

[339] Mannvit Engineering. (Accessed: January 3, 2012). *Anhydrous Refrigerated Ammonia Storage Tanks & Systems | Mannvit*. Available: http://www.mannvit.com/Industry/AmmoniaStorage/

[340] Lele GS. Ammonia Storage: Selection and Safety Issues. Chemical Industry Digest. 2008;Vol.:85-9.

[341] Pittsburgh Corning. Foamglas Industrial Insulation Handbook. 1st ed. Watterloo, Belgium: Pittsburgh Corning Europe; 1992.

[342] Webb D. (Accessed: February 13, *Large Scale Ammonia Storage and Handling*. Available: www.irc.wisc.edu/file.php?id=21

[343] Smil V. Enriching the Earth: Fritz Haber, Carl Bosch, and the Transformation of World Food Production. Cambridge, MA: MIT Press; 2001.

[344] Energy Information Administration. (Accessed: July 12, 2011). *Electric Power Monthly*. Available: http://www.eia.gov/cneaf/electricity/epm/epm_ex_bkis.html

[345] foxislandswind.com. (Accessed: February 10, 2012). *Fox Islands Wind Project*. Available: http://www.foxislandswind.com/

[346] The Cianbro Companies. (Accessed: February 12, 2011). *Fox Islands Wind Project*. Available: http://www.cianbro.com/ProjectsMarkets/PowerGenerationEnergy/FoxIslandsWindProject.aspx

[347] Bolinger M, "Community Wind: Once Again Pushing the Envelope of Project Finance," Ernest Orlando Lawrence Berkeley National Laboratory, Berkeley, CA. Report: LBNL-4193E, January 2011.

[348] U.S. Bureau of Labor Statistics. (Accessed: January 20, 2012). *Consumer Price Index (CPI)*. Available: http://www.bls.gov/cpi/

[349] U.S. Census Bureau. (Accessed: January 10, 2011). *NAICS Main Page*. Available: http://www.census.gov/eos/www/naics/

[350] Vestas Wind Systems. (Accessed: 2011). *Vestas V82 1.65 MW*. Available: http://www.vestas.com/files/filer/en/brochures/productbrochurev821_65_uk.pdf

[351] U.S. Bureau of Labor Statistics. (Accessed: 2012). *Producer Price Index Industry Data - Discontinued Series (NAICS Basis): Multi-Screen Data Search: US Bureau of Labor Statistics*. Available: http://data.bls.gov/cgi-bin/dsrv?nd

[352] Bolinger M, Wiser R, "Understanding Trends in Wind Turbine Prices Over the Past Decade," Ernest Orlando Lawrence Berkeley National Laboratory, Berkeley, CA. Report: LBNL-5119E, October 2011.

[353] Wiser R, Bolinger M, "2010 Wind Technologies Market Report," United States Department of Energy, Washington, D.C. Report: DOE/GO-102011-3322, June 2011.

[354] Elkinton CN. Offshore Wind Farm Layout Optimization [PhD]. Amherst, MA: University of Massachusetts; 2007.

[355] Dicorato M, Forte G, Pisani M, Trovato M. Guidelines for assessment of investment cost for offshore wind generation. Renewable Energy. 2011;Vol. 36:2043-51.

[356] Morthorst PE, Lemming J, Clausen N-E. Development of Offshore Wind Power – Status and Perspectives. In: Twidell J, Gaudiosi G, editors. Offshore Wind Power. Brentwood, Essex, UK: Multi-Science Publishing Co. Ltd.; 2010. p. 1-13.

[357] The Economist Online. The Big Mac index. The Economist. London, United Kingdom: The Economist; 2012.

[358] Anonymous. Economic Indicators. Chemical Engineering. 2012;Vol. 119:55.

[359] Officer LH, Williamson SH. (Accessed: January 21, 2011). *Choosing the Best Indicator to Measure Relative Worth*. Available: http://www.measuringworth.com/indicator.php

[360] Her Majesty's Treasury. (Accessed: January 21, 2012). *Latest Figures - HM Treasury*. Available: http://www.hm-treasury.gov.uk/data_gdp_fig.htm

[361] International Monetary Fund (IMF). (Accessed: June 24, 2012). *World Economic Outlook Database September 2011*. Available: http://www.imf.org/external/pubs/ft/weo/2011/02/weodata/index.aspx

[362] Danmarks Nationalbank. (Accessed: June 20, 2012). *Nationalbanken // Euro // Web Document // Introduction to the euro*. Available: http://www.nationalbanken.dk/DNUK/Euro.nsf/side/Introduction_to_the_euro!OpenDocument

[363] Shemilt I, Thomas J, Morciano M. A web-based tool for adjusting costs to a specific target currency and price year. Evidence & Policy. 2010;Vol. 6:51-9.

[364] European Commission, "Eurostat-OECD Methodological Manual on Purchasing Power Parities," Organization for Economic Cooperation and Development (OECD), Paris, France. Report: 2006.

[365] Taylor AM, Taylor MP. The Purchasing Power Parity Debate. Journal of Economic Perspectives. 2004;Vol. 18:135-58.

[366] Heston A, Summers R, Aten B. (Accessed: May 10, 2011). *Penn World Table Version 7.0*. Available: http://pwt.econ.upenn.edu/php_site/pwt70/pwt70_form.php

[367] Organization for Economic Co-Operation and Development (OECD). (Accessed: May 22, 2012). *4. PPPs and exchange rates*. Available: http://stats.oecd.org/Index.aspx?DataSetCode=SNA_TABLE4

[368] Van Der Temple J. Design of Support Structures for Offshore Wind Turbines [PhD]. Delft, The Netherlands: Technical University of Delft; 2006.

[369] American Petroleum Institute, "Recommended Practice for Planning, Designing and Constructing Fixed Offshore Platforms—Working Stress Design," American Petroleum Institute, Washington, D.C. Report: G2AWSD, 2000.

[370] Nielsen P, "Offshore Wind Energy Projects Feasibility Study Guidelines SEAWIND ALTENER PROJECT," EMD International A/S, Aalborg, Denmark. Report: 4.1030/Z/01-103/2001, 2003.

[371] Offshore Design Engineering (ODE) Limited, "Study of the Costs of Offshore Wind Generation: A Report to the Renewables Advisory Board (RAB) & DTI," Kingston-upon-Thames, UK. Report: URN Number 07/779, 2007.

[372] ABB Power Technologies AB. XLPE Cable Systems. In: ABB Power Technologies AB, editor. Karlskrona, Sweden: ABB Power Technologies AB; 2009.

[373] Jeppsson J, Larsen PE, Larsson A, "Technical Description Lillgrund Wind Power Plant," Vattenfall. Report: 2_1 LG Pilot Report, 2008.

[374] Nielsen OB, "Thanet Offshore Wind Farm – Case Study," presented at the Renewable UK Offshore Wind 2010, Liverpool, UK, 2010: Vattenfall UK Offshore Wind Power

[375] Office of the Gas and Electricity Markets (Ofgem), RBC Capital Markets. Preliminary Information Memorandum: Thanet Offshore Transmission Assets. http://wwwofgemgovuk/Networks/offtrans/rott/Documents1/Thanet%20-%20Project%20specific%20Preliminary%20Information%20Memorandum%20(PIM)pdf. London, UK: Ofgem; 2009.

[376] Christiansen P, Jørgensen KK, Sørensen AG, "Grid Connection and Remote Control for the Horns Rev 150MW Offshore Wind Farm in Denmark," presented at the EPSRC Offshore Wind Energy Network Workshop on Electrical Design of Offshore Wind Installations, Oxfordshire, UK, 2000: http://www.hornsrev.dk

[377] Dong Energy. (Accessed: July 12, 2012). *About the Project*. Available: http://www.dongenergy.com/Hornsrev2/EN/about_horns_rev_2/About_the_Project/Pages/about_the_project.aspx

[378] Prinses Amaliawindpark. (Accessed: July 12, 2012). *Windpark Q7*. Available: http://www.q7wind.nl/en/index.htm

[379] Gerdes G, Tiedemann A, Zeelenberg S, "Case Study: European Offshore Wind Farms - A Survey for the Analysis of the Experiences and Lessons Learnt by Developers of Offshore Wind Farms - Final Report," Pushing Offshore Wind Energy Regions (POWER), Groningen, The Netherlands. Report: 2005.

[380] Office of the Gas and Electricity Markets (Ofgem), RBC Capital Markets. Preliminary Information Memorandum: Gunfleet Sands Offshore Transmission Assets. Ofgem. London, UK: http://www.ofgem.gov.uk/Networks/offtrans/rott/Documents1/Gunfleet%20Sands%20-%20Project%20specific%20Preliminary%20Information%20Memorandum%20(PIM).pdf; 2009.

[381] power-technology.com. (Accessed: July 12, 2012). *Gunfleet Sands Windfarm - Power Technology*. Available: http://www.power-technology.com/projects/gunfleetsandswindfar/

[382] Lundberg S, "Performance comparison of wind park configurations," Chalmers University of Technology, Goteborg, Sweden. Report: 30R, 2003.

[383] Statistics Sweden. (Accessed: April 17, 2012). *HICP, (2005=100) - Statistics Sweden*. Available: www.scb.se/Pages/TableAndChart____33932.aspx

[384] Knodel B, "A high-level overview of offshore wind project development identifying current technologies, challenges, risks and costs.," presented at the IEEE Boston Power Energy Society, Boston, MA, November 16, 2010: IEEE Boston PES

[385] Short W, Sullivan P, Mai T, Mowers M, Uriarte C, Blaire N, et al., "Regional Energy Deployment System (ReEDS)," National Renewable Energy Laboratory, Golden, CO. Report: NREL/TP-6A20-46534, 2011.

[386] Halliday D, Resnick R, Walker J. Fundamentals of Physics. 6th ed. New York: John Wiley and Sons; 2001.

[387] Schachner J. Power Connections for Offshore Wind Farms. Leoben, The Netherlands: Delft University of Technology; 2004.

[388] Morgan CA, Snodin HM, Scott NC, "Offshore Wind: Economies of scale, engineering resource and load factors," Dept of Trade and Industry / Carbon Trust, Bristol, UK. Report: 3914/BR/01, December 18 2003.

[389] power-technology.com. (Accessed: July 12, 2012). *Robin Rigg Wind Farm - Power Technology*. Available: http://www.power-technology.com/projects/robinriggwind/

[390] Ocean Energy Institute. (Accessed: January 14, 2010). *Energy as a Complete System*. Available: http://www.oceanenergy.org/energysystem.asp

[391] National Data Buoy Center. (Accessed: February 10, 2012). *NDBC - Station MISM1*. Available: http://www.ndbc.noaa.gov/station_page.php?station=mism1

[392] MassGIS. (Accessed: December 2, 2011). *OLIVER*. Available: http://maps.massgis.state.ma.us/map_ol/oliver.php

[393] WinWinD. (Accessed: June 11, 2012). *The New WinWinD 3 - WinWinD*. Available: http://www.winwind.com/en/offering/winwind-3/#detailed-data

[394] Short W, Packey DJ, Holt T, "A Manual for the Economic Evaluation of Energy Efficiency and Renewable Energy Technologies," National Renewable Energy Laboratory, Golden, CO. Report: TP-462-5173, 1995.

[395] Branker K, Pathak MJM, Pearce JM. A Review of Solar Photovoltaic Levelized Cost of Electricity. Renewable & Sustainable Energy Reviews. 2011;Vol. 15:4470-82.

[396] OpenEI. (Accessed: June 20, 2012). *Transparent Cost Database | Transparent Cost Database*. Available: http://en.openei.org/apps/TCDB/

[397] ISO New England. (Accessed: July 6, 2012). *ISO New England - Locational Marginal Pricing*. Available: http://www.iso-ne.com/nwsiss/grid_mkts/how_mkts_wrk/lmp/index.html

[398] ISO New England. (Accessed: July 12, 2011). *ISO New England - Markets*. Available: http://www.iso-ne.com/markets/hrly_data/selectHourlyLMP.do

[399] Argonne National Laboratory. GREET Transportation Fuel Cycle Analysis Model. 1.8b ed. Argonne, IL: Argonne National Laboratory; 2008.

[400] Energy Information Administration. (Accessed: June 25, 2012). *United States Natural Gas Industrial Price (Dollars per Thousand Cubic Feet)*. Available: http://205.254.135.7/dnav/ng/hist/n3035us3a.htm

[401] Schnitkey G. (Accessed: March 22, 2012). *FarmdocDaily: Seasonal Fertilizer Prices*. Available: http://www.farmdocdaily.illinois.edu/2012/01/seasonal_fertilizer_prices.html

[402] Cumalioglu I, Ertas A, Ma Y, Maxwell T. State of the Art: Hydrogen storage. Journal of Fuel Cell Science and Technology. 2008;Vol. 5:(034001-1)-10.

[403] Osterle JF. The Thermodynamics of Compressed Air Exergy Storage. Journal of Energy Resources Technology. 1991;Vol. 113:7-11.

[404] Ibrahim H, Ilinca A, Perron J. Energy storage systems—Characteristics and comparisons. Renewable and Sustainable Energy Reviews. 2008;Vol. 12:1221–50.

[405] Dunn B, Kamath H, Tarascon J-M. Electrical Energy Storage for the Grid: A Battery of Choices. Science. 2011;Vol. 334:928-35.

[406] U.S. Department of Energy. Federal Energy Management Program - Quick Guide: Renewable Energy Certificates. In: U.S. Department of Energy - Energy Efficiency and Renewable Energy (EERE), editor. http://wwwnrelgov/docs/fy11osti/52105pdf. 1st ed. Washington, D.C.: U.S. Department of Energy; 2011.

[407] U.S. Department of Energy Office of Energy Efficiency and Renewable Energy Federal Energy Management Program. Renewable Energy Requirement Guidance for EPACT 2005 and Executive Order 13423. Washington, D.C.: U.S. Department of Energy; 2008.

[408] The 102nd US Congress. Energy Policy Act of 1992 (Public Law 102-486). In: Congress US, editor. 106 Statute 2776. Washington, D.C.: United States; 1992.

[409] Holt EA, Wiser R, "The Treatment of Renewable Energy Certificates, Emissions Allowances, and Green Power Programs in State Renewables Portfolio Standards," Ernest Orlando Lawrence Berkeley National Laboratory, Berkeley, CA. Report: LBNL-62574, April 2007.

[410] American Wind Energy Association. Production Tax Credit (PTC). In: American Wind Energy Association, editor. http://aweaorg/issues/federal_policy/upload/PTC_April-2011pdf. Washington, D.C.: AWEA; 2011.

[411] U.S. Department of Energy. (Accessed: June 15, 2011). *Alternative Fuels and Advanced Vehicles Data Center: Alternative and Advanced Fuels*. Available: http://www.afdc.energy.gov/afdc/fuels/index.html

[412] Harper JP, Karcher MD, Bolinger M, "Wind Project Financing Structures: A Review & Comparative Analysis," Ernest Orlando Lawrence Berkeley National Laboratory, Berkeley, CA. Report: LBNL-63434, September 2007.

[413] Google.com. (Accessed: June 15, 2012). *wind ethanol plant - Google Search*. Available: https://www.google.com/search?sugexp=chrome,mod=11&ix=h9&sourceid=chrome&ie=UTF-8&q=wind+ethanol+plant

[414] Cory K, Schwabe P, "Wind Levelized Cost of Energy: A Comparison of Technical and Financing Input Variables," NREL, Golden, CO. Report: NREL/TP-6A2-46671, 2009.

[415] Wiser R, Bolinger M, "Renewable Portfolio Standards in the United States: A Status Report with Data through 2007," Lawrence Berkeley National Laboratory, Berkeley, CA. Report: LBNL-154E, April 2008.